Magnetic properties of the Itinerant helimagnets MnSi and FeGe

Gregory, Christopher Ian

Magnetic Properties of the Itinerant Helimagnets MnSi and FeGe

Christopher Ian Gregory, B.Sc. (Dunelm)

A thesis submitted to the University of Durham in candidature for the degree of Doctor of Philosophy

December 15, 1992

Abstract

This thesis describes high quality magnetisation measurements made on single crystals of MnSi, FeGe and $ZrZn_2$ using a vibrating sample magnetometer. The measurements on MnSi have also been complemented with neutron scattering experiments.

MnSi is a heavily investigated itinerant helimagnet which exhibits a variety of interesting phenomena associated with formation of a helical spin density wave propagating along $< 111 >$ directions. Magnetisation measurements were performed as a function of magnetic field at fixed temperatures stepping through the magnetic transition observed at 29.1 ± 0.05K. These were found to be highly anisotropic and included observation of the so-called 'Phase A' consistent with measurements using other techniques and providing explanation of apparent anomalies in previous magnetisation data (Kadowaki *et al.* (1981)). Further investigation of 'Phase A' using small angle neutron scattering (SANS) was successful in determining the magnetic state of MnSi within this regime in terms of helix reorientation which is shown to be broadly consistent with the expression for the free energy derived by Bak and Jensen (1980) and Plumer and Walker (1981). Reorientation of the helical spin density wave as a function of magnetic field was also studied using SANS to complement the magnetisation measurements. The second order process observed is similar to that predicted by Plumer and Walker (1981) and the form of their model for the magnetisation of is compared with the experimental results. Finally, anomalous magnetisation measurements close to the magnetic transition were further explored through neutron scattering. The results suggest a possible isotropic phase pre-empting the helical spin density wave formation.

Cubic FeGe is also capable of supporting a static helical spin density wave and has a critical temperature of 278.7K with helix propagating along $< 100 >$ directions above 211K and along $< 111 >$ directions below 211K (for decreasing temperatures). Magnetisation measurements were made on cubic FeGe with magnetic field applied parallel to the $< 100 >$ direction and the magnetic phase diagram determined. Coupled with the SANS data of Lebech *et al.* (1989) it shows similar processes in terms of helix reorientation in an applied magnetic field occur for both FeGe and MnSi. The magnetic phase diagram is in good agreement with that predicted by Plumer (1990) for magnetic field applied parallel to the $< 100 >$.

Bak P. and Jensen M. (1980), J. Phys. C**13**,L881-885.
Kadowaki K *et al.* (1981), J. Phys. Soc. Jpn. **53**, 3624.
Lebech B. *et al.* (1989), J. Phys.:Condensed Matter **1**, 6105-6122.
Plumer M.L. and Walker M.B. (1981), J. Phys. C**14**, 4689-4699.
Plumer M.L. (1990), J. Phys.:Condensed Matter **2**, 7503-7510.

Dedicated to my father.

Acknowledgements

I welcome this opportunity to express my gratitude to the many people who have supported me during this course of study. The research described in this thesis was carried out in the Solid State Laboratory at the University of Durham together with short periods of time spent at the Manchester VSM facility based at the Schuster Laboratory, Manchester University and the Department of Solid State Physics, Risø National Laboratory, Denmark. The work was done between October 1989 and November 1992. The financial support of the Science and Engineering Research Council is appreciated.

I am grateful to Professor A.W. Wolfendale and Professor A. Martin for the provision of the facilities of the Physics Department. I thank Professor B.K. Tanner for providing me with the opportunity to undertake this study, the facilities of his laboratory and the freedom to develop this work.

I would like to offer Professor B. Lebech, Dr. N. Bernhoeft and Dr. D. Lambrick special thanks for their continual support, encouragement and enthusiasm for condensed matter physics. I also gratefully acknowledge the work of Dr. S. Brown and Dr. S. Hayden in preparation of the samples used, without which this work would not have been possible. I also thank all my colleagues in the Solid State Group at Durham University who have contributed to my time in Durham, in particular Mr. C.M. Friend, Mr. J. Hudson and Mr. S.M. Westwood.

I am much indebted to the complete technical backing of the Physics Department at Durham. Mr. P. Foley and Mr. J. Scott for their keen assistance in the laboratory. The excellent support of all members of both the Student Workshop under the supervision of Mr. D. Jobling and Mr. P. Armstrong, and Electronics Workshop under the supervision of Mr. T. Jackson. The advice and assistance of Mr. M. Lee and Miss. V. Greener in the Audio Visual Workshop and Mrs. P. Russel in the Graphics Office is gratefully acknowledged, together with the work of secretarial staff of the department. Their geniality has been a great source of encouragement during this period.

I greatly appreciate the support of my family and friends during this time, in particular my sister, Miss. L. Backhurst and Mr. J. Wilkinson.

Declaration

I declare that the work contained in this thesis has not been submitted for a degree at this University or any other. All the work presented herein was conducted by the author unless stated otherwise.

C.I. Gregory

November, 1992.

Publications

'Magnetisation Study of the Magnetic Phase Diagram in MnSi'
C.I. Gregory, D.B. Lambrick and N.R. Bernhoeft,
J. of Magn. and Magn. Mat. **104-107** (1992), 689-690.

Contents

Chapter 1

Magnetism: an introduction

1.1 Introduction

The first evidence of magnetic phenomena relates to the use of a lodestone compass by the Chinese, dating back to the fourth century BC. During the nineteenth century it was found that a similar force was exerted between two current carrying wires. However, despite its long recorded history, it was not until the advent of quantum theory this century that magnetic order could be explained at an atomic level. Even today, although there exist numerous empirical relationships to describe the bulk magnetic behaviour of materials, no theory yet exists that can adequately describe the magnetisation of all materials.

To account for such phenomena, the existence of a magnetic field is postulated. When a substance is placed in a magnetic field $\underline{H}$, it has a resultant magnetisation due to this external field. This field will induce inside the medium a flux density $\underline{B}$ which will be dependent on the magnetisation per unit volume $\underline{M}$ of the medium. In cgs units, in free space $\underline{B}$ is numerically equal to $\underline{H}$. In any other medium

$$\underline{B} = (\underline{H_i} + 4\pi\underline{M}) \tag{1.1}$$

where $\underline{H_i} = \underline{H} - \underline{H_D}$ and $\underline{H_D}$ is the demagnetisation field due to the sample geometry.

The magnetisation density $\underline{M}$ of a quantum mechanical system of volume V, in thermal equilibrium at a temperature T, in a uniform magnetic induction H_i is defined to be:

$$\underline{M} = -\frac{1}{V}\frac{\partial F}{\partial H_i} \tag{1.2}$$

where F is the magnetic Helmholtz free energy and H_i is the magnetic field acting on the body (see section *Demagnetising Field*).

Magnetic materials are usually classified according to the nature of their response to an applied magnetic field $\underline{H}$, that is according to their magnetic susceptibility χ. The susceptibility is a parameter characteristic of the substance considered. In this

thesis, the differential magnetic susceptibility is used and defined as:

$$\chi = \frac{\partial \underline{M}}{\partial \underline{H}_i} \tag{1.3}$$

and due to the above definition, is also:

$$\chi = -\frac{1}{V}\frac{\partial^2 F}{\partial \underline{H}_i^2} \tag{1.4}$$

1.2 Diamagnetism

Diamagnetism is the property of substances that have a negative magnetic susceptibility i.e. the magnetic field produced in the material opposes the applied magnetic field.

1.2.1 Susceptibility of Insulators with complete electron shells (Larmor Diamagnetism)

Consider a solid composed of ions or atoms with complete electronic shells. Such ions or atoms have a resultant spin and orbital angular momentum of zero in the ground state. On application of a magnetic field, a change is induced in the orbital motion of the electrons. In a manner analogous to Lenz's Law, this change produces a moment opposing the applied field and hence the magnetic susceptibility is negative. As all materials (apart from atomic hydrogen) consist of some complete electron shells, this response occurs in all materials, it is however usually very small and masked by other additional moments present.

1.2.2 Conduction Electron Diamagnetism (Landau Diamagnetism)

Diamagnetic affects arise from the coupling of the field to the orbital motion of the conduction electrons. In some high purity materials at low temperature and high magnetic field this motion is used to map the Fermi surface through the de Haas Van Alphen affect. Although at higher temperatures and in most materials the oscillations are not perceptible, the dependence of $\underline{M}$ on $\underline{H}$ does not average to zero and there is a net nonvanishing magnetisation antiparallel to $\underline{H}$. This is known as Landau diamagnetism and is due to the orbital electronic motion induced by the field.

1.3 Paramagnetism

Paramagnetism is the property of substances that have a positive magnetic susceptibility.

1.3.1 Susceptibility of Insulators containing ions with a partially filled electron shell

The circulatory motion of a filament current gives rise to a magnetic dipole moment. If a current i encloses an area $\underline{S}$ then the dipole moment produced is given by:

$$\underline{m_d} = i\underline{S} \tag{1.5}$$

A single electron will have a magnetic dipole moment associated with its motion, both its angular momentum $\underline{l}$ and also its intrinsic angular momentum or spin $\underline{s}$. This is written as:

$$\begin{aligned} \underline{m_d} &= \underline{m_l} + \underline{m_s} \\ &= (\frac{e}{2m})\underline{l} + g_s(\frac{e}{2m})\underline{s} \end{aligned} \tag{1.6}$$

where e and m are the charge and mass of the electron respectively and g_s is the gyromagnetic ratio. The integral unit of magnetic moment for the electron, the Bohr magneton, μ_B, is that for the lowest orbital state i.e. $\mu_B = \frac{e\hbar}{2m}$. Therefore

$$\underline{m_d} = \mu_B \frac{(\underline{l} + g_s\underline{s})}{\hbar} \tag{1.7}$$

Thus in the case of insulators with a partially filled electron shell, each ion will have a resultant magnetic moment which is free to be orientated in any direction. The resultant moment of the ion is dependent on the order in which the one electron levels are filled in the outer electron shell.This determines both the total angular momentum $\underline{L}$ and total spin $\underline{S}$ of the ion. The degeneracy is lifted by electron-electron and electron spin-orbit interactions such that the order of filling is deteremined by Hund's rules. Thermal effects tend to randomise these orientations whereas the application of a magnetic field tends to align the magnetic moments. It can be shown (see for example *'Solid State Physics'* by Ashcroft and Mermin) that in the high field or low temperature limit:

$$\chi = \frac{1}{3}\frac{N}{V}\frac{\mu_B^2 P^2}{k_B T} \tag{1.8}$$

$$= \frac{C}{T} \tag{1.9}$$

where N are the number of such ions in a volume V, k_B is the Boltzman Constant, T is the temperature, C is the Curie Constant and P is the 'effective Bohr magneton number' given by P=$g_s(JLS)[J(J+1)]^{\frac{1}{2}}$ where J is the total angular momentum quantum number such that $(\underline{J} = \underline{L} + \underline{S})$.

This inverse dependence of the susceptibility with temperature and its independancy on field is known as Curie's Law. It characterises paramagnetic systems with 'permanent moments' whose alignment is favoured by field and opposed by temperature. It accurately describes the behaviour of insulating crystals containing rare earth ions which have partially filled electronic f-shells.

1.3.2 Susceptibility of Metals - Independant electron model (Pauli Paramagnetism)

The above model applies only to localised moments. However work on the metallic state with individual conduction electrons not spatially localised produced a band model. Assuming the electrons to be independent and neglecting their orbital angular momentum, then upon application of an external magnetic field, the magnetic energy of a conduction electron will be either $-B_0\mu_B$ if the spin points parallel to the field or $+B_0\mu_B$ if it points antiparallel. The effect of the field is to shift the energy of each electronic level by $\pm B_0\mu_B$ dependent on the spin. Since electron energy levels will be filled up to the Fermi energy, this results in more electrons with spin orientated parallel to the field and hence a resultant magnetisation. However for an electron to move from a spin down state to spin up state, it has to move to an unoccupied energy level above the highest filled level in the absence of an applied field i.e. its kinetic energy is increased. An equilibrium between reduction in magnetic energy and increase in kinetic energy is established which leaves an excess of up spins. The resultant magnetisation is

$$M = -\mu_B(n_+ - n_-) \tag{1.10}$$

where $n_\pm$ is the number of electrons per unit volume with spin parallel (+) or antiparallel (-) to B_0. Application of Fermi Dirac statistics shows that (see for example *'Solid State Magnetism'*, by Crangle):

$$\chi = \mu_B^2 n(E_F) \tag{1.11}$$

where $n(E_F)$ is the electron density of states at the Fermi energy.

This is known as Pauli paramagnetic susceptibility and is independant of magnetic field.

1.4 Ferromagnetism

Ferro/ferri/antiferro magnetism is the property of materials that exhibit spontaneous magnetic order. To explain the occurence of this spontaneous order observed in some materials below a critical temperature, Weiss (1907) proposed the existence of an internal field, a 'Weiss molecular field' which would align moments in a similar manner to an external field. In the local moment model this yields the Curie-Weiss law:

$$\chi = \frac{C}{T - \theta} \tag{1.12}$$

where θ the Curie temperature marking the onset of internal ordering.

1.5 The Exchange Interaction

The origin of such a 'molecular field' was unclear as, to explain alignment, the magnitude of the field had to be far greater than that generated by dipole interaction

within the solid. An interaction of sufficient energy was only discovered with the advent of quantum theory which also provided the necessary concept of electron spin.

The Pauli exclusion principle requires that the total wavefunction, Ψ, of a system of N electrons must be antisymmetric, linking the spin state of the system to its spatial wavefunction. Heisenberg (1928) was the first to demonstrate that this could lead to magnetic order when he considered the hydrogen molecule. As the Hamiltonian is spin independent, the solution wavefunction can be written as the product of an orbital stationary state and the components of electron spin in a given direction:

$$\Psi = \psi(r_1, r_2)\chi(1,2) \tag{1.13}$$

where ψ is the spatial function of two electrons at positions r_1 and r_2 and χ is their relative spin direction to a particular axis. If $\psi_a(r_1)$ and $\psi_b(r_2)$ are the spatial wavefunctions of the atomic electrons a and b respectively and α and β are the spin states up and down respectively, then possible solutions are:

$$\begin{aligned} \Psi &= \psi_{symmetric}\chi_{antisymmetric} \\ &= \frac{1}{2}(\psi_a(r_1)\psi_b(r_2) + \psi_a(r_2)\psi_b(r_1)) \qquad (\alpha(r_1)\beta(r_2) - \alpha(r_2)\beta(r_1)) \end{aligned}$$

or

$$\begin{aligned} \Psi &= \psi_{antisymmetric}\chi_{symmetric} \\ &= \frac{1}{2}(\psi_a(r_1)\psi_b(r_2) - \psi_a(r_2)\psi_b(r_1)) \qquad (\alpha(r_1)\alpha(r_2)) \\ &\qquad\qquad\qquad\qquad\qquad\qquad (\alpha(r_1)\beta(r_2) + \alpha(r_2)\beta(r_1)) \\ &\qquad\qquad\qquad\qquad\qquad\qquad (\beta(r_1)\beta(r_2)) \end{aligned}$$

In the case of $\psi_{antisym}$ the wavefunction vanishes for $r_1 = r_2$ so that the electrons in the spin triplet state tend to 'keep away' from each other and hence have a relatively small repulsion energy. However, for ψ_{sym} the wavefunction does not vanish for $r_1 = r_2$ and the electrons may be very close at certain times, experiencing a stronger repulsion than $\psi_{antisym}$, raising the energy of the state. The Pauli exclusion principle introduces a coupling between the space and the spin variables of the electrons which act as if they are moving under the influence of a force whose sign depends on the relative orientation of their spins and is known as the exchange force.

More generally, the exchange energy is described by the Heisenberg Hamiltonian which sums the interaction between neighbouring atoms i and j over all N atoms in the solid:

$$H_{ex} = -2\sum_{\substack{i=1 \\ i\neq j}}^{N}\sum_{\substack{j=1 \\ j\neq i}}^{N} J_{ij}S_i.S_j \tag{1.14}$$

where S_i is the spin quantum number of the ion. The exchange energy is governed by the sign and magnitude of J_{ij}, the exchange constant derived by considering the

spatial wavefunctions of the electrons from the atoms or ions. For ferromagnetism to occur J_{ij} must be positive.

The Heisenberg model of magnetism describes the origin of magnetic ordering through interatomic exchange interactions which tend to align neighbouring electrons at atomic sites either parallel or antiparallel. The model applies to moments fixed in magnitude on atoms which are well separated so they retain free atom characteristics but whose orientation may vary and has been used with some success to describe magnetism in insulating materials.

1.5.1 Types of Exchange

The Heisenberg model is an example of an interaction known as direct exchange. The development of magnetic theory has led to the prediction of other types of exchange coupling between spins. Superexchange is the coupling of the spins of magnetic atoms by nonmagnetic atoms via the electronic charge distribution on the nonmagnetic atoms. Indirect exchange is the coupling of the localised spins of unfilled inner electron shells via polarisation of the conduction electrons. Finally, itinerant exchange is that between the conduction electrons which are able to move within a metal crystal; its development is briefly outlined below.

1.5.2 Development of the Itinerant model of Magnetism

The magnetism of metals has been a controversial subject and the development of a workable model remains one of the major unsolved problems of solid state theory. The great difficulty is the fact that metallic magnetism is a truly cooperative phenomenon arising from the corellated motion of a large number of mutually interacting electrons.

The theory of ferromagnetism prevalent in the 1930s was that developed by Heisenberg (1928) involving localised electrons in direct exchange interactions. Application of this model to metals suggested that the mean magnetic moment should be an integral number of Bohr magnetons per atom however in the case of Nickel the experimentally observed value is 0.6 Bohr magnetons per atom. Van Vleck (1953) suggested the Heisenberg model to still be applicable by assuming the atoms to posses different electron configurations, i.e. be in different states of ionisation with d electrons being mobile. Mott (1935) postulated a band model to explain the experimental observation, with a very marked overlap between 4s and 3d bands leading to a non integral saturation magnetisation of 0.6 Bohr magnetons. The main problem with this idea was the explaination of or 'source' of ferromagnetism. According to Slater (1936) in early band calculations, it is the exchange interaction between electrons in the same atomic shell which produce a parallel orientation.

The first major contribution to the field of itinerant magnetism was made by Stoner (1938), (1939) through his collective electron model. The Heisenberg model had given physical interpretation to the molecular field proposed by Weiss. An alternative to this model could continue to use this molecular field hypothesis, leaving

it to later research to interpret this field under conditions of nonlocalisation. On this basis, and the assumption of Fermi statistics, Stoner produced a model in which the electrons are treated as unbounded or free, the influence of the periodic lattice potential is described by an effective mass of the electron and the many body interactions by a field which is parallel to the external field. The Stoner equations (see for example *'Introduction to the Theory of Magnetism'* by Wagner or Wohlfarth (1981)) result in an expression for the number of up/down spin electrons in an applied magnetic field to be

$$n\pm = \int_0^\infty N(E)[exp(\frac{E - \mu \mp \epsilon \mp \mu_B H}{k_B T}) + 1]^{-1} \tag{1.15}$$

where μ is the chemical potential, k_B the Boltzman constant, T the temperature, μ_B the Bohr magneton, H the applied magnetic field and ϵ the interaction parameter.

$$\epsilon = \frac{1}{2} n I \xi \tag{1.16}$$

where n is the total number of electrons ($n = n_+ + n_-$), I the effective interaction between particles and ξ the relative magnetisation i.e. the ratio of the number of excess parallel spins to the total number of potentially effective spins at full saturation. Stoner originally used an effective temperature θ' to represent the molecular field coefficient:

$$k_B \theta' = \frac{1}{2} n I \tag{1.17}$$

The problem was to solve for $\xi = \xi(T, H, I)$ on the basis of equation (1.17). By assuming the density of states curve to be of a parabolic shape, it can be shown (see for example *'Intoduction to the Theory of Magnetism'* by Wagner) that in the case of H=0, T=0, an expression for the spontaneous magnetisation ξ is obtained of the form:

$$\frac{2 k_B \theta'}{E_F} = (1 + \xi_0)^{\frac{2}{3}} - (1 - \xi_0)^{\frac{2}{3}} \tag{1.18}$$

where E_F is the Fermi energy. For ferromagnetism to occur at all, i.e. $\xi(0, 0, I) > 0$, the Stoner criterion must be satisfied:

$$I N(E_F) > 1 \tag{1.19}$$

Equation (1.20) has solutions with $\xi_0 \neq 0$ for certain values of the parameter I and those such that $\xi(0, 0, I) < 1$ define the state of weak itinerant ferromagnetism. This occurs if

$$\frac{2}{3} \leq \frac{k_B \theta'}{E_F} < 2^{-\frac{1}{3}} \tag{1.20}$$

Also in the paramagnetic state, the resulting susceptibility is given by:

$$\chi = \frac{\chi_p}{1 - \frac{3 k_B \theta'}{2 E_F}} \tag{1.21}$$

where χ_p is the noninteracting (Pauli) susceptibility. In the paramagnetic state, the value of the denominator lies between 0 and 1 and the susceptibility is enhanced by the exchange interactions. This is known as the Stoner enhancement.

Stoner theory is quite successful in explaining the ground state properties of itinerant systems but calculations of high temperature properties are too simplistic. It cannot account for the temperature dependance of the magnetisation and predicts transition temperatures far above those actually observed. Within the Stoner theory there is no reason why the susceptibility in the paramagnetic state should exhibit Curie-Weiss behaviour observed over a wide temperature range in weakly magnetic systems. In this model, because the electrons are independant, the only possible excitations are due to spin flip processes and this kind of excitation are known as Stoner excitations.

The importance of the interaction between the excited electrons and holes was first considerred by Slater (1937) in his theory of bound collective modes in ferromagnetic insulators. This was extended to ferromagnetic metals and developed by Herring (1952), within the so-called Random Phase Approximation (R.P.A.). The introduction of electron correlations resulted in the appearance of collective spin wave modes at large wavelengths and lower energies, before merging into the Stoner continuum at higher energies. The interaction between the spin waves was considered by Dyson (1956), producing an expression for the modification of the spin wave energies as a consequence.

Rhodes and Wohlfarth (1963) considered the ratio of the local moment obtained from the Curie-Weiss susceptibility above the Curie temperature (T_c) with the saturated low temperature moment. If the T_c is not too high, this ratio gives a useful measure of the itinerancy of the magnetic electrons. This ratio is expected to be unity for a localised system and larger than unity for intinerant materials.

A different theoretical approach is that via the development of a Landau Ginzburg model of ferromagnetism (Edward and Wohlfarth (1967)). For weak itinerant ferromagnets, the magnetisation $\underline{M}(T, B)$ can at all temperatures be regarded as an order parameter. The free energy can in general be expanded in terms of even powers of the order parameter due to the symmetry of the problem such that:

$$F(M) = F(0) + \frac{A}{2}M^2 + \frac{b}{4}M^4 + ... - M.H_i \tag{1.22}$$

assuming A and b are independant of magnetisation and field. This results in an equation of state where the magnetic field which stabilises a magnetisation M is given by:

$$H_i = AM + bM^3 \tag{1.23}$$

For zero magnetic field, this has two solutions:
M(T,0) = 0 above T_c in the paramagnetic state.
M(T,0) = $(\frac{-A}{b})^{\frac{1}{2}}$ below T_c where $A < 0$.

Also from this expression:

$$\chi_{\|}{}^{-1} = \frac{\partial H_i}{\partial M} = A + 3bM^2 \tag{1.24}$$

This model is successful in explaining some of the experimental properties of weak itinerant ferromagnets including linear 'Arrot Plots' of the form $M^2(T, B)$

vs $H_i/M(T,B)$ over a wide temperature range T and magnetic field range H_i (a consequence of the form of equation (2)). Also, qualitative agreement of the experimental behaviour of the magnetisation as a function of temperature can be obtained by suitable choice of the form of A(T).

Numerous attempts have been made to develop the above analysis by adding additional terms to the expression for the free energy. The free energy at fixed temperature T, volume V, number of particles nNa (Na is the number of atoms) and characterised by a particular magnetisation M can be written in the form (Taillefer (1986a)),

$$F(M) = F_0(M) + \Delta_0 F(M) + \Delta_1 F(M) \tag{1.25}$$

where $F_0(M)$ is the noninteracting free energy for a given single particle density of states. $\Delta_0 F(M)$ is the Hartree Fock correction due to particle interactions of the form

$$\Delta_0 F(M) = -\frac{1}{2}\lambda V M^2 \text{ where } \lambda \text{ is the interaction parameter} \tag{1.26}$$

Combined with the first term they define a Stoner theory in which elementary excitations may be thought of as uncorrelated particle hole pairs in the presence of a molecular field λM. The last term represents corrections to this Stoner theory arising from correlations in the motion of these excited particle-hole pairs. These give rise to thermally excited, enhanced magnetic fluctuations.

Previously, the problems of interacting electrons had been reduced to a problem of almost noninteracting quasiparticles. The developing model considers the interactions between electrons in terms of the spatial and temporal fluctuations in charge and spin densities (Herring (1966)). Both models are equally valid, simply different sides of the same coin and to descibe the system fully, both may be required. However, the latter description suggests that narrow band d metals and f metals may be understood with a single unified picture. The spectrum of magnetic fluctuations becomes the quantity of central interest, possibly being localised in real or reciprocal space.

The Random Phase Approximation, whilst predicting spin waves, takes no account of their effect upon the Stoner equilibrium state. This was done by Murato and Doniach (1972) and extended by Moriya and Kawabata (1973). However, full vector analysis was performed by Lonzarich and Taillefer (1985) who considerred both longitudinal and transverse fluctuations on the system.

Lonzarich and Taillefer (1985) use the local magnetic density as an order parameter but express it in terms of its mean value $\underline{M}$ and the slowly varying average of the deviation of the exact local magnetisation of the mean, $\underline{m}(\underline{r},t)$. It is then assumed that the local free energy can be expanded in terms of this slowly varying magnetisation (taking terms to 4th order in $\underline{M}$):

$$f(\underline{r}) = f_0 + \frac{a}{2}|\underline{M} + \underline{m}(r)|^2 + \frac{b}{2}|\underline{M} + \underline{m}(r)|^4 + \frac{c}{2}\sum_{\mu}|\Delta m_\nu(\underline{r})|^2 + \ldots\ldots \tag{1.27}$$

where $\underline{m}(\underline{r},t)$ is expanded in terms of its Fourier components. As the temperature is increased from 0K, the available thermal energy will induce excitation of certain

modes of the local magnetisation. For low temperatures and weakly ferromagnetic metals, long wavelength modes will dominate the excitations. In order to account for this, a temperature dependant wavevector cut-off is introduced to the model such that:

$$m(\underline{q}) = m(\underline{q}) \; q < q_c$$
$$m(\underline{q}) = 0 \text{ otherwise}$$

The choice of q_c is taken so that modes are excited thermally i.e. the elementary excitations involved obey Bose statistics (whereas Stoner excitations obey Fermi statistics).

At some temperature T, the spectrum observed in a particular metal is dependant on two elements. The extrinsic thermal energy available for excitation and the intrinsic susceptibility of the various modes to thermal excitation, contained in the expression for the dynamic susceptibility $\chi_\nu(q,\omega)$. By producing an expression for $\chi_\nu(q,\omega)$ based on the Random Phase Approximation but incorporating the affect of modes already excited, the resulting equation of state is:

$$H_i = AM + bM^3 \text{ where} A = a + b[3 < m_{||}{}^2 > +2 < m_{\perp}{}^2 >] \qquad (1.28)$$

$< m_{||}{}^2 >$ and $< m_{\perp}{}^2 >$ are the thermal variances of the local magnetisation parallel and perpendicular to the average magnetisation $\underline{M}$ respectively. a and b are two of four parameters of the complete theory, all of which are measurable experimentally. This model successfully accounts for:

1. Linear Arrot plots.
2. The T^2 fall of the magnetisation as the temperature is raised below T_c.
3. The Curie-Weiss paramagnetic susceptibility.
4. The magnitude of T_c.
5. The ratio of the magnetic moments in the ferro and paramagnetic states.
6. The form of the paramagnetic dynamical susceptibility.
7. The magnitude of the spin fluctuation contribution to the enhancement of the observed affective mass.

1.6 Demagnetising Field

Consider a specimen of finite size placed in a uniform magnetic field. The total flux density $\underline{B}$ is conserved and will be the same outside the specimen as in the material itself. If the applied field is $\underline{H_a}$ the magnetic field effectively acting internally on the material to produce a magnetic flux is less than the externally applied field. This is due to the 'demagnetising field' produced within the specimen, in opposition to its magnetisation. The demagnetising field is dependent on the magnitude of the magnetisation and the specimen geometry. The field H_i acting inside the body may be written:

$$\underline{H_i} = \underline{H} - \underline{H_D} \qquad (1.29)$$
$$(1.30)$$

where H_D is the demagnetising field. The demagnetising factor N_D is defined by:

$$\underline{H_D} = -N_D \underline{M} \tag{1.31}$$

1.7 Magnetocrystalline Anisotropy

The energy associated with the magnetisation of a ferro/ferri or antiferromagnet is dependent on the direction of magnetisation with respect to the crystallographic axes. The energy is lowest in an easy direction and a higher field must be applied to make the magnetisation lie in a harder direction. The spins are coupled to the electronic charge density via the spin orbit coupling and their energy therefore depends to some extent on their absolute orientation with respect to the crystal axes, as well as their relative orientation with respect to one another.

In an attempt to minimise the magnetocrystalline energy, a crystal may undergo a small deformation when magnetised and if not allowed to expand freely may cause internal stress in the crystal. Conversely the application of stress to a crystal will affect the lattice and hence the magnetocrystalline energy.

1.8 Magnetic Domains

In order to account for the magnetic properties of ferromagnetic materials, including the ability to have zero magnetisation both with and without an applied field and to display magnetic hysteresis, Weiss (1907) postulated the existence of magnetic domains - separate magnetised regions of macroscopic size in the sample. Each domain is intrinsically fully magnetised under the influence of exchange interactions. However, the demagnetised state corresponds to a collection of separate domains orientated with no net magnetisation. On application of relatively low fields there is an overall change in the magnetisation due to rearrangement of domains and the boundaries between them, involving two main processes. In one process, the volume of domains favourably orientated with respect to the applied field grows at the expense of those unfavourably orientated (i.e. there is a displacement of the domain walls). In the other, the magnetisation of the domain rotates toward the field direction. The two processes may occur either reversibly or irreversibly depending on the strength of the field and nature of the sample.

Landau and Lifshitz (1935) showed that the subdivision of a specimen into domains resulted in a considerable reduction in the magnetostatic energy, as opposed to the saturated condition, minimising the demagnetising field. This reduction in energy through domain formation does not continue indefinetly, as it must be offset against the increase in energy due to the necessary creation of new domain boundaries. The spin near the boundary of a domain will experience unfavourable exchange interactions with nearby spins in a neighbouring misaligned domain. However, because the exchange interaction is short ranged, only the spins near the domain boundaries will have their exchange energies raised. In contrast, the gain in

magnetic dipolar energy is a bulk effect - because of the long range of the interaction, the dipolar energy of every spin drops when domains are formed.

A domain wall consists of the transition layer which separates adjacent domains magnetised in different directions. The total angular displacement across a wall is commonly 180° or 90°. Generally the whole spin change takes place gradually, being a compromise between the opposing influences of exchange energy and magnetocrystalline anisotropy energy. In a crude classical model, the exchange energy of successive pairs of spins seperated by an angle $\frac{\pi}{n}$ will not be the minimum value $-JS^2$, but rather

$$\begin{aligned} E_{ex} &= -JS^2 cos(\frac{\pi}{n}) \\ &\approx -JS^2[1 - \frac{1}{2}(\frac{\pi}{n})^2] \end{aligned} \tag{1.32}$$

If it takes n steps to produce 180° spin reversal, the energy cost will be:

$$\begin{aligned} \Delta E &\approx n[-JS^2 cos\frac{\pi}{n} - (-JS^2)] \\ &\approx \frac{\pi^2}{2n} JS^2 \end{aligned} \tag{1.33}$$

which lowers with the steps taken, n. However this will result in more spins lying out of the the easy direction, increasing the anisotropy energy so that the domain wall width is the result of a compromise between the two opposing effects.

Thus domain formation results in a lowering of the total magnetic free energy.

1.9 References

Dyson F.J. (1956), Phys. Rev. **102**, 1217, 1230.
Edwards D.M. and Wohlfarth E.P. (1967), Proc. R. Soc. London **A303**, 127.
Heisenberg W. (1928), Z. Physik **49**,619.
Herring C. (1952), Phys. Rev. **87**,60.
Herring C. (1966), in *Magnetism Vol. 4*, editors Rado G.T. and Suhl H. (Academic —Press).
Landau L.D. and E.M. Lifshitz (1935), Phys. Z. Sowj. **8**,153.
Lonzarich G.G. and Taillefer L. (1985), J. Phys. **C18**,4339.
Murata K.K. and Doniach S. (1972), Phys. Rev. Lett. **29**,285.
Moriya T. and Kawabata A. (1973), J. Phys. Soc. Jpn. **34**,639.
Moriya T. (1979), J. Magn. Mag. Mat. **14**,1.
Rhodes P. and Wohlfarth E.P. (1963), Proc. R. Soc. London Ser. **A273**,247.
Slater J.C. (1936), Phys. Rev. **49**,537,931.
Slater J.C. (1937), Phys. Rev. **52**,198.
Stoner E.C. (1938), Proc. R. Soc. **A165**, 372.
Stoner E.C. (1939), Proc. R. Soc. **A169**, 339.
Taillefer L. (1986a), Ph.D. Thesis, University of Cambridge.
Van Vleck J.H. (1953), Rev. Mod. Phys. **25**,220.
Weiss P. (1907), J. de Physique **6**,661.
Wohlfarth E.P. (1980), Inst. Phys. Conf. Ser. No. 55, 161.

1.10 Bibliography

Introduction to the Theory of Magnetism, D. Wagner. Publ. Pergamon Press.
Physical Principles of Magnetism, F. Braislford. Publ. D. Van Nostrand Company —Ltd.
Physics of Atoms and Molecules, B.H. Bransden and C.J. Jochain. Publ. Longman —(ISBN 0-582-44401-2).
Solid State Magnetism, J. Crangle. Publ. E. Arnold (ISBN 0-340-54552-6).
Solid State Physics, N. Ashcroft and N. Mermin. Publ. HRW International Ed. —(ISBN 0-03-49346-3).

Chapter 2

Manganese Silicide and Cubic Iron Germanium: an Introduction

2.1 Previous work done on Manganese Silicide and Cubic Iron Germanium

2.1.1 Manganese Silicide

The metallic alloy MnSi has been the subject of numerous theoretical and experimental investigations pivotal in the development of the self consistent theories of itinerant magnetism.

In 1966 a paper appeared in the Journal of Applied Physics (Williams *et al.* (1966)) on the magnetic properties of the monosilicides of some 3d transition elements. MnSi was reported to order magnetically at 30K with a magnetisation curve which is linear up to a field of 6.2kOe where it saturates abruptly. It was also noted with interest that the saturation moment per Mn atom at 1.4K is $0.4\mu_B$ which is smaller than the value one obtains in the paramagnetic region. Brown *et al.* (1968) later reported that the neutron diffraction experiments on both powder and single crystal failed to show an antiferro or ferrimagnetic component to the moment so suggested that the total moment was derived from the saturation magnetisation. Fawcett *et al.* (1970) measured the thermal expansion and specific heat of MnSi and found the transition to be of second order.

After macroscopic magnetisation measurements in the range 2.5 - 900K and up to 20kOe, Levinson *et al.* (1972) reported that the measurements were incompatible with zero field ferromagnetism below the ordering temperature. Low field magnetic measurements below the critical temperature on a powder sample showed the magnetisation was not completely linear but was curved below the linear response in fields below 1.1kOe as shown in figure 2.1. Although such magnetic behaviour is more typical of an antiferromagnet below the transition temperature, neutron experiments failed to observe any additional magnetic reflections. This posed a problem; magnetisation measurements being inconsistent with simple ferromagnetism whilst other experiments strongly implied a ferromagnetic structure. To resolve the incon-

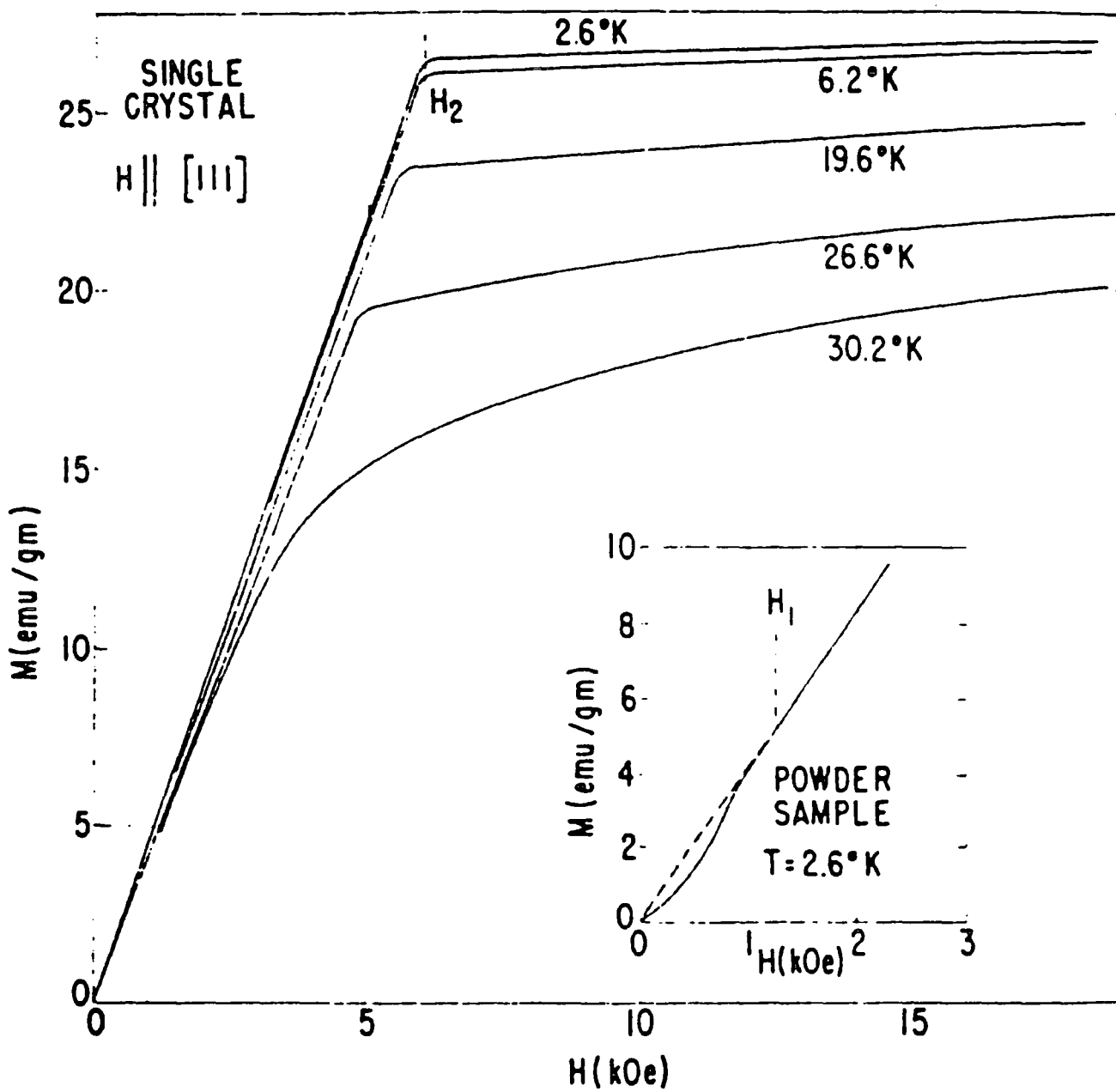

Figure 2.1 Magnetisation of MnSi as a function of applied magnetic field. (After Levinson *et al.* (1972)).

sistency, it was suggested (Levinson (1972)) that antiferromagnetic coupling existed between microscopic ferromagnetic regions. By measuring the depolarisation factor for polarised neutrons transmitted through a thin sample of MnSi, Levinson was also able to deduce that the size of each ferromagnetic domain was $\approx$ 500Å.

Wernick *et al.* (1972) and references therein also reported on the low saturation moment of MnSi and the abrupt manner in which it saturated at 6.2kOe. Magnetic properties determined by torque measurements suggested MnSi was antiferromagnetic in zero field at low temperatures while longitudinal magnetostriction studies indicated it was antiferromagnetic below 0.5kOe and ferromagnetic above 6.0kOe. NMR measurements also suggested that MnSi was not a simple ferromagnet in an external field of 6.0kOe.

After high magnetic field and high pressure measurements performed on MnSi, Bloch *et al.* (1975) pointed out that it could not be characterized as a simple, weak itinerant ferromagnet. Despite the difference in effective moments above and below the low critical temeprature and the lack of saturation at high fields, all consistent with weak itinerant ferromagnetic behaviour, they pointed out inconsistencies including the nonlinearity of the 'Arrot Plots'.

In 1976 Ishikawa *et al.* established the magnetic phase diagram of MnSi. Their neutron scattering studies carried out at the ILL in Grenoble revealed that MnSi had a helical spin structure with a long period of $180 \pm 3\mathring{A}$ in the equivalent $< 111 >$ directions at 4.2K. The helical spin density wave was found to align itself with an applied magnetic field when the strength exceeded about 2kOe before a cone like structure is stabilised and the magnetisation is saturated by the process of closing the cone. The magnetic behaviour above a critical field of about 6kOe is characteristic of an itinerant, weak ferromagnet. A phase diagram based on ultrasonic absorption data (and later published independently (Kusaka *et al.* (1976))) detailed the boundaries between ferromagnetic, helimagnetic and paramagnetic phases. It should be noted that the phase diagram, reproduced in figure 2.2 also contains points at 1.5kOe just below the transition temperature in the conical phase where an additional peak appeared in the ultrasonic absorption coefficient. This data corresponds to the magnetic field being applied parallel to the $< 001 >$ direction and is observation of the so-called 'Phase A', later reported by Kadowaki *et al.* (1981). The result of Ishikawa was confirmed by both ESR (Date *et al.* (1977)) and NMR (Matoya *et al.* (1976)(1978))

At about the same time, similar measurements on MnSi were being performed at Risø by Hanson (1976). Hanson (1977) also made magnetic measurements on a single crystal and showed the low field anisotropy in the magnetisation which is reproduced in figure 2.3. This was confirmed by Guy *et al.* (1979) through torque measurements on a single crystal of MnSi.

Despite the anomalies noted above, MnSi was then used as a typical weak itinerant ferromagnet in order to study the magnetic excitations in this type of system by Ishikawa *et al.* (1977). There had long been a debate on the electronic state of unpaired electrons in transition metals and alloys, reducing to whether they were itinerant or localised spin systems. In the case of an itinerant system, it was thought that single particle excitations called Stoner excitations would exist in addition to

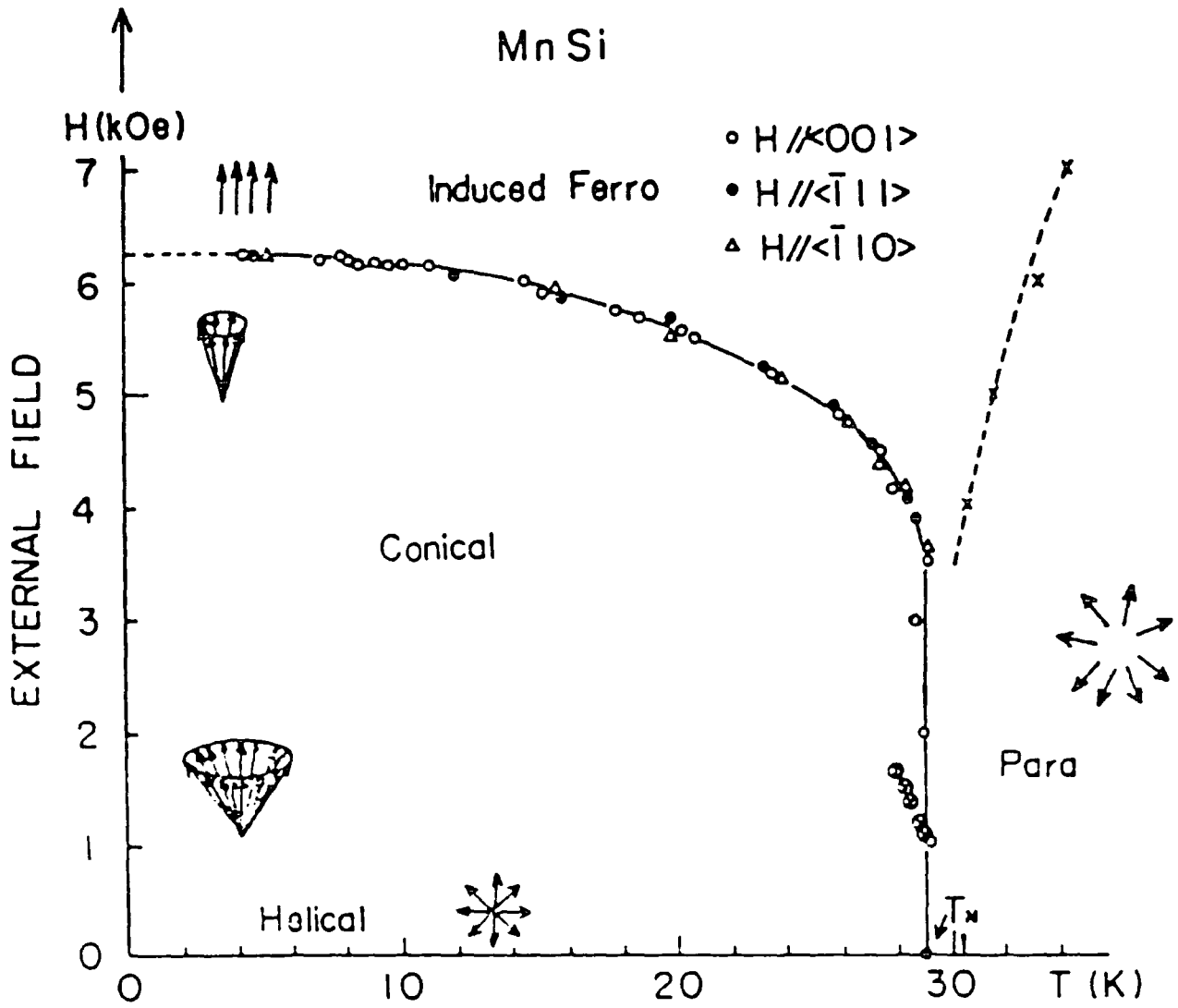

Figure 2.2 Magnetic phase diagram of MnSi determined by the attenuation of ultrasonic waves. (After Kusaka *et al.* (1976)).

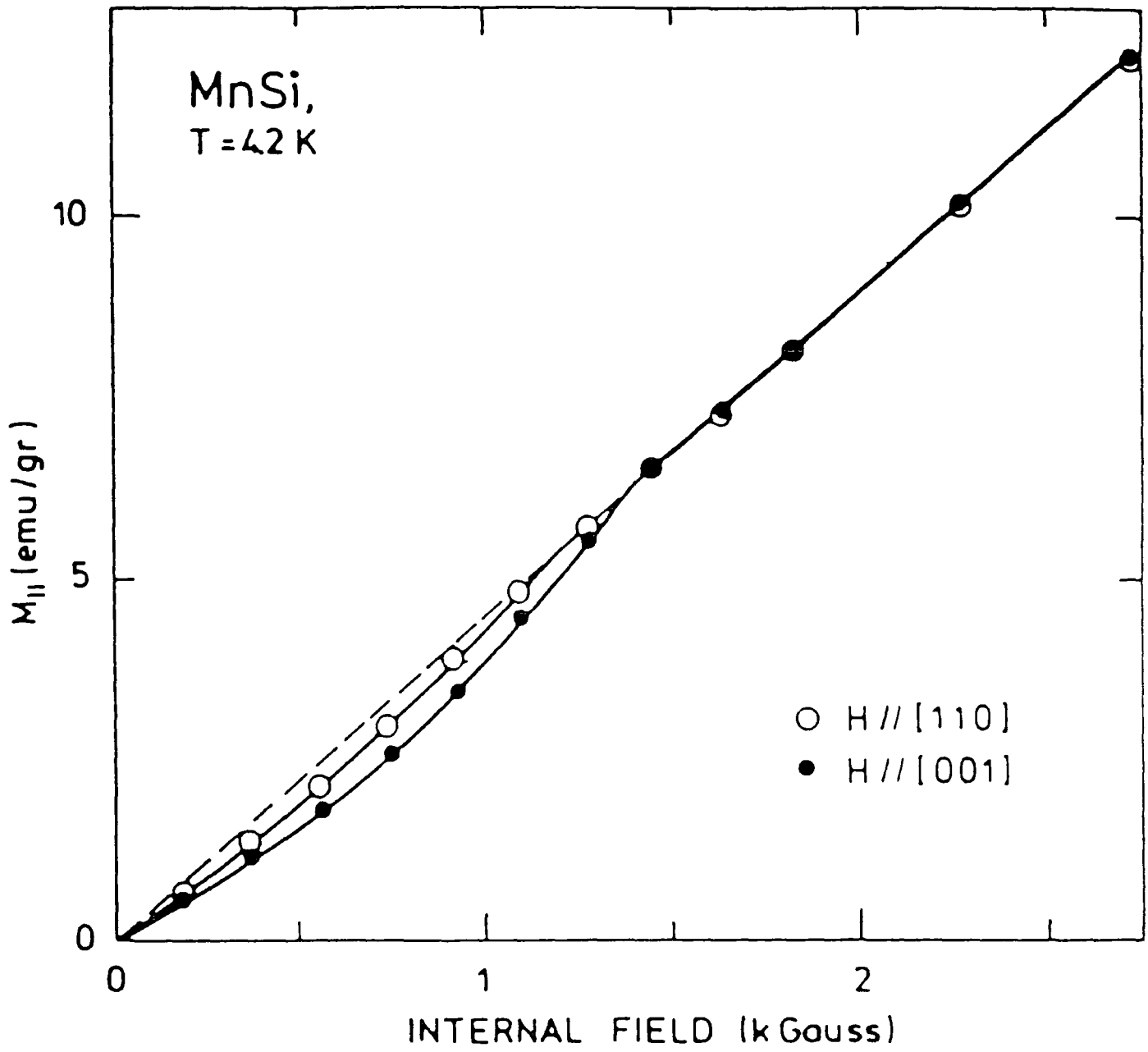

Figure 2.3 Magnetisation of MnSi as a function of applied magnetic field with magnetic field applied along particular crystallographic directions. (After Hansen (1977)).

collective spin wave excitations. These had not previously been observed because in metallic ferromagnets the Stoner excitations exist in a high energy regime (above 100meV). However, in the case of weak itinerant ferromagnets these excitations were thought to occur in a lower energy regime enabling the study of both collective and Stoner excitations through inelastic neutron scattering. The inelastic neutron scattering from MnSi revealed that well defined spin waves exist only below 2meV but above this, for increasing energies, the linewidth of the scattering broadens as shown in figure 2.4. This increase in linewidth was regarded as evidence for the Stoner boundary, observed as the excitations increased in energy and suggesting the itinerant model of magnetic carriers to be correct. The excitations in the Stoner continuum were found to remain almost unchanged even up to room temperature, whilst the spin wave excitations observed at 5K collapse into critical scattering above the transition temperature.

Following the work of Dzyaloshinsky (1958) and later that of Moriya (1960), Bak and Jensen (1980) pointed out that a helical spin structure can arise out of a Ginzberg Landau expansion of the free energy. Dzyaloshinsky had first recognised the existence of an antisymmetric spin interaction in magnetic insulators. Requiring that each term in the free energy satisfy the full crystal symmetry, the antisymmetric form was shown to be allowed in certain class of crystals of sufficiently low symmetry. The derivation of the antisymmetric interaction on the basis of a microscopic Hamiltonian was given by Moriya and extended to include spin orbit coupling in ionic crystals. Bak and Jensen produced a mechanism underlying the antisymmetric spin interactions in metallic systems. Although Nakanishi *et al.* also produced similar work, it was later discovered to be incorrect and a correct version was published by Kataoka (1984) together with the previous authors. From renormalisation theory, Bak and Jensen predicted the phase transition to be of first order.

The spin fluctuation spectrum in MnSi was further investigated by Ishikawa (1982). Emphasis was put on measurement of the collective spin wave excitations which were also found to exist above the transition temperature. Theoretical investigations by Moriya (1981) suggested the magnetic properties of itinerant electron systems at finite temperature could be understood in terms of the temperature variation of the mean squared magnetic moments $< M^2 >$. In contrast with the Heisenberg system where $< M^2 >$ is expected to be constant and independant of temperature, in a weakly magnetic system, an initial fall of $< M^2 >$ as the transition temperature is approached from below with moderate increase above the transition temperature was predicted. The data was interpreted within the framework of the selfconsistent renormalisation theory (SCR) of Moriya (1979) since in the paramagnetic phase the lack of distinction between the longitudinal and transverse components of the magnetisation becomes irrelevant. The data, excepting the low wavevector anisotropy associated with the incipient ordered state in the vicinity of the transition temperature, is also consistent with the more general model for the dynamical wavevector dependant susceptibility developed by Lonzarich and Taillefer (1985). This work by Ishikawa also interestingly included observation of spin correlations close to the transition temperature, developing as a ring of scattering around (0,0) and not the magnetic satellite.

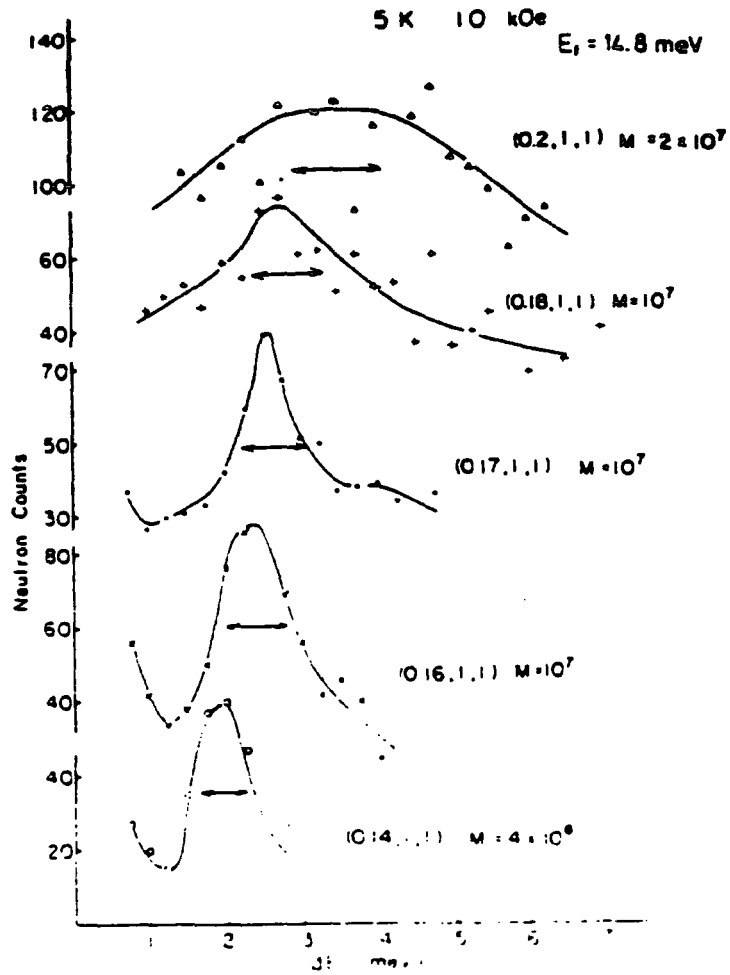

Figure 2.4 Constant q scans for MnSi in the [100] direction. The arrows indicate the width of the spectra that would be observed for spin waves with no broadening. (After Ishikawa *et al.* (1977)).

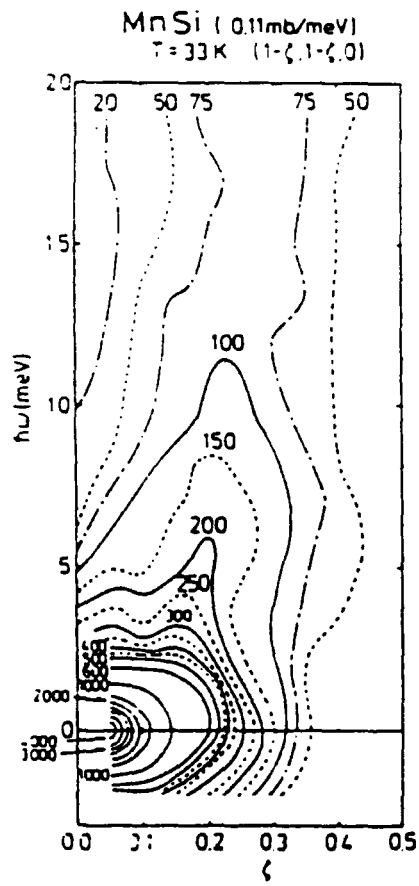

Figure 2.5 Contour map of the paramagnetic scattering along the [110] direction for MnSi for T=33K. (After Ishikawa *et al.* (1985)).

The experimental observation of spin fluctuations in the paramagnetic state was extended by Ishikawa (1985) a few years later by making a complete measurement of paramagnetic scattering for MnSi for the energy region 20meV. Figure 2.5 shows measurement of the scattering at T=33K using unpolarised neutrons. For small $\underline{q}$ the scattering contours are circular about $\underline{q} = 0$ but as $\underline{q}$ increases, a ridge of scattering can be found extending upwards in energy. This ridge exists for energies above about 3meV and is suggested to be the lower boundary of the Stoner continuum, initially observed in (1977). Reservations about this data, including experimental resolution and $\underline{q}$ dependant background, led to the work being repeated by Brown (1990).

Following these experiments on the fundamental nature of itinerant magnetism, more work was performed on the phase diagram of MnSi to further test the theoretical work of Moriya. Matsunga *et al.* (1982) measured the magnetovolume effect which was found to become positive above the transition temperature. The magnetisation and magnetoresistance of MnSi were studied by Kadowaki *et al.* (1981) and also by Sakakibara *et al.* (1981) in magnetic fields up to 500kOe. The work of Kadowaki observed anomalous peaks in the magnetisation and magnetoresistance just below the transition temperature in applied magnetic fields of 1.0 - 2.2kOe and suggested the existence of two new phases. The complete phase diagram, compiled using various techniques including ESR, ultrasonics and magnetisation (Kadowaki *et al.* (1981) and refs. therein) is reproduced in figure 2.6. It is important to note that the magnetisation data was recorded by fixing field and sweeping temperature and that no anisotropy was observed in relation to new phases when the field was applied along different crystallographic directions.

Following the theoretical work of Bak and Jensen (1980) and their prediction that the helix in MnSi must be only left or right handed depending on the sign of the Dzyaloshinsky term in the Hamiltonian, work was done to determine the handedness of the helix. Shirane *et al.* (1983) used the fact that a single handed helix only scatters a particular polarisation of the neutrons to deteremine that the spiral was right handed only. Tanaka *et al.* (1985) determined the chirality of MnSi crystal using convergent beam electron diffraction before Ishida *et al.* (1985) investigated the helicity using polarised neutron diffraction. All seven crystals grown from different seeds were found to belong to the left handed system and the neutron scattering showed that only the left handed spiral of the helical spin density wave existed. Thus the left handed spiral must be closely related to the left handed crystal structure.

Further investigation of the phase diagram of MnSi was performed by Ishikawa *et al.* (1984), particularly within the new phase close to the transition temperature and refered to as 'Phase A'. This work suggested that 'Phase A' was in fact an extension of the paramagnetic phase into the conical region where the magnetic correlations exhibited the same characteristics as those found at 29.5K in zero field, namely a diffuse ring of scatter. The work was performed using pulsed neutron beams with neutron wavelengths ranging from 3 - 11Å and only one crystallographic orientation was investigated. It was pointed out that the presence of such a phase was not predicted in the theoretical work of Bak and Jensen (1980) or Plumer and Walker

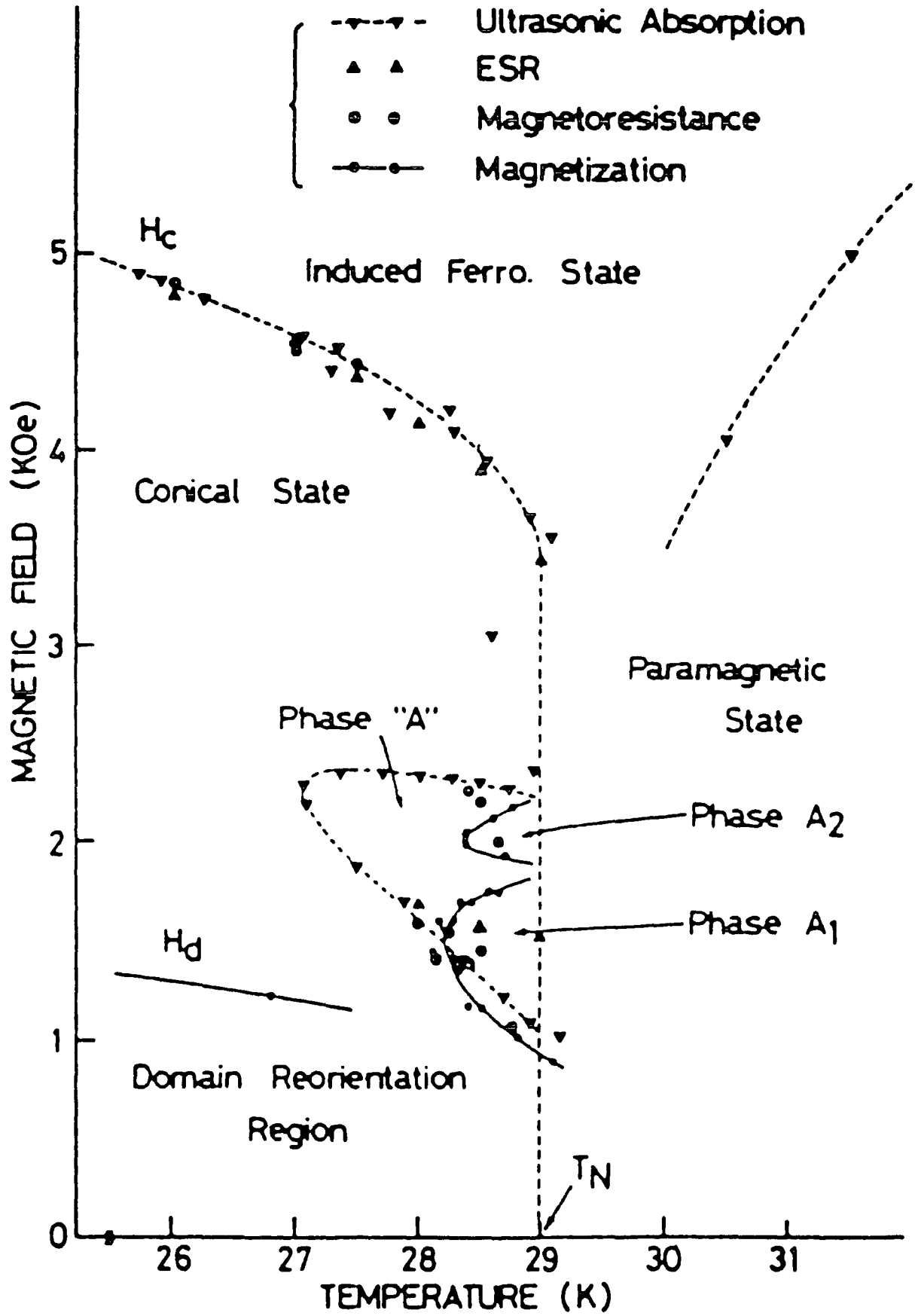

Figure 2.6 Phase diagram of MnSi near T_N as measured using various techniques. (After Kadowaki *et al.* (1981)).

(1981).

The electronic spectrum of MnSi was investigated by Taillefer (1986b) through band structure calculations and de Haas-van Alphen measurements. The high effective mass of the electron ($15m_0$) was noted. The de Haas van Alphen measurements were later developed by Brown (1990) at lower temperatures and higher fields.

Throughout the past decade, a series of theoretical papers was produced by Plumer and Walker. A mean field theory was presented and a study of the rotation of the helical spin density wave into the applied field direction performed (1981). The model assumes that the helix begins to rotate from $< 111 >$ direction towards the field direction on application of a magnetic field. The theoretical magnetisation was produced for magnetic field applied along different crystallographic directions, reproduced in figure 2.7 and is in good qualitative agreement with the experimental results of Hanson (1977), showing that rotation of the helix into the field direction could account for the unusual nonlinear dependence of the magnetisation observed below 1.5kOe. By incorporating magnetoelastic interactions within the expression for free energy, (Plumer and Walker (1982)), an expression for the magnetostriction has been derived which compare well with the existing data of Matsunga *et al.* (1982). This model was also developed to produce a theory of the generalised susceptibility and spin dynamics associated with the helical spin density wave phase of MnSi by Plumer (1984). Finally, Walker (1989) has presented a paper which predicts the helical response as the magnetic field is reduced after being large enough to cause rotation of the helical spin density wave into this direction. He suggests the rotation of the wavevector from $< 001 >$ to $< 111 >$ direction would occur as a result of two successive phase transitions. Due to the symmetry considerations, the helix would first rotate into another direction before rotating into the $< 111 >$ direction.

More recently, Shekhtman *et al.* (1992) have further commented on the Dzyaloshinsky Moriya interaction and its relevance for the spin anisotropies in La_2CuO_4 (a 'high T_c' superconductor). This demonstrates the universality of the symmetry breaking in MnSi where its consequence can be studied with out the complications of 'high T_c' superconductivity.

Throughout this review, there has been little agreement as to the 'type' of ferromagnetism exhibited by MnSi although most agree it does not arise from localised magnetic moments of fixed amplitude. This is apparent in the panel discussion on '3d Magnetism at Finite Temperatures' (Arrot (1983)). The problem can be resolved by considering a unified magnetic fluctuation picture as described by Taillefer (1986a). The origin of ferromagnetism in metals lies in the interaction between conduction electrons and in the resulting correlation in their motion. The interaction between electrons can be treated in terms of spatial and temporal fluctuations in the charge and spin densities. This makes the spectrum of magnetic or spin fluctuations the quantity of central interest and the difference in behaviour arises from the variation in the spatial character of the important fluctuations in spin and charge within the class of metals. At one end, there are the weakly ferromagnetic metals such as Ni_3Al or $ZrZn_2$ for which all the large fluctuations at low temperatures have long wavelengths. At the other end, there are the 'heavy fermions' such as UPt_3 where

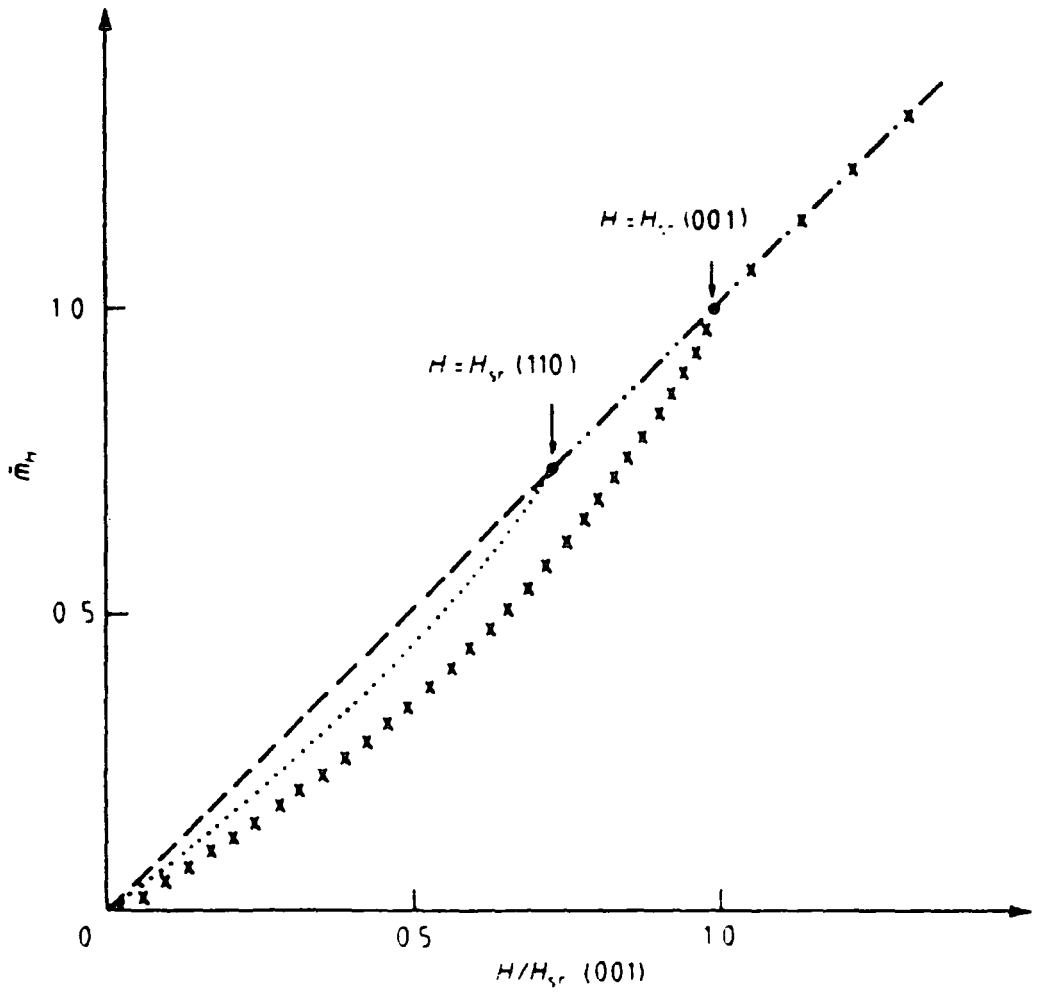

Figure 2.7 The magnetisation in the spin density wave phase versus magnetic field at a temperature well below T_N for H $\|$ < 001 > (broken curve), H $\|$ < 110 > (dotted curve) and H $\|$ < 001 > (crosses). (After Plumer *et al.* (1981)).

modes of all wavelengths are nearly equally strong. In the intermediate regime one finds MnSi where shorter wavelengths are becoming more important. Consequently it is then tempting to stretch the definition of the end categories to include MnSi in both.

2.1.2 Cubic Iron Germanium

The amount of work performed on cubic FeGe is far less extensive than that on MnSi, possibly owing to the difficulty of growing single crystals of cubic FeGe.

An excellent, concise review is given by Lebech (1989) summarising work up to 1989. Lebech studied the magnetic structure of cubic FeGe extensively using small angle neutron scattering. The metal was observed to order magnetically at a temperature of 278.7K into a long range spiral of period 683 - 700Å propagating along $< 100 >$ directions at high temperatures and along equivalent $< 111 >$ directions at low temperatures. The transition at which the direction of the spiral turns was observed to take place in a temperature interval of 40K and show pronounced hysteresis ($T_2 decr. = 211K, T_2 incr. = 245K$). Applied magnetic fields of 200 - 400 Oe, depending on temperature and direction cause the spiral axis to rotate into the direction of the field. As the field is further increased, the amplitude of the antiferromagnetic spiral decreases and the ferromagnetic component increases until cubic FeGe becomes magnetically saturated.

Following the neutron diffraction data of Lebech, Plumer (1990) analysed the magnetic reordering in the helical spin density wave phase of cubic FeGe in terms of a Landau-type free energy, similar to that previously used to study MnSi. A magnetic phase diagram was predicted and is shown in figure 2.8.

More recently, Lebech (1992) suggests that reorientation of the helix into the field direction in FeGe can occur as a first or second order process (figure 2.9 and figure 2.10) and is dependant on the angle between the applied field and the initial modulation vector $\underline{q}$. Investigations using SANS at both 250K and 140K (i.e. in both phases with $\underline{q}||\overline{<} 100 >$ directions (250K figure 2.9) and $\underline{q}|| < 111 >$ directions (140K figure 2.10)) show that with a magnetic field applied initially perpendicular to the helix, a first order transition or 'flip' occurs whereas with $\underline{q}$ initially at smaller angles, a second order rotation occurs.

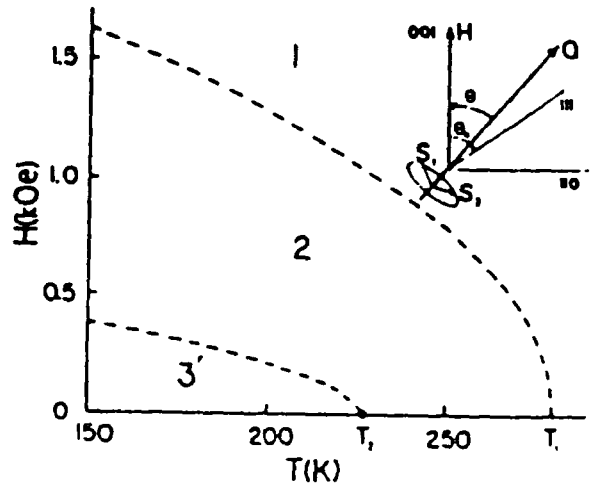

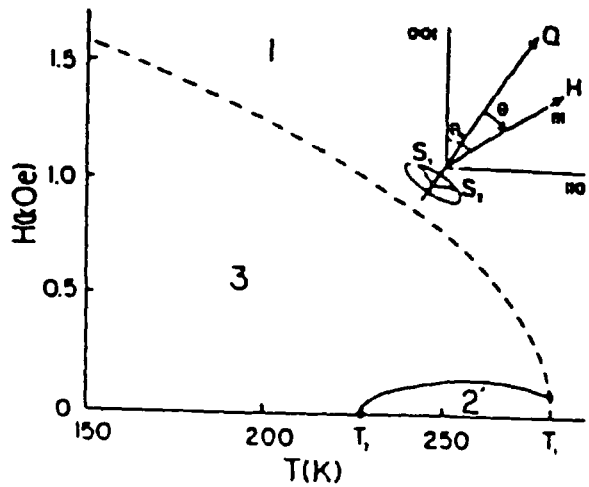

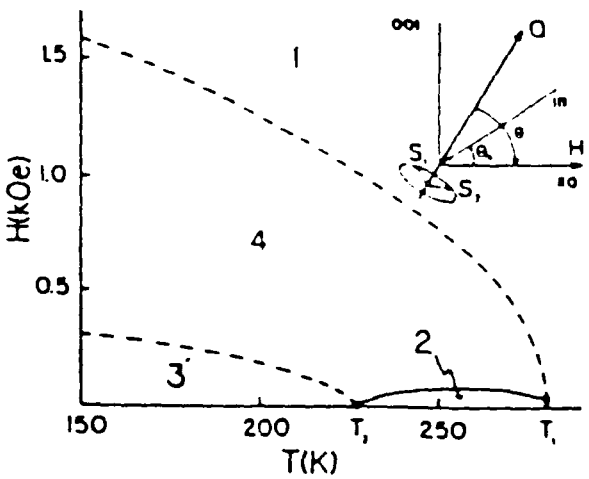

Figure 2.8 Phase diagrams for FeGe (a) H $\parallel$ [001] with paramagnetic phase 1, conical phase (2) with $\theta = 0$ Q $\parallel$ [001] and ordered state 3′ with $0 < \theta < \theta_0$; (b) H $\parallel$ [111] with paramagnetic phase (1), conical phase (3) with $\theta = 0$ and ordered state (2′) with $0 < \theta < \theta_0$; (c) H $\parallel$ [110] showing the paramagnetic phase (1), conical phase (4) with $\theta = 0$ and ordered states (3′) with $0 < \theta < \theta_0$ and (2) $\theta = \frac{\pi}{2}$. (After Plumer (1990)).

Figure 2.9 Field dependancies of the angle θ, between modulation vector $\underline{q}$ and the direction of the applied magnetic field $\underline{H}$ at 250K in cubic FeGe. The insets show the relevant parts of reciprocal space and define the orientations of the initial modulation vector $\underline{q}(0)$ and the modulation vector $\underline{q}(\underline{H})$ for a field $\underline{H}$ along [011]. Both these vectors lie in a vertical plane parallel to the area sensitive detectors. (After Lebech (1992)).

Figure 2.10 Field dependancies of the angle θ, between the modulation vector $\underline{q}$ and the direction of the magnetic field $\underline{H}$ at 140K in cubic FeGe. The insets show the relevant parts of reciprocal space and define the orientations of the initial modulation vector $\underline{q}(0)$ and the modulation vector $\underline{q}(\underline{H})$ at a field $\underline{H}$ along [011]. Both these vectors lie in a vertical plane parallel to the area sensitive detector. (After Lebech (1992)).

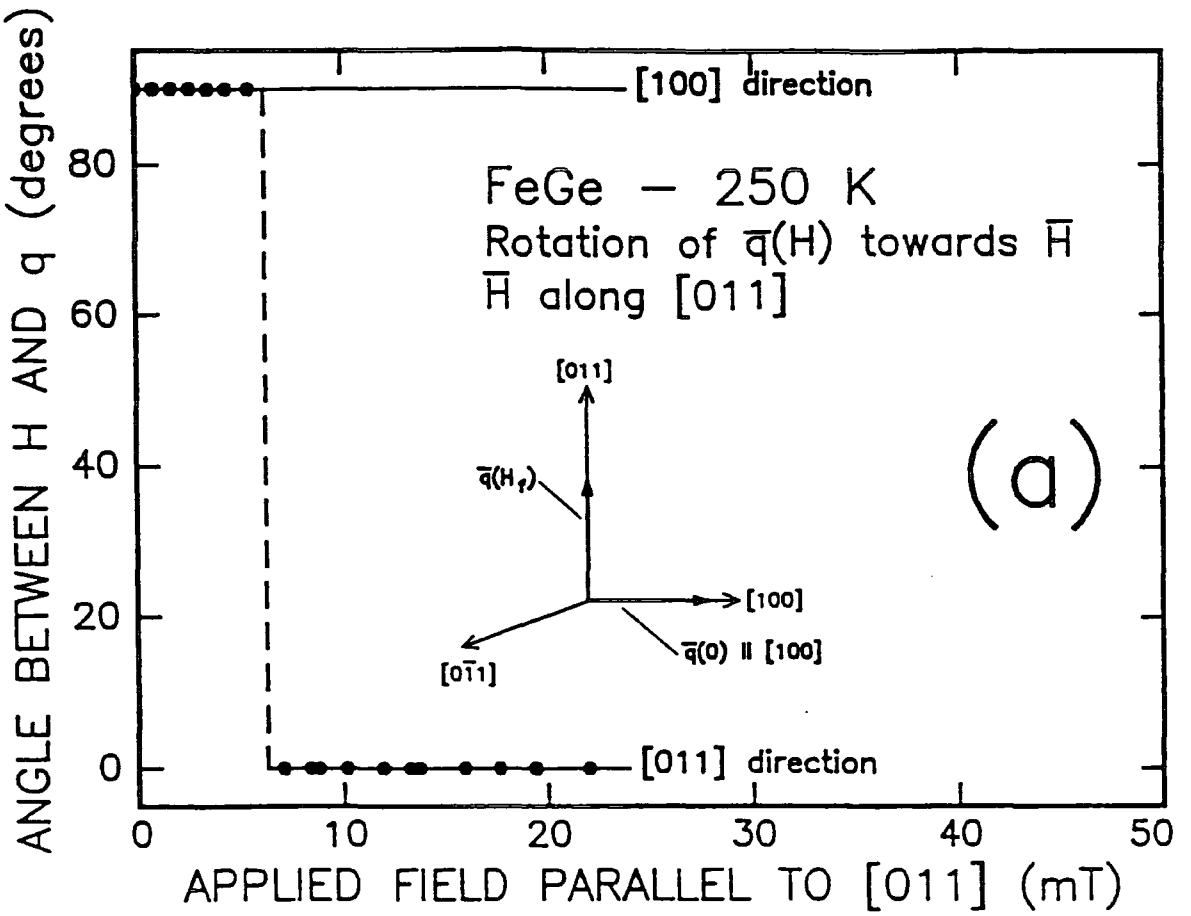
[100] direction
FeGe – 250 K
Rotation of q̄(H) towards H̄
H̄ along [011]
[011]
q̄(H≠)
[100]
q̄(0) ∥ [100]
[0$\bar{1}$1]
(a)
[011] direction
ANGLE BETWEEN H AND q (degrees)
APPLIED FIELD PARALLEL TO [011] (mT)
0
10
20
30
40
50
0
20
40
60
80

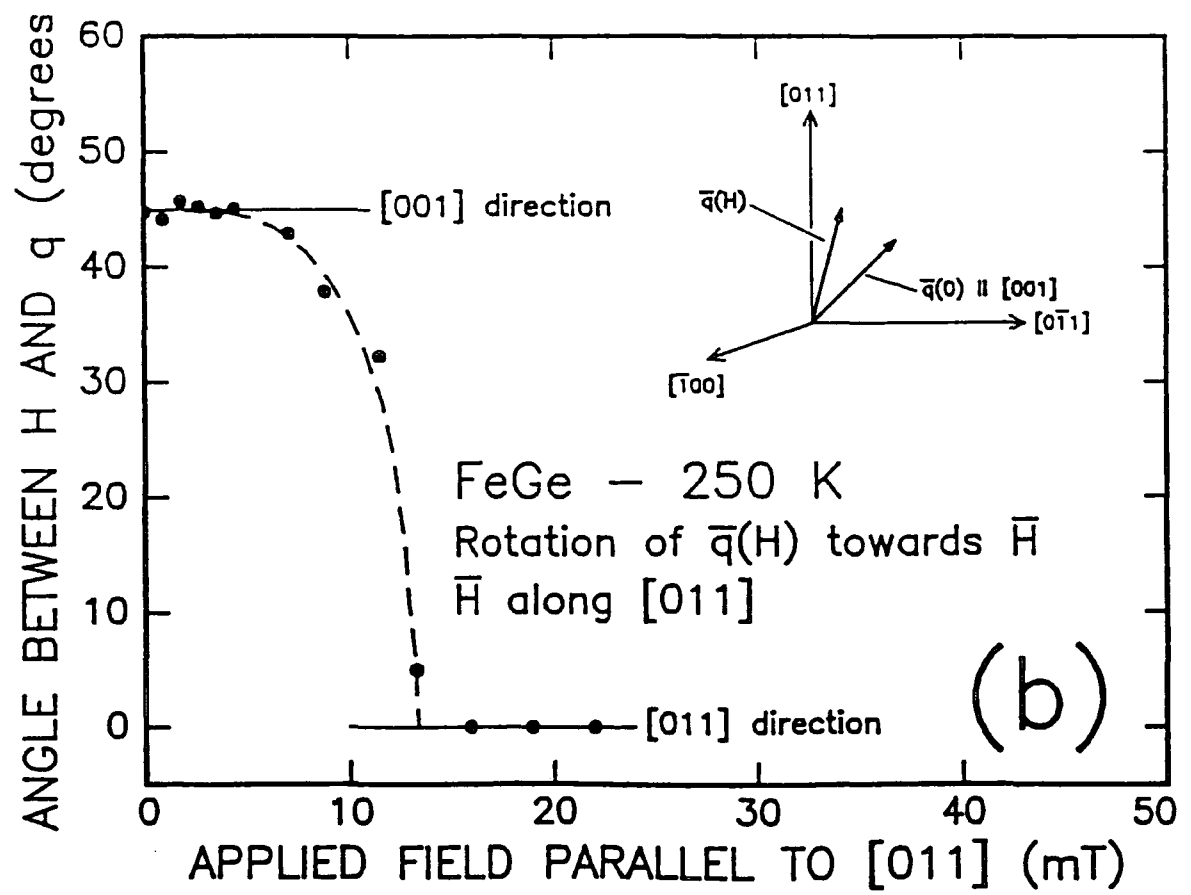
[001] direction
[011]
q̄(H)
q̄(0) ∥ [001]
[0$\bar{1}$1]
[$\bar{1}$00]
FeGe – 250 K
Rotation of q̄(H) towards H̄
H̄ along [011]
[011] direction
(b)
ANGLE BETWEEN H AND q (degrees)
APPLIED FIELD PARALLEL TO [011] (mT)
0
10
20
30
40
50
60

Figure 2.9

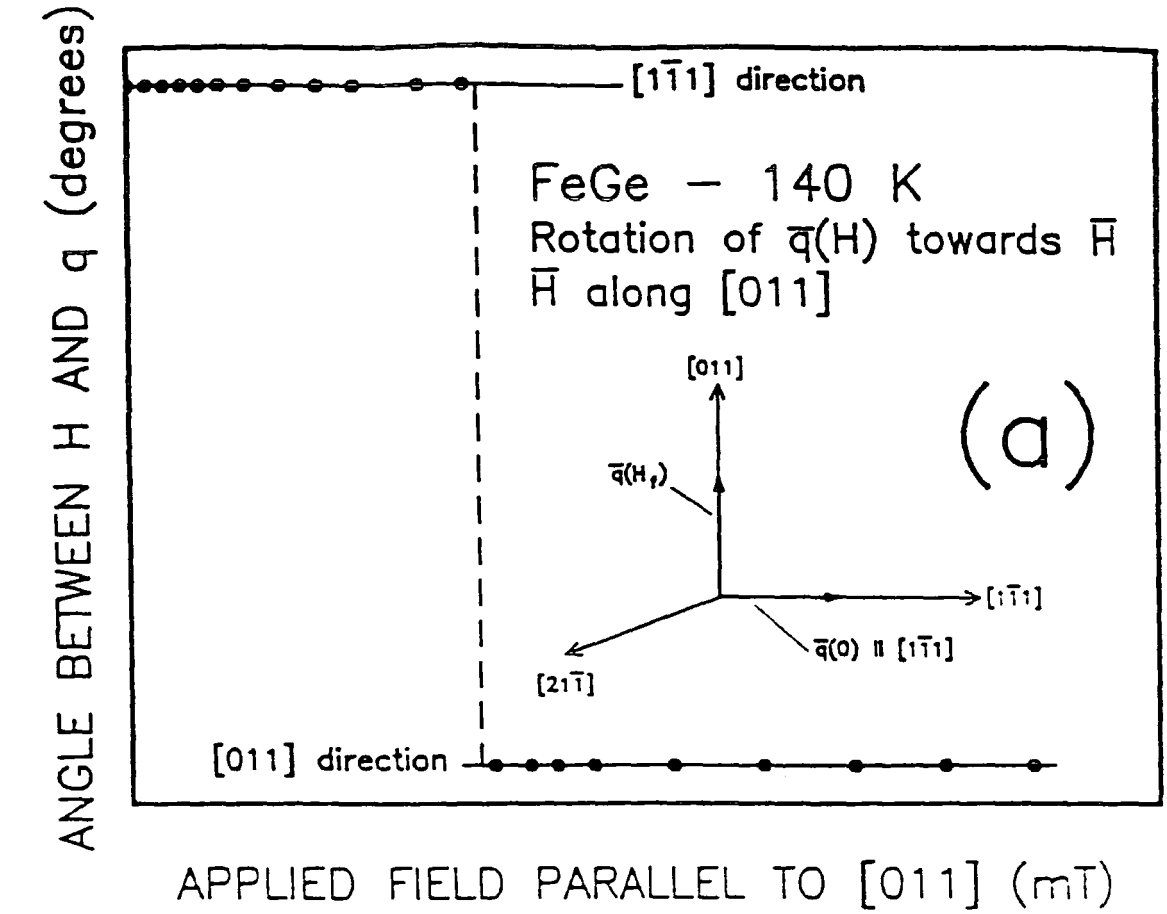
ANGLE BETWEEN H AND q (degrees)
[1$\bar{1}$1] direction
FeGe – 140 K
Rotation of $\bar{q}$(H) towards $\bar{H}$
$\bar{H}$ along [011]
[011]
$\bar{q}(H_f)$
(a)
[1$\bar{1}$1]
$\bar{q}$(0) ∥ [1$\bar{1}$1]
[21$\bar{1}$]
[011] direction
APPLIED FIELD PARALLEL TO [011] (mT)

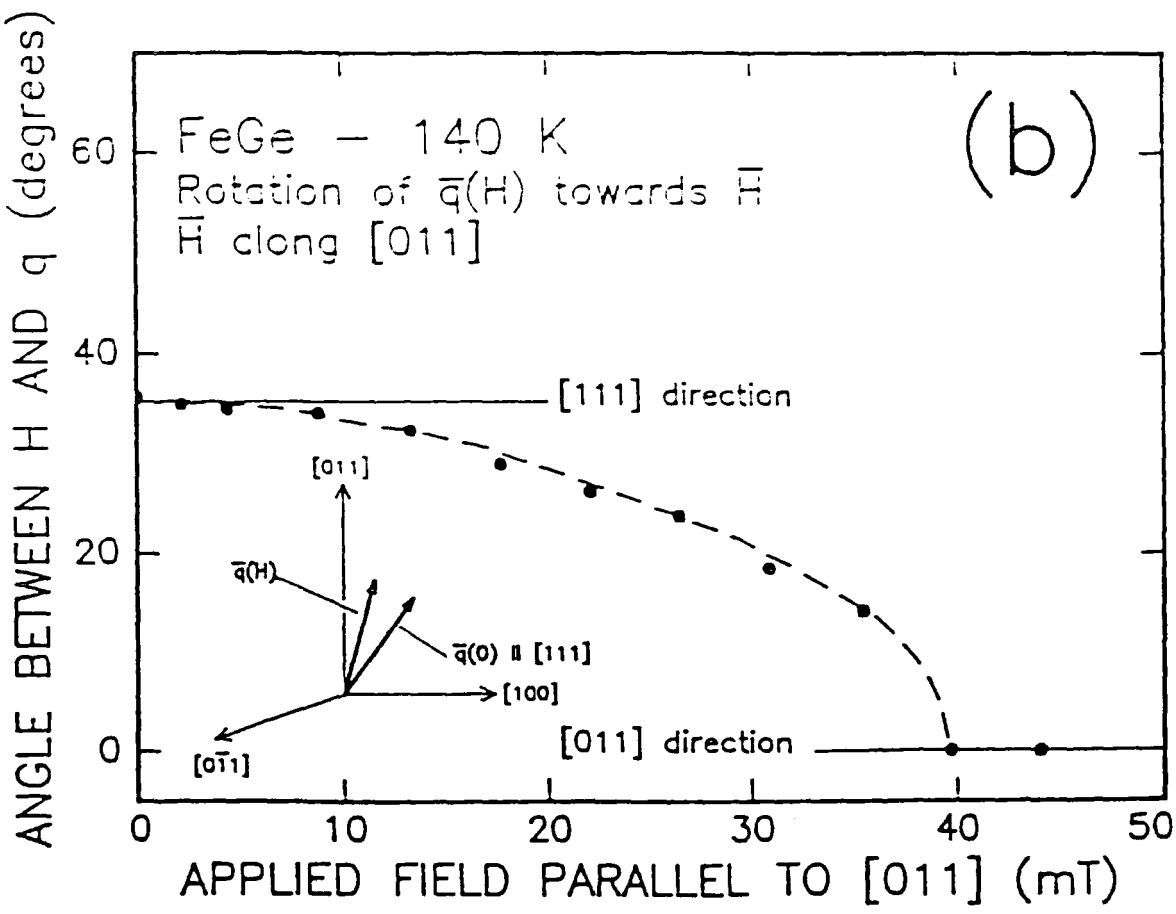
ANGLE BETWEEN H AND q (degrees)
60
40
20
0
FeGe – 140 K
Rotation of $\bar{q}$(H) towards $\bar{H}$
$\bar{H}$ along [011]
(b)
[111] direction
[011]
$\bar{q}$(H)
$\bar{q}$(0) ∥ [111]
[100]
[0$\bar{1}$1]
[011] direction
0
10
20
30
40
50
APPLIED FIELD PARALLEL TO [011] (mT)

Figure 2.10

2.2 Structure of the Unit Cell

Both MnSi and cubic FeGe have the B_{20} cubic structure as shown in figure 2.11. The structure belongs to the space group $P2_13$ and lacks inversion symmetry. In MnSi, the unit cell has sides a=4.558Å and in FeGe 4.700Å. The position of the atoms in the unit cell are (u,u,u),($\frac{1}{2}$+u,$\frac{1}{2}$-u,-u), (-u,$\frac{1}{2}$+u,$\frac{1}{2}$-u) and ($\frac{1}{2}$-u,-u,$\frac{1}{2}$+u) where u_{Mn} is 0.138, u_{Si} is 0.845 and u_{Fe} is 0.135, u_{Ge} is 0.842. This structure lacks inversion symmetry and the unit cell can exist in two chiral forms.

2.3 Origin of the Helical Spin Density Wave in MnSi and FeGe

The origin of the helical spin density wave HSDW in MnSi and FeGe is still not clearly understood and numerous peculiarities exist. The wavelength of the spiral decreases as the temperature is increased (Ishikawa (1984)) and also the helix is believed to only have one handedness. There are also anomalies close to the transition temperature in MnSi, with a double transition apparent in the thermal expansion data of Matsunga (1981) and the ultrasonic attenuation data of Kusaka (1976) at ambient pressure. Ishikawa (1984) has tried to relate this to the appearance of a spherical shell of scattering observed in a magnetic field close to the transition temperature (the so-called 'Phase A') without success.

Following the work of Dzyaloshinsky (1964) it was pointed out by Bak and Jensen (1980) that a helical spin structure can arise out of a Ginzberg Landau expansion for the free energy. The free energy can be expanded in terms of a slowly varying spin density $\underline{S}(\underline{r})$ with respect to the symmetry operations of the $P2_13$ space group. The most general form for the Free Energy to fourth order in S_i and to second order in $\frac{\partial S_i}{\partial i}$ is:

$$\begin{aligned} F(\underline{r}) &= \frac{1}{2}A({S_x}^2 + {S_y}^2 + {S_z}^2) + \\ &+ \quad b\underline{S}.(\underline{\nabla} \times \underline{S}) + \frac{1}{2}B_1\left[(\underline{\nabla}{S_x}^2 + \underline{\nabla}{S_y}^2 + \underline{\nabla}{S_z}^2\right] \\ &+ \quad \frac{1}{2}B_2\left[\left(\frac{\partial S_x}{\partial x}\right)^2 + \left(\frac{\partial S_y}{\partial y}\right)^2 + \left(\frac{\partial S_z}{\partial z}\right)^2\right] \\ &+ \quad C({S_x}^2 + {S_y}^2 + {S_z}^2)^2 + D({S_x}^4 + {S_y}^4 + {S_z}^4) \end{aligned} \tag{2.1}$$

Due to lack of inversion symmetry this includes a Dsyaloshinsky term of the form $\underline{S}.(\underline{\nabla} \times \underline{S})$ whose origin lies in the relativistic spin spin interactions $\underline{S}_i \times \underline{S}_j$ which are expected to be small compared to the Heisenberg term $\underline{S}_i.\underline{S}_j$.

In the case where $b = 0$, $B_1 > 0$ and $B_2 > 0$ the free energy is minimised through ferromagnetism however for $b \neq 0$ and a slowly varying spin density, the free energy may be minimised by spin densities of the form:

$$\underline{S}(\underline{r}) = \frac{1}{\sqrt{2}}\left[\underline{S}_k exp(i\underline{k}.\underline{r}) + \underline{S}_k{}^* exp(-i\underline{k}.\underline{r})\right] \tag{2.2}$$

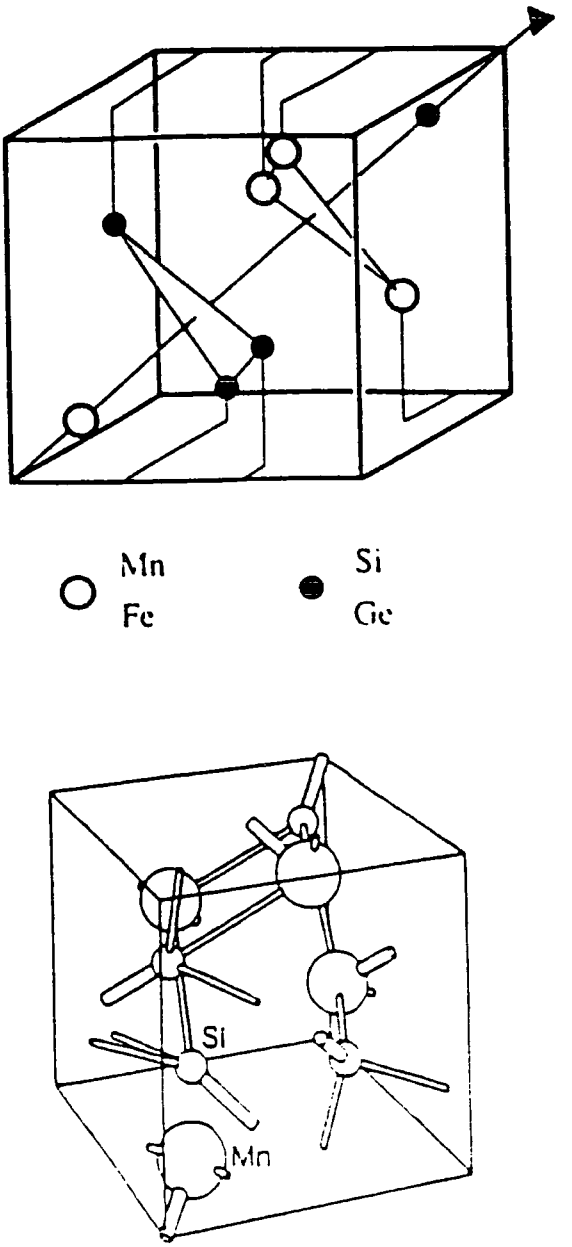

Figure 2.11 The cubic B_{20} structure of MnSi and FeGe.

The expression for the free energy becomes:

$$F(\underline{k}) = \frac{1}{2}A|\underline{S}_k|^2 + \frac{1}{2}b\underline{k}.(\underline{S}_k \times \underline{S}_k^*) + \frac{1}{2}B_1k^2|\underline{S}_k|^2$$
$$+\frac{1}{2}B_2\left(k_x{}^2|Sk_x|^2 + k_y{}^2|Sk_y|^2 + k_z{}^2|Sk_z|^2\right) + \text{higher order terms} \qquad (2.3)$$

If $\underline{S}_k = \alpha_k + i\beta_k$ then the free energy is minimised $\frac{\partial F}{\partial S}|_k = 0$ when $\alpha_k \perp \beta_k$, $|\alpha_k| = |\beta_k|$ and $k \times (\alpha_k \times \beta_k) = 0$. The sign of b then determines the handedness of the spiral.
$(b > 0)$ $\underline{k}$ antiparallel to $\alpha_k \times \beta_k$
$(b < 0)$ $\underline{k}$ parallel to $\alpha_k \times \beta_k$

The direction of $\underline{k}$ is fixed by the sign of the second order anisotropic term. In MnSi $\underline{k}$ lies parallel to [111] and so B_2 must be negative. For FeGe this constant is temperature dependant with a critical temperature of 278.7K with the helix propagating along equivalent $< 100 >$ directions above 211K and along equivalent $< 111 >$ directions below 211K for decreasing temperatures.

The free energy simplifies to the form:

$$F(k) = (\frac{1}{2}A - |b|k)|S_k|^2 + (\frac{1}{2}B_1 + \frac{1}{6}B_2)k^2|S_k|^2 \qquad (2.4)$$

Minimising this expression $\frac{\partial F}{\partial k}|_{S_k} = 0$ results in the magnitude of the HSDW

$$|k| = \frac{|b|}{B_1 + \frac{1}{3}B_2} \qquad (2.5)$$

In MnSi the wavevector is $\approx$ 180Å whereas in FeGe it is $\approx$ 700Å.

Although this approach predicts that a HSDW should exist, the magnitude of the parameter b is unknown as is the exact microscopic origin of that term in the free energy expansion. This work has been extensively expanded in the literature (Plumer and Walker (1981)) and appears to be able to account for some of the behaviour of the HSDW under an applied field in terms of the reorientation of the HSDW however both the temperature dependant behaviour and 'Phase A' remain unaccounted for.

2.4 Domains in MnSi and FeGe

In the introduction, the concept of domains was introduced as a region in a ferromagnet where the moments are locally aligned. Domains have been observed in antiferromagnets, for example Patterson (1985) and hence they may exist in MnSi and FeGe. Consider MnSi where within the cubic crystal structure there are eight equivalent $< 111 >$ directions along which the helical spin density wave can propagate. A domain is defined as a region of the crystal where the helix propagates along a particular direction. They are thought to exist because of temperature variations across the sample when passing through the critical temperature, as well as due to various stress variations within the specimen due to dislocations within the lattice.

The wavelengths of the helical spin density wave in both MnSi and FeGe are exceptionally long magnetic structures. Although domain size will be dependant on sample quality, Levinson (1972) measured the length scale of the domains to be 500Å i.e. a similar order of magnitude to the helical spin density wave. Within MnSi a complete wavelength extends across 22 unit cells so it is understandable that Collins (1989) describes MnSi as a 'long period modulation of a ferromagnetic structure rather than antiferromagnetic'.

2.5 References

Arrot A.S. *et al.* (1983), J. Magn. Magn. Mater. **31-34**, 313-319.
Bak P. and Jensen M. (1980), J. Phys. C **13**, L881-885.
Bloch D. *et al.* (1975), Phys. Lett. **A51**, 259-261.
Brown P.J. *et al.* (1968), J. Appl. Phys. **39**, 1331.
Brown S.A. (1990), Ph. D. thesis, University of Cambridge (unpublished).
Collins (1989),*Magnetic Critical Scattering*,(Oxford University Press).
Date M. *et al.* (1977), J. Phys. Soc. Jpn. **42**, 1555.
Dzyaloshinsky I. (1958), J. Phys. Chem. Solids **4**, 241.
Fawcett E. *et al.* (1970), Int. J. Magn. **1**,29.
Guy C.N. *et al.* (1979), J. Appl. Phys. **50**, 1667-1668.
Hansen P.A. (1976), Int. Conf. on Magnetism, Amsterdam, September 6-10.
Hansen P.A. (1977), Risø Report number 360 (thesis), Risø
National Laboratory, DK 4000 Roskilde, Denmark.
Ishida M. *et al.* (1985), J. Phys. Soc. Jpn. **54**, 2975-2982.
Ishikawa Y. *et al.* (1976), Solid State Comm. **19**,525-
Ishikawa Y. *et al.* (1977), Phys. Rev. B **16**, 4956-4970.
Ishikawa Y. *et al.* (1982), Phys. Rev. B **25**, 254.
Ishikawa Y. *et al.* (1984), J. Phys. Soc. Jpn. **53**, 2726-2733.
Ishikawa Y. *et al.* (1985), Phys. Rev. B **31**, 5884.
Kadowaki K. *et al.* (1981), J. Phys. Soc. Jpn. **51**, 2433-2438.
Kataoka M. (1984), J. Phys. Soc. Jpn. **53**,3624.
Kusaka S. *et al.* (1976), Solid State Comm. **20**, 925-927.
Lebech B. *et al.* (1989), J. Phys.:Condensed Matter **1**, 6105-6122.
Lebech B. (1992), presented at symposium on *Recent Progress in Material Physics*,
— Osaka, Japan. To be published in *Recent advances in Magnetism of Transition*
— *Metal Compounds*, World Scientific Publishing Co.
Levinson L.M. *et al.* (1972), American Institute of Physics
— Conf. Proc. **10**, 1138-1147.
Lonzarich G.G. and Taillefer L. (1985), J. Phys. C **18**, 4339.
Matoya K. *et al.* (1976), Solid State Commun. **19**, 529.
Matoya K. *et al.* (1978), J. Phys. Soc. Jpn. **44**,833.
Matsunga M. *et al.* (1982), J. Phys. Soc. Jpn. **51**, 1153-1161.
Moriya T. (1960), Phys. Rev. **120**, 91.
Moriya T. (1981), *Magnetism in Narrow Band Systems* ed. by T. Moriya
—(Springerverlag;Berlin), 2-27.
Patterson C. *et al.*(1985), Solid State Commun. **55**, 81-84.
Plumer M.L. and Walker M.B. (1981), J. Phys. C. **14**, 4689-4699.
Plumer M.L. and Walker M.B. (1982), J. Phys. C. **15**, 7181-7191.
Plumer M.L. (1984), J. Phys. C. **17**, 4663-4679.
Plumer M.L. (1990), J. Phys.:Condensed Matter **2**, 7503-7510.
Sakakibara T. *et al.* (1981), J. Phys. Soc. Jpn. **51**, 2439-2445.
Shekhtman L. *et al.* (1992), Phys. Rev. Lett. **69**,836.
Shirane G. *et al.* (1983), Phys. Rev. B **28**, 6251-6255.
Taillefer L. (1986a), Ph. D. Thesis, University of Cambridge, (unpublished).

Taillefer L. *et al.* (1986b), J. Magn. Magn. Mater. **54-57**, 957-958.
Walker M.B. (1989), Phys. Rev. B **40**, 9315-9317.
Williams H.J. *et al.* (1966), J. Appl. Phys. **37**, 1256

Chapter 3

Equipment

3.1 The Durham Vibrating Sample Magnetometer

3.1.1 Outline of the System

The principle investigative tool used in Durham was a Vibrating Sample Magnetometer (VSM). This instrument was designed and built in the laboratory by Drs. S.R.Hoon and S.N.M.Willcock and has been described in detail (Willcock(1985), Hoon and Willcock (1988)) consequently only a broad outline is given here.

The principle of the operation of a VSM was originally described by Foner (1956). In essence, the VSM detects the magnetic induction in the vicinity of a selected sample. The sample is placed in a static magnetic field and vibrated relative to a series of pick-up coils. This causes the flux through the detection coils to change and so induces an e.m.f. across them in accordance with Lenz's Law. This e.m.f. is proportional to the moment of the sample and the amplitude and frequency of vibration. The vibrator mechanism also provides an a.c. signal at the vibrational frequency which can be used as a reference signal for a phase-sensitive detector. Hence provided that the amplitude and frequency of vibration maintained constant, the signal is proportional to the magnetic moment of the sample. Calibration of the system with a known magnetic moment means the magnetisation of the sample can be measured.

Figure 3.1 shows the principle components of the Durham VSM as used with a 12kOe electromagnet. The vibration mechanism is achieved by means of an electric motor and crank mechanism. The 180° double throw arrangement of the crank assembly provides a significant improvement on previous systems in amplitude and frequency stability, low vibrational noise and high inertial loading. The vibrating head mechanism is isolated from the rest of the system by a pneumatic seating.

The detection coils are mounted on the pole tips of an 8 inch Newport Instrument Type D air cooled electromagnet. The geometry of the detection coils is that due to Mallinson (1986) consisting of two vertical pairs of pancake coils mounted parallel

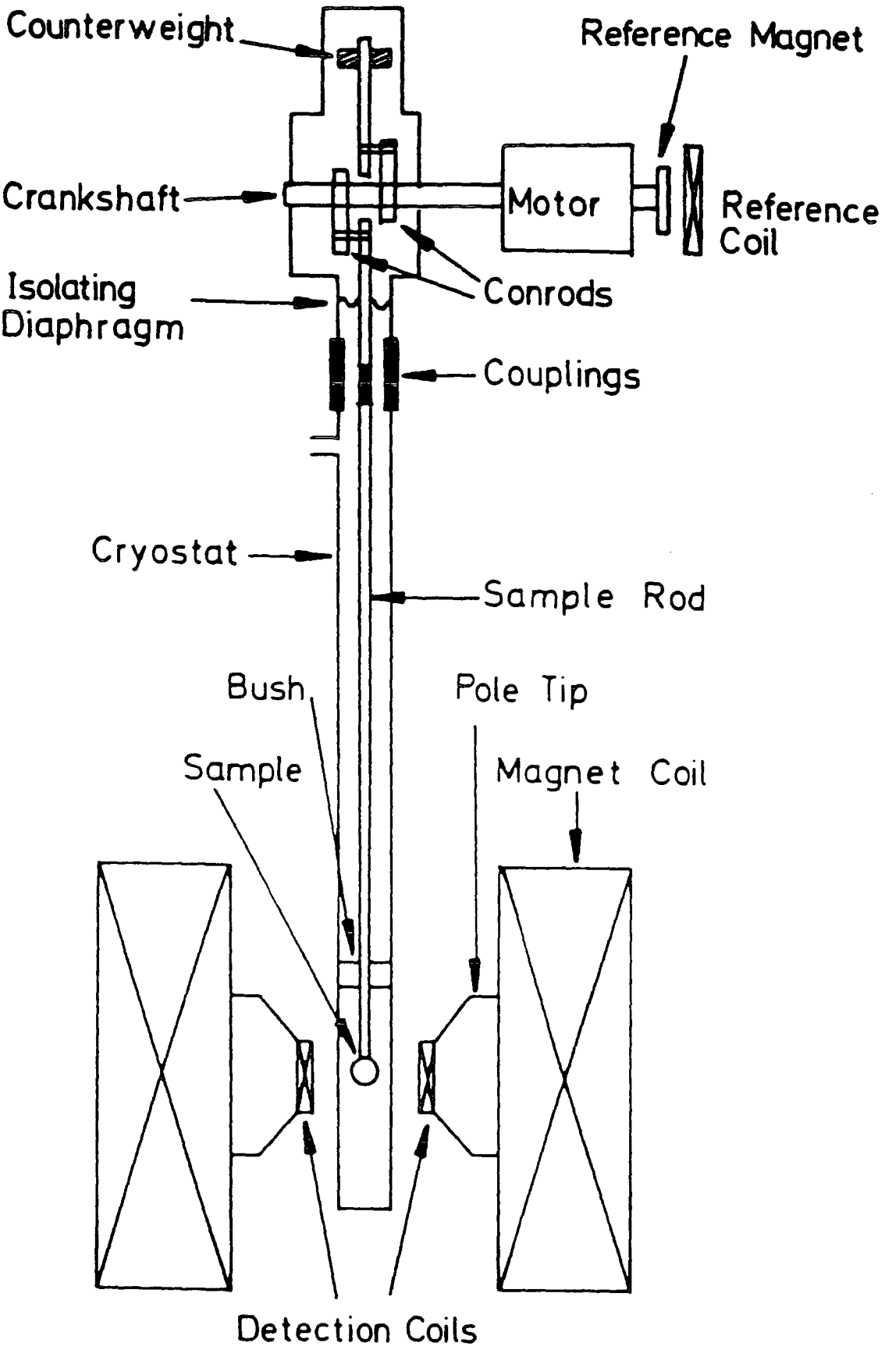

Figure 3.1 The principal elements of the Durham VSM.

to the faces of the pole tips. Data acquisition was via a Brookdeal 5206 lock-in amplifier used in common mode rejection to detect the signal from the two pairs of coils. A Hall effect Bell 640 Gaussmeter connected to a Fluke 8860a digital voltmeter was used to measure the magnetic field. An IBM compatible personal computer obtained data from these instruments via the IEEE 488 communication bus and controlled the magnet power supply (a KSM (SCT)) via a Bede Scientific Instruments Minicam interface system and a purpose built control panel, designed and built in the Physic Department Electronic Workshop.

The cryostat used was an Oxford Instruments CF1200 gas flow cryostat with seperate exchange gas filled sample space and controlled by an Oxford Instruments 3120 or ITC4 temperature controller. The sample was located centrally in the cryostat by a perforated polytetrafluorethylene (PTFE) bush, the cryostat itself being mounted centrally on the magnet axis.

Calibration was done by means of a Nickel sample. After accounting for demagnetisation factors, a standard was chosen for the magnetisation of Nickel (Pauthenet (1982)).

3.1.2 Enhancement of VSM Sensitivity

The Newport magnet and coils on the VSM were initially individually grounded via the lock-in amplifier which infact held them at a common potential but not earth.

It was found that the sensitivity of the VSM was dramatically increased by changing the above arrangement. The magnet was earthed directly using thick braid and then the coils linked directly to the magnet. There was a large reduction in noise, permitting a reduction in the time-constant used on the lock-in from 1s to 100ms, dramatically increasing the speed of data acquisition.

3.1.3 Data Acquisition System

The VSM at Durham was originally automated by Dr. S.N.M.Willcock using a PET microcomputer to communicate with Brookdeal 5206 Phase Sensitive Detector, an 8860a Fluke multimeter and Bede Scientific Minicam Crate which in turn controlled a Newport Power Supply. Over the passage of time, the computer had become obsolete and a new power supply (KSM (KCT)) had been obtained for the electromagnet. As a result, the system was overhauled and new control software was written by Mr. C.I. Gregory.

The PET was replaced by an 'IBM compatible' Elonex 286 PC fitted with a Scientific Solutions IEEE interface card. The source code of the program controlling the entire system was written in Turbo Pascal. Routines had previously been written for IEEE, Fluke, Brookdeal and Minicam individually by Dr. D.B.Lambrick and these were moulded into a complete control program.

An entire package of programs was written for the VSM to undertake various tasks and incorporated with a user guide. This descibes the apparatus used in the system, how it is computer controlled, each program in the package and what it can

do, and how to set-up the system before taking data (see Appendix A). Data is is stored in a matrix format and programs to display the data using the PC-Matlab software package are also included.

In short, the package allows the recording of magnetisation as a function of time, temperature and manually or automatically altered magnetic field. The complete control program allows for three field regions where the density of data points can be varied. It also requires the number of repeated measurements at each field and the delay between each in terms of the number of time constants to be input. There is real time display of data in the form of a graph on the screen in all programs. Well annotated listings of all the programs written are included in Appendix A.

One limitation of the system is that with the KSM power supply there is a region of 200Oe close to the remnant field which is unobtainable when the current polarity is switched. In order to overcome this, a control program was written incorporating a smaller Kepco bipolar operational powersupply/amplifier. This program, also included in Appendix A, is similar to the others and controls the Kepco via the dac board of a Bede Scientific Instrument Minicam system. The maximum field obtained is smaller than that using the KSM so the program moves in fixed field steps but would require little development to incorporate the field regions of the original program.

3.2 Oxford 120kOe VSM Facility

Some measurements were made in collaboration with Dr. D. B. Lambrick at Manchester Polytechnic using the Manchester VSM facility. This comprises of an Aerosonic VSM and Oxford solenoid 120kOe superconducting magnet. All measurements were taken in step mode using a typical time constant of 240ms and a field settle time of 3s. The sample enviroment was provided by an Oxford CF1200 cryostat providing a temperature range of 2-1200K. Temperatures were monitored by a Au(0.03%)Fe Cr thermocouple and controlled by an Oxford ITC4 temperature controller.

Calibration of the magnetic field at low fields was performed using a Bell 640 gaussmeter because a small amount of hysteresis due to flux pinning was observed in the magnet.

3.3 Small Angle Neutron Scattering at Risø

Small Angle Neutron Scattering (SANS) was undertaken at the Risø National Laboratory, Denmark in collaboration with Professor Bente Lebech of the Physics Department.

The SANS facility used is on the reactor DR3 at Risø. This is a heavy-water-modulated 10MW thermal neutron research reactor. Neutron beams emerge from horizontal through tubes tangential to the reactor core, the flux being about $3.5 * 10^{13} n/cm^2/s$ in the centre of the 7 inch diameter tubes. The thermal neutron flux, in

equilibrium with the heavy water moderator has a Maxwellian distribution peaking at 1.1Å.

The beam used for SANS is then scattered using a so-called cold source (a chamber filled with a supercritical hydrogen gas at 16 atmospheres and 38K) which enhances the long wavelength region when compared for example to a thermal water scatterer. The beam is shared, with a 20m long cold-neutron guide-tube providing three ports in the 'Neutron House'. Only neutrons that have undergone total internal reflection from the Ni coated glass plates in the bent guide tube arrive at the end in the 'Neutron House'. As the angle of total reflection is proportional to the neutron wavelength almost no neutrons below a 'critical' wavelength are transmitted. SANS benefits from both a high flux at long wavelengths and low background enviroment.

The SANS monochromator consists of a mechanical velocity selector giving access to wavelengths in the range 3 - 24Å with a resolution of 10 - 20%. The 6m long collimation section allows the neutron source point to be moved from 1 - 6m away from the sample. Thus the arrangement allows for a suitable choice of scattering vector range and enables tuning to optimum flux for a given resolution.

The area-sensitive multi-wire proportional detector used has been developed at Risø. The active volume is 60cm in diameter, 4.5cm thick and the total gas volume is 15.2l. The normal filling is 1 atm ^{3}He plus 1.5 atm Ar and Methane, which combines high efficiency and spatial resolution together with low γ-ray sensitivity. The anode grid is used for one coordinate and the two other cathode grids, coupled in parallel after the pre-amplifiers are used for the other coordinate, resulting in $1cm^2$ pixels. A beam stop was placed in front of the detector to remove unscattered neutrons.

The sample enviroment was provided by a 50kOe split coil, top loading superconducting magnet. This offered a temperature range between 4.2 - 300K and 0 - 50kOe vertical field. This was the first occasion the 50kOe magnet had been used on SANS.

3.4 Triple Axis Neutron Scattering at Risø

The triple axis spectrometer used at Risø was TAS1 which shares the cold neutron beam with the guide tube for cold neutrons to the Neutron House. The instrument has four fixed-incidence take-off angles from the monochromator, which for the (002) reflection in pyrolytic graphite corresponds to incident energies of the first order neutrons of 13.7meV, 7.2meV, 5.0meV and 3.6meV. The instrument is fully automated and operated by means of the fortran program TASCOM running on a PDP11 computer. The curved monochromator and the planar analyser crystals are composed of 1cm high (002) slabs of pyrolytic graphite. $\frac{\lambda}{2}$ filters of Be can be inserted either infront of or behind the sample. The instrument moves on air cushions and all angles may be set with a precision of a few hundredths of a degree. The collimations can easily be adjusted to suit the experiment. The background can be minimized by means of adjustable diaphragms.

The monochromator axis consists of a motorised turntable and a goniometer

mounted on a turntable. The sample axis consists of a turntable with a goniometer ($\pm$ 15 deg) and an X-Y translation ($\pm 12mm$). The analyser unit is mounted on air cushions. The take-off angle from the analyser is continuously variable. The shielding wedges around the analyser crystal are lifted pneumatically to allow for automatic change of the analyser setting.

3.5 References

Foner S. (1956), Rev. Sci. Instrum. **27**, 548.
Hoon S.R. and Willcock S.N.M. (1986), J. Phys. E:Sci. Instrum. **21**, 722.
Mallinson J. (1966), J. Appl. Phys. **37**, 2614.
Pauthenet R. (1982), J. Appl. Phys. **53**, 8187.
Willcock S.N.M. (1985), Ph.D. Thesis, University of Durham.

Chapter 4

Magnetic Measurements on $ZrZn_2$

4.1 Introduction

Magnetic measurements were made on a single crystal of $ZrZn_2$ and are included within this thesis for numerous reasons.

MnSi was used as a typical weak, itinerant ferromagnet by Ishikawa (1977) in order to study the magnetic excitations in this type of system, both above and below the critical temperature. However, as discussed in Chapter 2, the assumption that MnSi is such a material is controversial. $ZrZn_2$ on the other hand, is arguably the best example known of a typical, weak (Wohlfarth (1971)), itinerant (Pickart (1964)) ferromagnet and has a transition temperature between 20 and 28K i.e. very similar to that of MnSi. In order to investigate any differences, the magnetisation of $ZrZn_2$ was measured close to the transition temperature.

Both FeGe and MnSi have cubic B_{20} structures and are capable of supporting long range spin density waves at low temperatures. The helix propagate along high symmetry directions in the crystals and are extremely long range, with repeat distances ranging from 45 to 175 lattice units. This means that locally the spin arrangement can be considerred ferromagnetic. $ZrZn_2$ can be regarded as a similar ferromagnetic structure but of infinite wavelength.

Finally, although magnetic measurements have previously been performed on $ZrZn_2$ (for example Knapp *et al.*(1971)) and reproduction can be found in general magnetism texts (Crangle (1991)), there is no report of a detailed study close to the transition temperature.

4.2 Review of Previous work on $ZrZn_2$

Attention was first excited to $ZrZn_2$ in 1958 when Matthias and Bozorth established that a compound of 'approximate composition' 1Zr:2Zn had become ferromagnetic at 35K. Previously it had been assumed that ferromagnetic intermetallic compounds must contain at least one of the ferromagnetic elements Fe, Co or Ni. The fact seemed remarkable that neither Zr or Zn were ferromagnetic, but infact

both superconductors in their pure metallic state. Since then, a great deal of experimental and theoretical interest has been focussed on accounting for the magnetic properties of this alloy system.

Pickart *et. al.* (1964) directly observed a large degree of delocalisation of the Zr spin density in $ZrZn_2$ by polarised neutron scattering. Blythe (1966) studied the paramagnetic susceptibility of $ZrZn_2$ above the transition temperature and found it to follow the Curie-Weiss law. Within this report however, there is reference to questionable results due to 'suspect' samples. The extremely sensitive nature of the magnetisation to sample quality is evident as Foner (1967) considered whether the magnetism was intrinsic because of the large differences between samples. It was the results of Blythe (1968) on high purity samples of $ZrZn_2$ that proved the ferromagnetism was intrinsic. Mattocks (1978) used the same samples as Blythe and extended the magnetic measurements to find no sign of saturation of $ZrZn_2$ in fields of up to 170kOe.

The magnetisation of $ZrZn_2$ and related alloys is discussed by Knapp *et al.* (1971). They calculated the effective local moment from the Curie Weiss response of $ZrZn_2$ above the Curie temperature and found $P_{eff} = 1.57\mu_B$ per Zr atom as opposed to a value of $0.16\mu_B$ at zero field and extrapolated to zero temperature. (Note this figure was ammended to $0.17\mu_B$ by Van Deursen (1986)). Their results suggest that the ferromagnetism observed in $ZrZn_2$ is a consequence of the Fermi level being close to a peak in the density of states curve. As a result, the extra kinetic energy required for the transfer of a given number of electrons from one spin state to the other is smaller than the net gain in exchange energy resulting from the imbalance in population of the two spin states. The density of states curve is such that this condition is only satisfied for the transfer of a small number of electrons.

The initial homogeneous pressure derivative of the Curie temperature of $ZrZn_2$ was measured by Wayne and Edwards (1969). The value obtained of $-(1.95 \pm 0.1)Kkbar^{-1}$ was found to be in good agreement with the relationship $T_c(P) = T_c(0)(1 - \frac{P}{P_c})^{\frac{1}{2}}$ derived from the theory of itinerant magnetism by Wohlfarth (1968). The experiment was later repeated by Smith *et al.* (1971) who recorded a critical pressure of 8.5kbars for the destruction of ferromagnetism.

Wohlfarth and Bartel (1971) showed that the thermal expansion, susceptibility and pressure effects on the magnetisation are indicative of weak correlation effects between the itinerant electrons. Clinton *et al.* (1975) used previously published data to determine the magnetic entropy. They pointed out that although the broad features of the behaviour of $ZrZn_2$ could be understood within the band model, modifications would be necessary to account for the partially localised character of the moments. This comment was reinforced by Brown *et al.* (1984) who used polarised neutrons to measure the magnetic structure factor. This was found to be consistent with a model in which 57% of the magnetisation is associated with strongly hybridised Zr 4d and 5p wavefunctions, with the remaining magnetisation very delocalised. Van Deursen *et al.* (1986) studied the Fermi surface of $ZrZn_2$ through de Haas van Alphen and compared the observed frequencies to band structure calculations. Their high field magnetisation data showed the 'Arrot Plots' to be curved, this being attributed to structure in the density of states.

Because of the considerable development in theories of weak itinerant ferromagnetism (Moriya (1979), Lonzarich *et al.* (1985)), Law (1988) investigated the spin density spectrum of $ZrZn_2$ through neutron scattering in order to test new ideas. Hayden (1991) also measured the low temperature magnetisation of $ZrZn_2$ and found results consistent with the model of Lonzarich and Taillefer (1985).

4.3 $ZrZn_2$ Structure and Sample

$ZrZn_2$ has the cubic Laves phase (C15) structure with a lattice parameter of 7.315Å, as shown in figure 4.1. This structure has inversion symmetry. The sample was prepared by melting high purity zone refined zirconium and zinc contained by Y_2O_3 crucible inside a tantalum bomb at 1200^oC. The mixture was cooled slowly through the melting point and then annealed at various temperatures above 500^oC over a period of 5 days. The resulting ingot was found to have resistance ratio ($\frac{\rho_{293K}}{\rho_{4.2K}}$) in the range 30-50. The bulk of the specimen was seen to be a single crystal and back-reflection Laue X-ray diffraction photos were used to align the crystal and showed that the crystal mosaic spread was small. The sample has previously been used by Law (1988) in neutron scattering experiments and more recently by Hayden (1991) to measure the ac susceptibility. This latter experiment determined a transition temperature of between 23 - 24K.

4.4 Magnetisation Measurements above the Transition Temperature

Magnetic measurements were performed on a single crystal of $ZrZn_2$, a disc of diameter 2.5mm and mass 22.5mg, cut such that the disc is a $(1\bar{1}0)$ plane. The magnetisation was found to be isotropic in the $< 111 >$ and $< 001 >$ directions both above and below the transition temperature. Data presented in this thesis were taken with the magnetic field and magnetisation measured parallel to the $< 001 >$ direction.

Figure 4.2 shows the magnetisation of $ZrZn_2$ close to the transition temperature in magnetic fields upto ± 0.25kOe. The raw data is plotted as points with a single line representing the average value of measurements for increasing and decreasing magnetic field. The magnetisation is paramagnetic and as the temperature is lowered the paramagnetism not only increases, but the curvature of the magnetisation becomes enhanced as demonstrated in figure 4.3 of the corresponding inverse susceptibility.

From figure 4.3 it is evident that the inverse susceptibility is parabolic with applied magnetic field in the temperature regime of 27 - 30K. As the temperature is lowered, not only does the curvature of the parabola increase, particularly in low fields of less than 2kOe, but also the spread of values or error associated with the inverse susceptibility reduces in low fields. As the temperature is reduced, for example at and below 25K, the inverse susceptibility changes from being parabolic

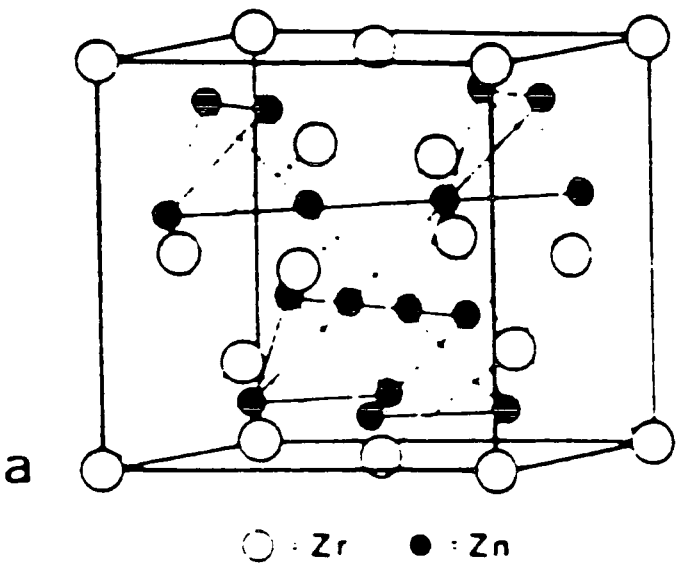

Figure 4.1 Structure of $ZrZn_2$.

In figures 4.2 - 4.4 the internal magnetic field ($H_i = H - H_D$) has been called B and given the units gauss. Magnetisation is measured in units of $emucm^{-3}$ and can be converted to units of $emug^{-1}$ using the density of $ZrZn_2$ which is $7.5gcm^{-3}$.

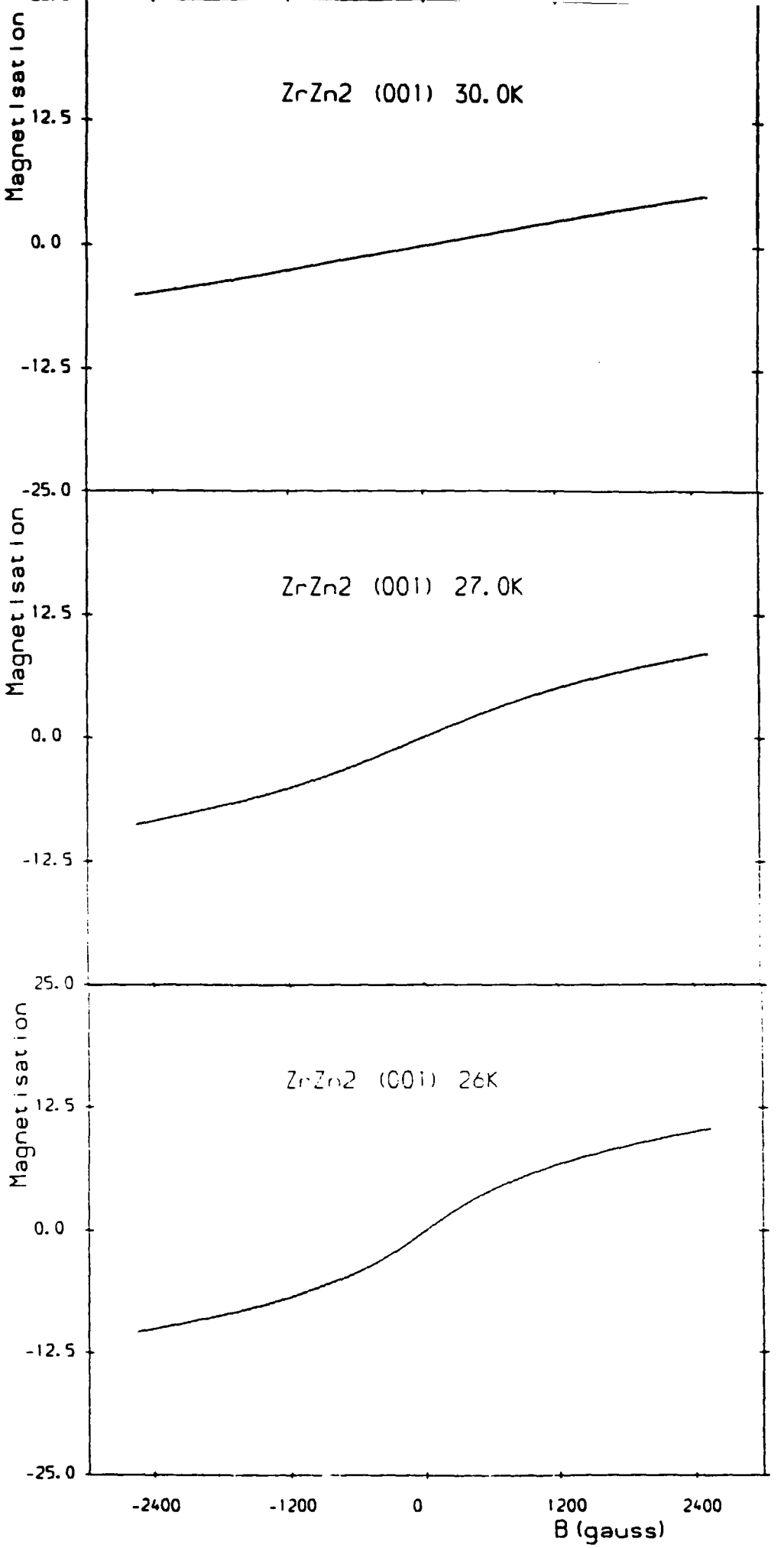
ZrZn2 (001) 30.0K
ZrZn2 (001) 27.0K
ZrZn2 (001) 26K
Magnetisation
12.5
0.0
-12.5
-25.0
-2400
-1200
0
1200
2400
B (gauss)

Figure 4.2 (a) - (c)

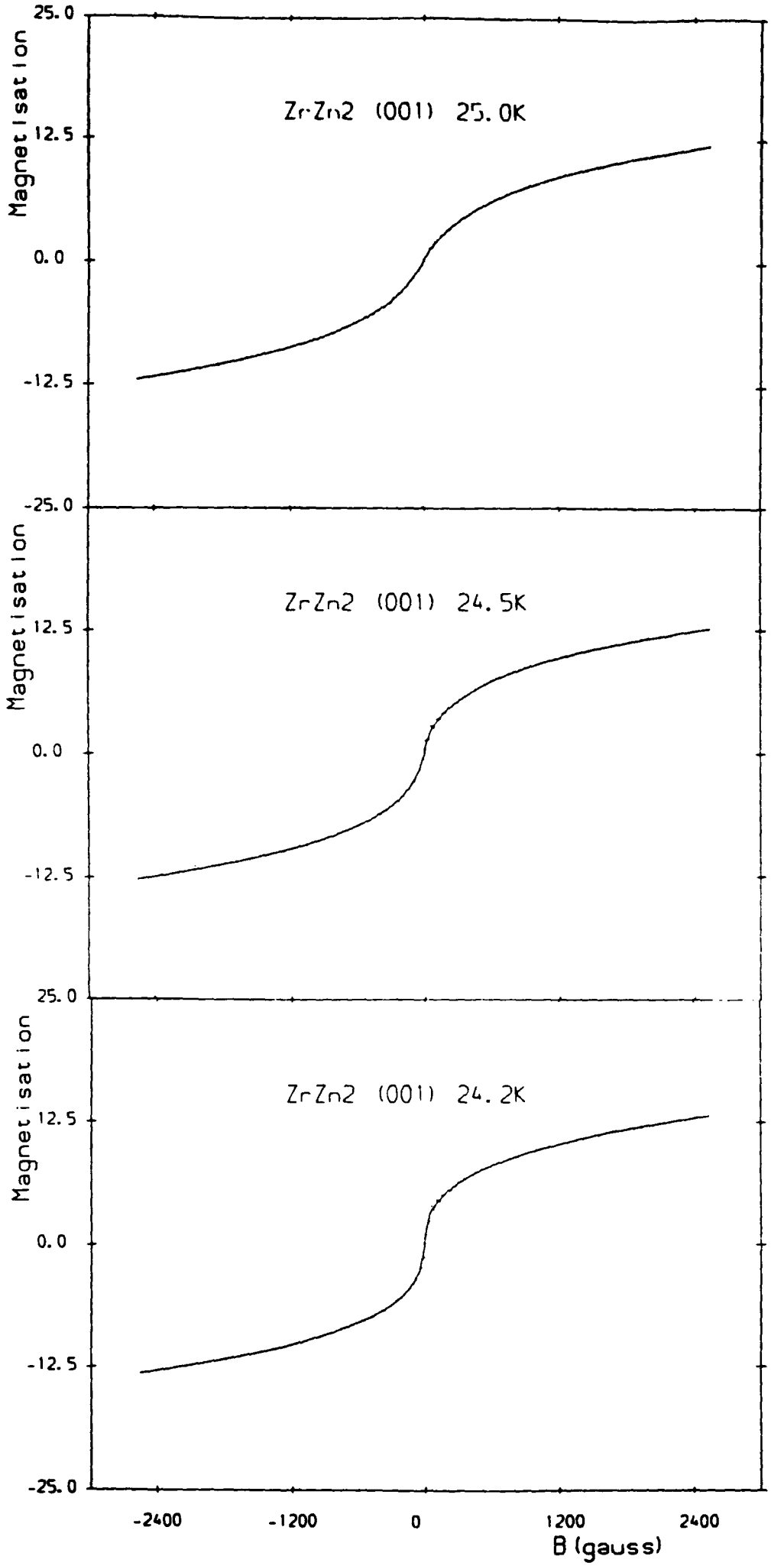
ZrZn2 (001) 25.0K
ZrZn2 (001) 24.5K
ZrZn2 (001) 24.2K
Magnetisation
25.0
12.5
0.0
-12.5
-25.0
-2400
-1200
0
1200
2400
B (gauss)

Figure 4.2 (d) - (f)

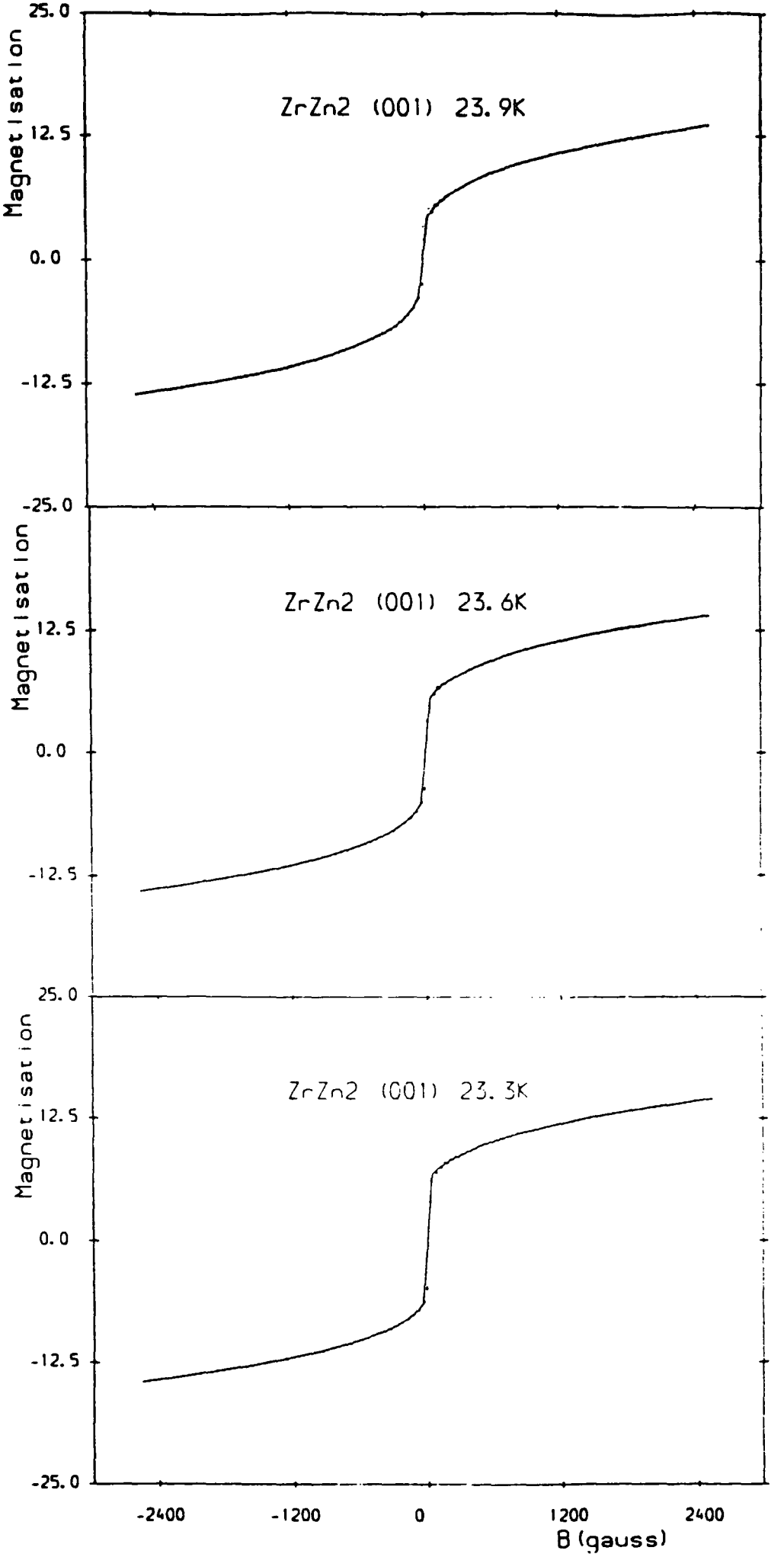
ZrZn2 (001) 23.9K
ZrZn2 (001) 23.6K
ZrZn2 (001) 23.3K
Magnetisation
25.0
12.5
0.0
-12.5
-25.0
-2400
-1200
0
1200
2400
B (gauss)

Figure 4.2 (g) - (i)

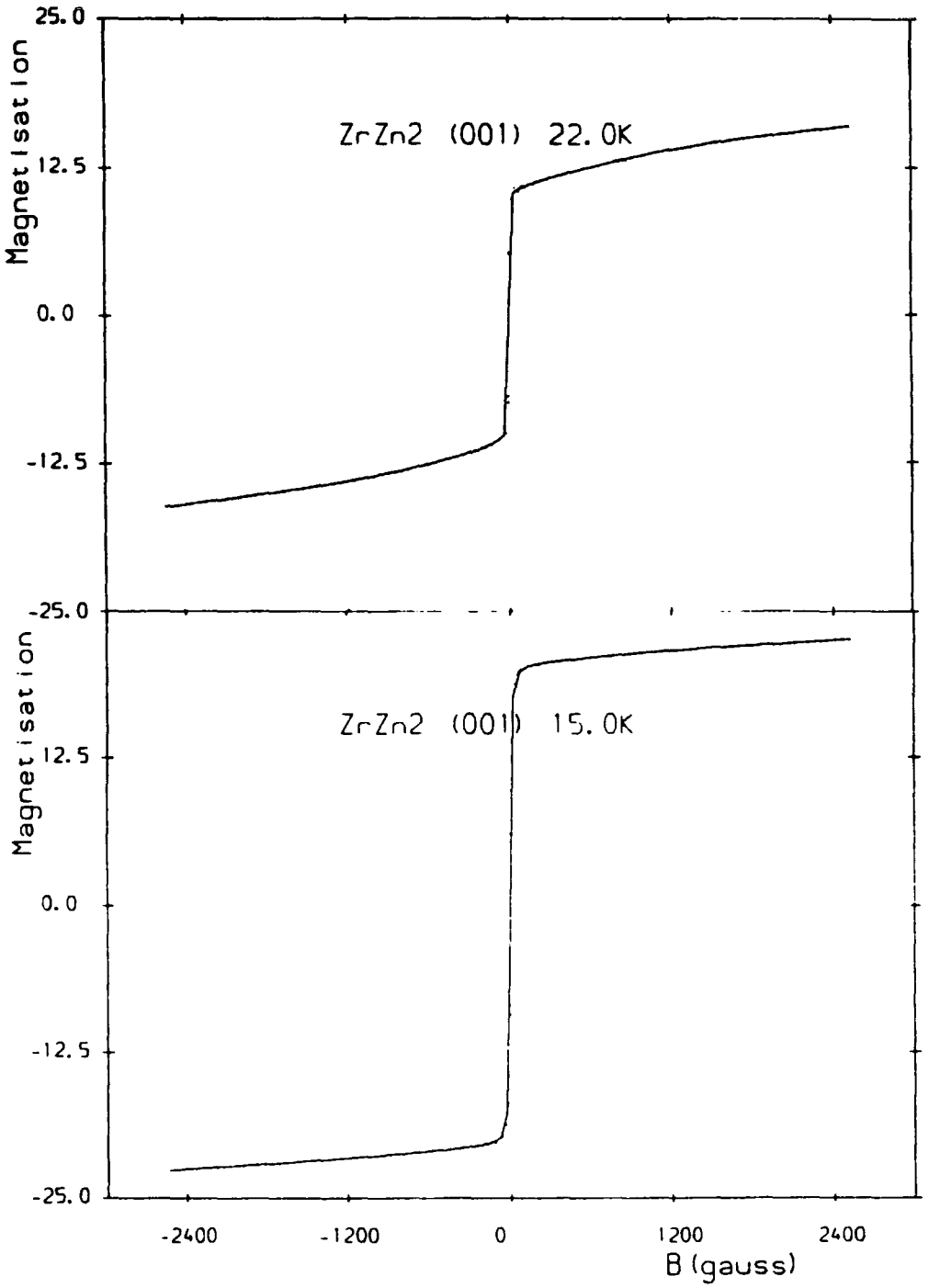

Figure 4.2 Magnetisation of $ZrZn_2$ as a function of applied magnetic field. Measurements were taken for decreasing temperature with field steps of 50Oe. The solid line is an average through the data points for a particular field. (a) 30.0K; (b) 27.0K; (c) 26.0K; (d) 25.0K; (e) 24.5K; (f) 24.2K; (g) 23.9K; (h) 23.6K; (i) 23.3K; (j) 22.0K; (k) 15.0K.

Figure 4.3 Inverse susceptibility of $ZrZn_2$ (derived from the data of fig. 4.2) as a function of applied magnetic field. The points on the graphs are the raw data The solid line is an average through the data points for a particular field value. (a) 30.0K; (b) 27.0K; (c) 26.0K; (d) 25.0K; (e) 24.5K; (f) 24.2K; (g) 23.6K; (h) 23.3K; (i) 22.0K.

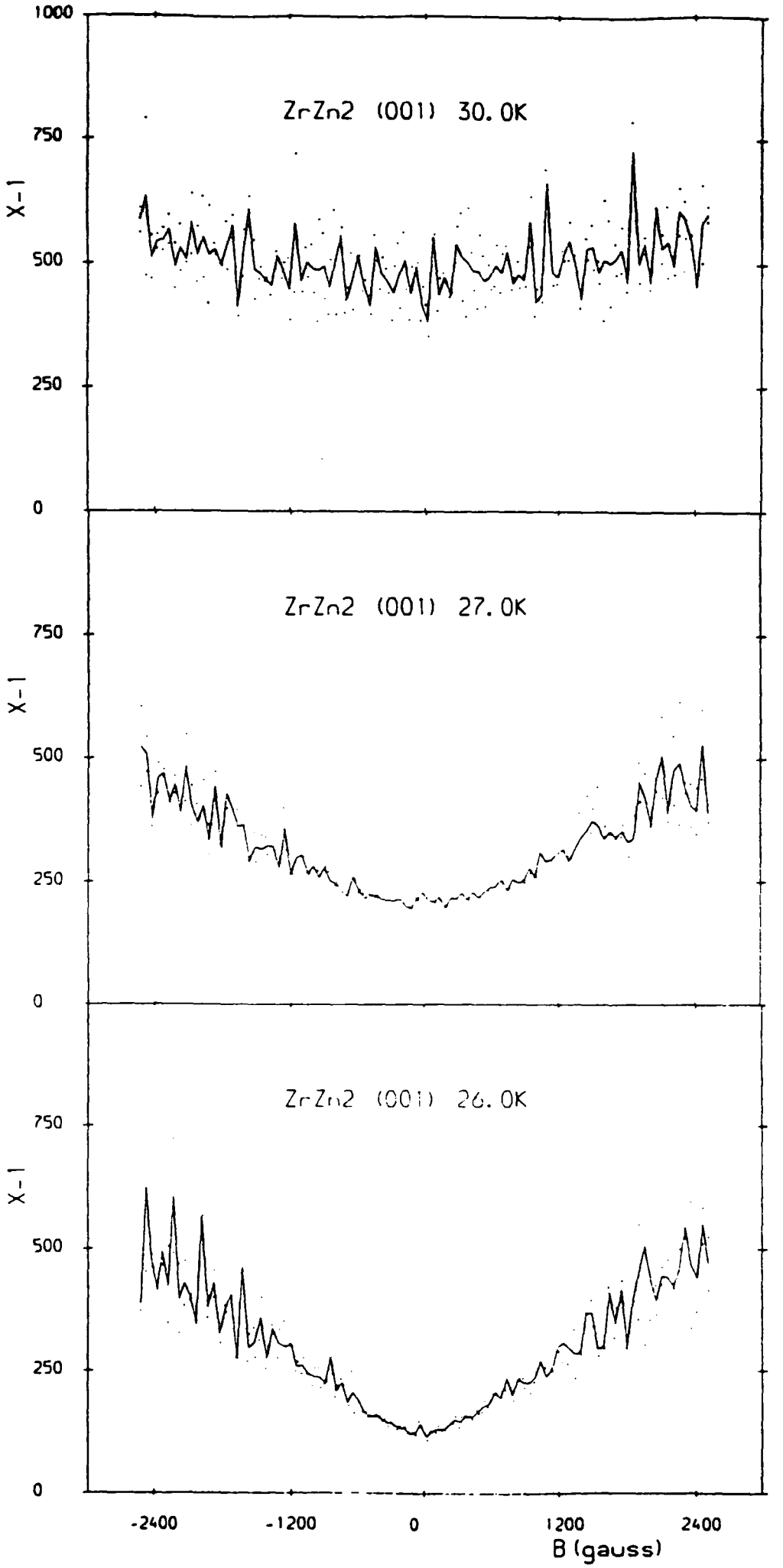
ZrZn2 (001) 30.0K
ZrZn2 (001) 27.0K
ZrZn2 (001) 26.0K
X-1
1000
750
500
250
0
-2400
-1200
0
1200
2400
B (gauss)

Figure 4.3 (a) - (c)

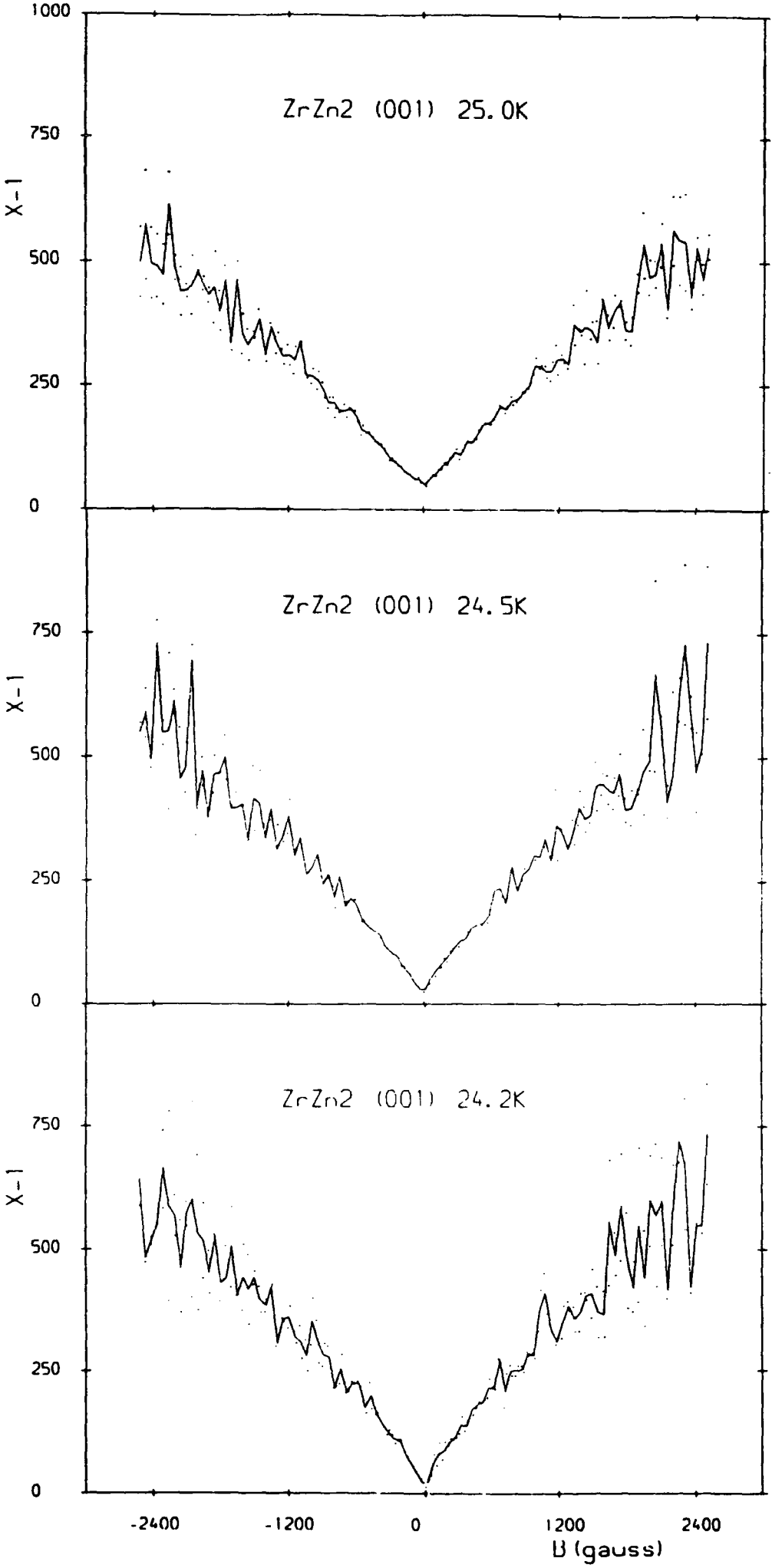
ZrZn2 (001) 25.0K
ZrZn2 (001) 24.5K
ZrZn2 (001) 24.2K
X-1
1000
750
500
250
0
-2400
-1200
0
1200
2400
B (gauss)

Figure 4.3 (d) - (f)

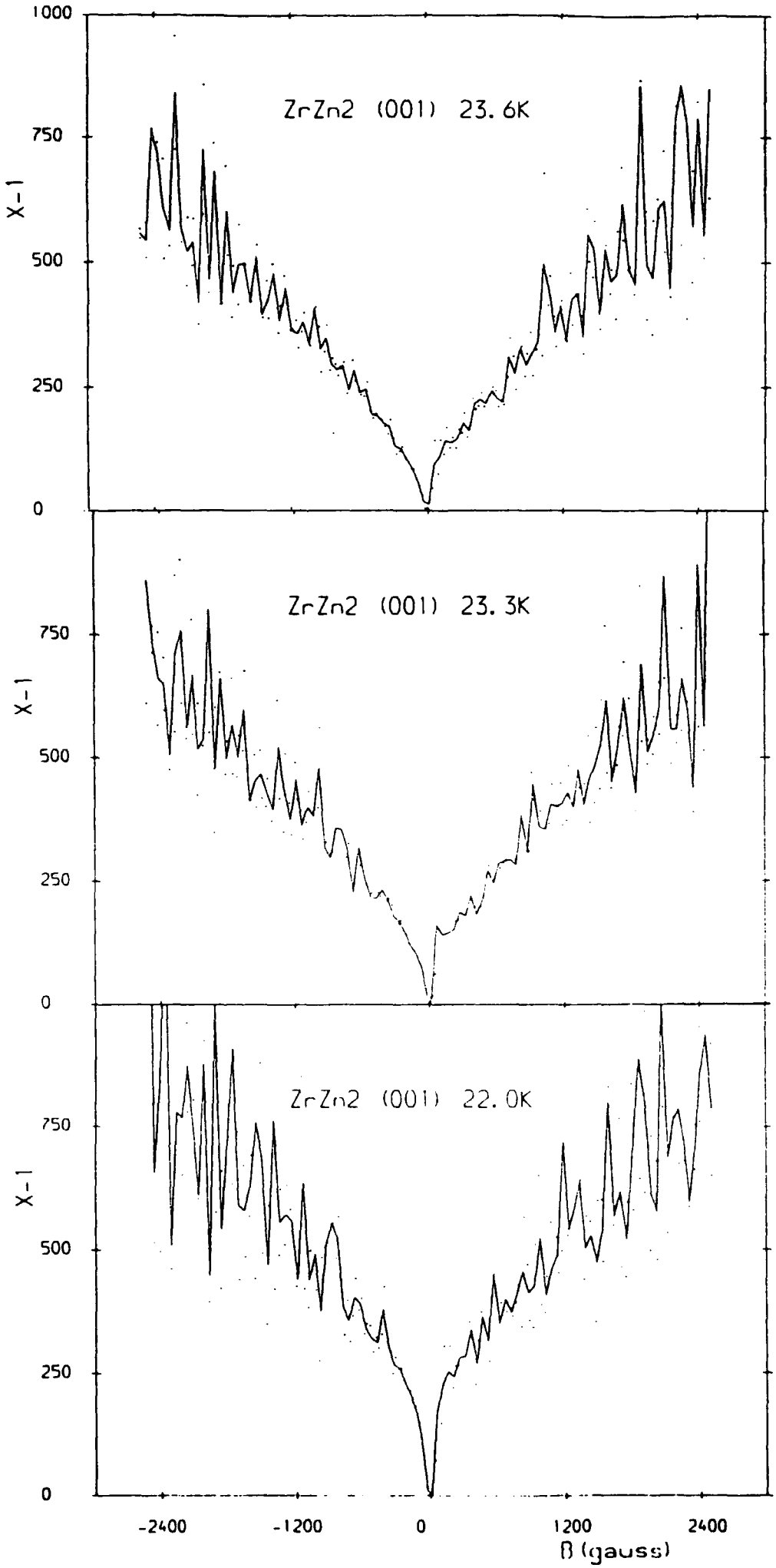
ZrZn2 (001) 23.6K
ZrZn2 (001) 23.3K
ZrZn2 (001) 22.0K
X-1
1000
750
500
250
0
-2400
-1200
0
1200
2400
B (gauss)

Figure 4.3 (g) - (i)

to a 'V' shape, owing to the zero field inverse susceptibility lowering rapidly with temperature whereas the high field values remain approximately fixed. This trend continues until at 24.5K the inverse susceptibility is convex with applied field and a minimum value in zero field.

Figure 4.5 shows magnetisation measurements in a similar temperature regime but extended to higher fields of 80kOe. Again points mark the raw data with a single line representing the average value of the magnetisation for a particular magnetic field. Within this field scale, the paramagnetic response appears to increase uniformly as the temperature is lowered. Note also that the magnetisation shows no sign of saturation above the transition temperature, even upto fields of 80kOe.

4.5 Magnetisation Measurements at and below the Transition Temperature

As the transition temperature is approached, the low field paramagnetic response increases and becomes enhanced until at a temperature between 24.5 - 24.2K the magnetisation becomes ferromagnetic i.e. finite in zero magnetic field (as shown in figure 4.2) although no hysteresis is observed. The transition temperature was determined by plotting M^2 against $\frac{B}{M}$ (the 'Arrot Plot'), which are linear at fixed temperature upto a field of 2.5kOe as shown in figure 4.4. By noting the highest temperature at which the plot intercepts the M^2 axis (implying a finite magnetisation in zero field), the ferromagnetic transition temperature of $ZrZn_2$ was determined. Figure 4.6 shows the 'Arrot Plots' of some high field magnetisation measurements. These are curved, consistent with Van Deurson (1986). Below the transition temperature there is a dramatic increase in the zero field magnetisation as the temperature is reduced, demonstrated in figure 4.2. The inverse susceptibility below the transition temperature is similar to that above, except that the low field limit approaches zero due to the sharpness of the response as the field switches direction, shown in figure 4.3. Again the inverse susceptibility is convex as the field is increased. The high field magnetisation data at and below the transition temperature (figure 4.5) shows that the magnetisation does not saturate below the transition temperature, even at fields of upto 80kOe.

The magnetisation data on $ZrZn_2$ was taken by fixing temperature and altering magnetic field. As the fields at which the magnetisation was measured were identical at each temperature, rearrangement of the data allows comparison of the magnetisation as a function of temperature. Figure 4.7 shows the magnetisation of $ZrZn_2$ between 24 - 28K i.e. just above the Curie temperature. In low fields of up to 250 Oe the magnetisation remains approximately constant until a temperature of 26K, below which it increases as the transition temperature is approached. As the field is increased, the temperature at which the magnetisation begins to increase rises until at a field of 400Oe (figure 4.7(c)) it increases over the complete temperature regime studied. In fields of upto 1kOe, the rate at which the magnetisation increases as the Curie temperature is approached is far greater than in higher fields. The curvature of the magnetisation against temperature reduces as the field is increased until, in

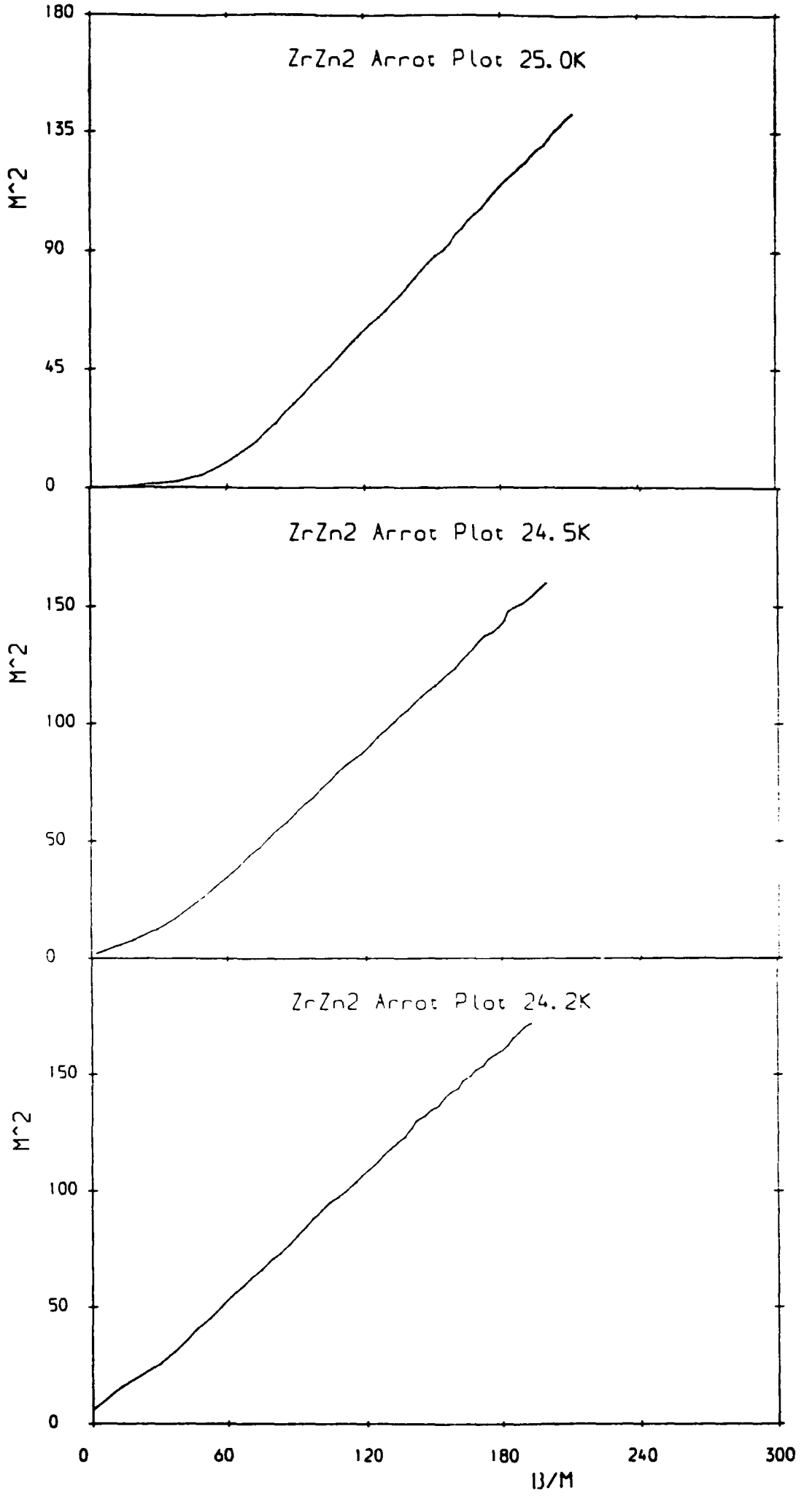
ZrZn2 Arrot Plot 25.0K
M^2
180
135
90
45
0
ZrZn2 Arrot Plot 24.5K
M^2
150
100
50
0
ZrZn2 Arrot Plot 24.2K
M^2
150
100
50
0
0
60
120
180
240
300
B/M

Figure 4.4 (a) - (c)

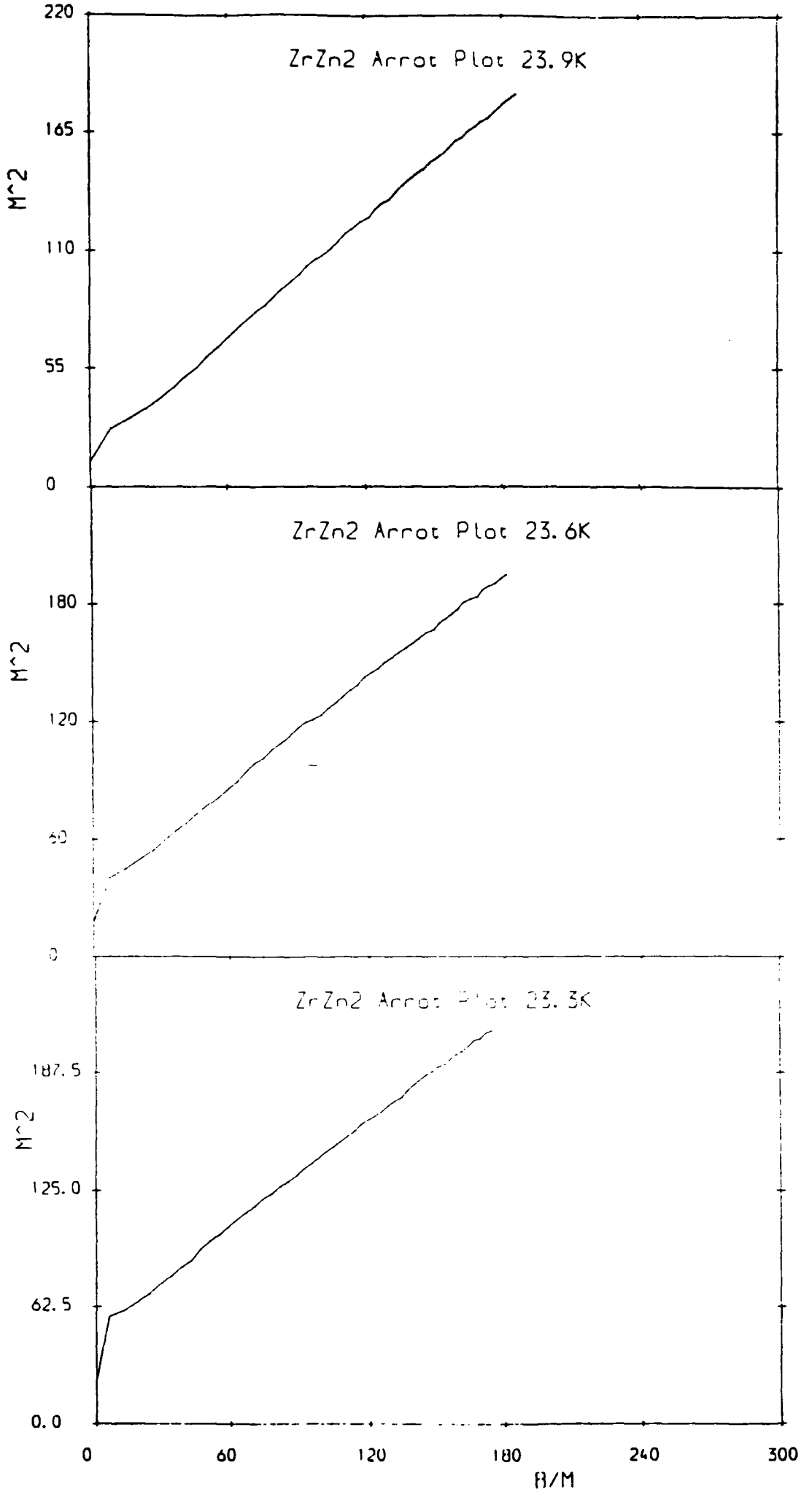
ZrZn2 Arrot Plot 23.9K
M^2
220
165
110
55
0
ZrZn2 Arrot Plot 23.6K
M^2
180
120
60
0
ZrZn2 Arrot Plot 23.3K
M^2
187.5
125.0
62.5
0.0
0
60
120
180
240
300
B/M

Figure 4.4 (d) - (f)

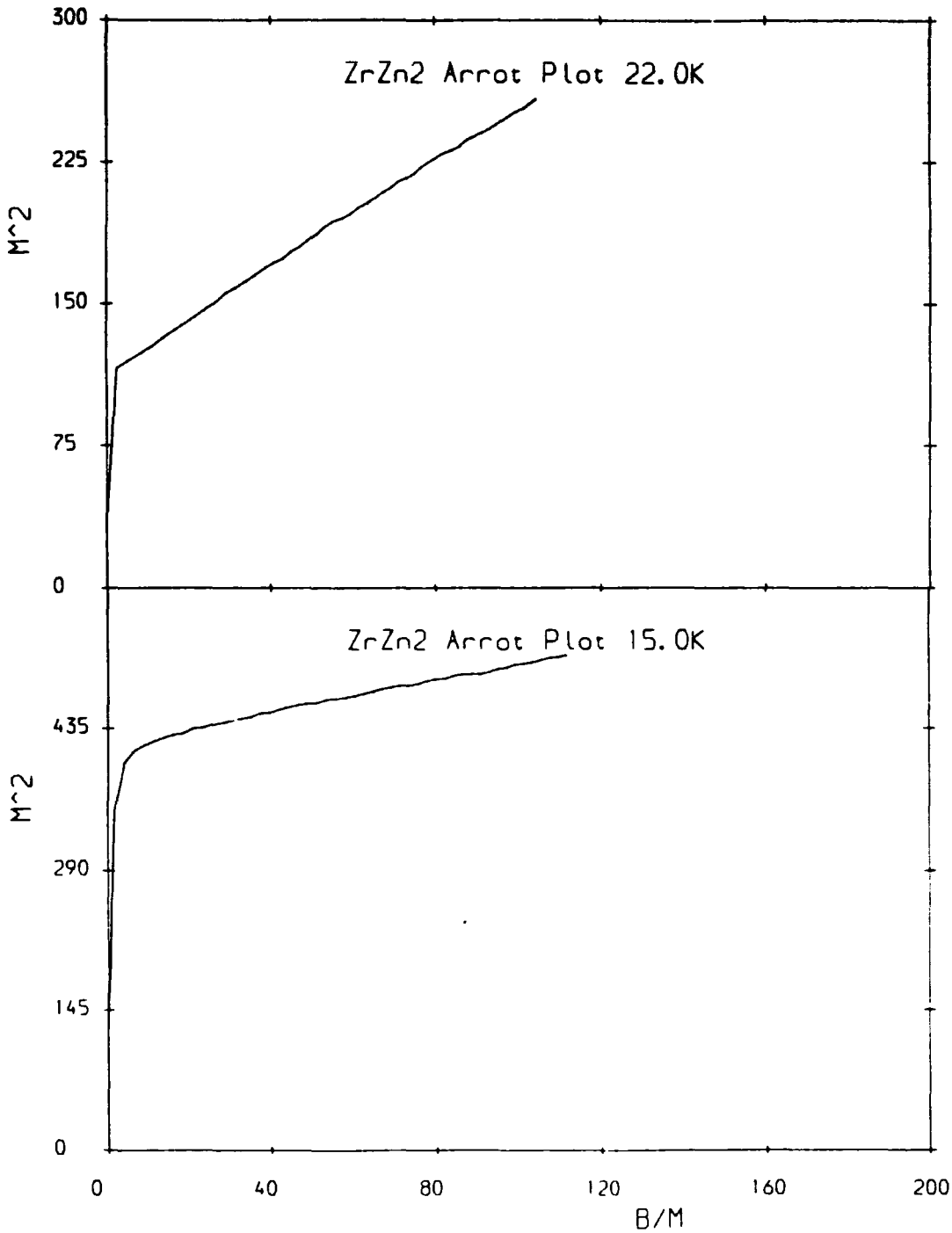

Figure 4.4 Arrot Plots for $ZrZn_2$ derived from the data of fig. 4.2. A solid line connects the raw data points. (a) 25.0K; (b) 24.5K; (c) 24.2K; (d) 23.9K; (e) 23.6K; (f) 23.3K; (g) 22.0K; (h) 15.0K.

In figures 4.5 - 4.6 the applied magnetic field (H) has been called B and given the units gauss. Magnetisation is measured in units of $emucm^{-3}$ and can be converted to units of $emug^{-1}$ using the density of $ZrZn_2$ which is $7.5gcm^{-3}$.

Figure 4.5 High field magnetisation measurements on $ZrZn_2$. A solid line connects the raw data points. (a) 28.0K; (b) 27.0K; (c) 26.0K; (d) 25.5K; (e) 25.0K; (f) 24.0K; (g) 23.5K; (h) 23.0K; (i) 22.0K.

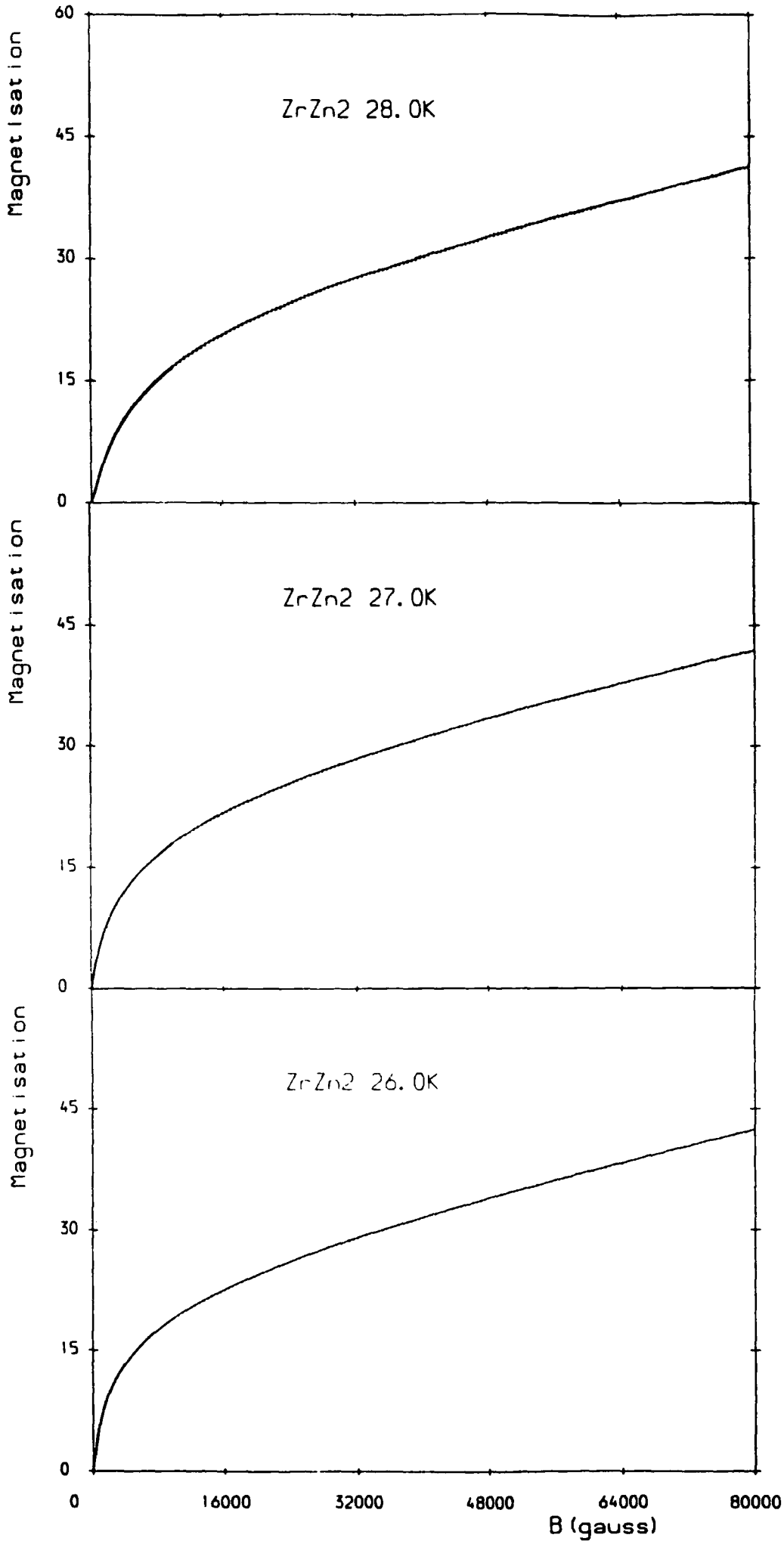
ZrZn2 28.0K
ZrZn2 27.0K
ZrZn2 26.0K
Magnetisation
60
45
30
15
0
0
16000
32000
48000
64000
80000
B (gauss)

Figure 4.5 (a) - (c)

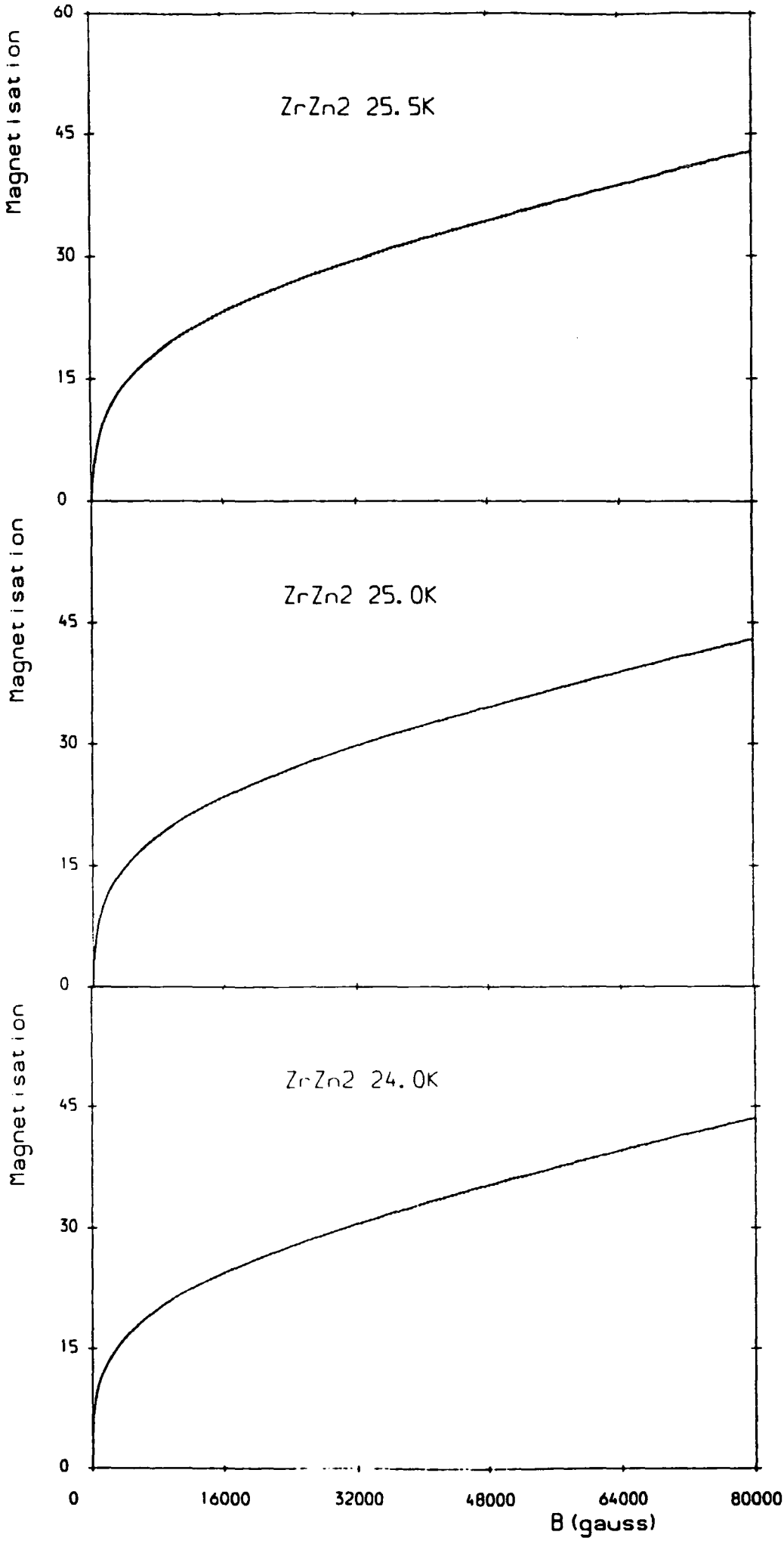
ZrZn2 25.5K
ZrZn2 25.0K
ZrZn2 24.0K
Magnetisation
60
45
30
15
0
0
16000
32000
48000
64000
80000
B (gauss)

Figure 4.5 (d) - (f)

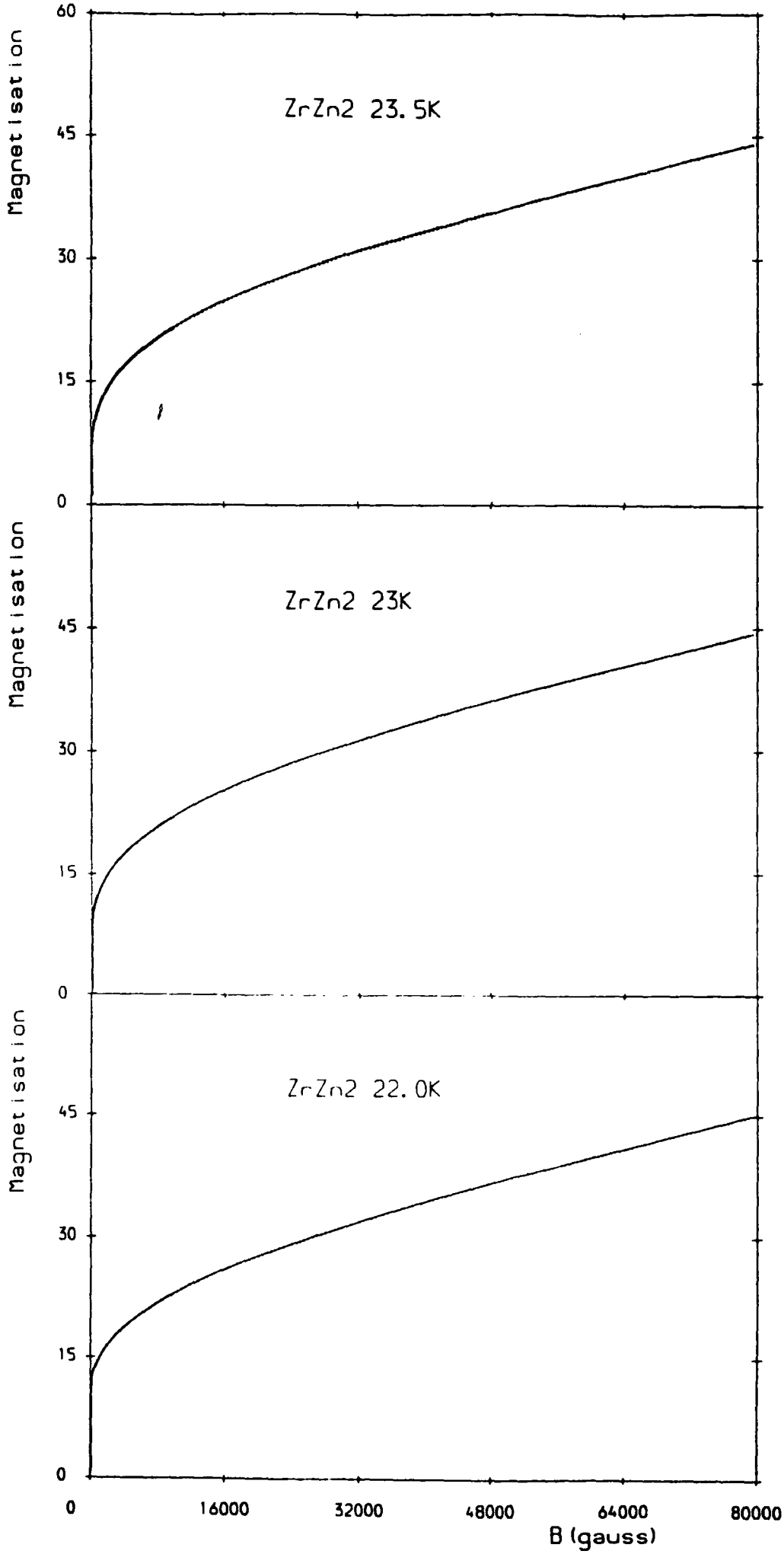
ZrZn2 23.5K
ZrZn2 23K
ZrZn2 22.0K
Magnetisation
60
45
30
15
0
0
16000
32000
48000
64000
80000
B (gauss)

Figure 4.5 (g) - (i)

Figure 4.6 Arrot Plots for $ZrZn_2$ derived from the data of figure 4.5. A solid line connects the raw data points. (a) 26.0K; (b) 25.0K; (c) 24.0K; (d) 23.5K; (e) 23.0K; (f) 22.0K.

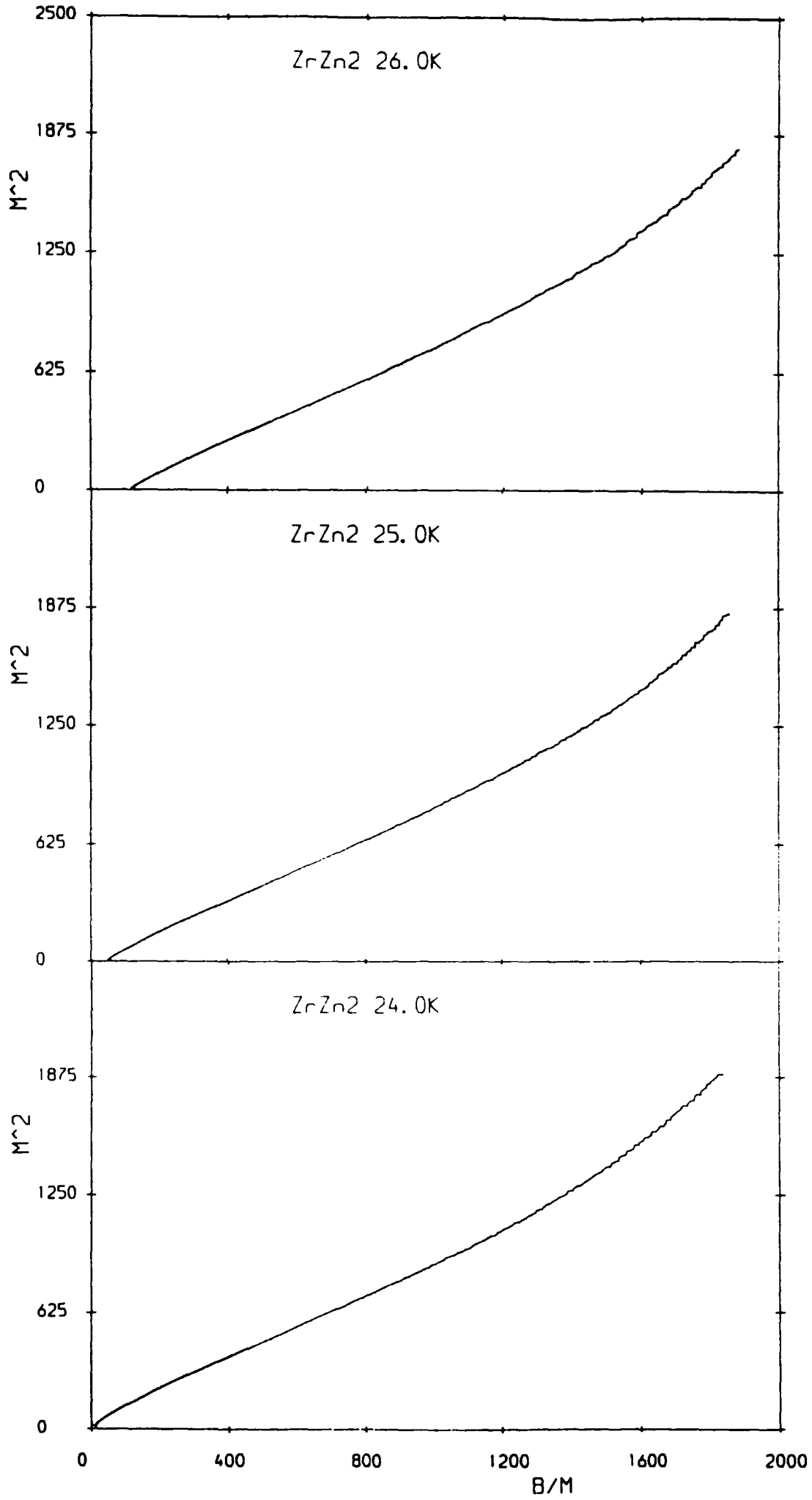
ZrZn2 26.0K
ZrZn2 25.0K
ZrZn2 24.0K
M^2
2500
1875
1250
625
0
0
400
800
1200
1600
2000
B/M

Figure 4.6 (a) - (c)

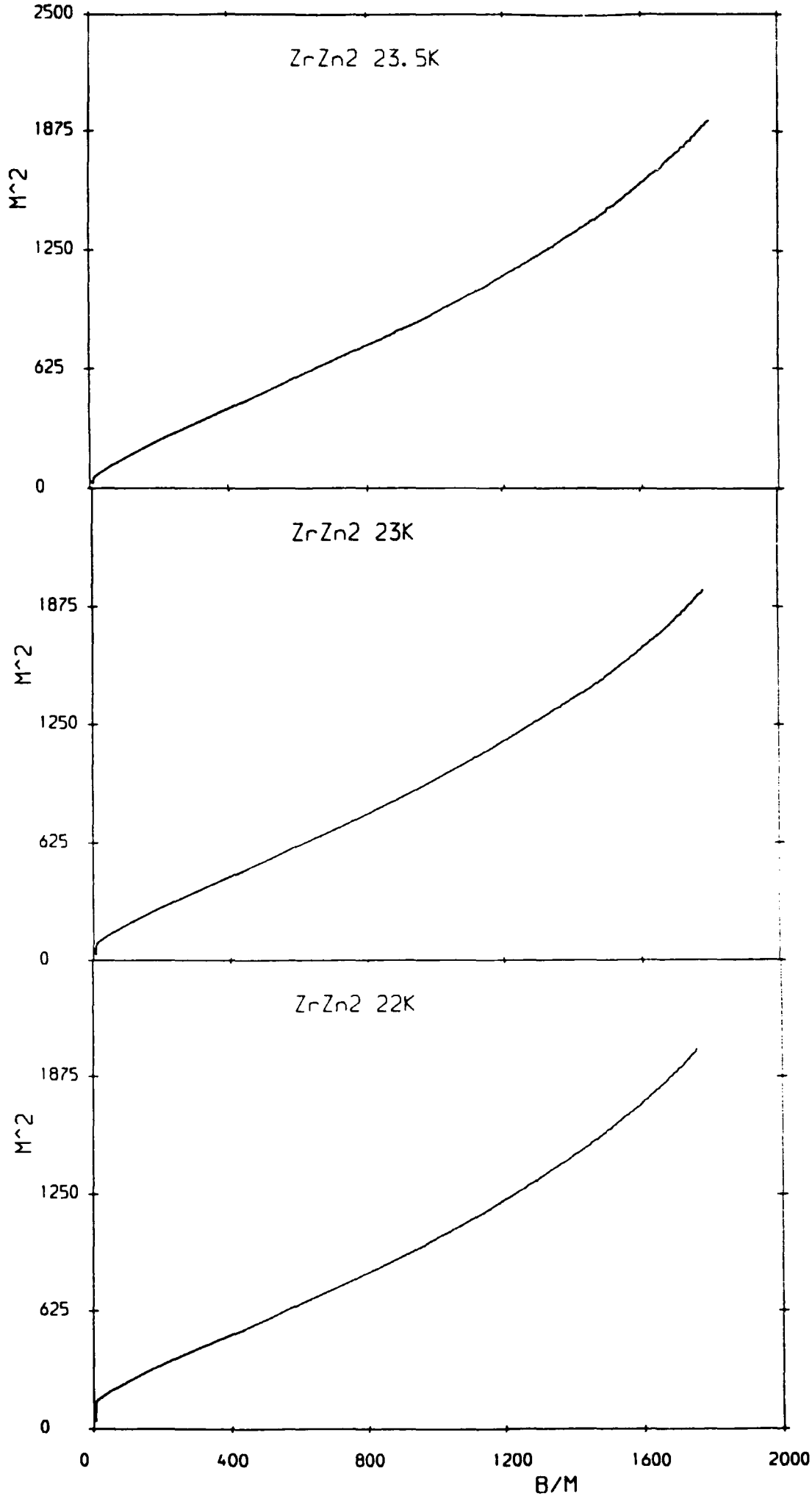
ZrZn2 23.5K
ZrZn2 23K
ZrZn2 22K
M^2
2500
1875
1250
625
0
400
800
1200
1600
2000
B/M

Figure 4.6 (d) - (f)

fields in excess of 1.8kOe, the magnetisation increases approximately linearly as the temperature is lowered, demonstrated in figure 4.7(f). The magnetisation remains linear with temperature as the field is increased up to 8kOe although the gradient of this line gradually reduces with increasing field. This is summarised in figure 4.8 where the rate of change of magnetisation with temperature, in a fixed magnetic field is plotted against the field. The rate of change of magnetisation was calculated by curve fitting to the data (note that in fields greater than 1.4kOe the fit was a straight line). From this it is evident that there is only a dramatic increase in magnetisation as the transition temperature is approached in applied magnetic fields less then 8kOe and that this reduces as the field is increased. In fields in excess of 10kOe, the increase remains approximately constant, reducing only slightly by a magnetic field of 80kOe.

In figure 4.7 the applied magnetic field has been called B and given units of gauss.

Figure 4.7 Magnetisation of $ZrZn_2$ as a function of temperature close to the transition temperature. (a) 150Oe; (b) 300Oe; (c) 400Oe; (d) 800Oe; (e) 1kOe; (f) 1.8kOe; (g) 5kOe; (h) 8kOe; (i) 10kOe; (j) 24kOe; (k) 40kOe; (l) 50kOe; (m) 60kOe; (n) 80kOe.

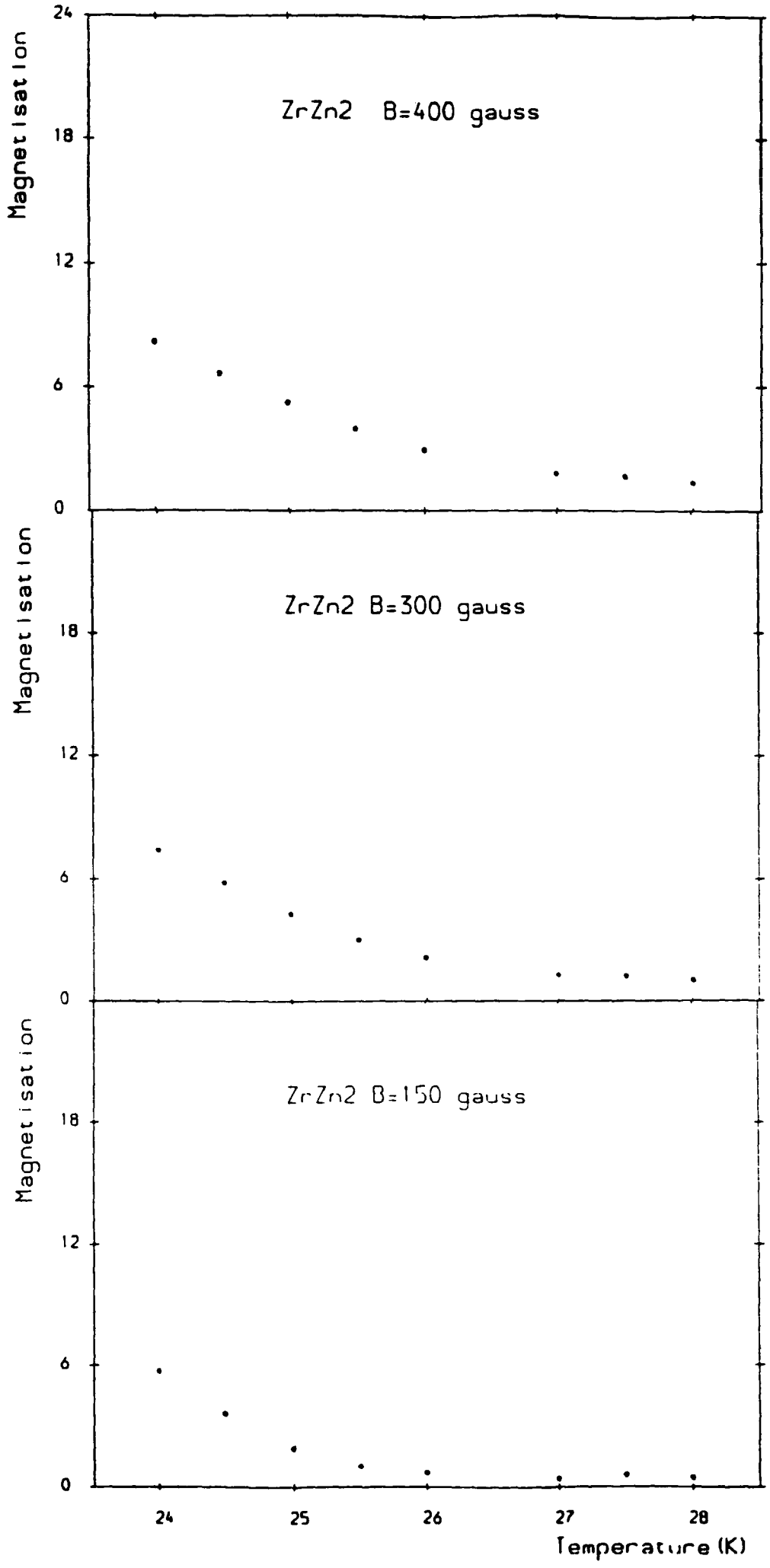
ZrZn2 B=400 gauss
ZrZn2 B=300 gauss
ZrZn2 B=150 gauss
Magnetisation
24
18
12
6
0
24
25
26
27
28
Temperature (K)

Figure 4.7 (a) - (c)

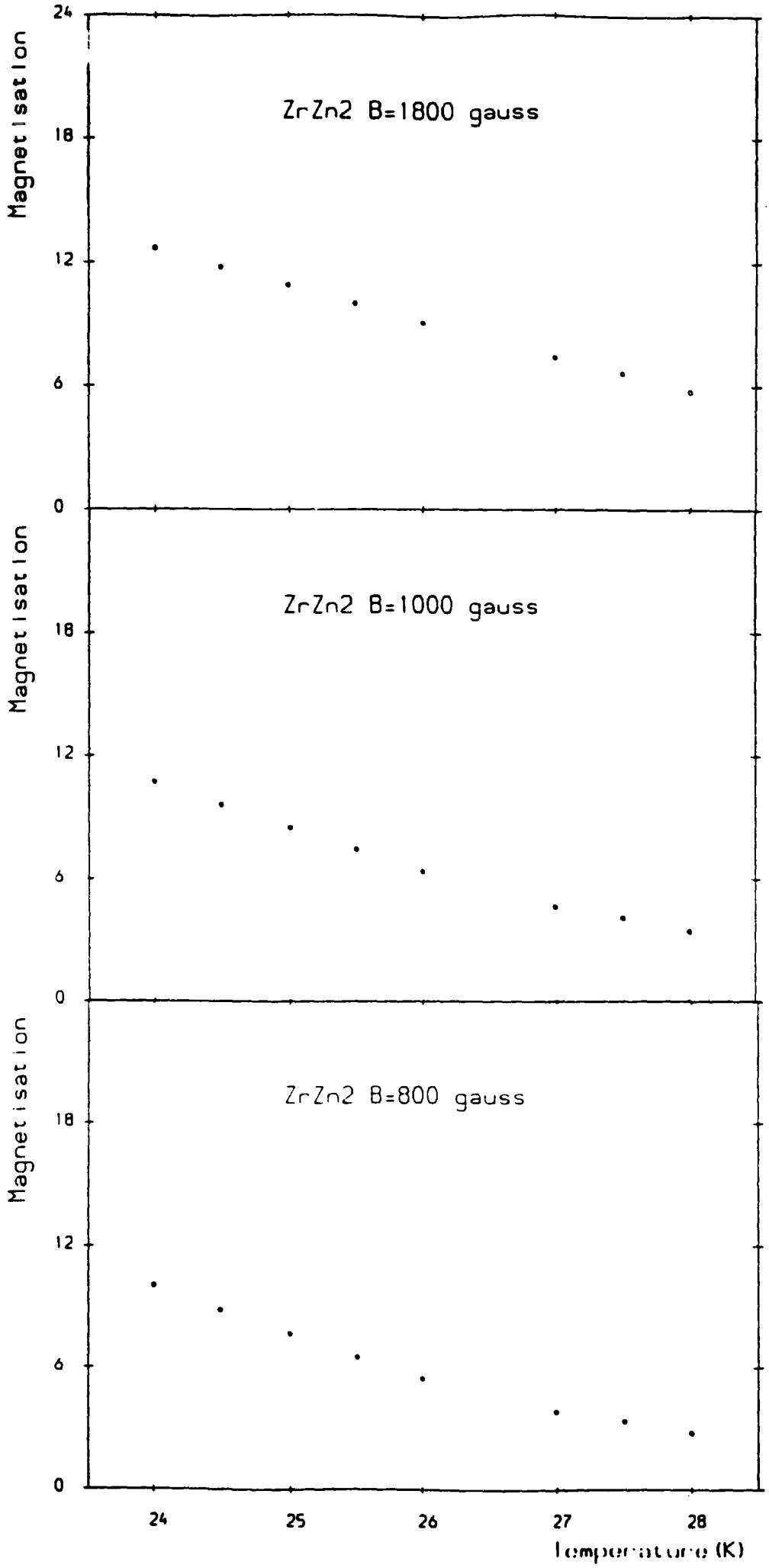
ZrZn2 B=1800 gauss
ZrZn2 B=1000 gauss
ZrZn2 B=800 gauss
Magnetisation
24
18
12
6
0
24
25
26
27
28
Temperature (K)

Figure 4.7 (d) - (f)

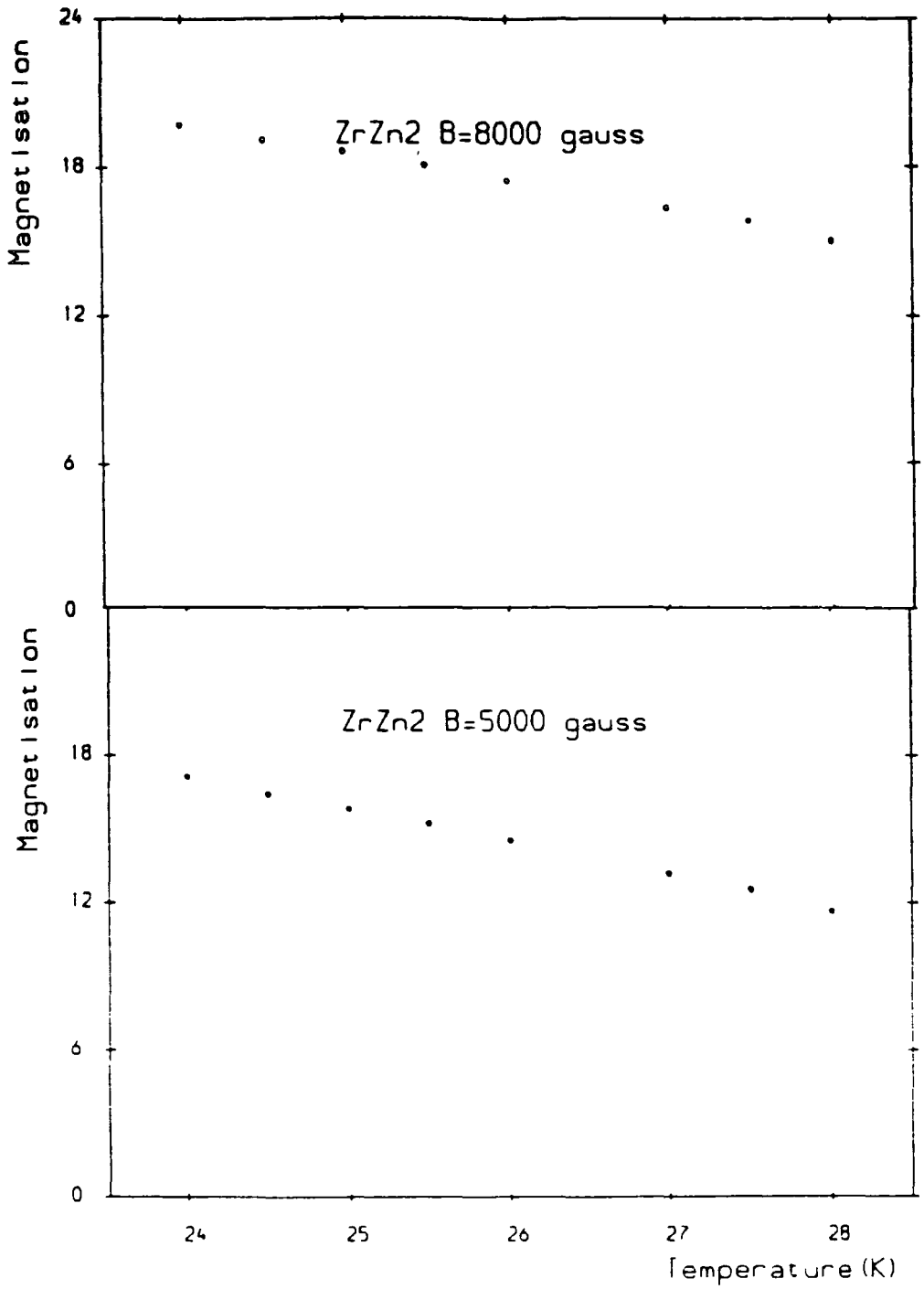

Figure 4.7 (g) and (h)

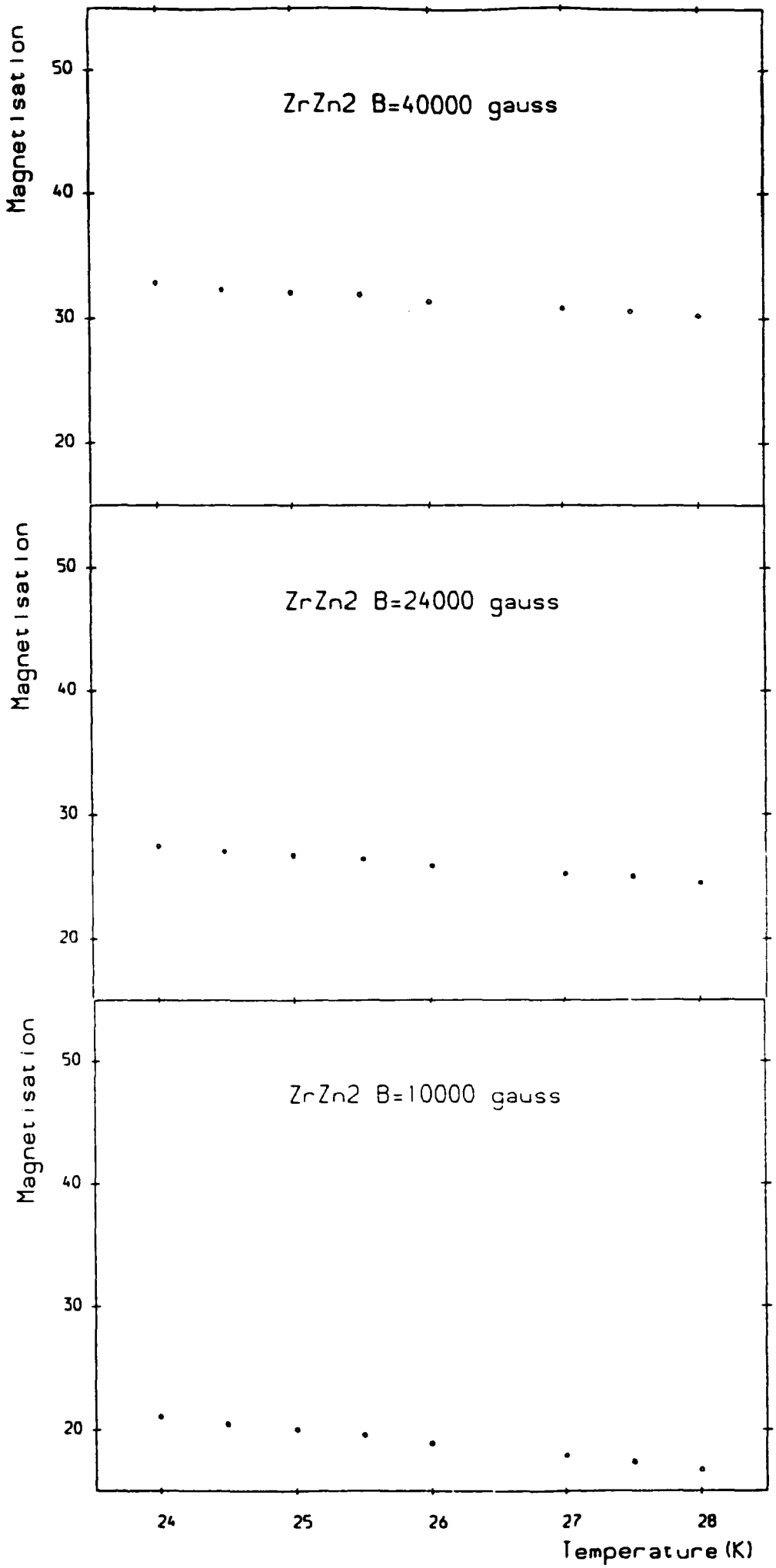
ZrZn2 B=40000 gauss
ZrZn2 B=24000 gauss
ZrZn2 B=10000 gauss
Magnetisation
50
40
30
20
24
25
26
27
28
Temperature (K)

Figure 4.7 (i) - (k)

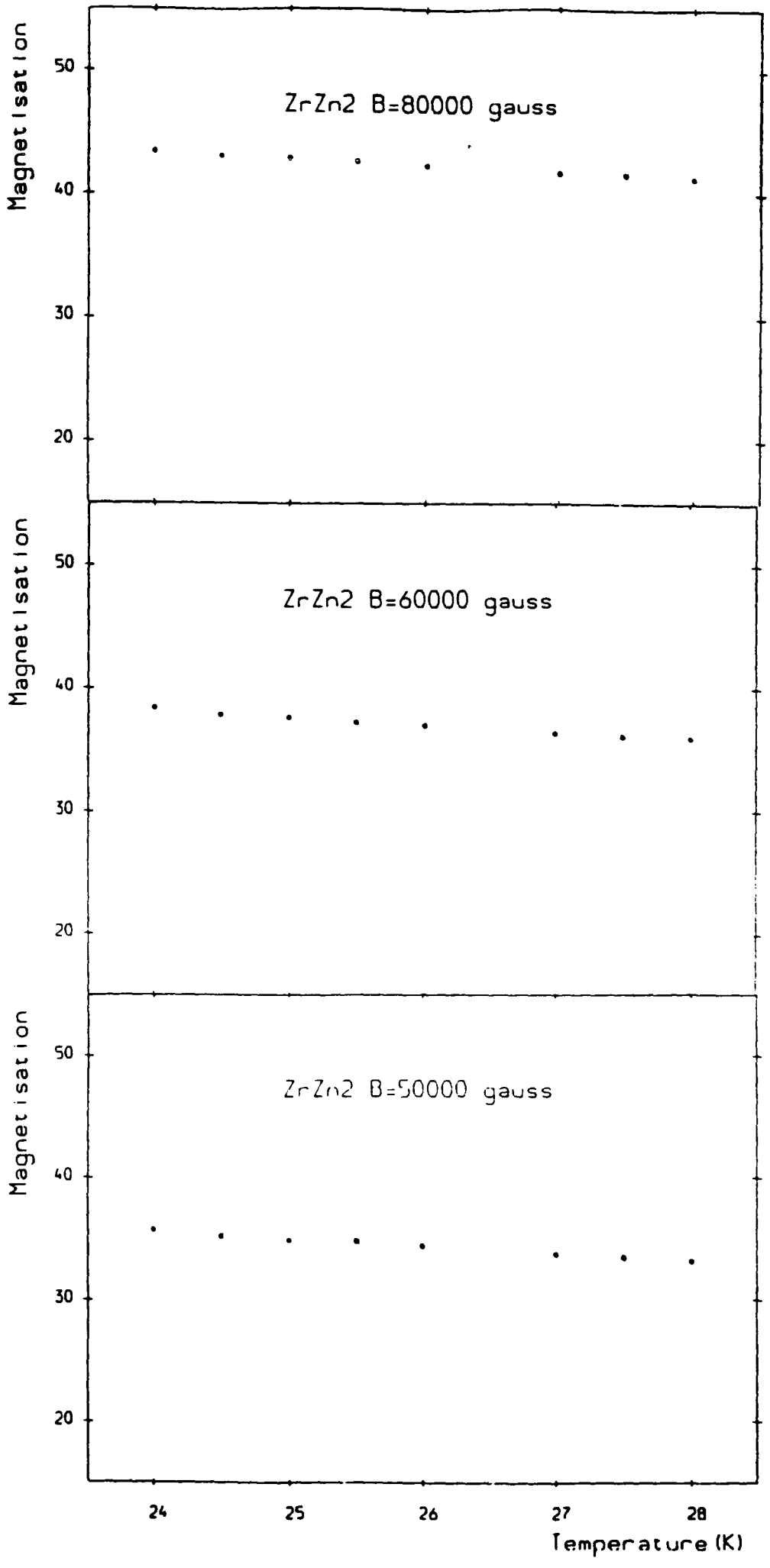
Magnetisation
ZrZn2 B=80000 gauss
Magnetisation
ZrZn2 B=60000 gauss
Magnetisation
ZrZn2 B=50000 gauss
50
40
30
20
24
25
26
27
28
Temperature (K)

Figure 4.7 (l) - (n)

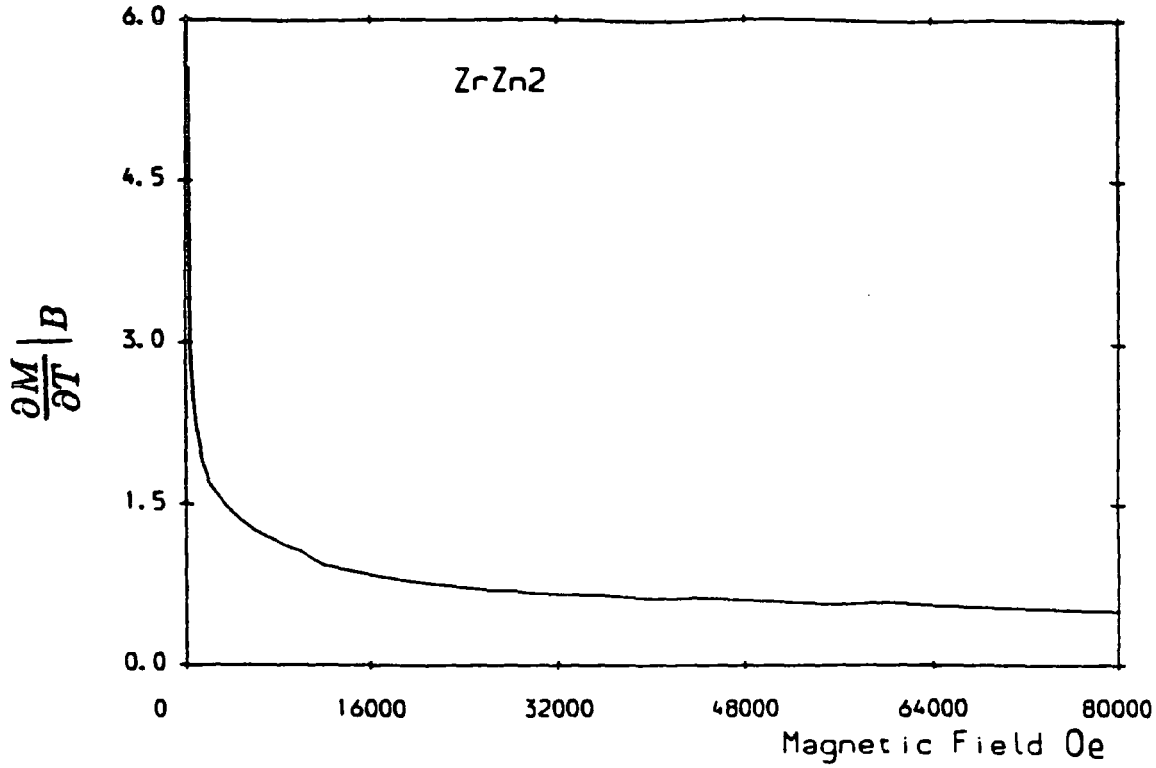

Figure 4.8 $\frac{\partial M}{\partial T}|_B$ vs magnetic field from the data of figure 4.7 and other similar measurements close to the transition temperature. A solid line connects the data points.

4.6 References

Blythe H.J.(1966), Phys. Letts **21**, 144.
Brown P.J. *et al.*(1984), J. Magn. Magn. Mat. **42**,12.
Crangle J.(1991) *'Solid State Magnetism'*, Publ. E. Arnold ISBN 0-340-54552-6
Foner S. *et al.*(1968), J. Appl. Phys. **39**, .
Hayden S.M. *et al.*(1990), Physica B, **165-166**,201.
Knapp G.S.(1971), J. Appl. Phys. **42**,1341.
Law S.A.(1988), Ph.D. Thesis, University of Cambridge.
Lonzarich G.G. and Taillefer L.(1985), J. Phys. **C18**,4339.
Matthias B.T. and Bozorth R.M.(1958), Phys. Rev. **109**,604.
Mattocks P.G. and Melville D.(1978), J. Phys. F.:Metal Phys, **8**,1291.
Smith T.F. *et al.*(1971), Phys. Rev. Lett. **27**,1732.
Van Deursen A.P.J. *et al.*(1986), J. Magn. Magn. Mat. **54-57**,1113.
Wayne R.C. and Edward L.R.(1969), Phys. Rev. **188**,1042.
Wohlfarth E.P.(1968), J. Appl. Phys. **39**,1061.
Wohlfarth E.P. and Bartel L.C.(1971), Phys. Letts. **34A**,303.

Chapter 5

Magnetic Measurements on Manganese Silicide (MnSi)

5.1 The Sample of Manganese Silicide

Observation of the intrinsic behaviour of highly correlated systems including MnSi close to the magnetic phase transition places extremely stringent requirements on sample purity and homogeneity. The single crystal used for these measurements was prepared to a high standard of purity by Simon Brown at the Cavendish Laboratory, Cambridge. It was grown by the Czochralski Technique under ultra high vacuum (Brown (1990)) to ensure an extremely clean enviroment. The sample used was a 2.5mm diameter, 0.7mm thick disk, spark machined from a larger single crystal with a mass of 22.9mg.

Preliminary characterisation was made by X-ray crystallography. The electrical residual resistance ratio ($\frac{\rho 293K}{\rho 4.2K}$) was measured to be 200. The samples have been used in other experiments, for example Fermi surface studies by the de Haas-van Alphen method (Brown (1990)).

The disc was cut in a $(1\bar{1}0)$ plane. In order to measure the magnetisation of the sample in the two crystallographic directions $< 111 >$ and $< 001 >$ the crystal was rotated about the $[1\bar{1}0]$ axis, maintaining the demagnetisation factor approximately constant. When measuring the magnetisation in the $< 110 >$ direction, the crystal was orientated with the $(1\bar{1}0)$ plane perpendicular to the applied field thus changing the demagnetisation factor.

The magnetic measurements were made taking field increments of 50Oe. The points plotted on the graphs are the raw data and the solid line drawn through them is the average for increasing and decreasing field measurements.

5.2 Magnetisation Study of MnSi close to its Critical Temperature

The inverse susceptibilities in the < 001 > and < 111 > major crystal symmetry directions are shown in figure 5.1. The most striking observations are the directional anisotropy of the response, extreme non-linearity and the narrow temperature range over which this behaviour occurs.

The magnetisation and inverse susceptibility derived from adjacent values of magnetisation and field is shown in figures 5.2(a) and 5.3(a) for a temperature of 30.0K for the two major symmetry directions. The inverse susceptibility exhibits a smooth, concave-upward response in both directions showing the magnetisation to be isotropic above the transition temperature.

In the interval $29.0 \pm 0.2K$, over a field sweep of $\pm$ 3.3kOe, we observe the start of the non-linear response in inverse susceptibility (figures 5.2(b) and 5.3(b)) with both the directions exhibiting four distinct rounded minima. The high field turning points may be associated with an induced ferromagnetic state (Bloch (1975)); on cooling below 29.0K these turning points move out of the selected display window and are of no further interest to our discussion here.

Cooling below 28.8K and down to 27.4K we see further qualitative and quantitve changes in the magnetic response as shown in figures 5.2(c) - (e) and 5.3(c) - (e). In the < 001 > direction at 28.8K there is the onset of a pair (symmetric in positive and negative field) of three minima, a pair of low field rounded minima and two pairs of sharp discontinuities at higher fields. Continued cooling to 27.2K and below leaves only the rounded minima. In between these temperatures the critical field (where the second sharp discontinuity occurs) remains fixed, with the position of the first evolving to higher fields.

In < 111 > direction a pair of low field minima persist from 29.0 - 28.8K where a new pair of sharp minima occur and then disappear by 28.2K, leaving the inverse susceptibility with a slow, monotonic, concave field dependence. The anisotropy of the response with respect to the crystallographic direction is marked.

Consider first the magnetic response at the temperature 27.2K (figure 5.2(f) and 5.3(f)), approximately 2K below the critical temperature. In MnSi, the axis of the helix lies along the < 111 > directions (Ishikawa (1976)) below the critical temperature and from this and neutron scattering it appears the magnetic response in this direction may be due cone formation of the moments towards the field direction.

In fields above 1400Oe, the magnetisation in the two directions is very similar, even down to the values of inverse susceptibility. This suggests a similar process may be occuring in these field regions. The magnetisation in the < 001 > direction is clearly different below 1400Oe and can be divided into two regions; one with the inverse susceptibility decreasing (approximately linearly) and the second with it increasing. Numerous processes may be occuring in these regions, including domain wall motion and domain rotation, but there is evidence that these processes result in the rotation of the helix or coning system into the direction of the applied field.

In figures 5.1 - 5.3 the internal magnetic field ($H_i = H - H_D$) has been called B and given the units gauss. Magnetisation is measured in units of $emucm^{-3}$ and can be converted to units of $emug^{-1}$ using the density of MnSi which is $5.82gcm^{-3}$.

Figure 5.1 Displayed in the left hand frame is the inverse magnetic susceptibility of MnSi as measured with an applied magnetic field parallel to the < 001 > direction at temperatures close to the transition temperature. Complementary values are given in the right hand frame for the < 111 > direction. The solid line is an average through the data points for a given field value and is a measure of the experimental uncertainty.

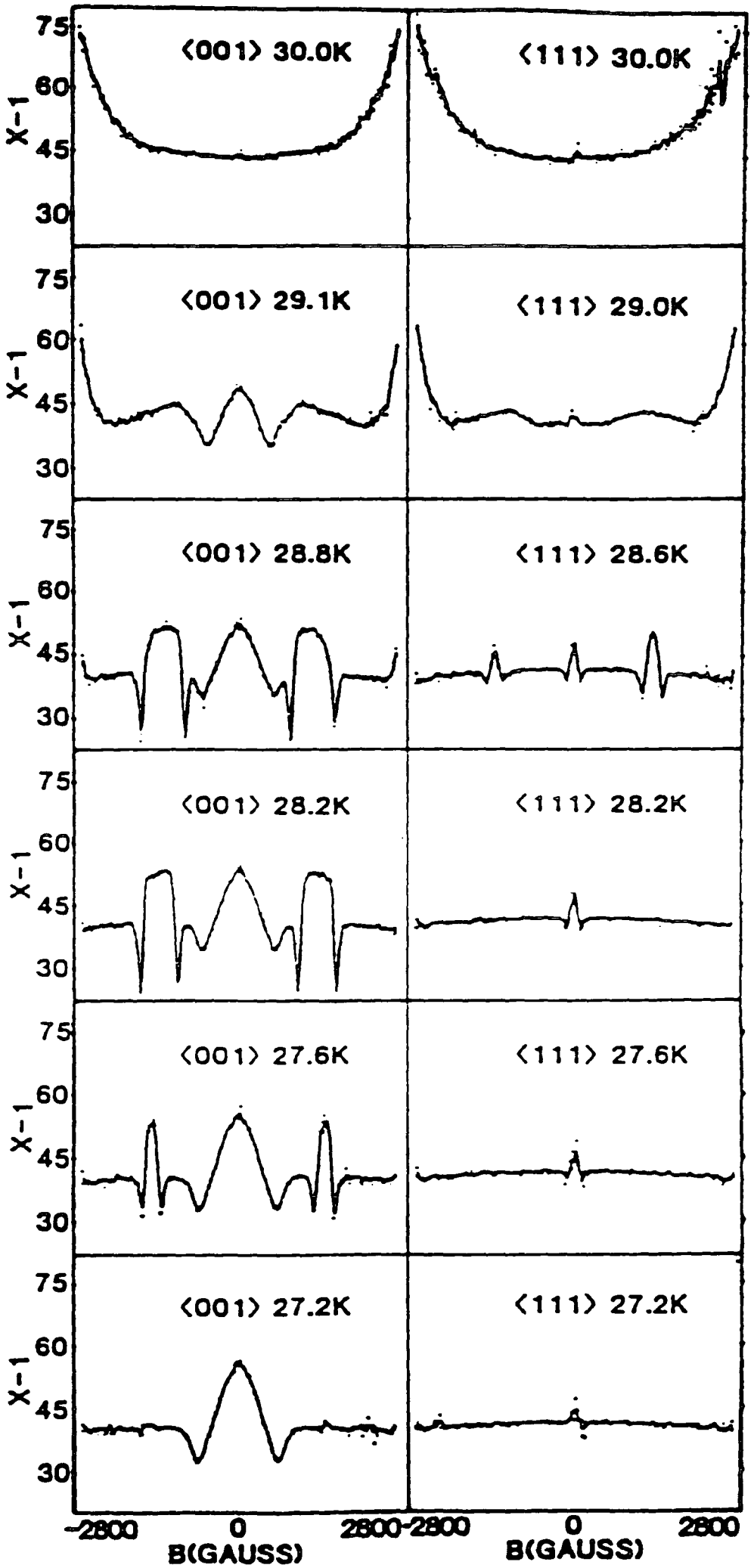
⟨001⟩ 30.0K
⟨111⟩ 30.0K
⟨001⟩ 29.1K
⟨111⟩ 29.0K
⟨001⟩ 28.8K
⟨111⟩ 28.6K
⟨001⟩ 28.2K
⟨111⟩ 28.2K
⟨001⟩ 27.6K
⟨111⟩ 27.6K
⟨001⟩ 27.2K
⟨111⟩ 27.2K
X-1
75
60
45
30
-2800
0
2800
B(GAUSS)

Figure 5.1

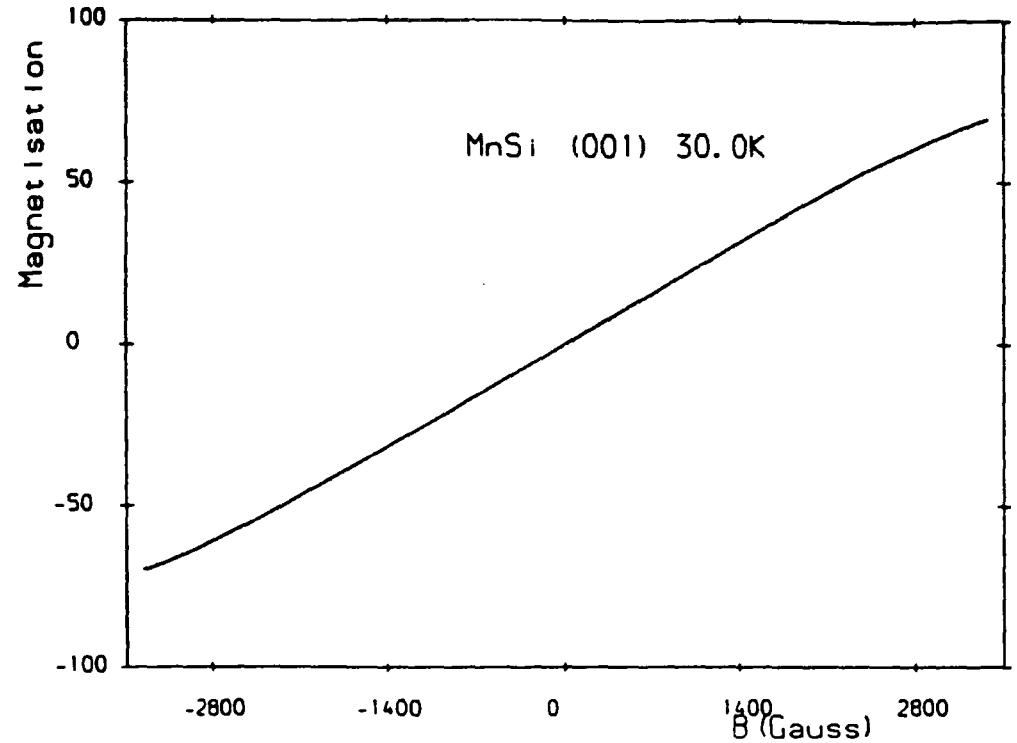
MnSi (001) 30.0K
Magnetisation
100
50
0
-50
-100
-2800
-1400
0
1400
2800
B (Gauss)

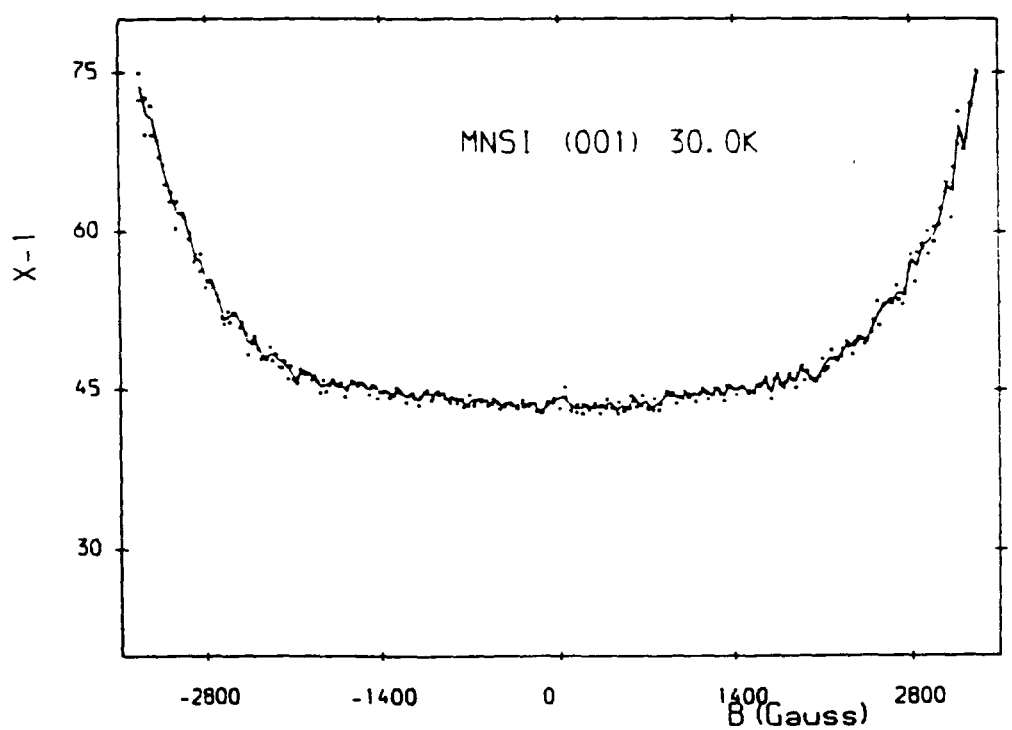
MNSI (001) 30.0K
X-1
75
60
45
30
-2800
-1400
0
1400
2800
B (Gauss)

Figure 5.2 (a)

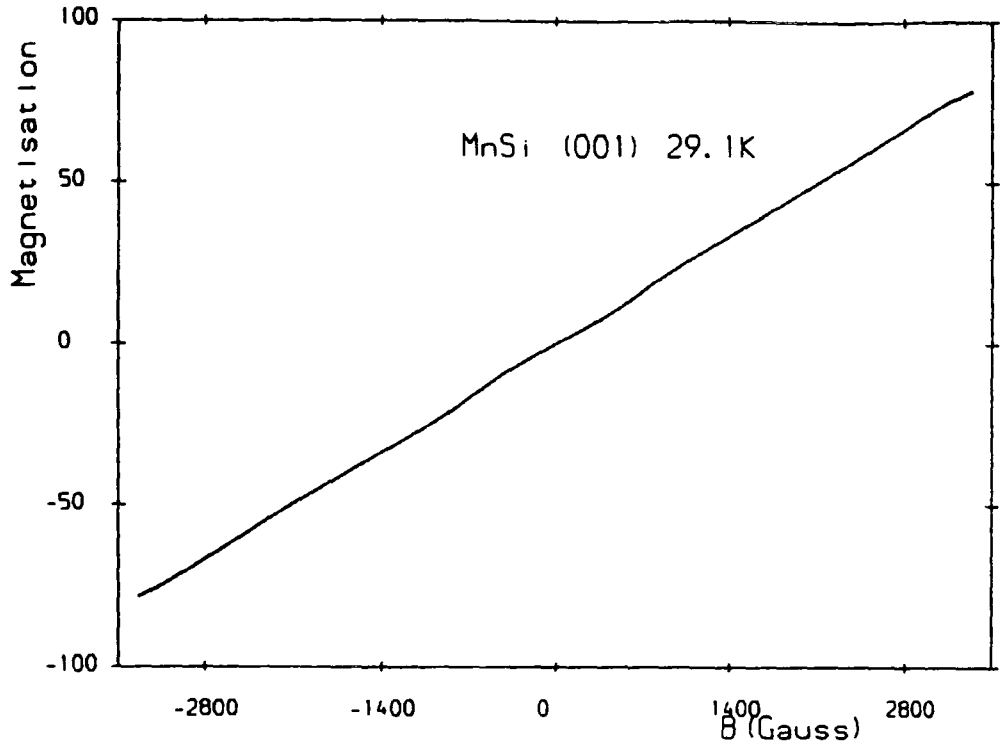
MnSi (001) 29.1K
Magnetisation
100
50
0
-50
-100
-2800
-1400
0
1400
2800
B (Gauss)

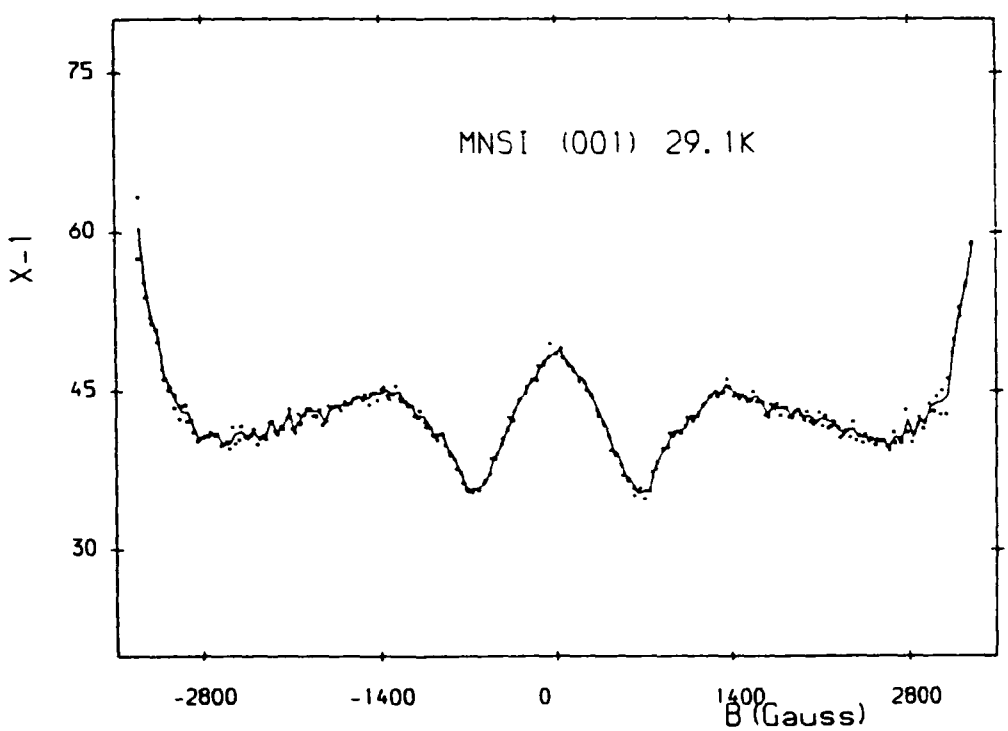
MNSI (001) 29.1K
X-1
75
60
45
30
-2800
-1400
0
1400
2800
B (Gauss)

Figure 5.2 (b)

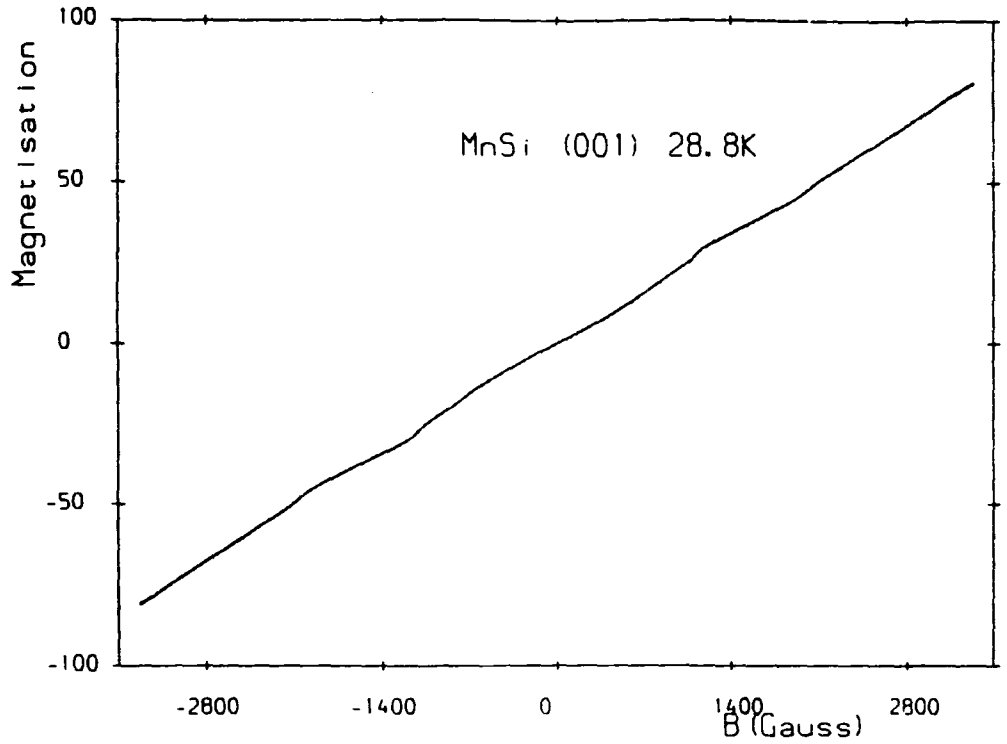
MnSi (001) 28.8K
Magnetisation
100
50
0
-50
-100
-2800
-1400
0
1400
2800
B (Gauss)

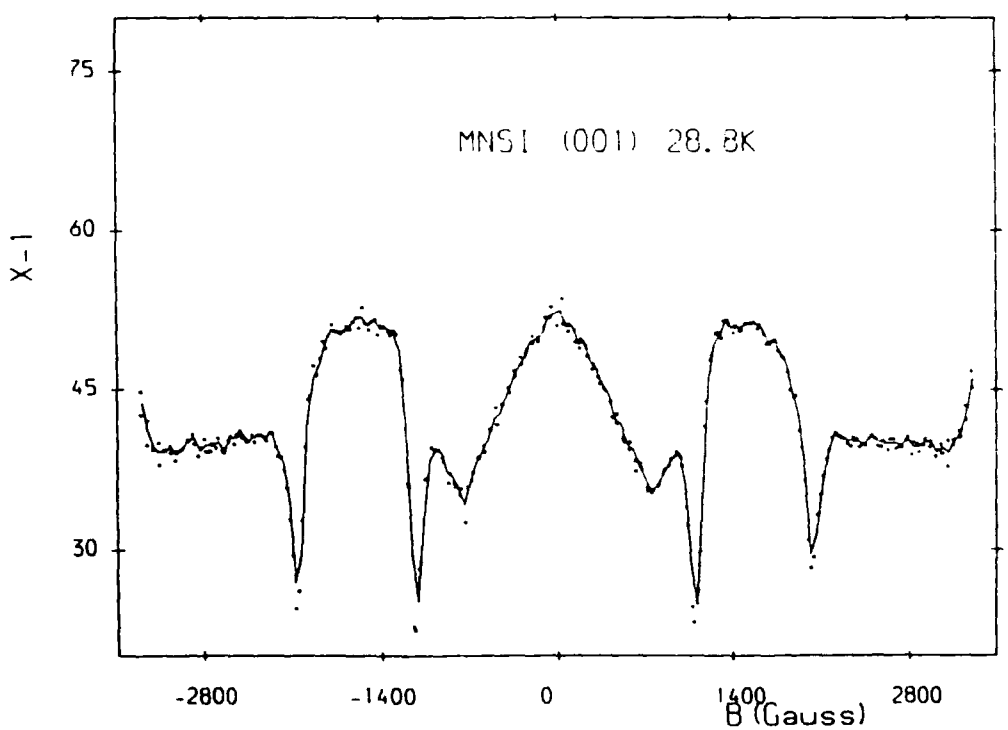
MNSI (001) 28.8K
X-1
75
60
45
30
-2800
-1400
0
1400
2800
B (Gauss)

Figure 5.2 (c)

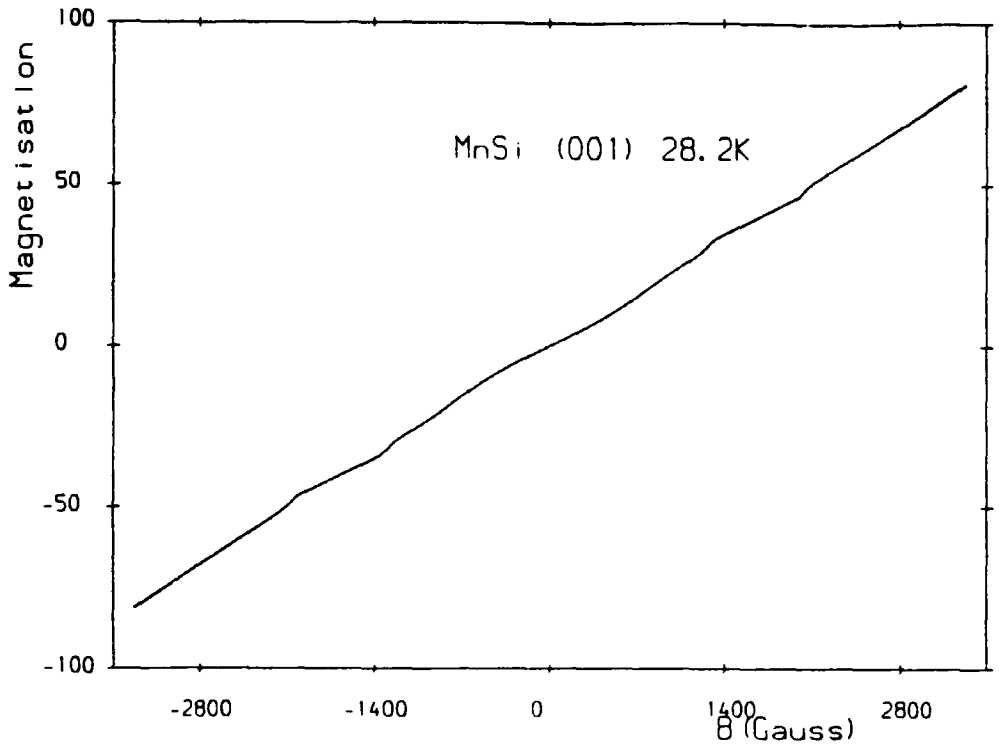
MnSi (001) 28.2K
Magnetisation
100
50
0
-50
-100
-2800
-1400
0
1400
2800
B (Gauss)

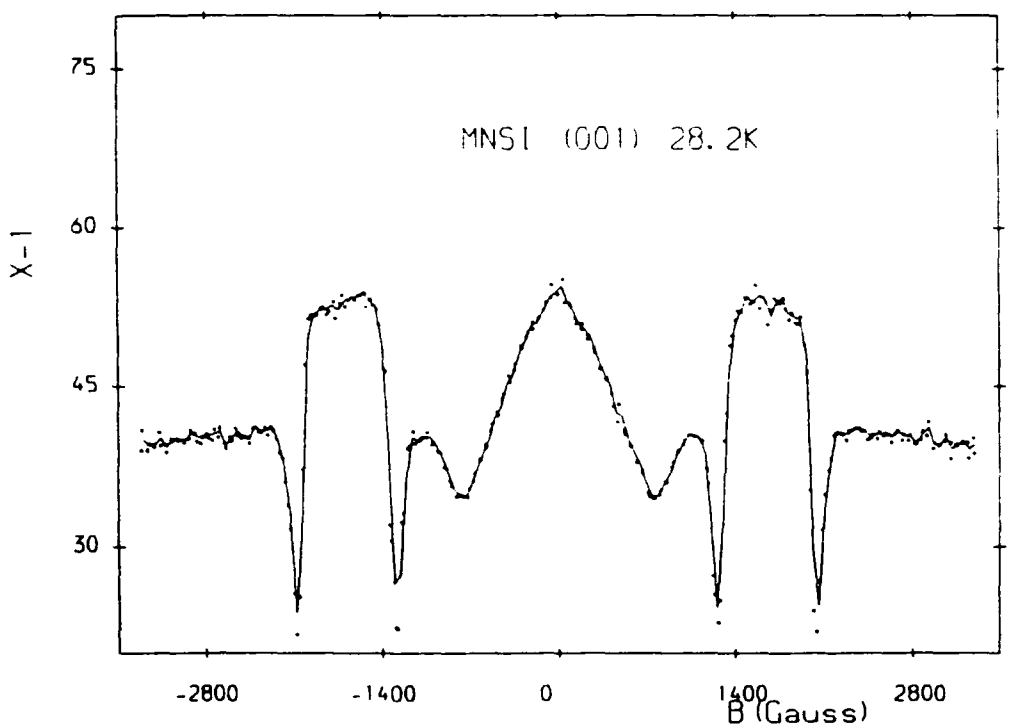
MNSI (001) 28.2K
X-1
75
60
45
30
-2800
-1400
0
1400
2800
B (Gauss)

Figure 5.2 (d)

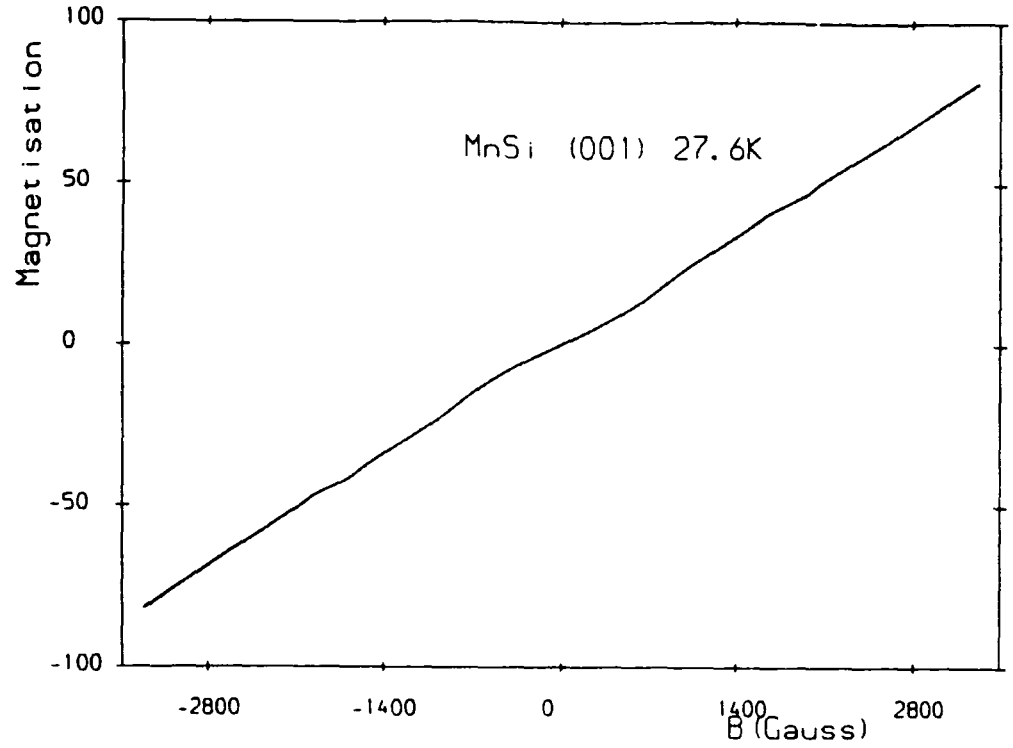
MnSi (001) 27.6K
Magnetisation
100
50
0
-50
-100
-2800
-1400
0
1400
2800
B (Gauss)

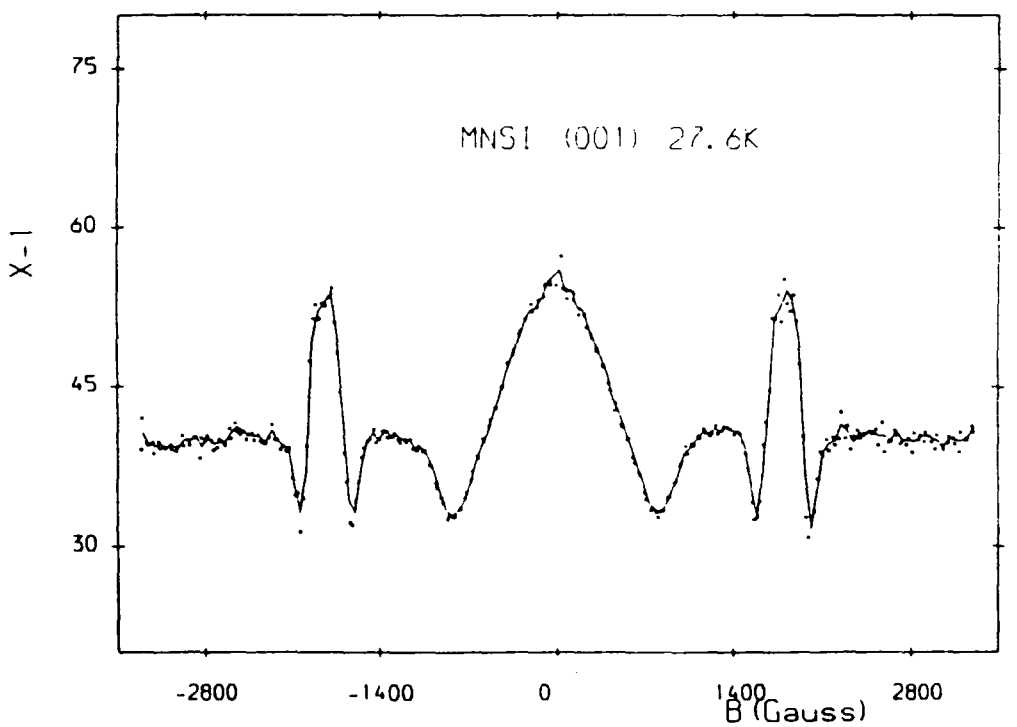
MNSI (001) 27.6K
X-1
75
60
45
30
-2800
-1400
0
1400
2800
B (Gauss)

Figure 5.2 (e)

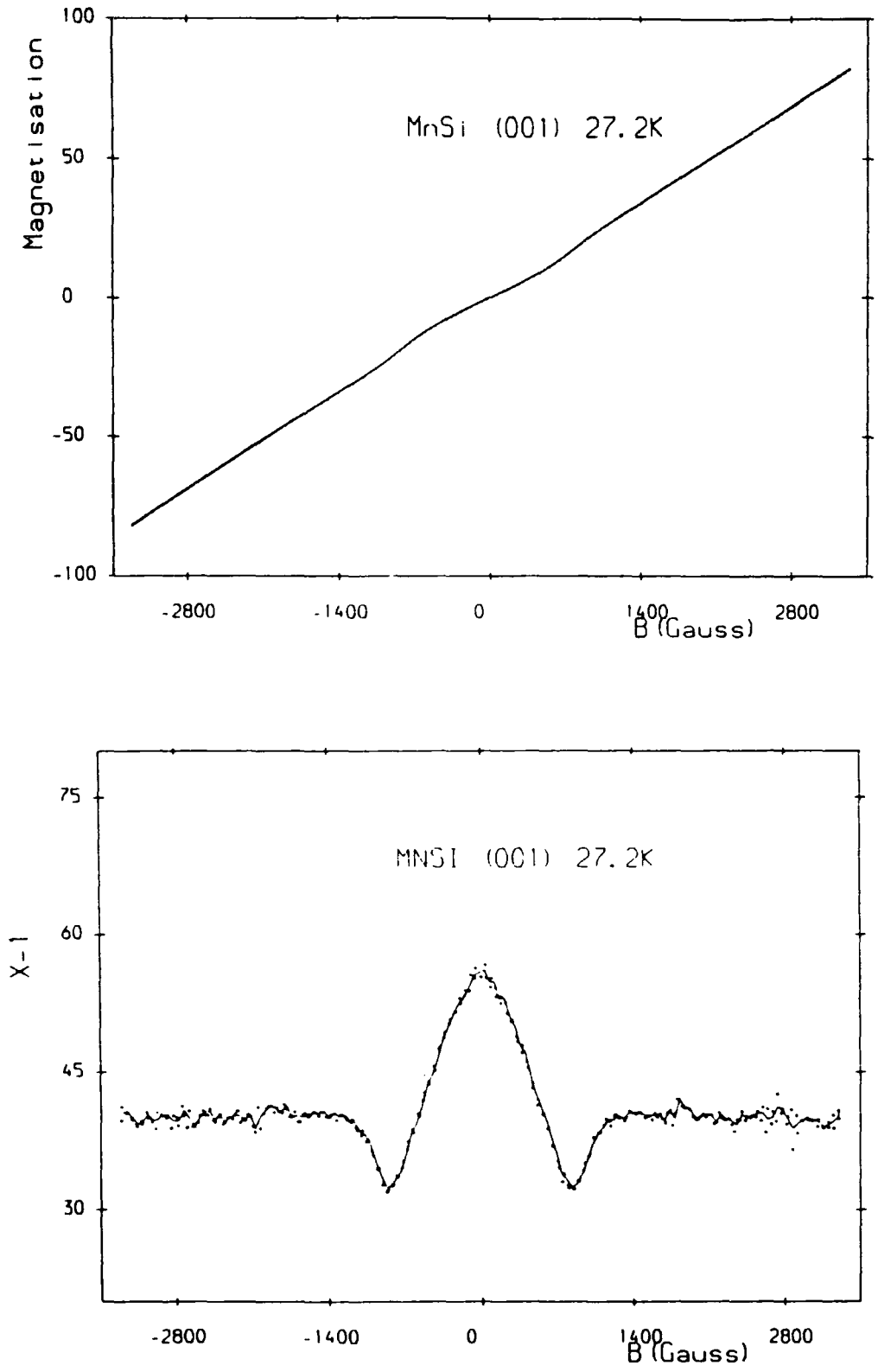

Figure 5.2 The magnetisation of MnSi with magnetic field applied parallel to the < 001 > direction together with the inverse magnetic susceptibility derived from the magnetisation data. The solid line is an average through the data points for a given field value and is a measure of the experimental uncertainty. (a) 30.0K; (b) 29.1K; (c) 28.8K; (d) 28.2K; (e) 27.6K; (f) 27.2K.

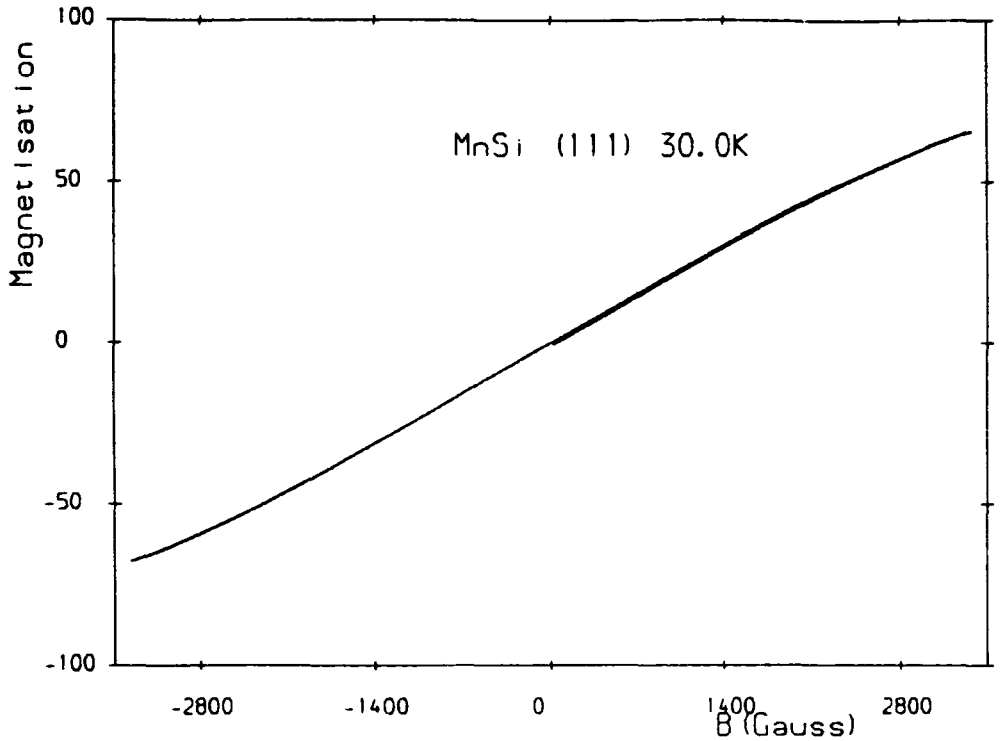
MnSi (111) 30.0K
Magnetisation
100
50
0
-50
-100
-2800
-1400
0
1400
2800
B (Gauss)

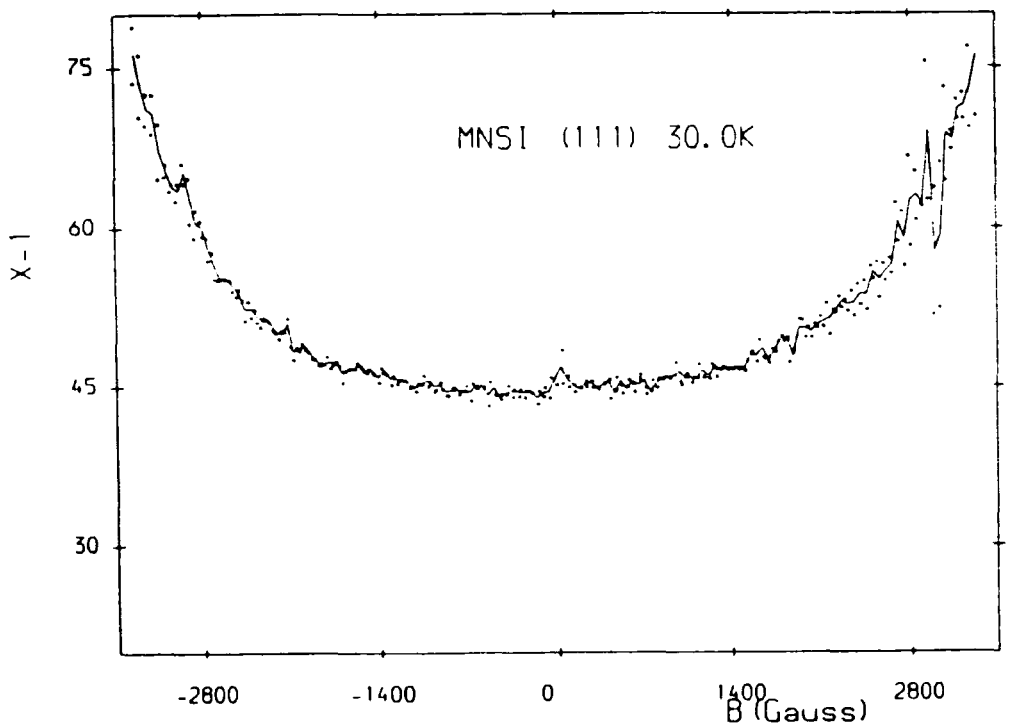
MNSI (111) 30.0K
X-1
75
60
45
30
-2800
-1400
0
1400
2800
B (Gauss)

Figure 5.3 (a)

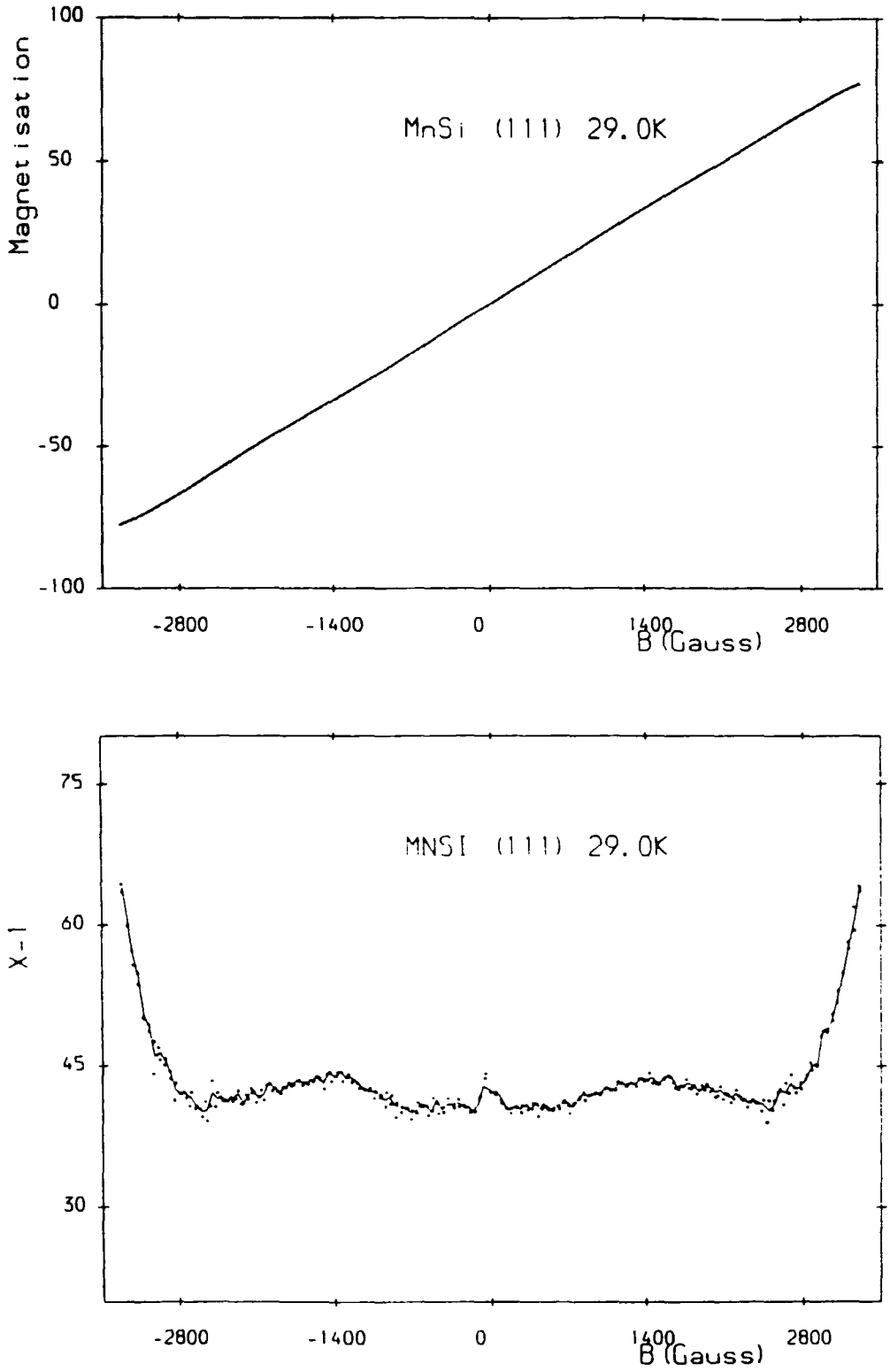
MnSi (111) 29.0K
Magnetisation
100
50
0
-50
-100
-2800
-1400
0
1400
2800
B (Gauss)
MNSI (111) 29.0K
X-1
75
60
45
30
-2800
-1400
0
1400
2800
B (Gauss)

Figure 5.3 (b)

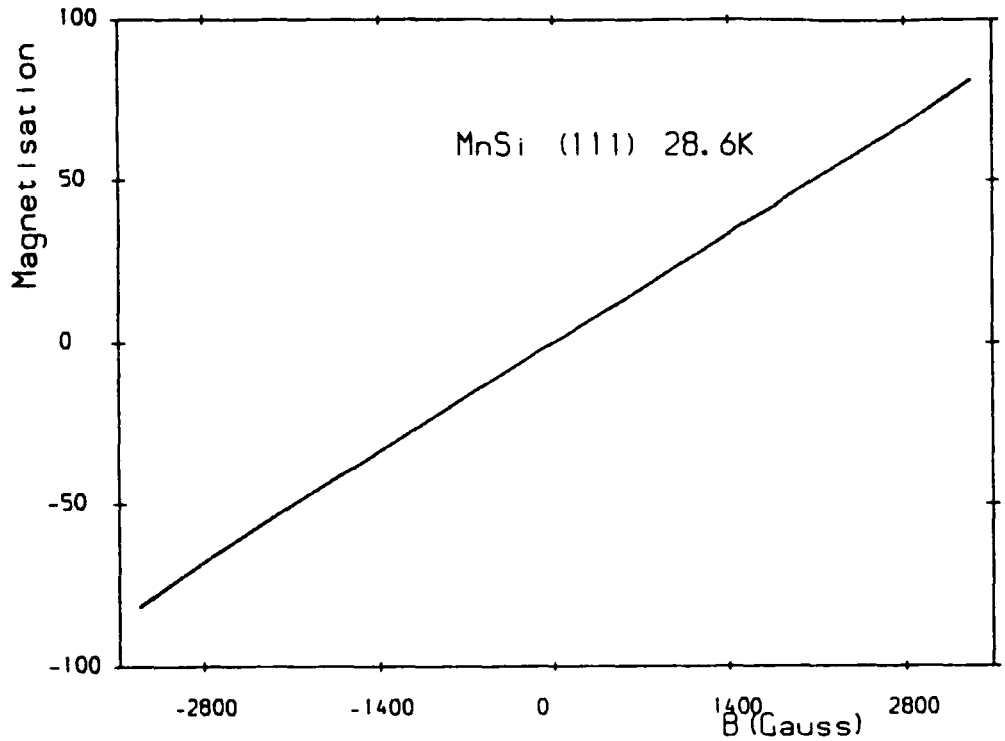
MnSi (111) 28.6K
Magnetisation
100
50
0
-50
-100
-2800
-1400
0
1400
2800
B (Gauss)

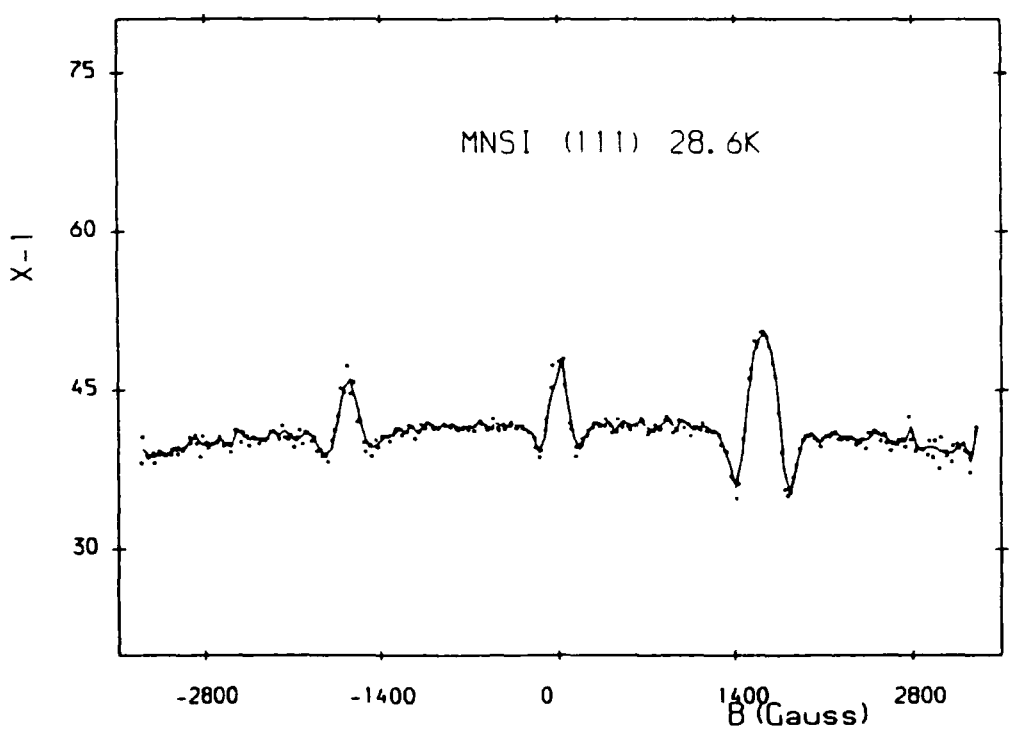
MNSI (111) 28.6K
X-1
75
60
45
30
-2800
-1400
0
1400
2800
B (Gauss)

Figure 5.3 (c)

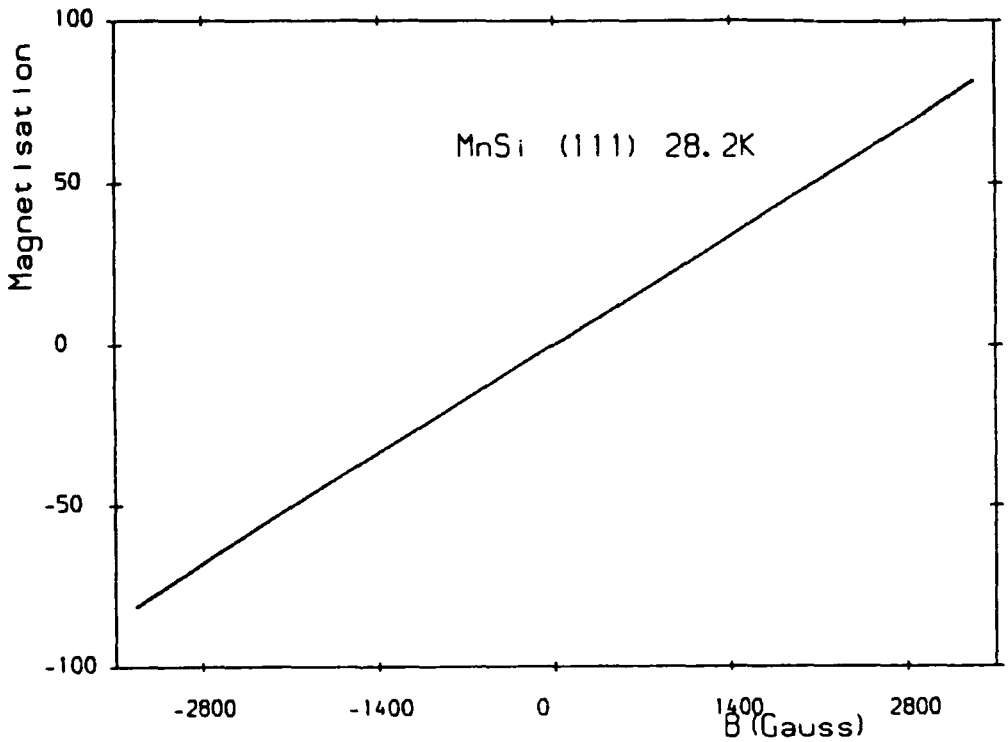
MnSi (111) 28.2K
Magnetisation
100
50
0
-50
-100
-2800
-1400
0
1400
2800
B (Gauss)

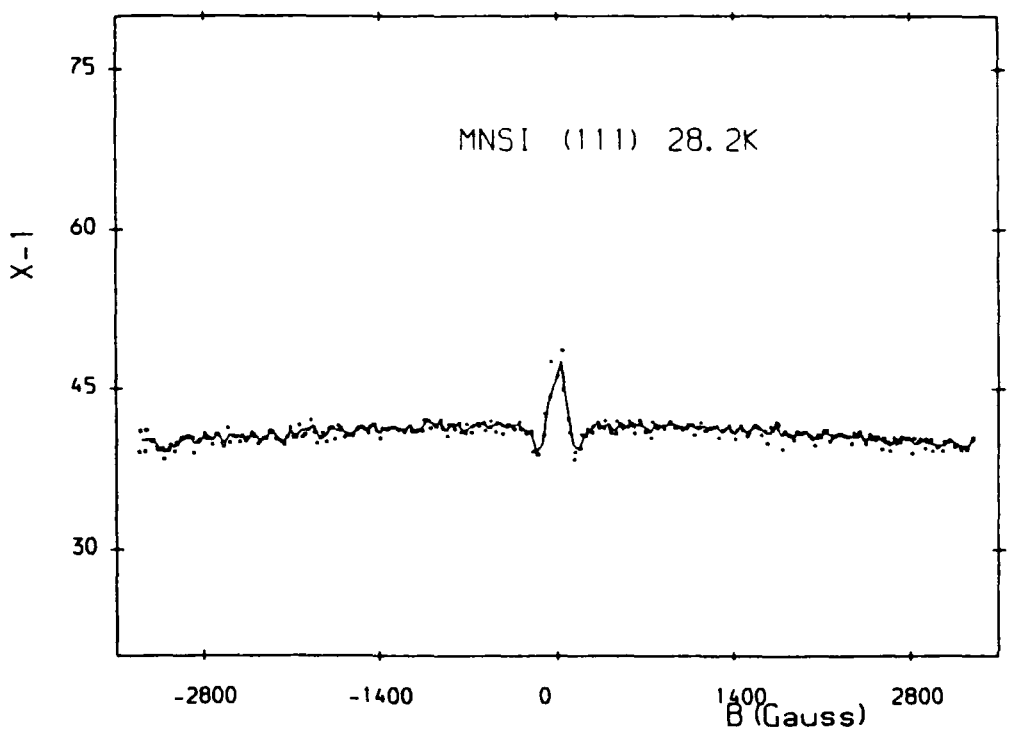
MNSI (111) 28.2K
X-1
75
60
45
30
-2800
-1400
0
1400
2800
B (Gauss)

Figure 5.3 (d)

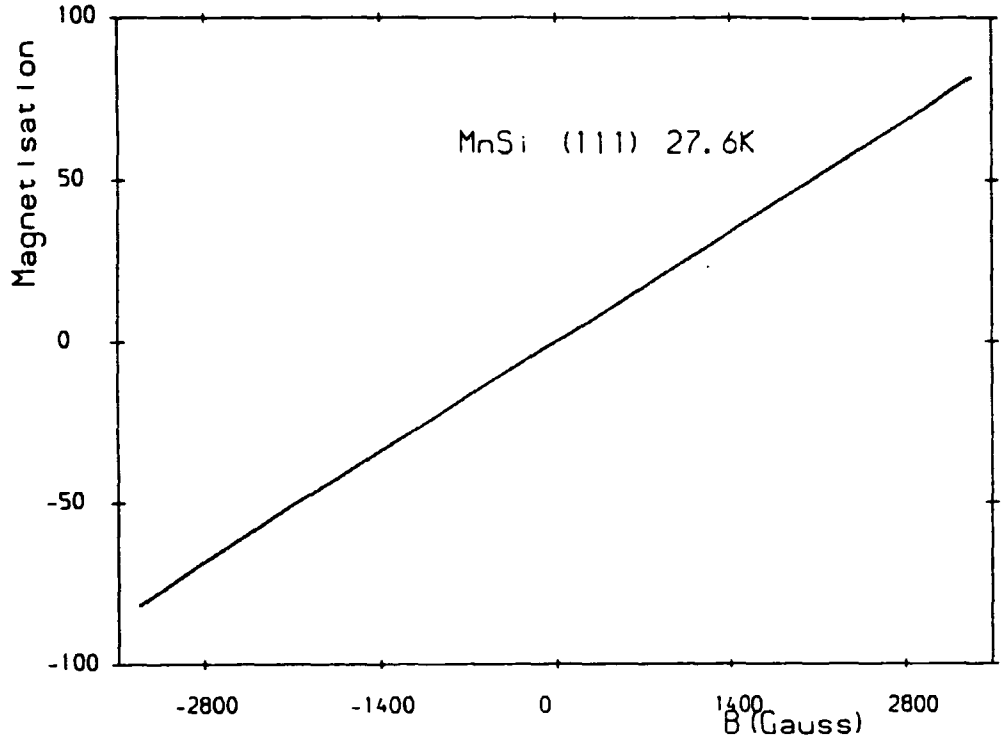
MnSi (111) 27.6K
Magnetisation
100
50
0
-50
-100
-2800
-1400
0
1400
2800
B (Gauss)

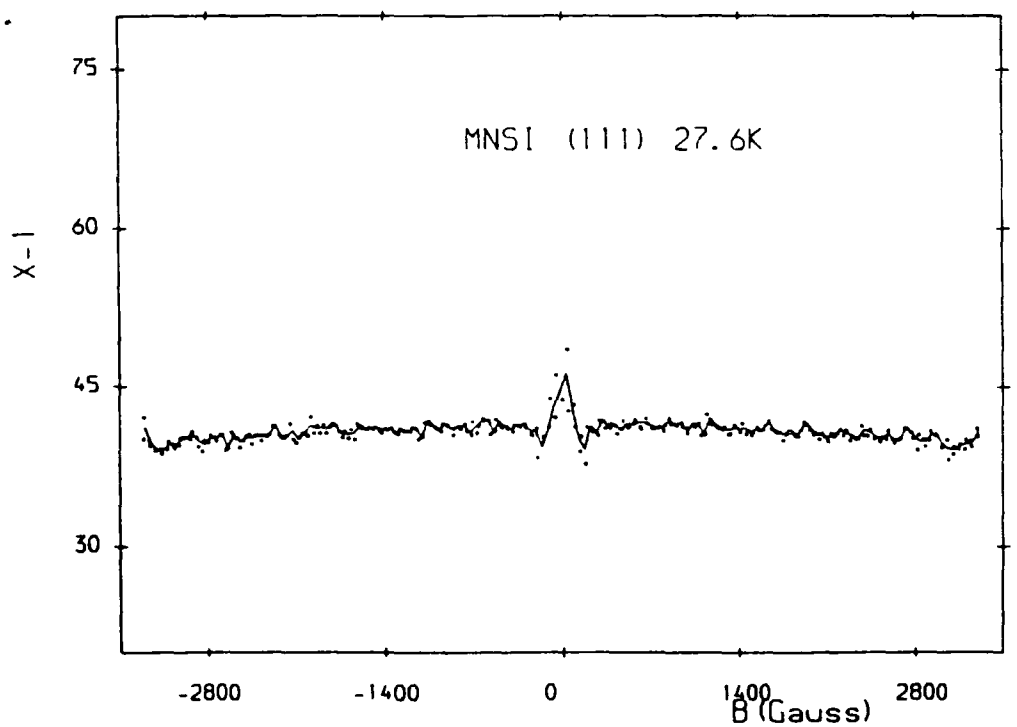
MNSI (111) 27.6K
X-1
75
60
45
30
-2800
-1400
0
1400
2800
B (Gauss)

Figure 5.3 (e)

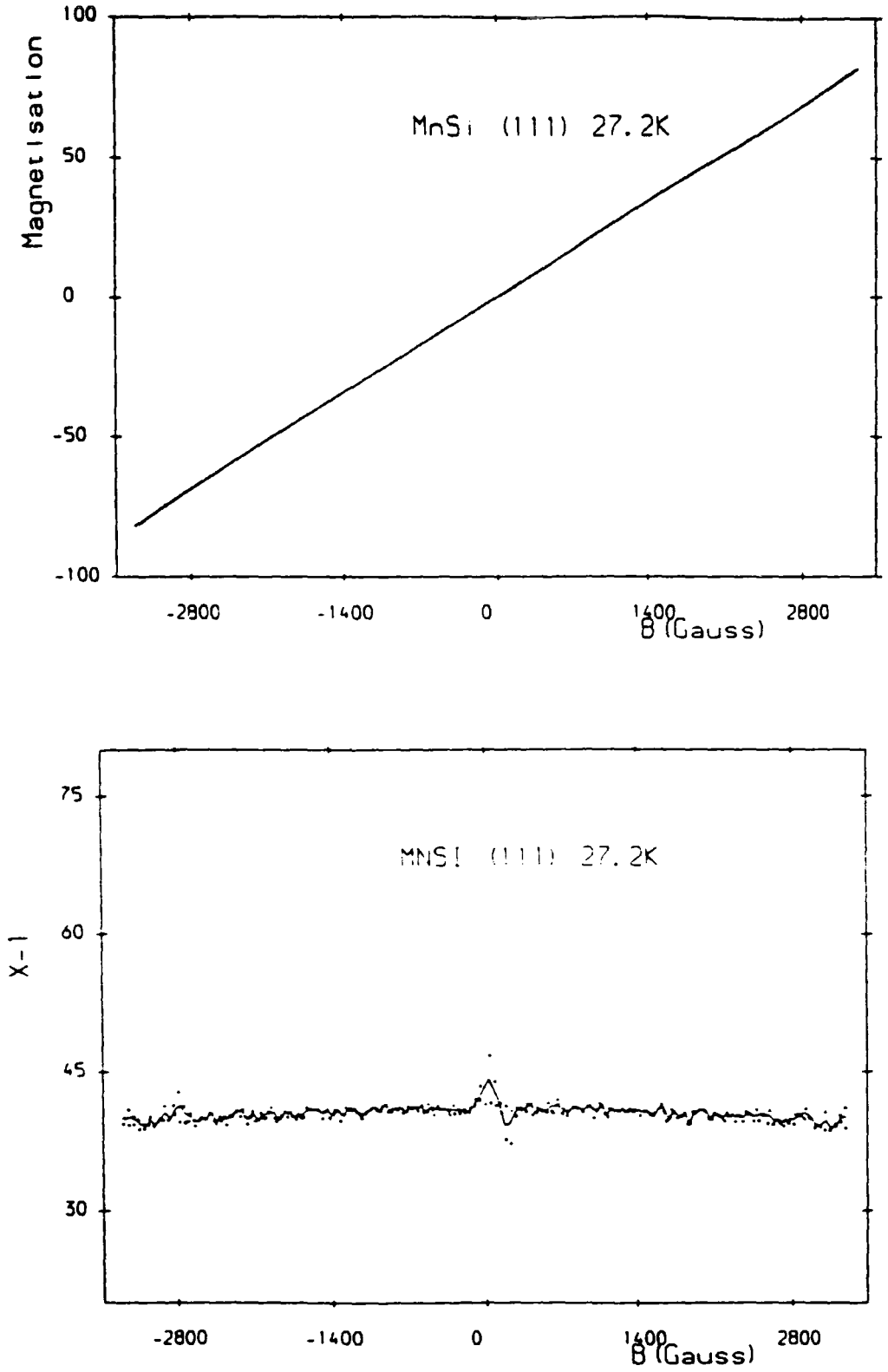

Figure 5.3 The magnetisation of MnSi with magnetic field applied parallel to the < 111 > direction together with the inverse magnetic susceptibility derived from the magnetisation data. The solid line is an average through the data points for a given field value and is a measure of the experimental uncertainty. (a) 30.0K; (b) 29.0K; (c) 28.6K; (d) 28.2K; (e) 27.6K; (f) 27.2K.

Let us now consider the magnetisation around 29.0K close to the critical temperature (figures 5.2(b) and 5.3(b)). The inverse susceptibility is very different to that observed 2K below this and there is a great deal of curvature to it. This response may be isotropic as similar behaviour is observed in the inverse susceptibility along the < 110 > direction. The temperature difference of 0.1K between the data sets is significant. It is suggested that this magnetic behaviour may indicate a new phase or commencement of the helical phase and raises the question of how the critical temperature should be defined.

In the temperature range 28.8 - 27.6K (figures 5.2(c) - (e) and 5.3(c) - (e)) we regard the sharp discontinuity in the inverse susceptibility observed in the < 001 > direction as a phase transition and believe it to be the 'Phase A' as reported by Kadowaki (1981), observed using ultrasonic absorption and ESR. This transition has not previously been seen in magnetic measurements at a fixed temperature. The transition is marked by a sudden increase in magnetisation to a region of lower susceptibility, with inverse magnetic susceptibility similar to the zero field value, and remains approximately constant throughout the phase. The magnetic response of 'Phase A' is strongly anisotropic and occurs after the 'new phase' behaviour close to the critical temperature. The transition to 'Phase A' occurs after the magnetic response corresponding to rotation of the helix into the direction of the applied magnetic field.

The resultant phase diagram of MnSi close to the critical temperature with magnetic field applied along the < 001 > direction is shown in figure 5.4. The lower points mark the position of minima in the inverse susceptibility corresponding to domain wall motion and rotation whereas the higher ones mark the position of the sharp discontinuities thought to be a phase transition. These findings are in broad agreement with previous work of Kadowaki (1981). Since this technique selects information on the zero wavevector, static magnetisation density whilst other techniques used in determining the magnetic phase diagram are sensitive to a range of wavevector components (possibly both static and dynamic) small differences may be anticipated.

5.3 Magnetisation of MnSi in 'Phase A'

Figure 5.5 shows the magnetisation of a single crystal of MnSi measured in the < 111 > and < 001 > directions in the field regime where 'Phase A' is observed in the < 001 > direction, at a temperature of 28.6K. In the < 001 > direction the magnetisation sharply increases but to a region of lower susceptibility than that in < 111 > direction and this lower susceptibility remains constant for a further 800Oe at 28.6K. The sudden change in susceptibility occurs within 100Oe, so that in total the field span in which the magnetisation is different in the two directions (after domain reorientation) is 1000Oe at 28.6K. Because the magnetisation increases to a region of lower susceptibility, the response in the < 001 > direction is initially greater than that in the < 111 > direction. There then follows a field region where it is similar in the two directions (still in 'Phase A') and finally the magnetisation in the < 001 > direction is lower than that in the < 111 > direction. When 'Phase A'

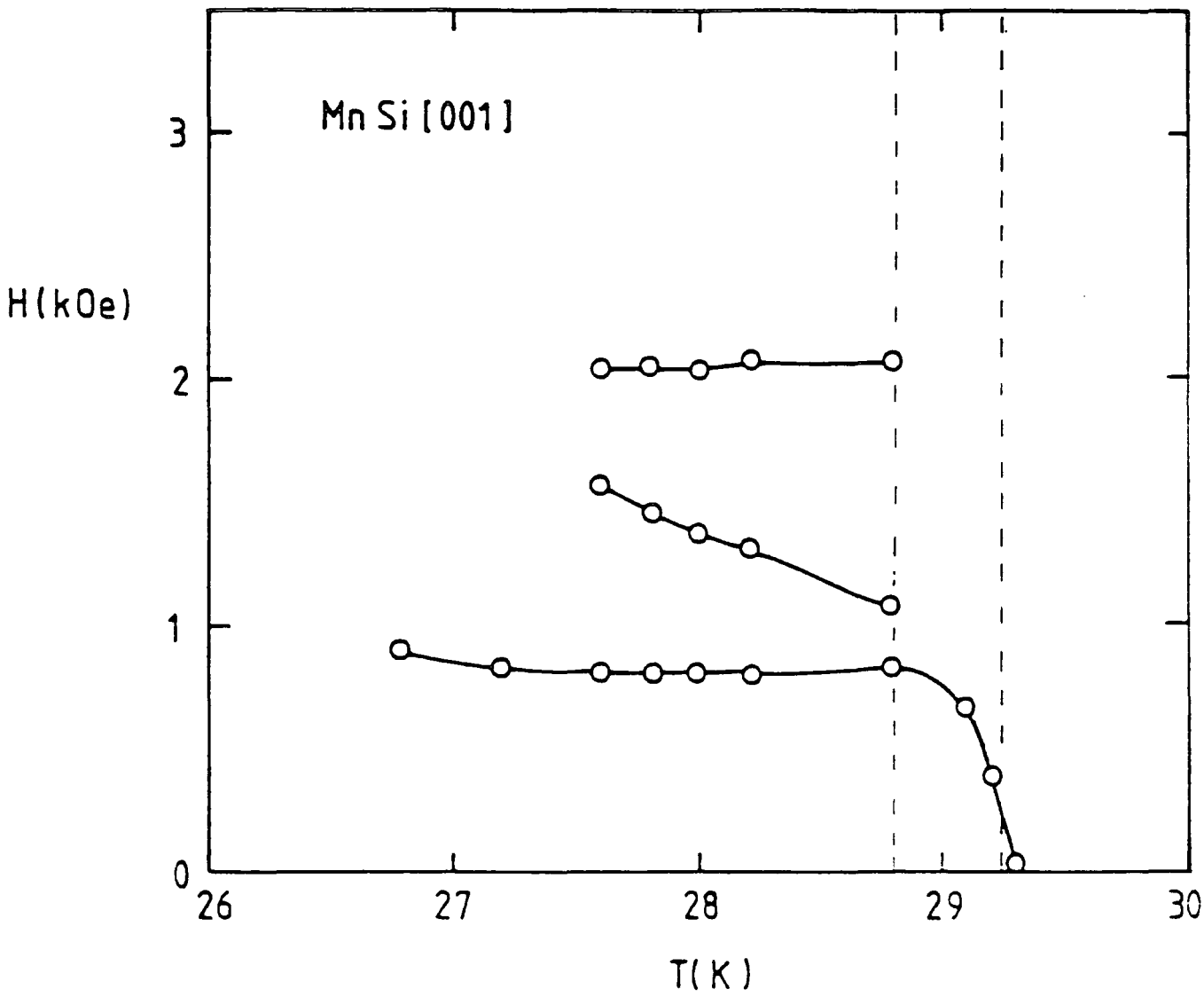

Figure 5.4 The positions of field minima of the inverse susceptibility in the < 001 > direction displayed as a function of internal field and sample temperature.

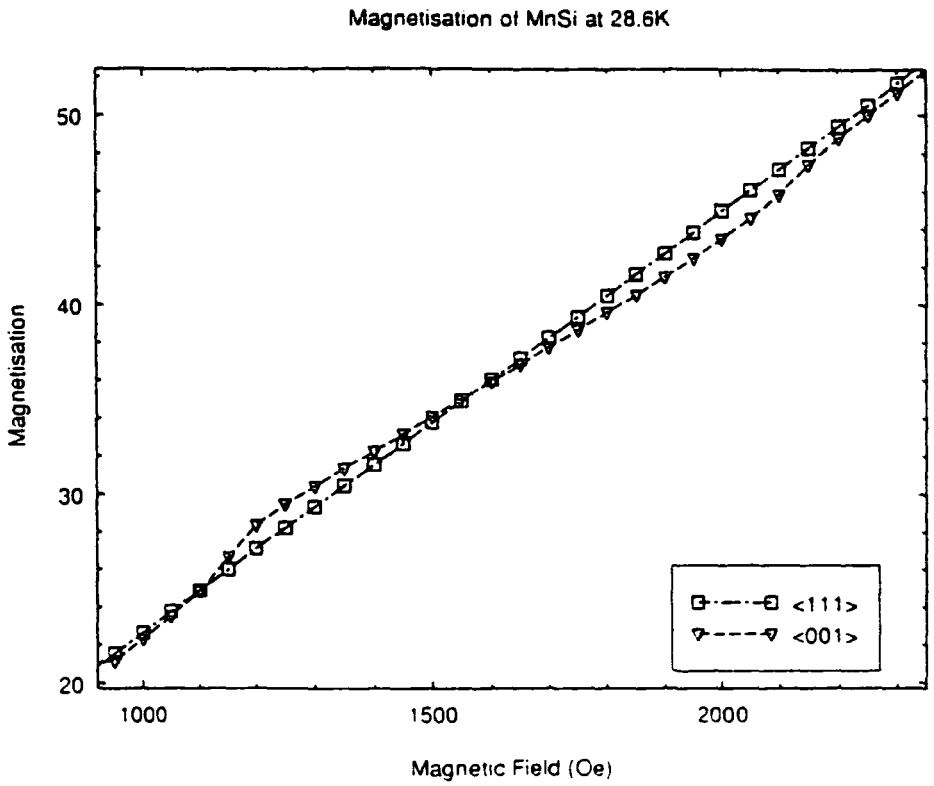

Figure 5.5 The magnetisation of MnSi with magnetic field applied parallel to the $< 001 >$ (triangles) and $< 111 >$ (squares) direction at a temperature of 28.6K i.e. in the temperature and field regime where 'Phase A' is observed in the $< 001 >$ direction.

is complete, the magnetisation increases sharply, again over a field range of 100Oe and returns to being identical in the two directions.

5.4 Magnetisation Below the Critical Temperature

Thorough investigation of the magnetisation of MnSi at 25K (i.e. well below the critical temperature) shows anisotropy between the $< 111 >$, $< 001 >$ and $< 110 >$ directions studied.

The magnetisation in the $< 111 >$ direction as shown in figure 5.6 (together with the inverse magnetic susceptibility and the differential of the inverse magnetic susceptibility) increases linearly with applied magnetic field upto the maximum field applied of ($\pm$3500Oe). The inverse susceptibility is constant and has a value of 42.1 ± 0.7.

The magnetic response in the $< 001 >$ direction (figure 5.7) can be divided into two regions; the first below 1300Oe is curved lower than that in the $< 111 >$ direction while the second region is linear with applied field up to the maximum field applied. The inverse susceptibility (figure 5.7(b)) corresponding to the first region can also be subdivided into two regions, both of which are linear with magnetic field. It has a maximum value of 59.3 ± 0.7 in zero field and decreases linearly to a minimum value of 29.5 ± 0.6 at a field of 880 ± 20Oe. The inverse magnetic susceptibility then linearly increases to a value of 41.6 ± 1.3 i.e. the region where it remains constant.

The magnetisation in the $< 110 >$ direction (figure 5.8) can also be subdivided into two regions and although similar to that in the $< 001 >$ direction, is not identical. The most striking difference is the hysteretic behaviour observed in this direction. This is evident from a temperature of 27K and yet is not observed about zero field. The magnetisation can again be divided into two regions; the first below 1000Oe is curved lower than that in the $< 111 >$ direction, but greater than that in the $< 001 >$ direction. This is evident in figures 5.9 and 5.10 where the magnetisation in each of the directions is plotted for increasing and decreasing magnetic field at a temperature of 25K. Above 1000Oe the behaviour is linear up to the maximum field applied of $\pm$2500Oe. Hysteresis is evident over the curved region of the magnetisation and thus the inverse susceptibility over this region is different for increasing and decreasing applied fields. The inverse susceptibility has a maximum value in zero field of 55 ± 2 and decreases gradually until, at a field of 300Oe there is a dramatic decrease over a range of 100Oe to a minimum value of 35.8 ± 0.8, where it remains constant for a short field region. This dramatic decrease is evident from the differential of the inverse susceptibility as a sharp peak. The inverse susceptibility then linearly increases to a value of 42.5 ± 0.8 where it remains constant over the field region studied. For a decreasing field, the inverse susceptibilty is very similar to that in the $< 001 >$ direction. At a field of 1000Oe it linearly decreases to a minimum value of 35.8 ± 0.6 at a field of 714 ± 50Oe from which it linearly increases to a maximum value of 55 ± 2 in zero field.

In figures 5.6 - 5.10 the internal magnetic field ($H_i = H - H_D$) has been called B and given the units gauss. Magnetisation is measured in units of $emucm^{-3}$ and can be converted to units of $emug^{-1}$ using the density of MnSi which is $5.82gcm^{-3}$.

Figure 5.6 (a) The magnetisation of MnSi with magnetic field applied parallel to the $< 111 >$ direction at a temperature of 25K; (b) the inverse magnetic susceptibility of MnSi at 25K derived from the magnetisation data; (c) the differential of the inverse magnetic susceptibility of MnSi at 25K. The solid line is an average through the data points for a given field and direction and is a measure of the experimental uncertainty.

Figure 5.7 (a) The magnetisation of MnSi with magnetic field applied parallel to the $< 001 >$ direction at a temperature of 25K; (b) the inverse magnetic susceptibility of MnSi at 25K derived from the magnetisation data; (c) the differential of the inverse magnetic susceptibility of MnSi at 25K. The solid line is an average through the data points for a given field and direction and is a measure of the experimental uncertainty.

Figure 5.8 (a) The magnetisation of MnSi with magnetic field applied parallel to the $< 110 >$ direction at a temperature of 25K; (b) the inverse magnetic susceptibility of MnSi at25K derived from the magnetisation data; (c) the differential ofthe inverse magnetic susceptibility of MnSi at 25K. The solid line is an average through the data points for a given field and direction and is a measure of the experimental uncertainty.

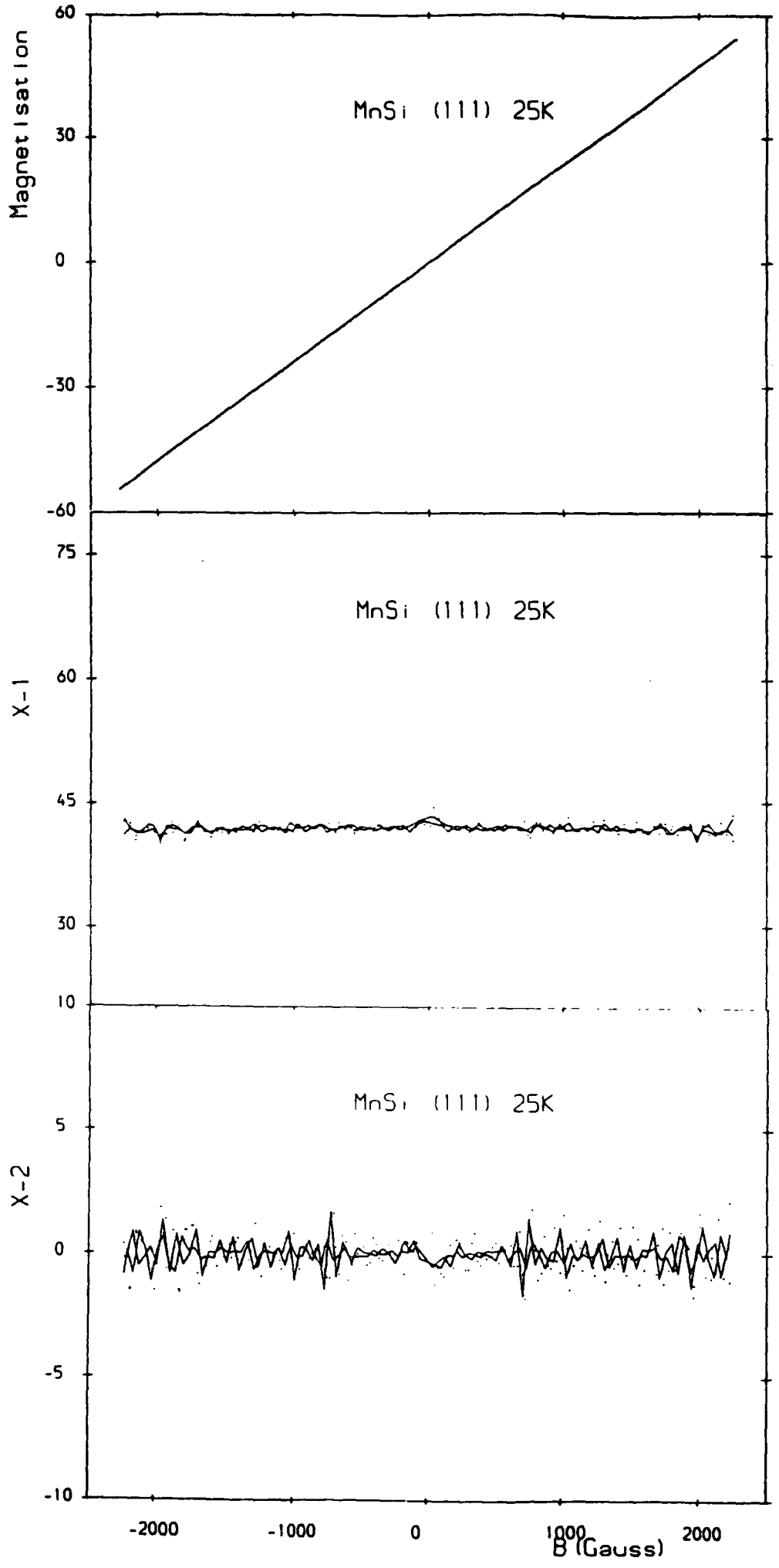
Magnetisation
60
30
0
-30
-60
MnSi (111) 25K
X-1
75
60
45
30
10
MnSi (111) 25K
X-2
5
0
-5
-10
MnSi (111) 25K
-2000
-1000
0
1000
2000
B (Gauss)

Figure 5.6 (a) - (c)

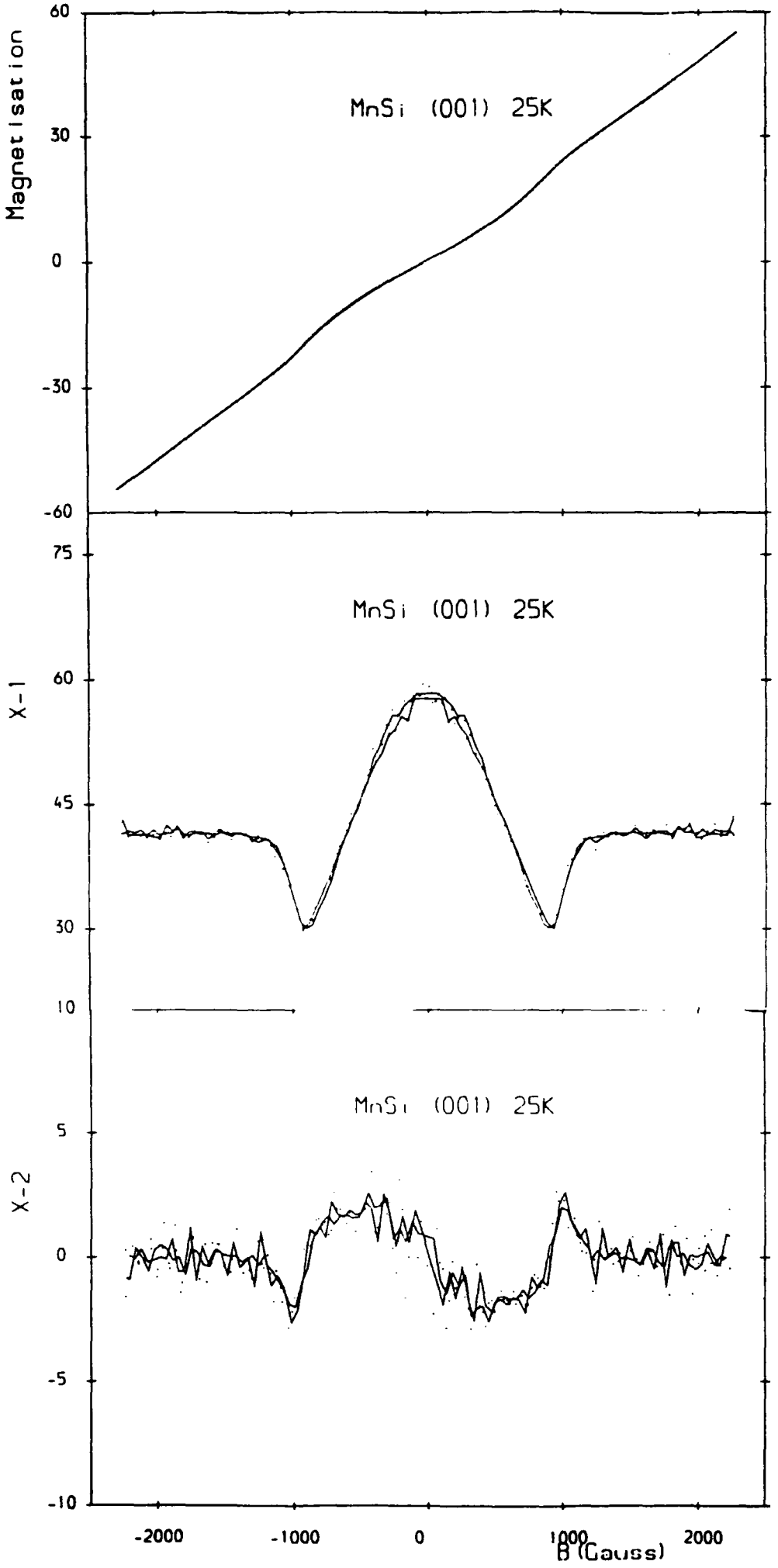
Magnetisation
60
30
0
-30
-60
MnSi (001) 25K
X-1
75
60
45
30
10
MnSi (001) 25K
X-2
5
0
-5
-10
MnSi (001) 25K
-2000
-1000
0
1000
2000
B (Gauss)

Figure 5.7 (a) - (c)

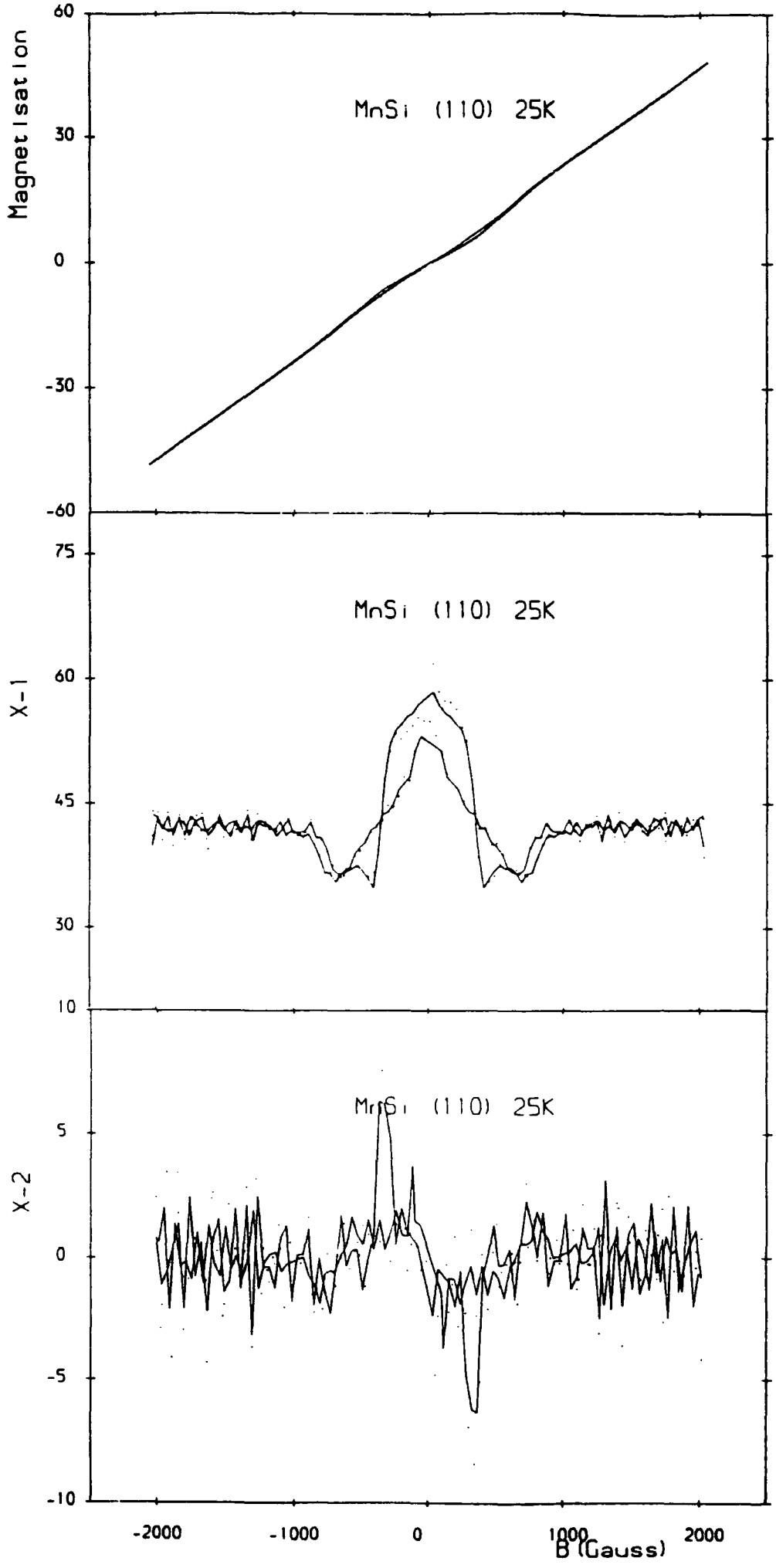
Magnetisation
60
30
0
-30
-60
MnSi (110) 25K
X-1
75
60
45
30
MnSi (110) 25K
X-2
10
5
0
-5
-10
MnSi (110) 25K
-2000
-1000
0
1000
2000
B (Gauss)

Figure 5.8 (a) - (c)

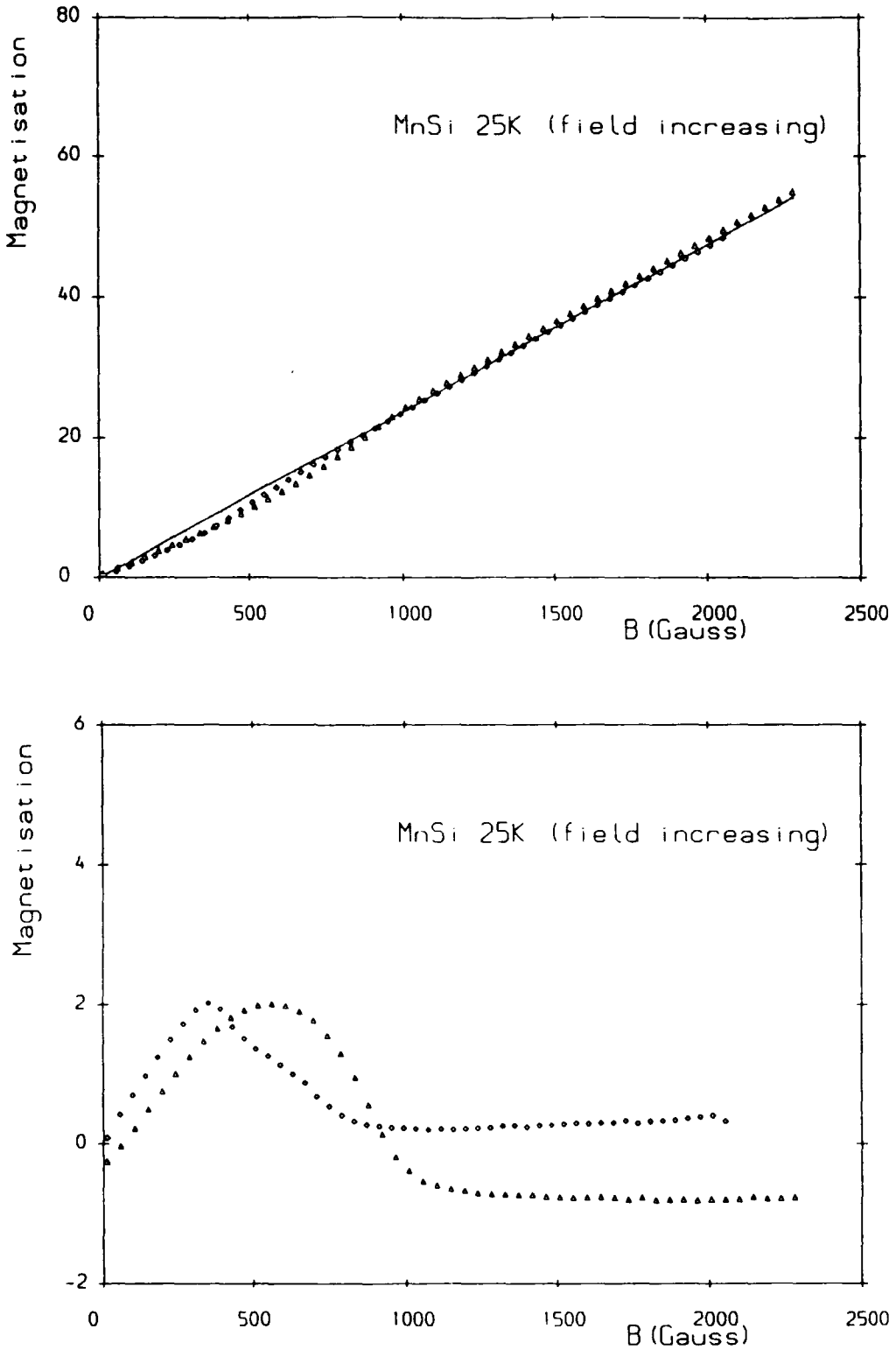

Figure 5.9 (a) The magnetisation of MnSi for an increasing magnetic field applied parallel to the < 111 > (complete line), < 001 > (triangles) and < 110 > (circles) at a temperature of 25K; (b) the subtraction of the magnetisation of MnSi (for an increasing field) with magnetic field applied parallel to the < 001 >(triangles)/< 110 >(circles) from the magnetisation with magnetic field applied parallel to the < 111 > direction.

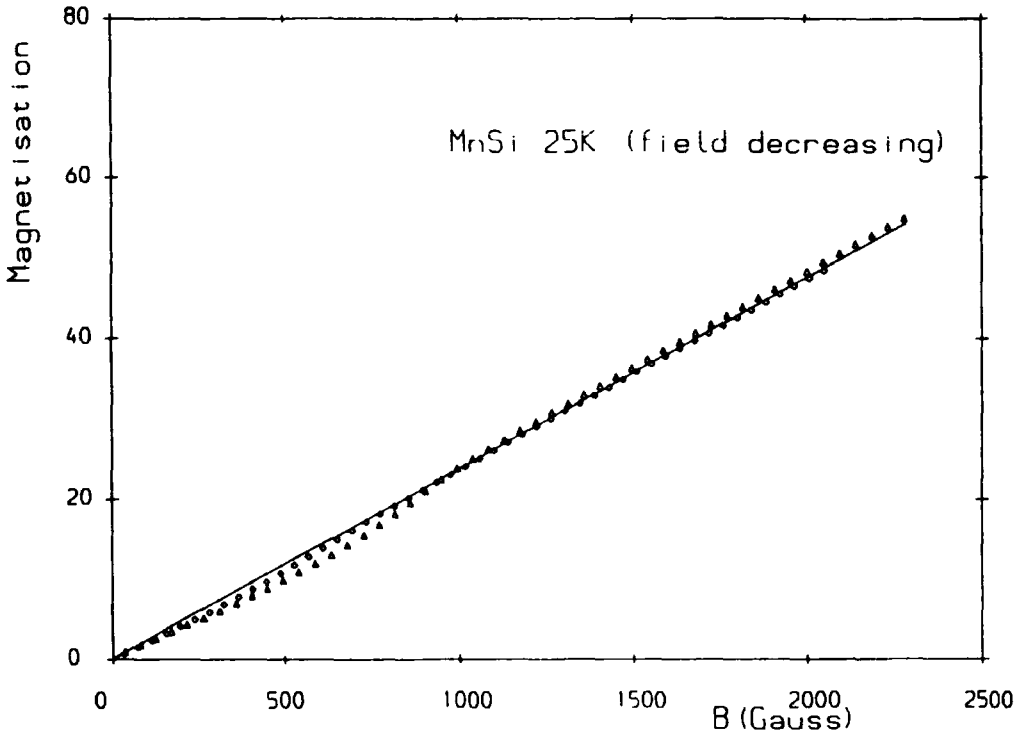

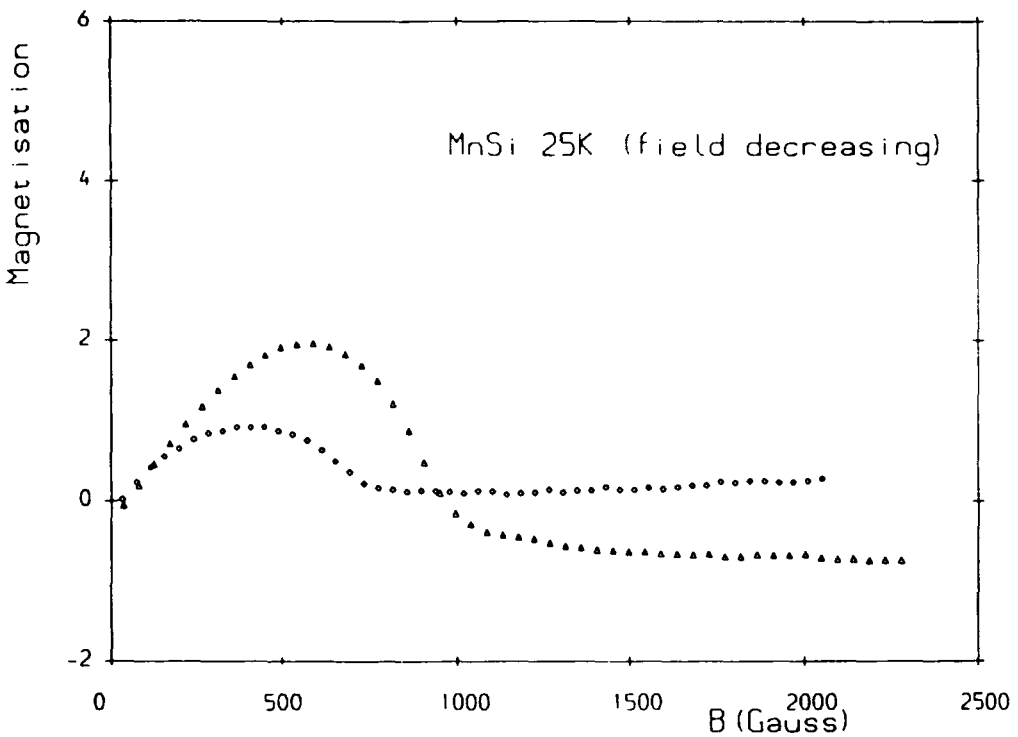

Figure 5.10 (a) The magnetisation of MnSi for a decreasing magnetic field applied parallel to the < 111 > (complete line), < 001 > (triangles) and < 110 > (circles) at a temperature of 25K; (b) the subtraction of the magnetisation of MnSi (for an decreasing field) with amgnetic field applied parallel to the < 001 >(triangles)/< 110 >(circles) from the magnetisation with magnetic field applied parallel to the < 111 > direction.

In order to investigate further the anisotropic nature of the response, figures 5.9 and 5.10 show the magnetisation in the three principle directions investigated, together with magnetisation in the < 110 > and < 001 > directions subtracted from that in < 111 > direction for increasing (figure 5.9) and decreasing (figure 5.10) fields, at a temperature of 25K. The difference of the magnetisation between < 111 > and < 001 > directions is similar for both increasing and decreasing field, however that between < 111 > and < 110 > directions varies in both form and magnitude.

5.5 Observation of Hysteresis in MnSi

As stated above, hysteresis was observed in the magnetisation of MnSi when measured at 25K in the < 110 > direction. This increases as the temperature is lowered (see for example the magnetisation in this direction at 17K and below as shown in figures 5.13 and 5.16).

In the < 111 > direction the behaviour is identical to that described at 25K with no hysteresis observed, demonstrated in figures 5.11 and 5.14.

In the < 001 > direction at 17K, shown in figure 5.12, hysteresis is now observed in the region 900 - 1300Oe but not about zero field. This is made apparent by the inverse susceptibility varying for increasing and decreasing applied field. The magnetisation for increasing field is similar to that descibed at 25K in this direction. As the field is reduced however, the region where the inverse susceptibility remains constant now extends to a lower field by approximately 250Oe. Here a sudden, dramatic decrease is observed, to a minimum value which is now lower than for increasing field. Finally the inverse susceptibility linearly increases with similar gradient to that for increasing field.

In the magnetisation measured in the < 110 > direction at 17K (shown in figure 5.13), the hysteresis observed at 25K is enhanced. It extends from 100 - 1000Oe but is not observed about zero field. The form of the inverse susceptibility for increasing and decreasing fields is similar to that described at 25K but as in the < 001 > direction with decreasing field, the region where the inverse susceptibility is constant extends to a lower field. It then sharply decreases to a minimum value which is lower than for increasing field.

As the temperature is further reduced down to 10K, figures 5.14 - 5.16, the hysteresis observed in both the < 001 > and < 110 > directions increases whereas there is still no evidence of it in the < 111 > direction.

5.6 High Field Magnetisation Measurements on MnSi

Figure 5.17 shows the results of magnetisation measurements performed on MnSi at high magnetic fields upto 80kOe. Both above and below the transition tem-

In figures 5.11 - 5.16 the internal magnetic field ($H_i = H - H_D$) has been called B and given the units gauss. Magnetisation is measured in units of $emucm^{-3}$ and can be converted to units of $emug^{-1}$ using the density of MnSi which is $5.82gcm^{-3}$.

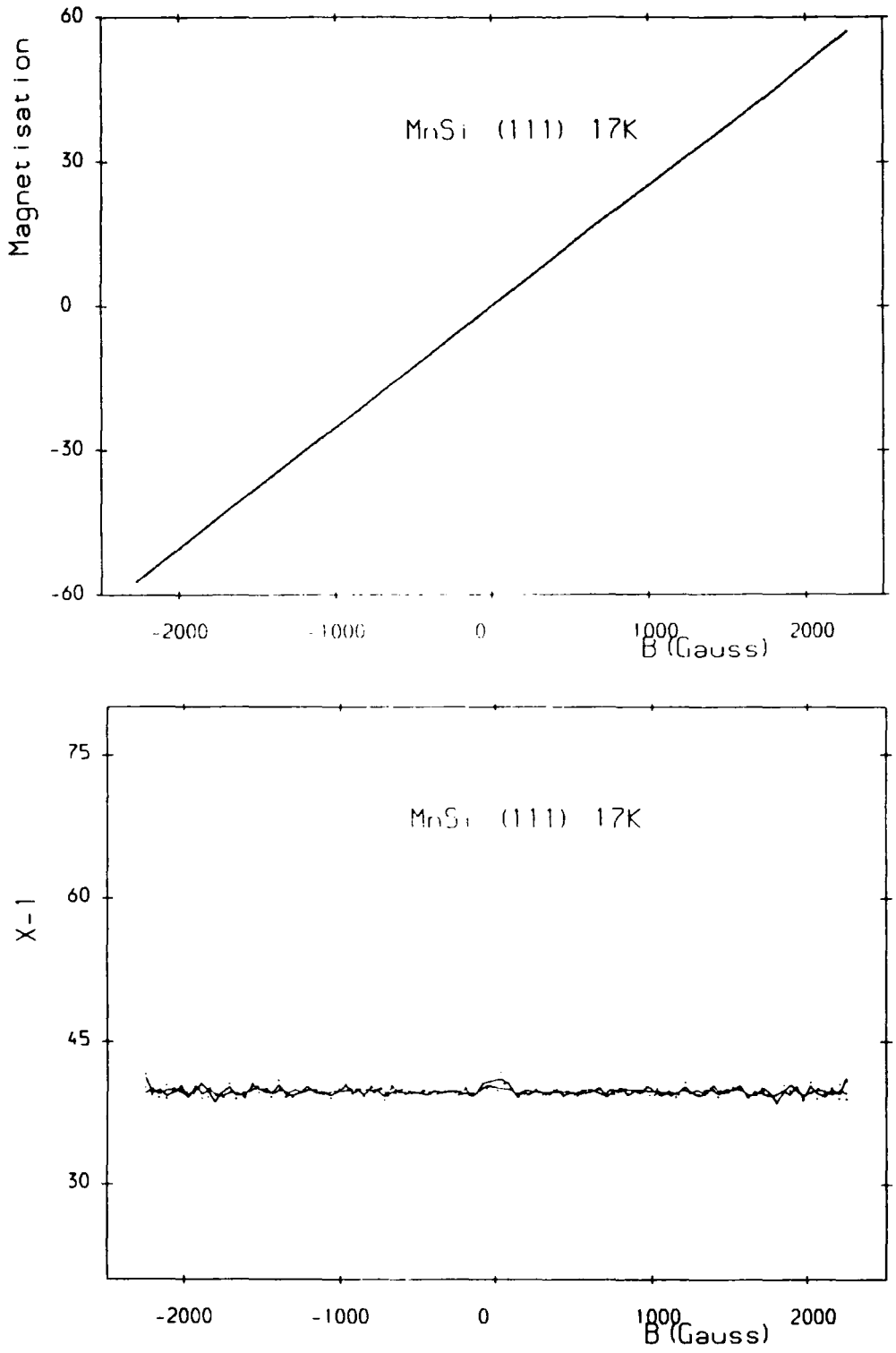

Figure 5.11 (a) The magnetisation of MnSi with magnetic field applied parallel to the < 111 > dierection at a temperature of 17K; (b) the inverse magnetic susceptibility of MnSi at 17K derived from the magnetisation data. The solid line is an average through the data points for a given field value and direction and is a measure of the experimental uncertainty.

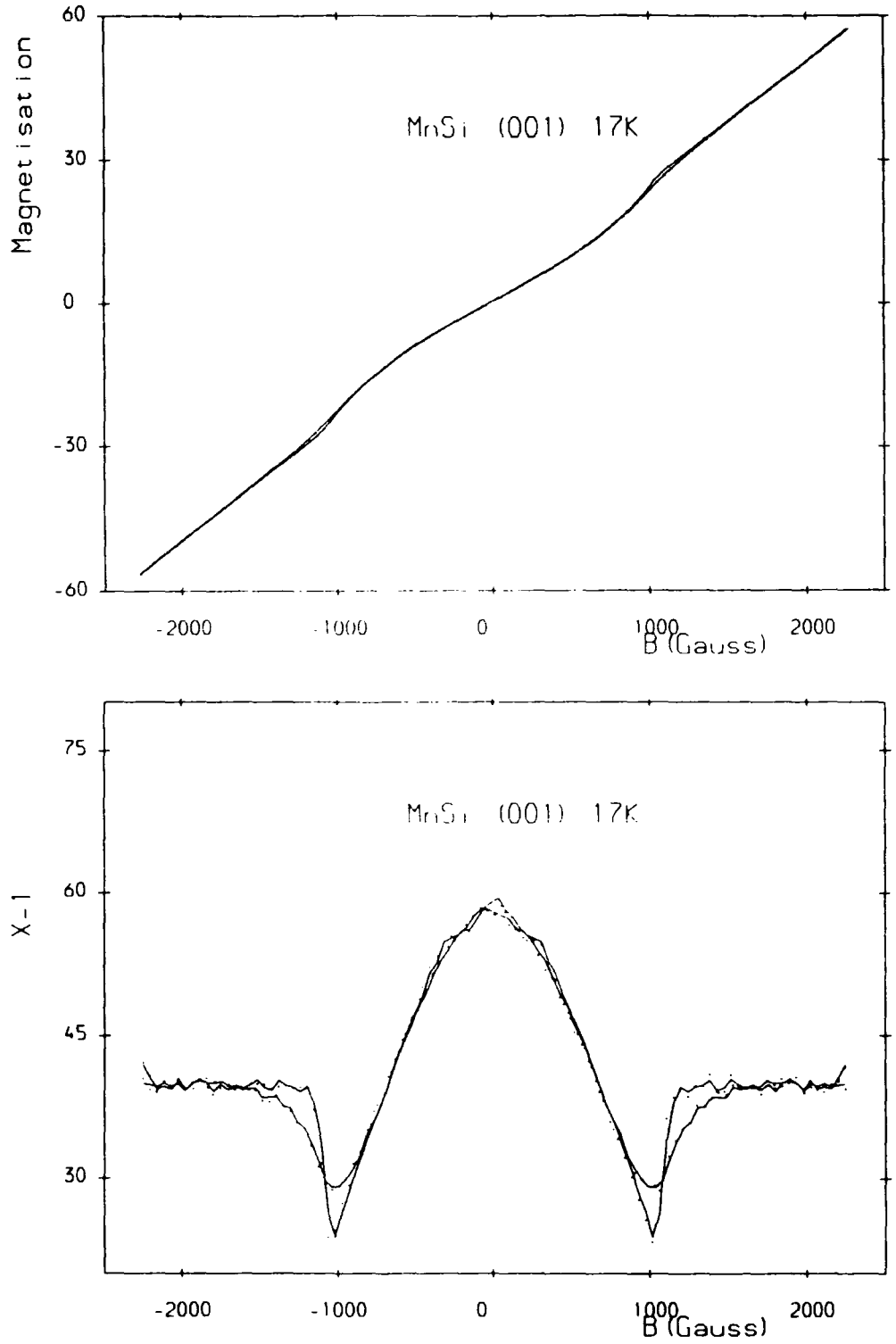

Figure 5.12 (a) The magnetisation of MnSi with a magnetic field applied parallel to the < 001 > direction at a temperature of 17K; (b) the inverse magnetic susceptibility of MnSi at 17K derived from the magnetisation data. The solid line is an average through the data points for a given field value and direction and is a measure of the experimental uncertainty.

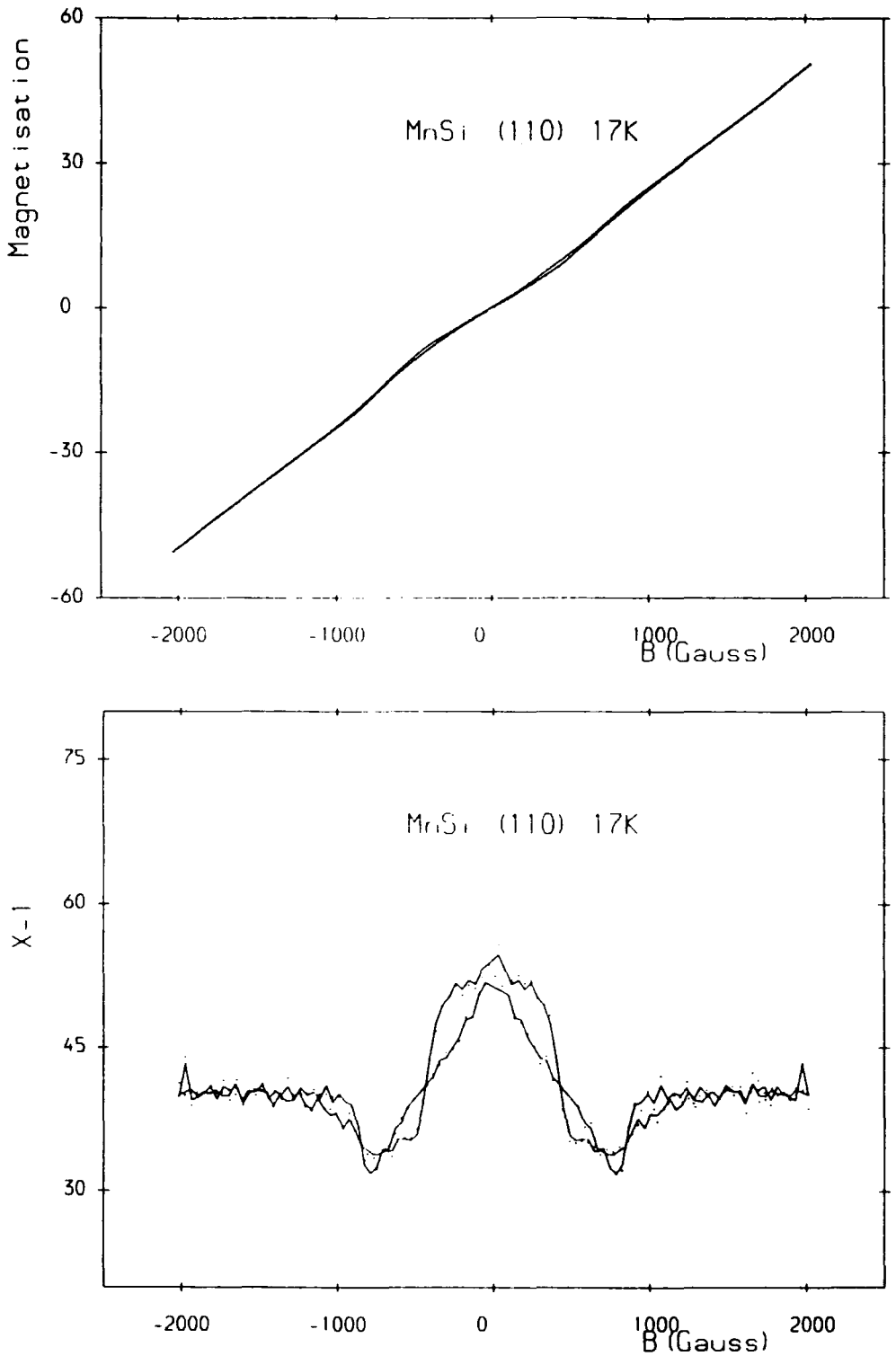

Figure 5.13 (a) The magnetisation of MnSi with a magnetic field applied parallel to the < 110 > direction at a temperature of 17K; (b) the inverse magnetic susceptibility of MnSi at 17K derived from the magnetisation data. The solid line is an average through the data points for a given field value and direction and is a measure of the experimental uncertainty.

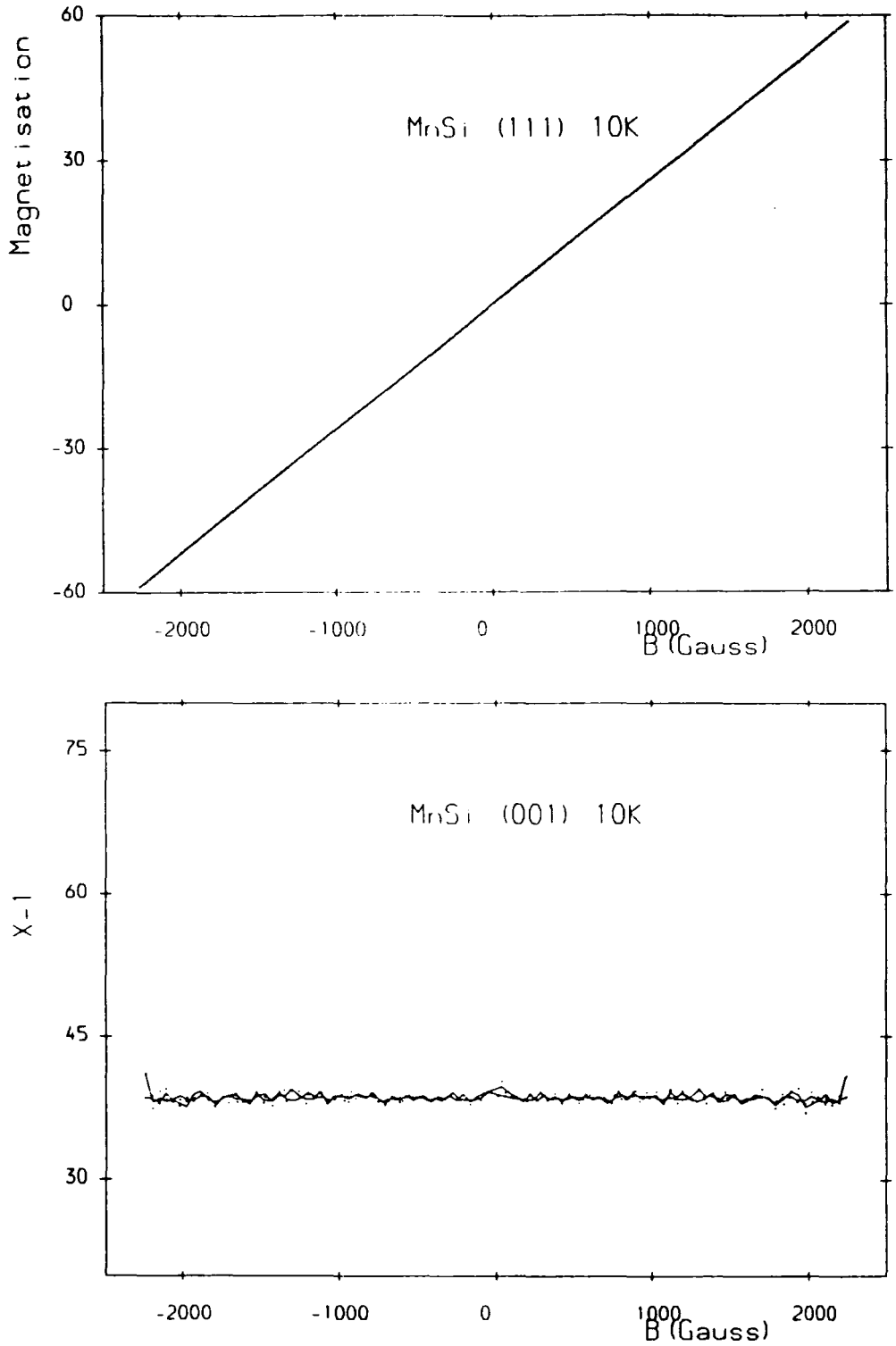

Figure 5.14 (a) The magnetisation of MnSi with a magnetic field applied parallel to the < 111 > direction at a temperature of 10K; (b) the inverse magnetic susceptibility of MnSi at 10K derived from the magnetisation data. The solid line is an average through the data points for a given field value and direction and is a measure of the experimental incertainty.

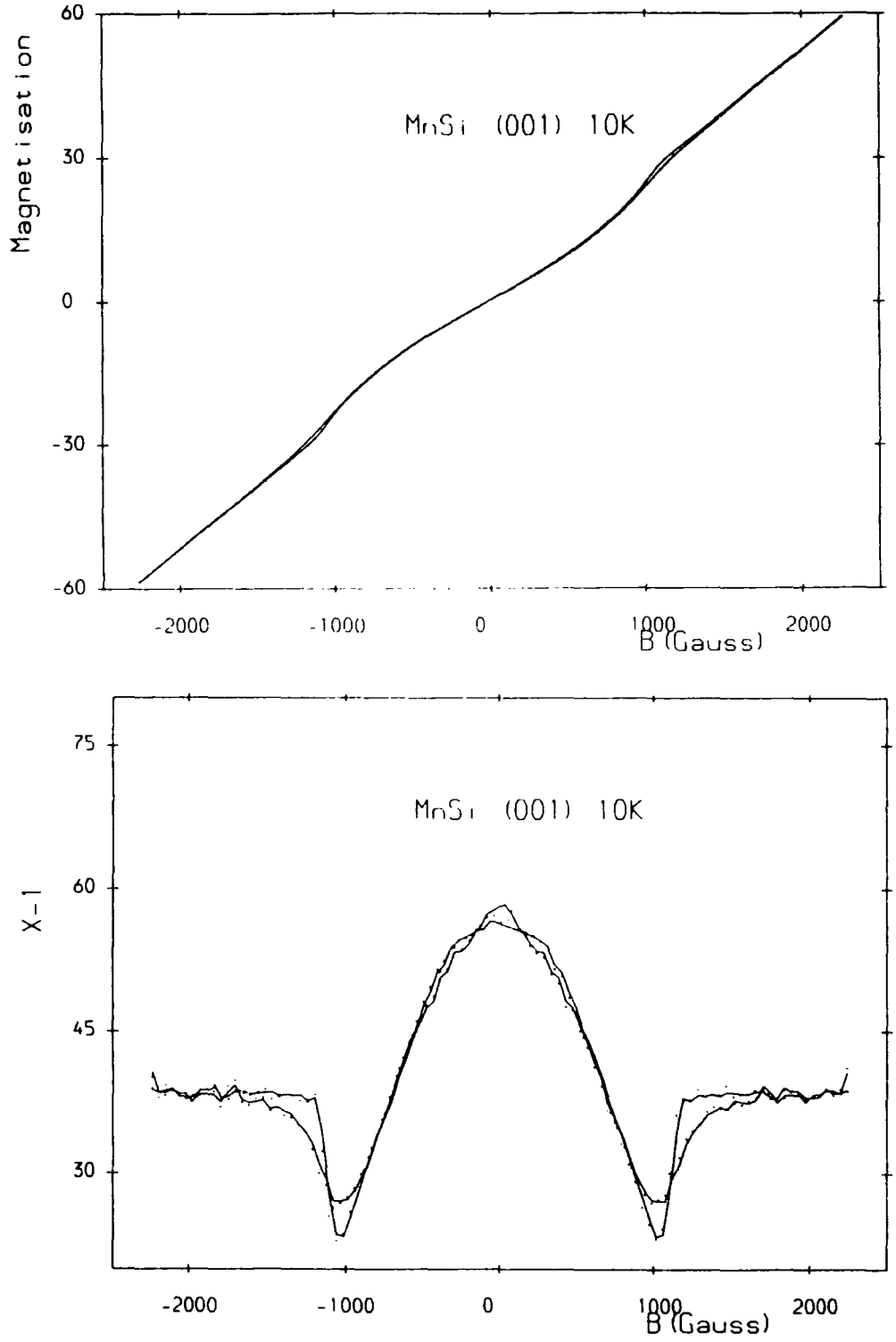

Figure 5.15 (a) The magnetisation of MnSi with a magnetic field applied parallel to the < 001 > direction at a temperature of 10K; (b) the inverse magnetic susceptibility of MnSi at 10K derived from the magnetisation data. The solid line is an average through the data points for a given field value and direction and is a measure of the experimental uncertainty.

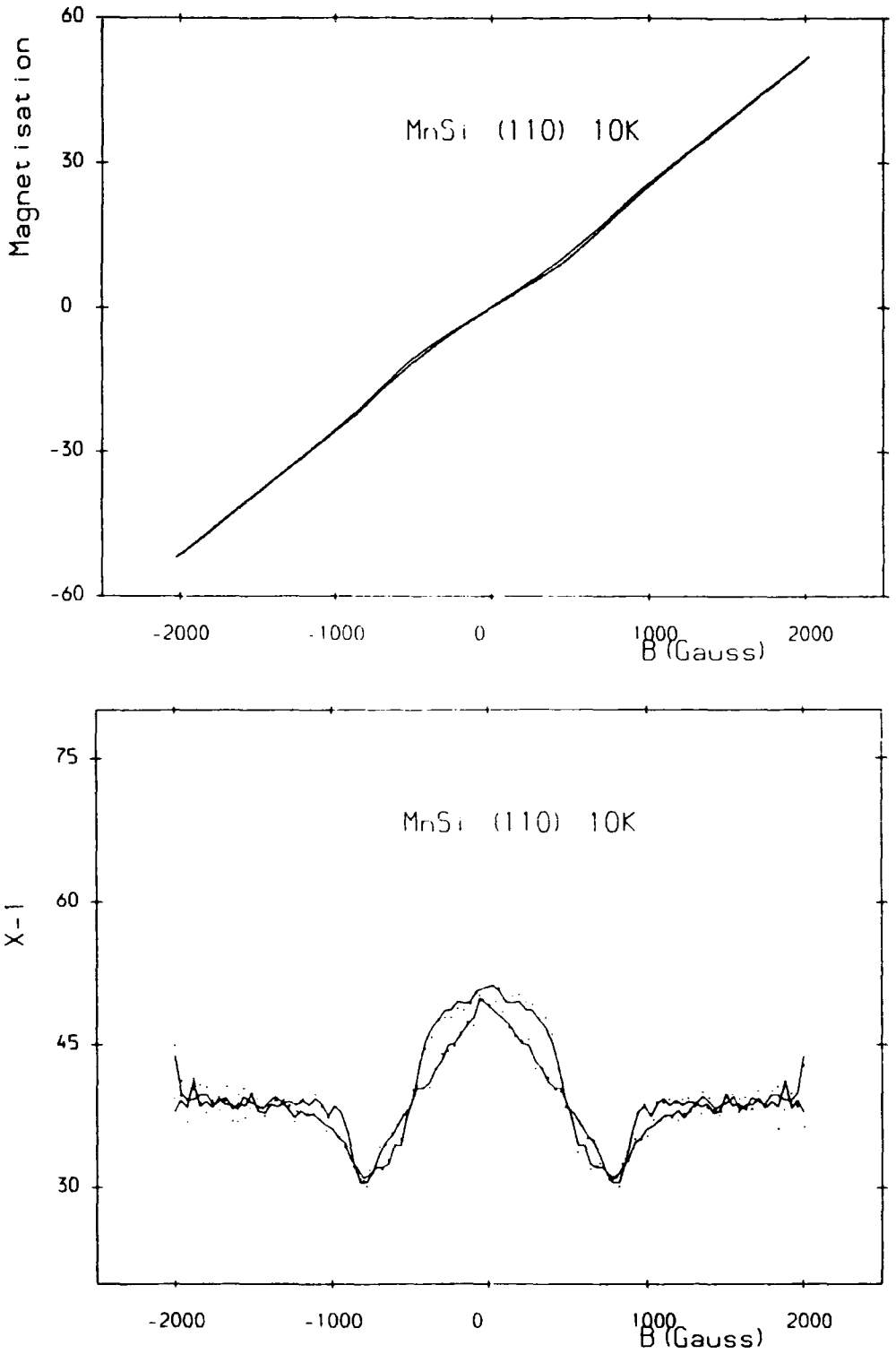

Figure 5.16 (a) The magnetisation of MnSi with a magnetic field applied parallel to the < 110 > direction at a temperature of 10K; (b) the inverse magnetic susceptibility of MnSi at 10K derived from the magnetisation data. The solid line is an average through the data points for a given field value and direction and is a measure of the experimental uncertainty.

perature, the magnetisation shows no sign of saturating in the field range studied. Below the transition temperature, the magnetisation increases linearly upto a field of approximately 5kOe at which point there is a 'knee' in the response. The magnetisation however, does increase significantly as the field is increased above this. In fields greater then ≈5kOe the magnetisation of MnSi is similar in form to that of $ZrZn_2$ (see Chapter 4). This is also evident from the 'Arrot Plot' shown in figure 5.17(b) which is almost linear for magnetic fields above 5kOe and similar to that of $ZrZn_2$. This suggests that the magnetisation of MnSi is displaying some of the characteristics of a weak itinerant ferromagnet in magnetic fields in excess of 5kOe.

As this magnetisation study was concerned with the low magnetic field properties of MnSi (i.e. in fields less than 3kOe), the 'Arrot Plots' of this data correspond to the initial region of figure 5.17(b) where the value of B/M is approximately constant. Figures 5.18(a) - (c) show the 'Arrot Plots' for a range of temperatures close to the transition temperature in both the $< 001 >$ and $< 111 >$ directions whereas figures 5.18(d) and (e) are of temperatures well below this. There is curvature to the plots above the transition temperature, however below this and at higher fields (higher field $\rightarrow M^2$ large) the plots are linear with a steep negative gradient. The intercept of this linear region on the B/M axis does decrease gradually as the temperature is lowered. The reason for the difference in the two directions at lower magnetisation is due to domain reorientation in the $< 001 >$ direction and also 'Phase A' at 28.2K.

5.7 Magnetisation as a Function of Temperature close to the Critical Temperature

The magnetisation data on MnSi was recorded by fixing temperature and varying the magnetic field. As the fields at which the magnetisation was measured were identical at each temperature, rearrangement of the data allows comparison of the magnetisation as a function of temperature. The data considered close to the critical temperature was taken within two days and the values of magnetic field quoted do not take into account demagnetisation factors. Plots compare the magnetisation in the two directions with $M_{<111>}$ and $M_{<001>}$ refering to the magnetisation measured with magnetic field applied in the respective directions.

When a low field (74Oe) is applied to the sample, the magnetisation in the two directions as shown in figure 5.19(a) is anisotropic over the temperature range considered. $M_{<001>}$ peaks at $29.3 \pm 0.1K$ while $M_{<111>}$ has a maximum value within the range 29.3 - 29.0K. This peak is regarded as marking the onset of a phase transition.

$M_{<111>}$ is greater than $M_{<001>}$ below 29.0K as expected, due to the curved magnetisation below 1000Oe in $< 001 >$ direction compared to the linear response in $< 111 >$ direction. In the $< 001 >$ direction, the magnetisation dramatically decreases after peaking and levels off down to 27.0K whereas in the $< 111 >$ direction, it has already started to increase again by 27.0K.

As the field is increased to 177Oe (figure 5.19(b)), the response in the two di-

In figures 5.17 - 5.18 the internal magnetic field has been called B and given units of gauss.

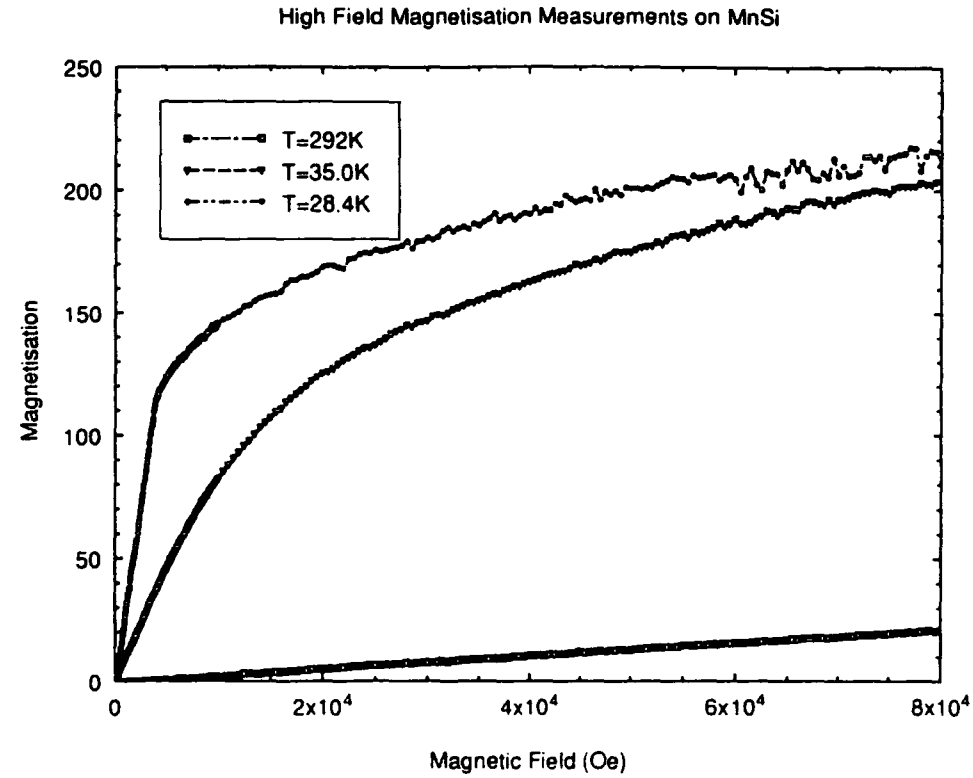

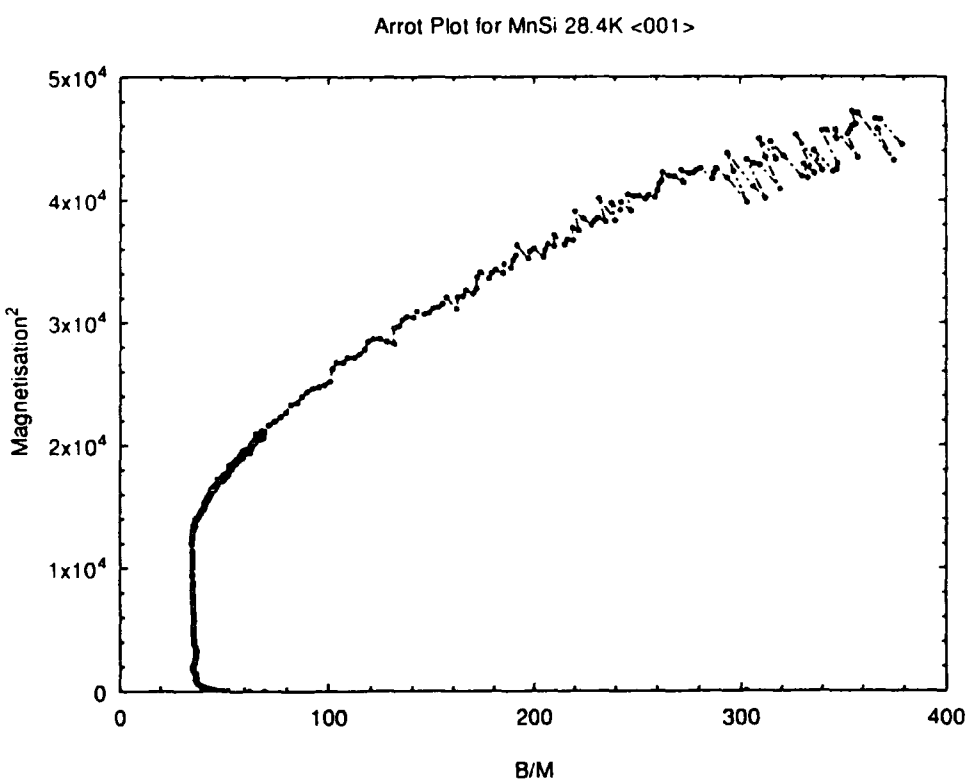

Figure 5.17 (a) High field magnetisation measurements on MnSi with magnetic field applied parallel to the < 001 > direction for temperatures 292K (squares), 35.0K (triangles) and 28.4K (circles); (b) the 'Arrot Plot' for MnSi at 28.4K derived from the high field magnetisation data with magnetic field applied parallel to the < 001 > direction.

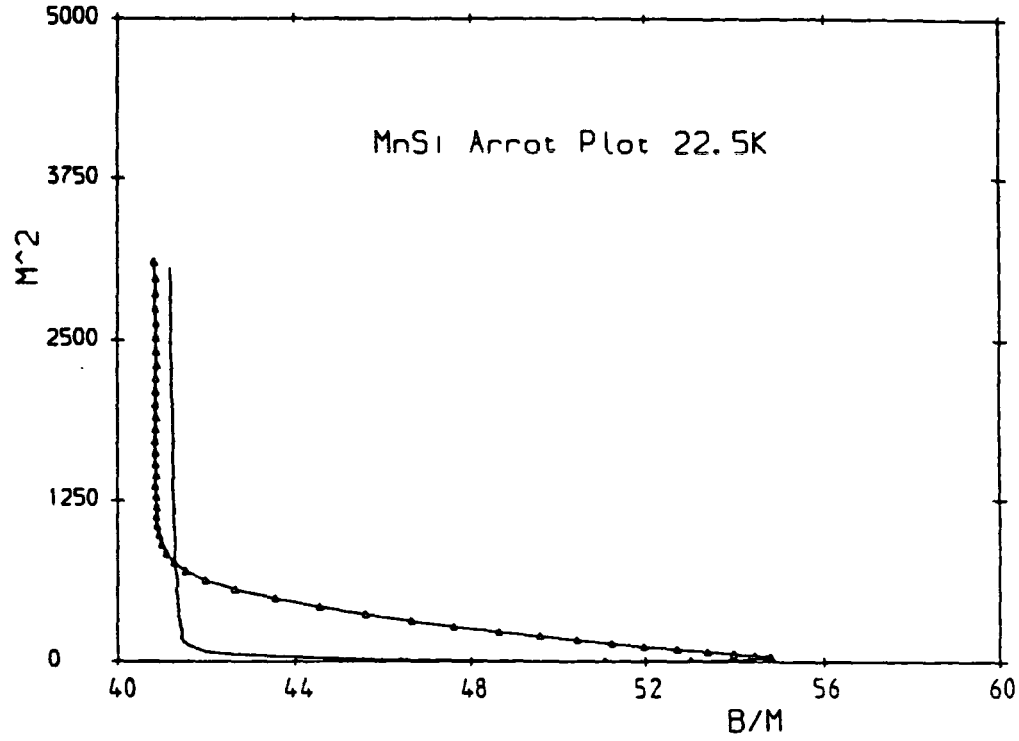

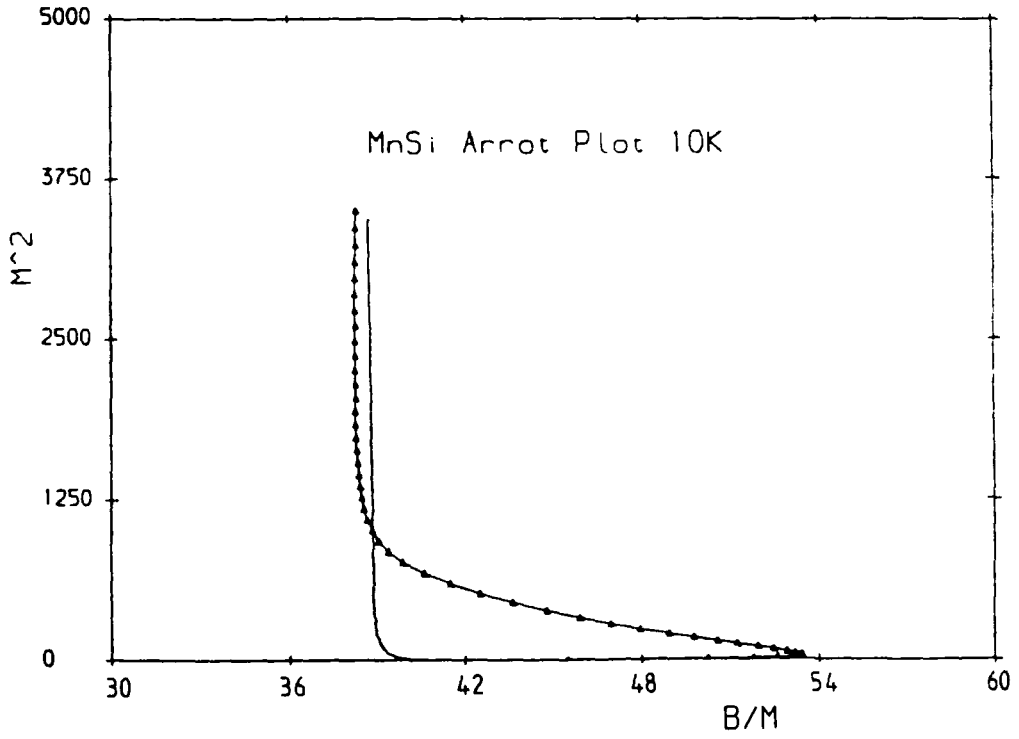

Figure 5.18 'Arrot Plots' for MnSi derived from the magnetisation data with magnetic field applied parallel to the < 111 > (points)/< 001 > (triangles). (a) 30.0K; (b) 29.1K; (c) 28.2K; (d) 22.5K; (e) 10.0K.

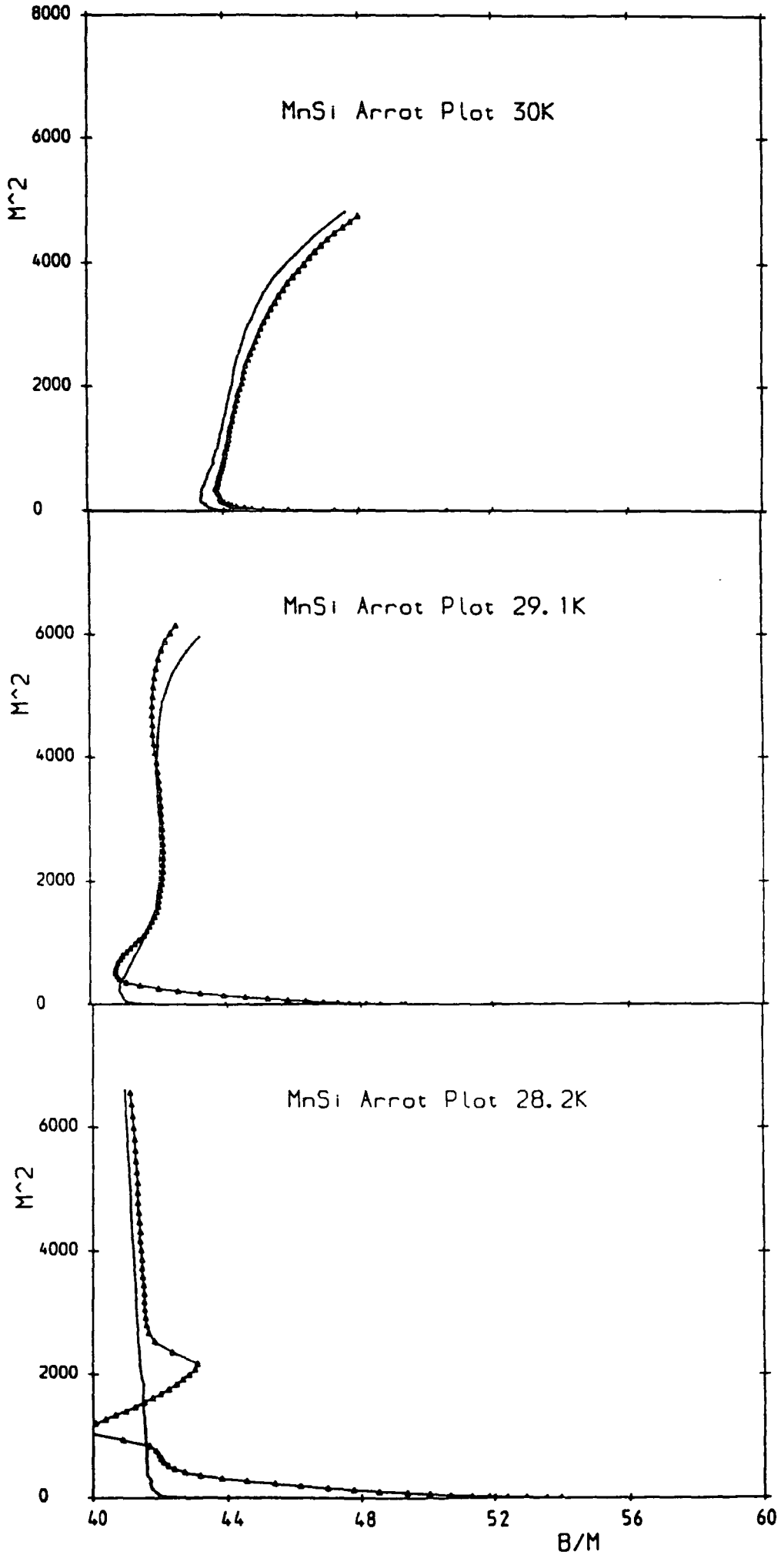

Figure 5.18 (a) - (c)

rections remains similar to that at lower fields although the peak in the < 111 > direction is increasingly less defined. In a field of 329Oe (figure 5.19(c)) there is a slight shift in the position of the peak in magnetisation towards 29K. $M_{<001>}$ then decreases, again dramatically at first whereas there is a step in the magnetisation in the < 111 > direction after the peak, below which the response remains approximately constant. With an applied field of 885Oe as shown in figure 5.19(d), the peak in the magnetisation has again shifted towards 29.0K and the magnitude of the difference in response in the two directions has reduced. This trend continues until in a field of 1090Oe (figure 5.19(e)) the magnetisation is isotropic.

On application of a field of 1191Oe (figure 5.19(f)) the magnetisation in the two directions is similar apart from a single data point in the $M_{<001>}$ at 28.9K which is greater than $M_{<111>}$. This marks the onset of 'Phase A' in the < 001 > direction with the crystal in this phase between 29.1 - 28.9K. There is no evidence of this transition in the < 111 > direction. As the field is further increased between 1344 - 1698Oe (figures 5.19(g) - (h)), the position of this second peak in $M_{<001>}$ lowers in temperature. The transition at 29K in both directions is now marked by a 'shoulder' in the magnetisation.

A short field region, between 1848Oe and 1920Oe follows (figure 5.19(i)) where the magnetisation of the crystal is isotropic. This region is short lived and in a field of 1948Oe the peak in $M_{<001>}$ is followed by a decrease in the magnetisation in this direction. In $M_{<111>}$ there is a shoulder at 29.0K below which the magnetisation gradually increases. The response in < 001 > direction is lower than in the < 111 > direction down to a temperature of 27.5K after which the magnetisation is identical. This behaviour continues in the field range 2050 - 2255Oe (figure 5.19(k)), though the magnitude of the variation decreases. Finally, at a field of 2353Oe (figure 5.19(l)) the magnetisation is isotropic with a shoulder at approximately 29.0K.

In the field region 1200 - 2400Oe the magnetisation of MnSi varies dramatically as a function of temperature and direction close to the transition temperature. To summarise, an isotropic response is followed by $M_{<001>}$ being greater than $M_{<111>}$. A small field range where the magnetisation in the two directions is similar precedes a regime where $M_{<001>}$ is lower than $M_{<111>}$ and finally the response is identical.

This behaviour is due to the 'Phase A' magnetisation in the < 001 > direction. As a function of magnetic field, the magnetisation in the < 001 > direction shows a sudden, dramatic increase above that in the < 111 > direction but to a region of lower susceptibility. Hence in fields initially after the onset of 'Phase A' $M_{<001>}$ is greater than $M_{<111>}$. There then follows a small field regime in which the magnetisation is similar in both directions. Finally, the $M_{<001>}$ is lower than $M_{<111>}$ before returning to an isotropic magnetisation.

This goes a long way to explaining the results reported by Kadowaki *et al.* (1981). The combination of assuming that the magnetisation is isotropic and noting the position of peaks in the response while sweeping temperature in a fixed field would result in the apparent observation of the two phases, 'Phase A_1' and 'Phase A_2'. 'Phase A_1' corresponds to the region where the $M_{<001>}$ is greater than $M_{<111>}$ and 'Phase A_2' is the regime where it is lower.

In figure 5.19 the applied magnetic field has been called B and given the units gauss.

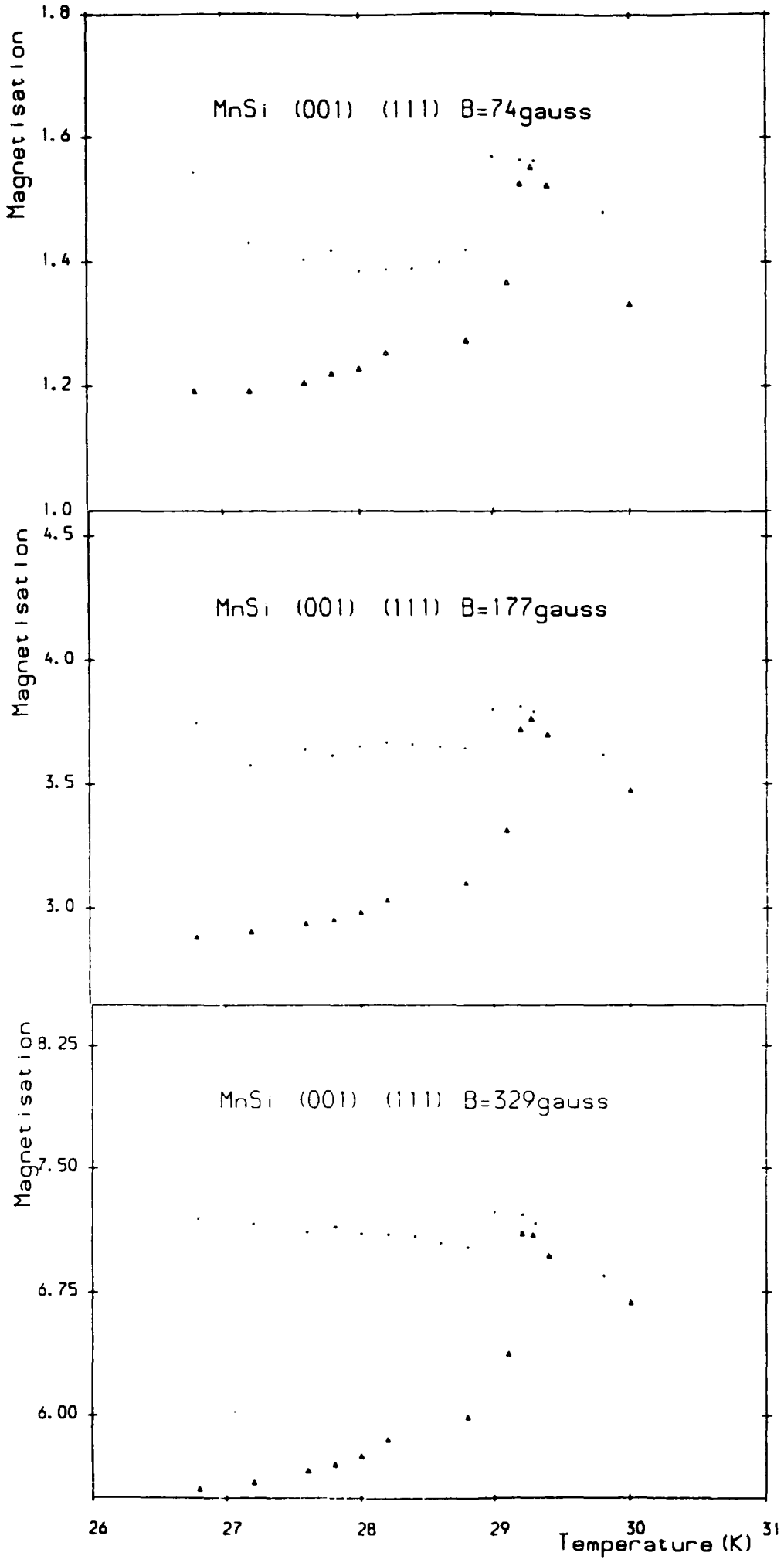

Figure 5.19 (a) - (c)

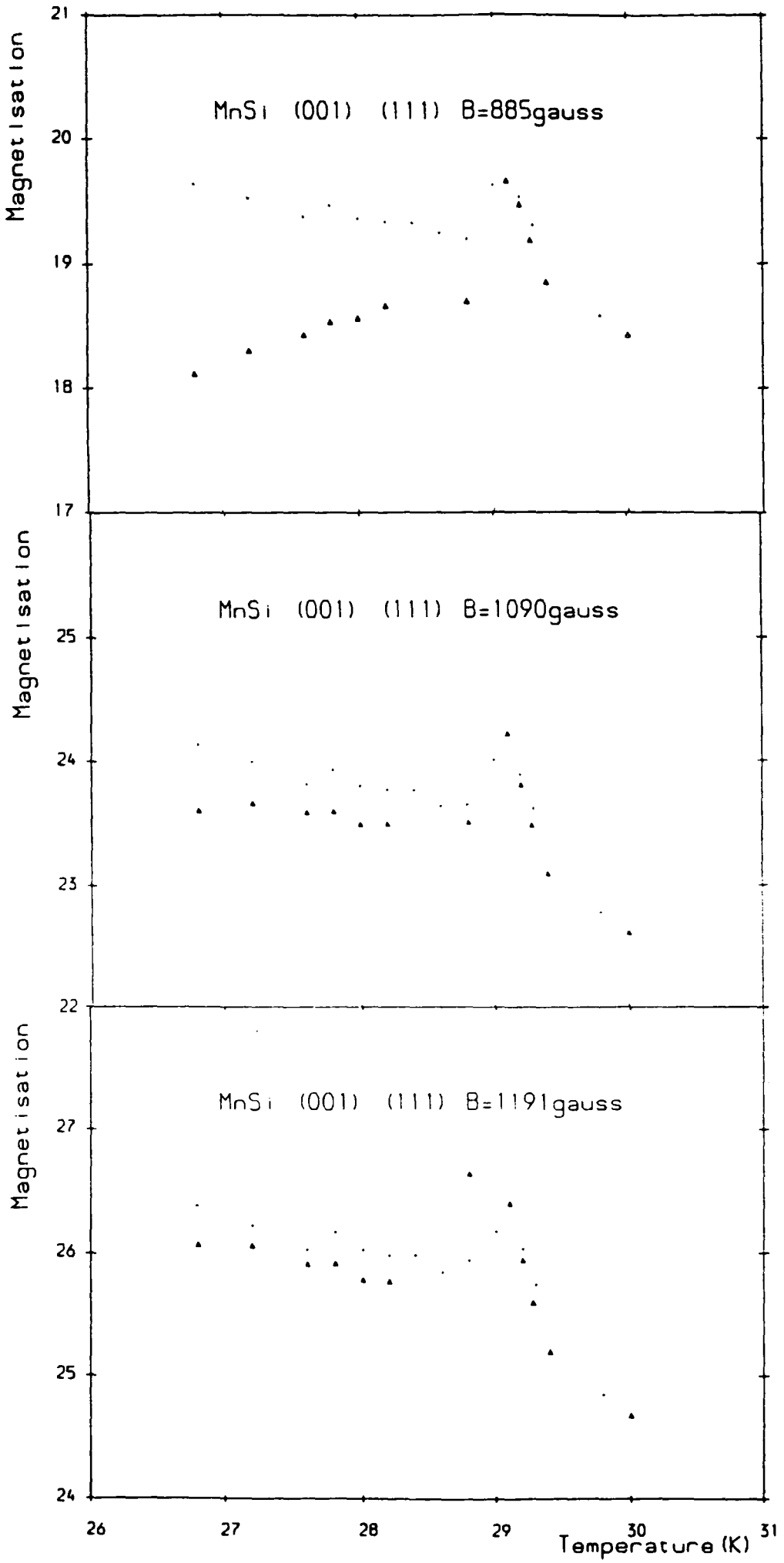

Figure 5.19 (d) - (f)

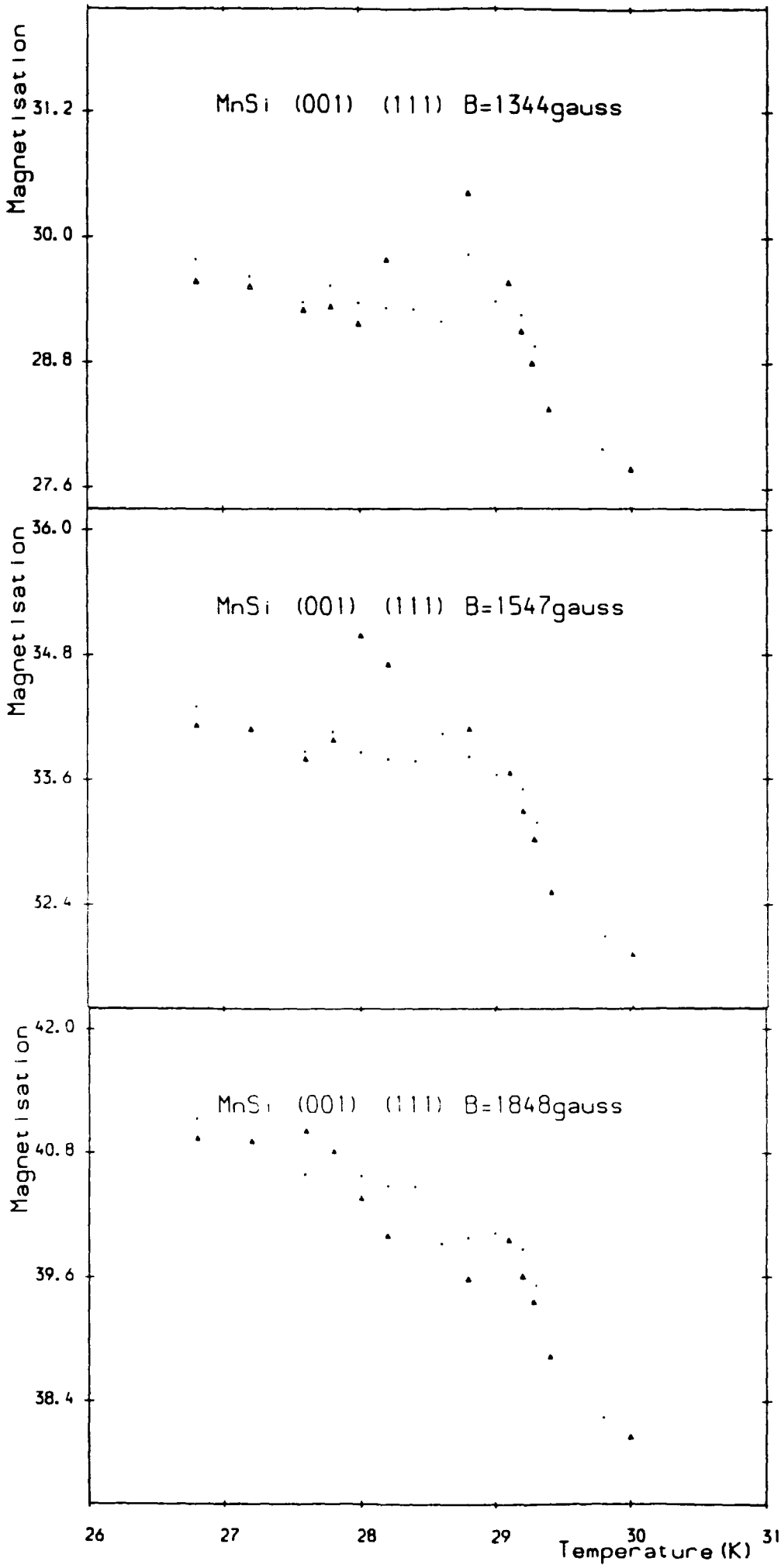

Figure 5.19 (g) - (i)

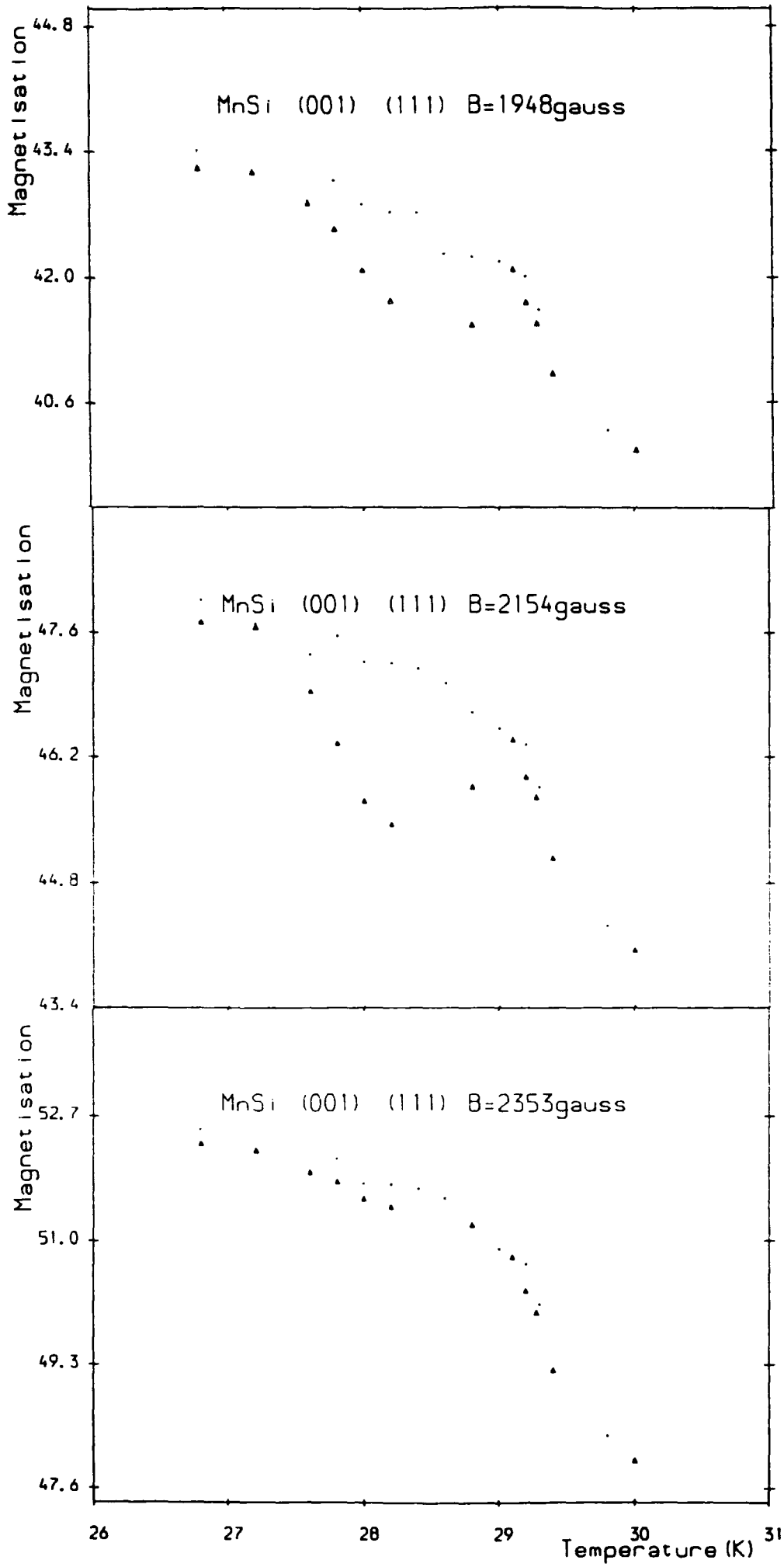

Figure 5.19 (j) - (l)

5.8 Combination of the Results

Figures 5.20 and 5.21 show three-dimensional plots of the inverse susceptibility as a function of both applied magnetic field and temperature close to the magnetic phase transition into the helimagnetic state for both < 001 > and < 111 > directions respectively. In the < 001 > direction above the transition temperature, the magnetisation is paramagnetic with a large increase in inverse susceptibility at higher fields associated with an induced ferromagnetic state. The central larger peak in the inverse susceptibility is believed to be due to domain reorientation while 'Phase A' occurs in larger magnetic fields and for a finite temperature range only, close to the transition temperature i.e. either side of the central peak.

Above the transition temperature the paramagnetic response is identical in both directions considered although the anisotropy is obvious below this. The small rises observed in the inverse magnetic susceptibility in the < 111 > direction, close to the transition temperature, are in comparable field regimes to similar features in the < 001 > direction and may be due to misalignment of the crystal. It is important, however, to note that the rises exist over a much shorter temperature region than the domain reorientation and 'Phase A' observed in the < 001 > direction. This is more likely an isotropic response due to either another phase before, or onset of the helical phase.

5.9 The Inverse Initial Susceptibility of MnSi

Figure 5.22 shows the inverse initial susceptibility as a function of temperature for the < 001 >, < 110 > and < 111 > principle directions studied. Above the critical temperature there is Curie-Weiss behaviour resulting in a value of θ_N of $29.1 \pm 0.1 K$. The measurement errors involved at higher temperatures are larger than those below the transition temperature as the signal obtained from the sample is much smaller. In addition, the results obtained in the < 110 > direction involve measurements along the cylinder axis and hence involve a different demagnetisation factor. The values of the initial inverse susceptibility are obtained from the low field magnetic measurements which are greatly affected by the magnetic domains present and hence quality of the sample of MnSi.

The inverse initial susceptibility undergoes a minimum response of 21.0 ± 1.0 at a temperature of 29.2K below which the response is anisotropic. The response initially increases in all directions below the minimum value but to different extents: In < 111 > direction (figure 5.22(a)) the inverse initial susceptibility increases at the lowest rate and peaks at a value of 28.2 ± 1.0 at a temperature of 28.0K before decreasing and levelling at a value of 15.6 ± 1.0 which remains constant at the lowerst temperatures measured.
In < 001 > direction (figure 5.22(b)), the inverse initial susceptibility increases and reaches a maximum value of 35.0 ± 1.0, again at 28.0K, before slightly dipping and then remaining approximately constant at 35.4 ± 1.0 over the lower temperatures measured.

Figure 5.20 The inverse magnetic susceptibility of MnSi as a function of both magnetic field and temperature close to the transition temperature, derived from the magnetisation data with field applied parallel to the < 001 >.

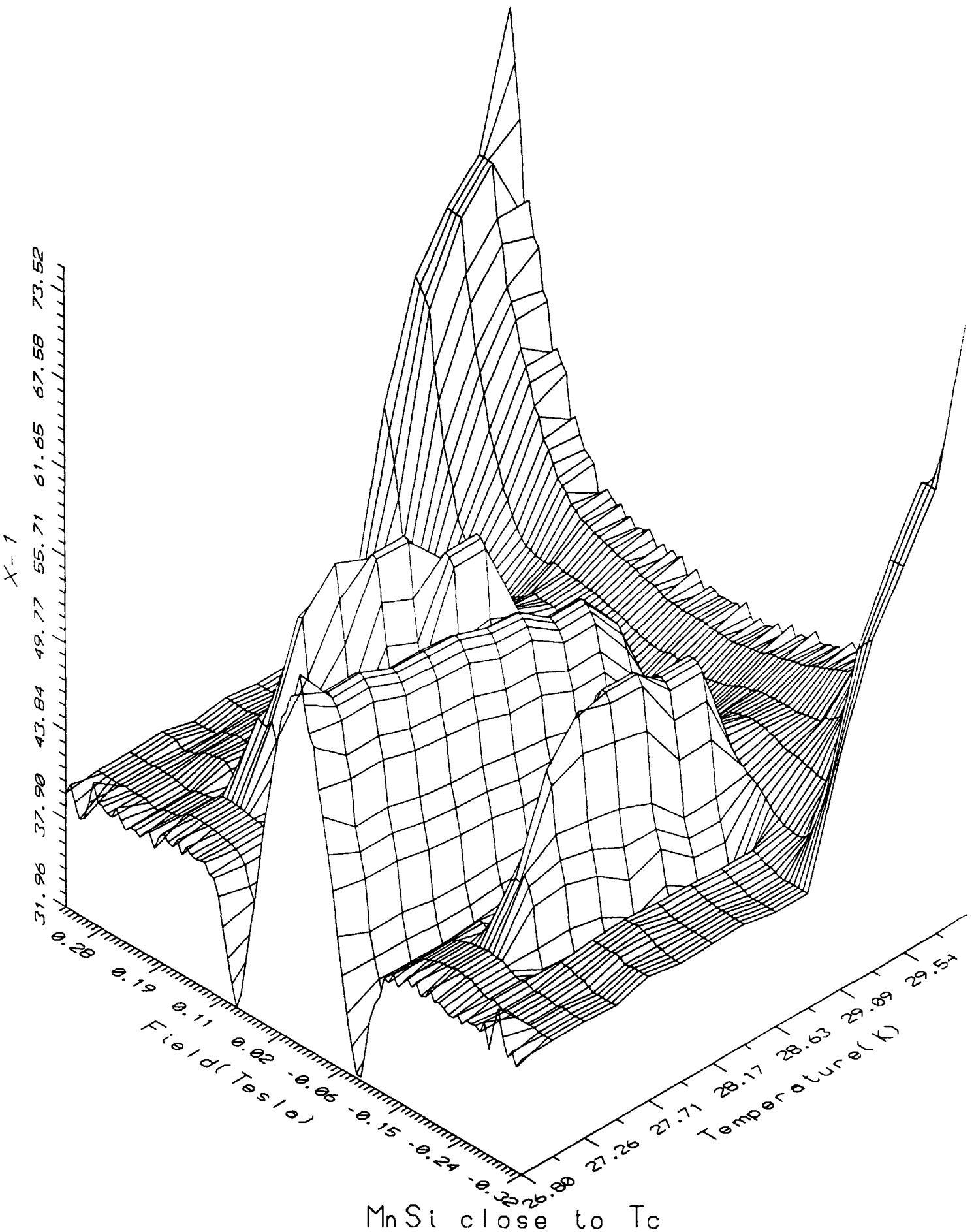

Figure 5.21 The inverse magnetic susceptibility of MnSi as a function of both magnetic field and temperature close to the transition temperature, derived from the magnetisation data with field applied parallel to the < 111 >.

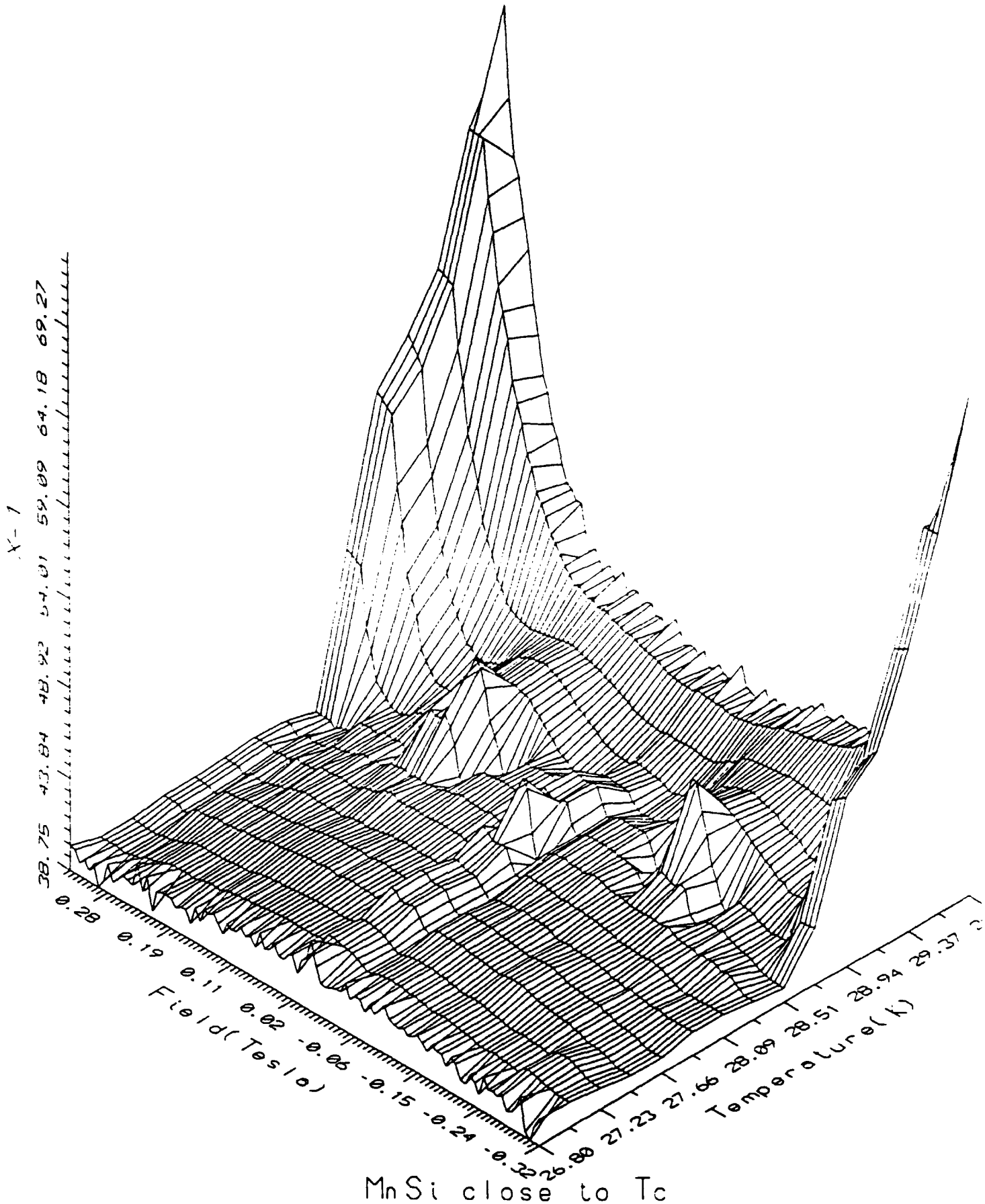

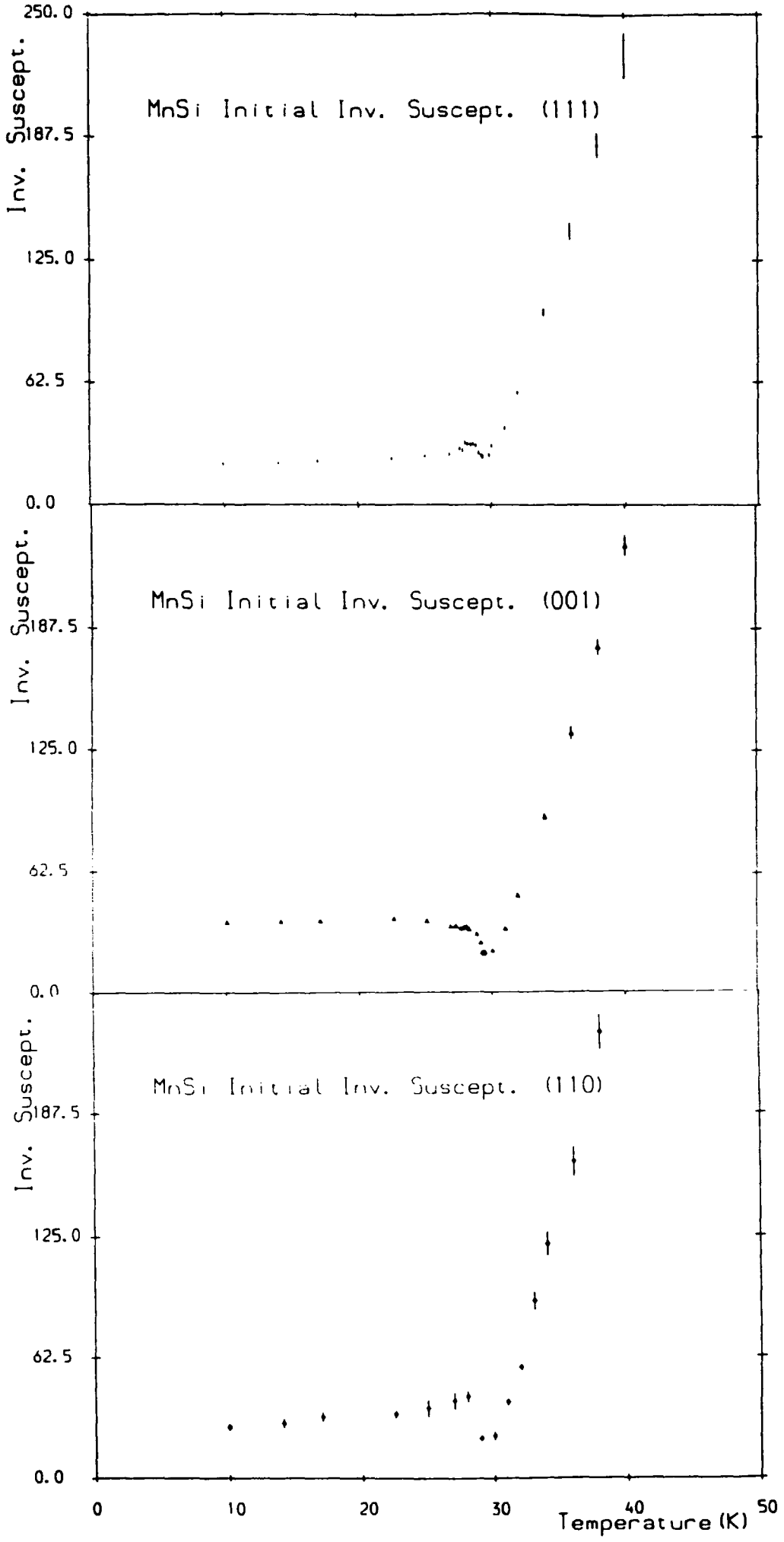

Figure 5.22 (a) - (c)

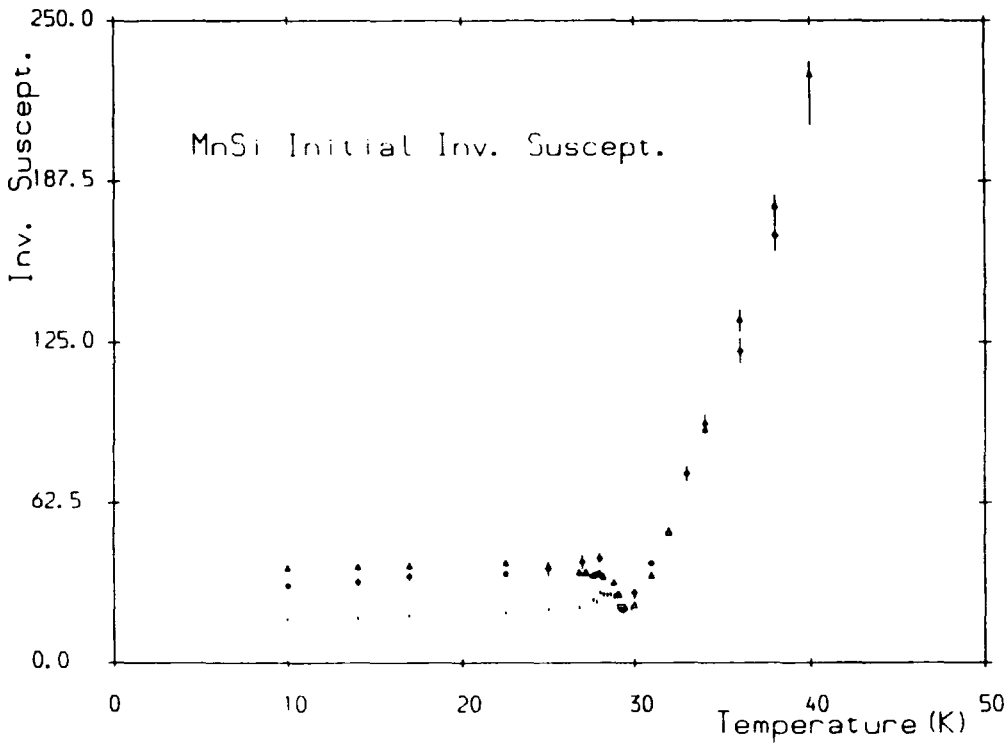

Figure 5.22 The inverse of the initial susceptibility of MnSi as a function of temperature. (a) Magnetic field applied parallel to the < 111 > direction; (b) magnetic field applied parallel to the < 001 > direction; (c) magnetic field applied parallel to the < 110 > direction; (d) combination of the results with magnetic field applied to the < 111 >(points), < 001 >(triangles) and < 110 >(circles) direction.

Unfortunately there is less data available in the < 110 > direction (figure 5.22(c)) close to the transition temperature. The inverse initial susceptibility increases and reaches a maximum value of 36.0 ± 1.0, again at a temperature of 28K. This slowly decreases and levels at a value of 28.1 ± 1.0 at 10K.

From figure 5.22(d), well below the transition temperature the value of inverse susceptibility increases from < 111 > direction through < 110 > to < 001 > direction. This is due to increasing curvature of the magnetisation away from the linear behaviour in the < 111 > direction.

The initial 'bump' in the inverse susceptibility after the minima in the response for a temperature range of 2.8K and most apparent in < 111 > direction is perhaps an indication of either a seperate new phase close to the transition temperature or the onset of the helical phase.

5.10 Further Work on MnSi

It is suggested that further magnetisation measurements be performed on MnSi with magnetic field applied along the < 011 > direction, particularly close to the transition temperature. The main reason for this is the nature of the magnetisation for increasing magnetic field, especially in fields of less than 1000Oe where the response is curved. This is shown in figure 5.8(b) of the inverse suceptibility below the transition temperature. Of particular interest is the sudden decrease in inverse susceptibility at a field of 300 ± 30Oe at 25.0K as compared to the gradual decrease in inverse susceptibility over the corresponding field range when applied along the < 001 > direction.

Another area of investigation currently untouched is magnetic measurements on MnSi close to the transition temperature but with an emphasis on increasing temperature, in order to investigate how the helical phase collapses in to the paramagnetic state.

Finally, magnetic measurements could be performed on MnSi with magnetic field applied along a non principle crystallographic direction in order to study the incommensurate nature of the helix.

5.11 References

Bloch D. *et al.*(1975), Phys. Lett **A51**, 259-261.
Brown S.(1990), Ph. D. Thesis, University of Cambridge.
Ishikawa Y.*et al.*(1976), Solid State Commun. **19**,525-528.
Kadowaki K. *et al.*(1981), J. Phys. Soc. Jpn. **51**, 2433-2438.

Chapter 6

Magnetic Measurements on Cubic Iron-Germanium (FeGe)

6.1 The Iron-Germanium Sample

Magnetic measurements were performed on a single crystal of FeGe which was also used for the small angle neutron scattering work of Lebech *et al.* (1989). It was grown by Richardson (1967) using a method based on a halogen chemical transport reaction. The crystal is of somewhat irregular shape which can be approximated to a flattened sphere of diameter 1mm, and had a mass of 46.5mg. It was orientated on the Risø four-circle neutron diffractometer and measurements reported in this thesis are with magnetic field applied along a $< 100 >$ direction. Measurements were performed for decreasing temperatures and with field steps of 50Oe unless otherwise stated. The points on the graphs are the raw data and the solid line drawn through them is the average for a particular magnetic field.

6.2 Magnetisation of FeGe close to the Critical Temperature

Above the critical temperature, the magnetisation of FeGe is paramagnetic (see figure 6.1(a)), though at 279K not linear with field. It shows a large amount of curvature with no apparent saturation observed in the field range studied. The inverse susceptibility (figure 6.2(a) and (d)) reflects this, showing a a parabolic response in applied field with minimum in zero field, a value of 9.2 ± 0.5

As the temperature is reduced below the transition temperature ($\approx 278K$) where a helical spin density wave forms in equivalent $< 100 >$ directions (Lebech (1989)), a sharp increase in magnetisation occurs in low magnetic fields (figure 6.1(b) and (c)), after a 'knee' in the response is observed at a field of 128Oe. The magnetisation below this increases linearly with field, and above it, although increasing in a much reduced manner, shows no sign of saturation. This is apparent in magnetisation measurements in fields of up to 120kOe (see figure 6.16(a)) and characteristic of

In figures 6.1 - 6.2 the internal magnetic field ($H_i = H - H_D$) has been called B and given the units gauss. Magnetisation is measured in units of $emucm^{-3}$ and can be converted to units of $emug^{-1}$ using the density of FeGe which is $8.25gcm^{-3}$.

Figure 6.1 The magnetisation of FeGe with applied magnetic field parallel to the $< 100 >$ direction. The solid line is an average through the data points for a given field value and is a measure of the experimental uncertainty. (a) 279K; (b) 278K; (c) 277.6K.

Figure 6.2 The inverse magnetic susceptibility of FeGe with field applied parallel to the $< 100 >$, derived from the magnetisation data. The solid line is an average through the data points for a given field value and is a measure of the experimental uncertainty. (a) 279K, field range $\pm$2500Oe; (b) 278K, field range $\pm$2500Oe; (c) 277.6K, field range $\pm$2500Oe; (d) 279K, field range $\pm$500Oe; (e) 278K, field range $\pm$500Oe; (f) 277.6K,field range $\pm$500Oe.

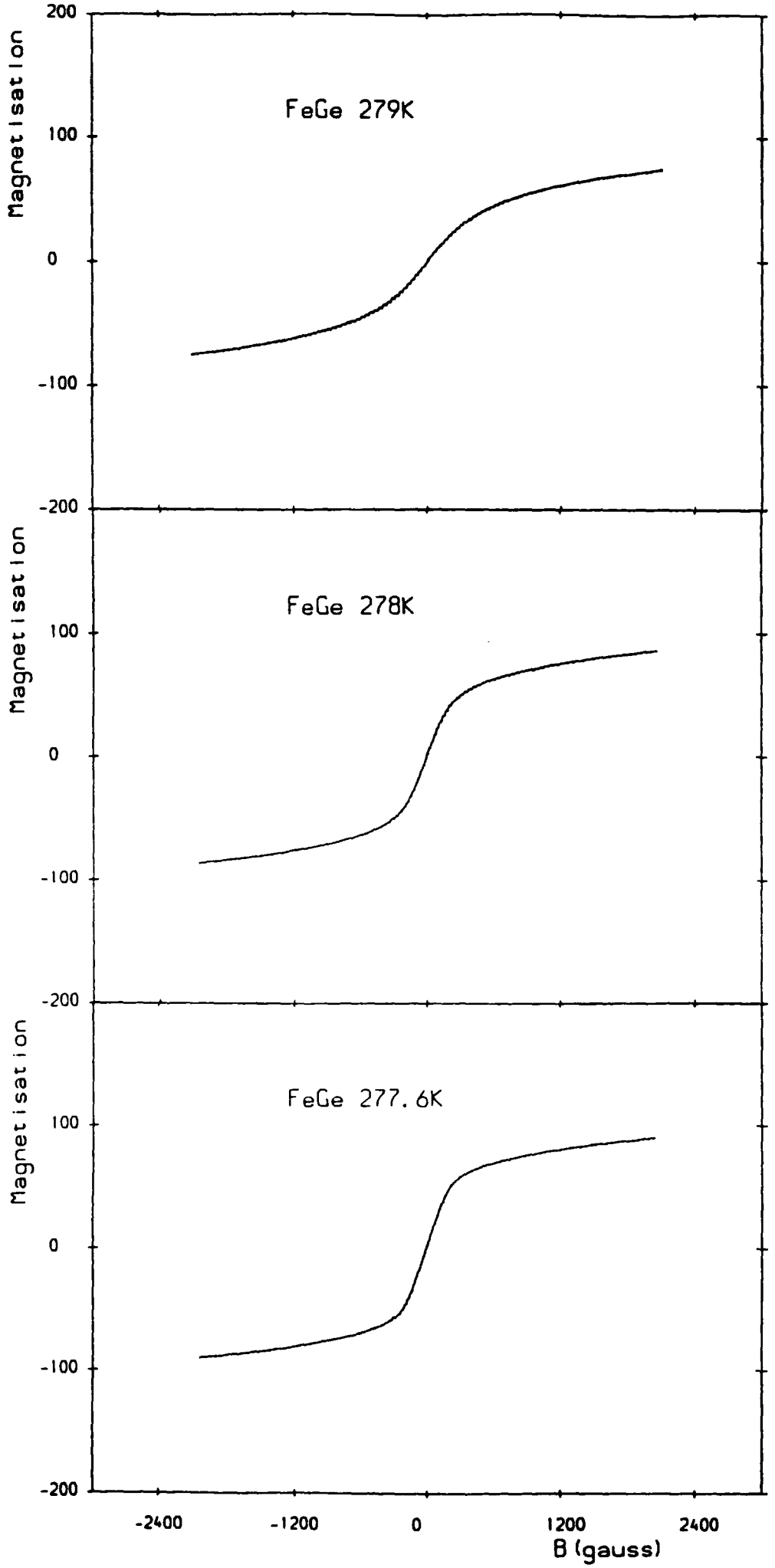
FeGe 279K
FeGe 278K
FeGe 277.6K
Magnetisation
200
100
0
-100
-200
-2400
-1200
0
1200
2400
B (gauss)

Figure 6.1 (a) - (c)

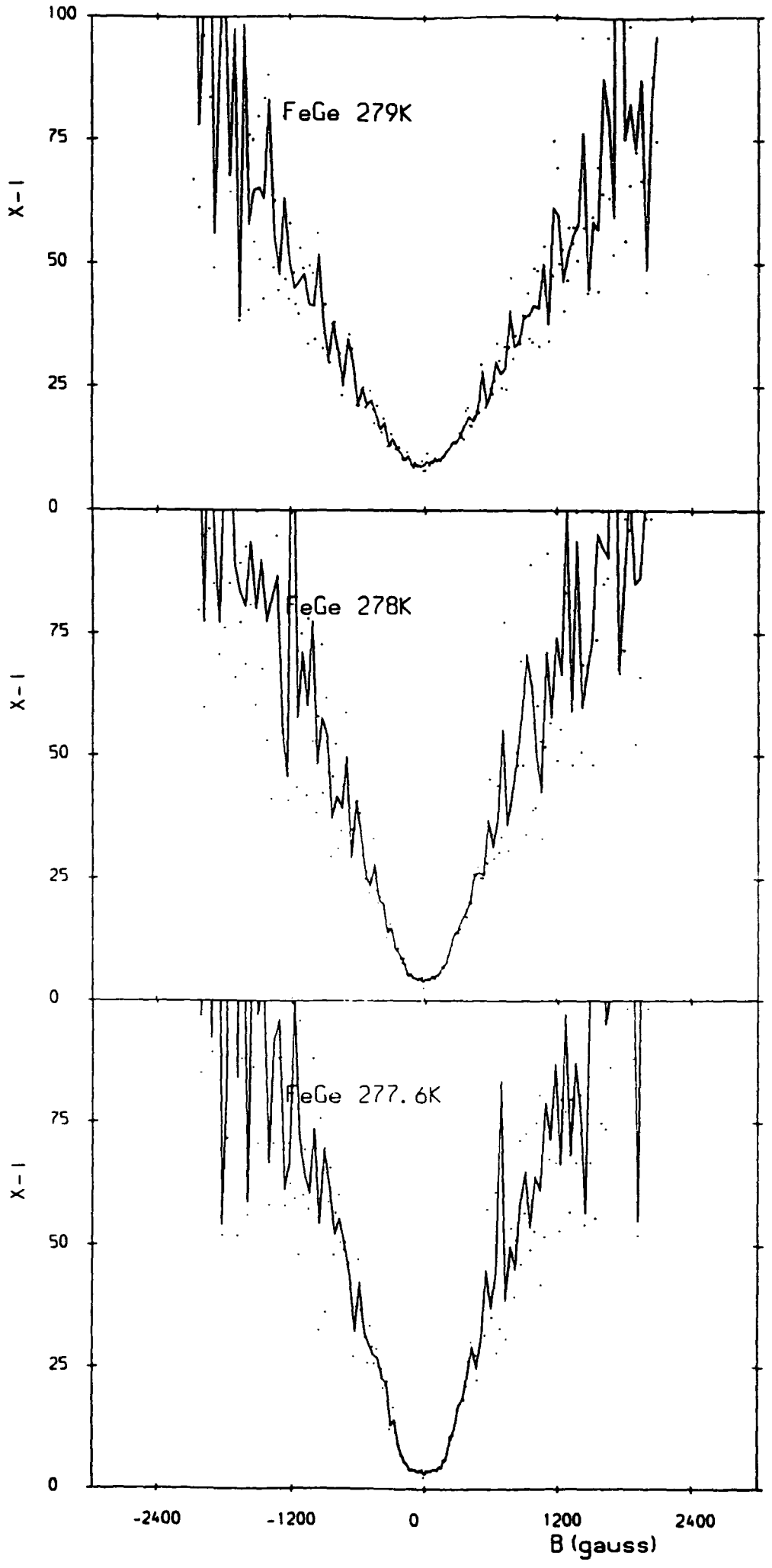
FeGe 279K
FeGe 278K
FeGe 277.6K
X-1
100
75
50
25
0
-2400
-1200
0
1200
2400
B (gauss)

Figure 6.2 (a) - (c)

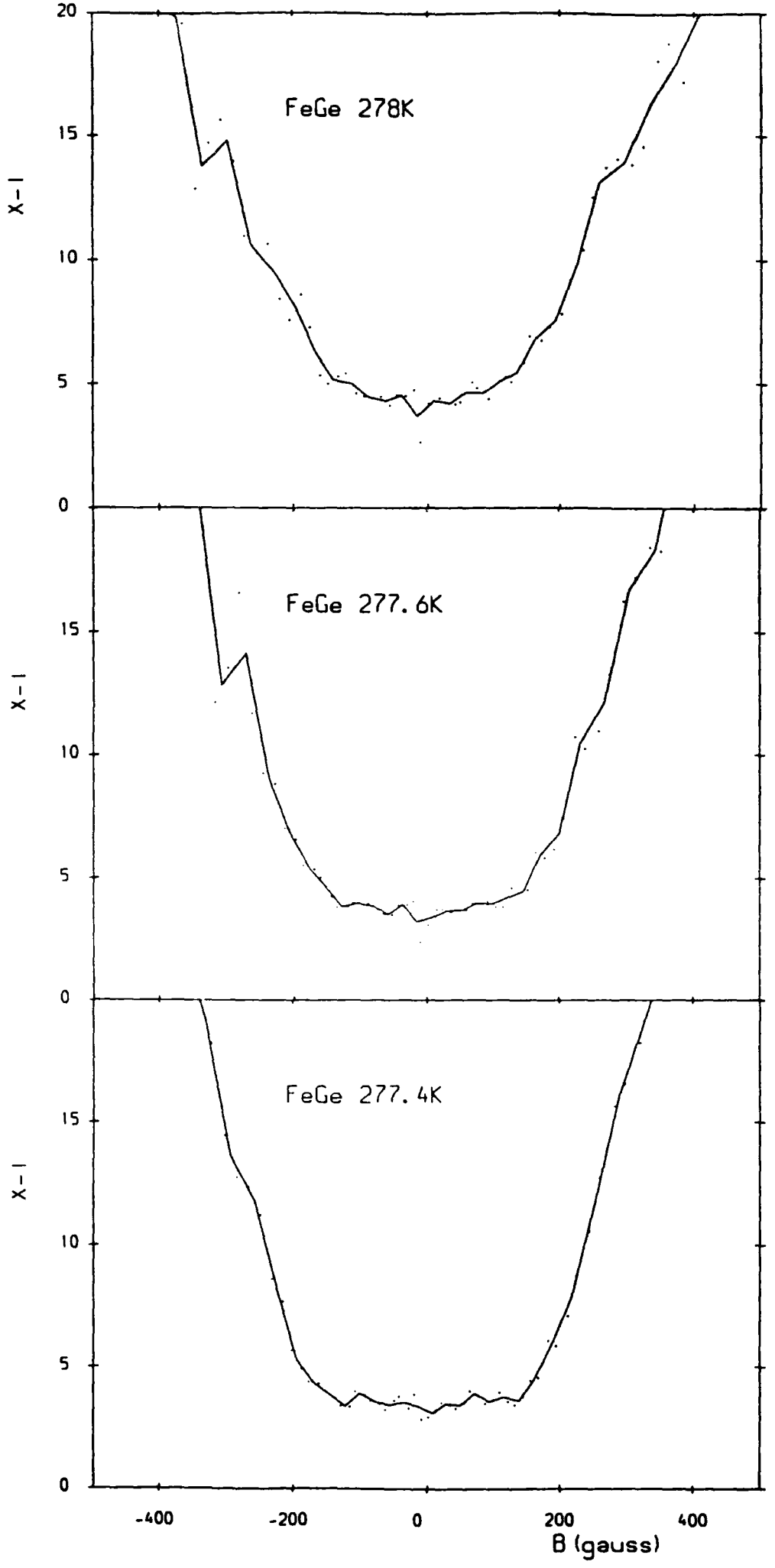
FeGe 278K
FeGe 277.6K
FeGe 277.4K
X-I
20
15
10
5
0
-400
-200
0
200
400
B (gauss)

Figure 6.2 (d) - (f)

itinerant systems. The response of the inverse susceptibility is similar to that above the transition (figure 6.1(b), (c), (e) and (f)), though remains constant in the low field regime at a value of 4.2 ± 0.5. As the temperature is lowered, again the nature of the magnetisation remains similar although the low field, linear region extends to increasingly higher fields.

6.3 Observation of a Field Induced Phase Close to the Upper Transition Temperature

In cubic FeGe, the magnetic response is very sensitive to small changes in applied field and 'saturation' occurs in a much lower field than in the helimagnet MnSi (N.B. although there is a well defined 'knee' in the magnetisation, application of large magnetic fields shows the system is in fact far from saturation). Consequently field steps of 20Oe were used to characterise the magnetisation of FeGe close to but below the transition temperature.

Figure 6.3 reveals the magnetisation in low magnetic fields (i.e.$<$ 320Oe) is not linear with applied field but has a 'shoulder' in the field region of 60 - 200Oe where the inverse susceptibility is greater than the other low field region. This occurs in a temperature range of 277 - 274K. The points on the graphs of inverse susceptibility in figure 6.4 are raw data derived from the magnetisation while the solid line is the data after being smoothed (see Appendix B). The distribution of points about the line gives an indication of the errors involved. It is evident there is a sudden increase in the inverse susceptibility, well above the noise level. The fields at which this step occurs are shown in figure 6.6 against temperature, together with the 'saturating' magnetic field. At a temperature of 273.4K (figure 6.5) there is no evidence of this 'shoulder'.

This is tentatively regarded as a field induced phase transition, similar to the so called 'Phase A' observed in MnSi (see Chapters 5 and 7). It is marked by a region of higher inverse susceptibility and the field at which it commences gradually increases as the temperature is lowered whereas the magnetic field at which it is complete remains approximately fixed.

6.4 Magnetic Measurements above the Lower Transition Temperature

At the temperatures down to 210K, the magnetisation in the low field region increases linearly with field (apart from the small temperature and field space described above and shown in figure 6.6), the inverse susceptibility having a value of 3.3 ± 0.3. The lower transition corresponds to rotation of the helical spin density wave into equivalent $< 111 >$ directions as described by Lebech *et al.* (1989). There is 'pronounced temperature hysteresis' of the transition and therefore the magnetic response of FeGe was recorded for both increasing and decreasing temperature in

In figures 6.3 - 6.5 the internal magnetic field ($H_i = H - H_D$) has been called B and given the units gauss. Magnetisation is measured in units of $emucm^{-3}$ and can be converted to units of $emug^{-1}$ using the density of FeGe which is $8.25gcm^{-3}$.

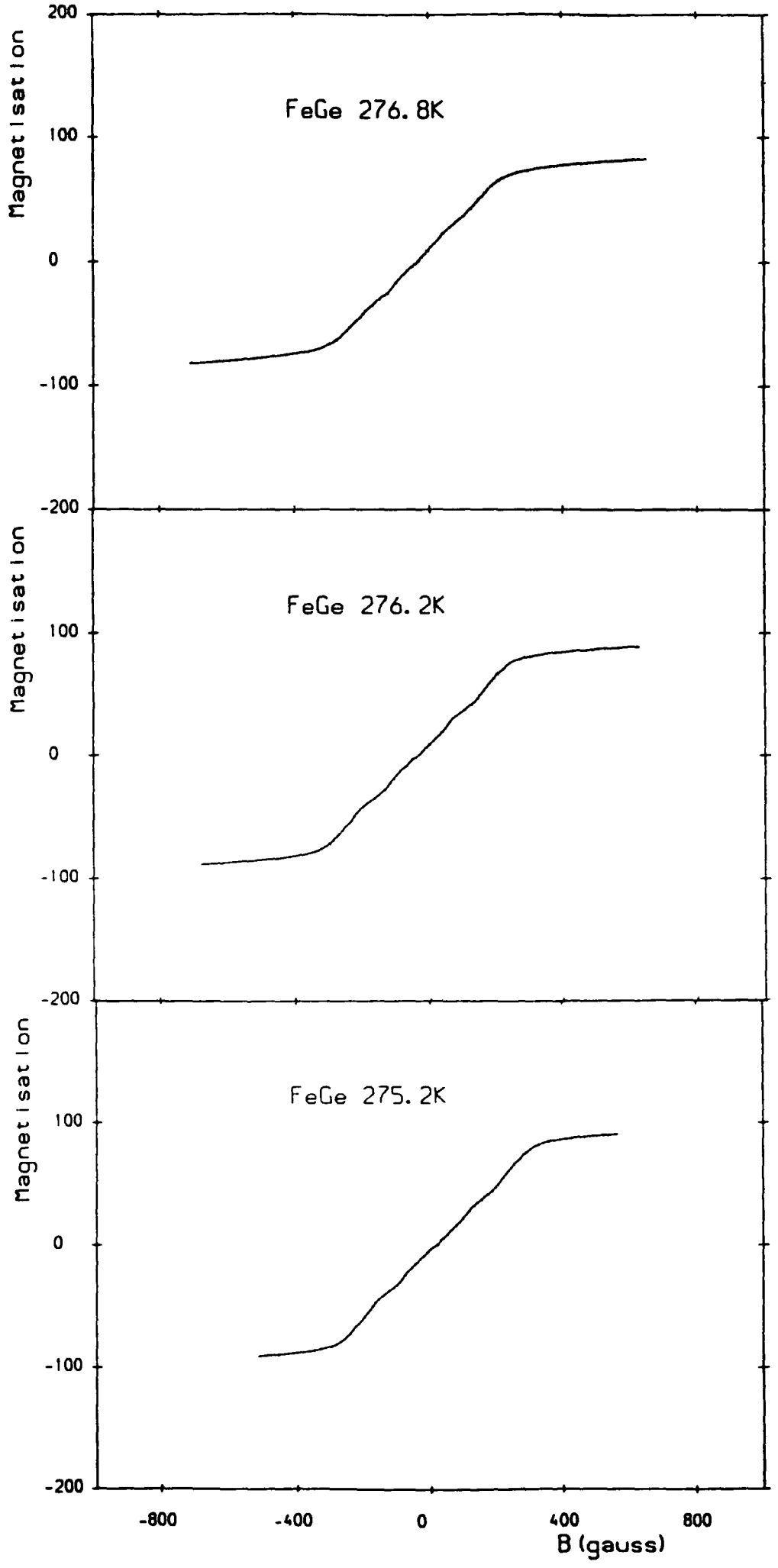
FeGe 276.8K
FeGe 276.2K
FeGe 275.2K
Magnetisation
200
100
0
-100
-200
-800
-400
0
400
800
B (gauss)

Figure 6.3 (a) - (c)

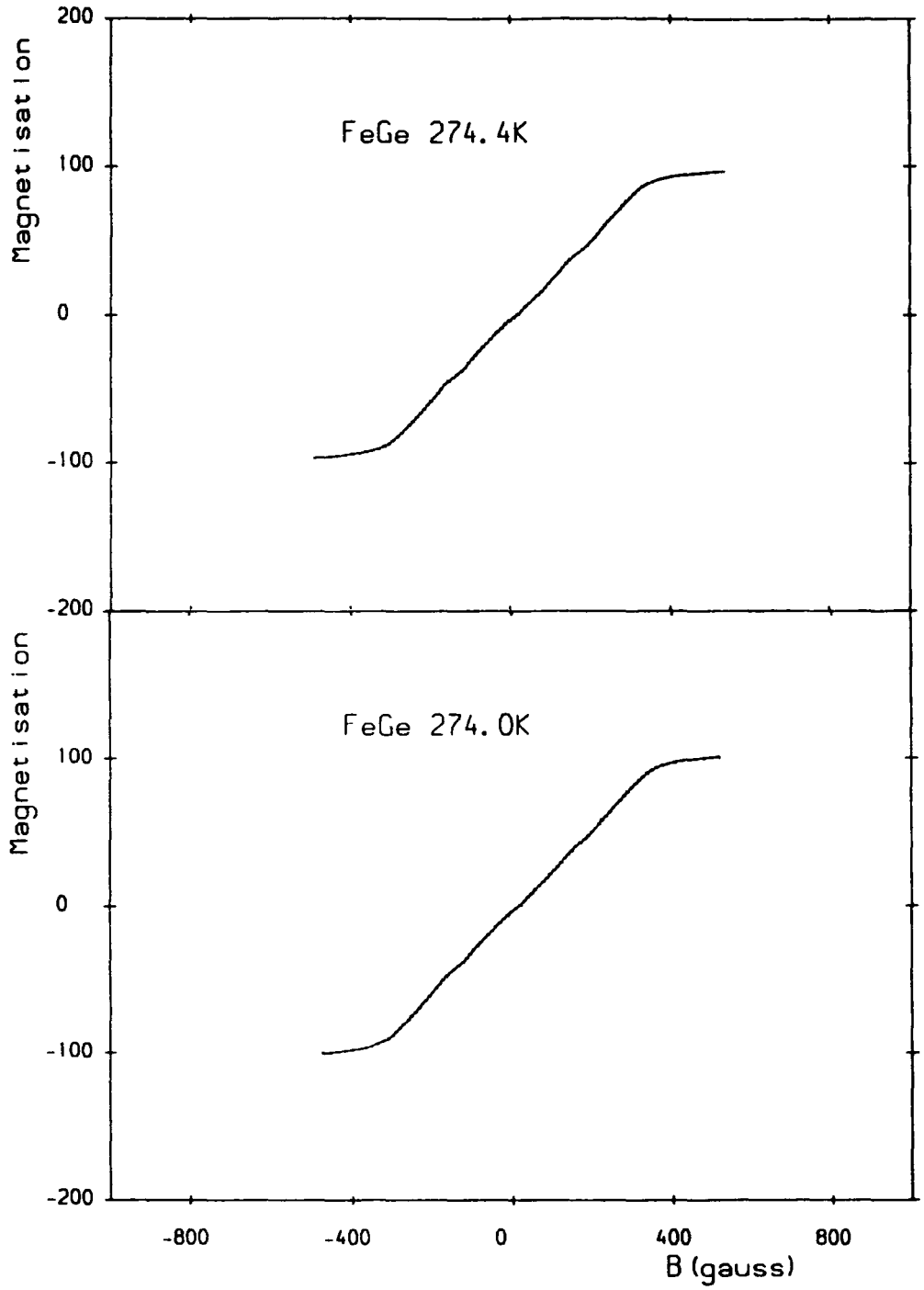

Figure 6.3 The magnetisation of FeGe with applied magnetic field parallel to the < 100 > direction. The solid line is an average through the data points for a given field value and is a measure of the experimental uncertainty. (a) 276.8K; (b) 276.2K; (c) 275.2K; (d) 274.4K; (e) 274.0K.

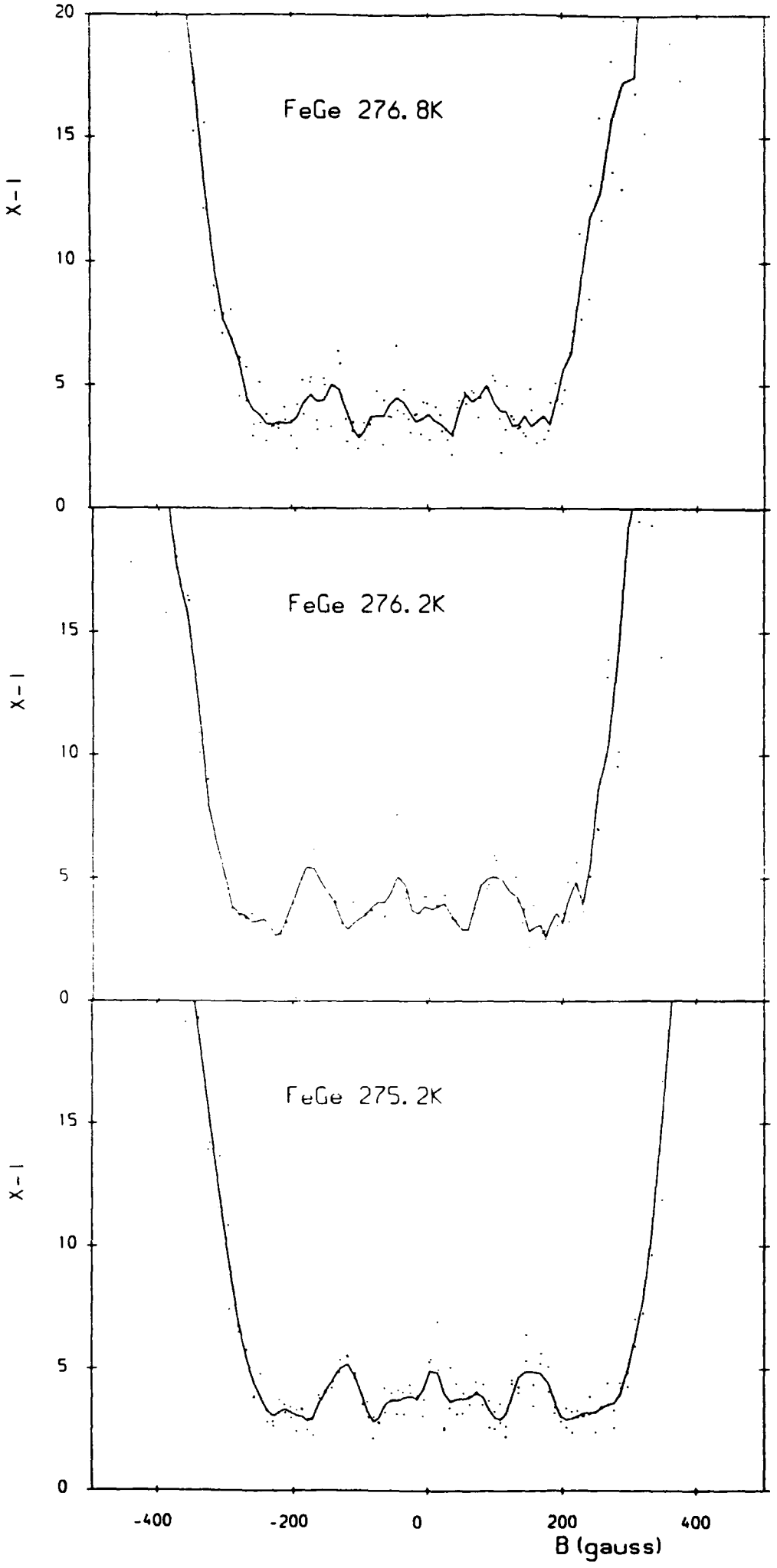
FeGe 276.8K
FeGe 276.2K
FeGe 275.2K
X-I
20
15
10
5
0
-400
-200
0
200
400
B (gauss)

Figure 6.4 (a) - (c)

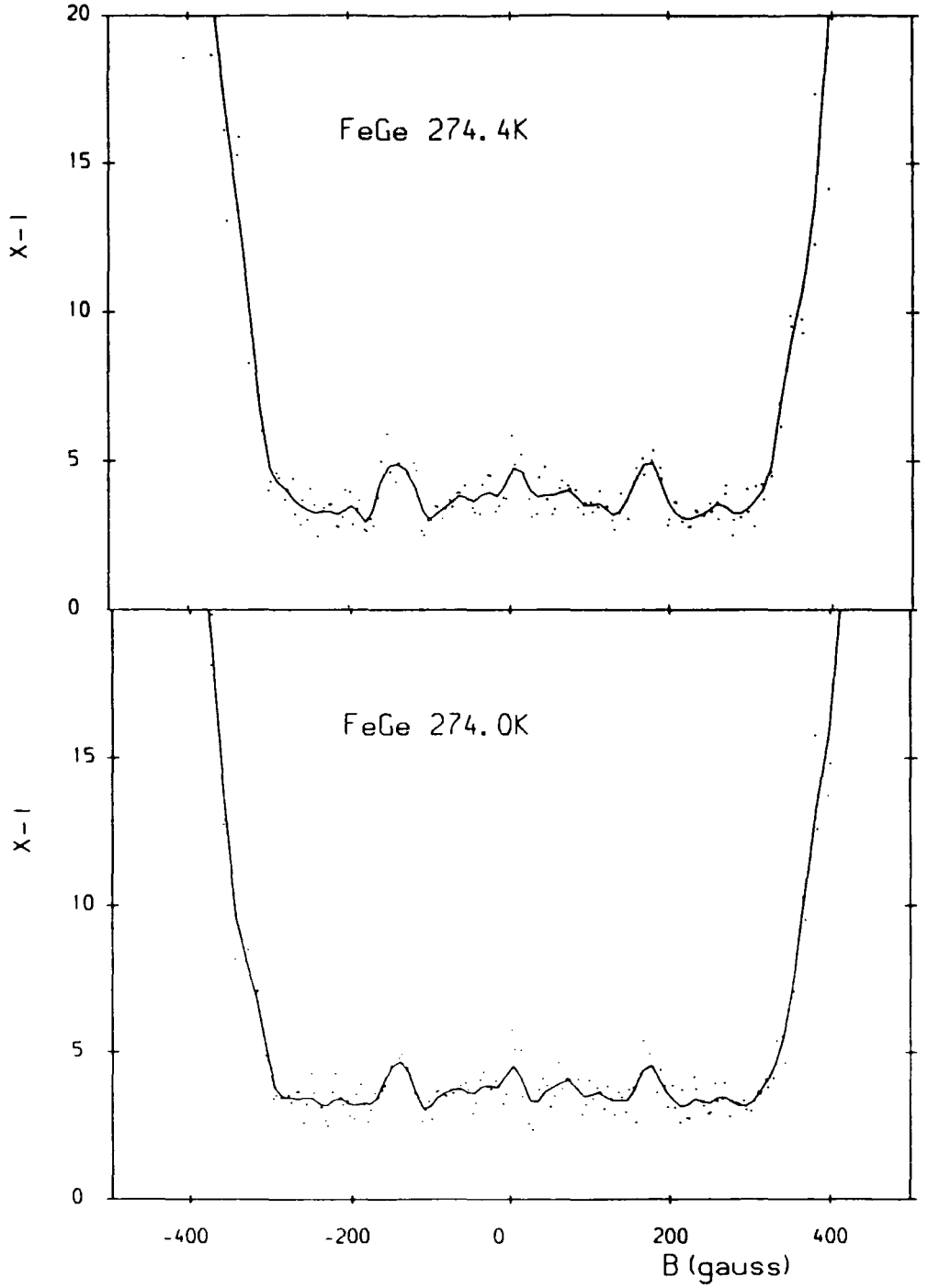

Figure 6.4 The inverse magnetic susceptibility of FeGe with field applied parallel to the < 100 >, derived from the magnetisation data. The solid line is the data (points) after being smoothed (see Appendix 2). (a) 276.8K; (b) 276.2K; (c) 275.2K; (d) 274.4K; (e) 274.0K.

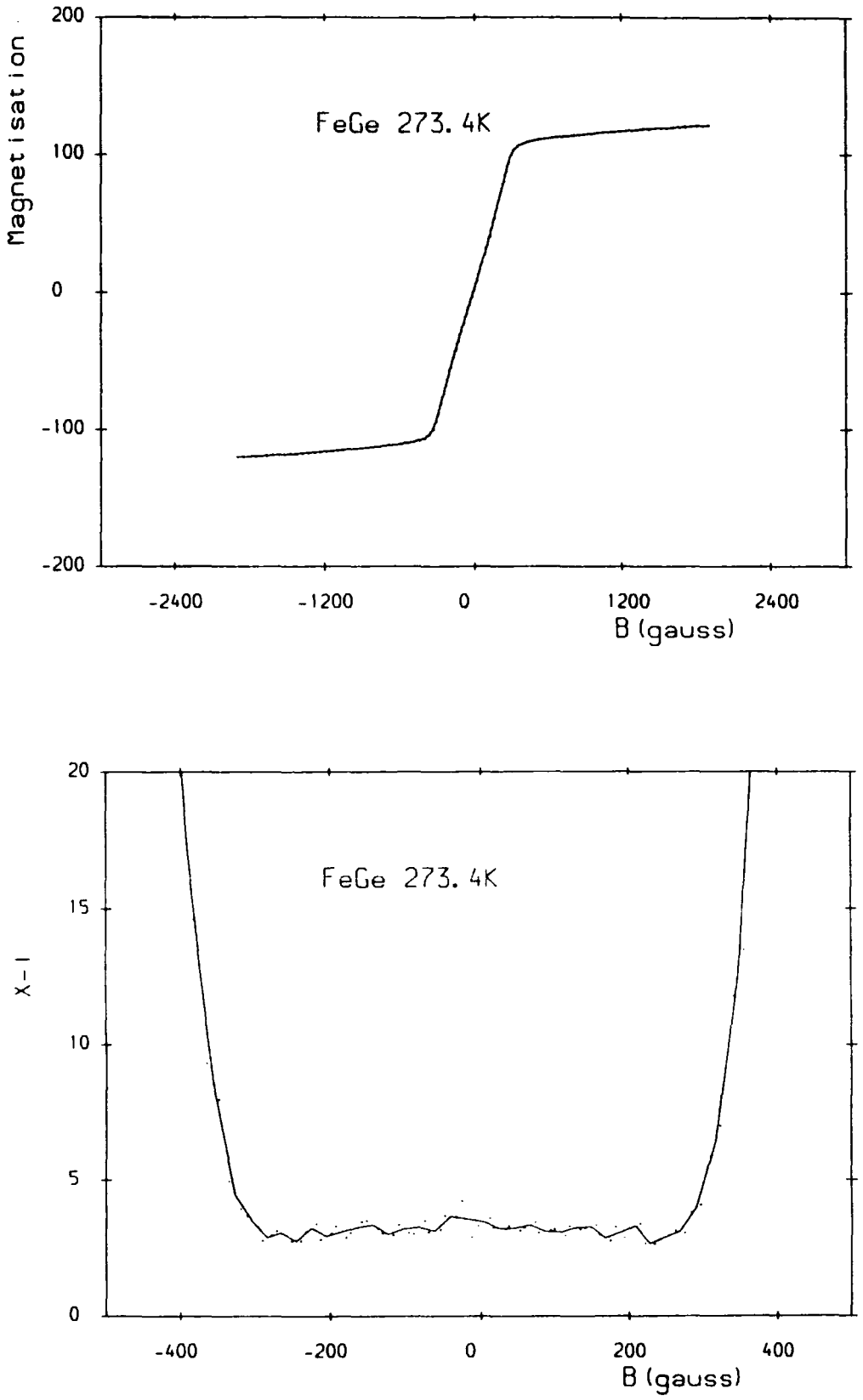

Figure 6.5 (a) The magnetisation of FeGe with magnetic field applied parallel to the < 001 > direction at a temperature of 273.4K; (b) the inverse magnetic susceptibility of FeGe with field applied parallel to the < 100 > at a temperature of 273.4K derived from the magnetisation data. In both cases, the solid line is an average through the data points for a given field value and is a measure of the experimental uncertainty.

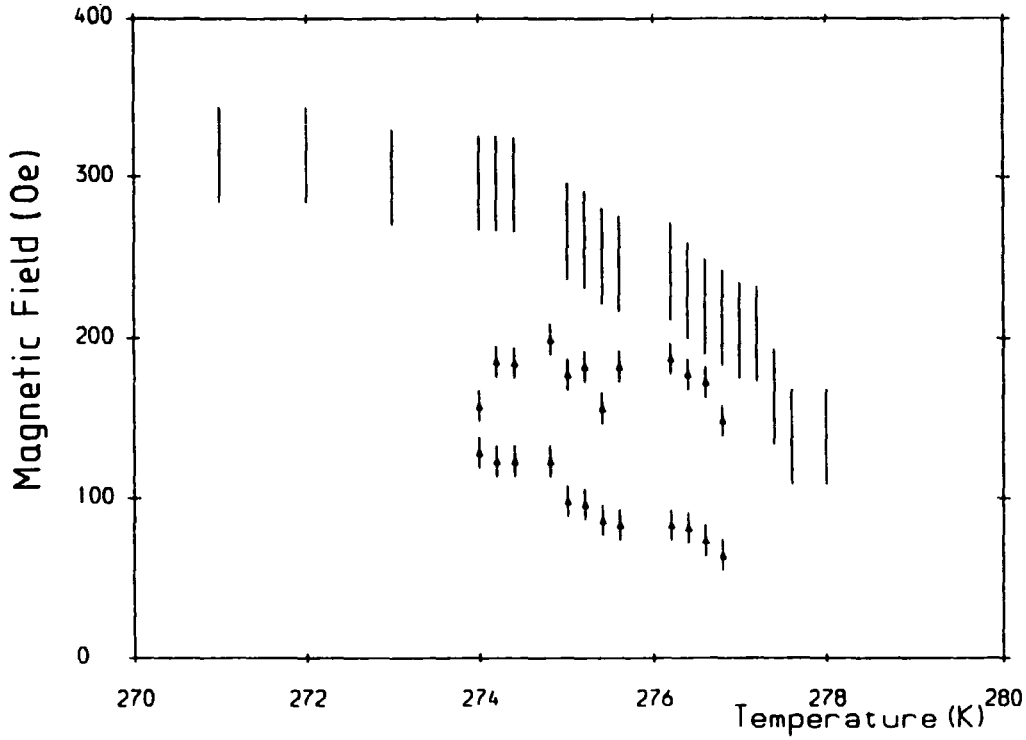

Figure 6.6 Field position of the 'knee' in the magnetisation of FeGe with field applied parallel to the < 100 > direction (points) and the field positions of the onset and conclusion of the region of increased inverse susceptibility (triangles) in an applied magnetic field close to the transition temperature.

the range 245 - 210K. The temperature was in fact lowered to 180K i.e. well below the second transition temperature.

The low field magnetisation of cubic FeGe (figure 6.7 - 6.10) was linear in both cases however there is variation in the 'saturating' field for increasing and decreasing temperature data as shown in figure 6.9. Both values of field are shown for each temperature on figure 6.14 with the 'saturation' field for decreasing temperature being greater than that for increasing temperature. The linear magnetisation regions have the same value of inverse susceptibility of 3.3 ± 0.3 at all temperatures in this regime.

6.5 Magnetic Measurements Below the Lower Transition Temperature (211K for decreasing temperature)

Unlike MnSi, FeGe has two transitions with the helix propagating along $< 111 >$ directions below 211K (for decreasing temperature). Figure 6.11 shows the magnetisation below this temperature.

At 210K there is no evidence of this transition with low field behaviour remaining linear with applied field upto a 'saturation field' of 780Oe. However, at a temperature of 200K (figure 6.11(a)), the magnetisation below a field of 80Oe is a curved, concave response, before increasing linearly with magnetic field, with the same value of inverses susceptibility as above the lower transition temperature (3.3 ± 0.3), and finally 'saturating'. The curved region manifests itself as a peak in the inverse susceptibility, with maximum in zero field of 5 ± 0.5 (figure 6.12(a) and 6.13(a)) which then reduces linearly to a minimum before gradually increasing until 'saturation' of the magnetisation.

By 180K (figure 6.11(b)), this low field feature becomes more prominent, with curved magnetisation extending to a larger field before becoming linear and finally 'saturating'. This trend continues as the temperature is lowered (figure 6.11, 6.12 and 6.13) and at a temperature of 80K (figure 6.11(g), 6.12(g) and 6.13(g)) the curved region of magnetisation extends to a field of 400Oe. The inverse susceptibility is a maximum in zero field with a value of 7.2 ± 0.3 and decreases linearly to a minimum value of 2.9 ± 0.3 at a field of 290 ± 20Oe. It then gradually increases to a value of 5 though is still increasing at 'saturation' and is identical for both increasing and decreasing fields. The field position at which the minimum occurs in the response is plotted in figure 6.14(b) for temperatures below the lower transition.

6.6 Magnetic Phase Diagram of Cubic FeGe

The magnetic phase diagram of FeGe is shown in figure 6.14 with its constituents of 'saturation' field, domain reorientation field and field induced phase close to the first transition temperature.

In figures 6.7 - 6.13 the internal magnetic field ($H_i = H - H_D$) has been called B and given the units gauss. Magnetisation is measured in units of $emucm^{-3}$ and can be converted to units of $emug^{-1}$ using the density of FeGe which is $8.25gcm^{-3}$.

Figure 6.7 The magnetisation of FeGe with magnetic field applied parallel to the < 100 > direction for decreasing temperature. The solid line is an average through the data points and is a measure of the experimental uncertainty. (a) 240K; (b) 230K; (c) 220K.

Figure 6.8 The inverse magnetic susceptibility of FeGe with magnetic field applied parallel to the < 100 > direction for decreasing temperature, derived from the magnetisation data. (a) 240K; (b) 230K; (c) 220K.

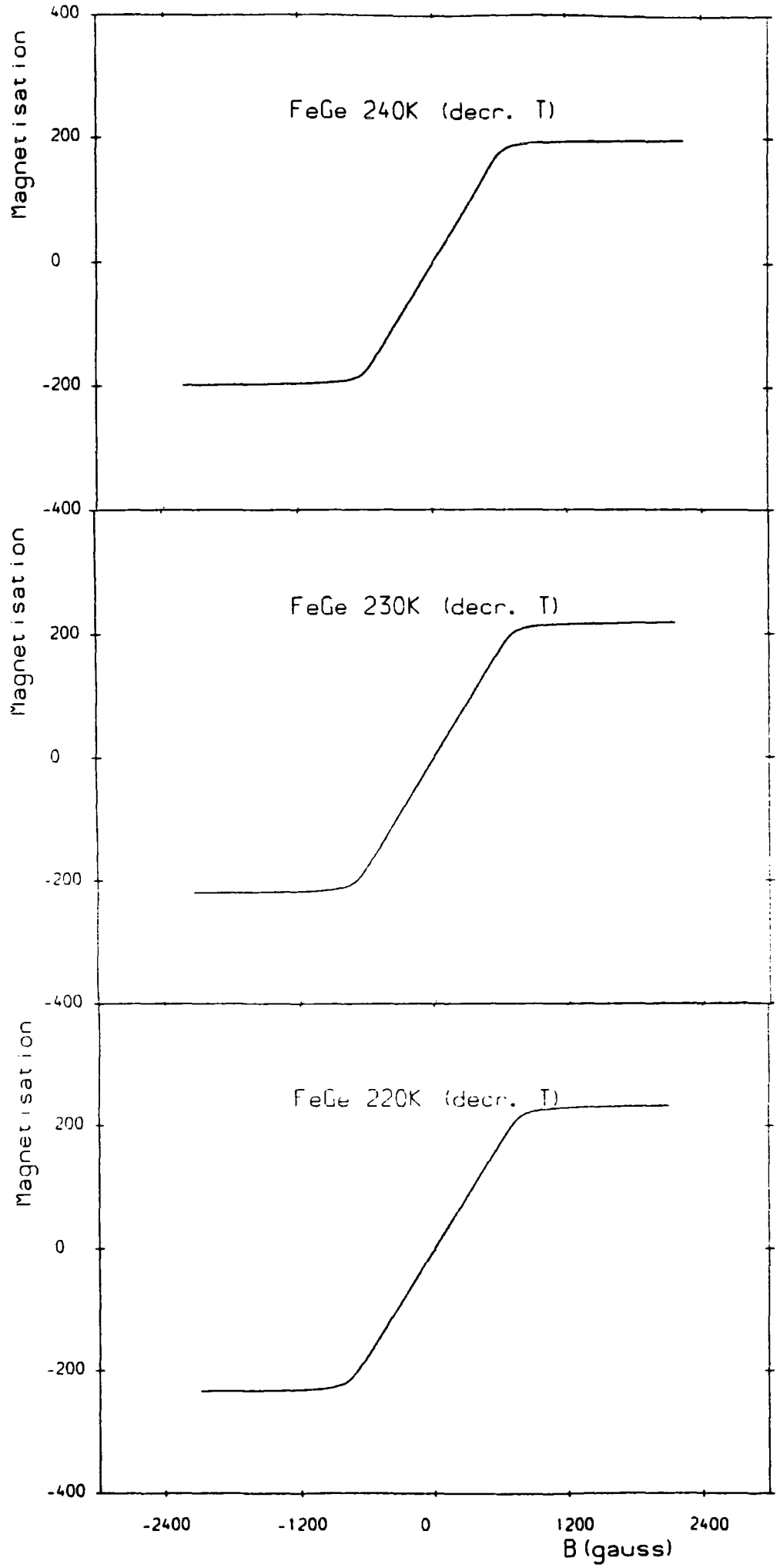
FeGe 240K (decr. T)
FeGe 230K (decr. T)
FeGe 220K (decr. T)
Magnetisation
400
200
0
-200
-400
-2400
-1200
0
1200
2400
B (gauss)

Figure 6.7 (a) - (c)

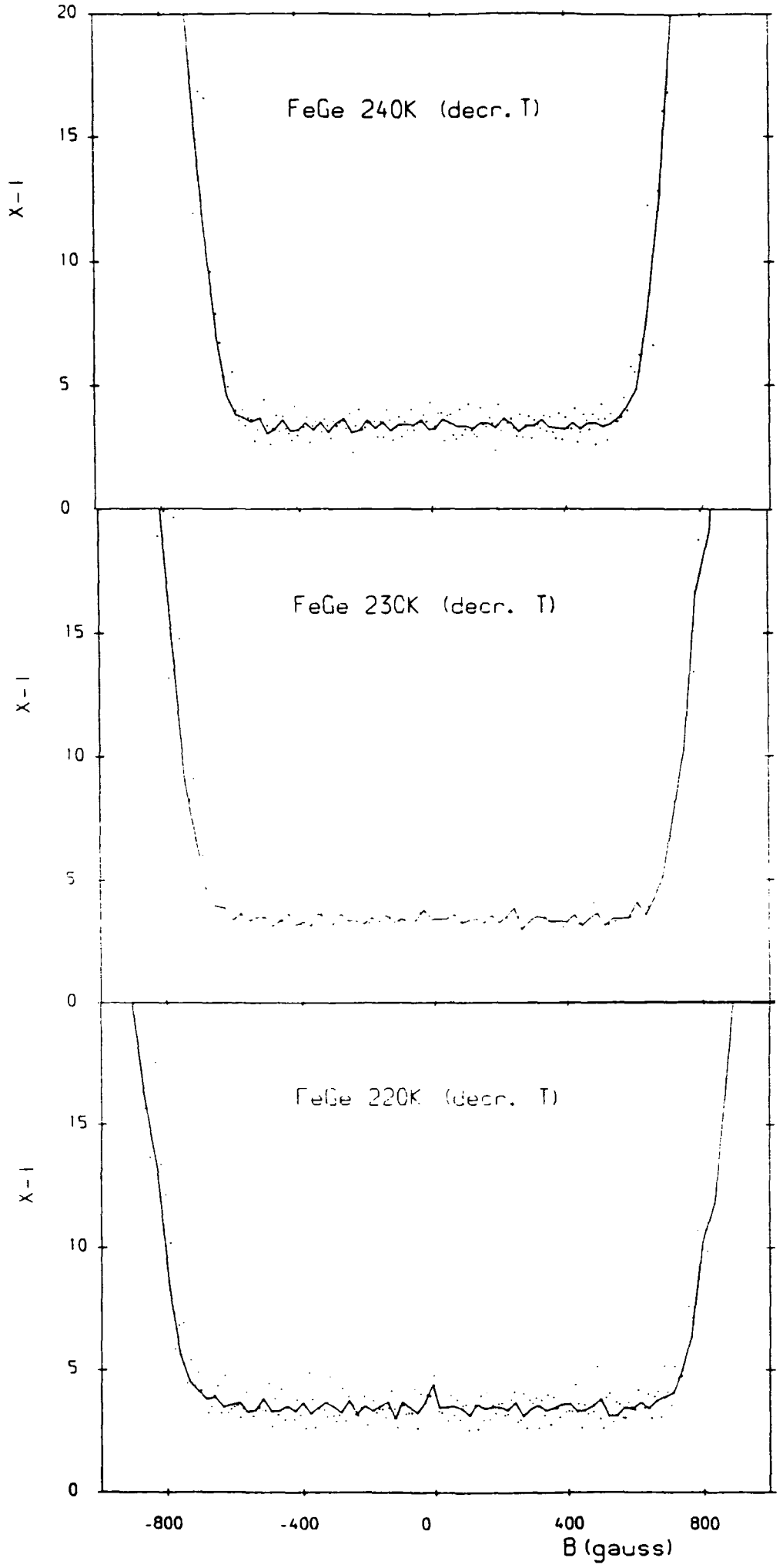
FeGe 240K (decr. T)
FeGe 230K (decr. T)
FeGe 220K (decr. T)
χ - 1
20
15
10
5
0
-800
-400
0
400
800
B (gauss)

Figure 6.8 (a) - (c)

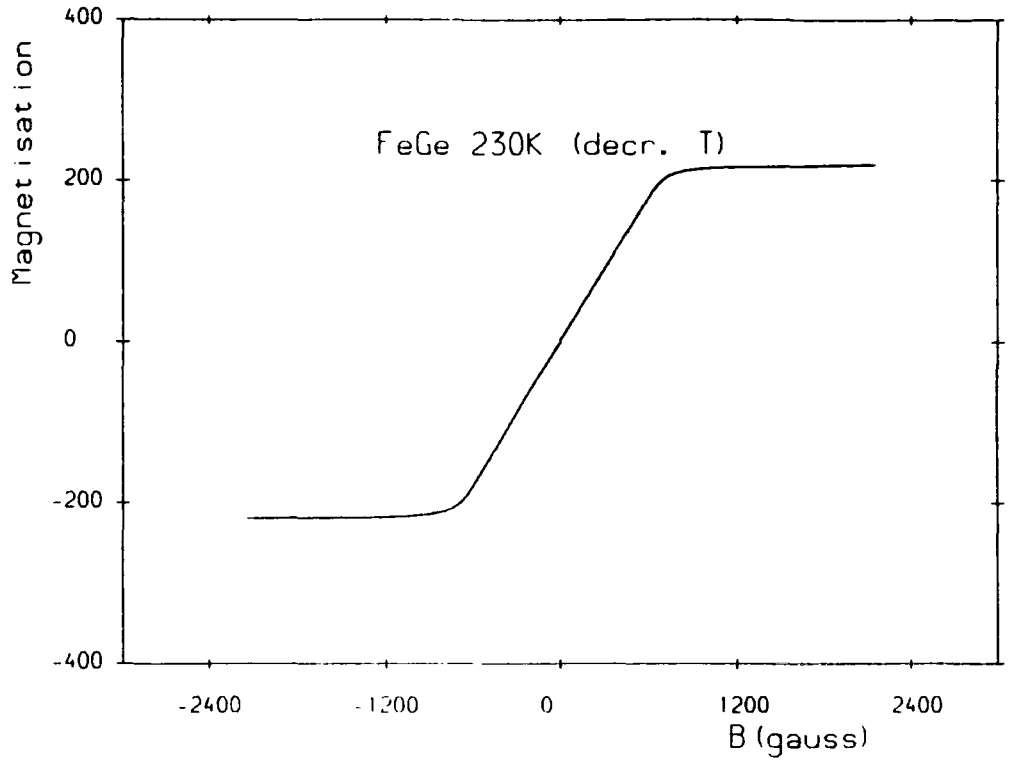

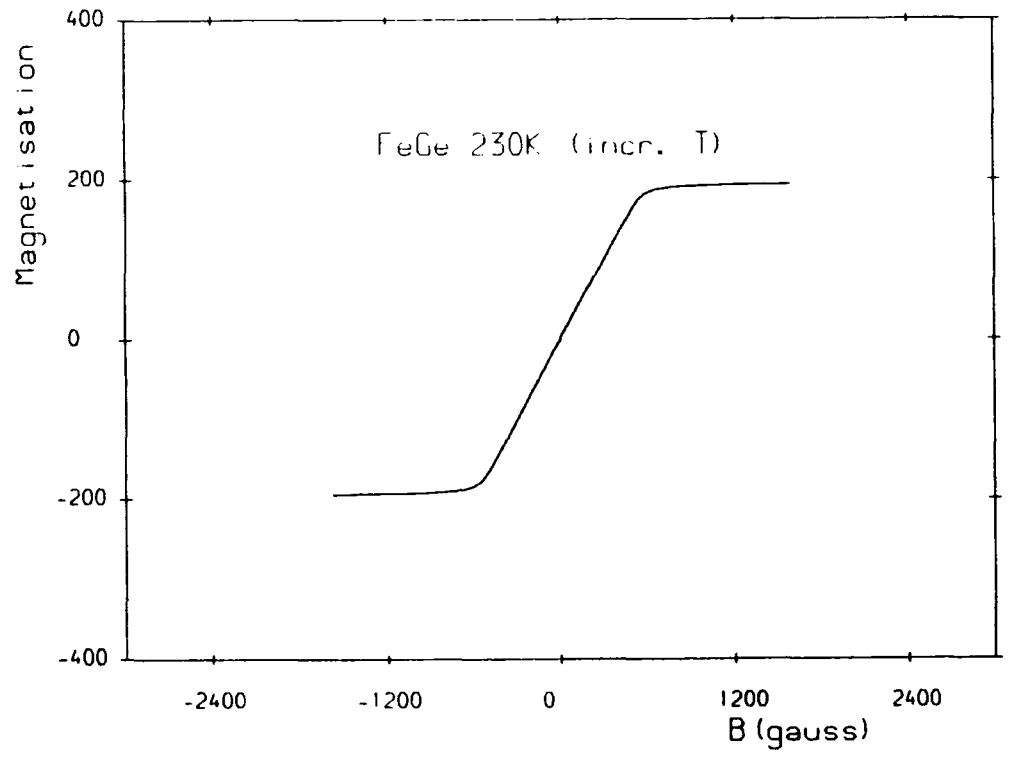

Figure 6.9 (a) The magnetisation of FeGe with magnetic field applied parallel to the < 100 > direction at 230K when lowering the temperature; (b) The magnetisation of FeGe with magnetic field applied parallel to the < 100 > direction at 230K but for increasing the temperature (from 180K).

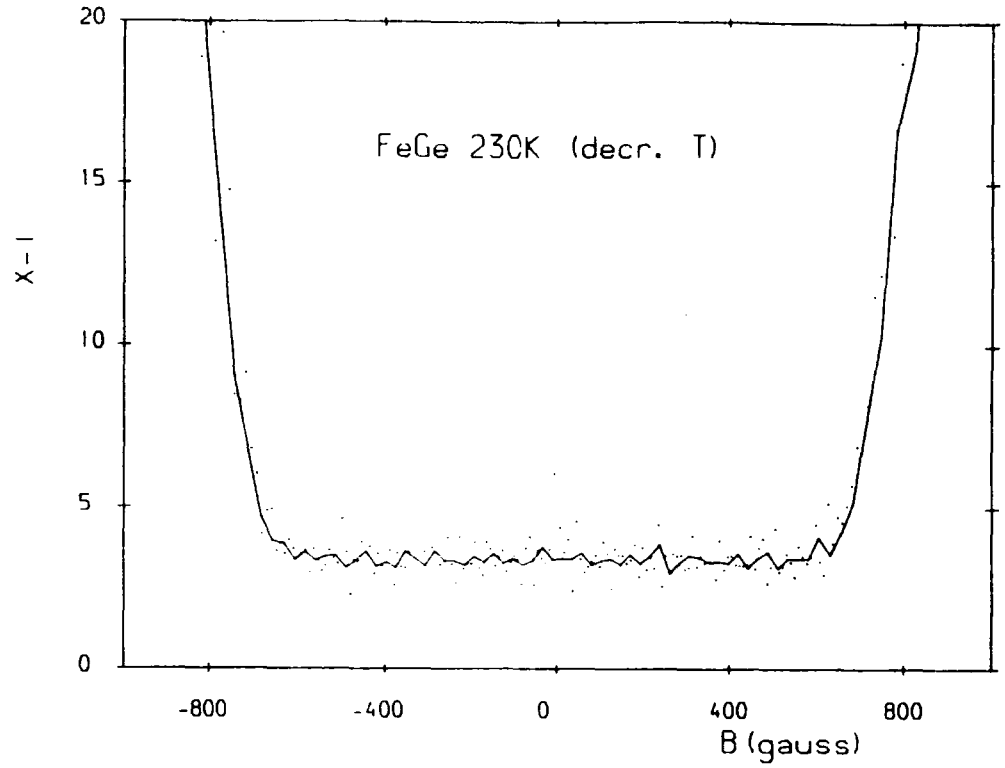

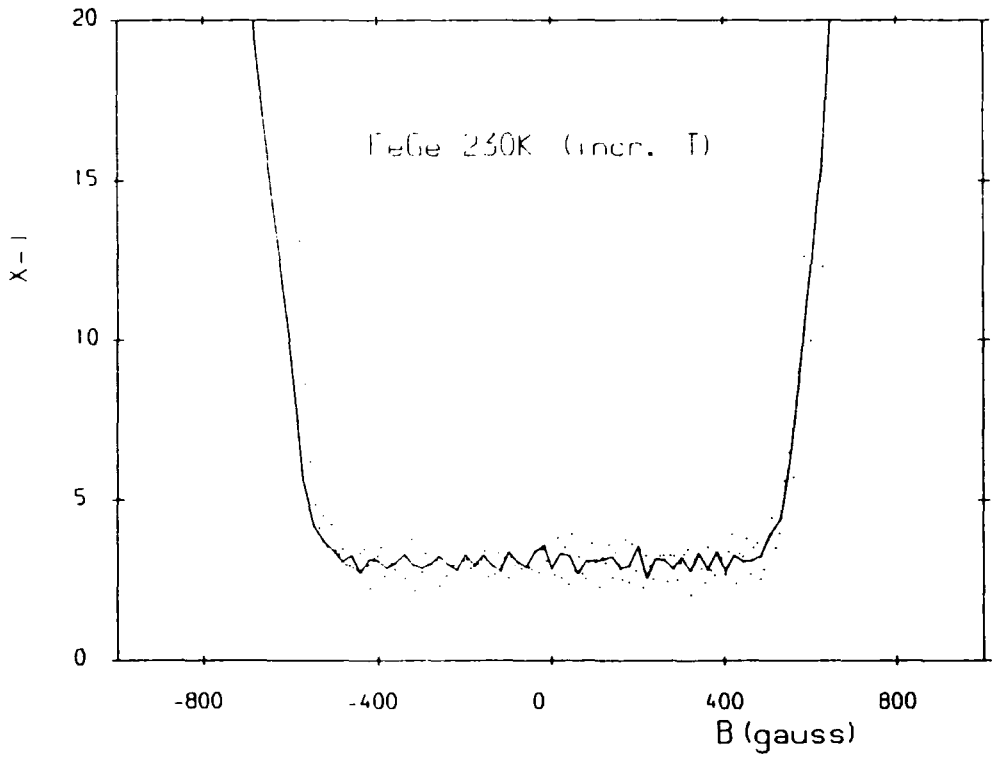

Figure 6.10 (a) The inverse magnetic susceptiblity of FeGe with magnetic field applied parallel to the < 100 > direction at 230K when lowering the temperature, derived from the magnetisation data; (b) the inverse magnetic susceptibility of FeGe with magnetic field applied parallel to the < 100 > direction at 230K when increasing the temperature, derived from the magnetisation data. The solid line is an average through the data points for a given field value and is a measure of the experimental uncertainty.

Figure 6.11 The magnetisation of FeGe with magnetic field applied parallel to the $< 100 >$ direction. (a) 200K; (b) 180K; (c) 160K; (d) 140K; (e) 120K; (f) 100K; (g) 80K; (h) 50K; (i) 20K.

Figure 6.12 The inverse magnetic susceptibility of FeGe with magnetic field applied parallel to the $< 100 >$ direction, derived from the magnetisation data. The solid line is an average through the data points for a given field value and is a measure of the experimental uncertainty. Magnetic field range $\pm 3500 Oe$. (a) 200K; (b) 180K; (c) 160K; (d) 140K; (e) 120K; (f) 100K; (g) 80K; (h) 50K; (i) 20K.

Figure 6.13 The inverse magnetic susceptibility of FeGe with magnetic field applied parallel to the $< 100 >$ direction, derived from the magnetisation data. The solid line is an average through the data points for a given field value and is a measure of the experimental uncertainty. Magnetic field range $\pm 1000 Oe$. (a) 200K; (b) 180K; (c) 160K; (d) 140K; (e) 120K; (f) 100K; (g) 80K; (h) 50K; (i) 20K.

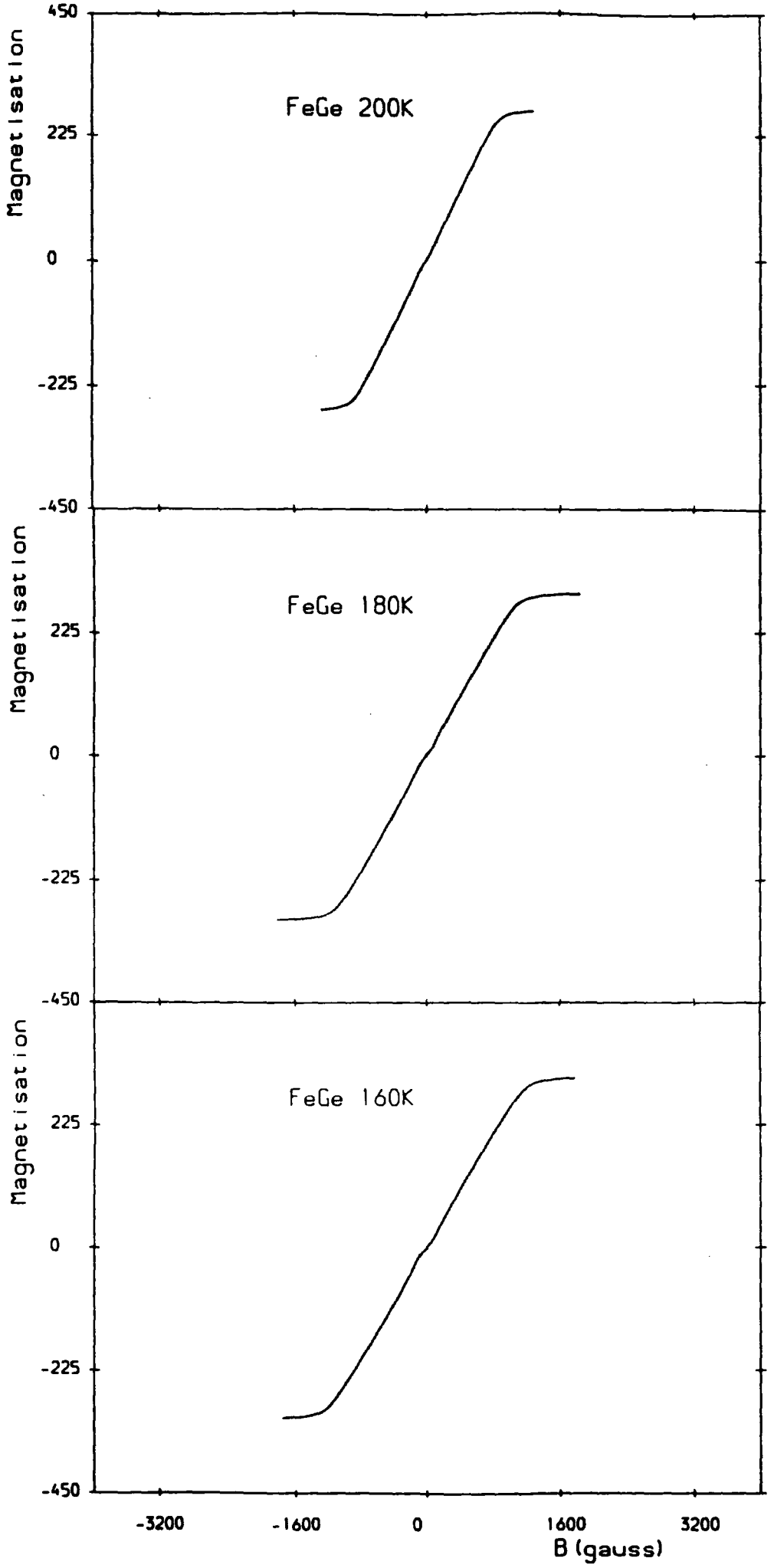

Figure 6.11 (a) - (c)

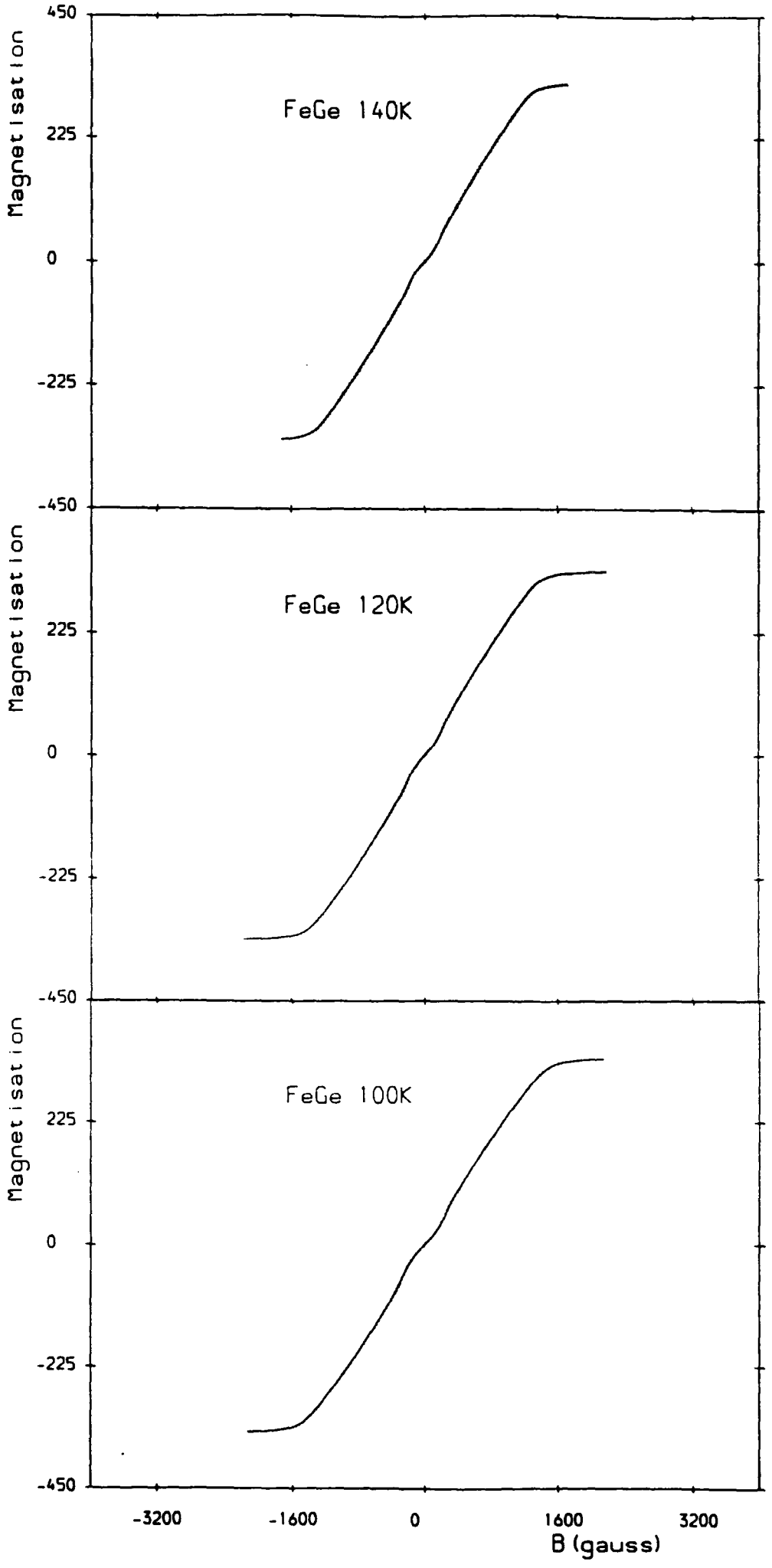

Figure 6.11 (d) - (f)

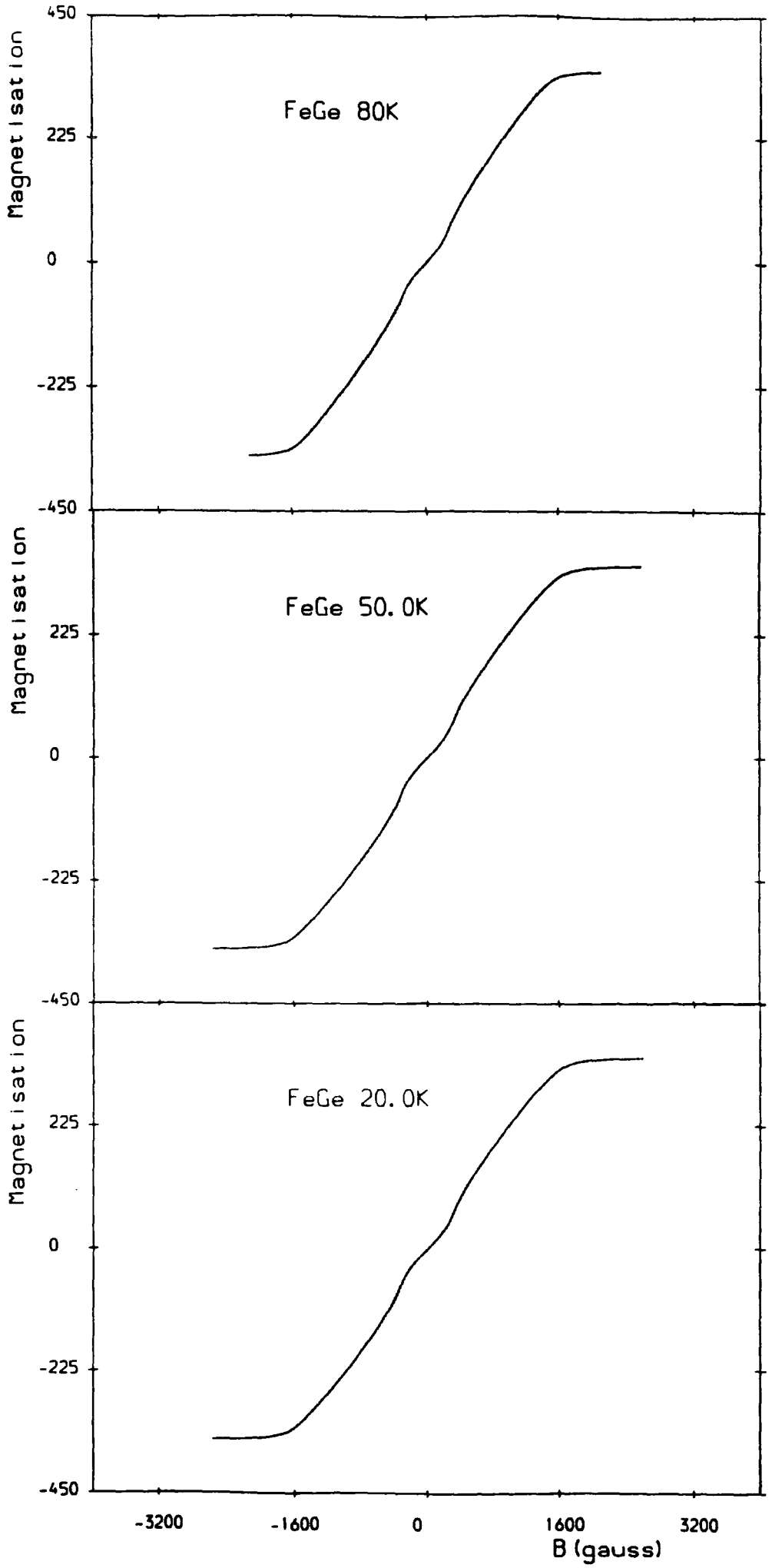

Figure 6.11 (g) - (i)

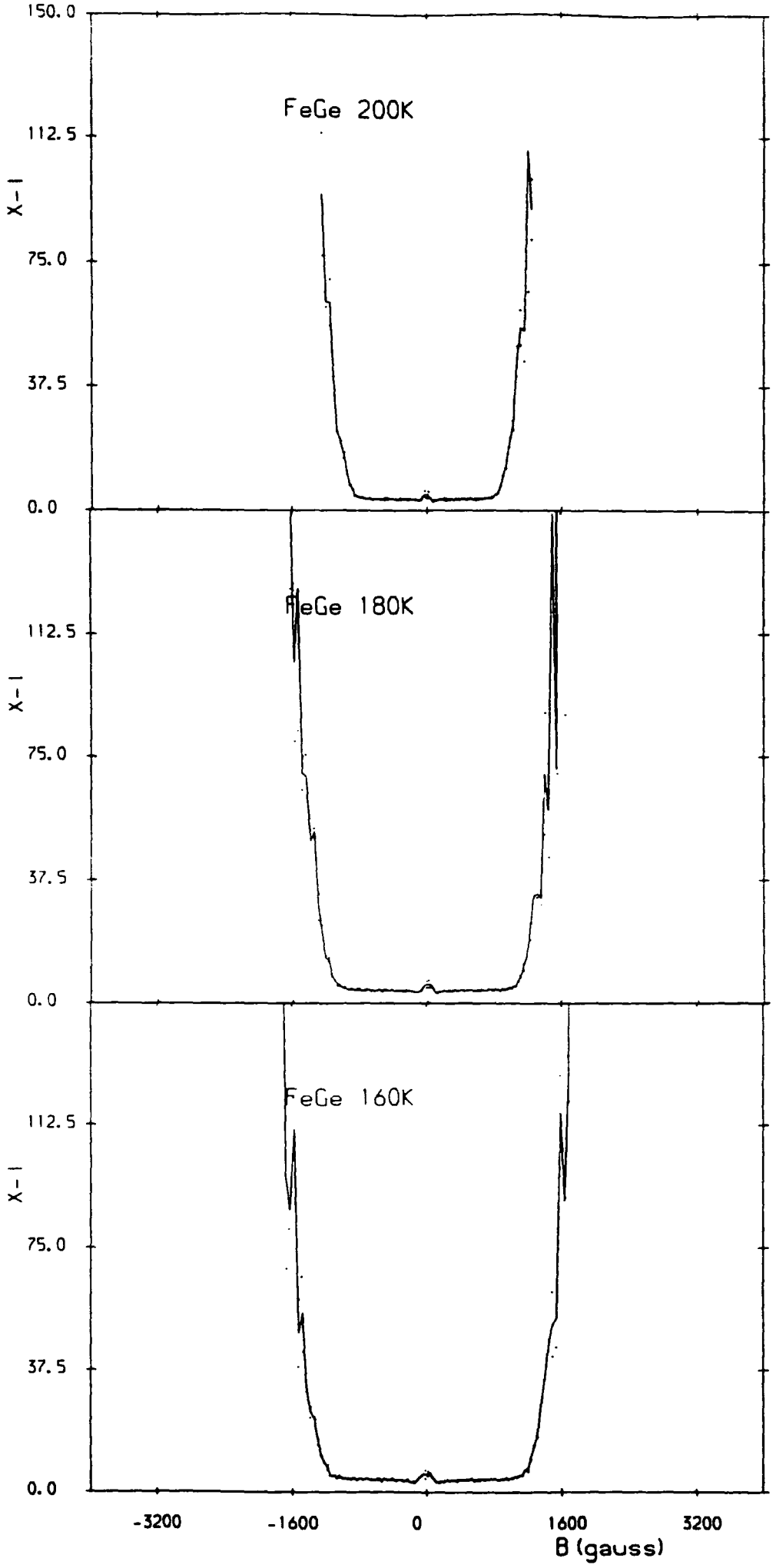

Figure 6.12 (a) - (c)

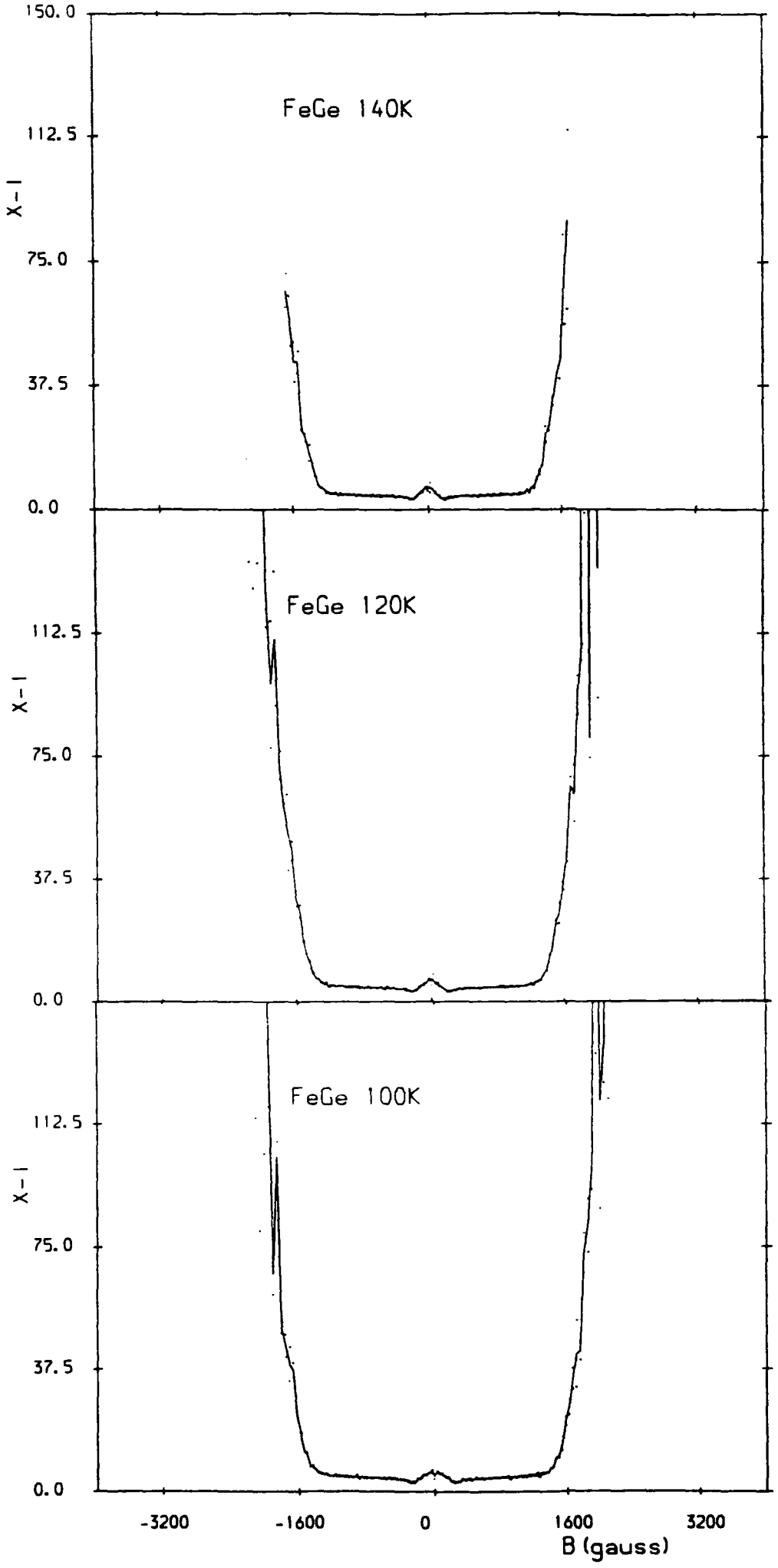

Figure 6.12 (d) - (f)

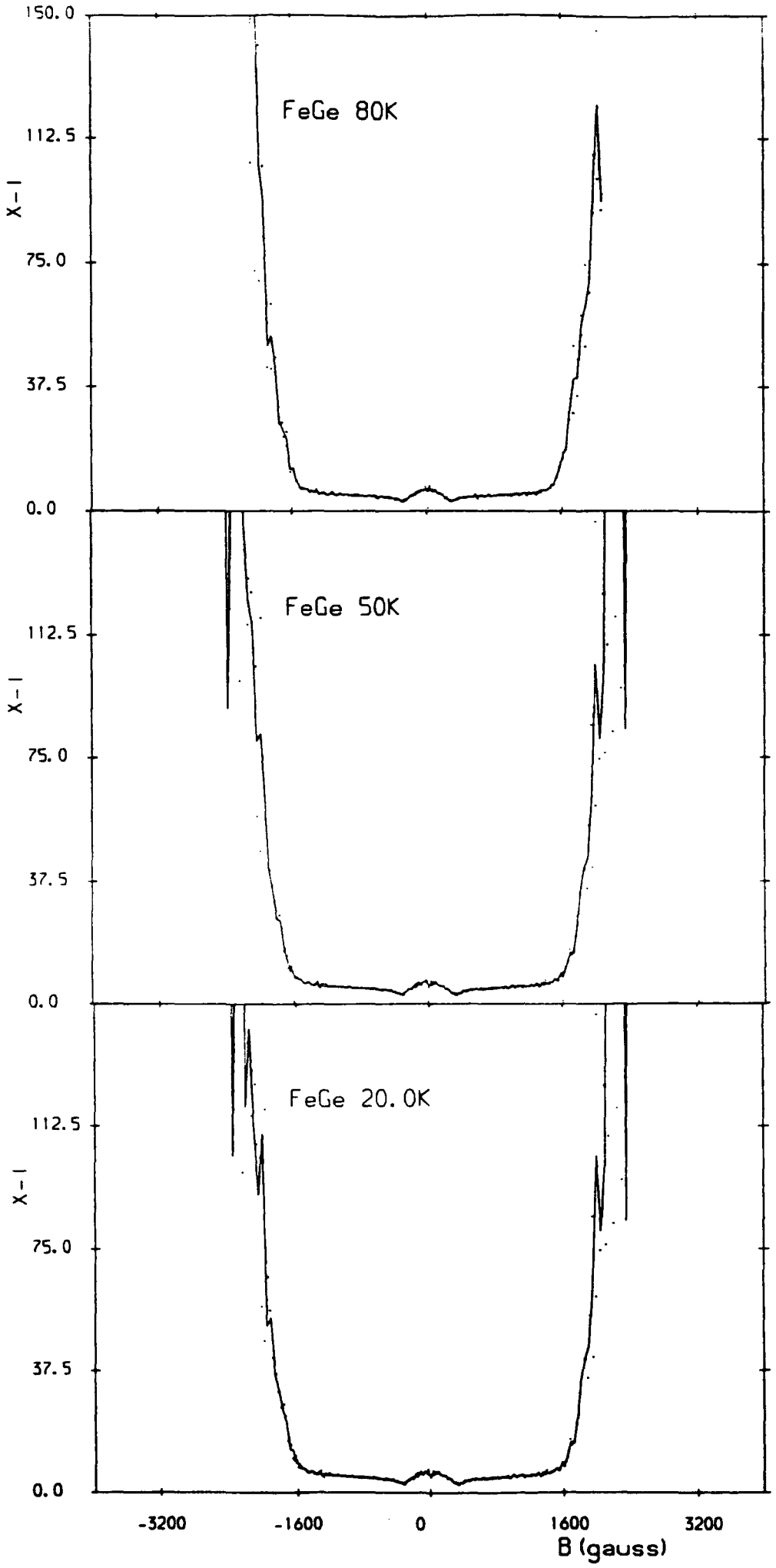

Figure 6.12 (g) - (i)

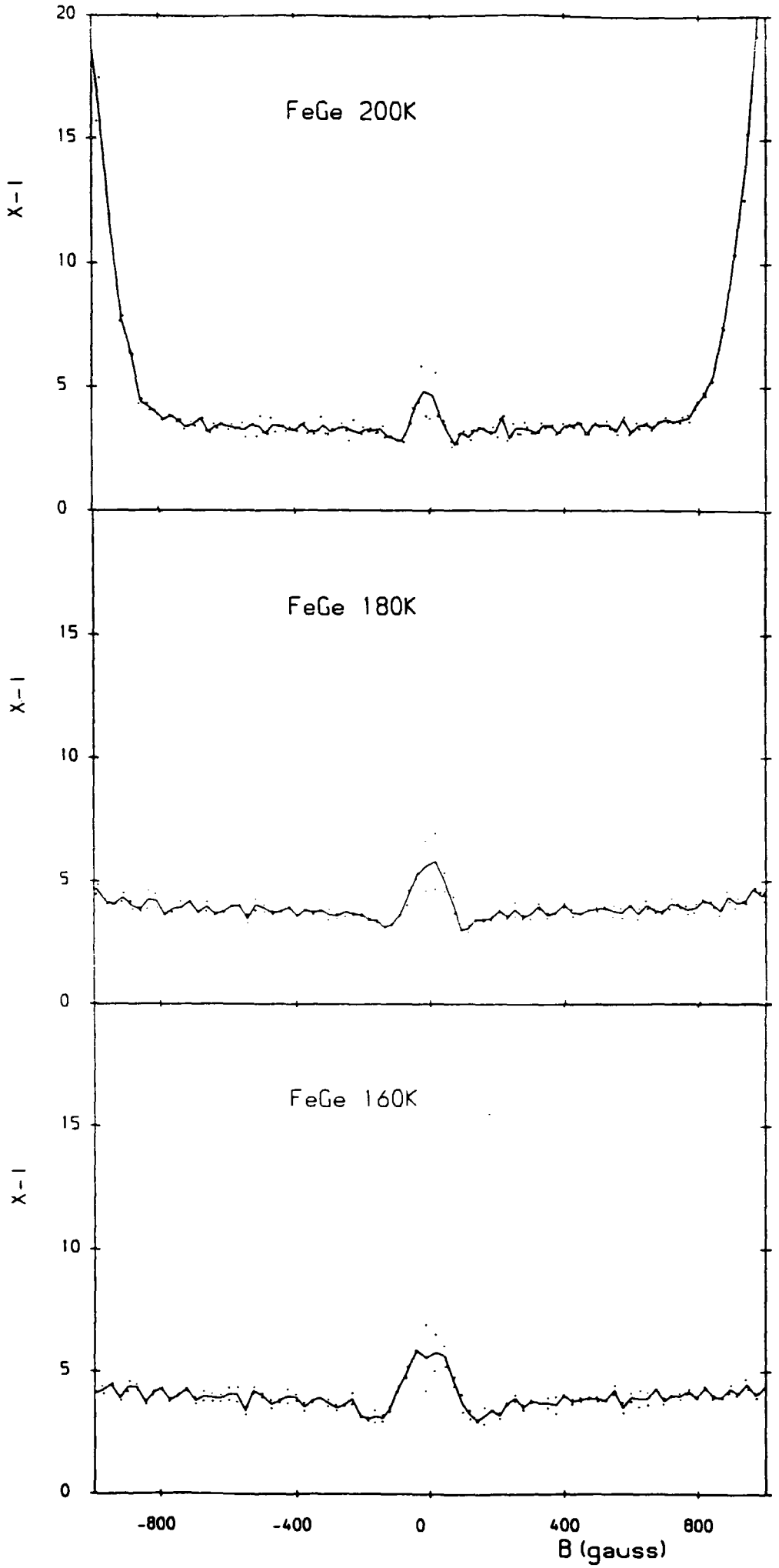

Figure 6.13 (a) - (c)

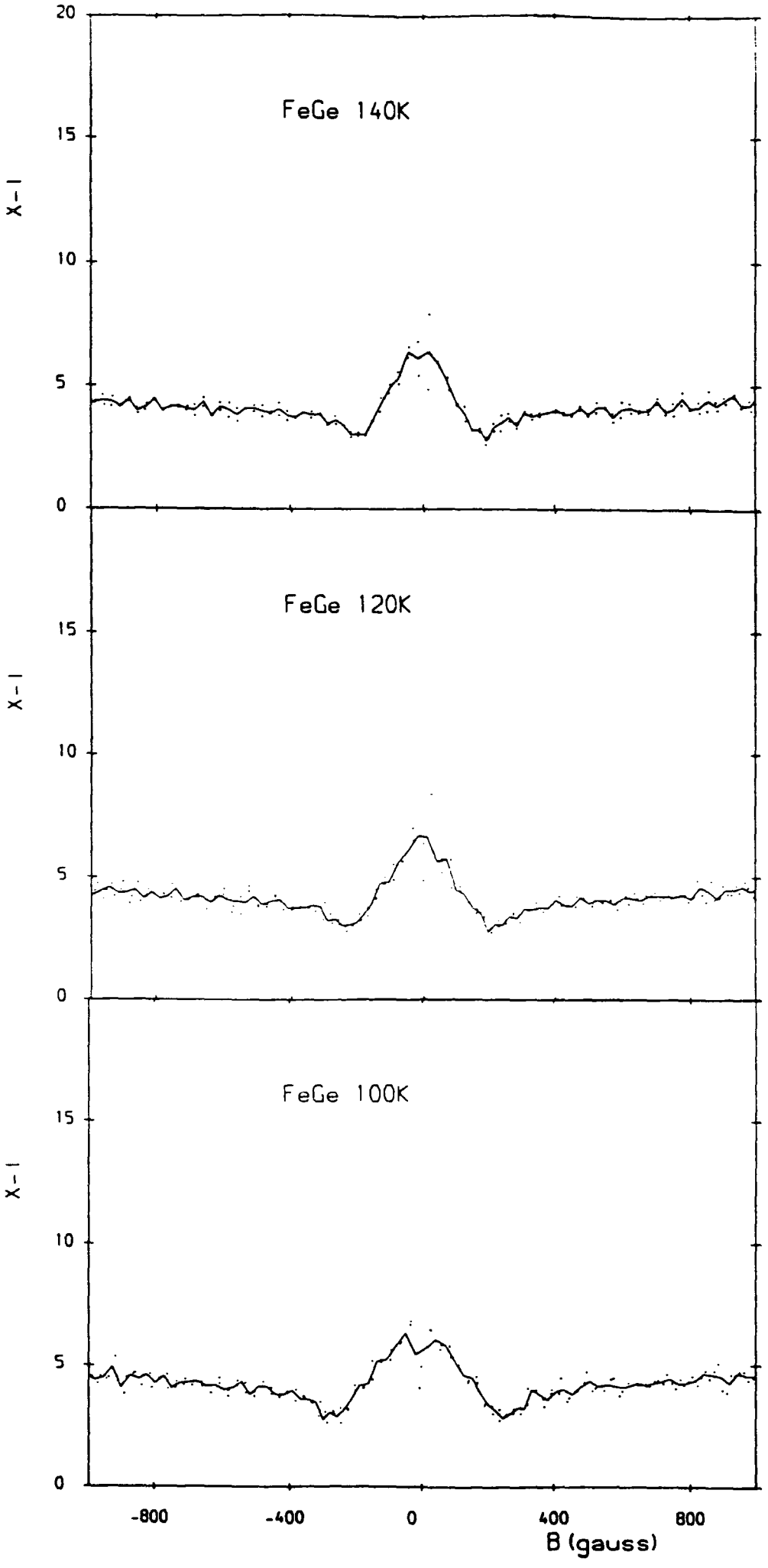

Figure 6.13 (d) - (f)

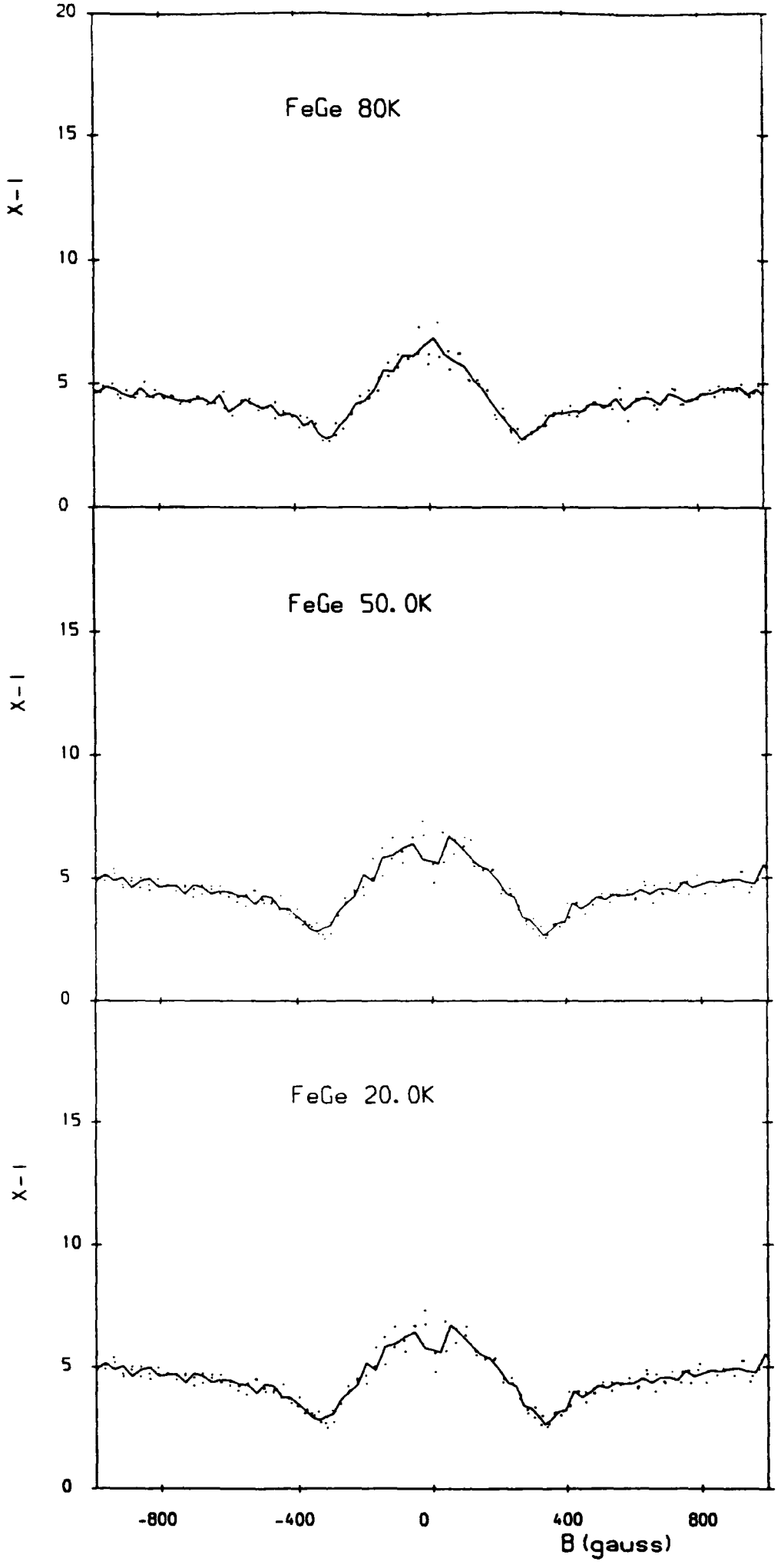

Figure 6.13 (g) - (i)

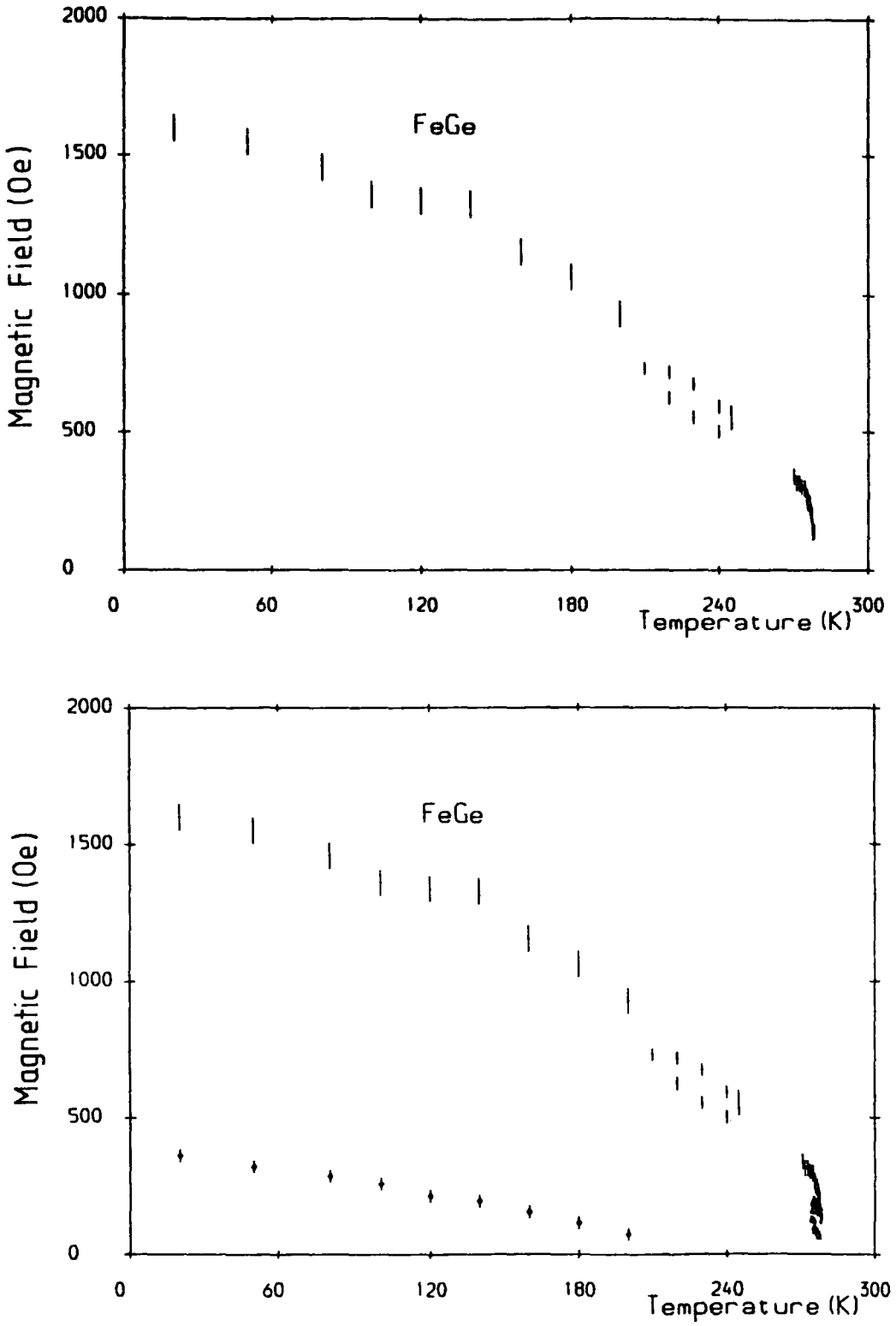

Figure 6.14 (a) Magnetic field position of the 'knee' in the magnetisation of FeGe with field applied parallel to the < 100 >; (b) complete magnetic phase diagram of FeGe with magnetic field applied parallel to the < 100 > direction including internal field position of the 'knee' in the magnetisation (points), position of the onset and conclusion of the increase in the inverse magnetic susceptibility close to the transition temperature (triangles) and the internal field position of minima in the inverse magnetic susceptibility below the second transition temperature (circles).

The field at which the 'knee' in the magnetisation occurs increases as the temperature decreases and there is a step in the response at the lower transition temperature. The fields marked are for decreasing temperature apart from the region 250 - 210K where increasing temperature are also plotted and are in fact lower. The errors increase below the second transition as larger field steps were used in measuring the magnetisation.

The field induced phase close to the first transition temperature is shown in figure 6.6 where the field at which the discontinuity in inverse susceptibility occurs is plotted together with saturation field in that temperature regime. The position of the second sharp discontinuity remains fixed while the field position of the first increases as the temperature is reduced until it is close to the second at the end of this temperature regime.

The low field points below the second phase transition represent the field position of minima in the inverse susceptibility corresponding to domain reorientation. The field position of this also increases as the temperature is lowered below the lower transition temperature.

6.7 High Field Magnetic Measurements on FeGe

Figure 6.16(a) shows the results of high field magnetistion measurements on FeGe close to, but above the transition temperature. The magnetisation shows no sign of saturating and is similar to that of MnSi and $ZrZn_2$. Unlike MnSi, this magnetisation study extends to the field where a 'knee' in the magnetisation is observed below the transition temperature. The magnetisation does however increase significantly as the field is increased above this. The resulting 'Arrot Plots' are shown in figures 6.16(b) and 6.17 and are similar in form to those of MnSi. At low magnetic fields, the value of B/M is approximately constant however, in fields greater than that at which the 'knee' in the magnetisation occurs, the 'Arrot Plot' is approximately linear, suggesting the magnetisation of FeGe shows some of the characteristics of a weak itinerant ferromagnet. Note that below the lower transition temperature the 'Arrot Plots' at low field differ from those above the upper transition temperature due to domain reorientation.

6.8 Comparison with Magnetic Measurements on Manganese Silicide

MnSi is a material in the same crystal class as cubic FeGe with the cubic B_{20} structure, however it has a transition temperature of $29 \pm 0.5K$, below which helical spin density waves propagate in equivalent $< 111 >$ directions (Ishikawa (1976)). In both materials, above the transition temperature the magnetisation is paramagnetic which, as the critical temperature is approached, becomes enhanced (similar to the super-paramagnetic response of small single domain particles) with the inverse magnetic susceptibility increasing in curvature.

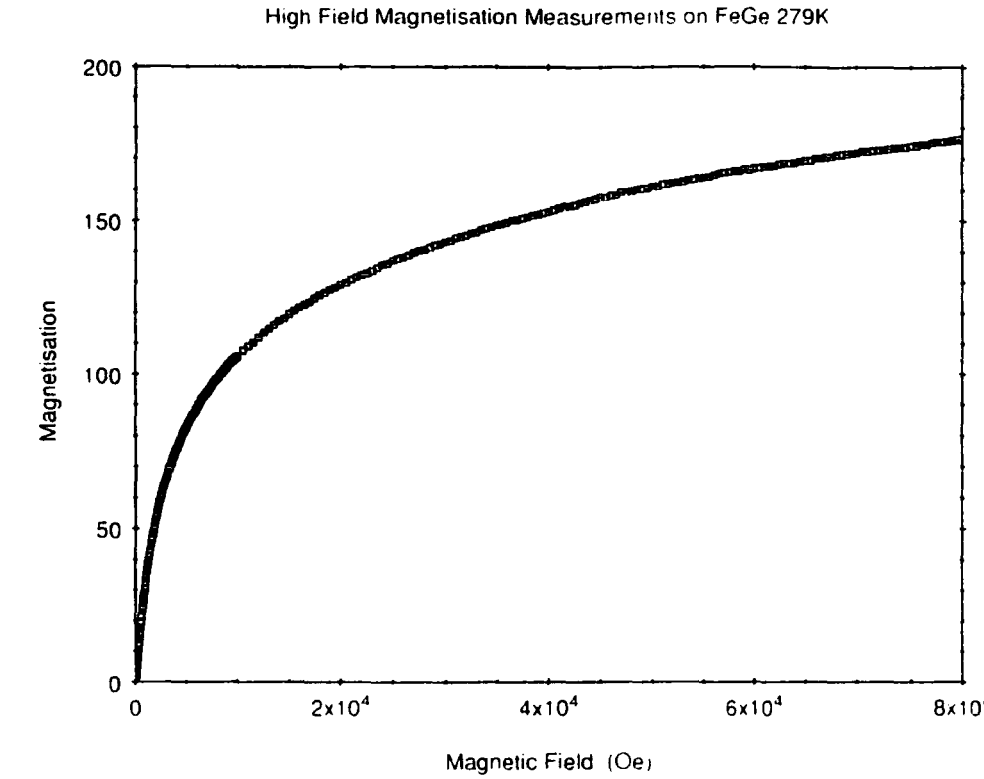

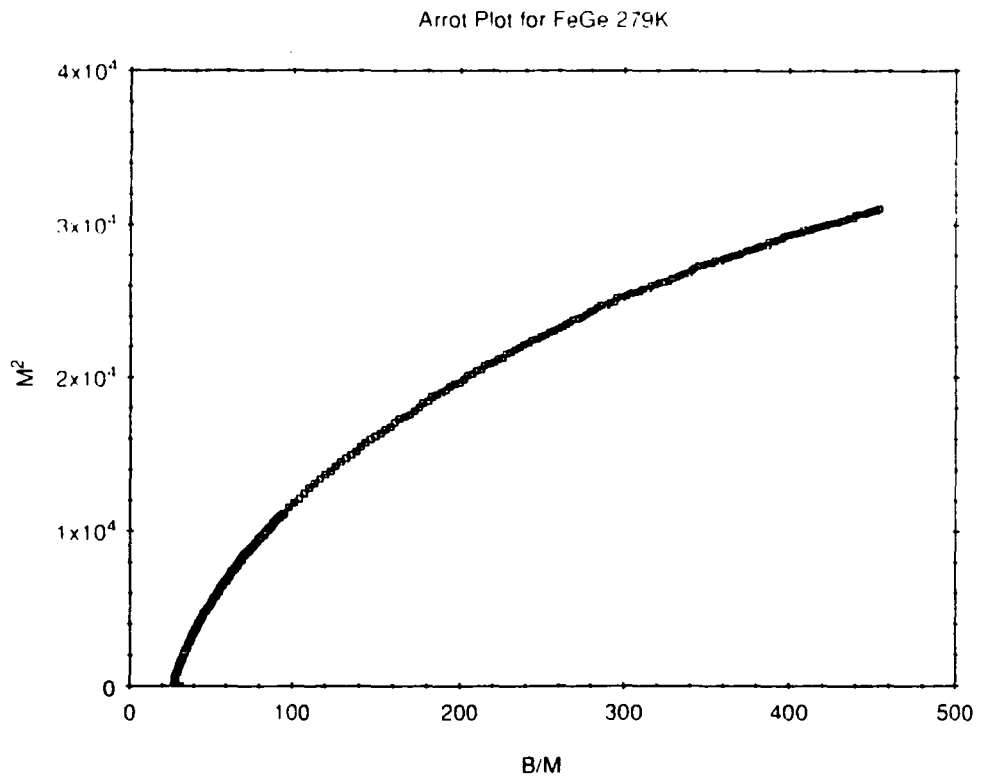

Figure 6.16 (a) high field magnetisation measurements on FeGe with magnetic field applied parallel to the < 100 > direction at 279K; (b) 'Arrot Plot' for FeGe at 279K derived from the high field magnetisation data.

In figure 6.17 the internal magnetic field ($H_i = H - H_D$) has been called B and given the units gauss. Magnetisation is measured in units of $emucm^{-3}$ and can be converted to units of $emug^{-1}$ using the density of FeGe which is $8.25gcm^{-3}$.

Figure 6.17 'Arrot Plots' for cubic FeGe derived from the magnetisation data with magnetic field applied parallel to the < 100 > direction for decreasing temperature. (a) 279K; (b) 278K; (c) 277.6K; (d) 240K; (e) 230K; (f) 210K; (g) 200K; (h) 140K; (i) 120K; (j) 80K; (k) 50K; (l) 20K.

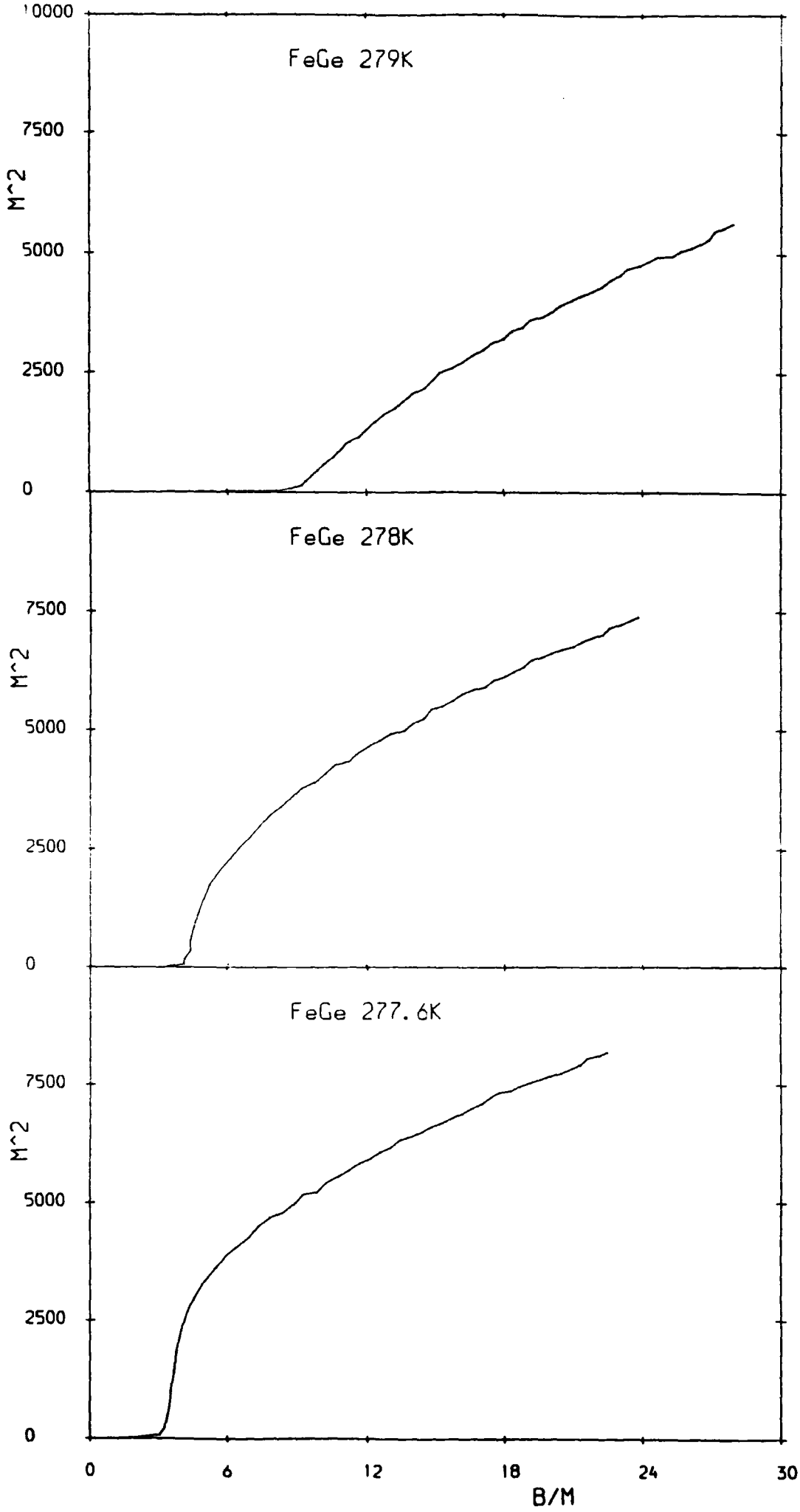

Figure 6.17 (a) - (c)

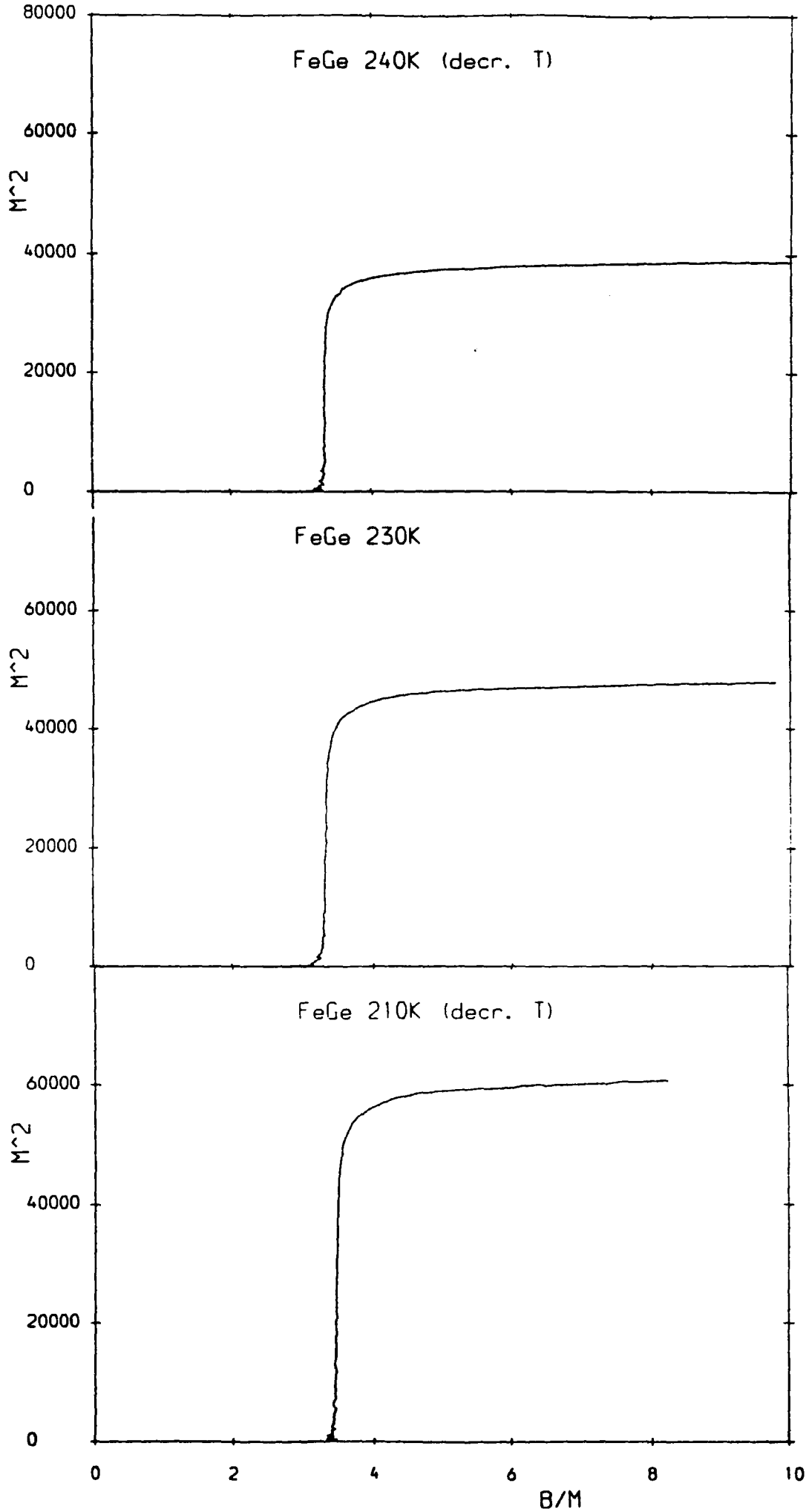

Figure 6.17 (d) - (f)

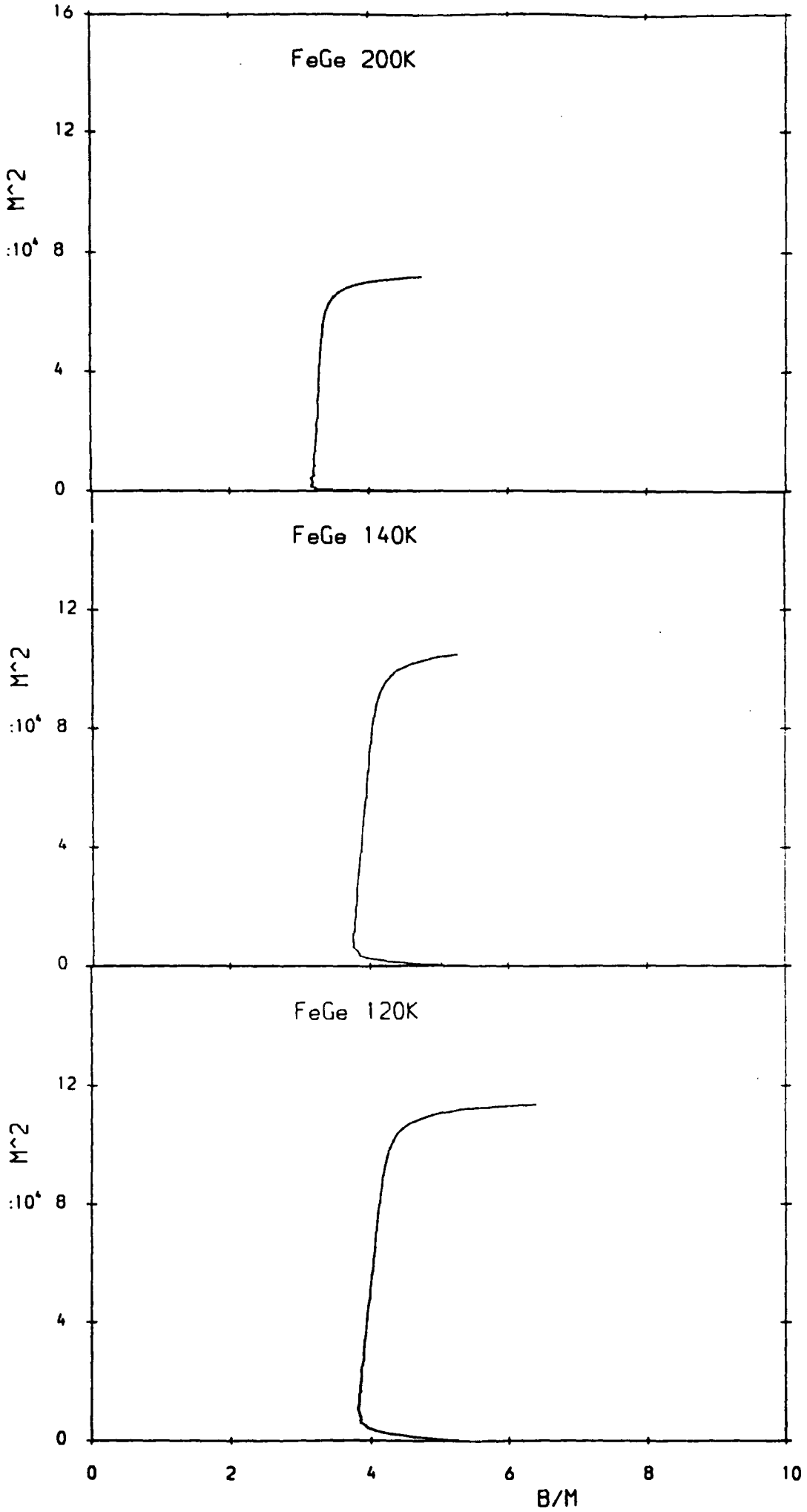

Figure 6.17 (g) - (i)

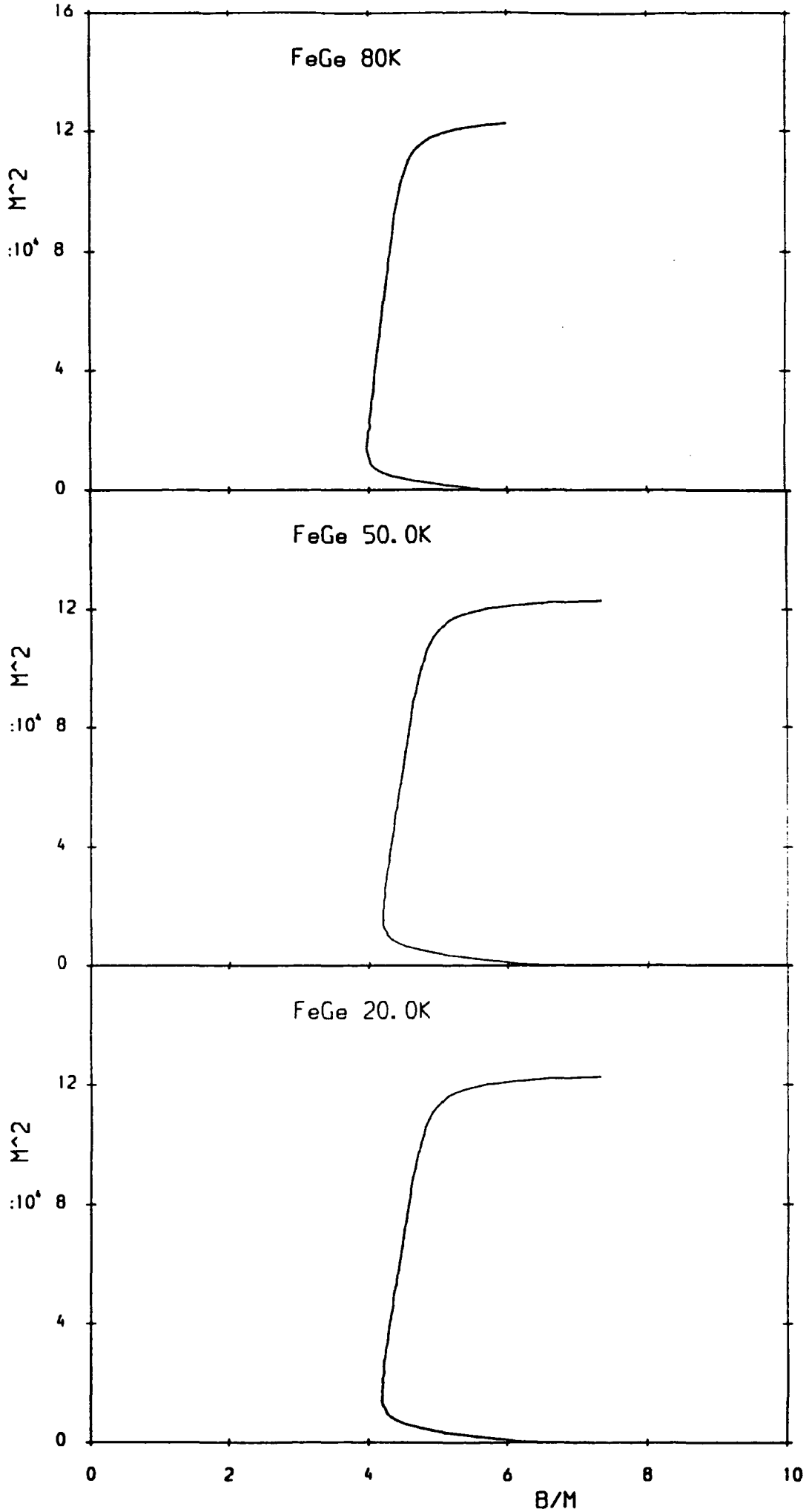

Figure 6.17 (j) - (l)

Just below the transition temperature, MnSi with field applied along the < 001 > direction and FeGe with field parallel to the < 100 > direction, both exhibit a field induced phase, manifest as a sharp increase in the inverse susceptibility. This phase is similar in both temperature and field regime relative to the 'saturation field' and transition temperature. An analogous region has been observed in the magnetic phase diagram of (Fe,Co)Si, a related compound (Ishimoto *et al* (1990)) which suggests that such a phase may be characteristic of all materials exhibiting cubic B_{20} crystal structure and supporting a helical spin density wave.

The magnetisation of cubic FeGe at a temperature between the upper and lower transition temperatures, with field applied along a < 100 > direction is similar to that of MnSi with magnetic field applied parallel to < 111 > direction. In both cases the helix lies parallel to the magnetic field and the low field magnetisation increases linearly with applied magnetic field.

Below the lower transition temperature in cubic FeGe, the helix no longer lies in the direction of the applied field but rather along the < 111 > direction. The magnetisation is similar to that observed in MnSi with field applied in the < 001 > direction i.e. is initially curved in low field. Comparison of the inverse susceptibility reveals these curved regions to be similar although at low temperatures, MnSi exhibits hysteresis with inverse susceptibility for increasing and decreasing magnetic fields being markedly different. FeGe does not exhibit this.

6.9 Further Work on FeGe

The most pressing future magnetisation work on cubic FeGe should consist of a similar study to that performed but with magnetic field applied parallel to other crystallographic directions. Firstly the field should be applied along the < 111 > direction, i.e. the direction of helical propagation below the lower transition temperature.

More recent work by Lebech (1992) on FeGe suggests that the reorientation of the helix into the field direction can occur as a first or second order process, depending on the angle between the applied field and the initial modulation vector $\underline{q}$. These magnetisation measurements are consistent with this, as a second order process is observed as the helix rotates 55° from the < 111 > direction into the applied field direction below the lower transition temperature. In order to investigate whether a first order 'flip' of the helix occurs and the affect of this on the magnetisation, measurements should also be performed with crystal orientation such that the helix is initially perpendicular to the applied field direction.

The behaviour of cubic FeGe has been thoroughly investigated close to the upper transition temperature however the results are limited around the lower. This transition should be further studied in greater detail for decreasing temperature to correspond with the SANS measurements on FeGe (Chapter 7) though it must be remembered that they correspond to the crystal in 'virgin state' with no magnetic field applied as the temperature is lowered.

Having completed a thorough investigation of the lower transition temperature,

it would then enable study of the temperature hysteresis reported by Lebech in the lower transition though application of the magnetic field destroying the 'virgin state' of the crystal will again be significant.

Finally, the variation of the 'saturation field' for increasing and decreasing temperature should be extended to include a far greater temperature regime.

6.10 References

Ishikawa Y. *et al.*(1976), Solid State Comm. **19**, 525.
Lebech B. *et al.*(1989), J. Phys.:Condensed Matter **1**, 6105-6122.
Lebech B. (1992), presented at symposium on *Recent Progress in Material Physics*, ——Osaka, Japan. To be published in *Recent Advances In Magnetism of Transition —-Metal Compounds*, World Scientific Publishing Co.
Richardson M. (1967), Acta Chem. Scand. **21**, 2305.

Chapter 7

Small Angle Neutron Scattering on MnSi and FeGe

7.1 Introduction

The neutron has a number of special properties which result in it being a unique tool in producing microscopic information about magnetic systems. It is a neutral particle so can penetrate deeply into most crystals, interacting via its magnetic moment with that of the electrons strongly enough to be measurably scattered, but without perturbing the magnetic system too severely. Thermal neutrons have wavelengths comparable with interatomic spacings and energies comparable with those of magnetic excitations in solids and so are ideally suited for studying both spatial arrangement and the dynamics of the magnetic moments.

7.2 Magnetic Neutron Scattering

Magnetic scattering arises from the interaction of the neutron magnetic moment μ_n with the local magnetic field $\underline{B}$ due to unpaired electrons in the atom. The operator corresponding to the magnetic dipole moment of the neutron is:

$$\underline{\mu}_n = -\gamma \mu_N \underline{\sigma} \tag{7.1}$$

where $\mu_N = \frac{e\hbar}{2m_p}$ is the nuclear magneton, $m_p$is the mass of the proton and e its charge. γ is the gyromagnetic ratio for the neutron with value $\gamma = 1.913$ and $\underline{\sigma}$ is the spin operator for the neutron in units of $\hbar$. The operator corresponding to the magnetic dipole moment of the electron is:

$$\underline{\mu}_e = -g\mu_B \underline{s} \tag{7.2}$$

where g is the gyromagnetic ratio of the electron with value g=2, μ_B is the Bohr magneton and $\underline{s}$ is the spin angular momentum operator for the electron in units of $\hbar$.

The magnetic field at a point $\underline{R}$ from the electron due to its magnetic dipole moment is:

$$\underline{B_s} = \text{curl}\underline{A} \tag{7.3}$$

where $\underline{A}$ is the magnetic vector potential and is defined by:

$$\underline{A} = (\frac{\mu_0}{4\pi})\frac{\underline{\mu_e} \times \underline{R}}{|R|^3} \tag{7.4}$$

The magnetic field due to the momentum of the electron is given by the Biot Savart law, such that the field from a current element $I\underline{dl}$ is

$$\begin{aligned} \underline{B_l} &= (\frac{\mu_0}{4\pi})I\frac{\underline{dl} \times \underline{R}}{|R|^3} \\ &= -(\frac{\mu_0}{4\pi})\frac{2\mu_B}{\hbar}\frac{\underline{p} \times \underline{R}}{|R|^3} \end{aligned} \tag{7.5}$$

The interaction potential with the neutron is given by:

$$V = -\underline{\mu}_n.\underline{B} = -\underline{\mu}_n.(\underline{B_l} + \underline{B_s}) \tag{7.6}$$

The differential cross section for a neutron scattering is given by the first Born Approximation (see for example Squires(1978)):

$$(\frac{d^2\sigma}{d\Omega dE'})_{\lambda\to\lambda'} = \frac{k'}{k}(\frac{m}{2\pi\hbar^2})^2| < \underline{k}'\lambda'|V|\underline{k}\lambda > |^2\delta(E_\lambda - E_{\lambda'} + E - E') \tag{7.7}$$

for a neutron with wavevector $\underline{k}$ incident on a scattering system characterised by an index λ. The neutron interacts via a potential V, the state of the neutron changes from $\underline{k}$ to $\underline{k}'$ and the scattering system changes from λ to λ'.

In the case of the magnetic potential, because it contains the spin operator $\underline{\sigma}$ explicitly it is therefore necessary to specify not only the wavevector $\underline{k}$ of the neutron but also its spin state σ:

$$(\frac{d^2\sigma}{d\Omega dE'})_{\lambda\sigma\to\lambda'\sigma'} = \frac{k'}{k}(\frac{m}{2\pi\hbar^2})^2| < \underline{k}'\sigma'\lambda'|V_m|\underline{k}\sigma\lambda > |^2\delta(E_\lambda - E_{\lambda'} + E - E') \tag{7.8}$$

where V_m is the potential between the neutron and all the electrons in the scattering system. It is convenient to treat spin and orbital parts of V_m seperately (V_m=V_l+V_s). It can be shown (see for example Squires(1978)):

$$< \underline{k}'|V_s|\underline{k} >= 4\pi exp(i\underline{K}.\underline{r}_i)\ [\hat{\underline{K}} \times (\underline{s}_i \times \hat{\underline{K}})] \tag{7.9}$$

where $\underline{K} = \underline{k} - \underline{k}'$ and is known as the scattering vector and $\hat{\underline{K}}$ is the unit vector in the direction $\underline{K}$.

The orbital contribution is given by:

$$< \underline{k}'|V_l|\underline{k} >= \frac{4\pi i}{\hbar K}exp(i\underline{K}.\underline{r}_i)\ (\underline{p}_i \times \hat{\underline{K}}) \tag{7.10}$$

Combining these we obtain:

$$\sum_i < \underline{k}'|V_s + V_l|\underline{k} >= 4\pi \underline{Q}_\perp \tag{7.11}$$

where

$$\underline{Q}_\perp = \sum_i exp(i\underline{K}.\underline{r}_i)\ [\hat{\underline{K}} \times (\underline{s}_i \times \hat{\underline{K}}) + \frac{i}{\hbar K}(\underline{p}_i \times \hat{\underline{K}})] \tag{7.12}$$

Collecting multiplying factors together, and defining the classical radius of the electron $r_0 = \frac{\mu_0}{4\pi}\frac{e^2}{m_e}$ then

$$(\frac{d^2\sigma}{d\Omega dE})_{\sigma\lambda\to\sigma'\lambda'} = (\gamma r_0)^2 \frac{k'}{k}| < \sigma'\lambda'|\underline{\sigma}.\underline{Q}_\perp|\sigma\lambda > |^2 \delta(E_\lambda - E_{\lambda'} + E - E') \tag{7.13}$$

The operator $\underline{Q}_\perp$ is related to the magnetisation of the scattering system. Separating $\underline{Q}_\perp$ into orbital and spin components:

$$\underline{Q}_{\perp s} = \sum_i exp(i\underline{K}.\underline{r}_i)\ [\hat{\underline{K}} \times (\underline{s}_i \times \hat{\underline{K}})] \tag{7.14}$$

Defining an operator $\underline{Q}_s$ by

$$\underline{Q}_{\perp s} = \hat{\underline{K}} \times (\underline{Q}_s \times \hat{\underline{K}}) \tag{7.15}$$

i.e. $\underline{Q}_\perp$ is the projection of the vector $\underline{Q}$ onto the plane perpendicular to the scattering vector, then

$$\underline{Q}_s = \sum_i exp(i\underline{K}.\underline{r}_i)\underline{s}_i \tag{7.16}$$

The vector operator $\underline{\rho}_s(r)$ gives the electron spin density:

$$\underline{\rho}_s(r) = \sum_i \delta(r - r_i)\underline{s}_i \tag{7.17}$$

so $\underline{Q}_s$ is the Fourier transform of $\underline{\rho}_s(r)$

$$\underline{Q}_s = \int \underline{\rho}_s(r) exp(i\underline{K}.\underline{r}) d\underline{r} \tag{7.18}$$

The spin magnetisation operator is defined by:

$$\underline{M}_s(r) = -2\mu_B \underline{\rho}_s(r) \tag{7.19}$$

so

$$\begin{aligned} \underline{Q}_s &= -\frac{1}{2\mu_B}\int \underline{M}_s(r) exp(i\underline{K}.\underline{r}) d\underline{r} \\ &= -\frac{1}{2\mu_B}\underline{M}_s(\underline{K}) \end{aligned} \tag{7.20}$$

The corresponding calculation for the orbital term is detailed in Squires (1978) and only quoted here:

$$\begin{aligned} \underline{Q}_l &= -\frac{1}{2\mu_B}\underline{M}_l(K) \\ &= \int \underline{M}_l(r) exp(i\underline{K}.\underline{r}) d\underline{r} \end{aligned} \tag{7.21}$$

Combining these results:

$$\begin{aligned} \underline{M}(K) &= \underline{M}_l(K) + \underline{M}_s(K) \\ &= 2\mu_B(\underline{Q}_l + \underline{Q}_s) \\ &= 2\mu_B\underline{Q} \end{aligned} \tag{7.22}$$

Thus $\underline{Q}$ is closely related to the fourier transform of the magnetisation density. Using the above equations it is possible to relate directly the neutron scattering to the magnetisation density.

7.3 Interaction of the Neutron with the Helical Spin Density Wave

From the above, the neutron scattering cross section is closely related to the fourier transform of the magnetisation density. The fourier transform of a helix of wavelength λ is a delta fuction, at a position $(\pm\frac{2\pi}{\lambda})$ along the direction of propagation which will be 'smeared' by the resolution of the apparatus. When in the $(1\bar{1}0)$ scattering plane, only two points are observed due to the tilting of the plane to satisfy the elastic condition.

7.4 SANS simulations

Several of the previous neutron scattering experiments on the helimagnets MnSi and FeGe report observation of a ring of scattering close to the transition temperature of both FeGe (Lebech *et al.*(1989)) and MnSi (Ishikawa *et al.*(1982)) as well as within 'Phase A' of MnSi in an applied magnetic field (Ishikawa *et al.*(1984)). In order to invetsigate the possible sources of this result and indeed others that may be obtained, a simulation program was written by Dr. N. R. Bernhoeft and the Author (see Appendix C) modelling the response expected from a helix of wavelength $\underline{q}$ propagating in equivalent $< 111 >$ directions and including resolution affects of the spectrometer.

The incident wavelength is input into the program together with a parameterised measure of the incident wavelength spread. The two dimensional 'simulated sample' is conceptionally divided into a grid (the sample shape and size should be altered within the program) from which the incident neutrons scatter. All final possible wavevectors are computed from each section of the sample to each segment of the detector in turn. From these the scattering wavevector $\underline{K}$ for each sample to detector path is calculated. These values are then filtered 'top hat' fashion on a range of acceptable $|\underline{K}| = |\underline{q}|$ input into the program corresponding to helical wavelength and taking into account the finite length of the helix. Figure 7.1 shows the simulated arrangement.

The direction for each $\underline{K}$ is then calculated using the angles θ and ω as defined in figure 7.1(b) and filtered on the values of θ and ω corresponding to helix propagation

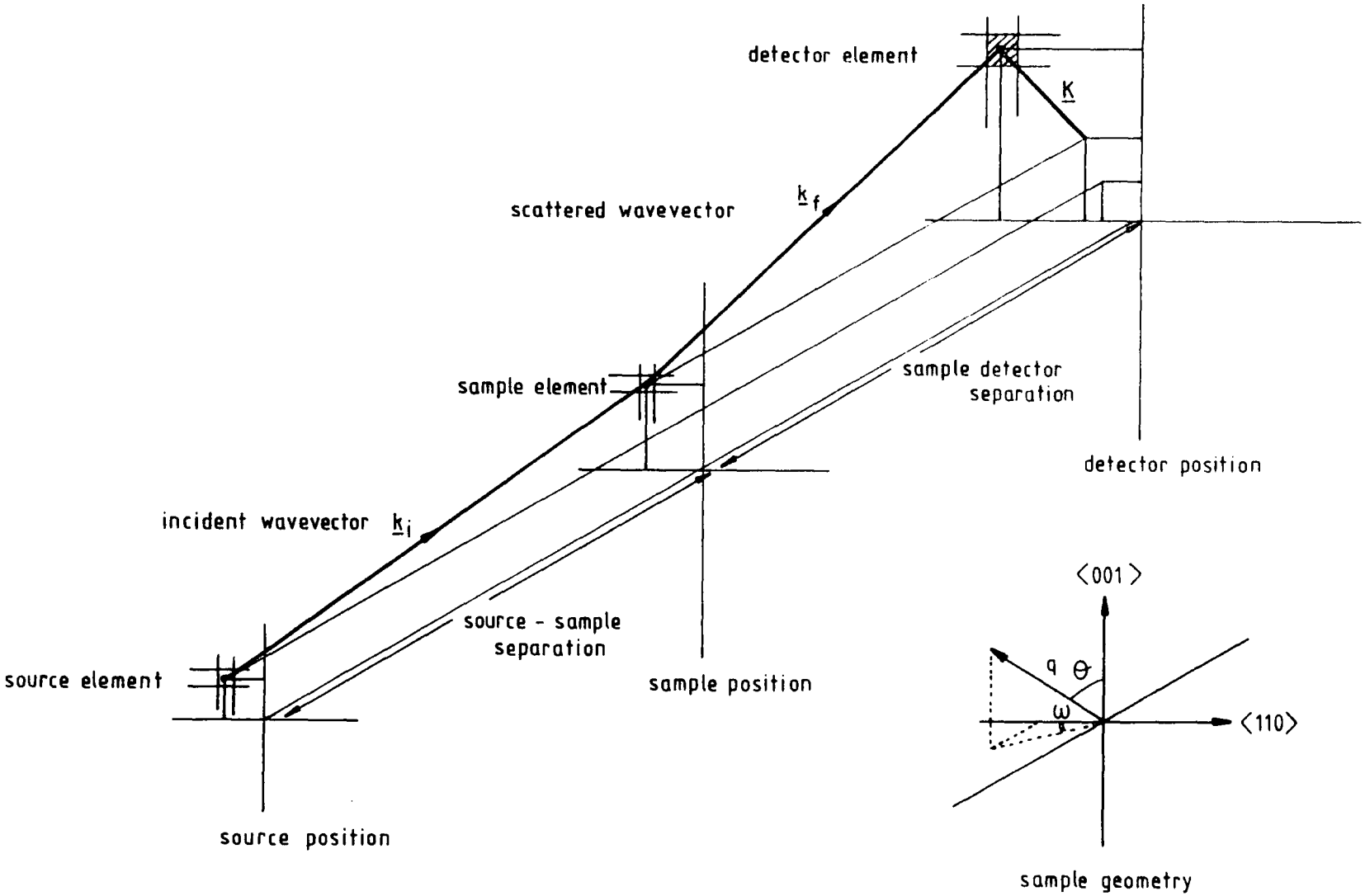

Figure 7.1 (a) Schematic outline of the method used to simulate the small angle neutron scattering results from both MnSi and FeGe. Source-sample and sample-detector separation are input into the program together with incident wavevector and range of acceptable $\underline{q}$. (b) Details of sample orientation together with the definition of angles ω and θ.

in equivalent < 111 > directions, but including a range of values to account for the mosaic spread of the crystal and collimation of the beam.

In the simulation we are assuming strictly elastic neutron scattering $|\underline{k}_f| = |\underline{k}_i|$. The scattering vector $\underline{K}$ is orientated slightly out of the detector plane by an angle α. In order to overcome this, the sample must be rotated by $\pm\alpha$ so that the scattered satellites are at the optimum position for the detector. In order to accomodate this, the program produces scattering assuming the sample has been rotated to optimum angle for either the left or right hand side or the value of sample rotation can be input into the program.

Finally, all the $\underline{K}$ satisfying the magnitude and angular restrictions necessary such that $\underline{K} = \underline{q}$ are summed.

Figures 7.2 and 7.3 show the simulated SANS results on the Risø spectrometer for MnSi and FeGe in zero magnetic field, below the transition temperature. Both simulations are for the crystals with $(1\bar{1}0)$ plane perpendicular to the incident neutrons with < 001 > axis vertical and rotated to optimise for the satellites on the right of the detector. With MnSi the conditions are such that two satellites are observed. Experimentally, however, all four are recorded, with two being weaker than the optimum pair (figure 7.6). This suggests the resolution conditions within the program are more stringent than those observed experimentally.

Figure 7.3 shows the simulated results for the FeGe crystal used in the work of Lebech *et al.* (1989), in the same crystallographic orientation as MnSi, at a temperature below the lower transition. Although the crystal is orientated such that the scattering from only two satellites is optimized it is evident that the resolution conditions or sample shape are such that this has little affect and all satellites in the scattering plane are observed. Comparing this simulation to the experimental results (figure 7.13) obtained, four satellites of similar intensity are observed though whether this was optimised for a particular pair is uncertain.

The helix is defined in real space by the angle θ (the angle the direction of helix propagation makes with the vertical) and ω (the angle of rotation of the scattering plane) as shown in figure 7.1b. By allowing relaxation of the constraints on these angles in turn, the following magnetic structures were simulated.

θ and ω fixed: Propagation of the helix in equivalent < 111 > directions. Figure 7.2a for MnSi and figure 7.3a for FeGe.

θ fixed, ω sweep: A cone of helix propagation vectors about the vertical axis. Figure 7.2b for MnSi and figure 7.3b for FeGe.

θ sweep, ω fixed: A disc of helix propagation vectors. In the crystal orientation used ($\omega = 0$) half the disc is in the scattering plane as the sample is rotated by the angle α. Figure 7.2c for MnSi and figure 7.3c for FeGe.

θ swept in a finite range, ω fixed: Two arcs of helix propagation vectors rather than the complete disc. Figure 7.14 for FeGe.

θ sweep, ω sweep: A sphere of helix propagation vectors. Figure 7.2d for MnSi and figure 7.3d for FeGe.

Table 7.1 lists the input parameters used in the SANS simulation program to

Figure 7.2 Simulated SANS results for MnSi for particular $\underline{q}$ arrangements. The scattering plane is a $(1\bar{1}0)$ plane with [001] vertical and [110] horizontal. The input parameters used were incident wavevector $0.090\mathring{A}^{-1}$, source sample separation 6000mm, sample detector separation 4000mm, upper limit to the wavevector $\underline{q}$ $0.036\mathring{A}^{-1}$ and lower limit $0.034\mathring{A}^{-1}$. These are very similar to the experimental conditions. The lowest contour is 100 counts and contour separation is 100 counts. (a) Helix ($\underline{q}$) propagating along equivalent < 111 > directions; (b) a cone of helix propagation vectors (ω sweep); (c) a plane of helix propagation vectors (θ sweep); (d) a sphere of helix propagation vectors (θ and ω sweep).

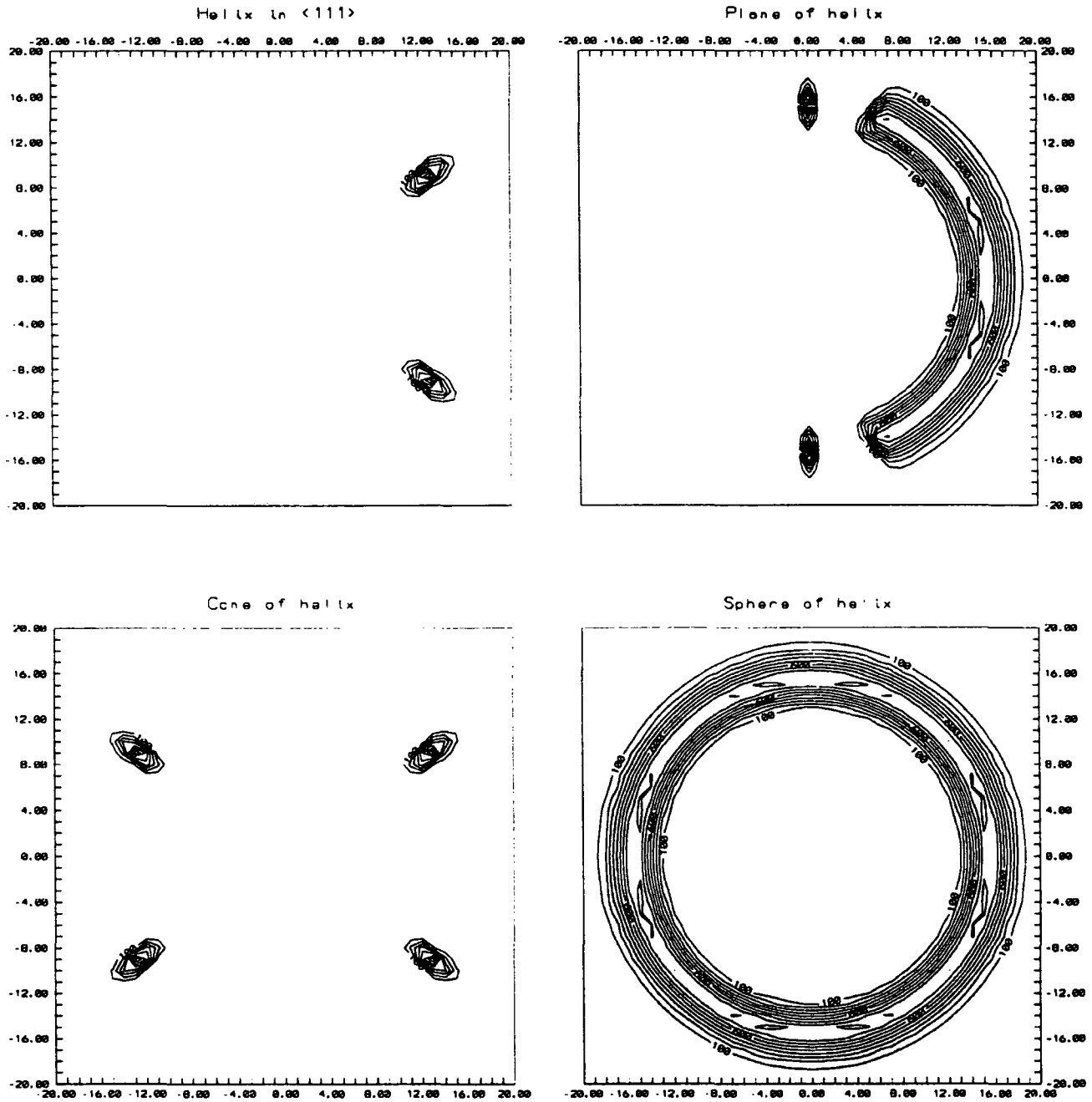

Figure 7.3 Simulated SANS results for FeGe for particular $\underline{q}$ arrangements. The scattering plane is a $(1\bar{1}0)$ plane with [001] vertical and [110] horizontal. The input parameters used were incident wavevector $0.3977\AA^{-1}$, source sample separation 6000mm, sample detector separation 6000mm, upper limit to the wavevector $\underline{q}$ $0.009199\AA^{-1}$ and lower limit $0.008975\AA^{-1}$. These are similar to the experimental conditions of Lebech *et al.* (1989). The lowest contour is 50 counts and the contour separation is 50 counts. (a) Helix propagating along equivalnet < 111 > directions; (b) a cone of helix propagation vectors (ω sweep); (c) a plane of helix propagation vectors (θ sweep); (d) a sphere of helix propagation vectors (θ and ω sweep).

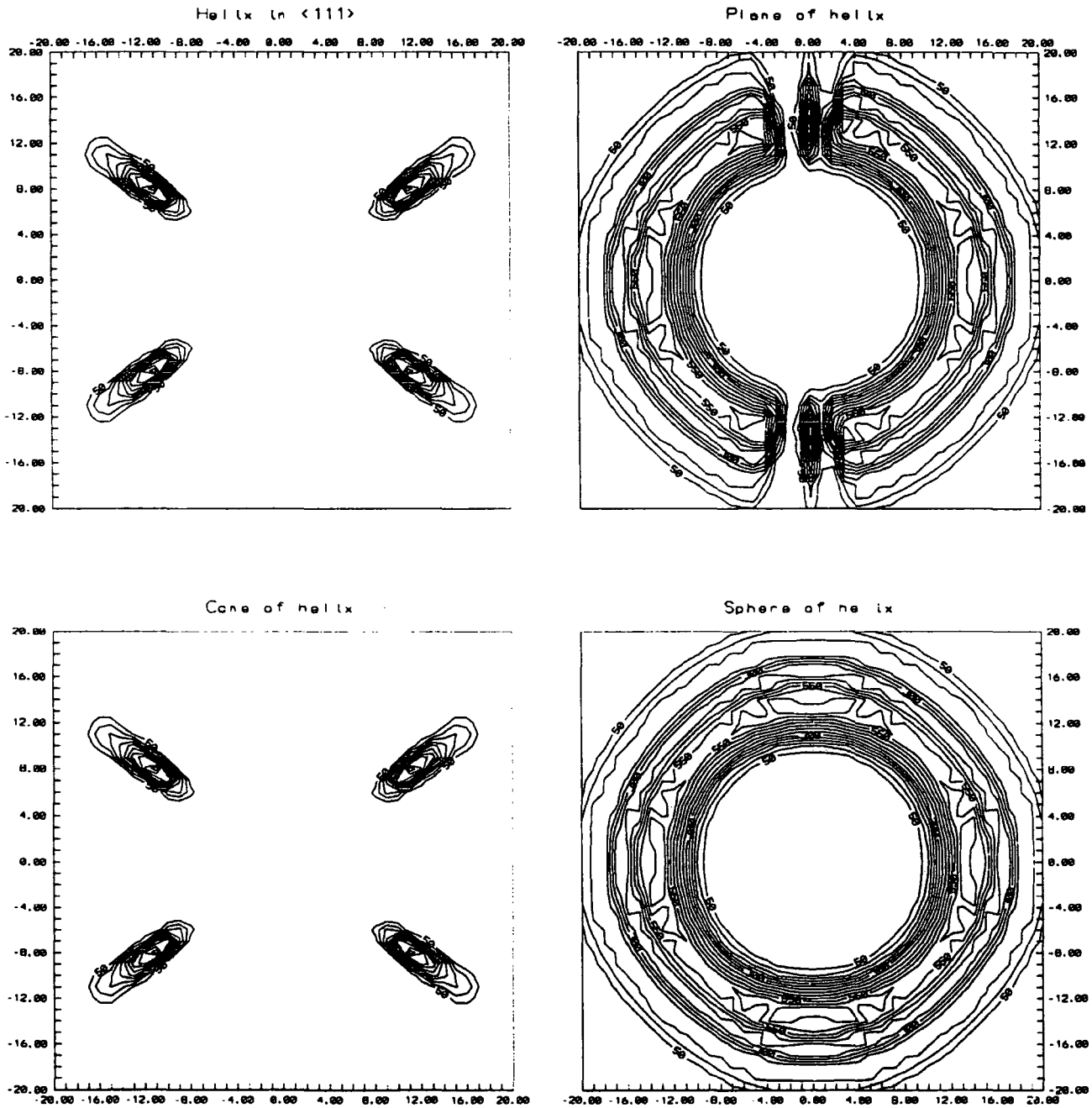

	MnSi	FeGe
incident wavevector/$\mathring{A}^{-1}$	0.09	0.3977
source sample separation/mm	6000	6000
sample detector separation/mm	4000	6000
range of acceptable q/$\mathring{A}^{-1}$	$0.036 > q > 0.034$	$0.009199 > q > 0.008975$

Table 7.1: The input parameters used for the SANS simulation program

produce the results of figures 7.2 and 7.3. These are very similar to the experimental conditions used by Lebech (1989) for FeGe and those used for the SANS on MnSi reported in this chapter. As the simulations corresponding to helicies propagating along equivalent $< 111 >$ directions are similar to the experimental SANS results obtained for both MnSi (this Chapter) and FeGe (Lebech(1989)), it suggests the predicted scattering of other helical arrangements to be accurate. The simulations also show that the sample and scattering conditions are more sensitive to the sample orientation for MnSi, maximising the scattering on one side of the detector only.

7.5 Experimental Details

The sample enviroment was provided by an Oxford 5kOe top loading, split superconducting magnet. The cryostat was made from Aluminium which had been strengthened using Lithium. Unfortunately, the dispersion of Al_2Li scatters the neutrons as shown in figure 7.4(a) producing a ring of scattering centred at a radius of $0.015\mathring{A}^{-1}$. This scatter produces a similar intensity to the satellites obtained from the helical spin density waves however these were situated at a larger radius. Figure 7.4(b) shows subtraction of two residuals and that the ring disappears, but noise level is very high, especially over the region where the ring of scatter is. Although residuals were subtracted, numerous orientations of the crystal were investigated as well as in various applied magnetic fields and it was impossible to record all necessary. This limited the sensitivity of the results obtained.

The incident neutron wavelength was set at 7.1Å i.e. above the Bragg cut off. Count times were 30 minutes and all results are normalised to the monitor.

7.6 SANS on MnSi in zero Field

Figure 7.5 shows the resultant SANS obtained from MnSi in zero magnetic field and at a temperature of 4.2K. The sample used in zero field work was the same as for the magnetic measurements of chapter 4 i.e. a 2.5mm diameter disc with $(1\bar{1}0)$ perpendicular to the incident neutron beam and [001] direction vertical.

The sample is orientated in this scan such that four satellites of equal intensity are observed (infact all lie slightly out of the plane of the detector) along the equivalent

Figure 7.4 (a) Equal intensity contours, SANS data (log-scale) obtained at 40K showing the substantial background scattering from the cryomagnet. (b) Equal intensity contours (log-scale) on subtraction of the residual scatter at 40K from that at 45K. Although the ring disappears, the noise level is very high.

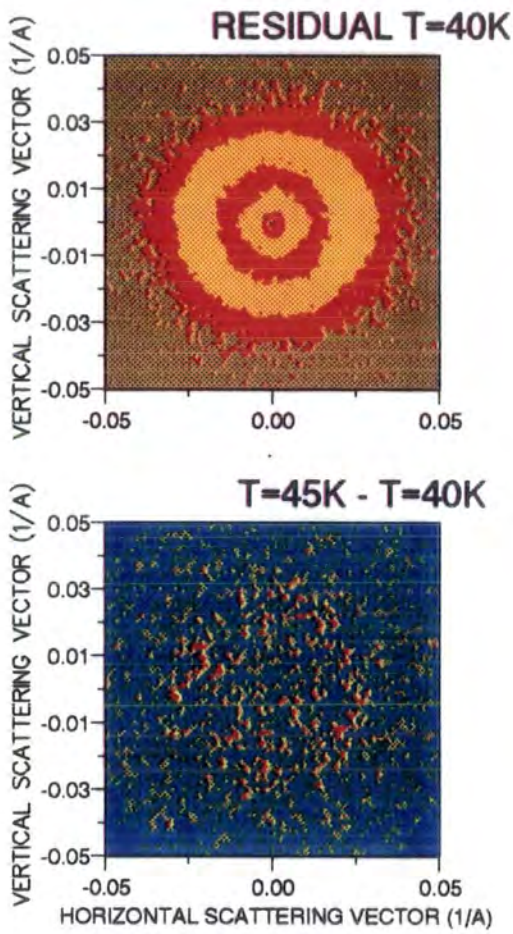
RESIDUAL T=40K
VERTICAL SCATTERING VECTOR (1/A)
0.05
0.03
0.01
-0.01
-0.03
-0.05
-0.05
0.00
0.05
T=45K - T=40K
VERTICAL SCATTERING VECTOR (1/A)
0.05
0.03
0.01
-0.01
-0.03
-0.05
-0.05
0.00
0.05
HORIZONTAL SCATTERING VECTOR (1/A)

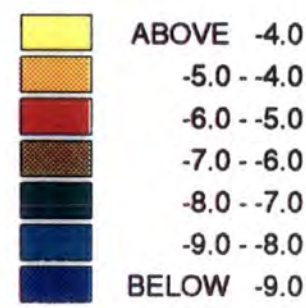
ABOVE -4.0
-5.0 - -4.0
-6.0 - -5.0
-7.0 - -6.0
-8.0 - -7.0
-9.0 - -8.0
BELOW -9.0

$< 111 >$ directions, with secondary satellites along the [110] direction and another pair existing outside the detector along the [001] direction.

The satellites are due to the neutrons diffracting from the helical spin density wave. The presence of the secondary satellites which are much weaker than the primary, may be a consequence of a number of processes. Multiple scattering may be ocurring within the crystal. Within the MnSi crystal, the domains result in the helical spin density waves only being a finite length. As a result, the helix will also consist of numerous harmonics and the secondary satellite may be measuring the second harmonic of the 'wave packet'. Also, when in a magnetic field there may be some moment reorientation in order to reduce the energy within the arrangement. This so called 'squaring' of the helix would contribute to the above effect and result in increasing measure of the second harmonic. Despite this, both explainations would seem unlikely as the secondary satellite does not lie in the direction of the helical propagation vector and the intensity does not increase in the presence of a magnetic field. Another feasable explanation is the existence of two seperate helicies within MnSi and obviously requires further investigation.

7.7 Study of the Magnetic Satellites Close to the Transition Temperature

Figure 7.6 shows the results of a temperature study close to the magnetic transition for MnSi for decreasing temperature. The crystal is orientated such that the scattering vector for two of the helicies is in the plane of the detector i.e. satellites on the left hand side. The results show evidence of a helical spin density wave propagating along the $< 111 >$ direction at 29.1K, after which the intensity of the satellites dramatically increases as the temperature is lowered.

This is summarised in figure 7.7 which shows the integrated intensity of the detector area corresponding to the position of the top left satellite. Although the error margins are significant, the dotted line shows a parabola fitted to the data which acts as a smooth curve through the data points below the transition temperature. There was no evidence of the diffuse ring of scattering as observed by Lebech *et al.*(1989) close to but above the transition temperature of FeGe, although this may be due to the scatter from the cryostat resulting in a high background noise level.

7.8 SANS on MnSi in an Applied Magnetic Field

SANS was performed on MnSi in an applied magnetic field and figure 7.8 shows the results obtained at 4.2K. The sample used was a cylinder of diameter 2mm and length 5mm cut from the same crystal as the previous sample. The magnetic field was monitored by a Hall probe mounted close to the sample. Count times were 30 minutes.

Again the sample is orientated such that four satellites of equal intensity are observed in zero field, in the four equivalent $< 111 >$ directions and secondary

Figure 7.5 Equal intensity contours, SANS data (log-scale) obtained from MnSi at 4.2K. The crystal is orientated such that the scattering plane is $(1\bar{1}0)$ with [001] vertical and [110] horizontal. The background scattering from the cryomagnet has been subtracted. The magnetic satellite Bragg peaks are the red-yellow spots observed at $q \approx 0.035$

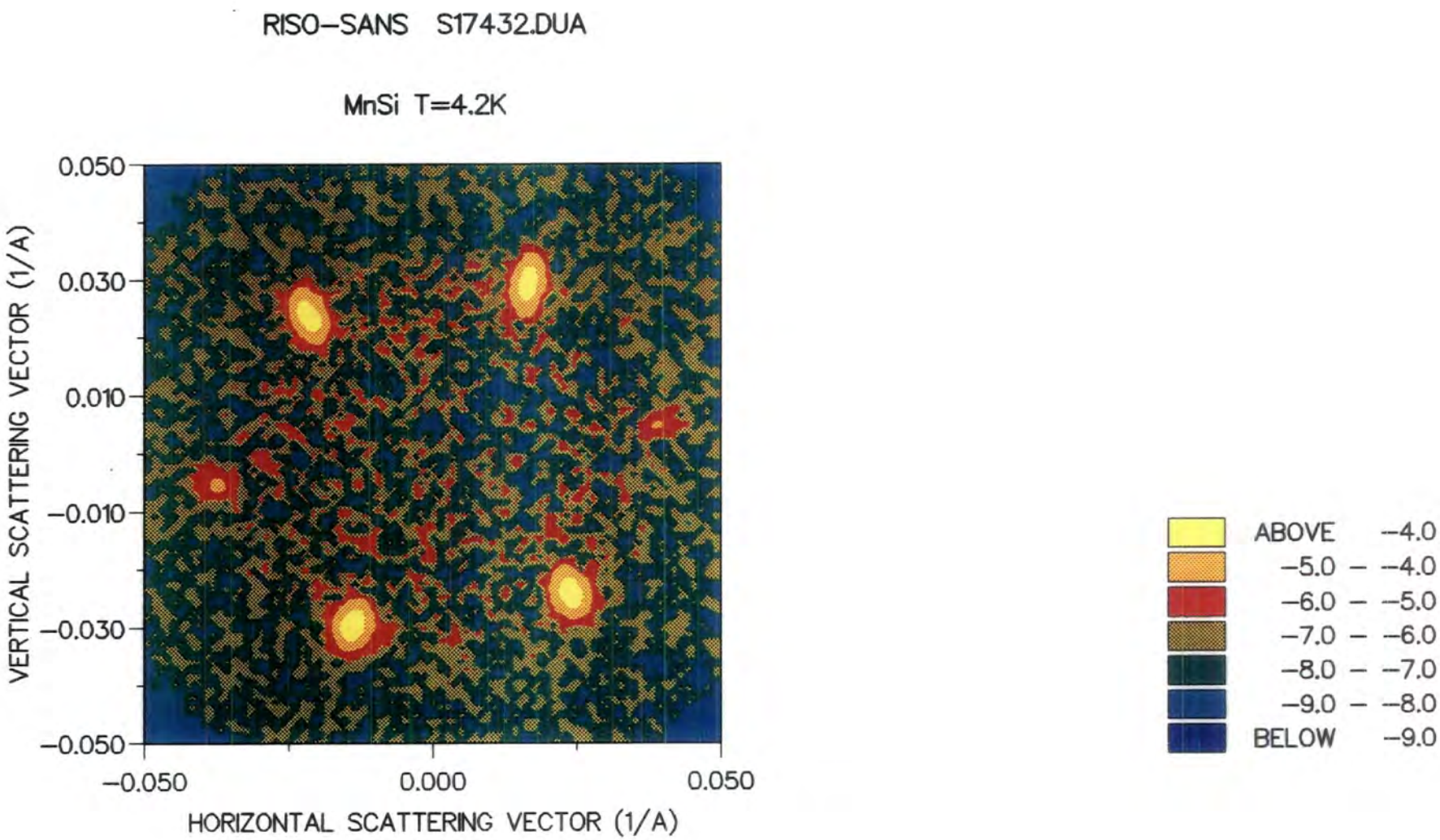
RISO–SANS S17432.DUA
MnSi T=4.2K
0.050
0.030
0.010
−0.010
−0.030
−0.050
VERTICAL SCATTERING VECTOR (1/A)
−0.050
0.000
0.050
HORIZONTAL SCATTERING VECTOR (1/A)
ABOVE −4.0
−5.0 – −4.0
−6.0 – −5.0
−7.0 – −6.0
−8.0 – −7.0
−9.0 – −8.0
BELOW −9.0

Figure 7.6 Equal intensity contours, SANS data (log-scale) obtained from MnSi close to the transition temperature. Again the background scattering from the cryomagnet has been subtracted. (a) 29.4K; (b) 29.2K; (c) 29.1K; (d) 29.0K; (e) 28.8K; (f) 28.7K

MnSi

Vary temperature through T_N
Zero field

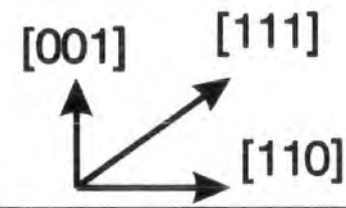

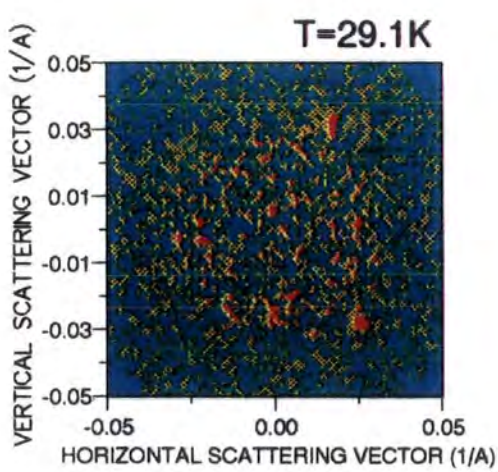

logarithmic intensity scale

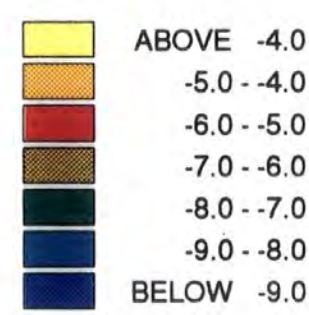

MnSi

Vary temperature through T_N
Zero field

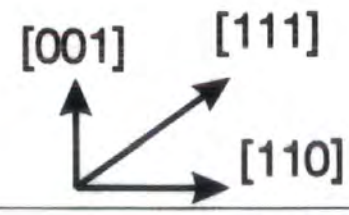

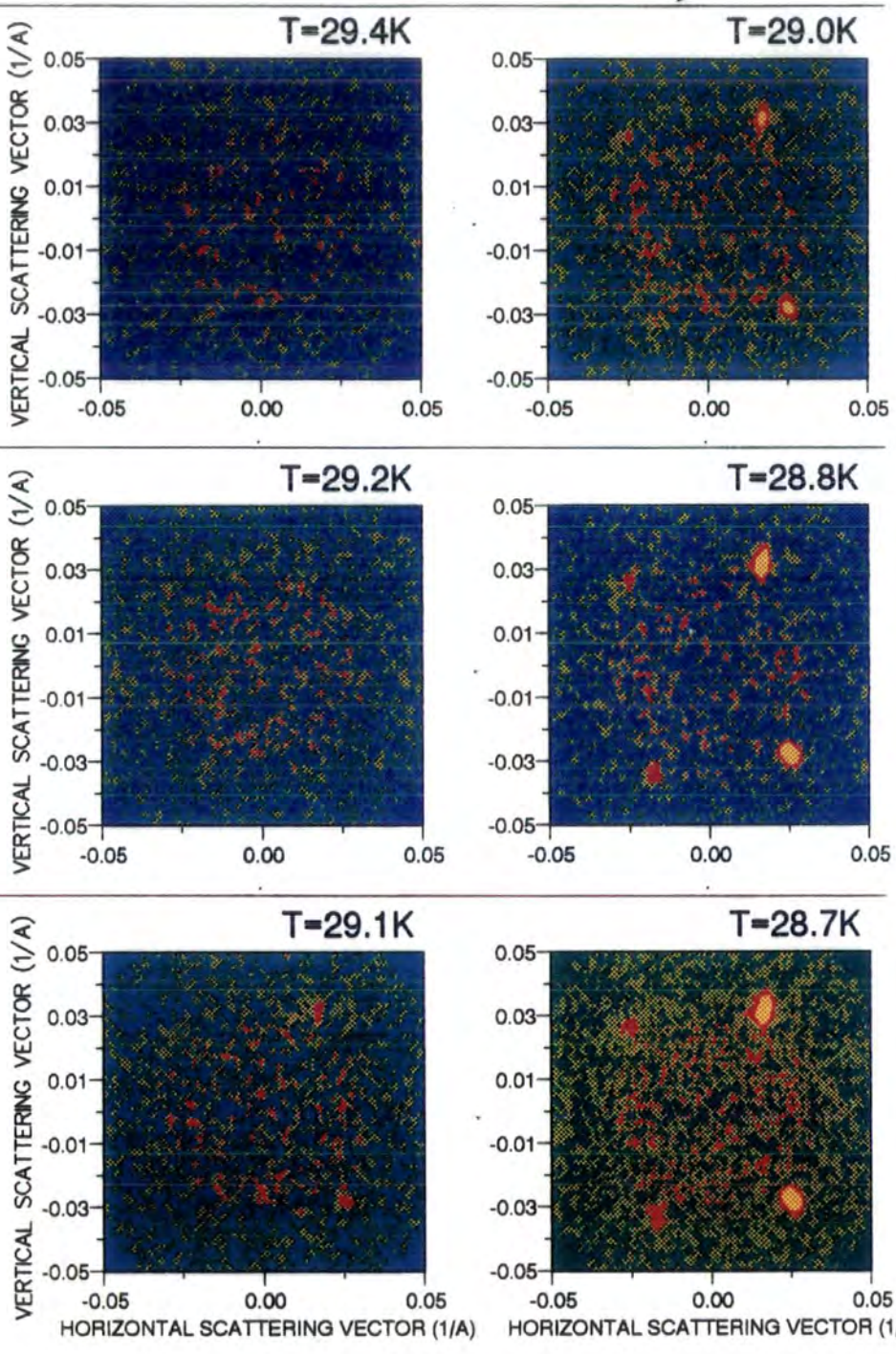

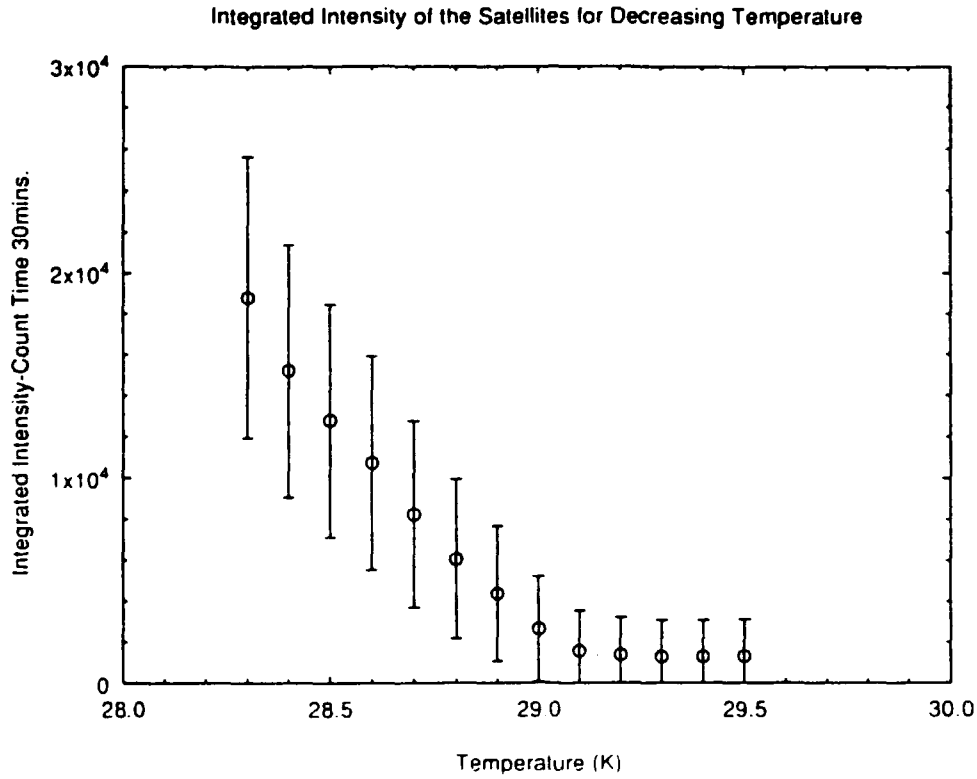

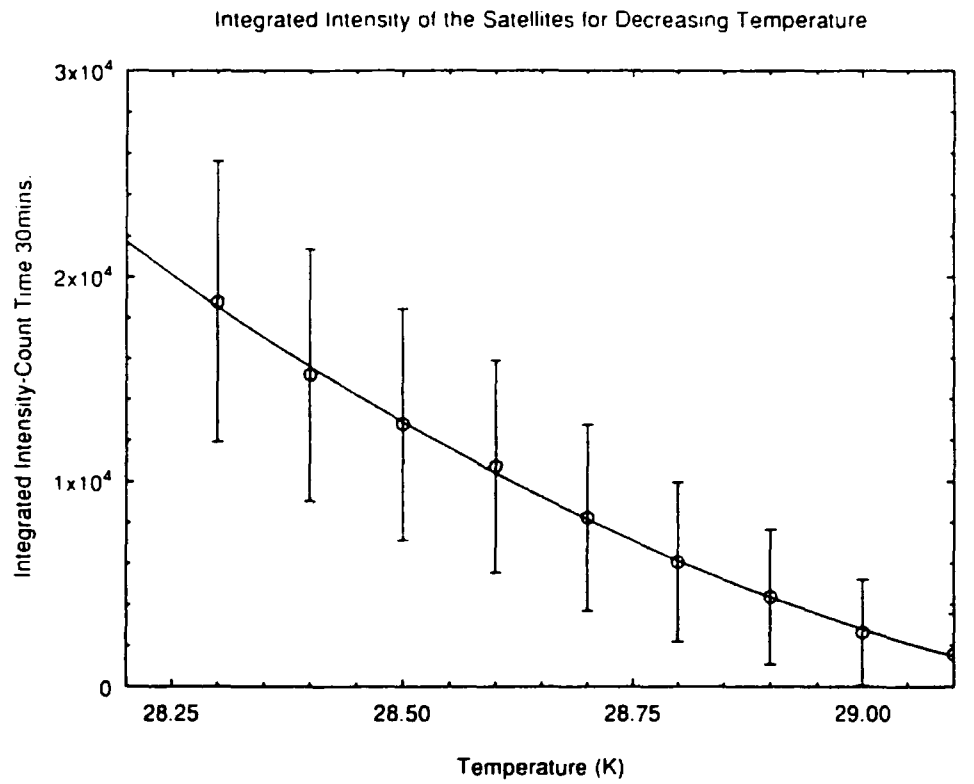

Figure 7.7 (a)Integrated intensity of the detector corresponding to the position of the top left magnetic Bragg satellite; (b) a parabolic fit to the data points below the transition temperature.

satellites are observed parallel to the [001] direction. Initially as the field is increased, the satellites remain fixed and apart from slight alteration in background (residuals at all orientations and fields could not be obtained), there is no change to the observed scattering from the sample. At a field of 500Oe rotation of the satellites towards the field direction commences, more noticeable by the movement of the secondary satellites. This trend continues as the field is increased until eventually at a field of 2160Oe rotation of the satellites is complete and they lie parallel to the field. This information is summarised in figure 7.9.

The rotation of the satellite corresponds to the curved region of the magnetisation with field applied parallel to the [001] direction. After the helix is rotated into the field direction the magnetisation is linear with applied field until saturation occurs. Although no rotations in the scattering plane were performed to follow the centre of the satellite as it rotated into the field direction, the intensity of the satellites remains approximately constant. This fact suggests that the moments remain perpendicular to the helical axis during this rotation process.

Rotation of the helical propagation direction to lie parallel with the applied field results in the magnetic moments being arranged perpendicular to the magnetic field. This is in fact the lowest energy arrangement of the magnetic moments. The magnetisation density of a quantum mechanical system of volume V, in thermal equilibrium at a temperature T in a uniform magnetic induction $(B_0)_i$ is defined to be:

$$\underline{M} = -\frac{1}{V}\frac{\partial F}{\partial (B_0)_i} \tag{7.23}$$

where F is the magnetic Helmholtz free energy. From Chapter 1, and the definition of the differential susceptibility then:

$$\chi = -\frac{1}{V}\frac{\partial^2 F}{\partial (B_0)_i^{\,2}} \tag{7.24}$$

The differential susceptibility can be divided into two components such that:

$$\chi = \chi_{\parallel} + \chi_{\perp} \tag{7.25}$$

Hence the magnetic free energy per unit volume is:

$$F = -\frac{1}{2}\chi_{\parallel}(B_0)_{i\parallel}^{\,2} - \frac{1}{2}\chi_{\perp}(B_0)_{i\perp}^{\,2} \tag{7.26}$$

This expression is minimised with maximum value of χ which corresponds to the moments being perpendicular to the applied magnetic field, as shown by the inverse susceptibility when the field is applied parallel to the $< 111 >$ direction (see Chapter5).

However, the magnetostatic and magnetocrystalline anisotropy should also be considered when concerning the resulting magnetic moment arrangement. In zero field, the helical propagation direction defines where the anisotropy energy is greatest since the moments are arranged perpendicular to this. The fact that the helix is able to rotate into the field direction in order to minimise the magnetic free energy is indicative that the anisotropy energy is low. Despite this, note that the rotation

Figure 7.8 Equal intensity contours, SANS data (log-scale) obtained from MnSi at 4.2K as a function of applied magnetic field. The background scattering from the cryomagnet has been subtracted. (a) 0T; (b) 0.042T; (c) 0.075T; (d) 0.100T; (e) 0.125T; (f) 0.141T; (g) 0.158T; (h) 0.166T; (i) 0.174T; (j) 0.183T; (k) 0.191T; (l) 0.216T.

MnSi 4.2 K

B

[001] [111] [110]

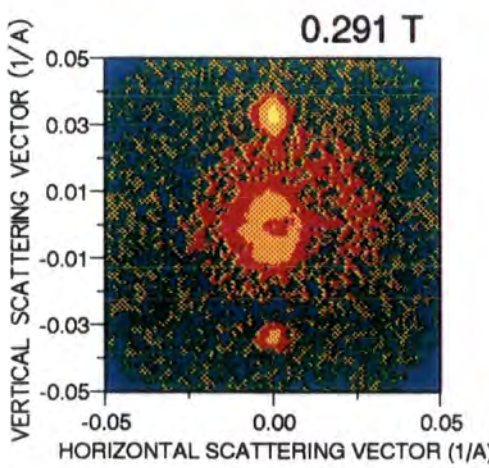

logarithmic intensity scale

ABOVE -4.0
-5.0 - -4.0
-6.0 - -5.0
-7.0 - -6.0
-8.0 - -7.0
-9.0 - -8.0
BELOW -9.0

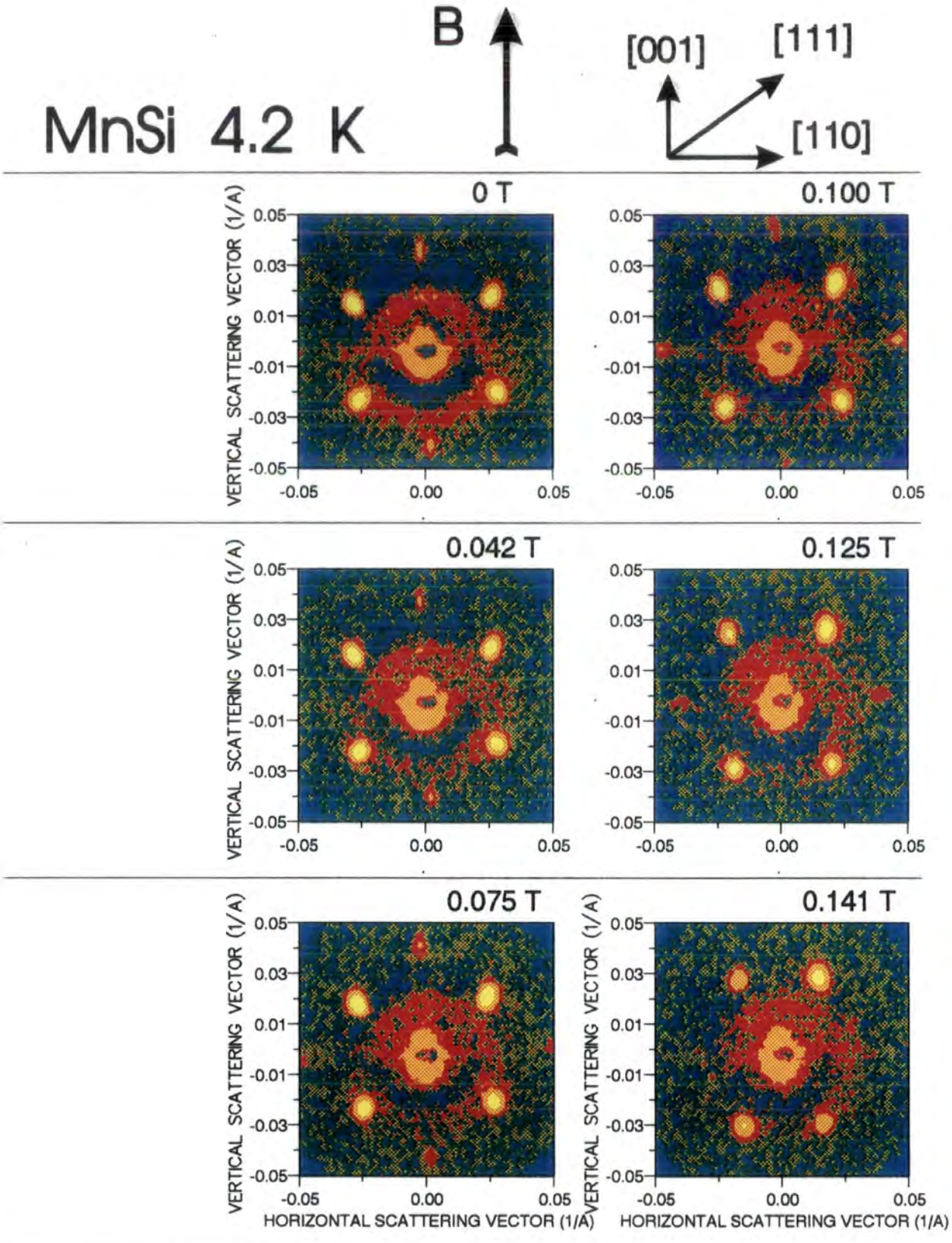
MnSi 4.2 K
B
[001]
[111]
[110]
0 T
0.100 T
0.042 T
0.125 T
0.075 T
0.141 T
VERTICAL SCATTERING VECTOR (1/A)
HORIZONTAL SCATTERING VECTOR (1/A)
0.05
0.03
0.01
-0.01
-0.03
-0.05
0.00

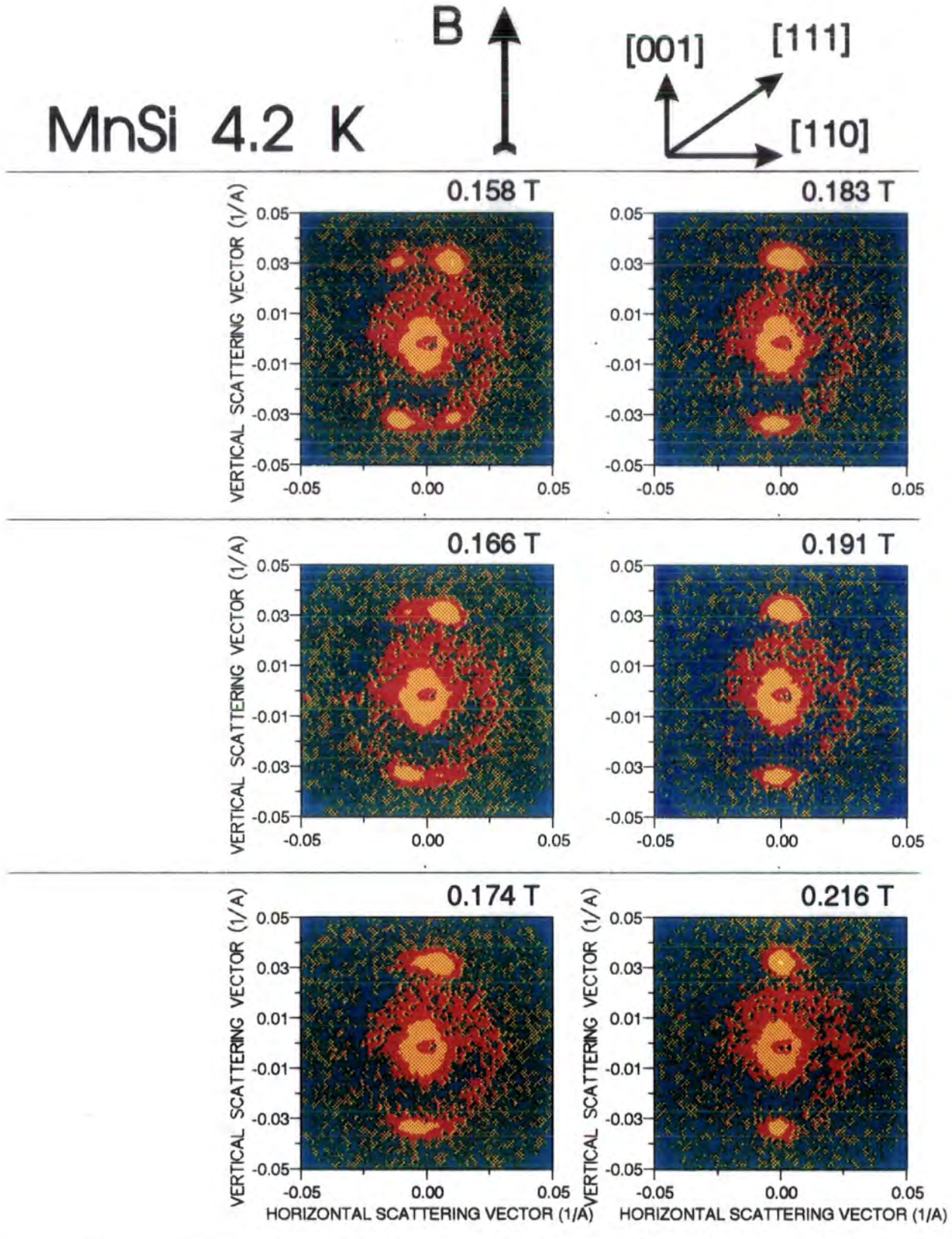
MnSi 4.2 K
B
[001]
[111]
[110]
0.158 T
0.183 T
0.166 T
0.191 T
0.174 T
0.216 T
VERTICAL SCATTERING VECTOR (1/A)
HORIZONTAL SCATTERING VECTOR (1/A)
0.05
0.03
0.01
-0.01
-0.03
-0.05
0.00

Figure 7.9 Field dependancies of the angle θ, between the modulation vector $\underline{q}$ and the direction of the applied field at 4.2K in cubic MnSi for two seperate experiments, (green and red) both with increasing magnetic field.

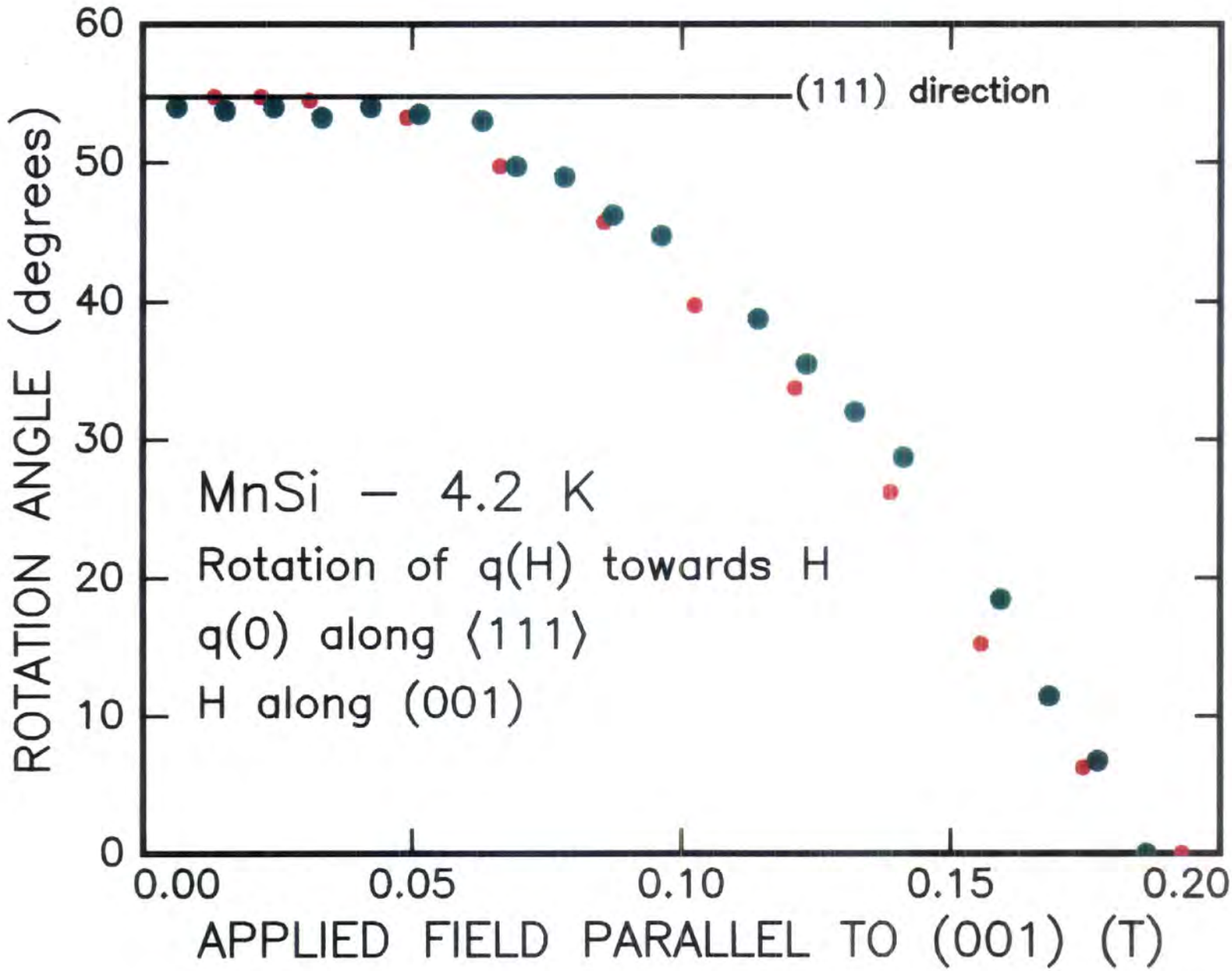
60
50
40
30
20
10
0
ROTATION ANGLE (degrees)
(111) direction
MnSi — 4.2 K
Rotation of q(H) towards H
q(0) along ⟨111⟩
H along (001)
0.00
0.05
0.10
0.15
0.20
APPLIED FIELD PARALLEL TO (001) (T)

is gradual and requires a minimum field of $\approx$ 400Oe before commencing. As the magnetic field is increased after helix reorientation, the magnetic moments cone towards the field direction in order to reduce the magnetostatic energy.

7.9 MnSi and 'Phase A'

In order to investigate 'Phase A' SANS was performed on MnSi in an applied magnetic field at a temperature of 28.5K as shown in the phase diagram of figure 7.10. The cylindrical sample was used and count times were 30 minutes.

Figure 7.11 summarises the results; note in particular the different scattering planes indicated at the top of the figure. In the $(1\bar{1}0)$ plane shown on the right, domain reorientation has occured at 0.14T and the satellites are parallel to the field direction. At 0.21T the crystal is in 'Phase A' and there is no evidence of the satellites in this plane but at 0.31T they return to lie parallel to the field.

Rotation of the scattering plane shows that within 'Phase A' the symmetry is broken and the helix propagates only along the two $< 100 >$ directions perpendicular to the field i.e. $\underline{q}$ || [100] and [010] directions. Above 'Phase A' the helix lies parallel to the field. This rotation of the helix occurs as a 'flip' i.e. no other intermediate orientations are occupied. At the boundary of 'Phase A' there is a field region where there exist some domains with helical orientation perpendicular to the field and some with it parallel to the field as shown in figure 7.12.

Within 'Phase A', as the helix lies perpendicular to the field then some of the moments will lie parallel to the field, increasing the energy of the system. Consequently there may be some squaring of the helix to reduce this (as shown in figure 7.18 in the case of FeGe), which may be evident in the increasing intensity of the secondary satellites but unfortunately they are situated outside of the detector.

This result is entirely consistent with the magnetisation measurements obtained in Chapter 5. The magnetisation of 'Phase A' is highly anisotropic, as shown in the magnetisation measured with magnetic field applied parallel to the $< 001 >$ direction but no evidence of it when the field is aligned in the $< 111 >$ direction. The SANS results show the response to be related to crystal structure as with field parallel to the $< 111 >$ direction there does not exist a $< 001 >$ direction perpendicular to the field. The magnetisation with field applied parallel to the $< 001 >$ direction in 'Phase A' shows a sudden increase but to a region of reduced susceptibility. When the spin density wave is perpendicular to the field, some of the moments will be parallel to the field and hence the sudden increase in magnetisation. However, once aligned their orientation will not vary greatly with field so the region has a lower susceptibility.

Previous studies by Ishikawa (1984) suggested that 'Phase A' was extension of the paramagnetic phase into the helical region although only the $(1\bar{1}0)$ scattering plane was investigated. The actual result is more closely related to current theories and can be explained by a field dependant anisotropy energy. It is also identical to the results reported on the magnetic phase diagram of (Fe,Co)Si by Ishimoto *et al.* (1990), a related helical structure.

Figure 7.10 Magnetic phase diagram of MnSi near T_N obtained from magnetisation measurements (see Chapter5). The red circles indicate schematically the field regions where the small angle neutron scattering data for MnSi were collected.

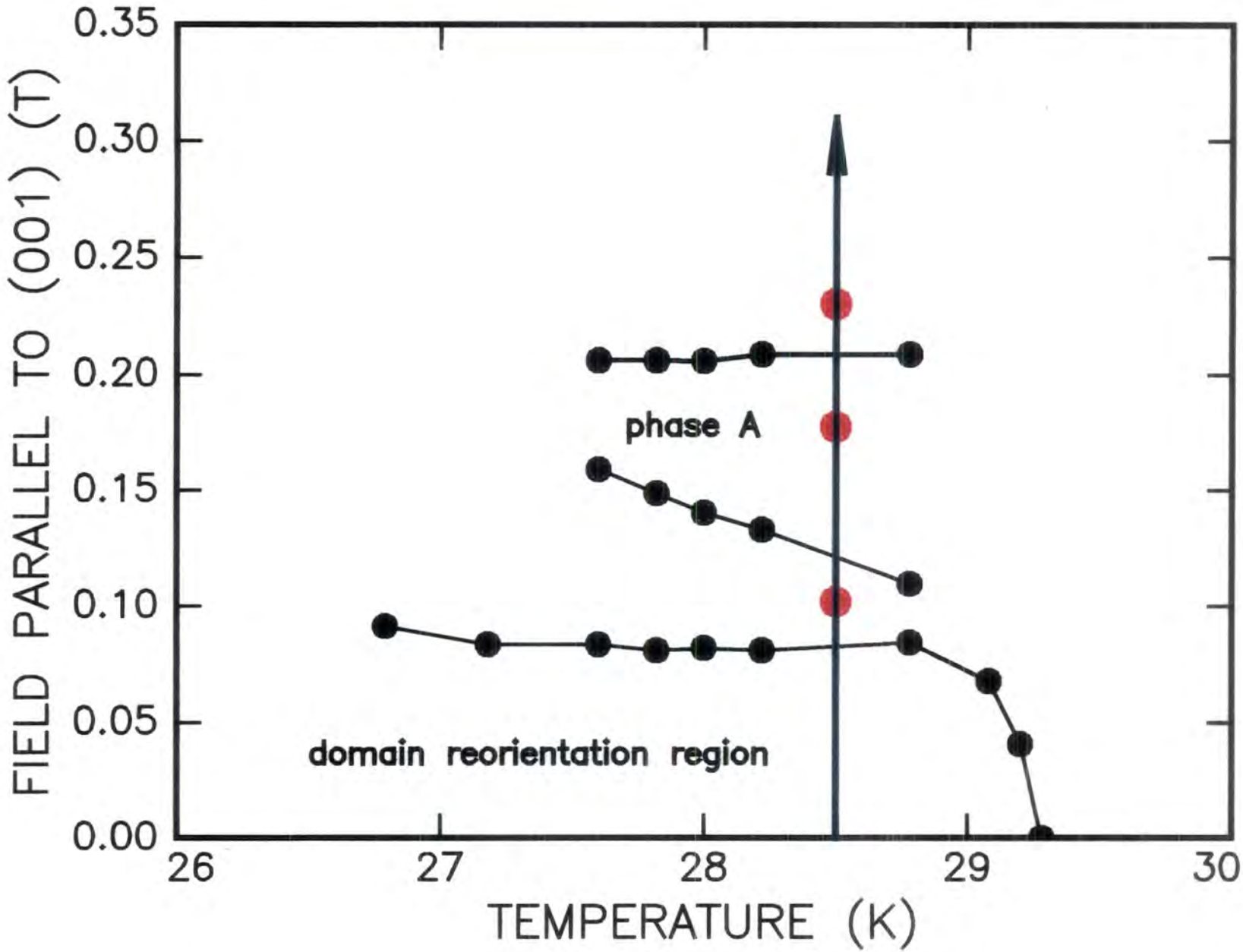
0.35
0.30
0.25
0.20
0.15
0.10
0.05
0.00
FIELD PARALLEL TO (001) (T)
phase A
domain reorientation region
26
27
28
29
30
TEMPERATURE (K)

Figure 7.11 Equal intensity contours, SANS data (log scale) observed in and out of 'Phase A' for two different crystal orientations (see text). The background scattering from the cryomagnet (which was substantial) has been subtracted. The magnetic satellite Bragg peaks are the red-yellow spots observed at $\underline{q} \approx 0.035\mathring{A}^{-1}$. The intense scattering around (0,0) in the right hand panel is presumably caused by insufficient subtraction of the central background.

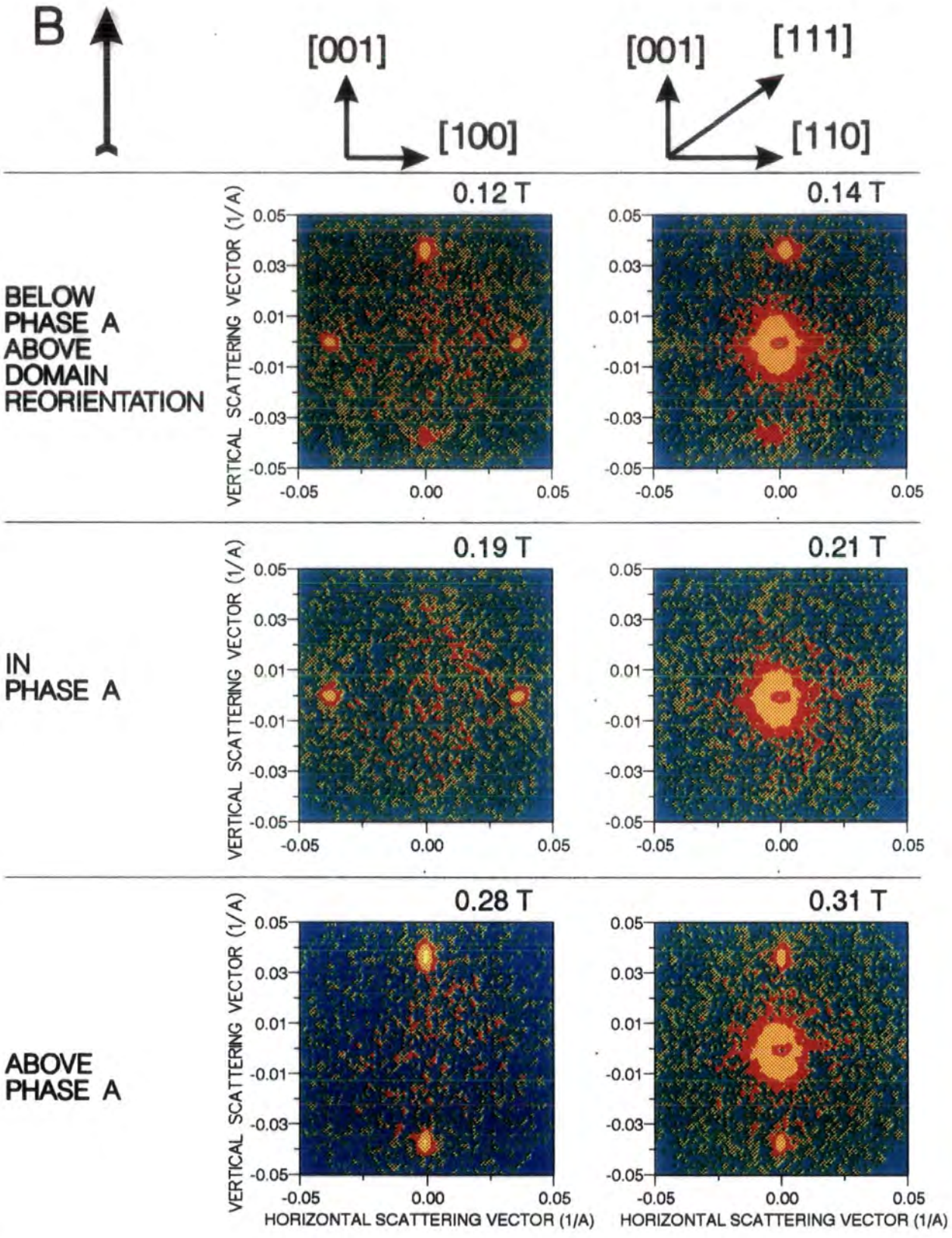
B
[001]
[100]
[001]
[111]
[110]
BELOW PHASE A ABOVE DOMAIN REORIENTATION
0.12 T
0.14 T
IN PHASE A
0.19 T
0.21 T
ABOVE PHASE A
0.28 T
0.31 T
VERTICAL SCATTERING VECTOR (1/A)
HORIZONTAL SCATTERING VECTOR (1/A)
0.05
0.03
0.01
-0.01
-0.03
-0.05
0.00

Figure 7.12 Equal intensity contours, SANS data (log scale) observed at the start of 'Phase A' in a magnetic field of 0.12T. The crystal is orientated such that the [001] is vertical and [100] horizontal in the scattering plane.

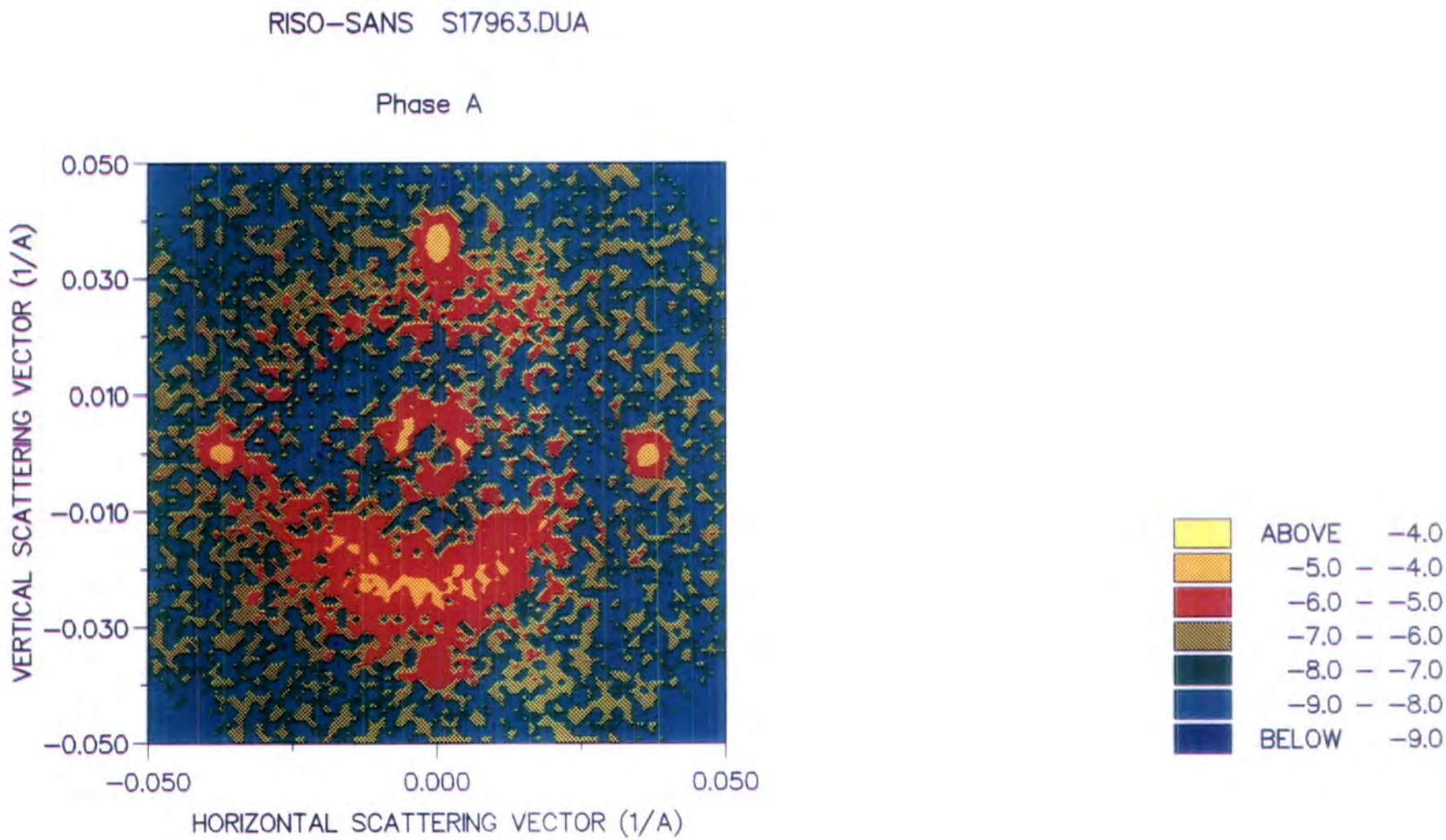
RISO–SANS S17963.DUA
Phase A
0.050
0.030
0.010
−0.010
−0.030
−0.050
VERTICAL SCATTERING VECTOR (1/A)
−0.050
0.000
0.050
HORIZONTAL SCATTERING VECTOR (1/A)
ABOVE −4.0
−5.0 – −4.0
−6.0 – −5.0
−7.0 – −6.0
−8.0 – −7.0
−9.0 – −8.0
BELOW −9.0

7.10 SANS on FeGe

Current understanding of the behaviour of FeGe (with cubic B_{20} structure) is dependant on the comprehensive study by Lebech *et al.* (1989) using SANS as a probe. Some of the results already published are reproduced here by kind permission of Professor Lebech in order to explain observations in the magnetisation measurements and also for comparison with MnSi.

7.11 SANS on FeGe in zero field

Figure 7.13 shows the results of a temperature study on the magnetic structure of FeGe using SANS. The start of the phase transition is marked at a temperature of 278.86K by a ring of diffuse scatter at a radius of $\underline{q}$, the wavevector of the helix in FeGe. As the temperature is lowered to 278.63K, satellites are seen to develop in the $< 100 >$ directions, initially with low intensity but dramatically increasing by a temperature of 278.31K. Further lowering the temperature, the satellite intensity gradually increases and their area becomes slightly larger.

At a temperature of 232.00K, the same satellites are still prominent, but now have a background of a much less intense ring of scatter. As the temperature is reduced in this regime, the intensity spreads from the satellites around the arcs of the ring although still with maxima at their old positions. The lengths of these arcs increases until at 211K two crescents centred at the previous satellite positions, covering most of the ring circumference and of uniform intensity exist.

The process occuring below this temperature can best be described as a gradual collapse of the ring to satellites along the [111] direction, together with secondary satellites along the [011] and [100] directions. Below 150K, higher orders of satellites are also observed.

In summary, in FeGe the direction of helical propagation changes with temperature. At temperatures below the upper magnetic ordering temperature and above the lower, the helix propagates along equivalent $< 100 >$ directions and along equivalent $< 111 >$ directions below the lower transition. The transition at which the spiral turns is 'sluggish', taking place in a temperature interval of 40K and shows pronounced hysteresis ($T_{2decr.temp}$=211K, $T_{2incr.temp}$ =245K).

The macroscopic theory developed by Bak and Jensen (1980) made after symmetry analysis of the P_{213} structure shows that a helical spin density wave may exist as a consequence of the Dzyalloshinsky instability and allowed for two propagation directions (the two observed in FeGe), depending on the sign of the anisotropy energy. The behaviour of FeGe can be 'explained' by the value of anisotropy energy being temperature dependant although no description of why this occurs is offered by the theory.

If the anisotropy energy changes sign continuously, then at some temperature it will be equal to zero with no defined propagation direction. Observations in the temperature range 221 - 190K show that the helix does not simply rotate from the

Figure 7.13 Equal intensity contours, SANS data (log scale) observed in the $(0\bar{1}1)$ plane of cubic FeGe at various temperatures below T_N=278.7K after background subtraction and normalisation. (After Lebech (1989)). (a) 278.86K; (b) 278.63K; (c) 278.31K; (d) 277.60K; (e) 256.75K; (f) 232.00K; (g) 226.44K; (h) 221.06K; (i) 219.65K; (j) 216.65; (k) 211.01; (l) 207.60; (m) 204.13; (n) 198.69K; (o) 190.55K; (p) 150.09K; (q) 118.77K; (r) 35.84.

FeGe 0 T

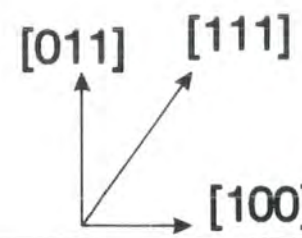

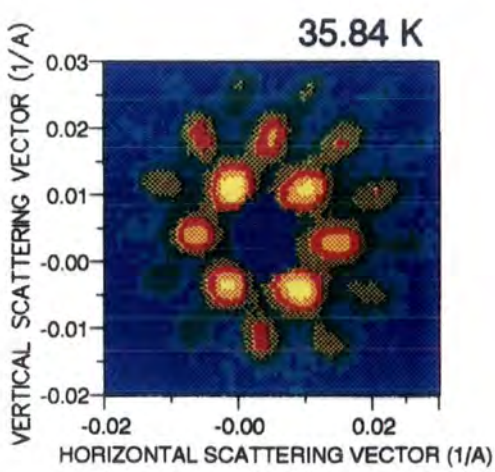

logarithmic intensity scale

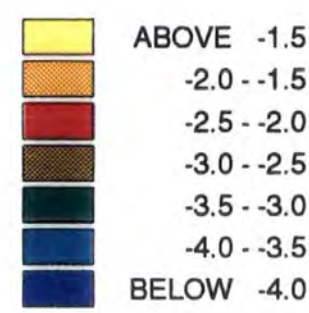

FeGe 0 T

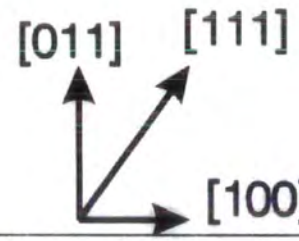
[011]
[111]
[100]

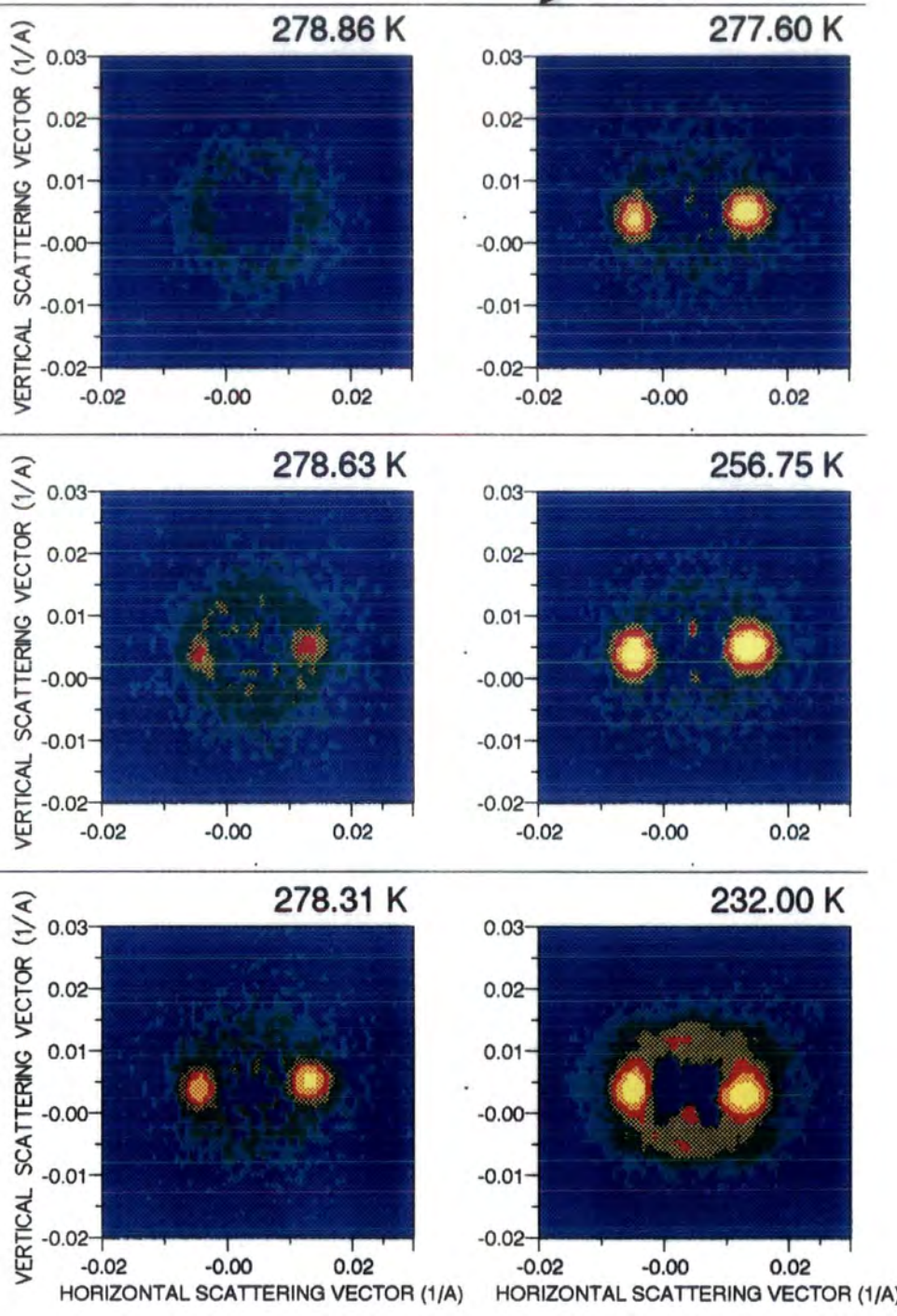
278.86 K
277.60 K
278.63 K
256.75 K
278.31 K
232.00 K
VERTICAL SCATTERING VECTOR (1/A)
0.03
0.02
0.01
-0.00
-0.01
-0.02
-0.02
-0.00
0.02
HORIZONTAL SCATTERING VECTOR (1/A)

FeGe 0 T

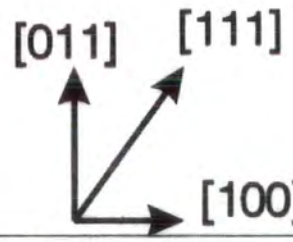
[011]
[111]
[100]

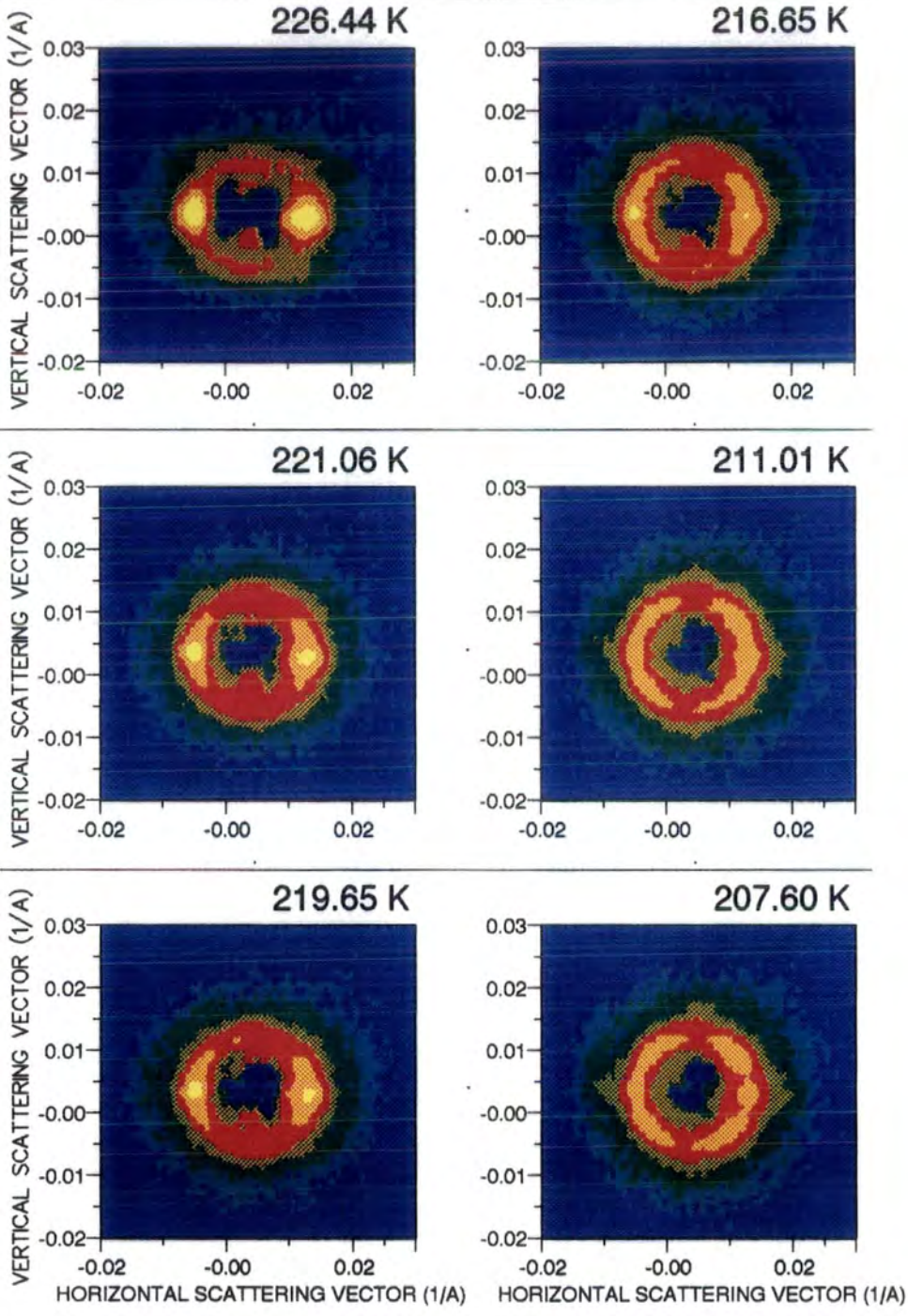
226.44 K
216.65 K
221.06 K
211.01 K
219.65 K
207.60 K
VERTICAL SCATTERING VECTOR (1/A)
0.03
0.02
0.01
-0.00
-0.01
-0.02
-0.02
-0.00
0.02
HORIZONTAL SCATTERING VECTOR (1/A)

FeGe 0 T

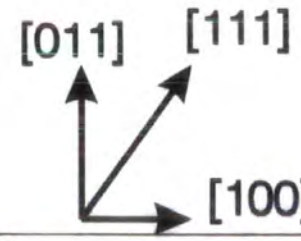
[011]
[111]
[100]

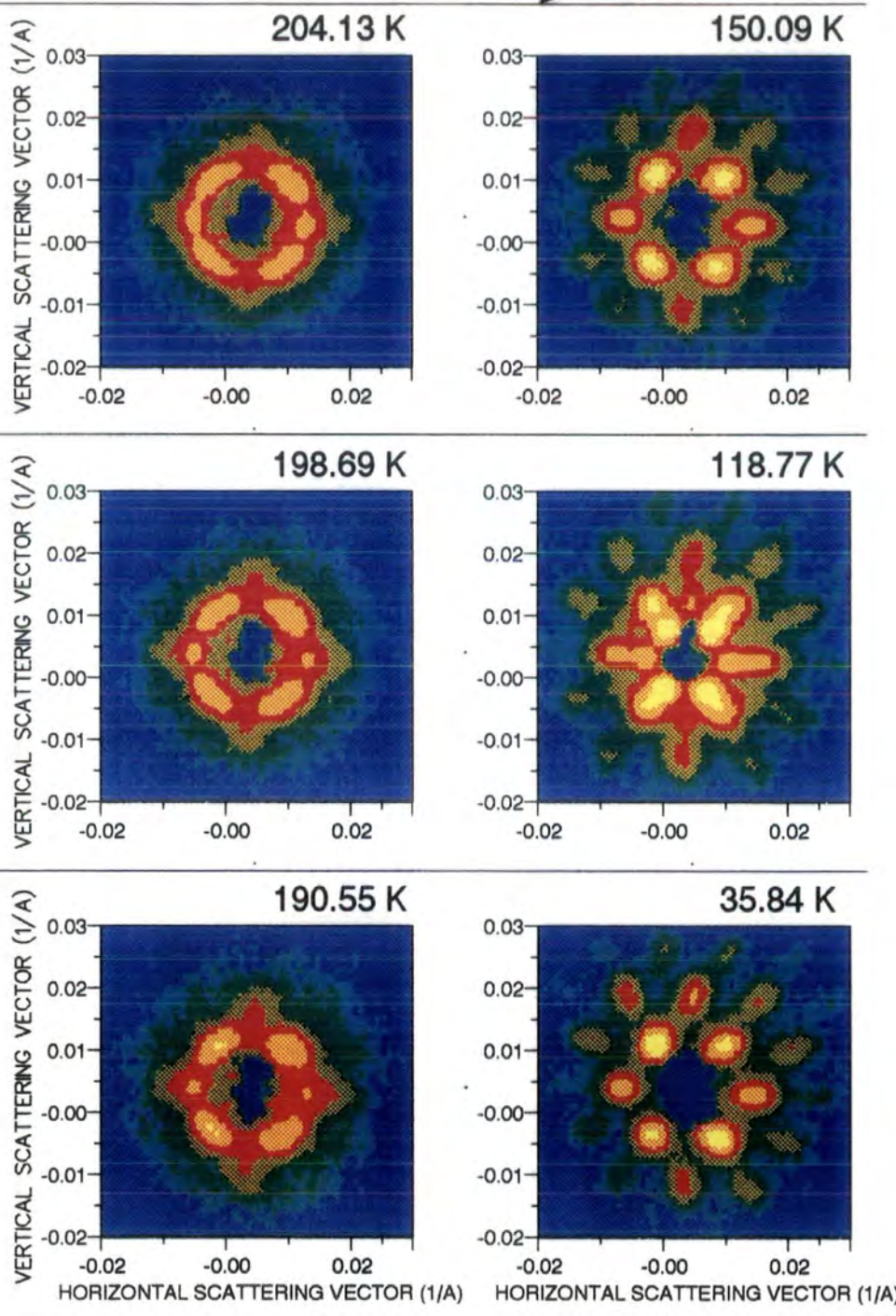
204.13 K
150.09 K
198.69 K
118.77 K
190.55 K
35.84 K
VERTICAL SCATTERING VECTOR (1/A)
HORIZONTAL SCATTERING VECTOR (1/A)
0.03
0.02
0.01
-0.00
-0.01
-0.02
-0.02
-0.00
0.02

[100] to [111] direction, as observed in MnSi for example in an applied magnetic field, but rather there is an intermediate regime corresponding to the two lobes of scattering at 207.60K. Although this is similar to the simulations produced for a disc of helical wavevectors in the scattering plane (figure 7.3), because of the resolution of SANS it is difficult to clearly differentiate between this and the simulation of an arc of helix propagation directions between [100] and [111] directions as shown in figure 7.14. A combination of the two processes may be occuring.

7.12 SANS on FeGe in an applied Magnetic Field

The SANS results obtained on FeGe in an applied magnetic field give some explanation of the magnetisation measurements. The magnetic measurements reported are those with magnetic field applied along the $< 100 >$ axis.

Below the upper transition temperature but above 211K, the crystal orientation corresponds to the field being applied along the helix propagation direction. The magnetisation is linear with applied field and is due to the coning of the moments into the field direction until FeGe becomes magnetically saturated.

Maintaining the magnetic field parallel to the$< 100 >$ direction below the lower transition temperature, the helix now propagates along $< 111 >$ directions and hence is initially orientated at an angle of $\approx 55^{o}$ to field direction. The magnetisation is now curved in low fields before becoming linear (with same susceptibility as above the lower transition temperature) and finally saturating. Figure 7.15 summarises the results of Lebech (1989) for FeGe at 140K and reveals that for this initial orientation, the magnetic field causes the spiral axis to rotate in to the field direction. This corresponds to the curved region of magnetisation. Analysis shows that the rotation of the helix is similar to that observed in MnSi (with helix not initially perpendicular to the field direction) in that it requires a finite field before the rotation begins and it is a second order process with intermediate orientations being occupied. During rotation into the field direction, the total intensity of the satellites remains 'nearly unchanged' which suggests the moments remain perpendicular to the propagation direction of the helix. When rotation is complete, the moments cone into the helix propagation direction.

7.13 Discussion

7.13.1 Helix rotation into the field direction

To understand the mechanisms behind helix rotation, consider the original work of Plumer and Walker (1981), *'Wavevector and spin reorientation in MnSi'*. From the assumption that in the presence of a homogeneous external magnetic field, the spin density (averaged over the unit cell) can be written as:

$$\underline{s}(\underline{r}) = \underline{m} + \underline{S}exp(i\underline{Q}.\underline{r}) + \underline{S}^{*}exp(-i\underline{Q}.\underline{r}) \qquad (7.27)$$

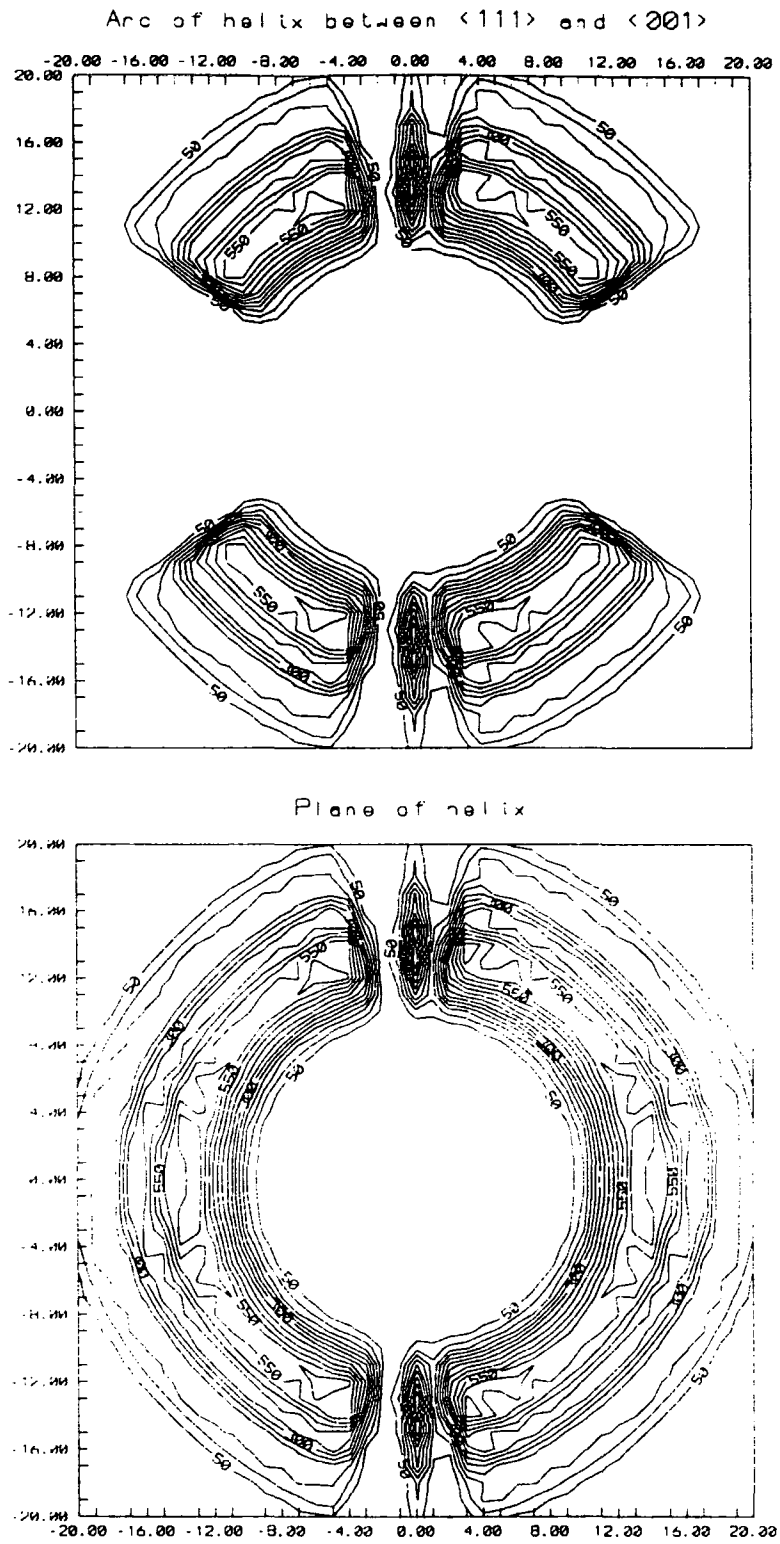

Figure 7.14 SANS simulation results for FeGe for particular $\underline{q}$ arrangements. The scattering plane was a $(1\bar{1}0)$ plane with [001] vertical and [110] horizontal. The input parameters used were incident wavevector $0.3977\AA^{-1}$, source sample seperation 6000mm, sample detector seperation 6000mm, upper limit to the wavevector $0.009199\AA^{-1}$ and lower limit $0.008975\AA^{-1}$. These are similar to the experimental conditions of Lebech *et al.* (1989). (a) Arc of possible $\underline{q}$ between the < 111 > and < 001 > directions in the scattering plane; (b) plane or disc of $\underline{q}$ in the scattering plane.

Figure 7.15 Field dependancies of the angle θ, between the modulation vector $\underline{q}$ and the direction of the magnetic field $\underline{H}$ at 140K in cubic FeGe. The insets show the relevant parts of reciprocal space and define the orientations of the initial modulation vector $\underline{q}(0)$ and the modulation vector $\underline{q}(\underline{H})$ along [011]. Both these vectors lie in a vertical plane parallel to the area sensitive detector.

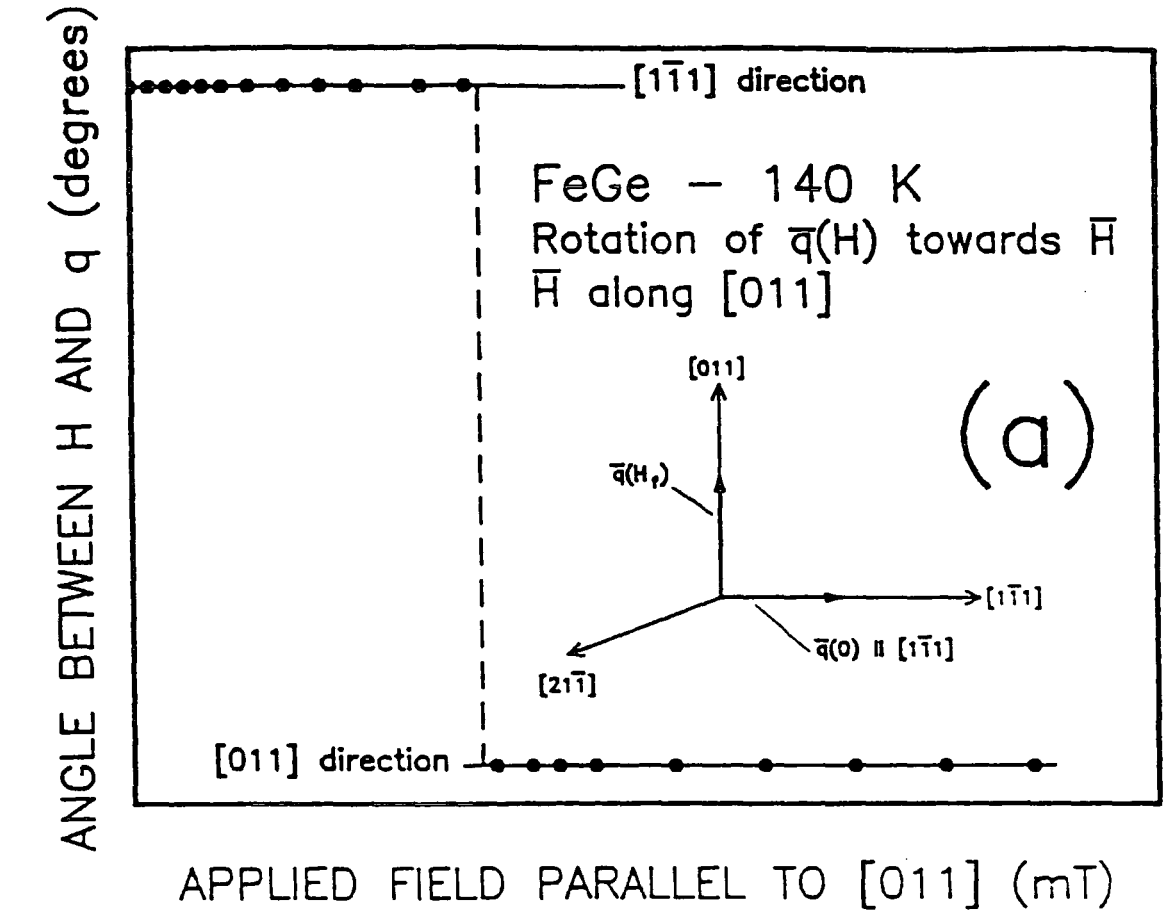
ANGLE BETWEEN H AND q (degrees)
[1$\bar{1}$1] direction
FeGe – 140 K
Rotation of $\bar{q}$(H) towards $\bar{H}$
$\bar{H}$ along [011]
[011]
$\bar{q}(H_c)$
(a)
[1$\bar{1}$1]
$\bar{q}$(0) ∥ [1$\bar{1}$1]
[21$\bar{1}$]
[011] direction
APPLIED FIELD PARALLEL TO [011] (mT)

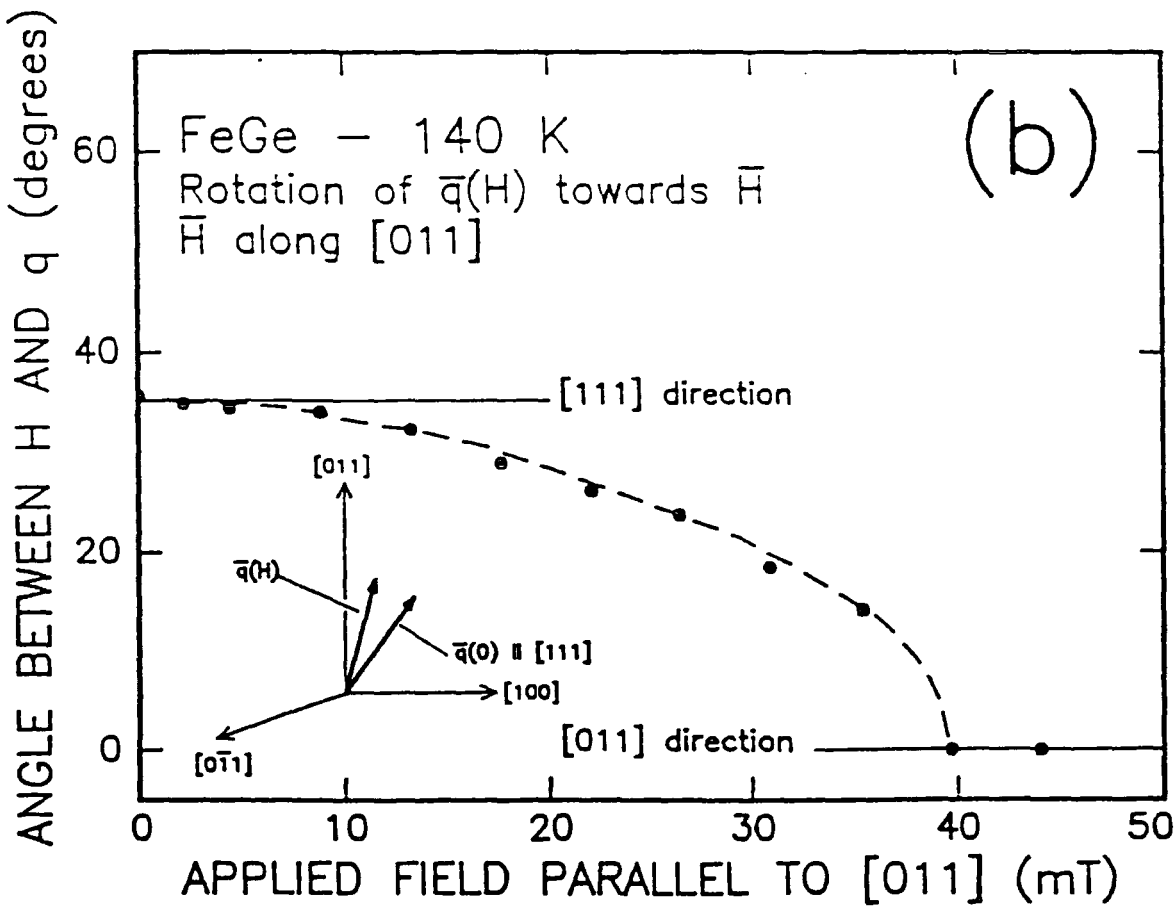
ANGLE BETWEEN H AND q (degrees)
60
40
20
0
FeGe – 140 K
Rotation of $\bar{q}$(H) towards $\bar{H}$
$\bar{H}$ along [011]
(b)
[111] direction
[011]
$\bar{q}$(H)
$\bar{q}$(0) ∥ [111]
[100]
[0$\bar{1}$1]
[011] direction
0
10
20
30
40
50
APPLIED FIELD PARALLEL TO [011] (mT)

Figure 7.15

where $\underline{S}$ is called the spin density wave polarisation vector, $\underline{Q}$ is the wavevector and $\underline{m}$ is the homogeneous contribution to the spin density wave which is induced by the external magnetic field $\underline{H}$. Assuming the free energy to be a function of $\underline{Q}$, $\underline{m}$ and $\underline{S}$, they obtain an expression for the free energy of:

$$\begin{aligned} F &= \frac{1}{2}A_0m^2 + A_QS^2 + Bn^2S^2 + BS^4 + \frac{1}{4}Bm^4 \\ &+ B'm_{\perp Q}{}^2S^2 + (\frac{1}{2}DQ^2S^2 + \frac{1}{4}ES^4)g - m_{\|Q}Hcos\theta - m_{\perp Q}Hsin\theta \quad (7.28) \end{aligned}$$

where $(\frac{1}{2}DQ^2S^2 + \frac{1}{4}ES^4)g$ is the anisotropy energy; β_1,β_2 and β_3 are the direction cosines of $\underline{Q}$ relative to the crystallographic axes; g=1+$\beta_1{}^4$ +$\beta_2{}^4$+$\beta_3{}^4$; θ is the angle between $\underline{Q}$ and the external field $\underline{H}$; $m_{\|Q}$ and $m_{\perp Q}$ are the components of $\underline{m}$ parallel and perpendicular to $\underline{Q}$; and all coefficients depend on temperature only. These definitions are not linked to terms mentioned in Chapter 1.

By minimising the expression for the free energy with respect to $m_{\perp Q}$, $m_{\|Q}$ and S^2 at fixed $\underline{Q}$ orientation they obtain solutions to first order in $\underline{H}$ of:

$$m_{\|Q} = \chi_{\|Q}Hcos\theta \text{ where } \chi_{\|Q} \approx (\Delta - \frac{Eg|A_Q|}{4B})^{-1} \quad (7.29)$$

$$m_{\perp Q} = \chi_{\perp Q}Hsin\theta \text{ where } \chi_{\perp Q} \approx (\Delta + \frac{B'}{B}|A_Q|)^{-1} \quad (7.30)$$

and $\Delta = |C|Q - A_2Q^2$.

When the field is applied at an angle θ to the helix propagation vector, the term $B'm_{\perp Q}{}^2S^2$ ($B' > 0$) in the free energy will increase. In order to reduce the contribution of this term, the helix rotates to cause $\underline{Q}$ to become parallel to the magnetic field direction, the lowering in free energy being greater than the increase in anisotropy energy which favours $\underline{Q}$ lying in the < 111 > direction. Note that when the helix is aligned with the field, $m_{\perp Q}$=0 since there is no magnetic field applied in this direction and the moment arrangement is antiferromagnetic in the plane perpendicular to $\underline{Q}$.

By reinserting the expressions for $m_{\|Q}$ and $m_{\perp Q}$ into that for the free energy, and assuming the helix rotation commences on application of a magnetic field (such that $sin^2\theta = \frac{(H_{SR}{}^2 - H^2)}{H_{SR}{}^2}$) where H_{SR} is the spin reorientation field, then an expression for the magnetisation along < 001 > is obtained:

$$m_{<001>} = \chi_{\|Q}H - \frac{2}{3}\Delta\chi\frac{(H_{SR}{}^2 - H^2)}{H_{SR}{}^2}H \text{ for} H < H_{SR} \quad (7.31)$$

From the above :

$$\begin{aligned} \underline{m} &= m_{\|Q}cos\theta + m_{\perp Q}sin\theta \\ &= \chi_{\|Q}Hcos^2\theta + \chi_{\perp Q}Hsin^2\theta \quad (7.32) \end{aligned}$$

By considering the difference in magnetisation measured along two different crystallographic directions:

$$\underline{m}_{<111>} - \underline{m}_{<001>} = \chi_{\|Q}H - (\chi_{\|Q}Hcos^2\theta + \chi_{\perp Q}Hsin^2\theta) \quad (7.33)$$

$$= sin^2\theta H(\chi_{\|Q} - \chi_{\perp Q}) \quad (7.34)$$

$$= \frac{2}{3}H\delta\chi - \frac{2}{3}\frac{H^3}{H_{SR}^2}\delta\chi \text{ (on substitution for } sin^2\theta.) \quad (7.35)$$

The form of this (assuming $\delta\chi$ is constant) is shown in figure 7.16 together with the experimental results obtained. The similarity is obvious and suggests the model of Plumer and Walker to be successful in this direction although it has certain limitations. It assumes that helix rotation commences on application of a small field whereas in fact this requires a finite field of 400Oe. The experimental observation of hysteresis in the field region of H_{SR} is in no way predicted. Also the experimental form of $m_{<111>}$ - $m_{<110>}$ as shown in chapter 5, is very different for increasing and decreasing fields which is also not predicted and the model in no way can account for the presence of 'Phase A' close to the transition temperature.

7.13.2 MnSi and 'Phase A'

Using the expression of Plumer and Walker (1981) for the free energy of the helical spin density wave, the anisotropy energy term is given by:

$$E_A = (\frac{1}{2}DQ^2S^2 + \frac{1}{4}ES^4)g \quad (7.36)$$

If E_A is positive, then g must be as small as possible hence the helix propagates along $< 111 >$ ($g = \frac{4}{3}$) as in MnSi in zero magnetic field. However, if E_A is negative, then g must be as large as possible and the helix propagates along $< 100 >$ (g=2), as in the upper magnetic phase of cubic FeGe. The variation in helix propagation direction with temperature in cubic FeGe can be explained by the anisotropy energy being a function of temperature and changing sign.

When considering the helical behaviour in a magnetic field, the terms of interest in the expression for the free energy are:

$$F = F' + B'm_{\perp Q}{}^2S^2 + (\frac{1}{2}DQ^2S^2 + \frac{1}{4}ES^4)g - m_{\|Q}Hcos\theta - m_{\perp Q}Hsin\theta \quad (7.37)$$

When the helix is aligned parallel to the magnetic field, this reduces to

$$F_{(Q\|H)} = F' + (\frac{1}{2}DQ^2S^2 + \frac{1}{4}ES^4)g - m_{\|Q}H \quad (7.38)$$

Within 'Phase A' when the helix 'flips' into $< 001 >$ perpendicular to the applied field, the free energy is

$$F_{(Q\perp H)} = F' + (\frac{1}{2}DQ^2S^2 + \frac{1}{4}ES^4)g + B'm_{\perp Q}{}^2S^2 - m_{\perp Q}H \quad (7.39)$$

At a particular field, the helical arrangement will favour the lowest free energy possible hence for the field and temperature regime of 'Phase A'

$$F_{Q\perp H} < F_{Q\|H} \quad (7.40)$$

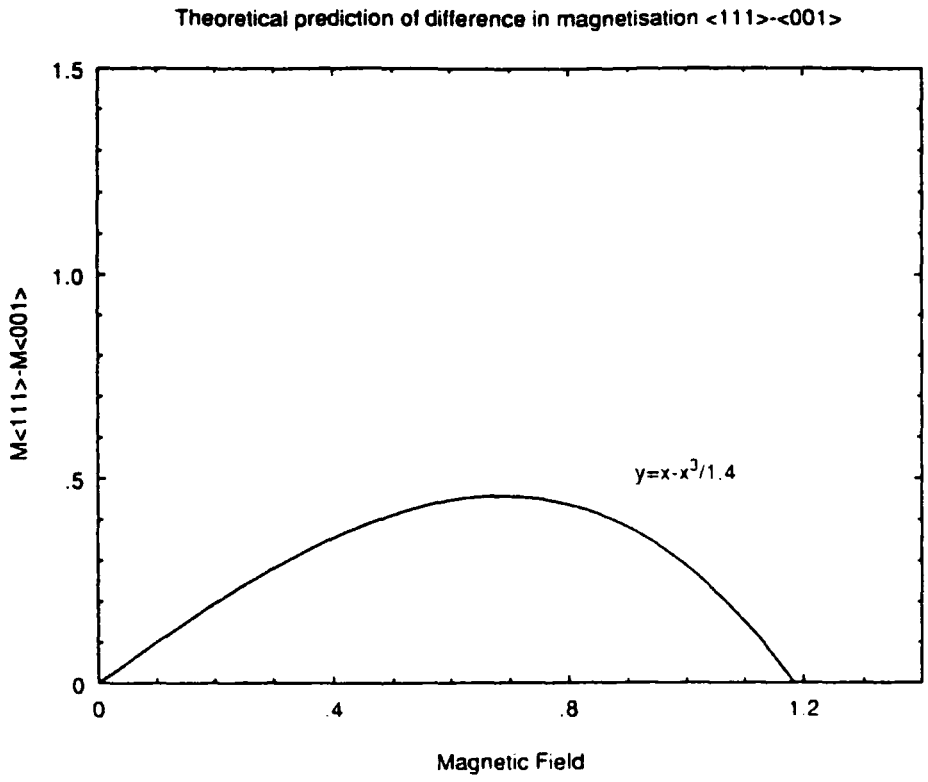

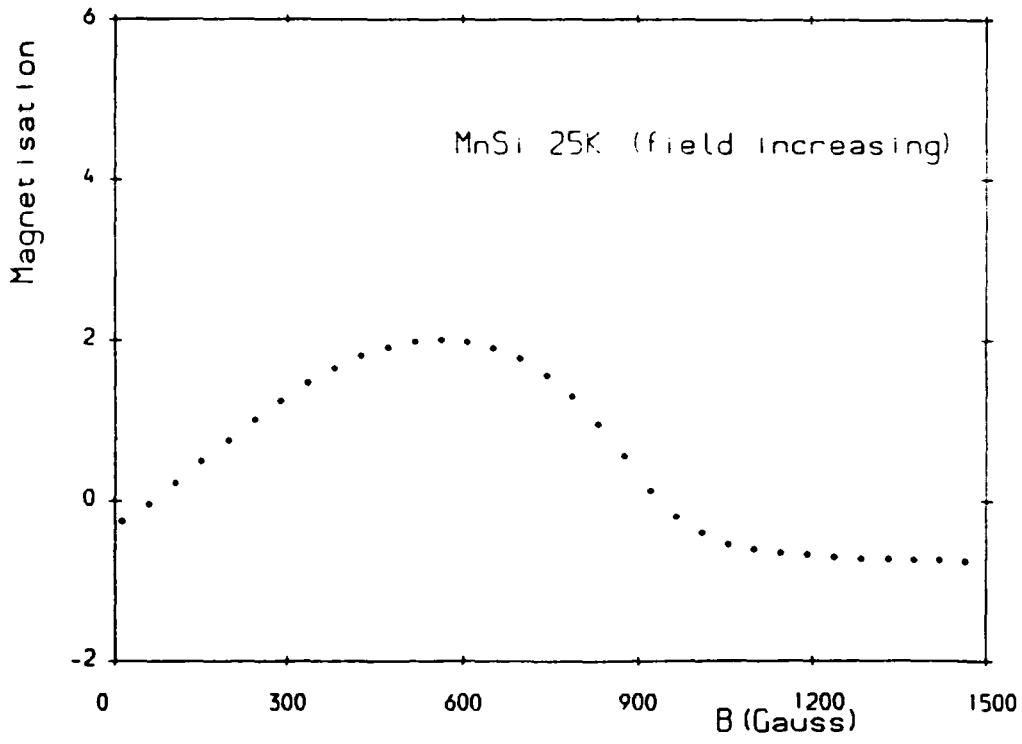

Figure 7.16 (a) Theoretical form of the difference in magnetisation measured with field parallel to the < 111 > and < 001 > directions developed from the work of Plumer *et al.* (1981); (b) experimentally determined difference in magnetisation measured with field applied parallel to the < 111 > and < 001 > directions.

From the magnetisation measurements in a fixed field close to the transition temperature (Chapter 5), within 'Phase A' by comparing the magnetisation in < 001 > and < 111 > directions there are temperature and field regions where $m_{\perp Q} > m_{\parallel Q}$ and regimes still in 'Phase A' where $m_{\perp Q} < m_{\parallel Q}$. In 'Phase A' with magnetisation along < 001 > direction there is a positive contribution to the free energy from the term $B' m_{\perp Q} S^2$ which suggests the only way the overall free energy can be lower is if the anisotropy energy has lowered and in fact become negative, causing the helix to 'flip' into a < 001 > direction perpendicular to the applied field.

Note that this is a first order transition, with the helix not occupying any interstitial sites which is very different to the second order rotation of the helix into the direction of the applied field where, although the anisotropy energy may vary with applied field, it is assumed to remain negative.

7.14 Theoretical Investigation of the Magnetic Phase Diagram of Cubic FeGe

Following the experimental work of Lebech *et al.*(1989), a theoretical paper on the behaviour of cubic FeGe was provided by M. L. Plumer (1990). FeGe is analysed in terms of a Landau-type free energy previously used to study the related phenomenon in MnSi (Plumer and Walker (1981)).

The model developed (in particular for magnetic field applied along the < 100 >) predicts a first order wavevector transition to occur at the transition from the upper phase with Q || < 100 > direction to the lower phase with Q || < 111 > direction. For magnetic field applied parallel to the < 100 > direction, the wavevector reorientation phase transition is predicted to be second order in the lower phase.

Results of the numerical minimisation of the free energy for the magnetic phase corresponding to field applied along the < 100 > direction are shown in figure 7.17. This is similar in form to the experimental results obtained from the magnetisation study in figure 6.14 although the values of field predicted at different temperatures are greater than those observed. Also the model does not predict the presence of the field induced phase close to the transition temperature.

7.15 Further SANS on MnSi

Although the behaviour of the helical spin density wave in MnSi has been determined as far as rotation into the field direction and 'Phase A', there now is a need for very detailed measurements. Firstly the integrated intensity of the satellites should be calculated as a function of field to determine whether the helix is deformed in a magnetic field or whether the amplitude of the spin density wave is a function of field as well as temperature. This is far from trivial, particularly as the helix propagation direction changes with field when not applied along the < 111 > direction. This should be performed at 4.2K and 28.8K when the crystal will enter 'PhaseA'.

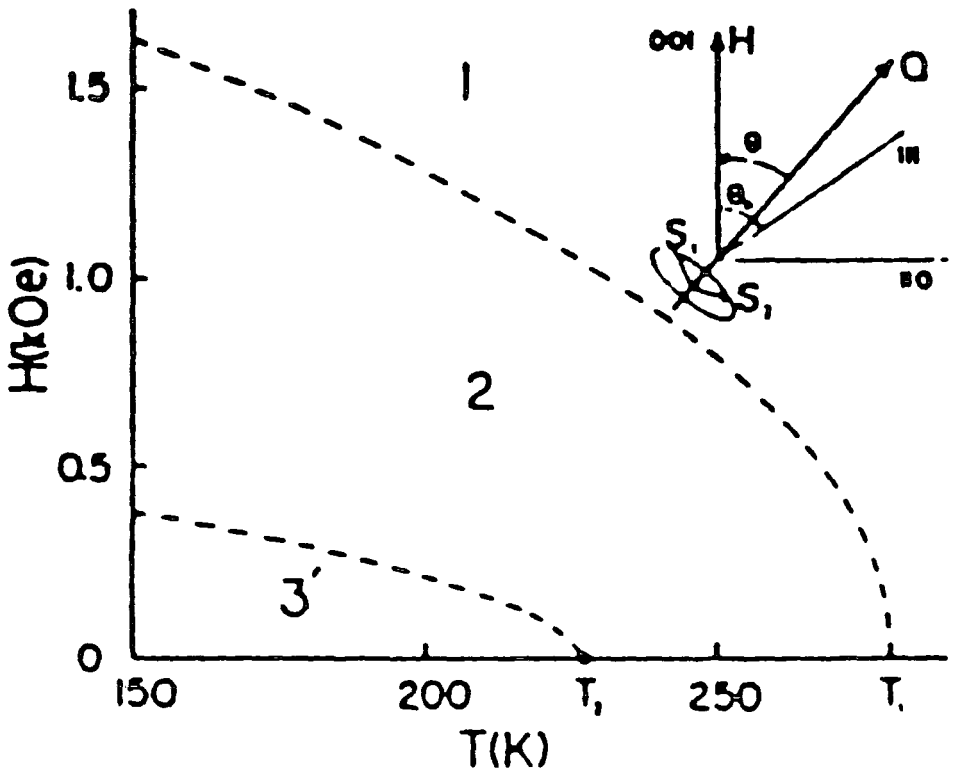

Figure 7.17 Numerically determined phase diagram of FeGe with $\underline{H} \parallel$ to [001]. (After Plumer (1990)).

The background noise level produced by the cryostat greatly affected the sensitivity of the SANS experiment and this will have been crucial close to the transition temperature. Because there is no necessity for magnetic field, these measurements could be repeated using different cryostat or displex in order to investigate the critical scattering close to the transition temperature and how the helical spin density wave develops from the paramagnetic phase.

Another observation of particular interest is the secondary satellites in the $< 001 >$ and $< 110 >$ directions in zero field. These may be observed for numerous reasons discussed earlier and in order to investigate this, MnSi should be cooled from above the transition temperature in an applied magnetic field. This will favour the growth of one domain and reveal more about the processes producing the secondary satellites.

Figure 7.18 shows arrangement of the helix propagation vector being perpendicular to the applied field direction for FeGe which corresponds to the helical arrangement observed in the field induced 'Phase A' in MnSi. In zero field, no secondary satellites are observed however in the field regime before the helix 'flips' into the field direction, they are seen to develop and then disappear. Since these satellites are in the same direction as the helix propagation direction and only appear when a magnetic field is applied to the sample, they are thought to be a consequence of 'squaring' of the helix or rearrangement of the moments. Because the helix propagation direction is perpendicular to the field, some of the moments will be parallel to the field and some perpendicular. In order to reduce the energy of this arrangement, the moments may reorder so they lie out of the field direction, possibly in two arcs centred perpendicular to the field (see Lebech (1992)). Similar investigations of secondary satellites should be performed on MnSi, especially while in 'Phase A' to see if a similar process is occuring.

Also MnSi could be cooled in a magnetic field within the 'Phase A' regime applied along the $< 001 >$ direction close to the transition temperature. This would shed more light on 'Phase A' and determine whether or not the helix would form parallel to the field before 'fliping' perpendicular into 'Phase A'.

Recent work by Lebech (1992) on FeGe suggests that reorientation of the helix into the field direction may occur as a first or second order process, depending on the angle between the applied field and the initial modulation vector. Investigations using SANS at both 250 and 140K show that with a magnetic field applied perpendicular to the helix, a first order transition or 'flip' of the helix occurs whereas with $\underline{q}$ initially at some smaller angle the rotation is a second order process. In order ot investigate whether the same behaviour occurs in MnSi, SANS should be performed with MnSi crystal orientated such that the $< 111 >$ direction is aligned perpendicular to the magnetic field and in the scattering plane.

Finally MnSi could be studied with magnetic field applied along a direction not corresponding to a principle crystallographic direction.

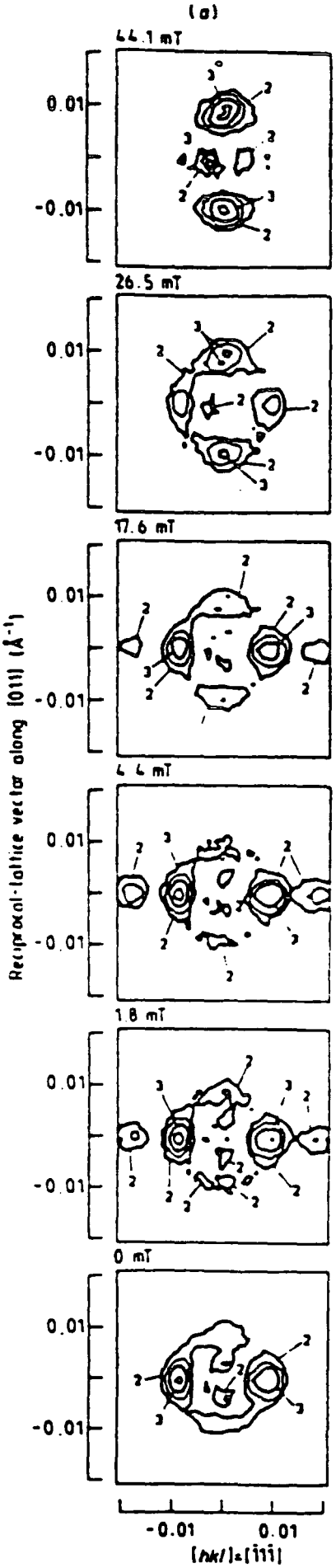

Figure 7.18 Equal intensity contours (logarithmic scale) observed in FeGe at 140K for various magnetic fields applied along the [011] vertical direction. The background has been subtracted and the data normalised. There are factors of 10 between the contour lines marked 1 and 2. This corresponds to a similar helix arrangement as observed in MnSi within 'Phase A' i.e. helix perpendicular to the magnetic field. (After Lebech *et al.* (1989)).

7.16 References

Bak P. and Jensen M. (1980), J. Phys. C **13**, L881-885.
Ishikawa Y. *et al.*(1984), J. Phys. Soc. Jpn. **53**, 2726-2733.
Ishimoto K. *et al.*(1990), J. Magn. Magn. Mat. **90-91**, 263-165.
Lebech B. *et al.*(1989), J. Phys.: Condensed Matter **1**, 6105-6122.
Lebech B. (1992), Presented at symposium on *Recent Progress in Material Physics*, ——Osaka, Japan. To be published in *Recent Advances in Magnetism of Transition ——Metal Compounds*, World Scientific Publishing Co.
Plumer M.L. and Walker M.B.(1981), J. Phys. C.: Solid State Phys **14**, 4689-4699.
Plumer M.L. (1990), J. Phys.: Condensed Matter **2**, 7503-7510.
Squires G. (1978), *Introduction to the theory of Thermal Neutron Scattering.* Publ. ——Cambridge University Press.

Chapter 8

Critical Magnetic Neutron Scattering on MnSi

8.1 Introduction to Critical Phenomena

Critical phase transitions were systematically investigated by Andrews (1869) through his studies of carbon dioxide. The phase boundary between vapour and liquid simply dies out at a point known as the critical point and the two phases, liquid and vapour become identical. There is a seemingly continuous transition from one phase to the other where vapour can become liquid without experiencing any discontinuous change in properties.

Phase transitions that pass through a critical point are known as critical phase transitions and phenomena observed close to this point are known as critical phenomena. In a magnetic system where a continuous phase transition occurs from an ordered ferromagnetic state to a paramagnetic state, the critical point is at zero applied field and at a temperature known as the Curie Temperature. In critical phase transitions, short lived microregions of one phase in the other are always found and if the two phases exhibit different 'densities', give rise to critical scattering. The linear extent of these regions (the correlation length) tends to infinity as the critical point is approached from any direction. The response time of the system i.e. the time taken to create or destroy such regions of local order also tends to infinity as the critical point is approached and is known as critical slowing down. Such transitions are generally descibed by an order parameter η, for example in the case of a ferromagnetic transition the parameter is the magnetisation. The order parameter is a continuous function of temperature; it is zero for temperatures above T_c and nonzero for temperatures below T_c.

8.2 Review of Previous Critical Scattering on MnSi

The critical scattering of MnSi has previously been studied by Ishikawa. Initially it was included in the study of low energy paramagnetic spin fluctuations above T_c (Ishikawa (1982)) which was performed with a triple axis spectrometer at Brookhaven. Figures 8.1 and 8.2 summarise the results, with figure 8.1 showing the development of a ring of scattering centred at (0,0) and the subsequent collapse into a helix propagating along the $< 111 >$ direction. Figure 8.2 shows the cross section of the ring as a function of temperature. As the temperature is increased 1K above that of helix formation, the ring disappears and the intensity of the scattering tends to increase with decreasing wavevector.

Ishikawa (1984) also studied the magnetic phase diagram of MnSi near the critical temperature by small angle neutron scattering. Again reference is made to a ring of scattering close to the transition temperature and is reproduced in figure 8.3. This ring of scattering was also thought to be present in 'Phase A' below the transition temperature in an applied magnetic field.

Hayden and Brown (1990) repeated a more detailed study of the cross section of this ring of scattering close to the transition temperature at the ILL in Grenoble and this is reproduced in figure 8.4.

Other measurements of interest close to the transition temperature include the ultrasonic study of the magnetic phase diagram of MnSi by Kusaka (1976) and also the magnetovolume effect in MnSi measured by Matsunga (1982). Figure 8.5 shows the temperature dependance of the attenuation of ultrasonic waves near the transition temperature in fixed magnetic field. It is evident that two peaks appear around 30K. The lower temperature transition is very sharp while the second is much broader and flatter. Simulatneous measurement of the attenuation and static susceptibility show that the sharp peak corresponds to where the temperature derivative of the susceptibility diverges and hence onset of the helical phase. Figure 8.6 reveals that the thermal expansitivity of MnSi also exhibits a two step transition. There is a sharp transition at 30K, followed by a broad bump one degree above it.

Makoshi (1979) has calculated the effect of spin fluctuations on the ultrasonic attenuation coefficient on the basis of previously developed theory of helical spin structure in itinerant electron systems. Although the double peak structure in the attenuation coefficient can be explained in terms of 'rather high magnetic fields', the presence in zero applied field remains unaccounted for.

Recent measurements of the heat capacity of MnSi by Bernhoeft *et al.* (1992) also reveal a similar two stage transition as shown in figure 8.7(a) and (b). Again the lower temperature transition is very sharp, followed by a broader peak. Finally, neutron scattering on MnSi by Brown (1990) suggests the intensity associated with this 'prephase' may be greater and temperature regime broader on application of homogeneous pressure to the sample. The results are reproduced in figure 8.8.

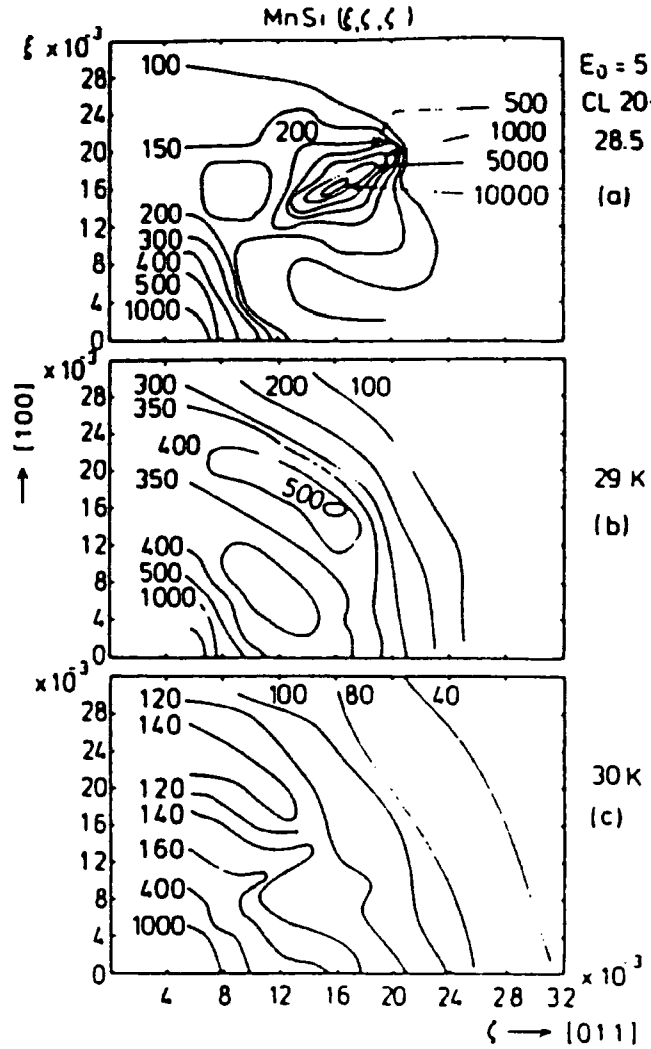

Figure 8.1 Contour maps of equal intensity of critical scattering of MnSi around a satellite point measured with E_i=5meV with $\hbar\omega$=0 at three different temperatures. (After Ishikawa *et al.* (1982)).

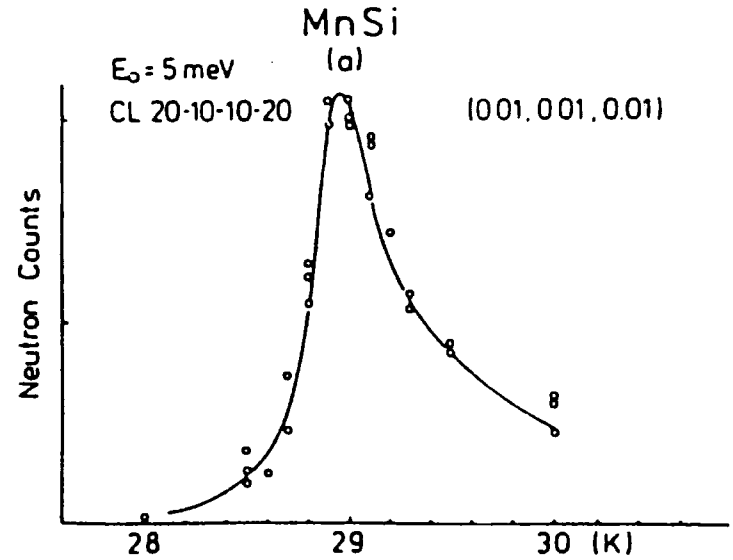

Figure 8.2 Temperature variation of peak intensities of MnSi at $\underline{q}$=(0.01,0.01,0.01)$\frac{2\pi}{a}$ measured with E_i=5meV. (After Ishikawa (1982)).

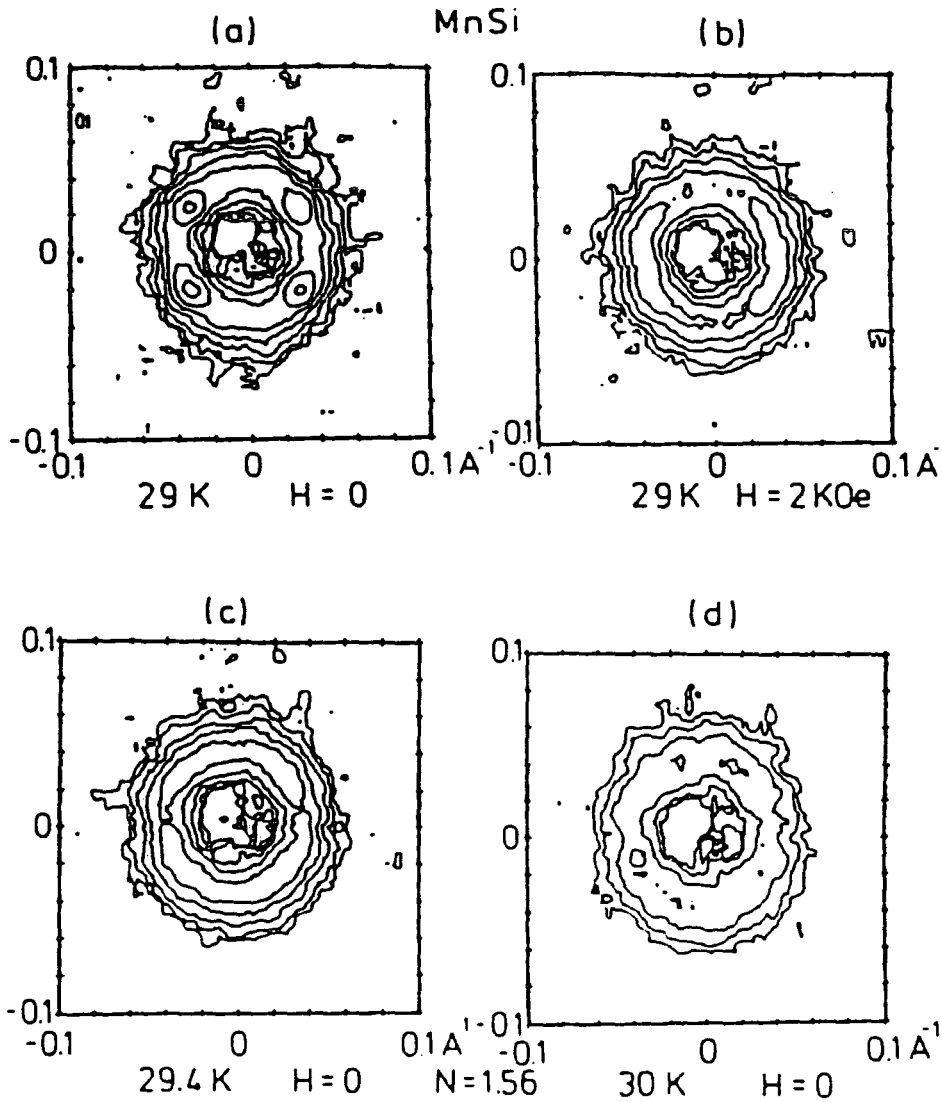

Figure 8.3 Contour maps of equal intensity of small angle neutron scattering on MnSi in the (110) reciprocal lattice plane of MnSi. Lines are plotted at intervals of 1/N of intensity with N=1.56. (a) 29K, $\underline{H}$=0; (b) 29K, $\underline{H}$=2kOe; (c) 29.4K, $\underline{H}$=0; (d) 30K, $\underline{H}$=0. (After Ishikawa *et al.* (1984)).

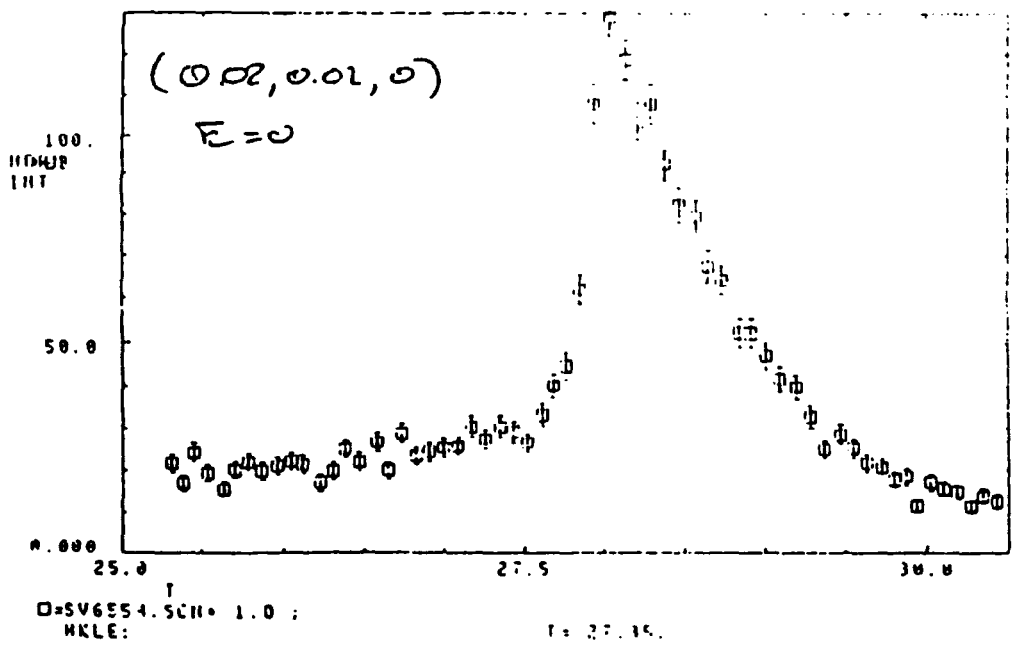

Figure 8.4 Temperature variation of peak intensities of MnSi at $\underline{q}$=(0.2,0.2,0) $\frac{2\pi}{a}$ and $\hbar\omega = 0$. (After Hayden *et al.* (1991)).

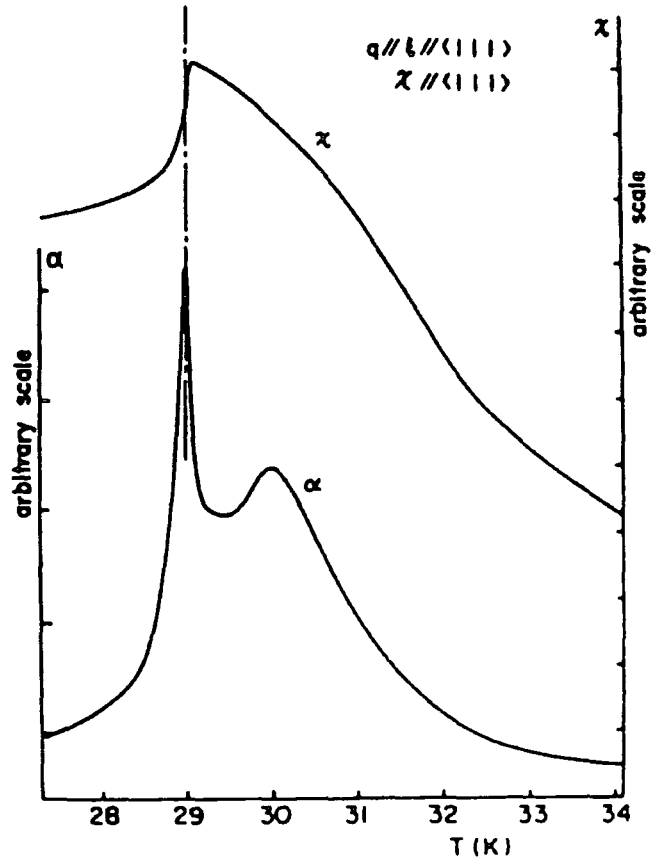

Figure 8.5 Simultaneous measurements of ultrasonic attenuation and static susceptibility of MnSi. Note the temperature where the sharp peak of attenuation agrees with the divergence of the temperature derivative of the static susceptibility. (After Kusaka *et al.* (1976)).

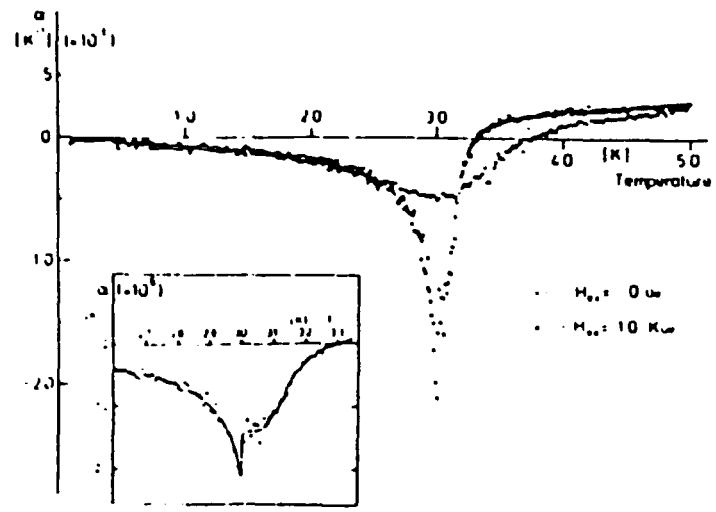

Figure 8.6 Thermal expansitivity α for MnSi below 50K measured for zero field and that for sample B at 10kOe. (α in zero field in the vicinity of T_N is enlarged in the inset.) (After Matsunaga *et al.* (1981)).

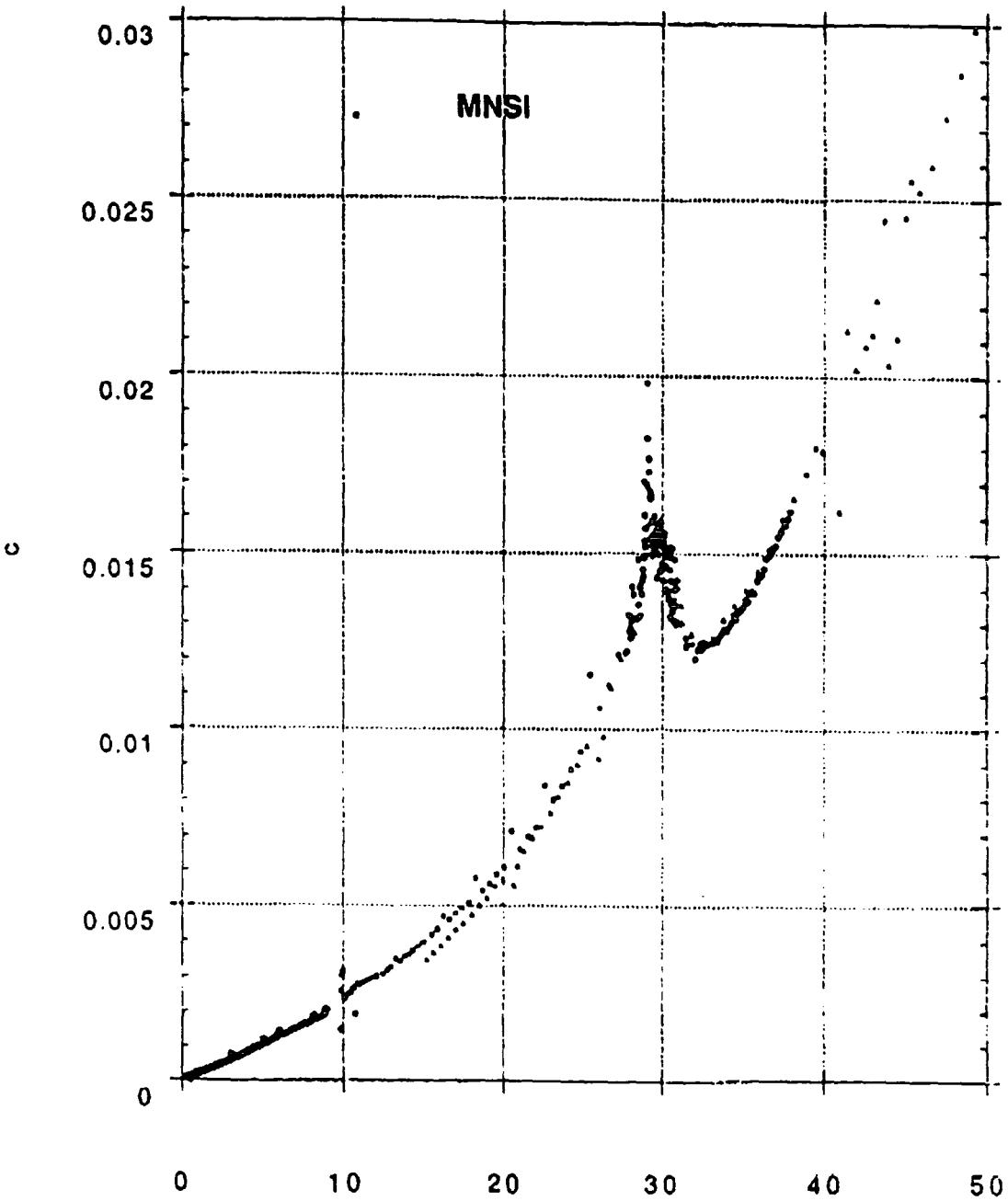

Figure 8.7 (a) Variation of the heat capacity of MnSi for increasing temperature. (After Bernhoeft *et al.* (1992)).

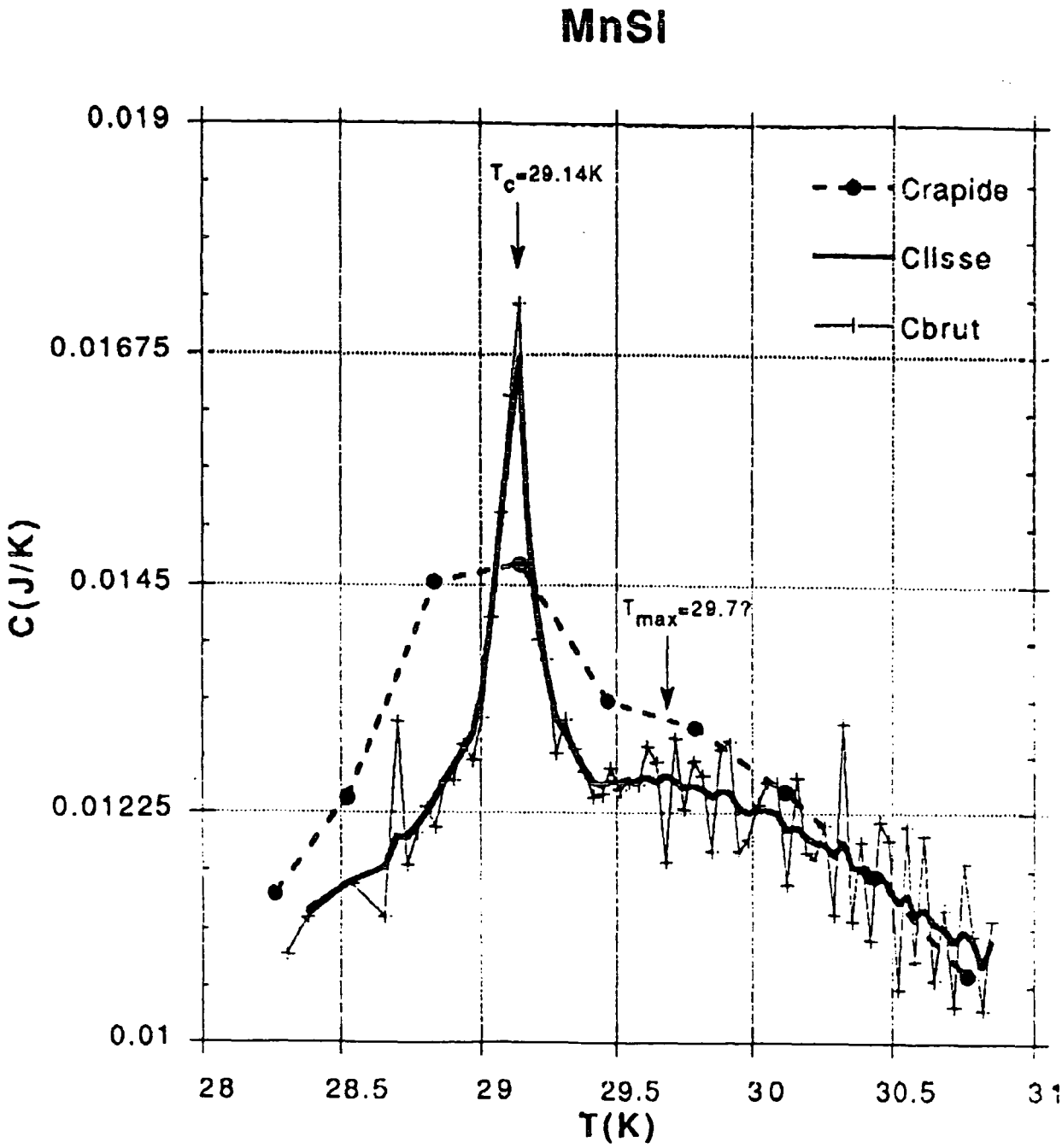

Figure 8.7 (b) Variation of the heat capacity of MnSi for increasing temperature close to T_N. (After Bernhoeft *et al.* (1992)).

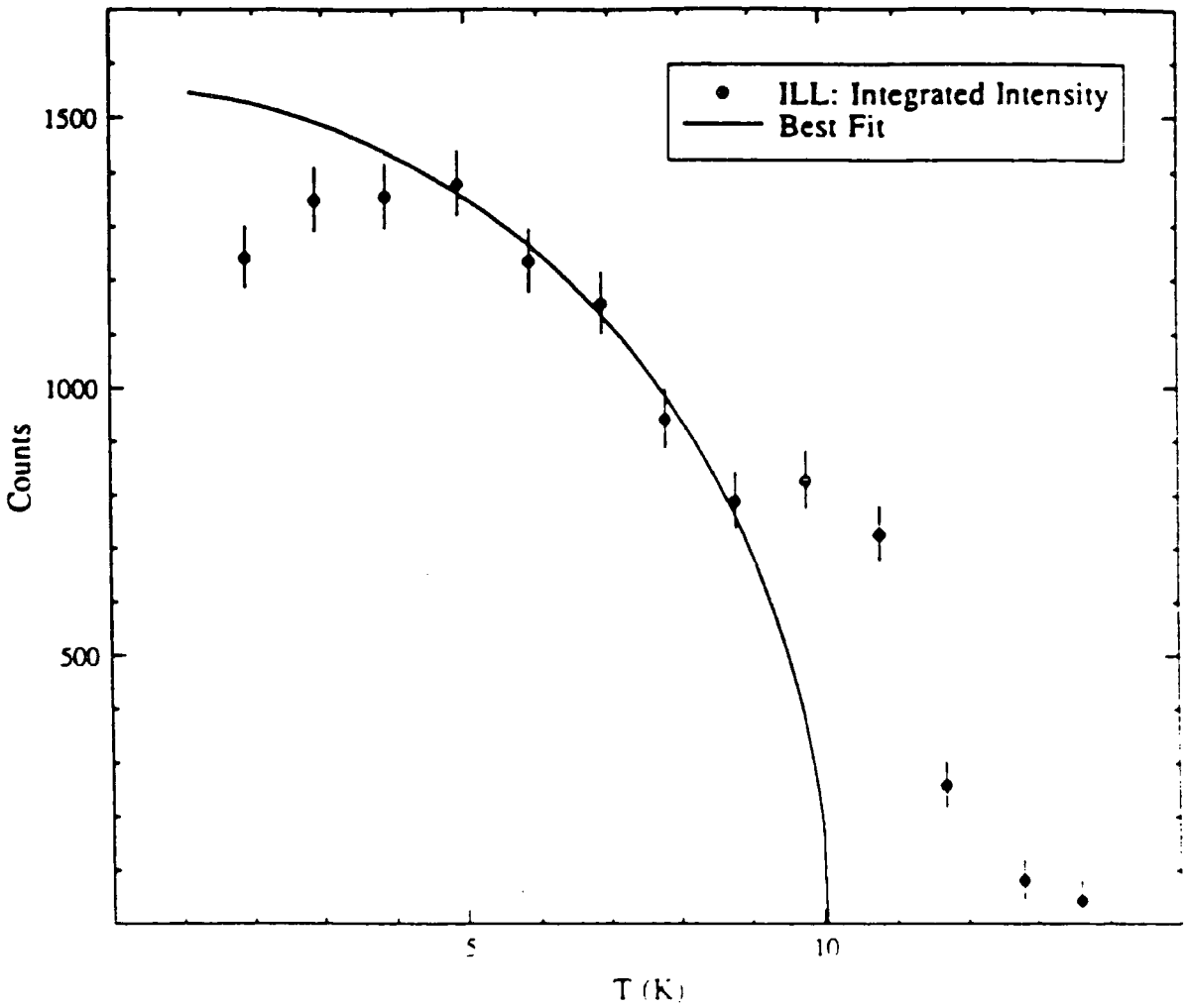

Figure 8.8 Variation of satellite intensity with temperature for MnSi at 12kbar. The intensity was obtained by integrating the number of counts at each temperature between q=0.071Å^{-1} and q=0.024Å^{-1} and then subtracting the 20K background. (After Brown (1990)).

8.3 Measurement of Magnetic Critical Scattering

Initial attempts to observe the critical scattering of MnSi were made on SANS at Risø as descibed in Chapter 7 in a similar manner to Lebech *et al.* (1989). However the sensitivity of this was limited by the scattering from the cryostat used. In order to overcome this, the experiment was repeated on a triple axis spectrometer using a displex to cool the sample.

8.3.1 The Triple Axis Spectrometer

The triple axis spectrometer is so called because neutrons are scattered about three parallel axis through angles $2\theta_M$, ϕ and $2\theta_A$ as shown in figure 8.9. A 'white' neutron beam is incident on a single crystal monchromator which is aligned so as to reflect neutrons of a particular wavelength $\underline{k}$. These neutrons are incident on the sample and scattered through an angle ϕ onto the analyser crystal which is arranged to reflect neutrons of wavevector $\underline{k}'$ into a detector. Within this experiment elastic neutron scattering is being studied and because of the angular degrees of freedom, the scattering function (see Chapter 7 for the magnetic scattering cross section) can be deteremined at any desired value of scattering vector $\underline{K}$ within the limits $0 \leq \underline{K} \leq 2\underline{k}_i$ and the geometrical limit of the spectrometer. Interest lies in values of $\underline{K}$ near to magnetic reciprocal lattice points and measurements were made by scanning $\underline{K}$ along some path in reciprocal space.

8.3.2 Experimental Details

The experiment was performed on the triple axis spectrometer TAS1 at the Risø National Laboratory in Denmark. The sample used was a single crystal described by Brown (1990) as 'sample 2' and used in the ambient pressure neutron experiments to investigate the spin fluctuation spectrum above the transition temperature. The single crystal has a maximum diameter of 8mm, length of 60mm and was the source of cylindrical sample used on the SANS in an applied magnetic field described in Chapter 7. The crystal was mounted in a sealed, helium filled can and placed in a displex. A calibrated Germanium thermometer was used as a temperature sensor and mounted close to the sample position. The temperature was controlled to within $\pm 0.01K$ by means of a Risø A1931a Digital Temperature Controller.

Both the curved monochromator and planar analyser used are pyrolytic graphite (crystal mosaicity of 30′) with the (002) Bragg reflection providing the required wavevector. Neutrons of incident energy 5meV were used with Be filters inserted infront of the sample to remove neutrons with integer fractions of the desired wavelength. The horizontal collimation of the neutron beam used was 60′/30′/30′/60′ and the vertical collimation was 120′/120′/120′/120′.

The crystal was orientated in the neutron beam such that the scattering plane was the $(1\bar{1}0)$ plane. Magnetic Bragg scattering from the sample at 15K around

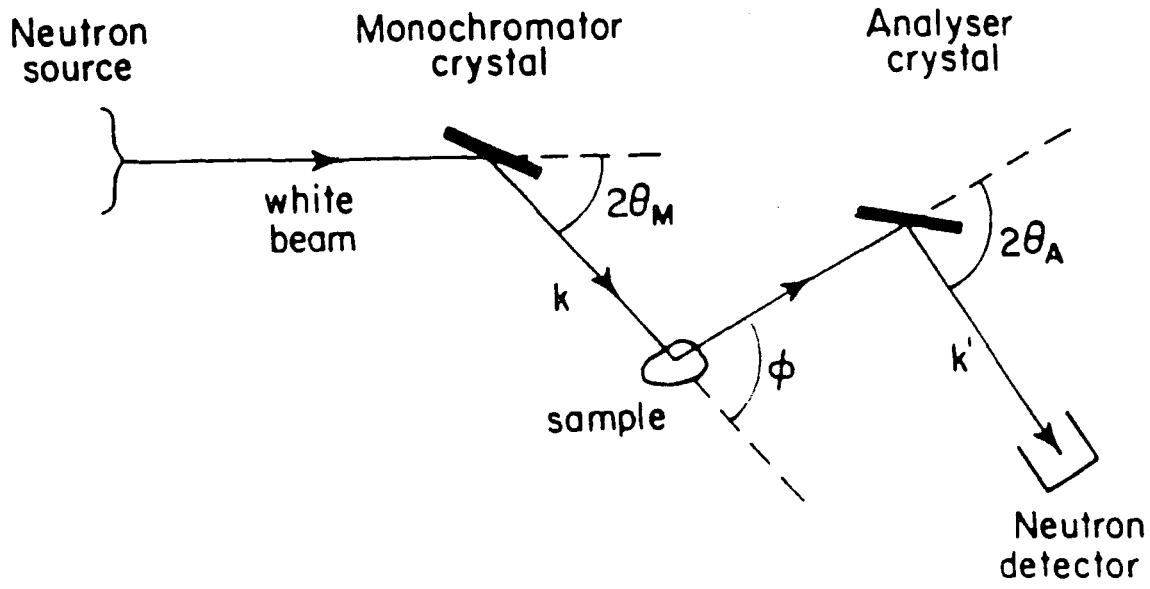

Figure 8.9 The triple axis spectrometer. A monochromator crystal scatters just those neutrons from a white source with wavevector $\underline{k}$. An analyser crystal sends to the detector just those neutrons scattered through an angle ϕ that have wavevector $\underline{k}'$.

	Scan	Calculated width $\AA^{-1}$	Measured width $\AA^{-1}$
(110) crystal Bragg peak (45K)	$\theta - 2\theta$	0.012	0.019
	ϕ	0.019	0.010
(111) magnetic Bragg peak (29K)	$\theta - 2\theta$	0.0180	0.015
	ϕ	0.0003	0.003

Table 8.1: Calculated and measured peak widths for both crystal and magnetic Bragg peaks.

the forward direction (0,0) was compared to that around the (110) reciprocal lattice point. Since the magnetic scatter around the (110) lattice point was weaker than around the straight through beam, the experiment was performed around (0,0). The bulk of the data was recorded measuring elastic scattering, scanning $\underline{K}$ along reciprocal space at a fixed temperature close to the transition. The $\underline{K}$ scans were performed along the [110] and [111] directions, passing radially through the (110) and (111) magnetic reciprocal lattice points from the (0,0) centre.

Figure 8.10(a) shows equal intensity contours of a compilation of scans of the (110) crystal Bragg reflection at 45K with scans taken along the marked lines. This was used to calculate the half width contour in figure 8.10(b). Table 1 shows the calculated (Lebech *et al.* (1975), Nielson *et al.* (1968)) and measured resolution widths for the (110) crystal Bragg peak at 45K and the (111) magnetic Bragg peak measured about (0,0) at 29K, also shown in figure 8.11(a) and (b).

From Table 1, the calculated and measured values for the (110) crystal Bragg peak at 45K are the same order of magnitude (particularly as the mosaicity of the crystal is unknown) and hence the peak is resolution limited. However the ϕ scan of the magnetic Bragg peak has a width over resolution of approximately a factor 10.

Residual scans were recorded at 45K and subtracted from the raw data at lower temperatures. A Gaussian function was fitted to the resulting data using the Risø program FGRAF which performed a least squares refinement to the fit. The parameters for the Gaussian fit at each temperature are listed in Table 2 for [110] scan and Table 3 for the [111] direction scan. Figure 8.12 shows some specific examples of the Gaussian fit to some of the data recorded along the [111] direction.

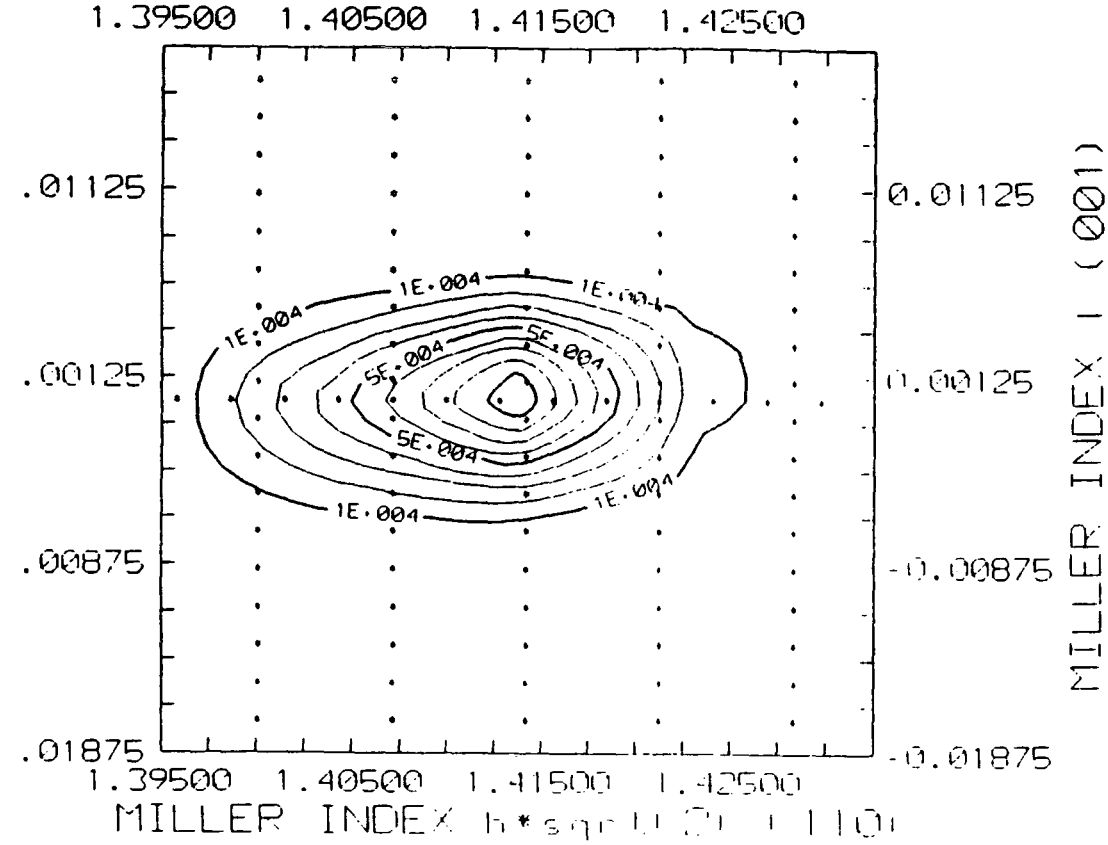

(110) 45 K FWHM CONTOUR I

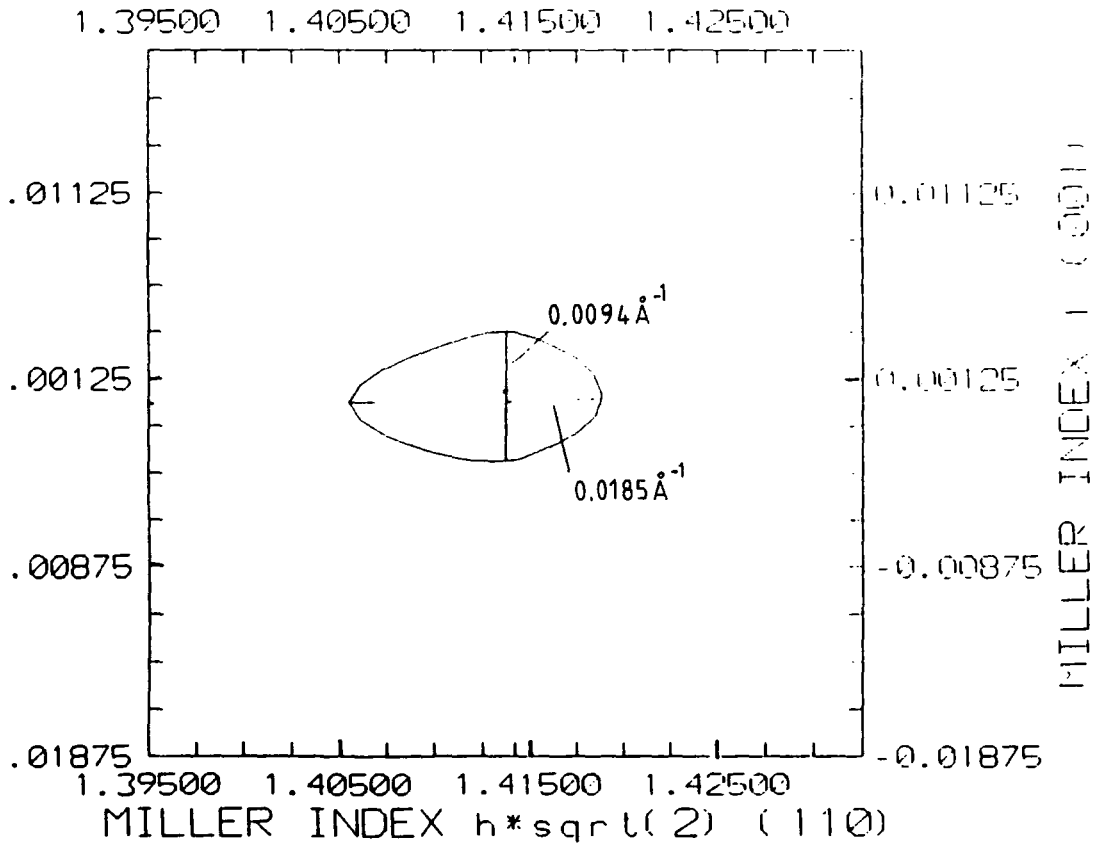

Figure 8.10 (a) Equal intensity contours of a compilation of scans of the (110) crystal Bragg reflection of MnSi at 45K with scans taken along the marked lines. This was used to calculate (b) the half width contour of the (110) crystal Bragg reflection at 45K.

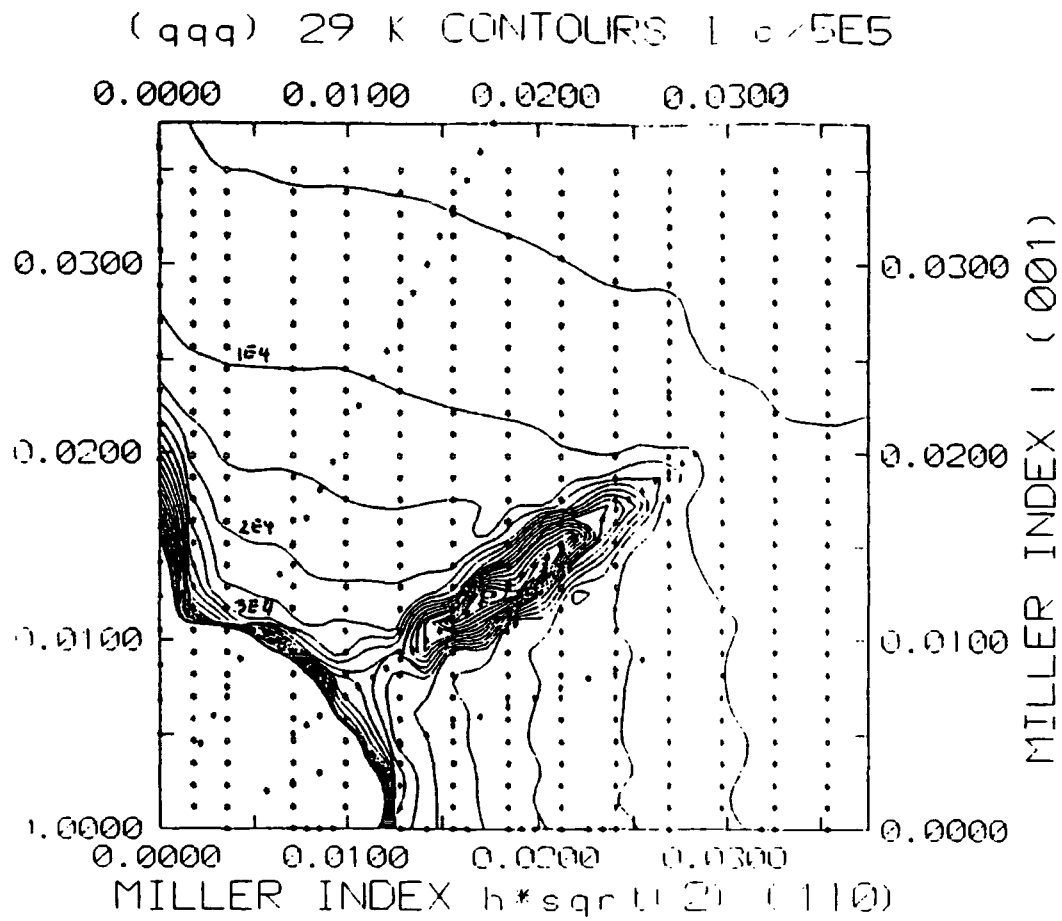

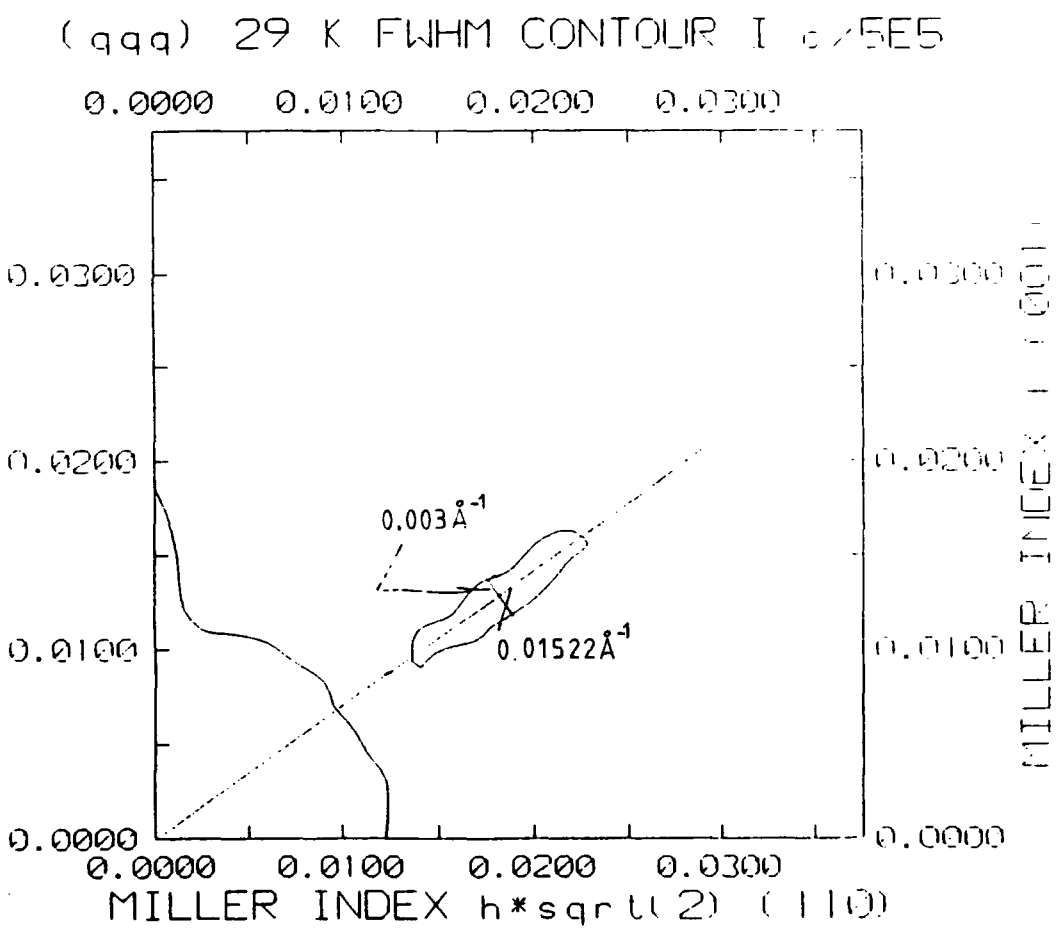

Figure 8.11 (a) equal intensity contours of a compilation of scans of the (111) magnetic Bragg reflection of MnSi at 29K with scans taken along the marked lines. This was used to calculate (b) the half width contour of the (111) magnetic Bragg reflection at 29K.

Figure 8.12 Specific examples of the Gaussian fits to the residual corrected critical scattering of MnSi close to T_N with $\underline{q}$ scan along the [111] direction. (a) T=32.0K; (b) T=31.0K; (c) T=30.0K; (d) T=29.6K; (e) T=29.4K; (f) T=29.3K; (g) T=29.1K; (h) T=29.0K; (i) T=28.9K; (j) T=28.8K; (k) T=28.4K; (l) T=28.0K; (m) T=27.0K; (n) T=26.0K; (o) T=25.0K.

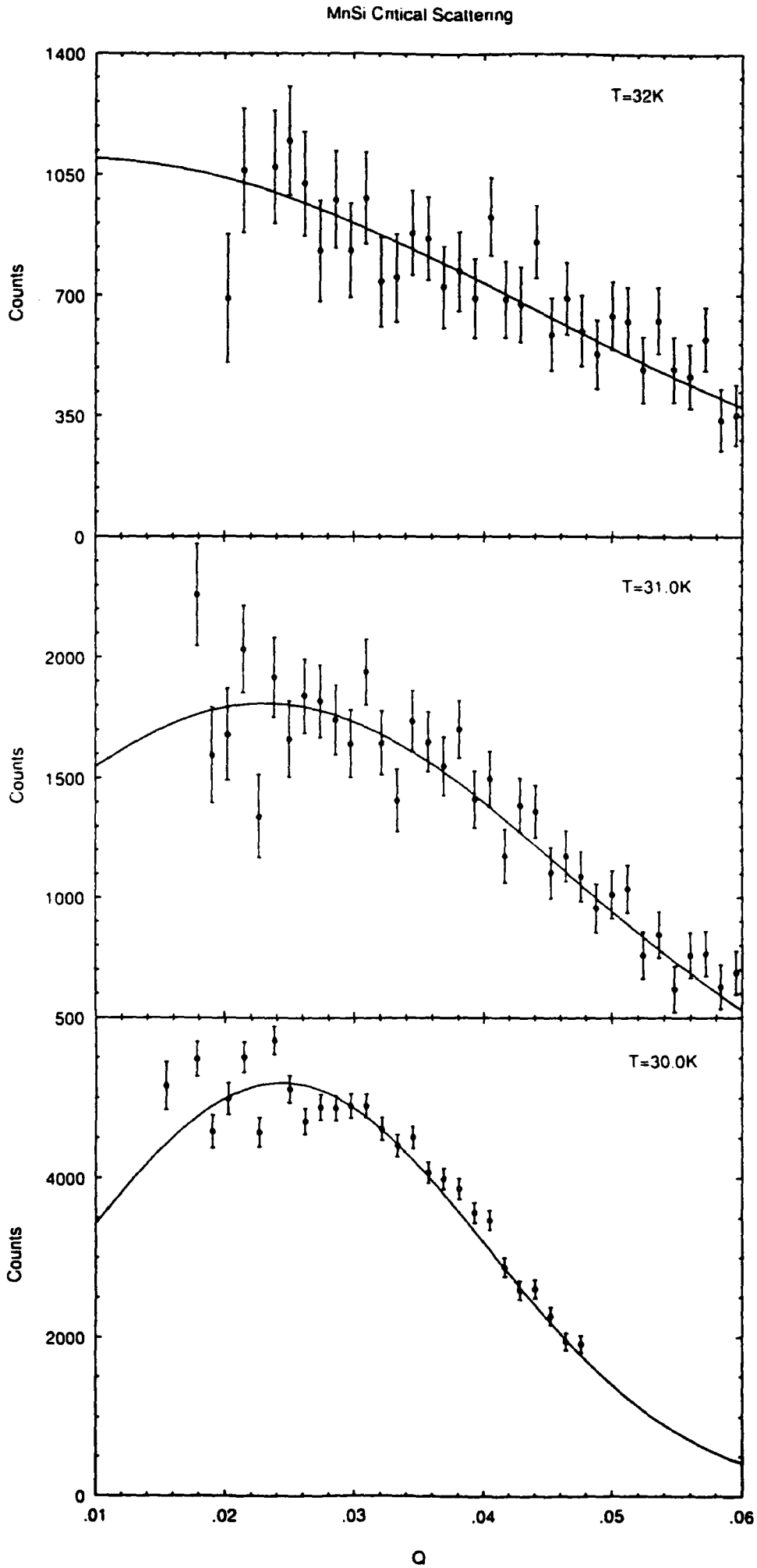

Figure 8.12 (a) - (c)

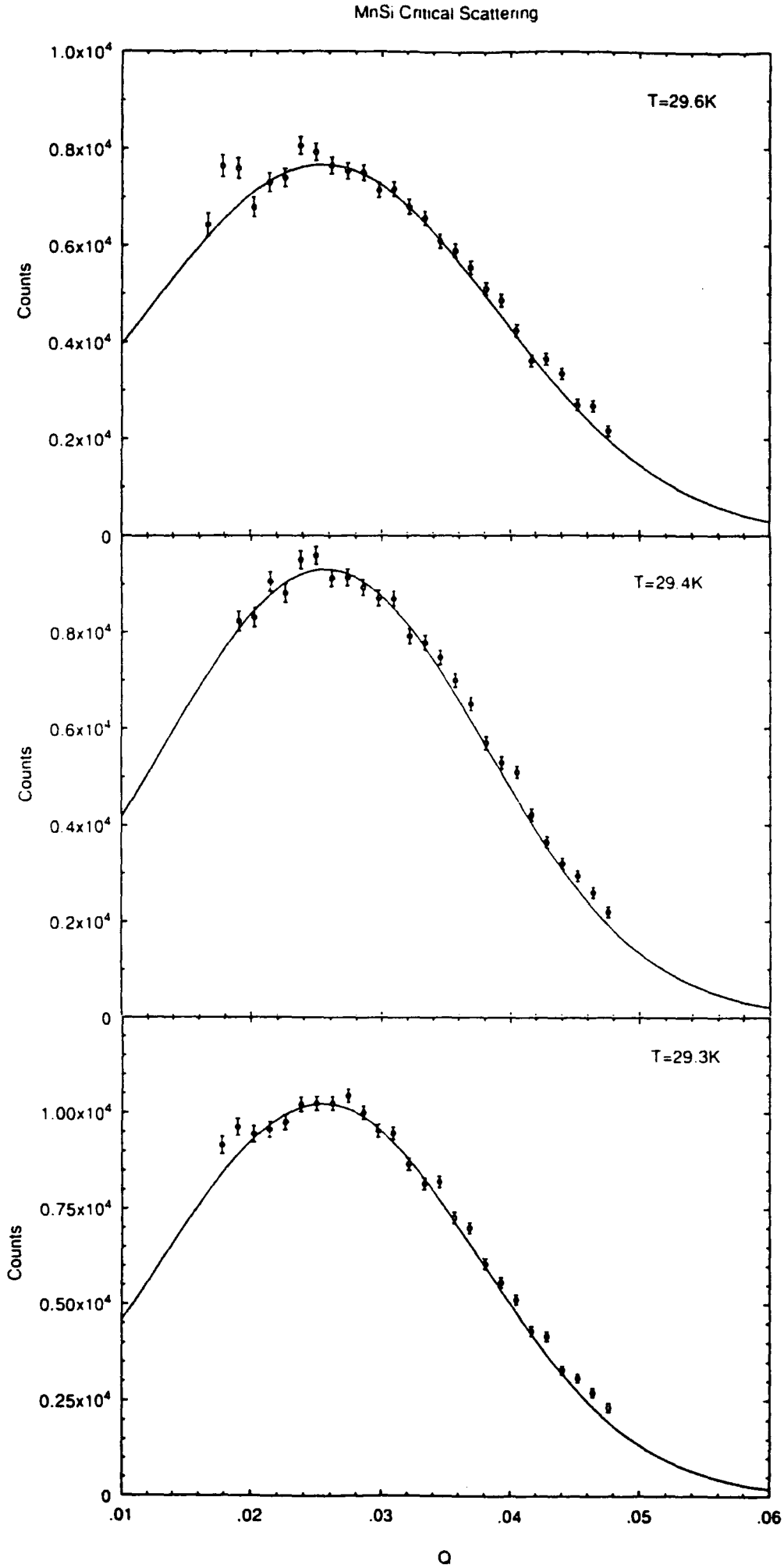

Figure 8.12 (d) - (f)

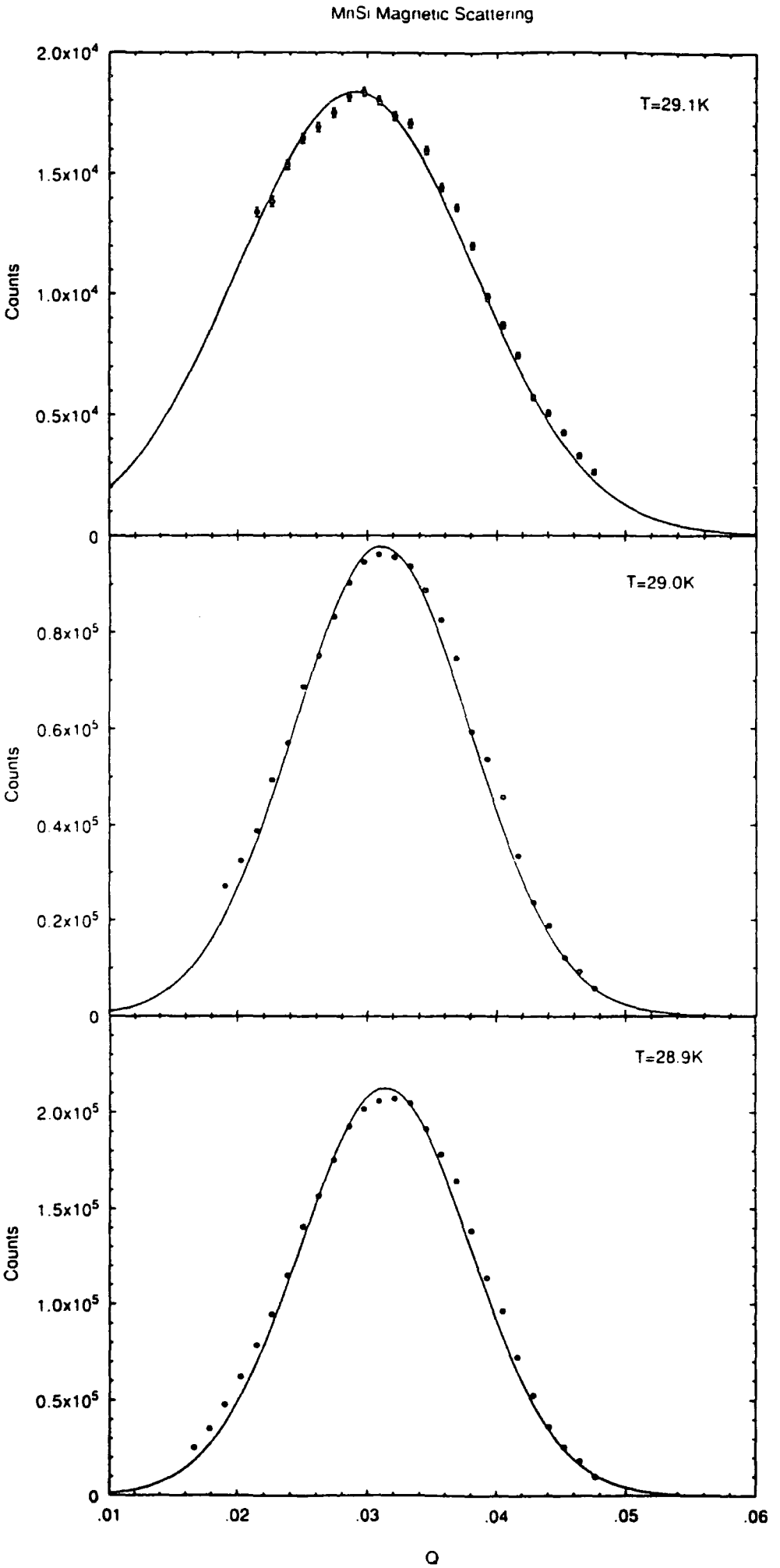

Figure 8.12 (g) - (i)

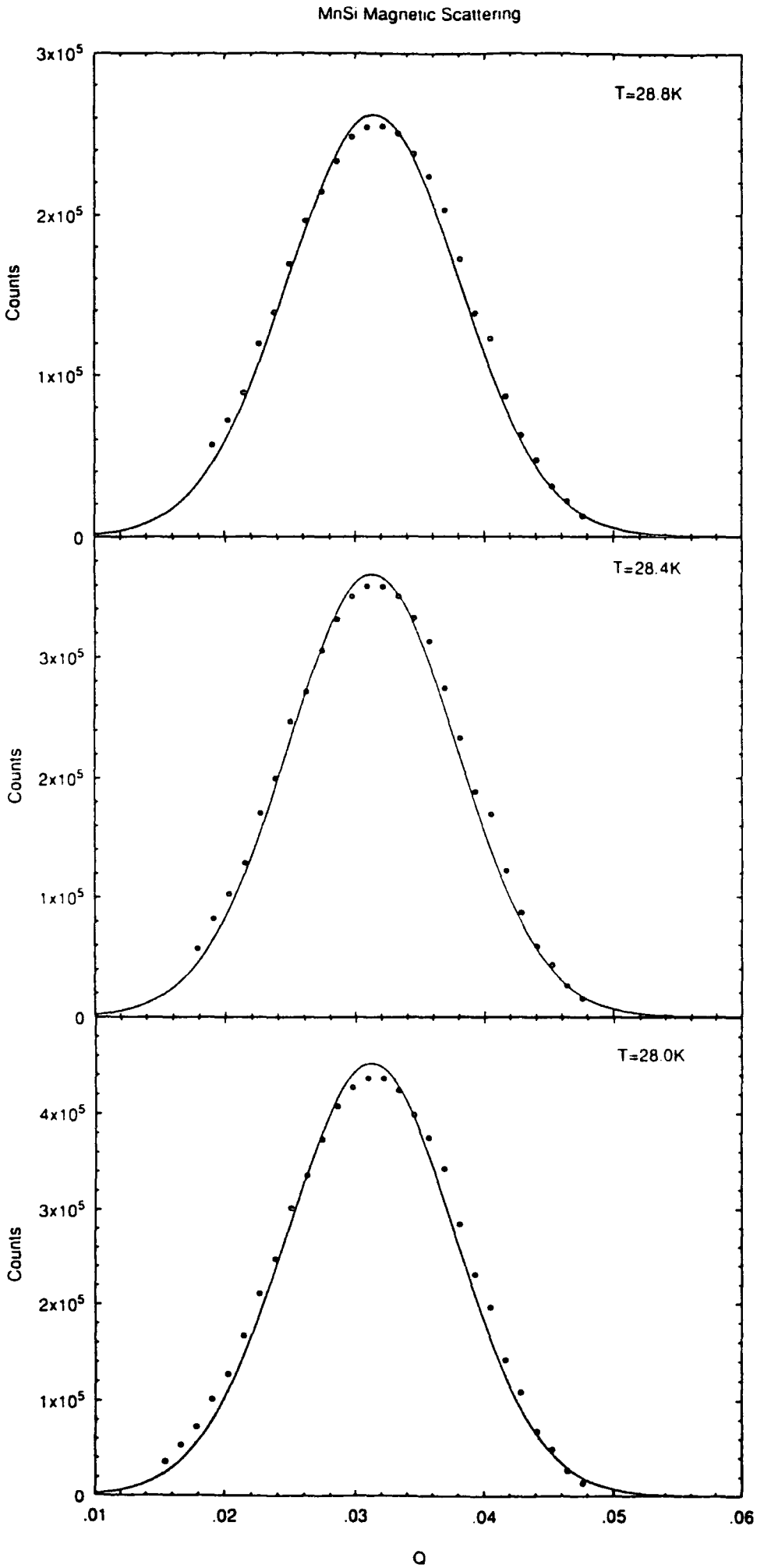

Figure 8.12 (j) - (l)

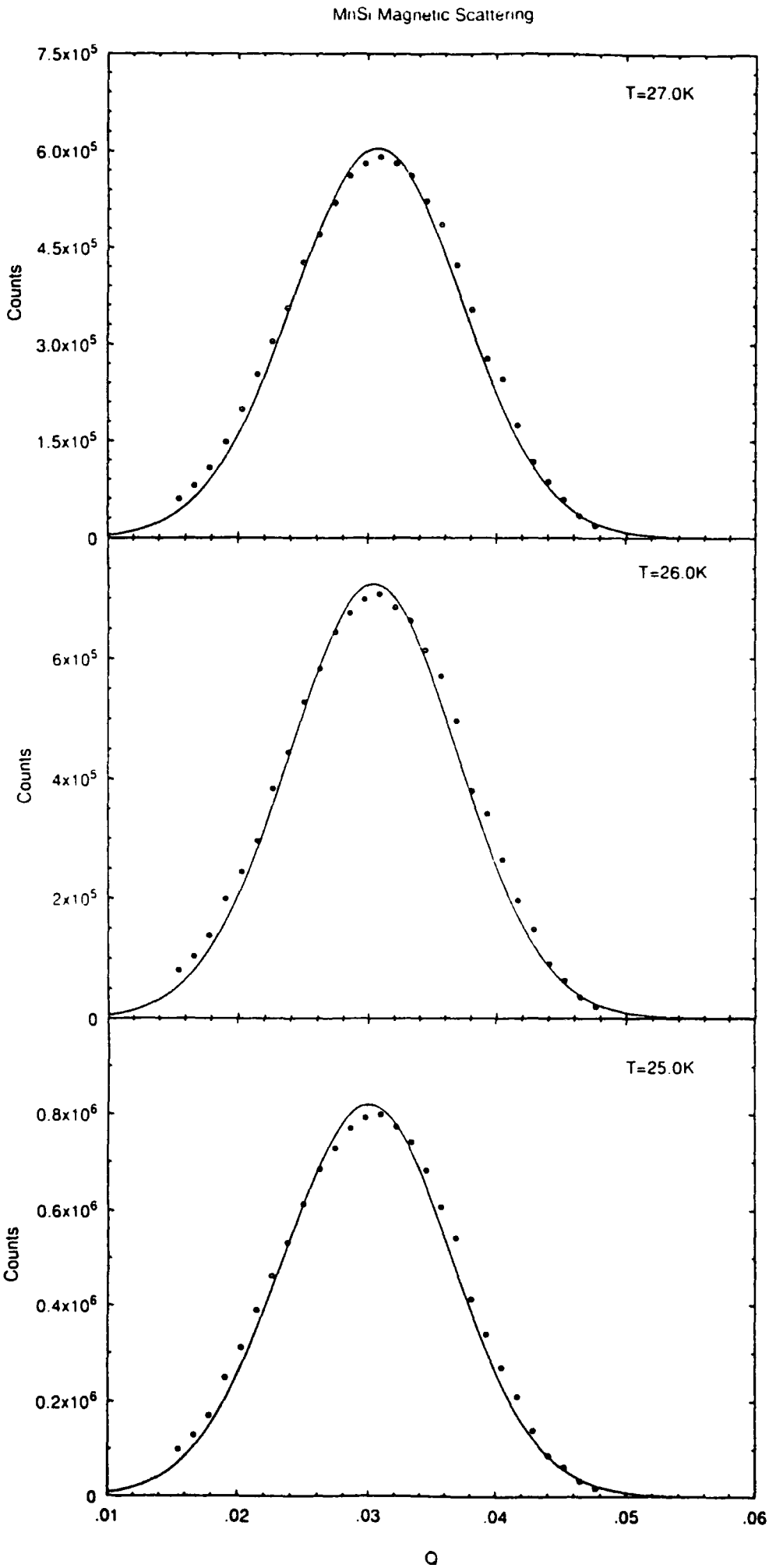

Figure 8.12 (m) - (o)

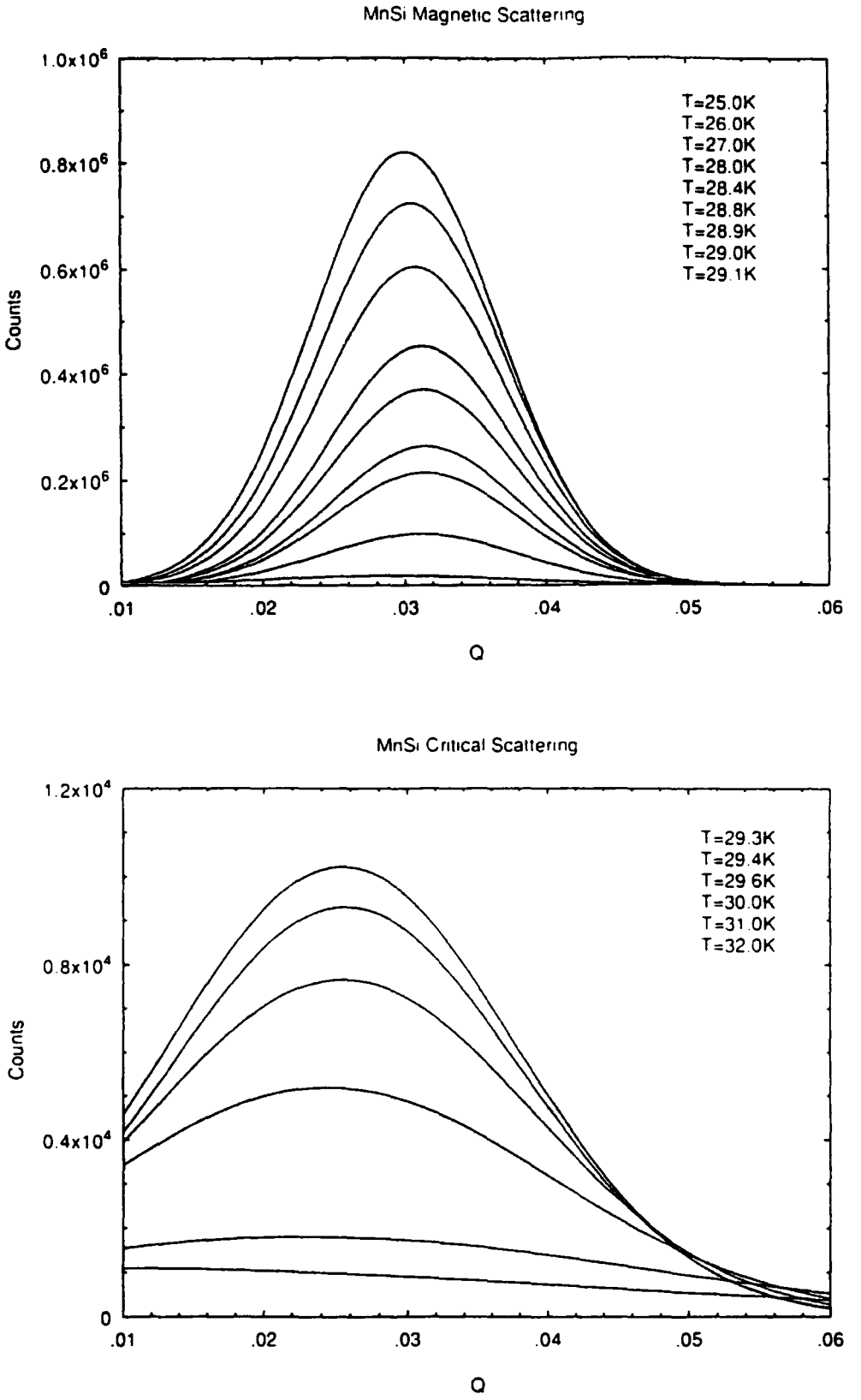

Figure 8.13 A selection of the Gaussian curves fitted to the residual corrected magnetic critical scattering from MnSi with $\underline{q}$ scanned along the [111] direction. (a) Below the transition temperature determined by SANS (see Chapter 7); (b) above the transition temperature determined by SANS.

Temp./K	Peak(c/2.5E6)	Error	Posn.($\AA^{-1}$)	Error	GFWHM($\AA^{-1}$)	Error
28.40	2192	102	0.0297	0.0024	0.0437	0.0038
28.50	2175	71	0.0330	0.0013	0.0379	0.0024
28.60	2453	64	0.0298	0.0012	0.0424	0.0020
28.70	2545	115	0.0277	0.0025	0.0461	0.0036
28.90	3661	130	0.0270	0.0018	0.0439	0.0026
29.00	6773	60	0.0297	0.0030	0.0305	0.0061
29.05	8684	224	0.0273	0.0011	0.0350	0.0015
29.05	8668	77	0.0294	0.0003	0.0294	0.0006
29.10	9468	207	0.0275	0.0087	0.0339	0.0013
29.10	9300	81	0.0293	0.0003	0.0295	0.0006
29.15	9700	216	0.0267	0.0091	0.0352	0.0013
29.15	9473	79	0.0287	0.0003	0.0308	0.0006
29.20	9306	61	0.0296	0.0022	0.0292	0.0042
29.30	8742	85	0.0291	0.0039	0.0309	0.0073
29.40	8038	63	0.0296	0.0031	0.0312	0.0061
29.50	7094	164	0.0277	0.0093	0.0371	0.0014
30.00	4220	118	0.0304	0.0013	0.0421	0.0022
30.20	3635	63	0.0299	0.0010	0.0412	0.0025
32.00	780	38	0.0375	0.0034	0.0555	0.0075
35.00	247	44	0.0435	0.0110	0.0540	0.0300

Table 8.2: Gaussian parameters for the curves fitted to the data measured in the [110] direction.

8.4 Critical Scattering Results

The peak height of the Gaussian fit to the critical scattering for the [111] and [110] directions are shown in figure 8.14(a) and (b) respectively, close to the transition temperature. Above a temperature of 29.2K the peak heights are identical in the two direction scanned. Below a temperature of 29.15K the peak height of the scattering in the [110] direction sharply decreases over a temperature interval of 0.3K whereas the scattering along the [111] direction continues to increase. The rate of increase is dramatic between 29.15 - 28.9K and the complete results are shown in figure 8.14(c).

Figure 8.15 shows the full width at half maximum (FWHM) of the Gaussian fit to the data in the two directions scanned close to the transition temperature. In the [111] direction, the FWHM of the Gaussian fit decreases smoothly with temperature from a maximum value of $0.085\AA^{-1}$ at 32K to a value of $0.025\AA^{-1}$ at 29.1K. There is then a sharp reduction in a temperature interval of 0.3K to a value of $0.015\AA^{-1}$ at 28.8K below which it remains constant over the remainder of the temperature regime studied.

In the [110] direction, the FWHM of the Gaussian fit to the data has a broad minimum with value of $0.03\AA^{-1}$ centred at 29.1K, probably due to this being the

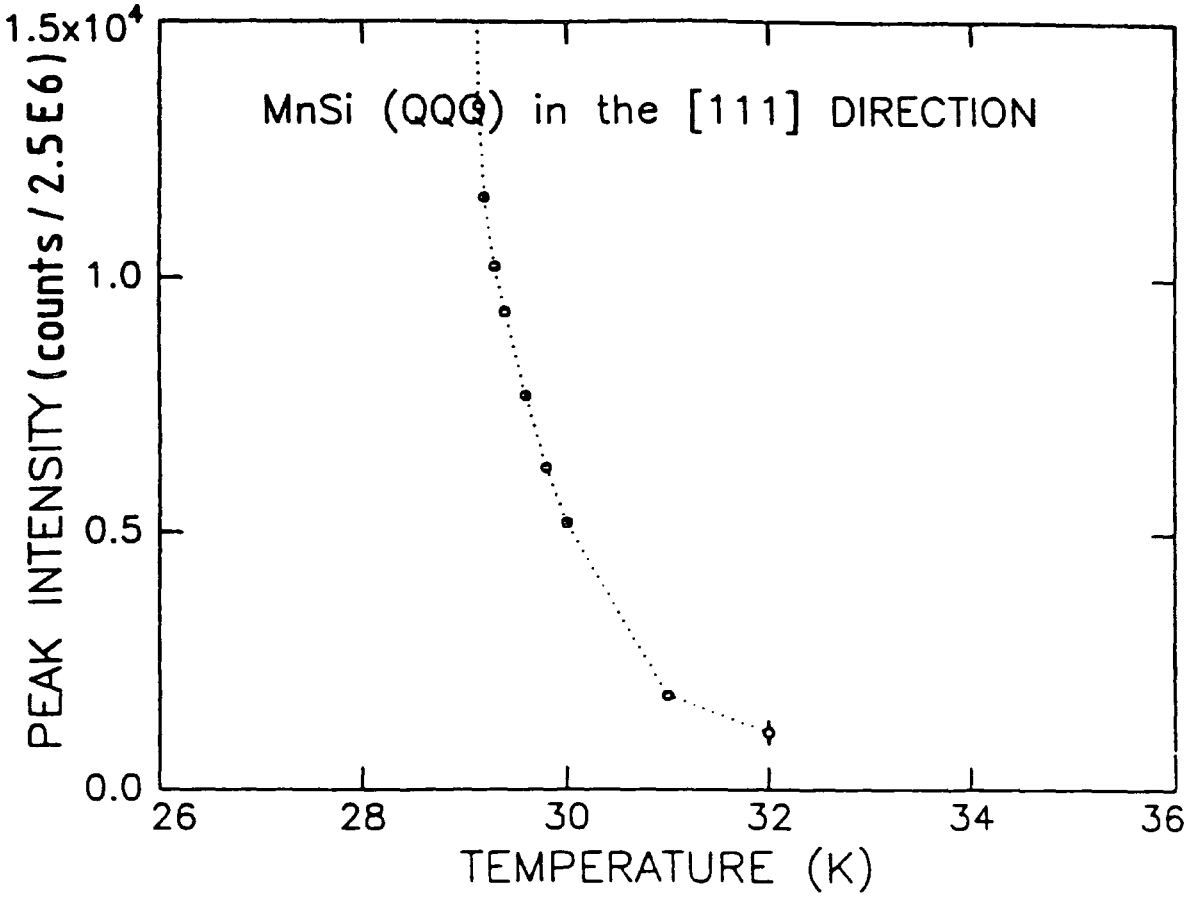

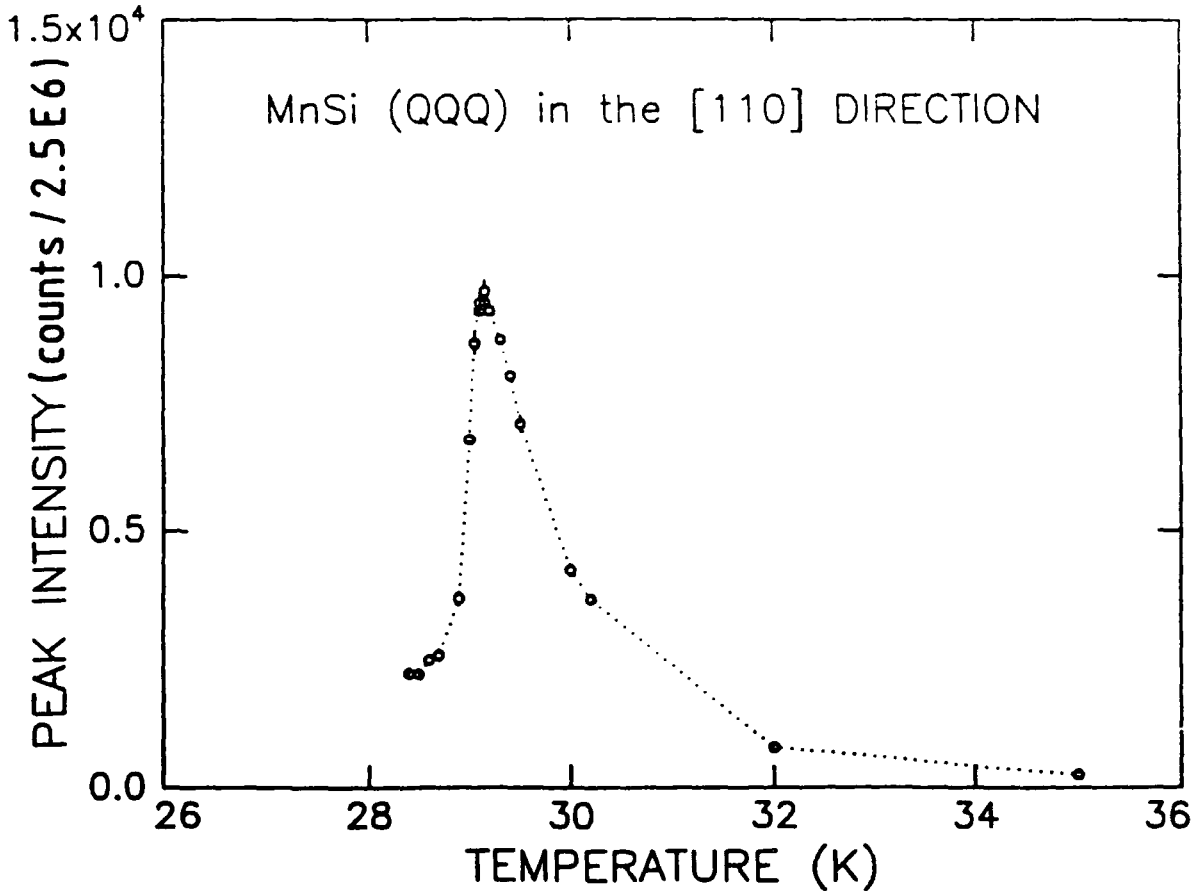

Figure 8.14 (a) and (b)

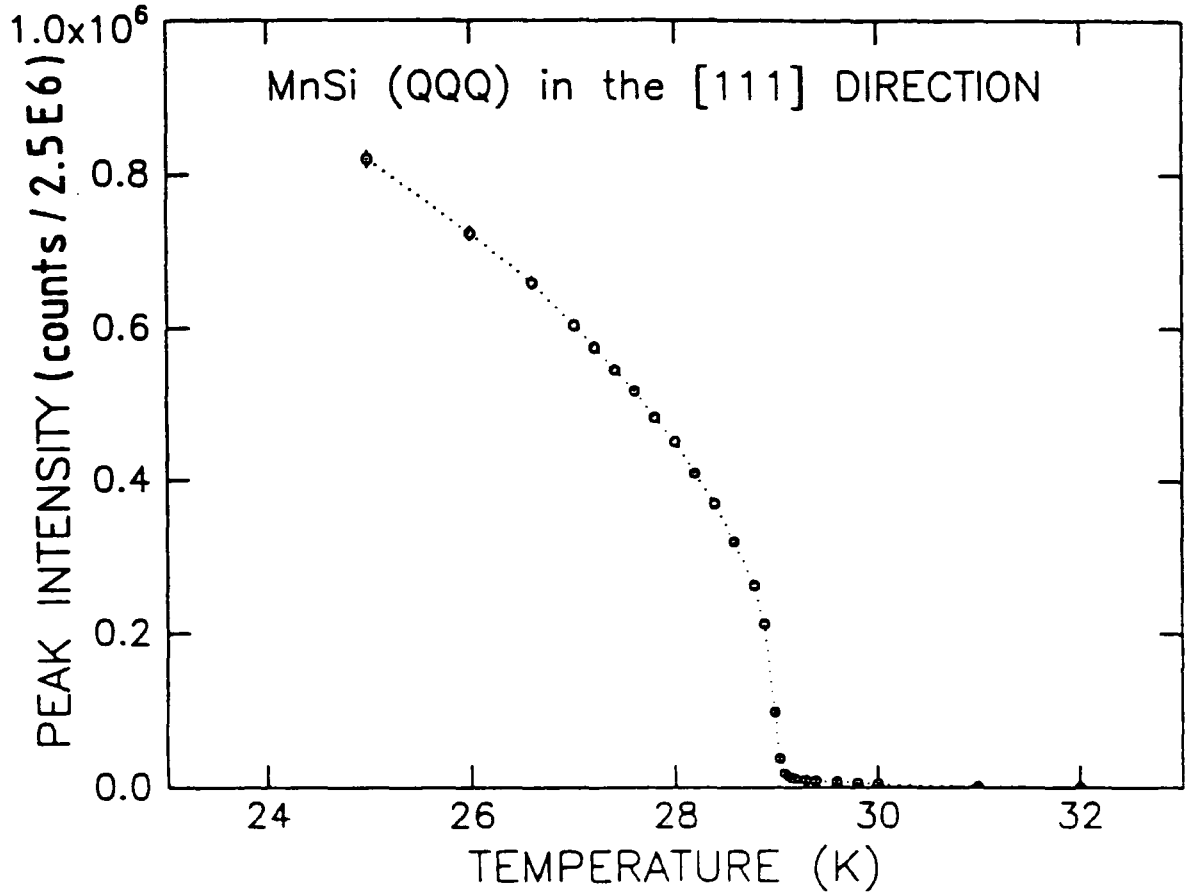

Figure 8.14 Peak height or intensity of the Gaussian fits to the residual corrected critical scattering of MnSi close to T_N. (a) $\underline{q}$ scan in the [111] direction; (b) $\underline{q}$ scan in the [110] direction; (c) $\underline{q}$ scan in the [111] direction (expanded scale).

regime of maximum scattering in this direction. At a temperature difference of $\pm\frac{1}{2}K$ from this the FWHM values are greater but show no obvious trend.

Figure 8.16 shows the peak position of the Gaussian fit to the data for the two directions scanned close to the transition temperature. In the [111] direction it is evident that the peak position increases smoothly to a value of $0.025\mathring{A}^{-1}$ until at a temperature of 29.15K there is a sharp increase of $0.006\mathring{A}^{-1}$ in a temperature interval of 0.3K. The peak position has a maximum $|\underline{Q}|$ value of $0.0361\mathring{A}^{-1}$ at a temperature of 28.9K after which it gradually decreases to a value of $0.0347\mathring{A}^{-1}$ at 25K. It is immediately pointed out that the observed peak position below 28.9K is consistent with the Q value of $0.035\mathring{A}^{-1}$ reported by Ishikawa (1984). Also the data is consistent with the fact that the wavelength of the helix increases as the temperature is lowered (Ishikawa (1984)). This behaviour is opposite to that of the spin density wave in Cr whose wavelength decreases as the temperature is lowered (see for example Fawcett (1988)).

The peak position of the data recorded in the [110] direction does not show any of the trends observed in the [111] direction as the temperature is varied. The values, especially between 28K and 30K are consistent with a single value of $0.0294\mathring{A}^{-1}$, note the same value of the peak position in the [111] direction before the dramatic increase at 29.1K. The errors associated with these values are a similar order of magnitude whereas the magnitude of the errors recorded in the [111] reduce, owed to the increased scattering and hence more accurate fitting of the Gaussian function.

8.5 Discussion

From the results of the magnetic critical scattering in the [111] direction it appears that there are three distinct regions over the temperature regime studied. This is evident from the logarithmic plot of peak height against temperature shown in figure 8.17(a). The first region, above 29.2K is characterised by broad scattering in reciprocal space, with low peak position which gradually increases as the temperature is lowered from 32K. There is both a gradual increase in the peak position and narrowing of the FWHM as the temperature decreases. There then follows a temperature regime of 0.3K where there is a dramatic increase in peak height coupled with sharp narrowing of FWHM and rapid increase in the peak position.

Measurements in the [110] direction appear very similar over the complete temperature range studied. The peak position remains approximately fixed and the FWHM shows no consistent behaviour apart from a slight decrease where the scattering is greatest. Although the peak height reduces sharply after 29.15K this is not as dramatic as the increase observed in the [111] direction as shown in figure 8.17(b).

In numerous phase transitions studied, various parameters including susceptibility and specific heat diverge as the critical point is approached (see for example Stanley (1971)). In an analogous way the magnetisation tends to zero, so the reciprocal of the magnetisation tends to infinity. In general, it is observed experimentally that (see for example Collins (1989)) the magnetisation (and numerous other pa-

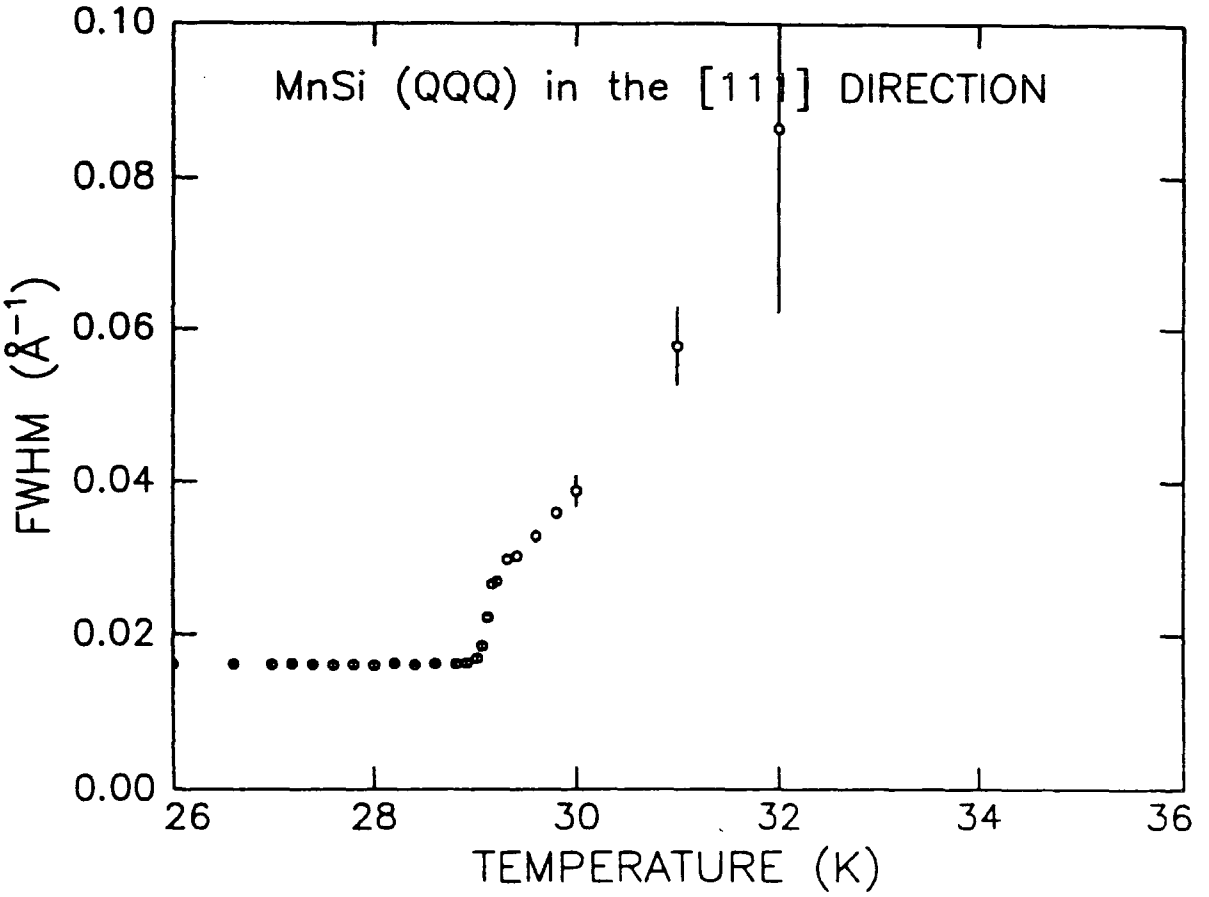

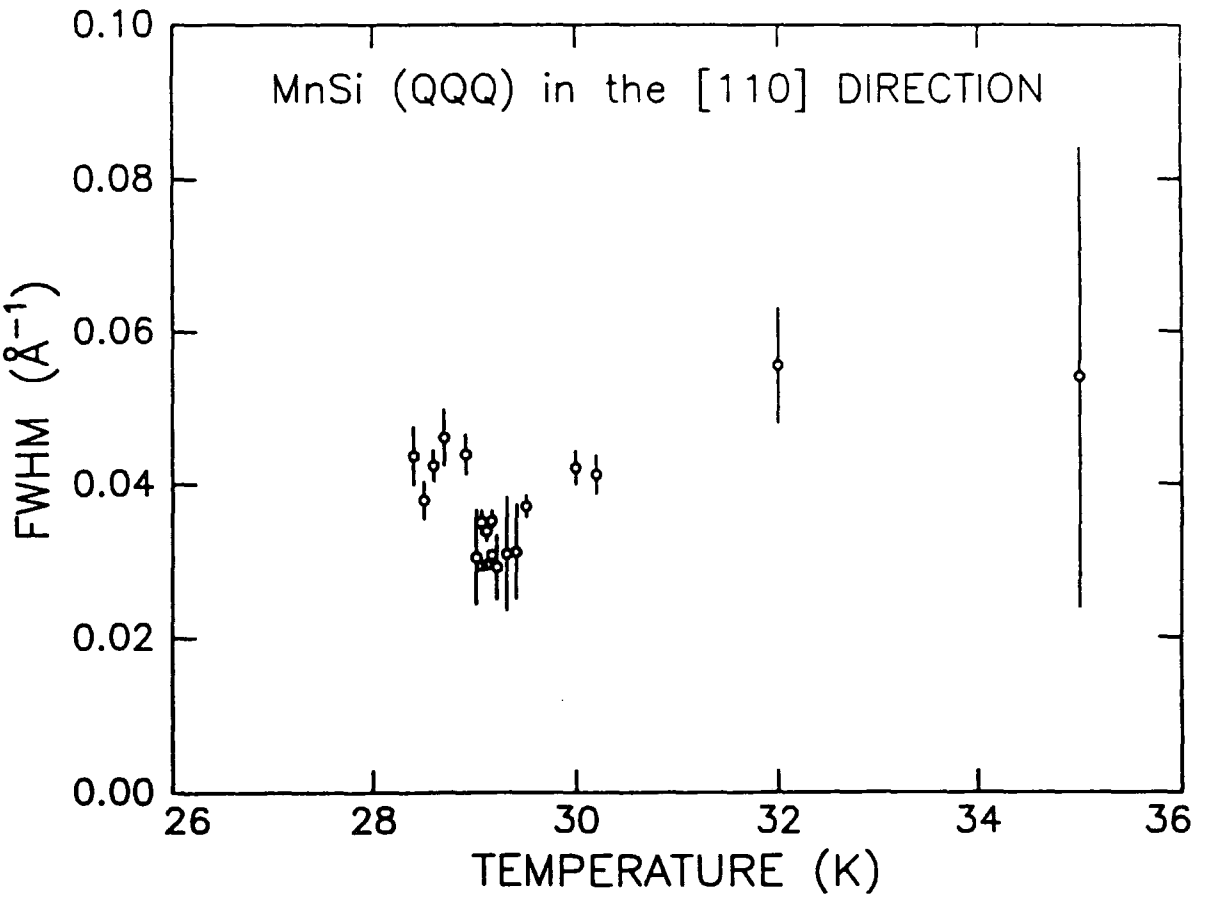

Figure 8.15 Full width at half maximum (FWHM) of the Gaussian fit to the residual corrected critical scattering of MnSi close to T_N. (a) $\underline{q}$ scan in the [111] direction; (b) $\underline{q}$ scan in the [110] direction.

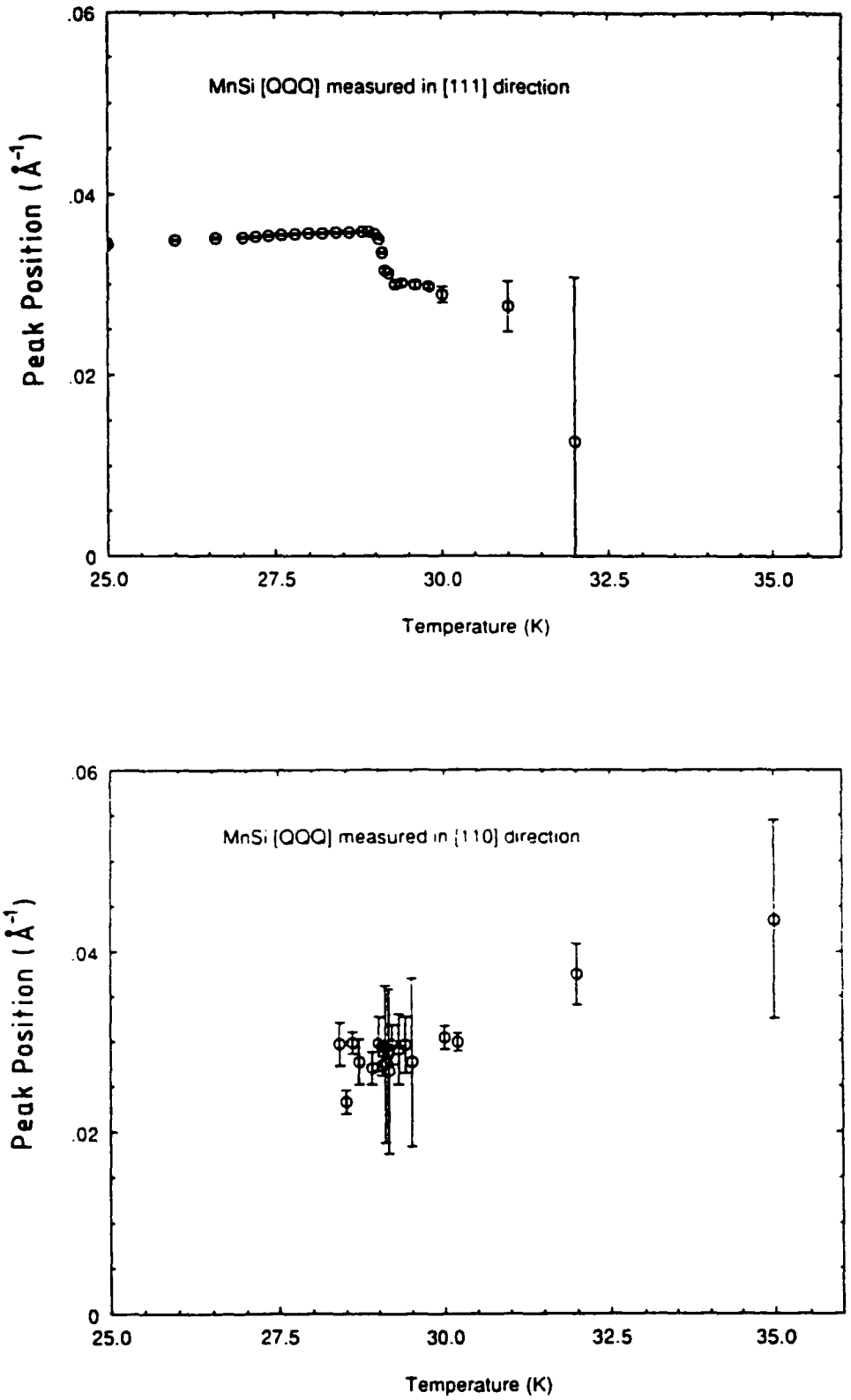

Figure 8.16 Peak position of the Gaussian fit to the residual corrected critical scattering of MnSi close to T_N. (a) $\underline{q}$ scan in the [111] direction; (b) $\underline{q}$ scan in the [110] direction.

Temp./K	Peak(c/2.5E6)	Error	Posn.($\AA^{-1}$)	Error	GFWHM($\AA^{-1}$)	Error
25.00	820256	10759	0.0347	0.0001	0.0161	0.0002
26.00	723603	9151	0.0351	0.0001	0.0161	0.0002
26.60	659214	7865	0.0353	0.0001	0.0161	0.0002
27.00	603565	7238	0.0354	0.0001	0.0161	0.0002
27.20	575122	7239	0.0355	0.0001	0.0162	0.0002
27.40	545701	6095	0.0356	0.0001	0.0161	0.0001
27.60	518053	6940	0.0357	0.0001	0.0160	0.0002
27.80	484321	5861	0.0358	0.0001	0.0161	0.0002
28.00	451534	6660	0.0359	0.0001	0.0160	0.0002
28.20	409373	4493	0.0359	0.0001	0.0162	0.0001
28.40	368684	4280	0.0360	0.0001	0.0161	0.0001
28.60	318726	3171	0.0360	0.0001	0.0162	0.0001
28.80	261959	2942	0.0361	0.0001	0.0162	0.0001
28.90	212552	2172	0.0361	0.0001	0.0163	0.0001
29.00	97818	1007	0.0358	0.0001	0.0169	0.0002
29.05	37718	347	0.0353	0.0001	0.0185	0.0002
29.10	18356	164	0.0338	0.0001	0.0222	0.0003
29.15	13331	151	0.0318	0.0003	0.0266	0.0005
29.20	11586	54	0.0315	0.0001	0.0270	0.0003
29.30	10222	69	0.0302	0.0003	0.0299	0.0005
29.40	9303	66	0.0304	0.0003	0.0303	0.0006
29.60	7660	64	0.0312	0.0004	0.0329	0.0008
29.80	6263	40	0.0300	0.0003	0.0359	0.0007
30.00	5186	34	0.0291	0.0009	0.0388	0.0020
31.00	1807	58	0.0278	0.0028	0.0577	0.0051
32.00	1099	224	0.0130	0.0181	0.0863	0.0240

Table 8.3: Gaussian parameters for the curves fitted to the data measured in the [111] dirrection.

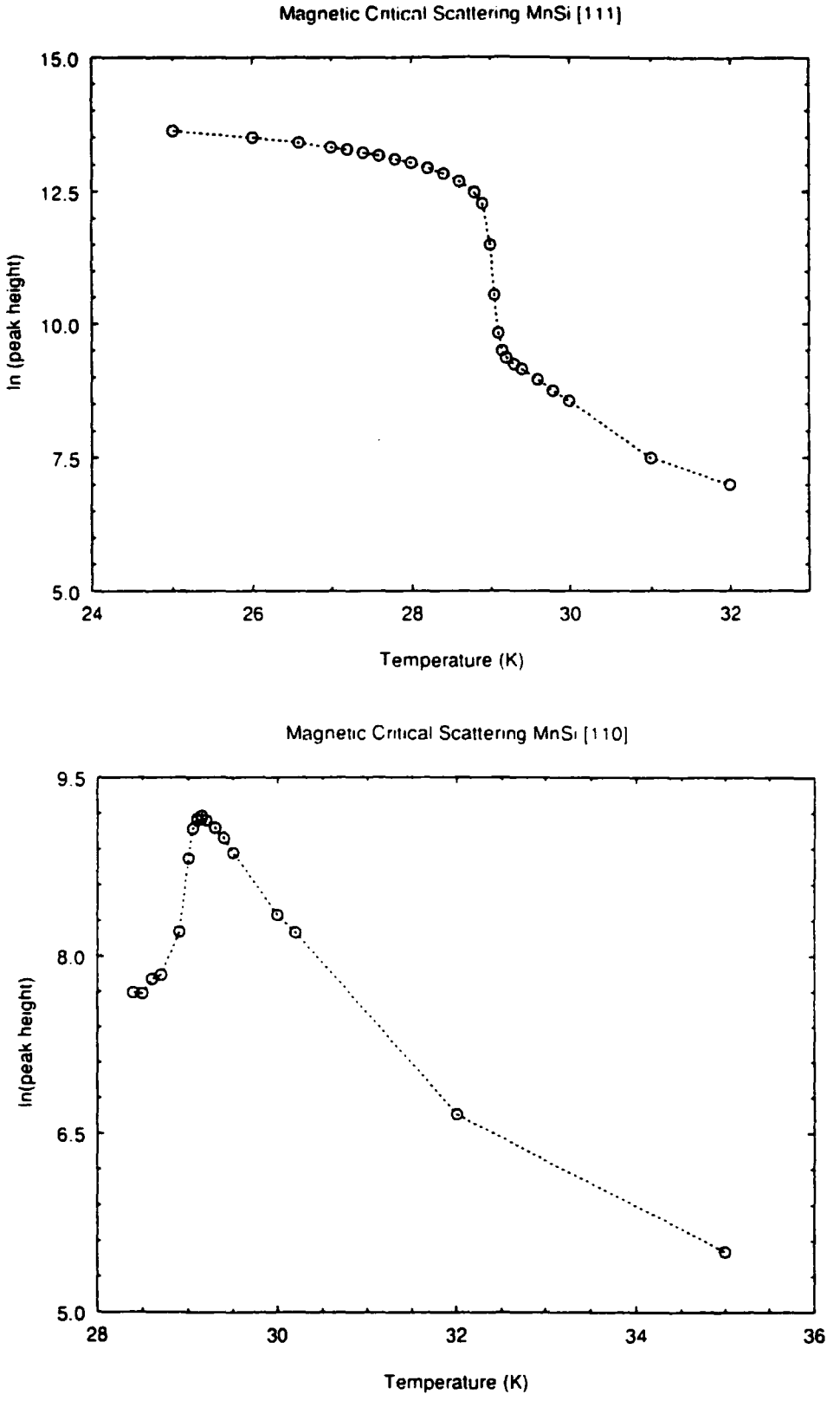

Figure 8.17 Natural log of the peak height of the Gaussian fit to the residual corrected critical scattering of MnSi close to T_N. (a) $\underline{q}$ scan in the [111] direction; (b) $\underline{q}$ scan in the [110] direction.

rameters) obey a simple power law and have a leading divergence close to the critical point of the form $(T_c - T)^\beta$ where β is defined as the critical exponent.

Considering the expression for the magnetic neutron scattering cross section (Chapter 7), the peak height is related to the magnetisation of the sample perpendicular to the scattering vector. It is thus regarded to be a measure of the 'order' or an 'order parameter' at the particular temperature.

SANS results of Chapter 7 suggest MnSi has a critical temperature of $29.1 \pm 0.1K$ however from these measurements magnetic scattering is observed as high as 32K. Thus in order to determine the transition temperature, an attempt is made to reduce the data to linear form as shown in figures 8.18(a) - (c) for numerous transition temperature values. From this it is evident that a linear form is obtained using a transition temperature close to 29.0K. Also note the curvature of the data and how it is dependant on the choice of transition temperature, even for $ln(T_c - T) > -1$. The further from the transition temperature, the closer the points from the individual graphs become, suggesting they would converge asymptotically. Although the graphs approach linear form over the temperature range studied, the resulting gradient of each is sensative to critical temperature used. The resulting value varies from 0.372 for a critical temperature of 28.6K to 0.536 for a critical temperature of 29.4K as demonstrated in figure 8.18(c). Figure 8.18(d) shows the resulting linear form of the data for a transition temperature of 29.04K, the value of critical exponent obtained being 0.435. This compares favourably with the range of experimental values of 0.2 - 0.4 observed for other critical magnetic systems (see for example Stanley (1971)). The onset of linearity of the data with a transition temperature of 29.04K appears entirely linked to the formation of the helical spin density wave along the $< 111 >$ directions and is consistent with the SANS results. However, it offers no explaination to the magnetic scattering observed above this temperature. This analysis suggests the helical spin density wave forms at a critical temperature of $29.04 \pm 0.05K$ below which the peak height of the neutron magnetic scattering increases with a critical exponent of 0.435, at least down to a temperature of 25.0K.

The magnetic critical scattering observed in the two directions above 29.2K is identical and different in form to that observed below 29.0K in the [111] direction. The peak position gradually increases from close to zero scattering vector which is opposite to the behaviour below 29.0K. This may be intuitively expected as it develops from the paramagnetic state. Also the peak height increases such that over the temperature region close to helix formation

$$\text{peak height} = Ae^{-T} \ (31K > T > 29.2K) \tag{8.1}$$

where A is a constant, as demonstrated in figure 8.19. This scattering may be related to the broad peak observed in the ultrasonic attenuation (Kusaka (1976)) and also in the magnetovolume effect (Matsunga (1982)) which prempts the helical spin density wave formation. It could possibly be linked to the structure of the inverse initial susceptibility of MnSi close to the transition temperature reported in Chapter 5. Since it is isotropic in the directions studied, the scattering is very similar to that observed by Ishikawa (1984) as a ring of scatter using SANS at 29.4K and also related to the similar observation on FeGe by Lebech (1989). The first evidence

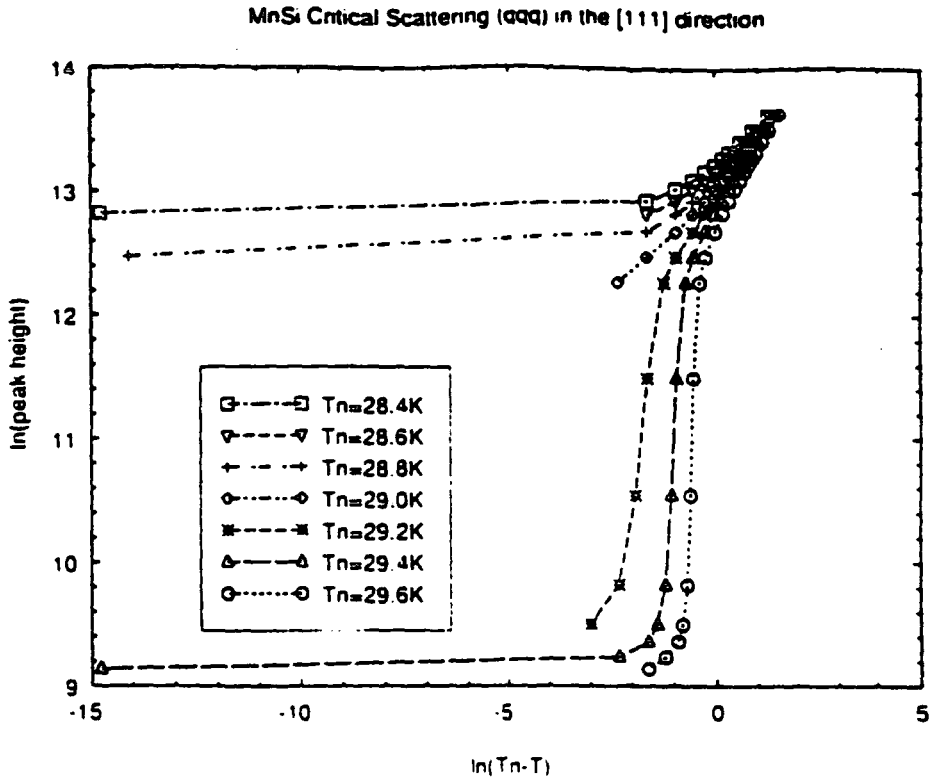

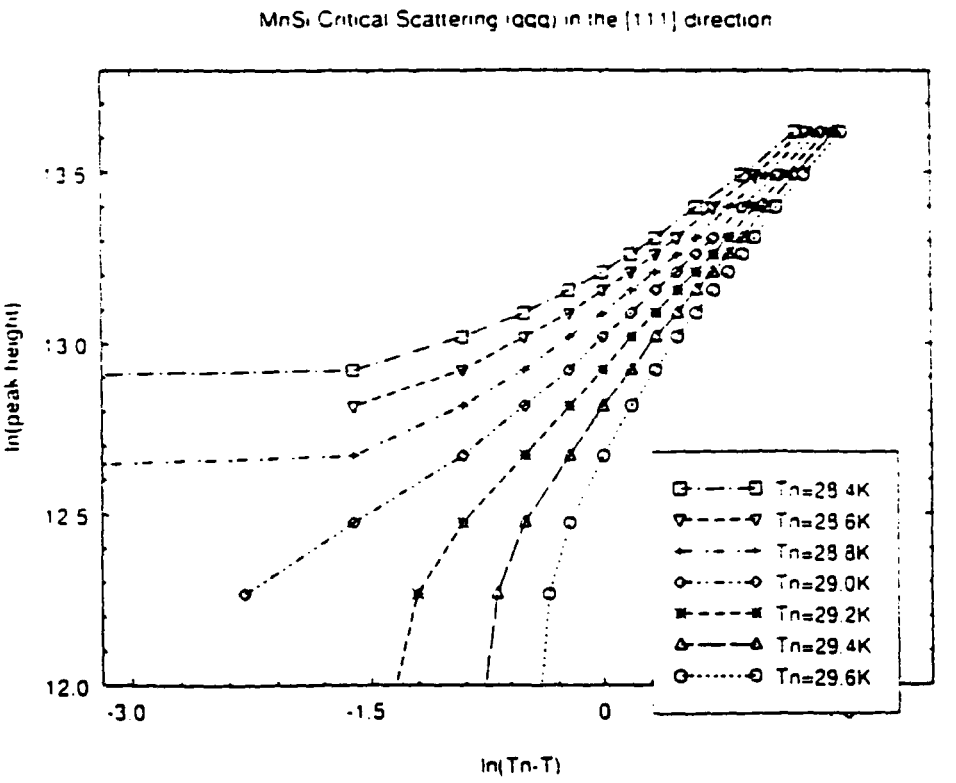

Figure 8.18 (a) and (b)

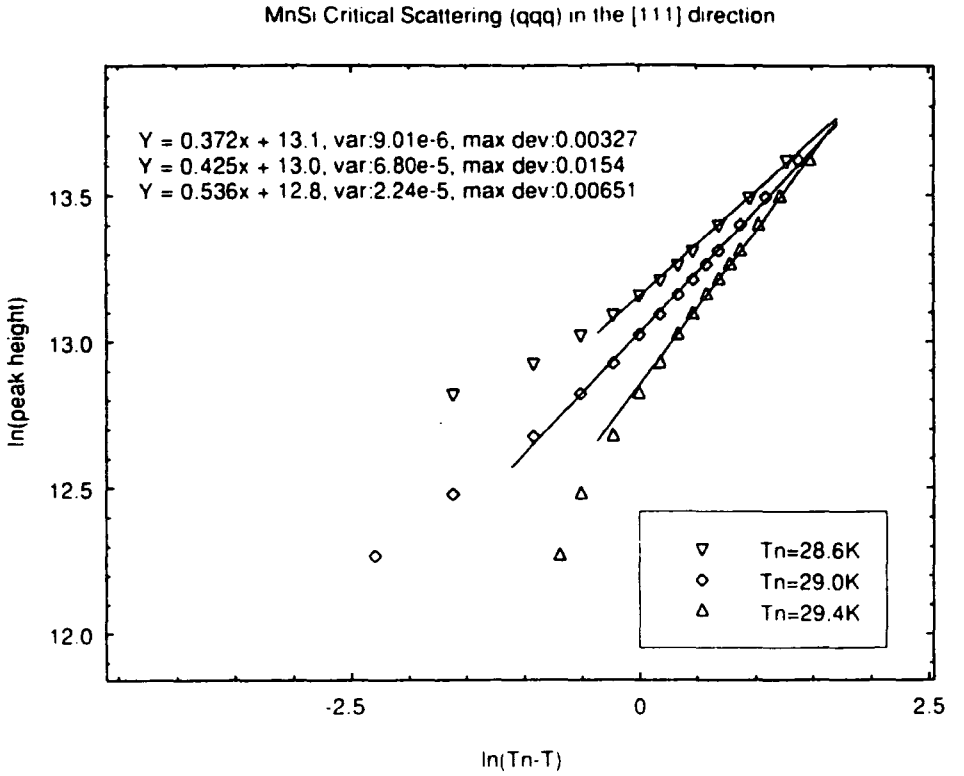

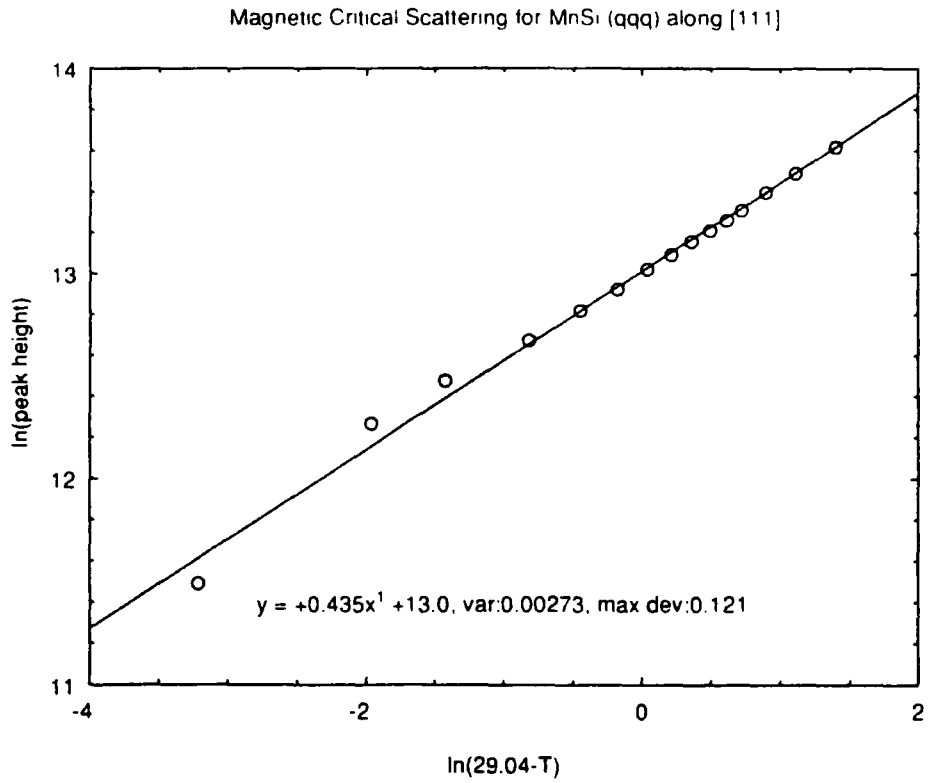

Figure 8.18 (a) and (b) Natural log of the peak height of the Gaussian fit to the residual corrected critical scattering of MnSi against natural log of (T_N-T) for various values of T_N in order to determine suitable T_N and critical exponent; (c) linear fits showing range of possible critical exponents; (d) linear fit assuming $T_N = 29.04K$.

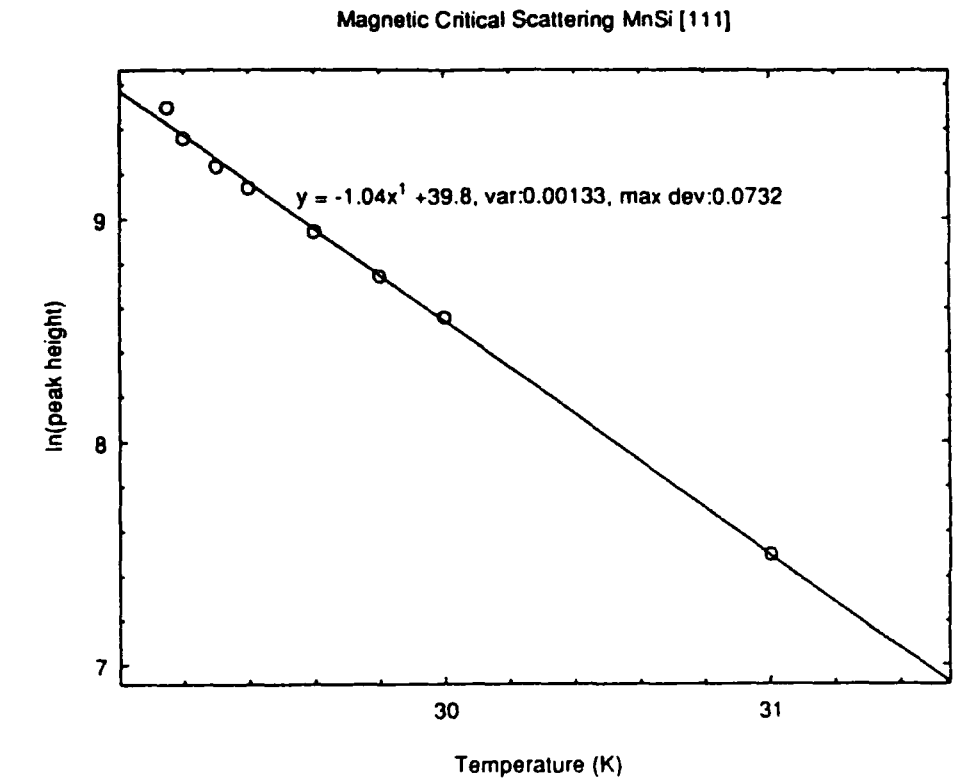

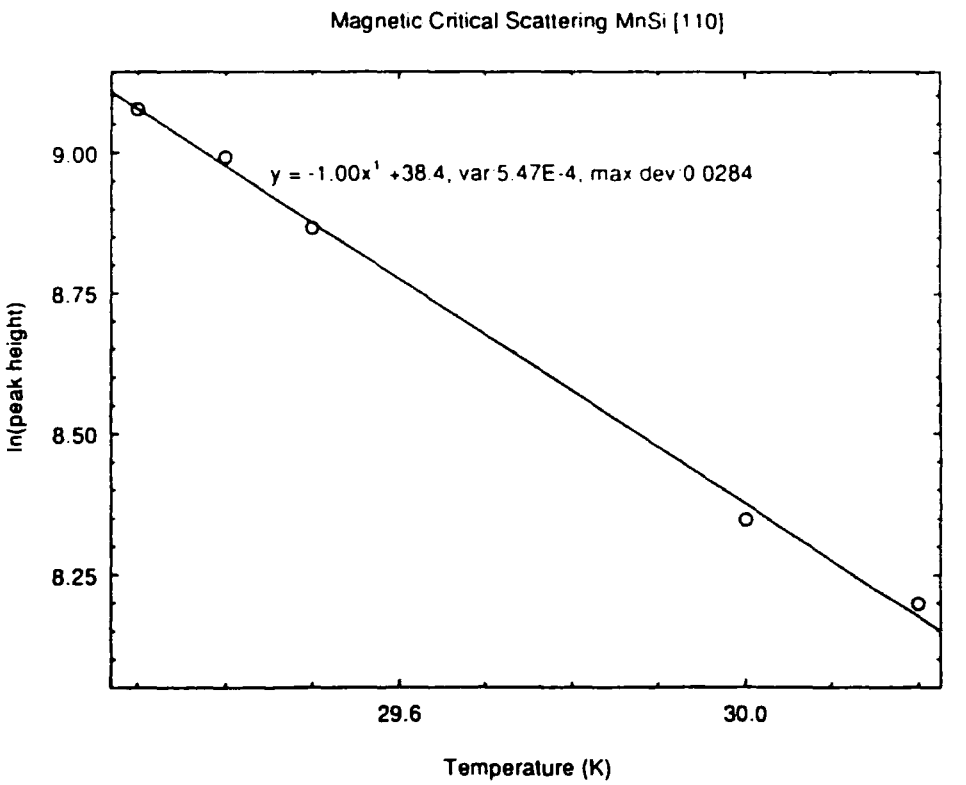

Figure 8.19 Natural log of the peak height of the Gaussian fit to the residual corrected critical scattering of MnSi against temperature together with least squares linear fit. (a) $\underline{q}$ scan along [111] direction; (b) $\underline{q}$ scan along [110] direction.

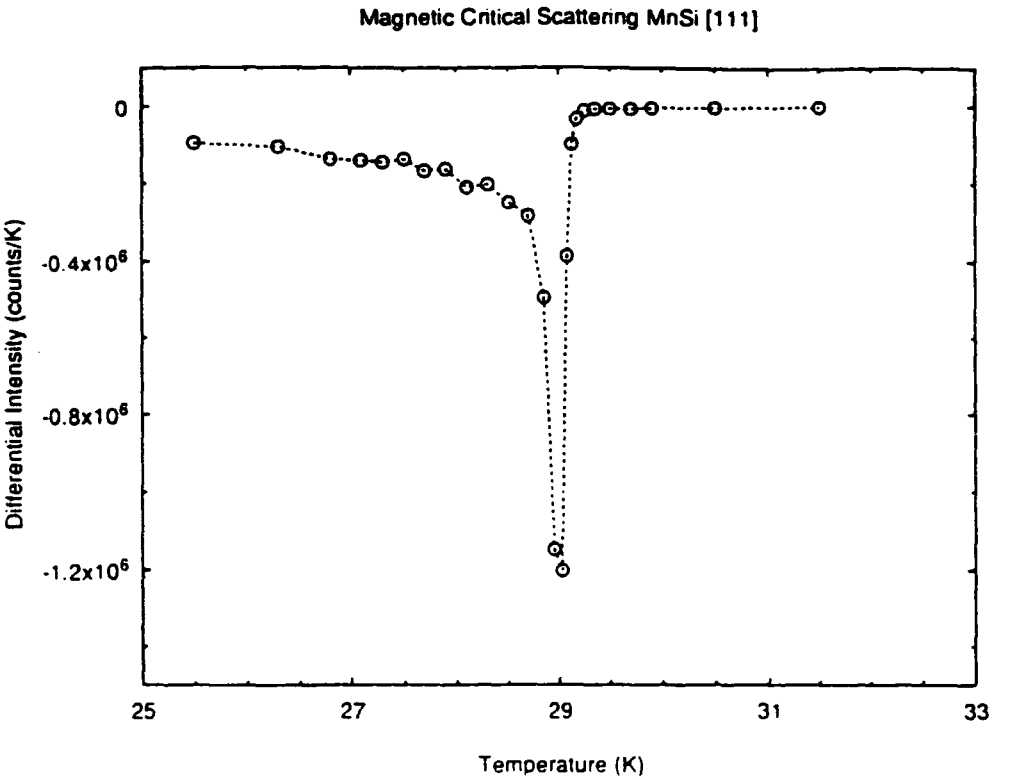

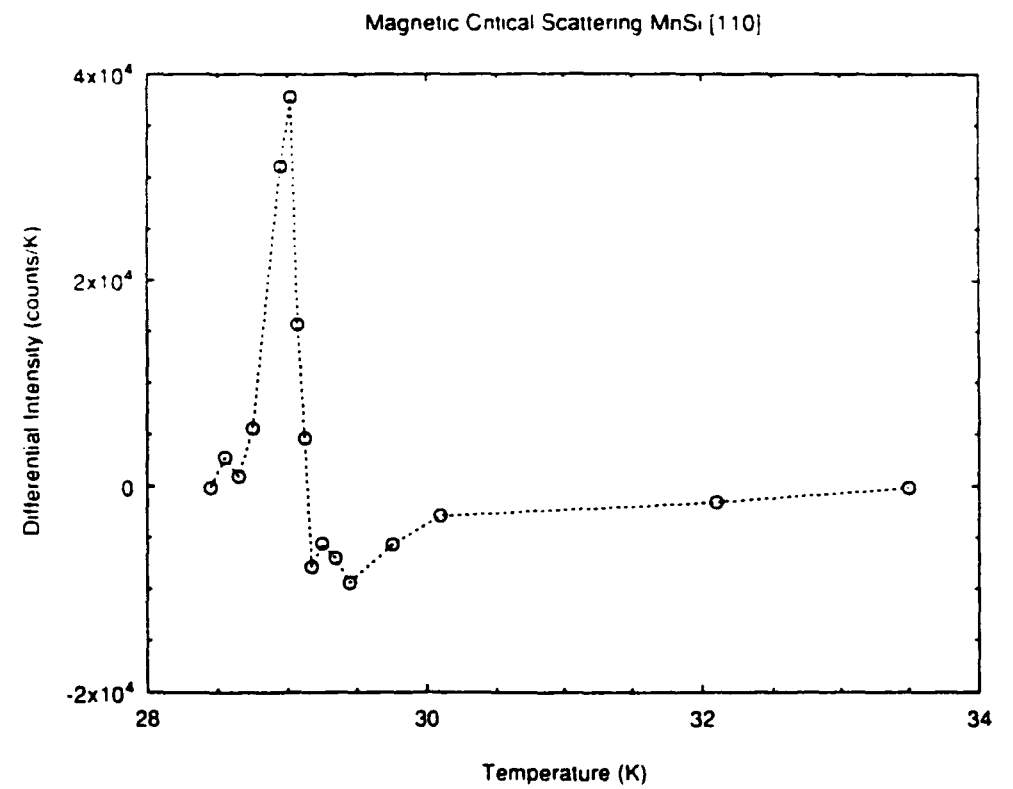

Figure 8.20 (a) and (b)

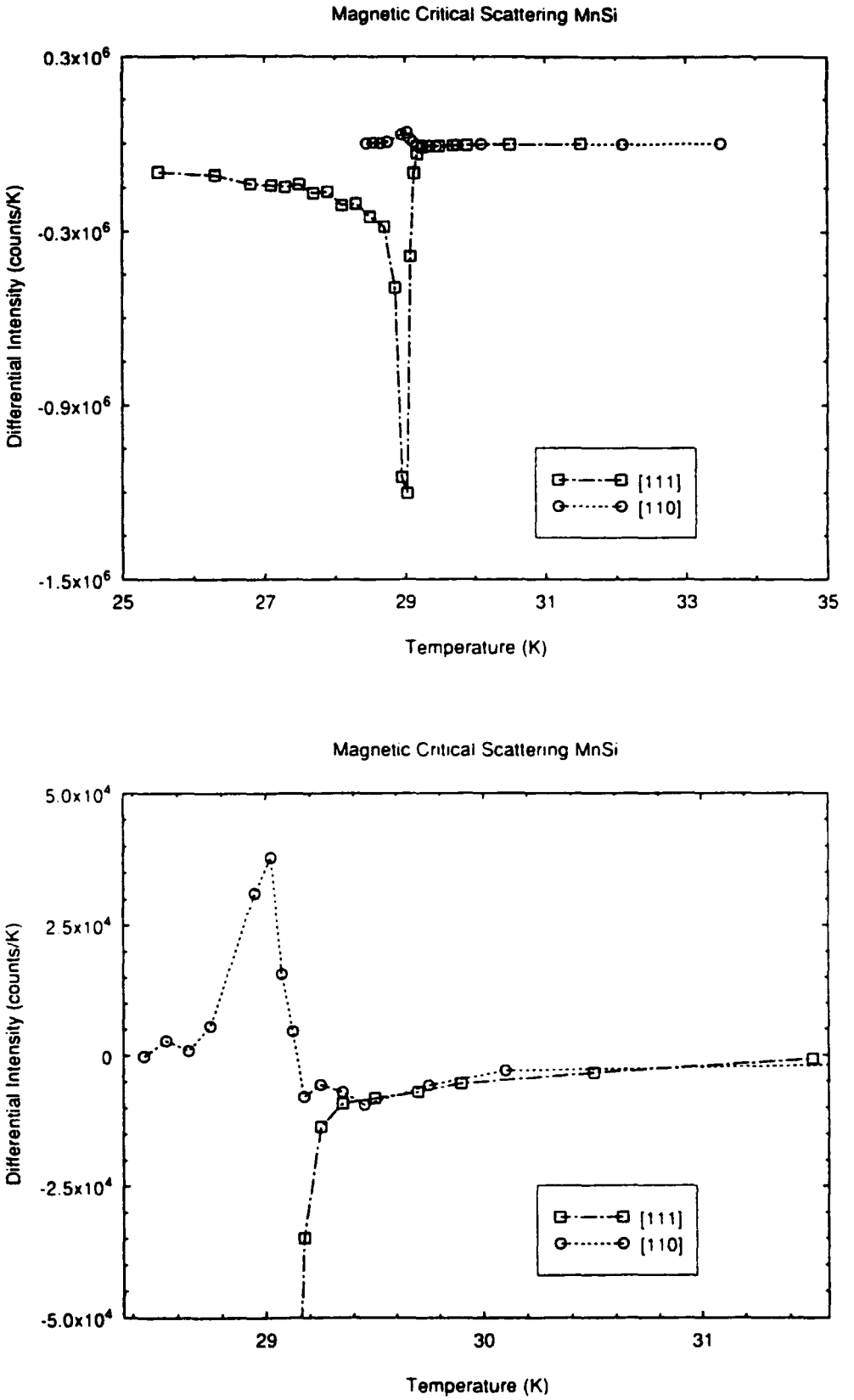

Figure 8.20 Differential intensity of the peak height of the Gaussian fit to the residual corrected critical scattering of MnSi close to T_N. (a) $\underline{q}$ scan along [111] direction; (b) $\underline{q}$ scan along [110] direction; (c) and (d) combined on the same figure.

of a peak in the scattering is at a temperature of 32K which corresponds to the temperature at which the heat capacity of MnSi begins to increase, as shown in figure 8.7(a).

This scattering may be onset or a prephase to helix formation. It is evident from Chapter 7 that application of a magnetic field ($\approx$ 1.5kOe) can cause reorientation of the helix to align it parallel to the field, which suggests the anisotropy energy is small. If initially the anisotropy energy is zero, then the helix could propagate in all directions, resulting in a ring of scatter from SANS (see neutron simulations, Chapter 7). As the anisotropy energy increases (perhaps due to a change in lattice constants), the sphere of helix may then collapse into the $< 111 >$ directions.

Finally, in the temperature regime 28.9 - 29.2K there is a dramatic increase in the scattering observed in the [111] direction which also corresponds to the region of sharp decrease in the peak height in the [110] direction. This temperature region is thought to be the phase transition into the helical phase. Figure 8.20 shows the differential intensity of the scattering in the two directions. Figure 8.20(c) shows how the magnitude in the [111] direction is far greater than that in the [110] direction and also demonstrates the similarity of the measurements at temperatures in excess of 29.2K.

8.6 Further Work

This work is a detailed study of the critical scattering initially observed in MnSi by Ishikawa (1982) however the study is only along the [111] and the [110] directions. As these directions correspond to major crystal symmetry directions, it is felt that further scans should be performed in other more random directions, one in the $(1\bar{1}0)$ scattering plane and the other out of this plane to investigate whether this scattering is truely isotropic. Another region of great interest is the temperature regime 28.9 - 29.2K which marks the transition between the types of scattering measured. In order to find the cause of this transition it may be worthwhile monitoring the lattice constants of MnSi in this temperature regime.

Finally, the work of Brown (1990) may suggest the intensity associated with this 'prephase' is greater and temperature regime broader on application of homogeneous pressure on MnSi. Thus in order to discover more about this phase it may be necessary to perform more measurements on MnSi under homogeneous pressure. With this in mind, a pressure cell was designed and built by the author to make magnetic measurements under uniaxial stress and homogeneous pressure. The design and initial measurements are described in detail in Appendix D.

8.7 References

Andrews T. (1869), Phil. Trans. R. Soc. **159**, 575.
Bernhoeft N.R., Marcenat C. and Calemizuk R. (1992), private communication.
Brown S. (1990), Ph.D. Thesis, University of Cambridge.
Collins M.F.(1989), *Magnetic Critical Scattering*, Oxford University Press.
Fawcett E. (1988), Rev. Mod.Phys. **60**, 209.
Hayden S. and Brown S. (1991), Private Communication.
Ishikawa Y. *et al.*(1982), Phys. Rev. B **25**, 254.
Ishikawa Y. *et al.*(1984), J.Phys. Soc. Jpn. **53**, 2726.
Kusaka S. *et al.*(1976), Solid State Commun. **20**, 925.
Lebech B. *et al.*(1989), J. Phys.: Condensed Matter **1**, 6105-6122.
Lebech B. and Nielson M.(1975), Presented at the Neutron Diffraction Conference, ——Petten, The Netherlands.
Makoshi K.(1979), J. Phys. Soc. Jpn. **46**, 1767.
Matsunga M. *et al.*(1982), J. Phys. Soc. Jpn. **51**, 1153.
Nielson M. *et al.*(1969), Acta Cryst. **A25**, 547.
Stanley H.E. (1971), *Introduction to Phase Transitions and Critical Phenomena*, ——Clarendon Press, Oxford.

Chapter 9

Conclusions

From this magnetisation study of MnSi, FeGe and $ZrZn_2$ it is evident that the magnetisation of MnSi in magnetic fields above ≈6kOe is very similar to that of $ZrZn_2$. The magnetisation of both $ZrZn_2$ and MnSi in this field regime are described by the model of Lonzarich and Taillefer (1985) which is discussed in Chapter 1. However, this study concentrates on the low field properties of MnSi where the magnetisation is very different to that of $ZrZn_2$. It is believed that the reason for this low field difference is the interaction of the itinerant electrons in MnSi with the lattice structure (Bak and Jensen (1980)), in particular due to the lack of inversion symmetry of the system.

Initial magnetisation measurements close to the magnetic transition temperature of MnSi observed anomalous behaviour between 29.1 - 29.0K. This was further investigated using neutron scattering which suggests that MnSi exhibits some magnetic order at temperatures as high as 32K, 3K higher than the generally accepted value of the transition temperature of $29.10 \pm 0.05K$ observed through small angle neutron scattering (SANS) and magnetisation measurements within this thesis. This is evident as a ring of scattering (possibly isotropic) about (0,0). The wavevector radius of this ring gradually increases until at a temperature of 29.1K the ring 'collapses' and the scattering observed in the [111] direction dramatically increases together with a sharp increase in wavevector. The neutron scattering associated with the formation of the helix in the [111] direction increases with a critical exponent of 0.435. The behaviour of the helical spin density wave is now consistent with previous measurements including wavevector of $q \approx 0.035\AA^{-1}$ (Ishikawa (1976)) which decreases as the temperature is lowered (Ishikawa (1984)).

On formation of the helical spin density wave, propagating along equivalent $< 111 >$ directions, the induced magnetisation under applied magnetic field becomes anisotropic. SANS reveals this to be due to reorientation of the helical spin density wave parallel to the applied magnetic field. This process results in an increase in the magnetic susceptibility of MnSi and hence reduction in the magnetic Helmholtz free energy. Although the reorientation causes an increase in the anisotropy energy of the arrangement, the total energy is reduced. The rotation of the helix is gradual with applied magnetic field and the magnetisation measurements are similar to those predicted by minimisation of the expression for free energy produced by Plumer and

Walker (1981). As the magnetic field is further increased, the magnetic moments cone towards the field direction in order to reduce the magnetostatic energy which becomes the dominant term in the expression for the free energy.

The magnetisation was also observed to be anisotropic in response to the so called 'Phase A', being evident only with magnetic field applied parallel to the $< 001 >$ direction, as a sharp increase in the magnetisation but to a region of reduced magnetic susceptibility. This explains the apparent anomalous magnetisation measurements of Kadowaki (1981) with 'Phase A_1' correponding to to the magnetic field regime where the magnetisation in the $< 001 >$ direction is greater than that in the $< 111 >$ direction, and 'Phase A_2' is the regime where the magnetisation is lower. SANS within 'Phase A' exposed the reason for the close link with crystal orientation. With magnetic field applied parallel to a $< 001 >$ direction, in 'Phase A' the helix 'flips' from parallel to the applied magnetic field to propagate along the two $< 100 >$ directions perpendicular to the field. This can be incorporated in the framework of the theory of Bak and Jensen (1980) and that of Plumer and Walker (1981) in terms of the anisotropy energy being both field and temperature dependent, changing sign within the temperature-magnetic field regime of 'Phase A'.

Consequently, the low field magnetisation of MnSi was measured and explained in terms of helical spin density wave orientation and can be understood within the framework of the models of Bak and Jensen (1980) and the expression for the free energy of Plumer and Walker (1981). The nature of the magnetic transition however, requires further investigation, in particular the magnetic order observed in MnSi above 29.1K.

The magnetisation measurements on cubic FeGe coupled with the SANS of Lebech (1989) highlights many similarities in behaviour between cubic FeGe and MnSi. Cubic FeGe also has the B_{20} crystal structure and hence is a candidate for supporting a helical spin density wave due to the lack of inversion symmetry of the lattice. The SANS results of Lebech (1989) reveal a helical spin density wave forms in FeGe at a temperature of $\approx$278K, propagating along equivalent $< 100 >$ directions although the propagation direction does change at $\approx$211K to $< 111 >$.

As the transition temperature of cubic FeGe is approached, a ring of scattering is observed in SANS which may correspond to the critical scattering observed in MnSi. Also, the magnetisation measurements suggest the possible existence of a field induced phase, close to but below the transition temperature similar to 'Phase A' observed in MnSi. From both the SANS and magnetisation measurements, it is evident that the response of the helical spin density wave to an applied magnetic field in both cubic FeGe and MnSi is identical. This includes linear magnetisation when the magnetic field is applied parallel to the helix propagation direction (below the 'knee' in magnetisation) and rotation of the helix into the field direction as a second order process when the orientation of both is neither parallel nor perpendicular.

The high field response above the 'knee' in the magnetisation of cubic FeGe is similar in form to the magnetisation of $ZrZn_2$ and MnSi in the corresponding regime. This is reinforced by comparison of the 'Arrot Plots' of cubic FeGe and MnSi and suggests the magnetisation of cubic FeGe above the 'saturating' field

is indicative of a weak itinerant ferromagnet. Finally, the form of the magnetic phase diagram of cubic FeGe predicted by Plumer (1990) using a similar model to that applied to MnSi is in good agreement with that determined through magnetic measurements.

Although further work has been suggested after each chapter, I feel one of the most pressing measurements required are SANS on MnSi with helix propagation direction initially perpendicualr to the applied magnetic field. This would determine whether the helix reorientation parallel to an applied magnetic field in MnSi is a first order 'flip' for helix perpendicular to the magnetic field as reported recently by Lebech (1992) in cubic FeGe. Another important experiment to be performed is SANS on FeGe close to the transition temperature in an applied magnetic field, to investigate whether a phase comparable to 'Phase A' in MnSi exists. If these phenomena were observed it would extend further the similarity of the behaviour of the helical spin density waves of MnSi and FeGe in an applied magnetic field. This generality may extend to all related materials. An anomalous region in the magnetic phase diagram of (Fe,Co)Si identical to that of 'Phase A' in MnSi has been reported by Ishimoto (1990).

Further investigation into the magnetic properties of other materials with cubic B_{20} crystal structure is also encouraged with emphasis on the reasons for range of magnetic behaviour as well as range of transition temperatures and wavelength for those supporting helical spin density waves.

It is evident from this thesis that there are many similarities between MnSi and cubic FeGe. The magnetisation of MnSi, both above the transition temperature and below in magnetic fields above which the 'knee' in the magnetisation occurs, is well described by the model of Lonzarich and Taillefer (1985) (see for example Taillefer (1986a)). Consequently, I recommend the growth of a larger crystal of cubic FeGe to enable investigation as to whether the magnetisation of cubic FeGe can also be decribed by the same model. This would also enable further study of the critical scattering from cubic FeGe.

9.1 References

Bak P. and Jensen M. (1980), J. Phys. C**13**, L881-885.
Ishikawa Y. *et al.* (1976), Solid State Comm. **19**, 525.
Ishikawa Y. *et al.* (1984), J. Phys. Soc. Jpn **53**, 2726-2733.
Ishimoto K. *et al.* (1990), J. Magn. Magn. Mat. **90-91**, 163-165.
Lebech B. *et al.* (1989), J. Phys.: Condensed Matter **1**, 6105-6102.
Lebech B. (1992), presented at symposium on *Recent Progress in Material Physics*, ——Osaka, Japan. To be published at *Recent Advances in Magnetism of Transition ——Metal Compounds'*, World Scientific Publishing Company.
Lonzarich G. and Taillefer (1985), J. Phys. C. **18**, 4339.
Plumer M.L. and Walker M.B. (1981), J. Phys. C. **14**, 4689-4699.
Plumer M.L. (1990), J. Phys.:Condensed Matter **2**, 7503-7510.
Taillefer L. (1986a), Ph.D. Thesis, University of Cambridge.

Appendix A
Programs Written to Automate the Durham VSM

This appendix consists of the computer programs (fully annotated) written to automate the Durham Vibrating Sample Magnetometer. It can be broadly split into three sections:

1. User manual for the Durham VSM.
2. Control programs written for the Durham VSM.
3. Constituent modules written by Dr. D. Lambrick.

Introduction

The Vibrating Sample Magnetometer being used was designed by Dr. S.R.Hoon and built by S.M.Willcock in 1984. A sample is placed in a static magnetic field and vibrated relative to a series of pick-up coils. The voltage induced is then compared to that produced by a sample of known magnetisation and thus the actual magnetisation is obtained.

Equipment used:

1. Computer (enabling automatic data collection.)

2. KSM power supply and control panel.

3. Minicam crate together with IEEE board, A-D board and GPOB.

4. EGandG 5206 two phase lockin analyser.

2. Fluke.

Programs available in this package and summary of what they do!

1. VSMTIME: Measures the in-phase signal from the pick-up coils after a given time increment. It can be used to see if a particular temperature has stabilized, decay of magnetisation or stability of the pick-up coils.

2. VSMTEMP: Measures the in-phase signal from the pick-up coils and INCREASING temperature as displayed on the fluke. The field should be set and temperature controller connected to the fluke (however any temperature sensor can be used as long as output is on the fluke.)

3. VSMTMPD: As above but with decreasing temperature.

4. VSMCONT: A control program for the VSM allowing manual field alteration before recording both field and induced voltage. Any power supply can be used.

5. VSMRUN: Complete control program allowing a full hysterisis curve to be recorded.

Displaying the Output.

Output can be displayed using the MATLAB maths package which requires a computer with a second coprocessor. Output data files are written in Matlab format with the first element being the number of actual data points recorded. Data starts at row four and there are four columns in each matrix. Columns are field, error on field, voltage, error on voltage for programs 4 and 5.Temperature, 0 , voltage, 0 for programs 2 and 3 and time, 0, voltage, 0 for program 1. Matlab programs have been written for each corresponding control program.

1. TIMPLT.M: plots time vs induced voltage.

2. TEMPLT.M: plots temperature vs induced voltage.

3. TEMPLT.M.

4 and 5. VLTPLT.M: after subtracting a residual, plots field vs induced voltage.

4and 5. MAGPLT.M: after subtracting a residual, plots magnetisation vs induced voltage.

FLUKE 8860a digital multimeter

The computer reads the display on the fluke. It is used in programs VSMCONT,VSMRUN,VSMTEMP and VSMTMPD displaying either field or temperature. The fluke may be used as a resistance meter so can be used with other temperature sensors eg RhFe resistor, to monitor the temperature together with computer.

IEEE address 16

This is set in PSD5206.pas in the routine from line 35 down.

LOCKIN AMPLIFIER

An EGandG 5206 lock-in amplifier is used. The computer reads the sensitivity ofit each time before reading channel 1 display and reads the time-constant at the start of the program.

The lock-in is to be set up by the operator. Firstly, to perform a device clear SELECT and SENSITIVITY should be depressed at the same time. It should then be PHASED on a large signal such as a nickel crystal and is done using the autofunctions with SELECTED on SET and then the RUNCLEAR button pressed. The phase should be recorded and compared to previous values as it's value should not change significantly between runs. For calibration purposes the signal produced by a sample of known magnetisation should be recorded eg a nickel crystal. This should be done in a field which saturates the magnetisation and in both positive and negative fields.

This process should be repeated at the start and end of the run and averaged incase the sensitivity of the VSM coils varied.

The lockin can be set-up as required by the operator but a typical set-up is to have NORMAL and LOW set as modes. There is no internal frequency and the external one is set on F. The phase is inserted i.e. the value obtained using the nickel. Typical time constants used are either 300ms or 1s. The sensitivity can be changed manually during the run or the AUTORANGE function used and to isolate all the keys, the remote button can be used.

The phase should not be alterred during a run nor the time constant!

IEEE address 10.

This is set in the program PSD5206.PAS from line 35 down!

Power Supply

A KSM (stabilised power supply type SCT) is used together with a control panel designed by SMT, BKT, DBL and Electronics workshop. The panel was then built by Chris Mullaney of EWS in Feb '91.

The manual box is self explanatory:- depressing a particular key results in that operation. The disable button overrides everything and the enable light must be OFF before logic is reversed.

The computer is linked via a minicam unit with particular lines performing corresponding tasks as above. An A-D board reads the logic state while the opto-isolated lines of a GPOB set lines low and high to operations ON and OFF. The minicam cards should NOT be earthed as accidental earting of the magnet coils will result in the driving current passing through the lockin, minicam and computer!!

When computer controlled, setting a line LOW results in the operation.

When the power supply is switched on, the control panel is switched on under manual control. This should not be switched to computer control until the computer program gives the necessary prompt.

The rate at which the field ramps is set by two oscillator frequencies, one each for both manual rate and computer rate which can be alterred seperately. However the computer program has been written with a particular frequency in mind and if the oscillator period is changed then the magnet must be recallobrated using the program CALIBR.PAS to obtain the tesla per second rate for the magnet.

MINICAM UNIT

A Bede minicam crate is used together with IEEE board, GPOP and A-D. The GPOP is used to set lines low or high thus operating the control panel as designed by EWS, and the A-D reads the logic state! The minicam crate must be turned OFF before removing any of the cards.

IEEE address of the minicam crate is 6. This is set in PSD5206.pas in the routine from line 35 down.

A-D board address 1. This is set as a constant at the beginning of the main control program.

GPOP (opto-isolated ports) address 41. Again set at the start of the main control program.

Process field-up, GPOP line 13, Input line 2 to supply,B sends line low

Process field-down, GPOP line 12, Input line 1 to supply,A sends line low

Process disable, GPOP line 14, Input line 3 to supply,D sends line low

Process reverse, GPOP line 15, input line 4 to supply,H sends line low

Process logic read, A-D board

Lines 30-33 of GPOP are common and go to line 6 of the supply. A line is then taken to give the A-D board a reference.

SETTING UP

Before starting a run, the VSM has to be set-up! Firstly the head should be elevated off the table by inflating the tyre! The nickel crystal should then be put on the rod in a field and set vibrating. The height of the rod should be adjusted (by inflating the tyre) until the signal obtained is a maximum. The position of the rod moving parallel to the field should be changed so as to maximise the signal and finally position of the rod perpendicular to the field alterred to minimise the induced voltage.

The gaussmeter should the be zeroed and junction of the thermocouple put in liquid nitrogen if temperature is to be monitored.

The lockin should then be phased using the nickel, recording phase and magnetisation in a saturating field.

When switching the powersupply and minicam on, check the control board is on manual in case it was switched off while under computer control.

VSMTEMP,VSMTMPD

This program measures the induced voltage in the pick-up coils and INcreasing/DEcreasing temperature which is displayed on the fluke. The field should be set and temperature controller connected to the fluke (however any temperature sensor can be used as long as output is displayed on the fluke.)

Data collection commences when the program is started. The input conditions required are the FINAL TEMPERATURE which is a real and the NUMBER of REQUIRED DATA POINTS which is an integer.

It is important to remember that the temperature sensor is NOT attached to the sample but a Be-Cu block at the bottom of the cryostat! Thus there will be a phase lag between voltage and temperature.

The data is in MATLAB format, ready for use with the package. It is a matrix with data starting on row 4 with format TEMPERATURE, 0, VOLTAGE, 0 and the program TEMPLT.M has been written to display the data. /end

VSMTIME

This program measures the signal from channel one of the lockin after a given time increment. It acn thus be used to see when the signal has stabilized perhaps because an equilibrium temperature has been reached, show the decay of magnetisation or stability of the pick-up coils.

The input data required is the time interval between points and the number of required points. The maximum time between points is 65s and both inputs are required as integers.

It is important to consider the time constant used with relation to the time between points as only one measurement is made per time interval.

The data is saved in MATLAB format for use with the package. This is a matrix with data starting at row 4, the format being TIME, 0, INDUCED VOLTAGE, 0. The TIME files have extension .TIM and the matlab program TIMPLT.M has been written to display the data. The real time display is more to give a feel for the data and show if anything is wrong!

VSMRUN

This program is the complete control program allowing a full hysterisis curve to be recorded. The program allows for three field regions where the density of data points can be varied. These are input as real numbers with the maximum field being 1T and the minimum field being greater then the remnant field. The computer then requires input of the number of data points in each region which in turn defines the fields to be set- these are input as integers. Finally it requires the number of repeated measurements at each point and the delay between each in terms of number of time constants- both again input as integers.

The system has numerous limitations which must be pointed out. Firstly, between ENABLE, positive logic and ENABLE, negative logic there is a region of approximately 200 gauss which is unobtainable. If this region is required it is suggested that the smaller power supply is used together with VSMCONT.

The system is very slow because of the long settle time of the power supply. A particular field is set by dividing the required field increment by 2 as the field is approached. If another power supply were used, the program could be speeded up by reducing the delay lenghts in procedure SET FIELD TO. Also the tesla per second calibrations used in the procedure SET LINE TIME are for one oscillator speed only, and if this is changed for computer control then the magnet should be recallobrated using CALIBR.(This raises a line for some length of time as set in the program and measures the field change because of this. A data point is taken by pressing any key except P which stops the program.) The one danger is that the program overshoots while setting a particular field, but if this occurs the program is stopped after saving the data!

Above 0.1T the program sets the field to within 1 percent of the new field. Below 0.1T the field is set to within 10 percent of the value and around 50 gauss to within 10 gauss. These conditions can be alterred in the program and are included in the procedure SET FIELD.

The enable light can't always be set easily and as there isn't a flag from this to

inform the computer then this must be set manually- resulting in the program not been fully automated. The computer actually reverses the logic when the enable light is OFF and prompts when ne. EWS hope to fit a the ENABLE light requires switching ON. EWS intend to fit a flag to the panel soon after which the program can be fully automated.

Finally, when the logic has been switched to positive the computer requires integer input of the number of field regions required before completion (1-3)! Thus when the program is complete, there is still current flowing through the magnet.

The output is in MATLAB format ready for use with the package. This is a matrix with data starting on row 4 with format FIELD, ERROR ON FIELD, VOLTAGE, ERROR on VOLTAGE. Matlab program VLTPLT.M also uses a residual run which it subtracts before displaying the data. MAGPLT.M uses a residual but then displays magnetisation vs field.

VSMCONT

This program for the VSM allows manual field alterration before recording both field and induced voltage. Any power supply can be used!

The input data required is the NUMBER of MEASUREMENTS to be made at each field and the number of TIME CONSTANTS delay between each one. Both should be input as integers! The computer reads the time constant at the start of the program so this should not be changed during the run however the sensitivity is read before channel 1 is read on each ocassion.

The field should be allowed to settle before data is taken, which commences when key P is pressed and the program terminated when key Z is pressed.

The output file is in MATLAB format to be used with the package and has an extension .VDT. This is a matrix with data beginning at row 4 and having format FIELD, ERROR on FIELD, VOLTAGE, ERROR on VOLTAGE. The Matlab program VLTPLT.M is written and requires a residual which is subtracted from the raw data and displays voltage vs field. The program MAGPLT.M is similar but displays magnetisation vs field.

ERROR MESSAGES

Within the control program there is an error procedure which can be called upon at any point in the program depending on whether a particular condition has been satisfied. Each error has a code, enabling the cause to be located and other error conditions included in the program. teh errors are:

1. The max. field input was greater than 1T. To get round this the condition can be alterred in the program if the power supply can produce such a field.

2. The minimum field step is less than 10 gauss. This can again be alterred and is dependant on the power supply used.

3. The number of points in the complete curve exceeds 600, which is the size of the data array. This condition can be alterred if the array is made bigger.

4. The field ranges have been input in the wrong order.

5. While trying to locate a particular field, the computer has exceeded the value! The point separations may be too small or the program may be trying to locate the field too precisely in which case the constant 'near enough' can be alterred in the procedure 'set field to'.

6. The remnant field is greater than the first field region so the first region must be lowered or magnet demagnetized.

It is intended that as the program is used and more errors become evident, that these be incorparated within the program.

```
(*************************************************************************)
(*                                                                       *)
(*   Program to find the magnetic field:current calibration for the      *)
(*   KSM power supply and large electromagnet for use in the VSM         *)
(*   program controlling the power supply.                               *)
(*   C.I.Gregory  15/06/91                                               *)
(*                                                                       *)
(*************************************************************************)


program field_pulse_calibration;

{$N+}

uses vsmglob,psd5206,fluke,crt,graph,dos,icccom,minicam;


var
{Temporarily stores voltage from the gauss meter}
fld_vlt                         :  double;
{Data stored in MATLAB format i.e. 4 column matrix}
data                            :  array[1..500,1..4] of real;
ndps,i                          :  integer;
{The time unit the field_up line is held low}
time                            :  word;
pp,testf                        :  char;
const
{Values sent to the minicam GPOP board to perform various tasks}
gpop_address            =       '41';{GPOP address in minicam crate}
high                    =       '0';{Sets all lines high}
field_up                =       'B';{Lowers the field_up line}
disable                 =       'D';{Lowers line to disable the control panel}

procedure get_data_point;
{Records voltage from the gaussmeter ten times, then calculates the average
and records this and compound time the field_up line has been low}
var
i           :integer;
fluke_val   :double;

begin
 fld_vlt:=0.0;
 for j:=1 to 10 do
 begin
 delay(1000);
 fluke_val:=read_fluke;
 fld_vlt:=fld_vlt+fluke_val;
 end;
 fld_vlt:=fld_vlt/10;
 data[i,1]:=fld_vlt;
 data[i,2]:=0.0;
 data[i,3]:=time*ndps;
 data[i,4]:=0.0;
end;


procedure set_line(gpop_address,state :str5;time    : word);
{procedure to set a particular line of the GPOP low for a given time and
the return all lines high}
var dumstr          :  str255;

begin
 dumstr:=dal(gpop_address,state);
 delay(time);
 dumstr:=dal(gpop_address,high);
end;



procedure save_data(ndps :  integer);
{Stores data in a file in MATLAB format}
var
i                       :   integer;
filnam                  :      str8;
filnamext               :     str12;
f                       :      text;

begin
writeln('-------------------------------------------------------');
writeln('    DATA STORAGE');
writeln('-------------------------------------------------------');
write('Name of file in which to store data (max 8 characters):');
readln(filnam);
filnamext:=filnam+'.vdt';
writeln('Storing data in ',filnamext);
assign(f,filnamext);
rewrite(f);
data[1,3]:=0.0;data[1,4]:=0.0;
data[2,1]:=0.0;data[2,2]:=0.0;data[2,3]:=0.0;data[2,4]:=0.0;
data[3,1]:=0.0;data[3,2]:=0.0;data[3,3]:=0.0;data[3,4]:=0.0;
for i:=1 to ndps-3 do
begin
  writeln(f,data[i,1]:12,' ',data[i,2]:11,' ',data[i,3]:12,' ',data[i,4]:11);
end;
close(f);
end;

{START OF MAIN PROGRAM}
begin

init_ieee;
set_line(gpop_address,high,1000);
{After setting all lines of GPOP high, the control panel is switched to
computer control}
writeln('Switch to computer control');
delay(2000);

repeat
init_fluke;
delay(500);
writeln('Did flke display all zeroes (y/n)?');readln(testf);
until testf='y';

ndps:=0;i:=1;time:=5000;{Time unit which field_up_line held low (5s)}

repeat
 get_data_point;
 ndps:=ndps+1;
 i:=i+1;
 set_line(gpop_address,field_up,time);
```

```
 delay(11000);
 pp:=readkey;
until pp='p';{Input character 'p' terminates the program}

data[1,1]:=ndps;
save_data(ndps);
end.
```

```
(*************************************************************************)
(*                                                                       *)
(*  Program to read 5206 lockin and fluke 8860A for VSM runs             *)
(*  with manual field alteration                                         *)
(*  by C.I.Gregory June'91                                               *)
(*                                                                       *)
(*************************************************************************)

{For annotation see VSMRUN.PAS which includes automatic field control}

program vsmtemp;

{$D+,L+}
{$N+}

uses vsmglob,psd5206,fluke,crt,graph,dos;

var
statusactive,
graphmodeset            : boolean;
fld_vlt                 : double;
mag_vlt,scfact,
xscale,yscale,
sderror_mag_vlt,
sderror_fld_vlt,
sensitivity,
old_sensitivity,
gauss_range_gauss,
gauss_range_tesla       : real;
data                    : array[1..200,1..4] of real;
i,graphmode,bdeal,flke,
ndps,xcen,p,m,flag4     : integer;
scX,scY,ycen,xborder1,
num_time_const,
num_measurements        : integer;
testf,pp                : char;
yt_str                  : str4;
mn_str,dy_str           : str2;
date_str                : str8;
t_const                 : longint;

procedure over_load;
var
   r   :integer;

begin
r:=0;
repeat
delay(1000);
r:=r+1;
until (lockin_ok);
if r > 1 then delay(t_const*6);
end;

procedure not_ready;

begin
repeat
delay(1000);
until lockin_ok;
end;

procedure get_data_point;
var
n                       :integer;
sumf,sumC1              :double;
sderror_fluke,sderror_Ch1,
var_fluke,var_Ch1       :real;
fluke,Ch1               :array[1..40] of real;

begin
 if statusactive then begin
       if autorange_set then not_ready
                        else over_load;
       sumf:=0;sumC1:=0;var_fluke:=0;var_Ch1:=0;
       for n:=1 to num_measurements do
          begin
            fluke[n]:=read_fluke*gauss_range_tesla;
            read_Ch1(Ch1[n]);
            sumf:=sumf+fluke[n];
            sumC1:=sumC1+Ch1[n];
            delay(t_const*num_time_const);
          end;
          fld_vlt:=sumf/num_measurements;
          mag_vlt:=sumC1/num_measurements;
          for n:=1 to num_measurements do
            begin
              var_fluke:=(fld_vlt-fluke[n])*(fld_vlt-fluke[n])+var_fluke;
              var_Ch1:=(mag_vlt-Ch1[n])*(mag_vlt-Ch1[n])+var_Ch1;
            end;
          sderror_fld_vlt:=sqr(var_fluke/(num_measurements-1))/sqr(num_measurements)
          sderror_mag_vlt:=sqr(var_Ch1/(num_measurements-1))/sqr(num_measurements);
          end
                else begin
                       fld_vlt:=fld_vlt-1.1;
                       mag_vlt:=0.9e-2*fld_vlt;
                     end;
end;

procedure save_data(ndpts : integer);
var
   i,nc                         : integer;
   year,month,day,daywk         : word;
   date_num                     : longint;
   f                            : text;
   filnam                       : str8;
   tm_str                       : str2;
   filnamext                    : str12;
   sammass,refmass,vref,fieldup : real;

begin
 restorecrtmode;
 writeln('-------------------------------------------------------------------');
 writeln('                        DATA STORAGE');
 writeln('-------------------------------------------------------------------');
 writeln;
 write('Mass of sample (g) = '); readln(sammass);
 write('Mass of ref (g) = '); readln(refmass);
 write('Ref voltage (V) = '); readln(vref);
 write('Field at which ref measured (T) = '); readln(fieldup);
```

```
 write('Name of file in which to store data ( max 8 chars):');
 readln(filnam);
 getdate(year,month,day,daywk);
 str(year,yr_str);
 str(month,mn_str);if month<10 then mn_str:='0'+copy(mn_str,1,1);
 str(day,dy_str);  if   day<10 then dy_str:='0'+copy(dy_str,1,1);
 tm_str:=copy(yr_str,3,2);
 date_str:=tm_str+mn_str+dy_str;
 val(date_str,date_num,nc);
 writeln('Date: ',date_num);
 filnamext:=filnam+'.vdt';
 writeln('Storing data in ',filnamext);
 assign(f,filnamext);
 rewrite(f);
 data[1,2]:=0.0; data[1,3]:=date_num; data[1,4]:=0.0;
 data[2,3]:=0.0; data[2,4]:=0.0; data[3,2]:=0.0; data[3,4]:=0.0;
 data[2,1]:=sammass; data[2,2]:=refmass;
 data[3,1]:=vref; data[3,3]:=fieldup;
 for i:=1 to ndps+3 do
 begin
   writeln(f,data[i,1]:12,' ',data[i,2]:10,' ',data[i,3]:12,' ',data[i,4]:10);
 end;
 close(f);
end;

procedure in_grph;
var
 graphdriver : integer;
 errorcode   : integer;

begin
 if (not graphmodeset) then begin
 graphmodeset:=true;
 graphdriver:=detect;
 initgraph(graphdriver,graphmode,'C:\tp5');
 errorcode:=graphresult;
 if errorcode <> grOK then
 begin
   writeln('Graphics error : ',grapherrormsg(errorcode));
   writeln('..program aborted...');
   halt(1);
 end;
 end
 else
 setgraphmode(graphmode);

 rectangle(0,0,getmaxX,getmaxY);
 setlinestyle(solidln,0,normwidth);
 restoreCRTMode;
end;

procedure set_scrn_plt(xread1,yread1,xsf : real; xaxis,yaxis : str10);
var
     xborderr,ybordert,yborderb,
     xlngth,yht,i,ii             : integer;
     xrmax                       : real;
     xlabel                      : str10;

begin
 in_grph;
 setgraphmode(graphmode);
 xborder1:=round(getmaxx/10);
 xborderr:=round(getmaxx-xborder1);
 ybordert:=round(getmaxy/10);
 yborderb:=round(getmaxy-ybordert);
 yht:=yborderb-ybordert;
 yscale:=yht/(2*yread1);
 xlngth:=xborderr-xborder1;
 if frac(xread1)<=1.5 then xrmax:=int(xread1)+0.5
                      else xrmax:=int(xread1)+1.0;
 xscale:=xlngth/(2*xrmax);
 ycen:=ybordert+(yht div 2);
 xcen:=xborder1+(xlngth div 2);
 rectangle(xborder1 div 2,ybordert div 2,xborderr+(xborder1 div 2),
                                         yborderb+(ybordert div 2));
 moveto(xcen,ybordert); lineto(xcen,yborderb);
 moveto(xborder1,ycen); lineto(xborderr,ycen);
 ii:=round(int(2*xrmax));
 settextstyle(smallfont,0,4);
 settextjustify(centertext,centertext);
 for i:=-ii to ii do
 begin
  moveto(round(i*0.5*xscale+xcen),ycen);
  lineto(round(i*0.5*xscale+xcen),ycen-(ycen div 25));
  moveto(round(i*0.5*xscale+xcen),ycen+(ycen div 25));
  str(i*0.5*xsf:3:1,xlabel);
  xlabel:=xlabel;
  outtext(xlabel);
 end;
 moveto(xborderr-(xborderr div 15),ycen+(ycen div 10));
 outtext(xaxis);
 moveto(xcen-(xcen div 10),ybordert+(yht div 10));
 settextstyle(smallfont,vertdir,4);
 outtext(yaxis);
 if flag4=0 then
      begin
      get_data_point;
      Moveto(round(xcen-fld_vlt*xscale),round(ycen-yscale*mag_vlt));
      end;
 if flag4=1 then
      begin
      Moveto(round(xcen+data[4,1]*xscale),round(ycen-yscale*data[4,3]));
      end;
 setcolor(4);
end;

procedure redraw;

begin
 set_scrn_plt(gauss_range_tesla*1.2,(old_sensitivity*1.2),1,'Field T','Magn (V)');
 for p:=4 to (ndps+2) do
 begin
 lineto(round(xcen+data[p,1]*xscale),round(ycen-yscale*data[p,3]));
 end;
end;

procedure plt_point(i:integer);

begin
   data[ndps+3,1]:=fld_vlt;
```

```
   data[ndps+3,2]:=sderror_fld_vlt;
   data[ndps+3,3]:=mag_vlt;
   data[ndps+3,4]:=sderror_mag_vlt;
   lineto(round(xcen+fld_vlt*xscale),round(ycen-yscale*mag_vlt));
   {writeln(data[i,1],' ',data[i,3]);}
 end;

{START OF MAIN PROGRAM}
begin
 graphmodeset:=false;
 statusactive:=true;
 if not statusactive then begin
                            fld_vlt:=-1.20;
                            mag_vlt:=1e-2;
                          end;
 if statusactive then
 begin
 writeln('-----------------------------------------------------');
 writeln(' PROGRAM TO OPERATE THE VSM (manual field alteration)');
 writeln('-----------------------------------------------------');
 writeln(' The program operates by reading the fluke and the');
 writeln('lock-in after the field has been alterred manually');
 writeln('When a data point is required i.e. the field is set,');
 writeln('by pressing key "p" this is done by the computer.');
 writeln('Key "z" completes the program.');
 writeln('Insert the number of points required at each field');
 writeln('must be greater than 1');
 readln(num_measurements);
 writeln('Insert number of time constant delay between points:-');
 readln(num_time_const);
 writeln('Insert gauss meter range (gauss):');
 readln(gauss_range_gauss);
 gauss_range_tesla:=gauss_range_gauss/1e4;
 init_ieee;
 repeat
   init_fluke;
   delay(150);
   writeln('Did the fluke display all zeroes?(y/n)');readln(testf);
   until testf='y';
 end;
 delay(100);
 get_time_const(t_const);
 delay(2000);
 get_sensitivity(sensitivity);
 old_sensitivity:=sensitivity;
 delay(200);
 flag4:=0;
 set_scrn_plt(gauss_range_tesla*1.2,(old_sensitivity*1.2),1,'Field (T)','Magn (V)');
 ndps:=0;
 repeat
   delay(500);
   get_data_point;
   ndps:=ndps+1;
   get_sensitivity(sensitivity);
   if (sensitivity > old_sensitivity) then
     begin
     old_sensitivity:=sensitivity;
     redraw;
     end;
   plt_point(ndps);
   sound(220); delay(150); nosound;
   repeat
   delay(40);
   pp:=readkey;
   until (pp='p') or (pp='z');
 until pp='z';

 data[1,1]:=ndps;
 repeat until keypressed;
 if statusactive then save_data(ndps);
end.
```

```
(*************************************************************************)
(*                                                                       *)
(*   Program for automatic data collection using the Durham VSM          *)
(*   C.I.Gregory June '91                                                *)
(*                                                                       *)
(*************************************************************************)

program vsmrun;

{$D+,L+}
{$N+}

uses vsmglob,minicam,ieee,icccom,psd5206,fluke,crt,graph,dos;

const
{constants which are sent to the GPOP to lower particular lines}
gpop_address       =  '41';{address of GPOP in minicam crate}
high               =   '0';{sets all lines high}
field_up           =   'b';{sets field_up line low}
field_down         =   'a';
disable            =   'd';
reverse            =   'h';

var
graphmodeset                :  boolean;
time                        :  word;
date_str                    :  str8;
state                       :  str5;
yr_str                      :  str4;
mn_str,dy_str               :  str2;
testf,pp                    :  str1;
{stores data in an array, max number of points set here (600)}
data                        :array[1..600,1..4] of real;
{stores field regions}
field_region                :array[0..3] of real;
{stores number of data points in each section}
number_points               :array[1..3] of integer;
{stores field separation between points in each region}
field_separation            :array[1..3] of real;
{flag-used to check if procedure remnant_field should be used
flag2-show logic has reversed and to get out of do loop
flag3-show passed through zero field without logic reversal ie -ve remnance
flag4-show procedure redraw is being used}
logic,i,flag,ndps,y,z,
flag2,n,increase,flag3,
total_number_points,a,
graphmode,bdeal,flke,
xcen,p,m,scX,scY,ycen,
xborder1,num_time_const,
num_measurements,flag4      : integer;
t_const                     : longint;
current_field,field,
fld_vlt                     : double;
next_field,mag_vlt,scfact,
xscale,yscale,sderror_mag_vlt,
sderror_fld_vlt,sensitivity,
old_sensitivity,
gauss_range_gauss,
gauss_range_tesla            :  real;
```

```
procedure set_line(gpop_address,state  : str5;time  :word);
{to set a particular line of GPOP high for a given time before
setting all low}
var
dumstr       :str255;

begin
 dumstr:=dal(gpop_address,state);
 delay(time);
 dumstr:=dal(gpop_address,high);
end;

procedure logic_read;
{to read A-D, reading the returned string upto chr(13) or (59)
which gives logic state}
var
dumstr,dummstr      :str255;
x                   :real;
code,p,q            :integer;

begin
 dumstr:=adl('1');
 p:=0;dummstr:='';
 repeat
   p:=p+1;
 until (dumstr[p]=chr(13)) or (dumstr[p]=chr(59));
 for q:=1 to (p-1) do
 begin
  dummstr:=dummstr+dumstr[q];
 end;
 val(dummstr,x,code);
 if x > 1000 then logic:=1 else logic:=-1;
end;

procedure reverse_logic;
{to read logic and attempt to reverse until this is successful}
var
old_logic:integer;

begin
 old_logic:=logic;
 repeat
   set_line(gpop_address,reverse,1000);
  delay(1500);
  logic_read;
 until logic<>old_logic;
end;

procedure try_reverse_logic;
{to attempt to reverse logic once only}

begin
 set_line(gpop_address,reverse,1000);
 delay(1500);
end;

procedure save_data(ndps : integer);
{to save data in MATLAB format in a file whose name is input}
var i,nc : integer;
   year,month,day,daywk : word;
```

```
    date_num : longint;
    f        : text;
    filnam : str8;
    tm_str     : str2;
    filnamext : str12;
    sammass,refmass,vref,fieldup : real;

begin
 restorecrtmode;
 writeln('-------------------------------------------------------------------');
 writeln('                        DATA STORAGE');
 writeln('-------------------------------------------------------------------');
 writeln;
 write('Mass of sample (g) = '); readln(sammass);
 write('Mass of ref (g) = '); readln(refmass);
 write('Ref voltage (V) = '); readln(vref);
 write('Field at which ref measured (T) = '); readln(fieldup);
 write('Name of file in which to store data ( max 8 chars):');
 readln(filnam);
 getdate(year,month,day,daywk);
 str(year,yr_str);
 str(month,mn_str);if month<10 then mn_str:='0'+copy(mn_str,1,1);
 str(day,dy_str);  if   day<10 then dy_str:='0'+copy(dy_str,1,1);
 tm_str:=copy(yr_str,3,2);
 date_str:=tm_str+mn_str+dy_str;
 val(date_str,date_num,nc);
 writeln('Date: ',date_num);
 filnamext:=filnam+'.vdt';
 writeln('Storing data in ',filnamext);
 assign(f,filnamext);
 rewrite(f);
 {first three lines of matrix:[1,1] number pts,[2,1] sample mass
 [2,2] reference mass,[3,1]induced voltage from reference,[3,3] field
 to obtain reference signal}
 data[1,2]:=0.0; data[1,3]:=date_num; data[1,4]:=0.0;
 data[2,3]:=0.0; data[2,4]:=0.0; data[3,2]:=0.0; data[3,4]:=0.0;
 data[2,1]:=sammass; data[2,2]:=refmass;
 data[3,1]:=vref; data[3,3]:=fieldup;
 for i:=1 to ndps+3 do
 {saves all data in matrix format
 field, error on field, voltage, error on voltage}
 begin
   writeln(f,data[i,1]:12,' ',data[i,2]:10,' ',data[i,3]:12,' ',data[i,4]:10);
 end;
 close(f);
end;

procedure error(error_number   :integer);
{to set all lines high ie OFF,save data taken then print error code
showing cause}

begin
 set_line(gpop_address,high,1000);
 if ndps > 1 then save_data(ndps) else restorecrtmode;
 writeln('The program has been alterred as an error has ocurred, error code');
 writeln(error_number);
 writeln('For information about this see the instruction manual');
 halt(0);
end;
```

```
procedure remnant_field(var p :integer);
{to read remnant field, calculate number points missedduo to this
and calculate next field in region to be measured returning the
integer to be used in the do loop}
var
rmnt_field      :double;
pts_missed      :real;

begin
rmnt_field:=read_fluke*gauss_range_tesla;
if abs(rmnt_field) > abs(field_region[1]) then error(6);
pts_missed:=abs(int(rmnt_field/field_separation[1]))+1;
if logic/rmnt_field < 0.0 then
                    begin
                    p:=-1*round(pts_missed)+1;
                    current_field:=pts_missed*field_separation[1]*(abs(rmnt_field)/r
                    end;
if logic/rmnt_field > 0.0 then
                    begin
                    p:=round(pts_missed);
                    current_field:=(pts_missed-1)*field_separation[1]*(abs(rmnt_fiel
                    end;
if p=0 then
      begin
        p:=1;
        current_field:=0.0;
      end;

next_field:=current_field-logic*field_separation[1];
flag:=1
end;

procedure raise_line_time(field_incr  :real;field :double);
{calculates the time required to raise a line to set a particular
field}
var
tesla_second      :real;

begin
 if abs(field)<=0.4 then tesla_second:=8.0e-4;
 if abs(field)>=0.7 then tesla_second:=4.0e-4;
 if (abs(field)>0.4) and (abs(field)<0.7) then tesla_second:=5.5e-4;
 time:=round((field_incr/tesla_second)*1000);
 if time>65000 then time:=65000;
 if time<1 then time:=1;
end;

procedure in_grph;
{Checks for and sets up graph mode}
var
 graphdriver : integer;
 errorcode   : integer;

begin
 if (not graphmodeset) then begin
 graphmodeset:=true;
 graphdriver:=detect;
 InitGraph(graphdriver,graphmode,'C:\tp5');
 errorcode:=graphresult;
 if errorcode <> grOK then
```

```
 begin
   writeln('Graphics error : ',grapherrormsg(errorcode));
   writeln('..program aborted...');
   halt(1);
 end;
 end
 else
 setgraphmode(graphmode);

 rectangle(0,0,getmaxX,getmaxY);
 setlinestyle(solidln,0,normwidth);
 restoreCRTMode;
end;

procedure over_load;
{if manually setting sensitivity, to check for overload and wait six
time constants after it is cleared}
var
   r   :integer;

begin
r:=0;
repeat
delay(1000);
r:=r+1;
until (lockin_ok);
if r > 1 then delay(t_const*6);
end;

procedure not_ready;
{if autoranging, waits until lockin is in state to transfer data}

begin
repeat
delay(1000);
until lockin_ok;
end;

procedure get_data_point;
{reads fluke and lockin when ready numerous times to get data
and error on data}
var
n                              :integer;
sumf,sumCl                     :double;
sderror_fluke,sderror_Chl,
var_fluke,var_Chl              :real;
fluke,Chl                      :array[1..40] of real;

begin
 if statusactive then begin
        if autorange_set then not_ready
                         else over_load;
        sumf:=0;sumCl:=0;var_fluke:=0;var_Chl:=0;
        for n:=1 to num_measurements do
           begin
             fluke[n]:=read_fluke*gauss_range_tesla;
             read_Chl(Chl[n]);
             sumf:=sumf+fluke[n];
             sumCl:=sumCl+Chl[n];
             delay(t_const*num_time_const);
             end;
             fld_vlt:=sumf/num_measurements;
             mag_vlt:=sumCl/num_measurements;
             for n:=1 to num_measurements do
               begin
                 var_fluke:=(fld_vlt-fluke[n])*(fld_vlt-fluke[n])+var_fluke;
                 var_Chl:=(mag_vlt-Chl[n])*(mag_vlt-Chl[n])+var_Chl;
               end;
             sderror_fld_vlt:=sqr(var_fluke/(num_measurements-1))/sqr(num_measurements)
             sderror_mag_vlt:=sqr(var_Chl/(num_measurements-1))/sqr(num_measurements);
             end
                   else begin
                          fld_vlt:=fld_vlt+0.1;
                          mag_vlt:=0.9e-2*fld_vlt;
                        end;
ndps:=ndps+1;
end;


procedure set_scrn_plt(xreadl,yreadl,xsf : real; xaxis,yaxis : str10);
{sets up graph axis, dependant on sensitivity of lockin}
var   xborderr,ybordert,yborderb,
     xlngth,yht,i,ii           : integer;
     xrmax                     : real;
     xlabel                    : str10;

begin
 in_grph;
 setgraphmode(graphmode);
 xborderl:=round(getmaxx/10);
 xborderr:=round(getmaxx-xborderl);
 ybordert:=round(getmaxy/10);
 yborderb:=round(getmaxy-ybordert);
 yht:=yborderb-ybordert;
 yscale:=yht/(2*yreadl);
 xlngth:=xborderr-xborderl;
 if frac(xreadl)<=0.5 then xrmax:=int(xreadl)+0.5
                      else xrmax:=int(xreadl)+1.0;
 xscale:=xlngth/(2*xrmax);
 ycen:=ybordert+(yht div 2);
 xcen:=xborderl+(xlngth div 2);
 rectangle(xborderl div 2,ybordert div 2,xborderr+(xborderl div 2),
                                         yborderb+(ybordert div 2));
 moveto(xcen,ybordert); lineto(xcen,yborderb);
 moveto(xborderl,ycen); lineto(xborderr,ycen);
 ii:=round(int(2*xrmax));
 settextstyle(smallfont,0,4);
 settextjustify(centertext,centertext);
 for i:=-ii to ii do
 begin
  moveto(round(i*0.5*xscale+xcen),ycen);
  lineto(round(i*0.5*xscale+xcen),ycen-(ycen div 25));
  moveto(round(i*0.5*xscale+xcen),ycen+(ycen div 25));
  str(i*0.5*xsf:3:1,xlabel);
  xlabel:=xlabel;
  outtext(xlabel);
 end;
 moveto(xborderr-(xborderr div 15),ycen+(ycen div 10));
 outtext(xaxis);
 moveto(xcen-(xcen div 10),ybordert+(yht div 10));
```

```
 settextstyle(smallfont,vertdir,4);
 outtext(yaxis);
 {if first time setup then gets data point and moves to it on axis}
 if flag4=0 then
 begin
 get_data_point;
 Moveto(round(xcen+fld_vlt*xscale),round(ycen-yscale*mag_vlt));
 end;
 {if using redraw moves to first data point as a reference}
 if flag4=1 then Moveto(round(xcen+data[4,1]*xscale),round(ycen-data[4,3]*yscale));
 setcolor(4);
end;

procedure redraw;
{redraws data on a new axis as sensitivity of lockin increased}

begin
 flag4:=1;
 set_scrn_plt(gauss_range_tesla*1.2,(old_sensitivity*1.2),1,'Field T','Magn (V)');
 for p:=4 to (ndps+2) do
 begin
 lineto(round(xcen+data[p,1]*xscale),round(ycen-yscale*data[p,3]));
 end;
end;


procedure  check_reverse;
{checks if attempt to reverse logic is successful ie enable light OFF,
then alters condition in program to get out of do loops and prompt
user to make sur enable light is on}
var
old_logic      :integer;

begin
 logic_read;
 old_logic:=logic;
 try_reverse_logic;
 logic_read;
 if (old_logic <> logic) and (flag3=0) then
   begin
   z:=1;
   y:=1;flag2:=1;i:=6;increase:=1;flag:=0;
   repeat
       restorecrtmode;
       writeln('Is the enable light on (y/n)?');readln(testf);
       delay(500);
   until testf='y';
   end;
 if (old_logic <> logic) and (flag3=1) then
    begin
       increase:=1;flag:=0;
       repeat
           restorecrtmode;
           writeln('Is the enable light on (y/n)?');readln(testf);
           delay(500);
       until testf='y';
    end;
writeln('after logic check');
redraw;
end;
```

```
procedure set_field_to(new_field  :real);
{to set field to a aparticular value}
var
field_incr,to_go,
near_enough                              :real;
old_field                                :double;

begin
 old_field:=read_fluke*gauss_range_tesla;
 field_incr:=abs(new_field-old_field)/10;
 if field_incr > 0.005 then  {to account for smallest step size-50gauss}
 begin
 {first moves to 60% of value}
  for i:=1 to 6 do
    begin
    field:=field+logic*increase*field_incr;
    raise_line_time(field_incr,field);
    if increase=1 then state:=field_up else state:=field_down;
    set_line(gpop_address,state,time);
    delay(5000);
    field:=read_fluke*gauss_range_tesla;
    if (y=1) and (increase=-1) then check_reverse;
    end;
 end;

if flag2=0 then
begin
 field:=read_fluke*gauss_range_tesla;
 repeat
 {divides field step by two and moves to this field. Repeat until
 within given percent of newfield}
   to_go:=abs(field-new_field);
   field_incr:=to_go/2;
   field:=field+logic*increase*field_incr;
   raise_line_time(field_incr,field);
   if increase=1 then state:=field_up else state:=field_down;
   set_line(gpop_address,state,time);
   delay(10000);
   field:=read_fluke*gauss_range_tesla;
   if (y=1) and (increase=-1) then check_reverse;
   if (increase=1) and ((abs(field))>(abs(new_field)*1.2)) then error(5);
   if (increase=-1) and ((abs(field)*1.2)<(abs(new_field))) and (abs(field) > 0.1) th
   near_enough:=0.01*new_field;{to within 1% of the field}
   if abs(new_field) <= 0.1 then near_enough:=0.1*new_field;
   if abs(new_field)< 0.001 then near_enough:=0.001;
 until ((abs(new_field-field)<=abs(near_enough))) or (flag2=1);
end;

end;


procedure plt_point(ndps:integer);
{stores result in array data then plots new point}
begin
   data[ndps+3,1]:=fld_vlt;
   data[ndps+3,2]:=sderror_fld_vlt;
   data[ndps+3,3]:=mag_vlt;
   data[ndps+3,4]:=sderror_mag_vlt;
   lineto(round(xcen+fld_vlt*xscale),round(ycen-yscale*mag_vlt));
```

```
   {writeln(data[i,1],' ',data[i,3]);}
 end;


{START OF THE MAIN PROGRAM}
begin
graphmodeset:=false;
statusactive:=true;
init_ieee;
{set minicam lines high before switching to computer control}
set_line(gpop_address,high,1000);
writeln('Switch to computer control');
delay(5000);

repeat
init_fluke;
delay(500);
writeln('Did fluke display all zeroes (y/n)?');readln(testf);
until testf='y';
delay(2000);

{check for positive logic}
logic_read;
{if logic<0 then reverse_logic;}

field_region[0]:=0.0;
{input required information}
writeln('Input first field region (Tesla):');readln(field_region[1]);
writeln('Input number of points in this region:');readln(number_points[1]);

writeln('Input second field region:');readln(field_region[2]);
writeln('Input number of points in this region:');readln(number_points[2]);

writeln('Input maximum field:');readln(field_region[3]);
if field_region[3] > 1.0 then error(1);
writeln('Input number of points in this region:');readln(number_points[3]);

writeln('Insert number of points required at each field');
writeln('Must be greater than one!');
readln(num_measurements);

writeln('Insert the number of time constants delay between points:-');
readln(num_time_const);

writeln('Input gauss meter range (gauss)');
readln(gauss_range_gauss);
gauss_range_tesla:=gauss_range_gauss/1e4;

{checking input data}
if (field_region[1]>=field_region[3]) or (field_region[1]>=field_region[2])
or (field_region[2]>=field_region[3]) then error(4);

total_number_points:=0;
for i:=1 to 3 do
begin
field_separation[i]:=(field_region[i]-field_region[i-1])/number_points[i];
if field_separation[i] < 10e-4 then error(2);
total_number_points:=total_number_points+number_points[i];
end;
if (total_number_points*4) > 600 then error(3);

for i:=1 to 3 do
begin
writeln(field_region[i]);
writeln(number_points[i]);
writeln(field_separation[i]);
end;

ndps:=0;flag:=0;flag4:=0;flag3:=0;flag2:=0;increase:=1;testf:='n';

repeat
writeln('Is the enable light on (y/n)?');readln(testf);
delay(500);
until testf='y';

delay(100);
{read lockin for required values}
get_time_const(t_const);
delay(2000);
get_sensitivity(sensitivity);
old_sensitivity:=sensitivity;
delay(200);
set_scrn_plt(gauss_range_tesla*1.2,(old_sensitivity*1.2),1,'Field (T)','Magn (V)');

ndps:=0;

get_data_point;
plt_point(ndps);

{first quadrant of curve}
for y:=1 to 3 do

 begin
 for z:=1 to number_points[y] do
    begin
    {calculates next field to be set}
    next_field:=z*field_separation[y]+field_region[y-1];
    if z=number_points[y] then next_field:=field_region[y];
    if flag=0 then remnant_field(z);
    {sets required field}
    set_field_to(next_field);
    {gets data point}
    get_data_point;
    {check if graph needs redrawing}
    get_sensitivity(sensitivity);
    if (sensitivity > old_sensitivity) then
        begin
        old_sensitivity:=sensitivity;
        redraw;
        end;
     {plots new point}
     plt_point(ndps);
    end;

 end;

increase:=-1;
{second quadrant}

for y:=3 downto 1 do
```

```
 begin
 n:=0;
 for z:=number_points[y] downto 1 do
   begin
   current_field:=field_region[y]-n*field_separation[y];
   next_field:=current_field-field_separation[y];
   set_field_to(next_field);
   get_data_point;
   get_sensitivity(sensitivity);
   if (sensitivity > old_sensitivity) then
        begin
        old_sensitivity:=sensitivity;
        redraw;
        end;
   plt_point(ndps);
   n:=n+1;
   end;

 end;

flag2:=0;testf:='n';flag3:=1;

get_data_point;
plt_point(ndps);
{third quadrant}

for y:=1 to 3 do

 begin
 for z:=1 to number_points[y] do
    begin
    next_field:=-1*z*field_separation[y]-field_region[y-1];
    if z=number_points[y] then next_field:=-1*field_region[y];
    if flag=0 then remnant_field(z);
    set_field_to(next_field);
    get_data_point;
    get_sensitivity(sensitivity);
    if (sensitivity > old_sensitivity) then
         begin
         old_sensitivity:=sensitivity;
         redraw;
         end;
    plt_point(ndps);
    end;

 end;

increase:=-1;flag3:=0;testf:='n';

{fourth quadrant}
get_data_point;

for y:=3 downto 1 do

  begin
  n:=0;
  for z:=number_points[y] downto 1 do
     begin
     next_field:=-1*field_region[y]+(n+1)*field_separation[y];
     set_field_to(next_field);
     get_data_point;
     get_sensitivity(sensitivity);
     if (sensitivity > old_sensitivity) then
        begin
        old_sensitivity:=sensitivity;
        redraw;
        end;
     plt_point(ndps);
     n:=n+1;
     end;
  end;

flag3:=1;flag2:=0;

{repeat as much of first quadrant as required}
restorecrtmode;
writeln('How many field regions do you want the computer to go positive?(1-3)');
readln(a);

redraw;

get_data_point;
plt_point(ndps);

for y:=1 to a do
 begin
 for z:=1 to number_points[y] do
    begin
    next_field:=z*field_separation[y]+field_region[y-1];
    if z=number_points[y] then next_field:=field_region[y];
    if flag=0 then remnant_field(z);
    set_field_to(next_field);
    get_data_point;
    get_sensitivity(sensitivity);
    if sensitivity > old_sensitivity then
         begin
         old_sensitivity:=sensitivity;
         redraw;
         end;
    plt_point(ndps);
    end;

 end;

data[1,1]:=ndps;
{save data in file}
save_data(ndps);

end.
```

```
(*************************************************************************)
(*                                                                       *)
(*  Program to record the induced voltage picked up in the coils as      *)
(*  a function of time.                                                  *)
(*  C.I.Gregory 10/09/90                                                 *)
(*                                                                       *)
(*************************************************************************)


program vsmtemp;
{$D+,L+}
{$N+}
uses vsmglob,psd5206,fluke,crt,graph;

var
graphmodeset                    : boolean;
statusactive                    : boolean;
tmp,temp                        : double;
time,time_interval              :integer;
sensitivity,
old_sensitivity,
final_temp,step_size,
mag_vlt,scfact,
xscale,yscale,tnr               : real;
data                            : array[1..400,1..4] of real;
i,graphmode,bdeal,flke,
ndps,p,nrps,flag4               : integer;
scX,scY,ycen,xborderl           : integer;
testf                           : char;

procedure get_data_point;
{Reads channel one of the lockin once only after a given time delay}
begin
 if statusactive then begin
                        read_Ch1(mag_vlt);
                      end
                 else begin
                        mag_vlt:=6e-5;
                      end;
end;

procedure save_data(ndpts : integer);
{Saves data in a .TIM file of MATLAB format}
var i      : integer;
   f      : text;
   filnam : str8;
   filnamext : str12;
   sammass,refmass,vref,fieldup : real;

begin
 RestoreCrtMode;
 TextColor(Cyan);
 writeln('-------------------------------------------------------------');
 writeln('                      DATA STORAGE');
 writeln('-------------------------------------------------------------');
 writeln;
 write('Mass of sample (g) = '); readln(sammass);
 write('Mass of ref (g) = '); readln(refmass);
 write('Signal from reference (V) = '); readln(vref);
 write('Field at which ref measured (T) = '); readln(fieldup);
 write('Temperature at which reference was measured (K) ='); readln(tnr);
 write('Name of file in which to store data ( max 8 chars):');
 readln(filnam);
 filnamext:=filnam+'.tim';
 writeln('Storing data in ',filnamext);
 assign(f,filnamext);
 rewrite(f);
 data[1,2]:=0.0; data[1,3]:=0.0; data[1,4]:=0.0;
 data[2,3]:=0.0; data[2,4]:=0.0; data[3,2]:=tnr; data[4,4]:=0.0;
 data[2,1]:=sammass; data[2,2]:=refmass;
 data[3,1]:=vref; data[3,3]:=fieldup;
 for i:=1 to ndps+3 do
 begin
   writeln(f,data[i,1]:12,' ',data[i,2]:10,' ',data[i,3]:12,' ',data[i,4]:10);
 end;
 close(f);
end;


procedure in_grph;
{Sets up graphics mode}
var
 graphdriver : integer;
 errorcode   : integer;
begin
if (not graphmodeset) then begin
 graphmodeset:=true;
 graphdriver:=detect;
 initgraph(graphdriver,graphmode,'C:\tp5');
 errorcode:=graphresult;
 if errorcode <> grOK then
 begin
   writeln('Graphics error : ',grapherrormsg(errorcode));
   writeln('..program aborted...');
   halt(1);
 end;
 end
 else
 setgraphmode(graphmode);

 rectangle(0,0,getmaxX,getmaxY);
 setlinestyle(solidln,0,normwidth);
 restoreCRTMode;
end;

procedure set_scrn_plt(xreadl,yreadl,xsf : real; xaxis,xunit : str5);
{Sets up graph axis dependant on lockin sensitivity for real time data
output}
var
xborderr,yybordert,yborderb,
xlngth,yht,i,ii                 : integer;
xrmax                           : real;
xlabel                          : str10;

begin
 in_grph;
 setgraphmode(graphmode);
 xborderl:=round(getmaxx/10);
 xborderr:=round(getmaxx-xborderl);
 ybordert:=round(getmaxy/10);
```

```
 yborderb:=round(getmaxy-ybordert);
 yht:=yborderb-ybordert;
 yscale:=yht/yread1;
 xlngth:=xborderr-xborderl;
 if frac(xread1)<=0.5 then xrmax:=int(xread1)+0.5
                      else xrmax:=int(xread1)+1.0;
 xscale:=xlngth/xrmax;
 ycen:=ybordert+(yht div 2);
 rectangle(xborderl div 2,ybordert div 2,xborderr+(xborderl div 2),
                                         yborderb+(ybordert div 2));
 moveto(xborderl,ybordert); lineto(xborderl,yborderb);
 moveto(xborderl,ycen);     lineto(xborderr,ycen);
 ii:=round(int(xrmax));
 settextstyle(smallfont,0,4);
 settextjustify(centertext,centertext);
 {for i:=1 to ii do
 begin
  moveto(round(i*xscale+xborderl),ycen);
  lineto(round(i*xscale+xborderl),ycen-(ycen div 25));
  moveto(round(i*xscale+xborderl),ycen+(ycen div 25));
  str(i*xsf:5:0,xlabel);
  xlabel:=xlabel+xunit;
  outtext(xlabel);
 end; }
 moveto(xborderr-(xborderr div 15),ycen+(ycen div 10));
 outtext(xaxis);
 if flag4=0 then
       begin
       get_data_point;
       Moveto(round(xborderl),round(ycen-yscale*mag_vlt));
       end;
 if flag4=1 then
       begin
       Moveto(round(xborderl),round(ycen-yscale*data[4,3]));
       end;
 setcolor(4);
end;

procedure plt_point(i:integer);
{Stores the recently taken data point in an array and plots this point
on the screen}

begin
   data[i,1]:=time_interval*ndps;
   data[i,2]:=0.0;
   data[i,3]:=mag_vlt;
   data[i,4]:=0.0;
   lineto(round(time_interval*ndps*xscale+xborderl),round(ycen-yscale*mag_vlt));
   {writeln(data[i,1],' ',data[i,3]);}
 end;

procedure redraw;
{Redraws the output on a larger scale if the sensitivity of the lockin is
increased}

begin
 set_scrn_plt(time,(old_sensitivity*2.5),500,'Time','s');
 for p:=4 to (ndps+4) do
 begin
 lineto(round((data[p,1]*(p-3))*xscale+xborderl),round(ycen-yscale*data[p,3]));
 end;
end;

{START OF THE MAIN PROGRAM}
begin
 graphmodeset:=false;
 statusactive:=true;
 if not statusactive then begin
                            mag_vlt:=2e-4;
                          end;
 if statusactive then
 begin
 ClrScr;
 writeln('-------------------------------------------------');
 writeln(' VSMTEMP:- a PROGRAM TO RECORD M vs TIME IN FIXED B');
 writeln('-------------------------------------------------');
 writeln(' ');
 writeln(' The program is used to measure magnetisation as a');
 writeln('function of time.');
 writeln('The program operates by reading the lock-in after');
 writeln('a given time delay');
 writeln('Care should be taken with choice of time constant');
 writeln('and time interval between points');
 writeln('Insert time interval between points\s:-');readln(time_interval);
 writeln('Insert number of data points');
 writeln('Maximum number of data points 200');
 readln(nrps);
 init_ieee;
 flag4:=0;
 time:=time_interval*nrps;
 get_sensitivity(sensitivity);
 old_sensitivity:=sensitivity;
{Sets axis on screen graph}
 set_scrn_plt(time,(sensitivity*2.5),time_interval,'Time',' s');
 ndps:=1;
 plt_point(4);

 for i:=4 to (nrps-3) do
 begin
   delay(time_interval*1000);
   get_sensitivity(sensitivity);
   if (sensitivity > old_sensitivity) then
        begin
        old_sensitivity:=sensitivity;
        redraw;
        end;
   ndps:=ndps+1;
   get_data_point;
   plt_point(i);
 end;

 data[1,1]:=ndps;
 save_data(ndps);
end.
```

```
(*************************************************************************)
(*                                                                       *)
(*  Program to read induced voltage on the lockin as a function of       *)
(*  temperature(Version 1.2 temperature decreasing)                      *)
(*  by C.I.Gregory  October '90                                          *)
(*                                                                       *)
(*************************************************************************)

{For annotation see version 1.1}

program vsmtemp;

{$D+,L+}
{$N+}

uses vsmglob,psd5206,fluke,crt,graph;

var
graphmodeset  : boolean;
statusactive                    : boolean;
tmp,temp                        : double;
temp_vlt,
sensitivity,
old_sensitivity,
final_temp,step_size,
mag_vlt,scfact,
xscale,yscale,tnr               : real;
data                            : array[1..200,1..4] of real;
i,graphmode,bdeal,flke,
ndps,p,nrps,flag4               : integer;
scX,scY,ycen,xborderl           : integer;
testf                           : char;

procedure get_data_point;

begin
 if statusactive then begin
                        temp_vlt:=read_fluke;
                        read_Ch1(mag_vlt);
                      end
                 else begin
                        temp_vlt:=temp_vlt-(0.05)*3.00;
                        mag_vlt:=6e-5/temp_vlt;
                      end;
end;

procedure save_data(ndpts : integer);
var
   i      : integer;
   f      : text;
   filnam : str8;
   filnamext : str12;
   sammass,refmass,vref,fieldup : real;

begin
 RestoreCrtMode;
 TextColor(Cyan);
 writeln('-------------------------------------------------------------');
 writeln('                       DATA STORAGE');
 writeln('-------------------------------------------------------------');
 writeln;
 write('Mass of sample (g) = '); readln(sammass);
 write('Mass of ref (g) = '); readln(refmass);
 write('Signal from reference (V) = '); readln(vref);
 write('Field at which ref measured (T) = '); readln(fieldup);
 write('Temperature at which reference was measured (K) ='); readln(tnr);
 write('Name of file in which to store data ( max 8 chars):');
 readln(filnam);
 filnamext:=filnam+'.tem';
 writeln('Storing data in ',filnamext);
 assign(f,filnamext);
 rewrite(f);
 data[1,2]:=0.0; data[1,3]:=0.0; data[1,4]:=0.0;
 data[2,3]:=0.0; data[2,4]:=0.0; data[3,2]:=tnr; data[4,4]:=0.0;
 data[2,1]:=sammass; data[2,2]:=refmass;
 data[3,1]:=vref; data[3,3]:=fieldup;
 for i:=1 to ndps+3 do
 begin
   writeln(f,data[i,1]:12,' ',data[i,2]:10,' ',data[i,3]:12,' ',data[i,4]:10);
 end;
 close(f);
end;


procedure in_grph;
var
 graphdriver : integer;
 errorcode   : integer;

begin
if (not graphmodeset) then begin
 graphmodeset:=true;
 graphdriver:=detect;
 initgraph(graphdriver,graphmode,'C:\tp5');
 errorcode:=graphresult;
 if errorcode <> grOK then
 begin
   writeln('Graphics error : ',grapherrormsg(errorcode));
   writeln('..program aborted...');
   halt(1);
 end;
 end
 else
 setgraphmode(graphmode);
 rectangle(0,0,getmaxX,getmaxY);
 setlinestyle(solidln,0,normwidth);
 restoreCRTMode;
end;

procedure set_scrn_plt(xreadl,yreadl,xsf : real; xaxis,xunit : str5);
var
     xborderr,ybordert,yborderb,
     xlngth,yht,i,ii          : integer;
     xrmax                    : real;
     xlabel                   : str10;

begin
 in_grph;
 setgraphmode(graphmode);
 xborderl:=round(getmaxx/10);
```

```
 xborderr:=round(getmaxx-xborderl);
 yborder:=round(getmaxy/10);
 yborderb:=round(getmaxy-yborder);
 yht:=yborderb-yborder;
 yscale:=yht/yreadl;
 xlngth:=xborderr-xborderl;
 if frac(xreadl)<=0.5 then xrmax:=int(xreadl)+0.5
                      else xrmax:=int(xreadl)+1.0;
 xscale:=xlngth/xrmax;
 ycen:=yborder+(yht div 2);
 rectangle(xborderl div 2,yborder div 2,xborderr+(xborderl div 2),
                                        yborderb+(yborder div 2));
 moveto(xborderl,yborder); lineto(xborderl,yborderb);
 moveto(xborderl,ycen);    lineto(xborderr,ycen);
 ii:=round(int(xrmax));
 settextstyle(smallfont,0,4);
 settextjustify(centertext,centertext);
 for i:=1 to ii do
 begin
  moveto(round(i*xscale+xborderl),ycen);
  lineto(round(i*xscale+xborderl),ycen-(ycen div 25));
  moveto(round(i*xscale+xborderl),ycen+(ycen div 25));
  str(i*xsf:5:0,xlabel);
  xlabel:=xlabel+xunit;
  outtext(xlabel);
 end;
 moveto(xborderr-(xborderr div 15),ycen+(ycen div 10));
 outtext(xaxis);
 if flag4=0 then
      begin
      get_data_point;
      Moveto(round(temp_vlt*xscale+xborderl),round(ycen-yscale*mag_vlt));
      end;
 if flag4=1 then
      begin
      Moveto(round(data[4,1]*xscale+xborderl),round(ycen-yscale*data[4,3]));
      end;
 setcolor(4);
 flag4:=1;
end;

procedure plt_point(i:integer);
begin
   data[i,1]:=temp_vlt*100.0;
   data[i,2]:=0.0;
   data[i,3]:=mag_vlt;
   data[i,4]:=0.0;
   lineto(round(temp_vlt*xscale+xborderl),round(ycen-yscale*mag_vlt));
 end;

procedure redraw;

begin
 set_scrn_plt(temp_vlt,(old_sensitivity*2.5),100,'Temp','K');
 for p:=4 to (ndps+4) do
 begin
 lineto(round((data[p,1]/100)*xscale+xborderl),round(ycen-yscale*data[p,3]));
 end;
end;
```

```
{START OF MAIN PROGRAM}
begin
 graphmodeset:=false;
 statusactive:=true;
 if not statusactive then begin
                            temp_vlt:=3.00;
                            mag_vlt:=2e-4;
                          end;
 if statusactive then
 begin
 ClrScr;
 writeln('-------------------------------------------------');
 writeln(' VSMTEMP:- a PROGRAM TO RECORD M vs T IN FIXED B');
 writeln('-------------------------------------------------');
 writeln(' ');
 writeln(' The program is used to measure magnetisation as a');
 writeln('function of temperature.');
 writeln('External output of the temperature controller is');
 writeln('inserted into the fluke and the program operates by');
 writeln('reading in turn the fluke and lock-in after a given ');
 writeln('temperature step.');
 writeln(' N.B. It must be remembered that the temperature ');
 writeln('displayed is not that of the sample but of the heat');
 writeln('exchanger. The slower the cooling rate, the closer');
 writeln('this temperature will be to that of the sample');
 writeln('temperature.');
 writeln('Version 1.2:-decreasing temperature,start program');
 writeln('at required temp');
 writeln('Insert final temperature/K:-');readln(final_temp);
 writeln('Insert number of data points');
 writeln('Maximum number of data points 200');
 readln(nrps);
   init_ieee;
   repeat
     init_fluke;
     delay(100);
     write('Did the fluke display all zeroes?(y,n)');readln(testf);
   until testf='y';
 end;
 flag4:=0;
 temp:=read_fluke;
 tmp:=temp*100;
 temp_vlt:=temp;
 step_size:=abs(tmp-final_temp)/nrps;
 get_sensitivity(sensitivity);
 old_sensitivity:=sensitivity;
 set_scrn_plt(temp_vlt,(old_sensitivity*2.5),100,'Temp',' K');
 get_data_point;
 plt_point(4);
 ndps:=1;

 for i:=5 to nrps do
 begin
   repeat
    tmp:=read_fluke;
    tmp:=tmp*100;
    delay(100);
   until ((abs(tmp-data[i-1,1]))>=step_size) or (tmp<final_temp);
   get_sensitivity(sensitivity);
   if (sensitivity > old_sensitivity) then
```

```
      begin
      old_sensitivity:=sensitivity;
      redraw;
      end;
    get_data_point;
    plt_point(i);
    ndps:=ndps+1;
  end;

  data[1,1]:=ndps;
  save_data(ndps);
end.
```

```
(*************************************************************************)
(*                                                                       *)
(*  Program to record induced voltage as a function of temperature       *)
(*  which is displayed on the fluke  (Version:1.1 increasing temp)       *)
(*  by C.I.Gregory October '90                                           *)
(*                                                                       *)
(*************************************************************************)

program vsmtemp;

{$D+,L+}
{$N+}

uses vsmglob,psd5206,fluke,crt,graph;

var
graphmodeset                  : boolean;
statusactive                  : boolean;
tmp,temp                      : double;
temp_vlt, {temporarily stores read temperature}
sensitivity,
old_sensitivity,
final_temp,step_size,
mag_vlt,scfact,  {temporarily stores induced voltage on lockin}
xscale,yscale,tnr             : real;
data                          : array[1..200,1..4] of real;
{array used to store all the data-array size set here}
i,graphmode,bdeal,flke,
ndps,p,nrps,flag4             : integer;
scX,scY,ycen,xborder1         : integer;
test:f                        : char;

procedure get_data_point;
{reads temperature displayed on the fluke and then induced voltage on
channel one}

begin
 if statusactive then begin
                        temp_vlt:=read_fluke;
                        read_Ch1(mag_vlt);
                      end
                 else begin
                        temp_vlt:=temp_vlt-(0.05)*3.00;
                        mag_vlt:=6e-5/temp_vlt;
                      end;
end;

procedure save_data(ndpts : integer);
{Stores data in an input file name in MATLAB format}
var
   i      : integer;
   f      : text;
   filnam : str8;
   filnamext : str12;
   sammass,refmass,vref,fieldup : real;

begin
 RestoreCrtMode;
 TextColor(Cyan);
 writeln('-----------------------------------------------------------------');
 writeln('                        DATA STORAGE');
 writeln('-----------------------------------------------------------------');
 writeln;
 write('Mass of sample (g) = '); readln(sammass);
 write('Mass of ref (g) = '); readln(refmass);
 write('Signal from reference (V) = '); readln(vref);
 write('Field at which ref measured (T) = '); readln(fieldup);
 write('Temperature at which reference was measured (K) ='); readln(tnr);
 write('Name of file in which to store data ( max 8 chars):');
 readln(filnam);
 filnamext:=filnam+'.tem';
 writeln('Storing data in ',filnamext);
 assign(f,filnamext);
 rewrite(f);
 data[1,2]:=0.0; data[1,3]:=0.0; data[1,4]:=0.0;
 data[2,3]:=0.0; data[2,4]:=0.0; data[3,2]:=tnr; data[4,4]:=0.0;
 data[2,1]:=sammass; data[2,2]:=refmass;
 data[3,1]:=vref; data[3,3]:=fieldup;
 for i:=1 to ndps+3 do
 begin
   writeln(f,data[i,1]:12,' ',data[i,2]:10,' ',data[i,3]:12,' ',data[i,4]:10);
 end;
 close(f);
end;


procedure in_grph;
{Checks for and sets up graphs mode}
var
 graphdriver : integer;
 errorcode   : integer;

begin
if (not graphmodeset) then begin
 graphmodeset:=true;
 graphdriver:=detect;
 initgraph(graphdriver,graphmode,'C:\tp5');
 errorcode:=graphresult;
 if errorcode <> grOK then
 begin
   writeln('Graphics error : ',grapherrormsg(errorcode));
   writeln('..program aborted...');
   halt(1);
 end;
 end
 else
 setgraphmode(graphmode);

 rectangle(0,0,getmaxX,getmaxY);
 setlinestyle(solidln,0,normwidth);
 restoreCRTMode;
end;

procedure set_scrn_plt(xreadl,yreadl,xsf : real; xaxis,xunit : str5);
{Sets up graph axis for screen output}
var
     xborderr,ybordert,yborderb,
     xlngth,yht,i,ii          : integer;
     xrmax                    : real;
     xlabel                   : str10;
```

```
begin
 in_grph;
 setgraphmode(graphmode);
 xborder1:=round(getmaxx/10);
 xborderr:=round(getmaxx-xborder1);
 ybordert:=round(getmaxy/10);
 yborderb:=round(getmaxy-ybordert);
 yht:=yborderb-ybordert;
 yscale:=yht/yread1;
 xlngth:=xborderr-xborder1;
 if frac(xread1)<=0.5 then xrmax:=int(xread1)+0.5
                      else xrmax:=int(xread1)+1.0;
 xscale:=xlngth/xrmax;
 ycen:=ybordert+(yht div 2);
 rectangle(xborder1 div 2,ybordert div 2,xborderr+(xborder1 div 2),
                                         yborderb+(ybordert div 2));
 moveto(xborder1,ybordert); lineto(xborder1,yborderb);
 moveto(xborder1,ycen);     lineto(xborderr,ycen);
 ii:=round(int(xrmax));
 settextstyle(smallfont,0,4);
 settextjustify(centertext,centertext);
 for i:=1 to ii do
 begin
  moveto(round(i*xscale+xborder1),ycen);
  lineto(round(i*xscale+xborder1),ycen-(ycen div 25));
  moveto(round(i*xscale+xborder1),ycen+(ycen div 25));
  str(i*xsf:5:0,xlabel);
  xlabel:=xlabel+xunit;
  outtext(xlabel);
 end;
 moveto(xborderr-(xborderr div 15),ycen+(ycen div 10));
 outtext(xaxis);
 if flag4=0 then
       begin
       get_data_point;
       Moveto(round(temp_vlt*xscale+xborder1),round(ycen-yscale*mag_vlt));
       end;
 if flag4=1 then
       begin
       Moveto(round(data[4,1]*xscale+xborder1),round(ycen-yscale*data[4,3]));
       end;
 setcolor(4);
 flag4:=1;
end;

procedure plt_point(i:integer);
{Stores the data in an array and then plots the point on the screen}

begin
   data[i,1]:=temp_vlt*100.0;
   data[i,2]:=0.0;
   data[i,3]:=mag_vlt;
   data[i,4]:=0.0;
   lineto(round(temp_vlt*xscale+xborder1),round(ycen-yscale*mag_vlt));
   {writeln(data[i,1],' ',data[i,3]);}
 end;

procedure redraw;
{Redraws the graph on the screen if the lockin sensitivity is increased}
begin
 set_scrn_plt(temp_vlt,(old_sensitivity*2.5),100,'Temp','K');
 for p:=4 to (ndps+4) do
 begin
 lineto(round((data[p,1]/100)*xscale+xborder1),round(ycen-yscale*data[p,3]));
 end;
end;

{START OF THE MAIN PROGRAM}
begin
 graphmodeset:=false;
 statusactive:=true;
 if not statusactive then begin
                            temp_vlt:=3.00;
                            mag_vlt:=2e-4;
                          end;
 if statusactive then
 begin
 ClrScr;
 writeln('-------------------------------------------------');
 writeln(' VSMTEMP:- a PROGRAM TO RECORD M vs T IN FIXED B');
 writeln('-------------------------------------------------');
 writeln(' ');
 writeln(' The program is used to measure magnetisation as a');
 writeln('function of temperature.');
 writeln('External output of the temperature controller is');
 writeln('inserted into the fluke and the program operates by');
 writeln('reading in turn the fluke and lock-in after a given ');
 writeln('temperature step.');
 writeln(' N.B. It must be remembered that the temperature ');
 writeln('displayed is not that of the sample but of the heat');
 writeln('exchanger. The slower the cooling rate, the closer');
 writeln('this temperature will be to that of the sample');
 writeln('temperature.');
 writeln('Version 1.1:-increasing temperature,start program');
 writeln('at required temp');
 writeln('Insert final temperature(K:-');readln(final_temp);
 writeln('Insert number of data points');
 writeln('Maximum number of data points 200');
 readln(nrps);
   init_ieee;
   repeat
     init_fluke;
     delay(100);
     write('Did the fluke display all zeroes?(y/n)');readln(testf);
   until testf='y';
 end;
 flag4:=0;
 temp:=read_fluke;
 tmp:=temp*100;
 temp_vlt:=final_temp/100;
 step_size:=abs(tmp-final_temp)/nrps;
 get_sensitivity(sensitivity);
 old_sensitivity:=sensitivity;
 set_scrn_plt(temp_vlt,(sensitivity*2.5),100,'Temp',' K');
 get_data_point;
 plt_point(4);
 ndps:=1;
```

```
 for i:=5 to nrps+3 do
 begin
   repeat
    tmp:=read_fluke;
    tmp:=tmp*100;
    delay(100);
   until ((abs(tmp-data[i-1,1]))>=step_size) or (tmp>final_temp);
  {Delay until required temperature is reached, fluke read every 0.1s}
   get_sensitivity(sensitivity);
   if (sensitivity > old_sensitivity) then
          begin
          old_sensitivity:=sensitivity;
          redraw;
          end;
   get_data_point;
   plt_point(i);
   ndps:=ndps+1;
 end;

 data[1,1]:=ndps;
 save_data(ndps);
end.
```

```
(*************************************************************************)
(*                                                                       *)
(*  Program to calibrate a Au-Fe thermocouple against a Rh-Fe            *)
(*  resistor. Reads voltage on a keithley 175 and four probe             *)
(*  resistance on a keithley 197                                         *)
(*  C.I.Gregory January '92                                              *)
(*                                                                       *)
(*************************************************************************)

program calibrate;

{$D+,L+}
{$N+}

uses dos,crt,keithley,vsmglob,psd5206;

var
data                                    : array[1..500,1..4] of real;
thermo_voltage,RhFe_resistance          : real;
ndpts                                   : integer;
pp                                      : char;

procedure get_data_point;
{Reads both keithleys in turn to record a data point}
var
range,range1      :str3;

begin
thermo_voltage:=k175_com(k175initstr,'R',range);
RhFe_resistance:=k197_com(k197initstr,'R',range1);
end;

procedure record_data_point(i: integer);

begin
data[ndpts+1,1]:=thermo_voltage;
data[ndpts+1,2]:=RhFe_resistance;
end;

procedure save_data(ndpts  : integer);
{saves data in a file whose name is input. Data stored in 2D matrix}
var
i        : integer;
filnam   :str8;
filnamext:str12;
f        :text;

begin
writeln('Data stored in a two dimensional array :thermo_voltage , RhFe resistance');
writeln('Input name of file in which to store data (max 8 characters):');
readln(filnam);
filnamext:=filnam+'.VDT';
writeln('Storing data in ',filnamext);
assign(f,filnamext);
rewrite(f);
data[1,2]:=0.0;
for i:=2 to ndpts+1 do
 begin
 writeln(f,data[i,1]:12,' ',data[i,2]:12);
 end;
close(f);
end;

begin
writeln('A program used to calibrate a AuFe therocouple by reading the');
writeln('thermocouple voltage and RhFe resistance on the Keithley meters.');
writeln('When a data point is required, press key "p" and key "z"');
writeln('terminates the program.');
ndpts:=0;
init_ieee;
init_k175;
init_k197;

repeat
get_data_point;
ndpts:=ndpts+1;
record_data_point(ndpts);
writeln('Data point number',ndpts);
writeln('Rh-Fe resistance',RhFe_resistance);
writeln('Thermocouple voltage',thermo_voltage);
writeln;

repeat
delay(40);
pp:=readkey;
until (pp='p') or (pp='z');

until pp='z';

data[1,1]:=ndpts;
save_data(ndpts);
end.
```

```
(*************************************************************************)
(*                                                                       *)
(*    program for automatic data collection using the Durham VSM         *)
(*    by C.I.Gregory June '91                                            *)
(*    ammended to use kepco as a power supply Jan ' 92                   *)
(*                                                                       *)
(*************************************************************************)

{The kepco is a bipolar power supply which can provide a field of +/- 0.5T
It is controlled by a DAC minicam board with an output of 0-4095, 2048
giving zero field. Because the fields obtained are small, the field steps
are fixed and dependant on the number of data points required. The step can
be as low as 2gauss}


program vsmkep;

{$D+,L+}
{$N+}

uses vsmglob,minicam,ieee,icccom,psd5206,fluke,crt,graph,dos;

const
dac_address                 = '531';
var
graphmodeset                 :  boolean;
time                         :  word;
date_str                     :  str8;
state,b                      :  str5;
yr_str                       :  str4;
mn_str,dy_str                :  str2;
testf,pp                     :  str1;
data                         :array[1..600,1..4] of real;
{flag4-show procedure redraw is being used}
i,ndps,
total_number_points,a,
graphmode,bdeal,flke,
xcen,p,m,scX,scY,ycen,
xborderl,num_time_const,
num_measurements,
flag4,z,r,o,q                : integer;
t_const                      : longint;
fld_vlt                      : double;
next_field,mag_vlt,scfact,
xscale,yscale,sderror_mag_vlt,
sderror_fld_vlt,sensitivity,
old_sensitivity,
gauss_range_gauss,
gauss_range_tesla             :  real;



procedure save_data(ndps : integer);
{to save data}
var i,nc : integer;
   year,month,day,daywk : word;
   date_num : longint;
   f      : text;
   filnam : str8;
   tm_str    : str2;
   filnamext : str12;
   sammass,refmass,vref,fieldup : real;

begin
 restorecrtmode;
 writeln('-------------------------------------------------------------------');
 writeln('                        DATA STORAGE');
 writeln('-------------------------------------------------------------------');
 writeln;
 write('Mass of sample (g) = '); readln(sammass);
 write('Mass of ref (g) = '); readln(refmass);
 write('Ref voltage (V) = '); readln(vref);
 write('Field at which ref measured (T) = '); readln(fieldup);
 write('Name of file in which to store data ( max 8 chars):');
 readln(filnam);
 getdate(year,month,day,daywk);
 str(year,yr_str);
 str(month,mn_str);if month<10 then mn_str:='0'+copy(mn_str,1,1);
 str(day,dy_str);  if   day<10 then dy_str:='0'+copy(dy_str,1,1);
 tm_str:=copy(yr_str,3,2);
 date_str:=tm_str+mn_str+dy_str;
 val(date_str,date_num,nc);
 writeln('Date: ',date_num);
 filnamext:=filnam+'.vdt';
 writeln('Storing data in ',filnamext);
 assign(f,filnamext);
 rewrite(f);
 {first three lines of matrix:[1,1] number pts,[2,1] sample mass
 [2,2] reference mass,[3,1]induced voltage from reference,[3,3] field
 to obtain reference signal}
 data[1,2]:=0.0; data[1,3]:=date_num; data[1,4]:=0.0;
 data[2,3]:=0.0; data[2,4]:=0.0; data[3,2]:=0.0; data[3,4]:=0.0;
 data[2,1]:=sammass; data[2,2]:=refmass;
 data[3,1]:=vref; data[3,3]:=fieldup;
 for i:=1 to ndps-3 do
 {saves all data in matrix format
 field, error on field, voltage, error on voltage}
 begin
   writeln(f,data[i,1]:12,' ',data[i,2]:10,' ',data[i,3]:12,' ',data[i,4]:10);
 end;
 close(f);
end;

procedure error(error_number   :integer);
{to set all lines high ie OFF,save data taken then print error code
showing cause}

begin
 if ndps > 1 then save_data(ndps) else restorecrtmode;
 writeln('The program has been alterred as an error has ocurred, error code');
 writeln(error_number);
 writeln('For information about this see the instruction manual');
 halt(0);
end;


procedure in_grph;
var
 graphdriver : integer;
 errorcode   : integer;
```

```
begin
 if (not graphmodeset) then begin
 graphmodeset:=true;
 graphdriver:=detect;
 InitGraph(graphdriver,graphmode,'C:\tp5');
 errorcode:=graphresult;
 if errorcode <> grOK then
 begin
   writeln('Graphics error : ',grapherrormsg(errorcode));
   writeln('..program aborted...');
   halt(1);
 end;
 end
 else
 setgraphmode(graphmode);

 rectangle(0,0,getmaxX,getmaxY);
 setlinestyle(solidln,0,normwidth);
 restoreCRTMode;
end;

procedure over_load;
{if manually setting sensitivity check for overload and wait six
time constants after it is cleared}
var r   :integer;
begin
r:=0;
repeat
delay(1000);
r:=r+1;
until (lockin_ok);
if r > 1 then delay(t_const*6);
end;

procedure not_ready;
{if autoranging, waits until lockin is in state to transfer data}
begin
repeat
delay(1000);
until lockin_ok;
end;

procedure get_data_point;
{reads fluke and lockin when ready numerous times to get data
and error on data}
var
n                              :integer;
sumf,sumCl                     :double;
sderror_fluke,sderror_Ch1,
var_fluke,var_Ch1              :real;
fluke,Ch1                      :array[1..40] of real;
begin
 if statusactive then begin
        if autorange_set then not_ready
                         else over_load;
        sumf:=0;sumCl:=0;var_fluke:=0;var_Ch1:=0;
        for n:=1 to num_measurements do
           begin
             fluke[n]:=read_fluke*gauss_range_tesla;
             read_Ch1(Ch1[n]);
             sumf:=sumf+fluke[n];
             sumCl:=sumCl+Ch1[n];
             delay(t_const*num_time_const);
           end;
           fld_vlt:=sumf/num_measurements;
           mag_vlt:=sumCl/num_measurements;
           for n:=1 to num_measurements do
             begin
               var_fluke:=(fld_vlt-fluke[n])*(fld_vlt-fluke[n])+var_fluke;
               var_Ch1:=(mag_vlt-Ch1[n])*(mag_vlt-Ch1[n])+var_Ch1;
             end;
           sderror_fld_vlt:=sqr(var_fluke/(num_measurements-1))/sqr(num_measurements)
           sderror_mag_vlt:=sqr(var_Ch1/(num_measurements-1))/sqr(num_measurements);
           end
                 else begin
                        fld_vlt:=fld_vlt+0.1;
                        mag_vlt:=0.9e-2*fld_vlt;
                      end;
ndps:=ndps+1;
end;


procedure set_scrn_plt(xread1,yread1,xsf : real; xaxis,yaxis : str10);
{sets up graph axis, dependant on sensitivity of lockin}
var   xborderr,ybordert,yborderb,
     xlngth,yht,i,ii           : integer;
     xrmax                     : real;
     xlabel                    : str10;
begin
 in_grph;
 setgraphmode(graphmode);
 xborder1:=round(getmaxx/10);
 xborderr:=round(getmaxx-xborder1);
 ybordert:=round(getmaxy/10);
 yborderb:=round(getmaxy-ybordert);
 yht:=yborderb-ybordert;
 yscale:=yht/(2*yread1);
 xlngth:=xborderr-xborder1;
 if frac(xread1)<=0.5 then xrmax:=int(xread1)+0.5
                      else xrmax:=int(xread1)+1.0;
 xscale:=xlngth/(2*xrmax);
 ycen:=ybordert+(yht div 2);
 xcen:=xborder1+(xlngth div 2);
 rectangle(xborder1 div 2,ybordert div 2,xborderr+(xborder1 div 2),
                                         yborderb+(ybordert div 2));
 moveto(xcen,ybordert); lineto(xcen,yborderb);
 moveto(xborder1,ycen); lineto(xborderr,ycen);
 ii:=round(int(2*xrmax));
 settextstyle(smallfont,0,4);
 settextjustify(centertext,centertext);
 for i:=-ii to ii do
 begin
  moveto(round(i*0.5*xscale+xcen),ycen);
  lineto(round(i*0.5*xscale+xcen),ycen-(ycen div 25));
  moveto(round(i*0.5*xscale+xcen),ycen+(ycen div 25));
  str(i*0.5*xsf:3:1,xlabel);
  xlabel:=xlabel;
  outtext(xlabel);
 end;
 moveto(xborderr-(xborderr div 15),ycen+(ycen div 10));
```

```
 outtext(xaxis);
 moveto(xcen-(xcen div 10),ybordert+(yht div 10));
 settextstyle(smallfont,vertdir,4);
 outtext(yaxis);
 {if first time setup then gets data point and moves to it on axis}
 if flag4=0 then
 begin
 get_data_point;
 Moveto(round(xcen+fld_vlt*xscale),round(ycen-yscale*mag_vlt));
 end;
 {if using redraw moves to first data point as a reference}
 if flag4=1 then Moveto(round(xcen+data[4,1]*xscale),round(ycen-data[4,3]*yscale));
 setcolor(4);
end;

procedure redraw;
{redraws data on a new axis as sensitivity of lockin increased}
begin
 flag4:=1;
 set_scrn_plt(gauss_range_tesla*1.2,(old_sensitivity*1.2),1,'Field T','Magn (V)');
 for p:=4 to (ndps+2) do
 begin
 lineto(round(xcen+data[p,1]*xscale),round(ycen-yscale*data[p,3]));
 end;
end;

procedure plt_point(ndps:integer);
{stores result in array data then plots new point}
begin
   data[ndps+3,1]:=fld_vlt;
   data[ndps+3,2]:=sderror_fld_vlt;
   data[ndps+3,3]:=mag_vlt;
   data[ndps+3,4]:=sderror_mag_vlt;
   lineto(round(xcen+fld_vlt*xscale),round(ycen-yscale*mag_vlt));
   {writeln(data[i,1],' ',data[i,3]);}
 end;

procedure dac_set(nstps  :  str5);
{procedure to raise the output of the dac by a fixed step after
each data point}

var
dumstr       :  str255;

begin
dumstr:=dal(dac_address,nstps);
end;


{start of main program}
begin
graphmodeset:=false;
statusactive:=true;
init_ieee;


repeat
init_fluke;
delay(500);
writeln('Did fluke display all zeroes (y/n)?');readln(testf);
until testf='y';
delay(2000);

writeln('Insert the total number of data points required:-');
readln(total_number_points);

writeln('Insert number of points required at each field');
writeln('Must be greater than one!');
readln(num_measurements);

writeln('Insert the number of time constants delay between points:-');
readln(num_time_const);

writeln('Input gauss meter range (gauss)');
readln(gauss_range_gauss);
gauss_range_tesla:=gauss_range_gauss/1e4;


if (total_number_points) > 600 then error(3);

r:=trunc(total_number_points/4);
o:=trunc((2046*4)/total_number_points);
q:=2047;
writeln(r,o,q);
delay(5000);


ndps:=0;flag4:=0;testf:='n';

delay(100);
{read lockin for required values}
get_time_const(t_const);
delay(2000);
get_sensitivity(sensitivity);
old_sensitivity:=sensitivity;
delay(200);
set_scrn_plt(gauss_range_tesla*1.2,(old_sensitivity*1.2),1,'Field (T)','Magn (V)');

get_data_point;
plt_point(ndps);

 for z:=1 to r do
    begin
    delay(20000);
    {gets data point}
    get_data_point;
    {check if graph needs redrawing}
    get_sensitivity(sensitivity);
    if (sensitivity > old_sensitivity) then
        begin
        old_sensitivity:=sensitivity;
        redraw;
        end;
     {plots new point}
     plt_point(ndps);
    ndps:=ndps+1;
    q:=q+o;
    str(q,b);
    dac_set(b);
    end;
```

```
q:=4095;

for z:=r downto -r do

  begin
  delay(20000);
  get_data_point;
  get_sensitivity(sensitivity);
  if (sensitivity > old_sensitivity) then
       begin
       old_sensitivity:=sensitivity;
       redraw;
       end;
  plt_point(ndps);
  q:=q-c;
  str(q,b);
  dac_set(b);
  end;

q:=0;

for z:=1 to (r+15) do

   begin
   delay(20000);
   get_data_point;
   get_sensitivity(sensitivity);
   if (sensitivity > old_sensitivity) then
        begin
        old_sensitivity:=sensitivity;
        redraw;
        end;
   plt_point(ndps);
   q:=q-c;
   str(q,b);
   dac_set(b);
   end;


data[1,1]:=ndps;
{save data in file}
save_data(ndps);

end.
```

```
%Program written in MATLAB using the MATLAB mathematics passage
%to display the data taken using the VSM.
%Program VLTPLT.M used to subtract a residual signal from the data
%and display the induced voltage as a function of field.
%For annotation see MAGPLT.M
!a:
dir
datfil=input('Data file (no ext):');
resfil=input('Residual file (") :');
ext='.vdt';
df=[datfil,ext];
rf=[resfil,ext];
eval(['load ',df]);
eval(['load ',rf]);
!c:
eval(['data=',datfil,';']);
eval(['resid=',resfil,';']);
ndps=data(1,1);
nrps=resid(1,1);
xd=data(4:ndps,1);
yd=data(4:ndps,3);
xr=resid(4:nrps,1);
yr=resid(4:nrps,3);
p=polyfit(xr,yr,1);
rfit=polyval(p,xd);
ydc=yd-rfit;
gr=polyfit(xd,ydcc,1);
yf=polyval(gr,xd);
plot(xd,ydc,'g',xd,rfit,'w',xd,yd,'o')
grid
xlabel('Field - Tesla')
ylabel('Signal-V')
```

```
%A program written in MATLAB which uses the MATLAB maths package to
%display data taken on the VSM.
%This program is TIMPLT.M which displays the induced voltage as a function
%of time.
%For annotation see MAGPLT.M
!a:
dir
datfil=input('Data file (no ext):');
ext='.tim';
df=[datfil,ext];
eval(['load ',df]);
!c:
eval(['data=',datfil,';']);
ndps=data(1,1);
time=data(4:ndps,1);
vlts=data(4:ndps,3);
plot(time,vlts,'g')
grid
xlabel('Time-s')
ylabel('Signal-V')
```

```
%A program written in MATLAB which uses the MATLAB maths package to
%display the data obtained on the VSM.
%This program is  TEMPLT.M which displays the induced voltage on the
%VSM as a function of temperature.
%For annotation see MAGPLT.M
!a:
dir
datfil=input('Data file (no ext):');
ext='.tem';
df=[datfil,ext];
eval(['load ',df]);
!c:
eval(['data=',datfil,';']);
ndps=data(1,1);
temp=data(4:ndps,1);
vlts=data(4:ndps,3);
plot(temp,vlts,'g')
grid
xlabel('Temperature-K')
ylabel('Signal-V')
```

```
%A program written in MATLAB which uses the MATLAB maths package to display
%the data obtained on the VSM.
%This is MAGPLT.M which subtracts a residual signal from the data and
%converts this to a measure of magnetisation using the value of
%nickel calibration.
!a:%Data read in on floppy disc.
dir
datfil=input('Data file (no ext):');%Two data sets are input-the data
resfil=input('Residual file (") :');%and a residual file.
ext='.vdt';
df=[datfil,ext];
rf=[resfil,ext];
eval(['load ',df]);
eval(['load ',rf]);
!c:
eval(['data=',datfil,';']);
eval(['resid=',resfil,';']);
%Extracts required information from the top of the data matrix.
ndps=data(1,1);%number of data points in the file.
nrps=resid(1,1);%number of data points in the residual file.
sammass=data(2,1);%mass of sample from the data file.
refmass=data(2,2);%mass of reference used from the data file.
vref=data(3,1);%induced voltage from the Ni sample.
temp=data(3,2);%temperature at which this was recorded.
td=1-6.64e-6*temp^1.5-1.85e-08*temp^2.5;%temperature dependance of the
magnetisation of Nickel.
mni=58.e8*td;%Magnetisation of Ni extrapolated to 0K.
cf=mni*refmass/(vref*1000*sammass);%conversion factor for sample voltage.
xd=data(4:ndps,1);%Applied magnetic field.
yd=data(4:ndps,3);%induced sample voltage.
yerr=data(4:ndps,4);%standard error on induced voltage.
xr=resid(4:nrps,1);%applied magnetic field to the residual.
yr=resid(4:nrps,3);%induced residual voltage.
p=polyfit(xr,yr,1);%first order poly fit to the residual signal.
ri=p(1)*xd+p(2);%residual voltage calculated at all fields the sample
got to.
ydc=yd-ri;%subtraction of the residual.
ydc=cf*ydc;%conversion of voltage to magnetisation.
yerr=cf*yerr;%conversion of standard error.
plot(xd,ydc,'g')
grid
xlabel('Field - Tesla')
ylabel('Magnetisation-J T Kg')
```

```
{any declarations following originated in "MINICAM.DEF"}

{type declarations for minicam interface functions}

unit minicam;
interface
uses vsmglob;

type
    minicamtype     = record
          call                          : str3;
          address,
          num,
          tim                           : integer;   {in minicam units!}
          result                        : str16;
                    end;


    motortype       = record   {applies to stepper and dc motors}
          motorclass                    : (stepper, dcmotor); {switch}
          name                          : str8;    {both}
          plus,minus,                              {either stepper
                                                    module addresses,
                                                    or dc databus values}
          address,                                 {dc module address}
          maxspeed,                                {steps/sec}
          backlash                      : integer; {steps; not yet used}
          units                         : str3;    {steppers}
          steps_per_unit, range, lowlimit : real;  {steppers}
          width, decpts,                           {steppers}
          windowpt                      : integer; {both}
          searchrange,                             {default values }
          firstrange,                              {on             }
          searchstep,                              {Peakfind.      }
          defaultscanrange,                        {defaults       }
          defaultstepsize               : real;    {on Scan        }
                    end;


    scalertype      = record
          scalername            : str8;
          gatetime              : real;            {seconds     }
          auto,                                    {bargraph display}
          switchedon            : boolean;         {on/off      }
          span,                                    {for display }
          Zoff                  : real;            {for display }
          address               : integer;
          Hz,                                      {count rate  }
          scanstopcount,
          searchstopcount       : real;            {peakfind criterion}
                    end;

    adctype         = record
          adcname               : str16;
          address,
          windowpt,
          range                 : integer;
          volt_range,
          units_per_volt        : real;
          units                 : str8;
                    end;

    dactype         = record
          dacname               : str16;
          address,
          windowpt,
          range,
          sense,
          channel               : integer;
          polarity              : char;
          v_ref,
          volts_per_unit        : real;
          units                 : str8;
                    end;

    relaytype       = record
          boardname             : str16;
          address,
          windowpt,
          relays_on             : integer;
          relay_on              : array[1..8] of boolean;
          relayname             : array[1..8] of str16;
                    end;

    gpiptype        = record    {digital input ports}
          gpipname              : str8;
          address, channels     : integer;
                    end;

    gpoptype        = record    {digital output ports}
          gpopname              : str8;
          address, channels     : integer;
                    end;

    Clock           = record
          hour,minute,second    :integer;
                    end;

    Calendar        = record
          day,month,year        :integer;
                    end;

    DosRec          = record
          ax,bx,cx,dx,bp,si,di,ds,es,flags   :integer;
                    end;


    gaussmetertype  = record
                range,
                units_per_volt  : real;
                units           : str6;
                windowpt        : integer;
                   end;

    magnettype      = record
              maxcurrent        : real;
              remanentfield     : real;
                    end;
```

```
    lockintype      = record
              datachannel          : integer;
              bandpass             : integer;
              sensitivity          : integer;
              dynreserve           : integer;
              timeconst            : integer;
                    end;

    filenames       = record
                      end;

    motors                         = array[0..8] of motortype;
    scalers                        = array[1..8] of scalertype;
    adcs                           = array[1..8] of adctype;
    dacs                           = array[1..8] of dactype;
    relayboards                    = array[1..8] of relaytype;
    gpips                          = array[1..8] of gpiptype;
    gpops                          = array[1..8] of gpoptype;
    gaussmeters                    = array[1..8] of gaussmetertype;
    magnets                        = array[1..8] of magnettype;
    lockins                        = array[1..8] of lockintype;
    filesettype                    = array[1..30] of filenames;

 The following are used by IEEE.I03}
type  laddr  = record
             pri : integer;
             sec : array[1..10] of integer;
                end;
      devadd = array[1..10] of laddr;
      stray  = array[1..10] of string[255];
      namfil = str12;

var
    intstat,my_addr,lastint1,dat,poll_resp,ieeestatus,srq : integer;
    bit,sense : integer;
    ecis,ters : char;
    cntrlr,last,my_flag : boolean;
    datastring : string[255];
    filnam : namfil;
    sar : stray;
    devla,devta : devadd;

    implementation
end.
```

```
(*************************************************************************)
(*                                                                       *)
(*  UNIT psd5206 - Brookdeal 5206 lockin amplifier routines              *)
(*  12/04/89  D.B.Lambrick                                               *)
(*  init_ieee and lock_int ammended by C.I.Gregory 12/06/91              *)
(*                                                                       *)
(*************************************************************************)

unit psd5206;

{-------------------------------------------------------------------------}

interface

uses vsmglob,ieee,utils,crt;

procedure init_ieee;
procedure psd_com(comstr : str12);
function  lock_in(instr:str12;rep:char):real;
procedure init_lockin;
procedure read_Ch1(var Ch1_value:real);
procedure ave_Ch1(var mean_Ch1:real);
function  lockin_ovld : boolean;
procedure set_sensitivity(n_val:integer);
procedure range_lockin;
procedure get_time_const(var t_const : longint);
procedure get_sensitivity(var sens_volt : real);
function lock_int(instr:str12;rep:char):real;
function autorange_set : boolean;
function lockin_ok : boolean;
{-------------------------------------------------------------------------}

implementation

procedure init_ieee;
begin
 ieee_add;
 controlr:=true;
 my_flag:=false;
 my_addr:=1;
 intistat:=0;
{These are the address numbers as used by the computer and are set below}
 bdeal:=1;
 fike:=2;
 mcam:=4;
 k175:=5;
 k197:=6;
{A very important section of the program set! The IEEE addresses of the devices
are changed here as far as the computer is concerned}
 devla[1].prim:=10;{converts the device at address 10 to address one for the
computer}
 devta[1].prim:=10;{10 is the lockin address. All lockins in the lab should be
at address 10. If not, then put address here}
 devla[2].prim:=16;{fluke address}
 devta[2].prim:=16;
 devla[4].prim:=6;{minicam address}
 devta[4].prim:=6;
 devla[5].prim:=3;{keithley 175 address}
 devta[5].prim:=3;
 devla[6].prim:=2;{keithley 197 address}
 devta[6].prim:=2;
 init;
end;

procedure psd_com( comstr : str12 );

begin
 init;
 eois:=chr(13);
 iors:='i';
 datastring:='';
 datastring:=comstr;
 wr_str(bdeal);
end;

{-------------------------------------------------------------------------}

function lock_in( instr : str12; rep : char ) : real;

var dumstr : str5;
    dummy  : real;

begin
 psd_com(instr);
 if rep = 'R' then begin
                   read_str(bdeal);
                   dummy:=decipher(datastring);
                   lock_in:=dummy;
                   end
              else lock_in:=0.0;
end;

{-------------------------------------------------------------------------}

procedure init_lockin;
var dummy : real;

begin
if statusactive then
  begin
    dummy:=lock_in('S','N');
    delay(3000);
  end else
    delay(50);
end;

{-------------------------------------------------------------------------}
procedure read_Ch1(var ch1_value : real);
var sensitivity : real;

begin
  ch1_value:=lock_in('Q1','R');
  delay(50);
  get_sensitivity(sensitivity);
  ch1_value:=(ch1_value/2000)*sensitivity;
end;


{-------------------------------------------------------------------------}
```

```
procedure ave_Ch1(var mean_Ch1 : real);

var sum,
    dummy   : real;
    t_const : longint;

begin
  sum:=0.0;
  {  get_time_const(t_const); }
  for i:=1 to 10 do
   begin
     read_Ch1(dummy);
     sum:=sum+dummy;
     delay(1000);
   end;
  mean_Ch1:=sum/10;
end;

{-------------------------------------------------------------------------}

function lockin_ovld : boolean;

var dummy : real;
    intdum : integer;

begin
  statusactive:=true;
  if statusactive then
  begin
    dummy:=lock_in('N','R');
    if (dummy <>0) then lockin_ovld:=true
                   else lockin_ovld:=false;
  end
  else
    delay(200);
end;

{-------------------------------------------------------------------------}

procedure set_sensitivity(n_val : integer);

var  dummy  : real;
     n      : integer;
     dumstr : str2;

begin
if statusactive then
  begin
    if n_val=0 then
      begin
        dummy:=lock_in('S0','N');
        delay(2500);
        n:=0;
        repeat
          n:=n+1;
          str(n:2,dumstr);
          dummy:=lock_in('S'+dumstr,'N');
          delay(2000);
        until lockin_ovld;
        if n<>24 then n:=n+1;
        str(n:2,dumstr);
        dummy:=lock_in('S'+dumstr,'N');
      end else
        begin
          str(n_val:2,dumstr);
          dummy:=lock_in('S'+dumstr,'N');
        end;
  end else
    delay(200);
end;

{-------------------------------------------------------------------------}

procedure range_lockin;

var dummy   : real;
    dum2    : integer;
    dumstr2 : str2;
    dumstr3 : str3;

begin
  if statusactive then
    begin
      if lockin_ovld then repeat
                            dumstr2:='';  dumstr3:='';
                            dummy:=lock_in('G','R');
                            dum2:=trunc(dummy);
                            if dum2<24 then dum2:=dum2+1;
                            str(dum2:2,dumstr2);
                            dumstr3:='G'+dumstr2;
                            dummy:=lock_in(dumstr3,'N');
                            delay(400);
                          until (not lockin_ovld) or (dum2=24);
    end else
      delay(200);
end;

{-------------------------------------------------------------------------
{function lockin_int returns a string of two values seperated by a ','.
This routine was ammended to seperate the two numbers and use the first
one returned}


function lock_int( instr : str12; rep :char ) : real;
var dumstr :str5;
   dummstr :str5;
   dummy  :real;
   p,Code,q :integer;
 begin
   psd_com(instr);
   if rep = 'R' then begin
                     read_str(bdeal);
                     p:=0; dummstr:='';
                     repeat p:=p+1;
                     until datastring[p]=',';
                     for q:=1 to (p-1) do
                       begin
                       dummstr:=dummstr+datastring[q];
                       end;
                     val(dummstr,dummy,Code);
```

```
                    lock_int:=dummy;
                    end
                else lock_int:=0.0;
    end;

{-------------------------------------------------------------------------}

procedure get_time_const;
var dummy : real;
    i     : longint;
begin
 dummy:=lock_int('T','R');
 i:=trunc(dummy);
 case i of
  0 : t_const:=100000;
  1 : t_const:=30000;
  2 : t_const:=10000;
  3 : t_const:=3000;
  4 : t_const:=1000;
  5 : t_const:=300;
  6 : t_const:=100;
  7 : t_const:=30;
  8 : t_const:=10;
  9 : t_const:=1;
 10 : t_const:=1;
 end;
end;

{-------------------------------------------------------------------------}

procedure get_sensitivity;
var dumr,dumi : real;
begin
 dumr:=lock_in('S','R');
 delay(40);
 dumi:=dumr-(trunc(dumr/3)*3)+1;
 if dumi=1 then dumi:=5;
 if dumi=2 then dumi:=1;
 sens_volt:=exp(-trunc(dumr/3)*ln(10))*dumi;
end;
{-------------------------------------------------------------------------}

function autorange_set : boolean;
var dummy :real;
begin
dummy:=lock_in('A1','R');
if dummy > 0.0 then autorange_set:=true
                   else autorange_set:=false;
end;

function lockin_ok : boolean;
var dummy : real;
  intdum : integer;

  begin
  dummy:=lock_in('Z','R');
  if dummy=32.0 then lockin_ok:=true
                else lockin_ok:=false;
  end;
```

```
(*************************************************************************)
(*                                                                       *)
(*  UNIT ieee - Pascal routines for Scientific Solutions RevD board      *)
(*  12/04/89 D.B.Lambrick                                                *)
(*                                                                       *)
(*  Rd_Byte Amended 7/7/88                                               *)
(*  Conversion to Turbo 5.0 21/3/89 - Unit conv. 12/04/89                *)
(*                                                                       *)
(*************************************************************************)

unit ieee;

{-------------------------------------------------------------------------}

interface

uses vsmglob;

 const Bdadd : integer = $310;

 type  laddr  = record
               prim : integer;
                sec : array[1..10] of integer;
                  end;
       devadd = array[1..10] of laddr;
       stray  = array[1..10] of string[255];

 var
     intlstat,my_addr,lastintl,dat,poll_resp,ieeestatus,srq : integer;
     bit,sense,i,nl : integer;
     eois,iors : char;
     cntrllr,last,my_flag,firstln,statusactive: boolean;
     datastring,petfile : str255;
     filnam : namfil;
     sar : stray;
     devla,devta : devadd;
     filvar : text;
     pcfile : str14;

 procedure ibclear;
 procedure wait12;
 procedure tci(comm:integer);
 procedure fetch_la(devnum:integer);
 procedure out_ta(devnum:integer);
 procedure init;
 procedure gtsby;
 procedure go_idle;
 procedure gtscnt;
 procedure abrt;
 procedure abort;
 procedure devclr;
 procedure getrigg(devnum:integer);
 procedure devloc(devnum:integer);
 procedure llo;
 procedure my_rsp(devnum:integer);
 procedure read_setup(devnum:integer);
 procedure read_end;
 procedure read_str(devnum:integer);
 procedure read_to_file(filnam:namfil;devnum:integer);
 procedure write_setup(devnum:integer);
 procedure wr_str(devnum:integer);
 procedure wr_from_file(filnam:namfil;devnum:integer);
 procedure rd_byte;
 procedure wr_byte(dat:integer);
 procedure par_poll;
 procedure unconfig;
 procedure disab_poll(devnum:integer);
 procedure read_bus_stat;
 procedure sel_dev_clr(devnum:integer);
 procedure sel_dev_rem(devnum:integer);
 procedure ser_poll(devnum:integer);
 procedure pp_en(devnum:integer);
 procedure all_loc;
 procedure all_rem;
 procedure trnsfr(devnum:integer);
 procedure my_la;
 procedure my_ta;
 procedure listen(devnum:integer);
 procedure talk(devnum:integer);
 procedure unlisten;
 procedure untalk;
 procedure tcsy;
 procedure tasy;
 procedure rcv_cntrl;
 procedure pass_cntrl(devnum:integer);
 procedure set_eoi;
 procedure rdsup(devnum:integer);
 procedure rd_arry(sar:stray;sep,lastchar:char;devnum:integer);
 procedure zero_add;
{-------------------------------------------------------------------------}

implementation

procedure ibclear;                    { Waits for the input buffer to clear }
var   dummy : integer;                { i.e. 9292 buffer }
begin
 repeat
  dummy:=Port[Bdadd+3];
 until (dummy and 2)<>2;
end;

procedure wait12;
var w12dum : integer;
begin
 repeat
  w12dum:=Port[Bdadd+1];
  until (w12dum and 2) = 2;
end;

procedure tci(comm:integer);
var   dummy : integer;
begin
 ibclear;
 Port[Bdadd+10]:=0;
 Port[Bdadd+3]:=comm;
 repeat
  dummy:=Port[Bdadd+12]
 until (dummy and 1) <> 0;
end;
```

```
procedure fetch_la;
var j :integer;
begin
  if devla[devnum].prim = my_addr then my_flag:=true
   else begin
          Port[Bdadd+0]:=devla[devnum].prim+$20;
          j:=1;
          while (devla[devnum].sec[j] <> 0) {or (j=1)} do
           begin
            Port[Bdadd+0]:=devla[devnum].sec[j]+$60;
            j:=j+1;
           end;
         end;
end;

procedure out_ta;
var j : integer;
begin
 wait12;
 Port[Bdadd+0]:=devta[devnum].prim+$40;
 j:=1;
 while (devta[devnum].sec[j] <> 0)  do
  begin
   wait12;
   Port[Bdadd+0]:=devta[devnum].sec[j]+$60;
   j:=j+1;
  end;
end;

procedure init;
var   dummy : integer;
begin
 dummy:=Port[bdadd];       { Clear IBF }
 ibclear;                  { Wait for IBF low }
 Port[Bdadd+9]:=$f2;       { Reset 9292 }
 Port[Bdadd+5]:=$2;        { Reset 9291A }
 Port[Bdadd+5]:=$25;       { Init TI delay }
 Port[Bdadd+1]:=$93;       { 9291A intrr enble 1 }
 Port[Bdadd+2]:=$0;        { 9291A intrr enble 2 }
 Port[Bdadd+3]:=$0;        { 9291A serial poll mode }
 Port[Bdadd+5]:=$80;       { 9291A Aux mode A }
 Port[Bdadd+5]:=$a1;       { 9291A Aux mode B, enable cpt }
 Port[Bdadd+6]:=$1;        { 9291A addr mode - bd is 1 }
 Port[Bdadd+6]:=$e0;       { Disable addr 1 }
 ibclear;
 Port[Bdadd+8]:=$0;        { Clr 9292 err mask }
 ibclear;
 Port[Bdadd+8]:=$a0;       { Enable tci }
 tci($e6);                 { Read 9292 cont status reg }
 repeat
  dummy:=Port[Bdadd+9]
 until (dummy and 1) <> 0;
 Port[Bdadd+4]:=$80;
 Port[Bdadd+5]:=$0;
end;

procedure gtsby;
begin
 tci($f6);
end;
```

```
procedure go_idle;
begin
 tci($f1);
end;

procedure gtsent;
begin
 tci($f4);
end;

procedure abrt;
begin
 ibclear;
 Port[Bdadd+9]:=$f9;
end;

procedure abort;
begin
 if cntrllr then abrt else
  begin
   tci($f9);
   Port[Bdadd+4]:=$80;
   Port[Bdadd+5]:=$0;
   cntrllr:=true;
  end;
end;

procedure devclr;
begin
 wait12;
 Port[Bdadd+0]:=$14;
end;

procedure getrlq;
begin
 wait12;
 Port[Bdadd+0]:=$3f;
 fetch_la(devnum);
 wait12;
 Port[Bdadd+0]:=$8;
end;

procedure devloc;
begin
 wait12;
 Port[Bdadd+0]:=$3f;
 fetch_la(devnum);
 wait12;
 Port[Bdadd+0]:=1;
end;

procedure llo;
begin
 wait12;
 Port[Bdadd+0]:=$11;
end;

procedure my_rsp;
begin
```

```
 out_ta(devnum);
 wait12;
 Port[Bdadd+0]:=my_addr+$20;
 wait12;
 Port[Bdadd+4]:=$40;
 Port[Bdadd+5]:=0;
 tci($f6);
end;

procedure read_setup;
var dummy : integer;
begin
 if eois='' then dummy:=13 else dummy:=ord(eois);
 Port[Bdadd+7]:=dummy;
 if iors='s' then Port[Bdadd+5]:=$86 else Port[Bdadd+5]:=$82;
 if my_flag then my_rsp(devnum);
 if cntrllr then begin
                  wait12;
                  Port[Bdadd+0]:=$3f;
                  my_rsp(devnum);
                 end;
 if not (my_flag or cntrllr) then repeat
                                   dummy:=Port[Bdadd+4];
                                  until (dummy and 4)=0;
end;

procedure read_end;
var dummy : integer;
begin
 if cntrllr then begin
                  tci($fd);
                  Port[Bdadd+4]:=$80;
                  Port[Bdadd-5]:=$3;
                  Port[Bdadd-5]:=$80;
                  Port[Bdadd-5]:=$0;
                 end
            else begin
                  Port[Bdadd-5]:=$80;
                  lastintl:=intlstat;
                  Port[Bdadd+5]:=$3;
                  dummy:=Port[Bdadd+0];
                 end;
end;

procedure read_str;
var iobyt : integer;
    achar : string[1];
begin
 read_setup(devnum);
 datastring:='';
 repeat
  intlstat:=port[Bdadd+1];
  if ((intlstat and 1)<>0) then
    begin
     iobyt:=Port[Bdadd+0];
     achar:=chr(iobyt);
     datastring:=datastring+achar;
    end;
 until ((intlstat and $10)=$10);
 read_end;
```

```
end;

procedure read_to_file;
var datout : file of char;
    iobyt : integer;
    achar : char;
begin
 assign(datout,filnam);
 rewrite(datout);
 read_setup(devnum);
 intlstat:=Port[Bdadd+1];
 while ((intlstat and 1)=1) and ((intlstat and $11)<>$11) do
  begin
   iobyt:=Port[Bdadd+0];
   achar:=chr(iobyt);
   write(datout,achar);
   intlstat:=Port[Bdadd+1];
  end;
 read_end;
 close(datout);
end;

procedure write_setup;
var dummy : integer;
begin
 if cntrllr then begin
                  wait12;
                  gtsby;
                  tcsy;
                  Port[Bdadd+0]:=my_addr-$40;
                  wait12;
                  Port[Bdadd+1]:=$3f;
                  fetch_ta(devnum);
                  wait12;
                  gtsby;
                 end
            else begin
                  repeat
                   dummy:=Port[Bdadd+4];
                  until ((dummy and 2)=2);
                  if not ((lastintl and 2)=2) then wait12;
                 end;
end;

procedure wr_str;
var iobyt,strcnt : integer;
    schar : string[1];
    achar : char;
begin
 write_setup(devnum);
 for strcnt:=1 to length(datastring)-1 do
  begin
   schar:=copy(datastring,strcnt,1);
   achar:=schar[1];
   iobyt:=ord(achar);
   Port[Bdadd+0]:=iobyt;
   wait12;
  end;
 schar:=copy(datastring,length(datastring),1);
 achar:=schar[1];
```

```
 iobyt:=ord(achar);
 if ters='i' then begin
                   Port[Bdadd+5]:=$6;
                   Port[Bdadd+0]:=iobyt;
                  end
             else begin
                   if achar <> eois then begin
                                          Port[Bdadd+0]:=iobyt;
                                          writeln(iobyt);
                                          wait12;
                                         end;
                   Port[Bdadd+0]:=ord(eois);
              {     writeln(ord(eois)); }
                  end;
 lastintl:=intlstat;
 if cntrllr then tcsy;
end;

procedure wr_from_file;
var datin : file of char;
    schar : string[1];
    achar : char;
begin
 assign(datin,filnam);
 reset(datin);
 write_setup(devnum);
 repeat
  read(datin,achar);
  while not eof(datin) do
   begin
    Port[Bdadd+0]:=ord(achar);
    wait12;
   end;
 until eof(datin);
 if ters='i' then begin
                   Port[Bdadd+5]:=$6;
                   Port[Bdadd+0]:=ord(achar);
                  end
             else begin
                   if achar <> eois then begin
                                          Port[Bdadd+0]:=ord(achar);
                                          wait12;
                                         end;
                   Port[Bdadd+0]:=ord(eois);
                  end;
 close(datin);
 lastintl:=intlstat;
 if cntrllr then tci($fd);
end;

procedure rd_byte;
begin
 repeat
  intlstat:=Port[Bdadd+1];
 until ((intlstat and 1)=1) or ((intlstat and $10)=$10);
 if (intlstat and $10)=$10 then begin
                   if (intlstat and $1)=$1 then begin
                                                 dat:=Port[Bdadd+0];
                                                 last:=true;
                                                end
                                           else
                                                begin
                                                  dat:=256;
                                                  last:=true;
                                                end;
                                      end
                                 else dat:=Port[Bdadd+0];

end;

procedure wr_byte;
begin
 Port[Bdadd+0]:=dat;
 if not last then wait12;
 if not last then write(chr(dat));
 if last then writeln(chr(dat));
end;

procedure par_poll;
var dummy : integer;
begin
 Port[Bdadd+4]:=$40;
 Port[Bdadd+5]:=0;
 repeat
  dummy:=Port[Bdadd+9];
 until ((dummy and 2)<>2);
 Port[Bdadd+9]:=$f5;
 repeat
  dummy:=Port[Bdadd+1];
 until ((dummy and 1)<>0);
 poll_resp:=Port[Bdadd+0];
 Port[Bdadd+4]:=$80;
 Port[Bdadd+5]:=0;
end;

procedure unconfig;
begin
 wait12;
 Port[Bdadd+0]:=$15;
end;

procedure disab_poll;
begin
 wait12;
 Port[Bdadd+0]:=$1f;
 fetch_la(devnum);
 wait12;
 Port[Bdadd+0]:=$5;
 wait12;
 Port[Bdadd+0]:=$70;
 unconfig;
end;

procedure read_bus_stat;
var dummy : integer;
begin
 tci($e7);
 Port[Bdadd+9]:=$e7;
 repeat
  dummy:=Port[Bdadd+9];
```

```
 until not ((dummy and 1)=0);
 ieeestatus:=Port[Bdadd+8];
 srq:=ieeestatus and 1;
end;

procedure sel_dev_clr;
begin
 wait12;
 Port[Bdadd+0]:=$3f;
 fetch_la(devnum);
 wait12;
 Port[Bdadd+0]:=$4;
end;

procedure sel_dev_rem;
begin
 wait12;
 gtsby;
 tosy;
{ Port[Bdadd+0]:=$3f;}
 tci($f8);
 fetch_la(devnum);
{  gtsby; }
end;

procedure ser_poll;
var dummy : integer;
begin
 wait12;
 Port[Bdadd+0]:=$3f;
 wait12;
 Port[Bdadd+0]:=$18;
 out_ta(devnum);
 wait12;
 Port[Bdadd-4]:=$40;
 Port[Bdadd+5]:=0;
 gtsby;
 repeat
  dummy:=Port[Bdadd+1];
 until not ((dummy and 1)=0);
 poll_resp:=Port[Bdadd+0];
 Port[Bdadd+4]:=$80;
 Port[Bdadd+5]:=$40;
 tci($fd);
 wait12;
 Port[Bdadd+0]:=$19;
end;

procedure pp_en;
begin
 wait12;
 Port[Bdadd+0]:=$3f;
 fetch_la(devnum);
 wait12;
 Port[Bdadd+0]:=$5;
 wait12;
 Port[Bdadd+0]:=$60+bit+sense;
end;

procedure all_loc;
begin
 tci($f7);
end;

procedure all_rem;
begin
 tci($f3);
end;

procedure trnsfr;
var dummy : integer;
begin
 wait12;
 Port[Bdadd+0]:=$3f;
 fetch_la(devnum);
 if not my_flag then
  begin
   out_ta(devnum);
   if eois='' then dummy:=13 else dummy:=ord(eois);
   Port[Bdadd+7]:=dummy;
   if iors='s' then Port[Bdadd+5]:=$87 else Port[Bdadd+5]:=$83;
   Port[Bdadd+4]:=$40;
   Port[Bdadd+5]:=$0;
   tci($f6);
   repeat
    intlstat:=Port[Bdadd-1];
   until not ((intlstat and $10)=0);
   tci($fd);
   Port[Bdadd-5]:=$80;
   Port[Bdadd-4]:=$3;
   Port[Bdadd-5]:=$0;
  end;
end;

procedure my_ta;
begin
 wait12;
 Port[Bdadd+0]:= my_addr + $20;
 wait12; }
 Port[Bdadd+5]:= $82;
 Port[Bdadd+4]:= $40;
 Port[Bdadd+5]:= $0;
 last:=false;
end;

procedure my_ta;
begin
 wait12;
 Port[Bdadd+0]:= my_addr + $40;
 wait12;
 last:=false;
end;

procedure listen;
begin
 fetch_la(devnum);
end;

procedure talk;
begin
```

```
 out_ta(devnum);
end;

procedure unlisten;
begin
 tcsy;
 wait12;
 Port[Bdadd+0]:=$3f;
 gtsby;
end;

procedure untalk;
begin
 tcsy;
 wait12;
 Port[Bdadd+0]:=$5f;
 gtsby;
end;

procedure tcsy;
begin
 tci($fd);
 Port[Bdadd+5]:=$80;
 Port[Bdadd+5]:=$3;
 Port[Bdadd+4]:=$80;
 Port[Bdadd+5]:=$0;
end;

procedure tasy;
begin
 tci($fc);
 Port[Bdadd+5]:=$80;
 Port[Bdadd+5]:=$3;
 Port[Bdadd+4]:=$80;
 Port[Bdadd+5]:=$0;
end;

procedure rcv_cntrl;
var dummy,comm : integer;
begin
 if not cntrllr then
  begin
   if not ((lastint1 and 128)=128) then repeat
                                         intlstat:=Port[Bdadd+1];
                                        until not ((intlstat and 128)=0);
   repeat
    dummy:=Port[Bdadd+4];
   until not ((dummy and 2)=0);
   comm:=Port[Bdadd+5];
   Port[Bdadd+5]:=$f;
   comm:=comm and 127;
   if comm =9 then begin
                    Port[Bdadd+4]:=$80;
                    Port[Bdadd+5]:=$0;
                    cntrllr:=true;
                    tci($fa);
                   end
              else begin
                    writeln('Error - undefined command');
                   end;
```

```
  end;
end;

procedure pass_cntrl;
begin
 if not cntrllr then begin
                      out_ta(devnum);
                      wait12;
                      Port[Bdadd+0]:=$9;
                      wait12;
                      Port[Bdadd+4]:=$1;
                      Port[Bdadd+5]:=$a1;
                      Port[Bdadd+5]:=$0;
                      lastint1:=0;
                      cntrllr:=false;
                      tci($f1);
                     end;
end;

procedure set_eoi;
begin
 Port[Bdadd+5]:=$6;
 last:=true;
end;

procedure rdsup;
var dummy : integer;
begin
 if my_flag then my_rsp(devnum);
 if cntrllr then begin
                  wait12;
                  Port[Bdadd+0]:=$3f;
                  my_rsp(devnum);
                 end;
 if not (my_flag or cntrllr) then repeat
                                   dummy:=Port[Bdadd+4];
                                  until (dummy and 4)=0;
end;

procedure rd_arry;
var dummy,iobyt,i : integer;
    achar         : string[1];
begin
 Port[Bdadd+5]:=$81;
 rdsup(devnum);
 repeat
  i:=i+1;
  sar[i]:='';
  repeat
   repeat
    dummy:=Port[Bdadd+1];
   until not ((dummy and 1)=0);
   iobyt:=Port[Bdadd+0];
   achar:=chr(iobyt);
   sar[i]:=sar[i]+achar;
   if (achar <> lastchar) then Port[Bdadd+5]:=$3;
  until (achar=sep) or (achar=lastchar);
 until (achar=lastchar);
end;
```

```
procedure zero_add;
var i : integer;
begin
 for i:=1 to 10 do
  begin
   with devla[i] do begin
                     prim:=0;
                     sec[1]:=0;
                     sec[2]:=0;
                     sec[3]:=0;
                     sec[4]:=0;
                     sec[5]:=0;
                     sec[6]:=0;
                     sec[7]:=0;
                     sec[8]:=0;
                     sec[9]:=0;
                     sec[10]:=0;
                    end;
   with devta[i] do begin
                     prim:=0;
                     sec[1]:=0;
                     sec[2]:=0;
                     sec[3]:=0;
                     sec[4]:=0;
                     sec[5]:=0;
                     sec[6]:=0;
                     sec[7]:=0;
                     sec[8]:=0;
                     sec[9]:=0;
                     sec[10]:=0;
                    end;
  end;
end;
{------------------------------------------------------------------------}
end.
```

```
(*************************************************************************)
(*                                                                       *)
(*       UNIT to communicate with FLUKE 8860A digital multimeter         *)
(*       12/04/89 D.B.Lambrick                                           *)
(*                                                                       *)
(*************************************************************************)
{$N+}
unit fluke;

{-----------------------------------------------------------------------}

interface

uses vsmglob,utils,ieee;

procedure fluke_com(comstr:str12);
procedure cr_eoi;
procedure init_fluke;
function read_fluke : double;

{-----------------------------------------------------------------------}

implementation

procedure fluke_com;
begin
  eois:=chr(10);
  iors:='i';
  datastring:=comstr+chr(13)+chr(10);
  init;
  wr_str(flke);
end;

procedure cr_eoi;
begin
  fluke_com('W2');
end;

procedure init_fluke;
begin
  eois:=chr(10);
  iors:='i';
  gtsby;
  tcsy;
  tci($f8);
  wr_byte($30);
  gtsby;
  tcsy;
  wr_byte($3f);
  wr_byte($5f);
  wr_byte($30);
  gtsby;
  wr_byte($2a);
  wr_byte($54);
  wr_byte($30);
  wr_byte($0d);
  set_eoi;
  last:=true;
  wr_byte($0a);
  last:=false;
  tcsy;
end;

function read_fluke;
var dum : double;
    ec  : integer;
begin
  eois:=chr(10);
  iors:='i';
  gtsby;
  tcsy;
  read_str(flke);
  datastring:=copy(datastring,1,length(datastring)-2);
  val(datastring,dum,ec);
  read_fluke:=dum;
end;
{-----------------------------------------------------------------------}
end.
```

```
(*************************************************************************)
(*                                                                       *)
(*   UNIT vsmglob - Global variables for VSM programs                    *)
(*   12/14/89 D.B.Lambrick                                               *)
(*   Updated by C.I.Gregory 10/06/91                                     *)
(*                                                                       *)
(*************************************************************************)

unit vsmglob;

{-------------------------------------------------------------------------}

interface
  type
      namfil = string[12];
       str1   = string[1];
       str2   = string[2];
       str3   = string[3];
       str4   = string[4];
       str5   = string[5];
       str6   = string[6];
       str8   = string[8];
       str10  = string[10];
       str12  = string[12];
       str14  = string[14];
       str16  = string[16];
       str20  = string[20];
       str80  = string[80];
       str255 = string[255];

   var
    ideal,flke,mcam,k197,k174 : integer;
{The above are arreviations of different devices on the IEEEbus.
The values are set in psd5206.pas                                       }

   const
    k197initstr   =    'G0K0D0T5';
    k175initstr   =    'G0K0D0T5';
{These are the constants sent to the keithley instruments in order to be
able to talk to them.                                                   }

{-------------------------------------------------------------------------}

implementation
{-------------------------------------------------------------------------}
end.
```

```
(*************************************************************************)
(*                                                                       *)
(*              Minicam Routines     -    Version One                    *)
(*                   D.B.Lambrick  August 1987                           *)
(*                                                                       *)
(*************************************************************************)

unit ieccom;
interface
uses vsmglob,minicam,psd5206,ieee;

function ad1(madd : str5) : str255;
function ad2(madd : str5) : str255;
function da1(madd,n : str5) : str255;
function da2(madd,n : str5) : str255;

type mcamstr = string[20];

var amstr : mcamstr;
        i : integer;
     volt : real;
     reply: str255;

implementation
{-------------------------------------------------------------------------}
procedure mcam_con( comstr : mcamstr );

begin
{ zero_add;
 cntrllr:=true;
 my_flag:=false;
 my_addr:=4;
 intlstat:=0;}
 eois:=chr(13);
 cors:='c';
  devla[4].prim:=6;
 devla[4].prim:=6;}
 datastring:=comstr+chr(13);
 init;
 wr_str(mcam);
 read_str(mcam);
end;

{-------------------------------------------------------------------------}

function st1(madd,t,n : str5): str255;
var comstr : mcamstr;
begin
  comstr:='ST1,'+madd+','+t+','+n;
  mcam_con(comstr);
  st1:=datastring;
end;

function st2(madd,t,n : str5) : str255;
var comstr : mcamstr;
begin
  comstr:='ST2,'+madd+','+t+','+n;
  mcam_con(comstr);
  st2:=datastring;
end;

function ad1(madd : str5) : str255;
var comstr : mcamstr;
begin
 comstr:='AD1,'+madd;
 mcam_con(comstr);
 ad1:=datastring;
end;

function ad2(madd : str5) : str255;
var comstr : mcamstr;
begin
 comstr:='AD2,'+madd;
 mcam_con(comstr);
 ad2:=datastring;
end;

function co1(madd,t : str5) : str255;
var comstr : mcamstr;
begin
 comstr:='CO1,'+madd+','+t;
 mcam_con(comstr);
 co1:=datastring;
end;

function co2(madd,t : str5) : str255;
var comstr : mcamstr;
begin
 comstr:='CO2,'+madd+','+t;
 mcam_con(comstr);
 co2:=datastring;
end;

function da1(madd,n : str5) : str255;
var comstr : mcamstr;
begin
 comstr:='DA1,'+madd+','+n;
 mcam_con(comstr);
 da1:=datastring;
end;

function da2(madd,n : str5) : str255;
var comstr : mcamstr;
    bdadd  : real;
    i      : integer;
begin
 val(madd,bdadd,i);
 bdadd:=bdadd+512;
 str(bdadd,madd);
 comstr:='DA2,'+madd+','+n;
 mcam_con(comstr);
 da2:=datastring;
end;

function gp1(madd : str5) : str255;
var comstr : mcamstr;
begin
 comstr:='GP1,'+madd;
 mcam_con(comstr);
 gp1:=datastring;
```

```
end;

function m00 : str255;
var comstr : mcamstr;
begin
 comstr:='M00';
 mcam_con(comstr);
 m00:=datastring;
end;

function m01 : str255;
var comstr : mcamstr;
begin
 comstr:='M01';
 mcam_con(comstr);
 m01:=datastring;
end;

function m02 : str255;
var comstr : mcamstr;
begin
 comstr:='M02';
 mcam_con(comstr);
 m02:=datastring;
end;

function m03 : str255;
var comstr : mcamstr;
begin
 comstr:='M03';
 mcam_con(comstr);
 m03:=datastring;
end;

function m04 : str255;
var comstr : mcamstr;
begin
 comstr:='M04';
 mcam_con(comstr);
 m04:=datastring;
end;

function m05 : str255;
var comstr : mcamstr;
begin
 comstr:='M05';
 mcam_con(comstr);
 m05:=datastring;
end;

function rd1 : str255;
var comstr : mcamstr;
begin
 comstr:='RD1';
 mcam_con(comstr);
 rd1:=datastring;
end;

function rd2(madd : str5) : str255;
var comstr : mcamstr;
begin
 comstr:='RD2,'+madd;
 mcam_con(comstr);
 rd2:=datastring;
end;

function vp1(madd,t,n : str5) : str255;
var comstr : mcamstr;
begin
 comstr:='VP1,'+madd+','+t+','+n;
 mcam_con(comstr);
 vp1:=datastring;
end;

function vp2(madd,t,n : str5) : str255;
var comstr : mcamstr;
begin
 comstr:='VP2,'+madd+','+t+','+n;
 mcam_con(comstr);
 vp2:=datastring;
end;
end.
```

```
(*********************************************************************)
(*                                                                   *)
(*  Unit keithley: to communicate with keithley 175 and 197.         *)
(*  M.R.Delap                                                        *)
(*  for complete listing see DELAP PhD Thesis                        *)
(*                                                                   *)
(*********************************************************************)

unit keithley;

{unit to talk to keithleys}

interface

uses ieee,crt,dos,vsmglob,psd5206;

function decipher_keithley(instr:str80; digits:integer): real;
function k197_com(comstr:str80; rep:char; var range:str3): real;
procedure init_k197;
function k197_range_check(intended:str3): boolean;
function k175_com(comstr:str80; rep:char; var range:str3): real;
function k175_range_check(intended:str3): boolean;
procedure init_k175;


{*********Keithley 197 & 175 routines*********************************** }

implementation

function decipher_keithley(instr:str80; digits:integer) : real;
var
  dummy  : real;
  dummy2 : integer;
  dumstr : str80;
begin
  dummy2:=digits+6;
  dumstr:=copy(instr,5,dummy2);
  val(dumstr,dummy,dummy2);
  decipher_keithley:=dummy;
end;


function k197_com(comstr:str80; rep:char; var range:str3) : real;
begin
{   init_ieee;  }
  eois:=chr(10);
  iors:='i';
  datastring:=comstr+'X'+chr(13);
  wr_str(k197);
  k197_com:=0.0;
  range:='   ';
  if (rep='R') then begin
                      read_str(k197);
                      k197_com:=decipher_keithley(datastring,5);
                      range:=copy(datastring,2,3);
                    end;
  end;


procedure init_k197;
var
  dummy  : real;
  dumstr : str3;
  k197initstr  : str8;
begin
  sel_dev_rem(k197);
  dummy:=k197_com(k197initstr,'N',dumstr);
end;


function k197_range_check(intended:str3) : boolean;
var
  dummy  : real;
  dumstr : str3;
begin
  dummy:=k197_com('G0','R',dumstr);
  if (dumstr<>intended) then k197_range_check:=false
                        else k197_range_check:=true;
end;


function k175_com(comstr:str80; rep:char; var range:str3) : real;
begin
 { init_ieee;}
  eois:=chr(10);
  iors:='i';
  datastring:=comstr+'X'+chr(13);
  wr_str(k175);
  k175_com:=0.0;
  range:='   ';
  if (rep='R') then begin
                      read_str(k175);
                      k175_com:=decipher_keithley(datastring,4);
                      range:=copy(datastring,2,3);
                    end;
 end;


function k175_range_check(intended:str3) : boolean;
var
  dummy  : real;
  dumstr : str3;
begin
  dummy:=k175_com('','R',dumstr);
  if (dumstr<>intended) then k175_range_check:=false
                        else k175_range_check:=true;
end;


procedure init_k175;
var
  dummy  : real;
  dumstr : str3;
  k175initstr : str8;
begin
  sel_dev_rem(k175);
  dummy:=k175_com(k175initstr,'N',dumstr);
end;
```

```
C dafix.for to smooth data using smooft.for and realft.for
C234567
      DIMENSION       Y(1024),B(1024),EB(1024),EY(1024)
      REAL PTS
C NUMBER OF DATA POINTS
      N=100
C SIZE OF SAMPLING WINDOW
      PTS=3
      DO 1 I=1,N
C READ IN THE DATA
      READ(1,*) B(I),Y(I)
    1 CONTINUE
C CALL THE SMOOTHING ROUTINE
      CALL SMOOFT(Y,N,PTS)
C WRITE OUT THE SMOOTHED FILE
      DO 3 I=1,N
    3 WRITE(2,*)B(I),Y(I)
   10 FORMAT(1H ,2E14.6)
      STOP
      END


      SUBROUTINE SMOOFT(Y,N,PTS)
      PARAMETER(MMAX=1024)
      DIMENSION Y(MMAX)
      M=2
      NMIN=N+2.*PTS
    1 IF(M.LT.NMIN)THEN
        M=2*M
      GO TO 1
      ENDIF
      IF(M.GT.MMAX) PAUSE 'MMAX too small'
      CONST=(PTS/M)**2
      Y1=Y(1)
      YN=Y(N)
      RN1=1./(N-1.)
      DO 11 J=1,N
        Y(J)=Y(J)-RN1*(Y1*(N-J)+YN*(J-1))
   11 CONTINUE
      IF(N+1.LE.M)THEN
        DO 12 J=N+1,M
          Y(J)=0.
   12   CONTINUE
      ENDIF
      MO2=M/2
      CALL REALFT(Y,MO2,1)
      Y(1)=Y(1)/MO2
      FAC=1.
      DO 13 J=1,MO2-1
        K=2*J+1
        IF(FAC.NE.0.)THEN
          FAC=AMAX1(0.,(1.-CONST*J**2)/MO2)
          Y(K)=FAC*Y(K)
          Y(K+1)=FAC*Y(K+1)
        ELSE
          Y(K)=0.
          Y(K+1)=0.
        ENDIF
   13 CONTINUE
      FAC=AMAX1(0.,(1.-0.25*PTS**2)/MO2)
      Y(1)=FAC*Y(1)
      CALL REALFT(Y,MO2,-1)
      DO 14 J=1,N
        Y(J)=RN1*(Y1*(N-J)+YN*(J-1))+Y(J)
   14 CONTINUE
      RETURN
      END
C
C
      SUBROUTINE REALFT(DATA,N,ISIGN)
C      REAL*8 WR,WI,WPR,WPI,WTEMP,THETA
      DOUBLE PRECISION WR,WI,WPR,WPI,WTEMP,THETA
      DIMENSION DATA(*)
      THETA=6.28318530717959D0/2.0D0/DBLE(N)
      C1=0.5
      IF (ISIGN.EQ.1) THEN
        C2=-0.5
        CALL FOUR1(DATA,N,+1)
      ELSE
        C2=0.5
        THETA=-THETA
      ENDIF
      WPR=-2.0D0*DSIN(0.5D0*THETA)**2
      WPI=DSIN(THETA)
      WR=1.0D0+WPR
      WI=WPI
      N2P3=2*N+3
      DO 11 I=2,N/2+1
        I1=2*I-1
        I2=I1+1
        I3=N2P3-I2
        I4=I3+1
        WRS=SNGL(WR)
        WIS=SNGL(WI)
        H1R=C1*(DATA(I1)+DATA(I3))
        H1I=C1*(DATA(I2)-DATA(I4))
        H2R=-C2*(DATA(I2)+DATA(I4))
        H2I=C2*(DATA(I1)-DATA(I3))
        DATA(I1)=H1R+WRS*H2R-WIS*H2I
        DATA(I2)=H1I+WRS*H2I+WIS*H2R
        DATA(I3)=H1R-WRS*H2R+WIS*H2I
        DATA(I4)=-H1I+WRS*H2I+WIS*H2R
        WTEMP=WR
        WR=WR*WPR-WI*WPI+WR
        WI=WI*WPR+WTEMP*WPI+WI
   11 CONTINUE
      IF (ISIGN.EQ.1) THEN
        H1R=DATA(1)
        DATA(1)=H1R+DATA(2)
        DATA(2)=H1R-DATA(2)
      ELSE
        H1R=DATA(1)
        DATA(1)=C1*(H1R+DATA(2))
        DATA(2)=C1*(H1R-DATA(2))
        CALL FOUR1(DATA,N,-1)
      ENDIF
      RETURN
      END
C
C
```

```
      SUBROUTINE FOUR1(DATA,NN,ISIGN)
C      REAL*8 WR,WI,WPR,WPI,WTEMP,THETA
      DOUBLE PRECISION  WR,WI,WPR,WPI,WTEMP,THETA
      DIMENSION DATA(*)
      N=2*NN
      J=1
      DO 11 I=1,N,2
        IF(J.GT.I)THEN
          TEMPR=DATA(J)
          TEMPI=DATA(J+1)
          DATA(J)=DATA(I)
          DATA(J+1)=DATA(I+1)
          DATA(I)=TEMPR
          DATA(I+1)=TEMPI
        ENDIF
        M=N/2
    1   IF ((M.GE.2).AND.(J.GT.M)) THEN
          J=J-M
          M=M/2
        GO TO 1
        ENDIF
        J=J+M
   11 CONTINUE
      MMAX=2
    2 IF (N.GT.MMAX) THEN
        ISTEP=2*MMAX
        THETA=6.283185307179586D0/(ISIGN*MMAX)
        WPR=-2.D0*DSIN(0.5D0*THETA)**2
        WPI=DSIN(THETA)
        WR=1.D0
        WI=0.D0
        DO 13 M=1,MMAX,2
          DO 12 I=M,N,ISTEP
            J=I+MMAX
            TEMPR=SNGL(WR)*DATA(J)-SNGL(WI)*DATA(J+1)
            TEMPI=SNGL(WR)*DATA(J+1)+SNGL(WI)*DATA(J)
            DATA(J)=DATA(I)-TEMPR
            DATA(J+1)=DATA(I+1)-TEMPI
            DATA(I)=DATA(I)+TEMPR
            DATA(I+1)=DATA(I+1)+TEMPI
   12     CONTINUE
          WTEMP=WR
          WR=WR*WPR-WI*WPI+WR
          WI=WI*WPR+WTEMP*WPI+WI
   13   CONTINUE
        MMAX=ISTEP
      GO TO 2
      ENDIF
      RETURN
      END
```

Appendix B
Data Smoothing

The concept of data 'smoothing' lies in a very murky area and is probably most justified as a graphical technique to guide the eye through a forest of data points. Consequently, when data was smoothed, (χ^{-1} vs B for FeGe in the temperature range 277 - 274K) it was only when absolutely necessary and included with the raw data.

The inverse magnetic susceptibility was calculated by subtraction of adjacent magnetisation and magnetic field values for both increasing and decreasing field. Since the magnetisation of FeGe is highly sensitive to field and the field width of the feature being investigated close to the transition temperature was so narrow (the field induced phase of FeGe figure 6.6), field steps of 20Oe were used as oppose to 50Oe for other measurements. This results in the error associated with the magnetisation being more significant in the difference between adjacent values, hence there is a greater spread of values calculated in the inverse magnetic susceptibility.

The routine to smooth the data was taken from the book 'Numerical Recipes Fortran', section 13.9- Smoothing Data and is listed. The programme removes any linear trend and then uses a fast fourier transform to low pass filter the data. The linear trend is reinserted at the end. The one user specified constant is the 'amount of smoothing', specified as the number of points over which the 'data smoothing window' should exist. In all cases, the value used for this was three, chosen because of the field width of the investigated phase.

```
C main.for to smooth data using smooft.for and realft.for
C234567
      DIMENSION       Y(1024),B(1024),EB(1024),EY(1024)
      REAL PTS
C NUMBER OF DATA POINTS
      N=100
C SIZE OF SAMPLING WINDOW
      PTS=3
      DO 1 I=1,N
C READ IN THE DATA
      READ(1,*) B(I),Y(I)
    1 CONTINUE
C CALL THE SMOOTHING ROUTINE
      CALL SMOOFT(Y,N,PTS)
C WRITE OUT THE SMOOTHED FILE
      DO 3 I=1,N
    3 WRITE(2,*)B(I),Y(I)
   10 FORMAT(1H ,2E14.6)
      STOP
      END


      SUBROUTINE SMOOFT(Y,N,PTS)
      PARAMETER(MMAX=1024)
      DIMENSION Y(MMAX)
      M=2
      NMIN=N+2.*PTS
    1 IF(M.LT.NMIN)THEN
        M=2*M
      GO TO 1
      ENDIF
      IF(M.GT.MMAX) PAUSE 'MMAX too small'
      CONST=(PTS/M)**2
      Y1=Y(1)
      YN=Y(N)
      RN1=1./(N-1.)
      DO 11 J=1,N
        Y(J)=Y(J)-RN1*(Y1*(N-J)+YN*(J-1))
   11 CONTINUE
      IF(N+1.LE.M)THEN
        DO 12 J=N+1,M
          Y(J)=0.
   12   CONTINUE
      ENDIF
      MO2=M/2
      CALL REALFT(Y,MO2,1)
      Y(1)=Y(1)/MO2
      FAC=1.
      DO 13 J=1,MO2-1
        K=2*J+1
        IF(FAC.NE.0.)THEN
          FAC=AMAX1(0.,(1.-CONST*J**2)/MO2)
          Y(K)=FAC*Y(K)
          Y(K+1)=FAC*Y(K+1)
        ELSE
          Y(K)=0.
          Y(K+1)=0.
        ENDIF
   13 CONTINUE
      FAC=AMAX1(0.,(1.-0.25*PTS**2)/MO2)
```

```
      Y(2)=FAC*Y(2)
      CALL REALFT(Y,MO2,-1)
      DO 14 J=1,N
        Y(J)=RN1*(Y1*(N-J)+YN*(J-1))+Y(J)
   14 CONTINUE
      RETURN
      END
C
C
      SUBROUTINE REALFT(DATA,N,ISIGN)
C     REAL*8 WR,WI,WPR,WPI,WTEMP,THETA
      DOUBLE PRECISION WR,WI,WPR,WPI,WTEMP,THETA
      DIMENSION DATA(*)
      THETA=6.28318530717959D0/2.0D0/DBLE(N)
      C1=0.5
      IF (ISIGN.EQ.1) THEN
        C2=-0.5
        CALL FOUR1(DATA,N,+1)
      ELSE
        C2=0.5
        THETA=-THETA
      ENDIF
      WPR=-2.0D0*DSIN(0.5D0*THETA)**2
      WPI=DSIN(THETA)
      WR=1.0D0+WPR
      WI=WPI
      N2P3=2*N+3
      DO 11 I=2,N/2+1
        I1=2*I-1
        I2=I1+1
        I3=N2P3-I2
        I4=I3+1
        WRS=SNGL(WR)
        WIS=SNGL(WI)
        H1R=C1*(DATA(I1)-DATA(I3))
        H1I=C1*(DATA(I2)-DATA(I4))
        H2R=-C2*(DATA(I2)+DATA(I4))
        H2I=C2*(DATA(I1)-DATA(I3))
        DATA(I1)=H1R+WRS*H2R-WIS*H2I
        DATA(I2)=H1I+WRS*H2I+WIS*H2R
        DATA(I3)=H1R-WRS*H2R+WIS*H2I
        DATA(I4)=-H1I+WRS*H2I+WIS*H2R
        WTEMP=WR
        WR=WR*WPR-WI*WPI+WR
        WI=WI*WPR+WTEMP*WPI-WI
   11 CONTINUE
      IF (ISIGN.EQ.1) THEN
        H1R=DATA(1)
        DATA(1)=H1R+DATA(2)
        DATA(2)=H1R-DATA(2)
      ELSE
        H1R=DATA(1)
        DATA(1)=C1*(H1R+DATA(2))
        DATA(2)=C1*(H1R-DATA(2))
        CALL FOUR1(DATA,N,-1)
      ENDIF
      RETURN
      END
C
C
```

```
      SUBROUTINE FOUR1(DATA,NN,ISIGN)
C      REAL*8 WR,WI,WPR,WPI,WTEMP,THETA
      DOUBLE PRECISION  WR,WI,WPR,WPI,WTEMP,THETA
      DIMENSION DATA(*)
      N=2*NN
      J=1
      DO 11 I=1,N,2
        IF(J.GT.I)THEN
          TEMPR=DATA(J)
          TEMPI=DATA(J+1)
          DATA(J)=DATA(I)
          DATA(J+1)=DATA(I+1)
          DATA(I)=TEMPR
          DATA(I+1)=TEMPI
        ENDIF
        M=N/2
    1   IF ((M.GE.2).AND.(J.GT.M)) THEN
          J=J-M
          M=M/2
        GO TO 1
        ENDIF
        J=J+M
   11 CONTINUE
      MMAX=2
    2 IF (N.GT.MMAX) THEN
        ISTEP=2*MMAX
        THETA=6.28318530717959D0/(ISIGN*MMAX)
        WPR=-2.D0*DSIN(0.5D0*THETA)**2
        WPI=DSIN(THETA)
        WR=1.D0
        WI=0.D0
        DO 13 M=1,MMAX,2
          DO 12 I=M,N,ISTEP
            J=I+MMAX
            TEMPR=SNGL(WR)*DATA(J)-SNGL(WI)*DATA(J+1)
            TEMPI=SNGL(WR)*DATA(J+1)+SNGL(WI)*DATA(J)
            DATA(J)=DATA(I)-TEMPR
            DATA(J+1)=DATA(I+1)-TEMPI
            DATA(I)=DATA(I)+TEMPR
            DATA(I+1)=DATA(I+1)+TEMPI
   12     CONTINUE
          WTEMP=WR
          WR=WR*WPR-WI*WPI+WR
          WI=WI*WPR+WTEMP*WPI+WI
   13   CONTINUE
        MMAX=ISTEP
      GO TO 2
      ENDIF
      RETURN
      END
```

Appendix C
SANS Simulation Program

This appendix consists of the SANS simulation program written by Dr. N.R. Bernhoeft and the Author.

```
C123457
C DIC9.FOR  SAS FOR MNSI 001 VERTICAL
C DIC9.FOR 1/05/92 SAS FROM DIC2.FOR 7/11/91
C RESOLUTION DETERMINED BY THE SAMPLE SIZE
C
C W ANGLE 0.02143=1.228DEG IS FOR KI=1,TH=54.74DEG,Q=.035
C OBTAINED BY SETTING 0,0;0,0 FOR BEAM AND CING OUT TH FILTER
      DIMENSION A(-2:2,-2:2),B(-2:2,-2:2),C(-20:20,-20:20),T12A(625)
      OPEN(1,FILE='RES5.DAT')
      N=0
      ZPI=3.1415927
C B2 IS SPREAD.B1 IS ROUGHLY INCIDENT KI. B10 IS INCIDENT KI
      B1=1.0
      B2=.15
      PRINT*,'INCIDENT KI    '
      READ(5,*)B10
      R1Z=6000.
      R3Z=6000.
      PRINT*,'SOURCE SAMPLE  '
      READ(5,*)R1Z
      PRINT*,'SAMPLE DETECT  '
      READ(5,*)R3Z
      PRINT*,'SPIRAL UPPER Q    '
      READ(5,*)SUQ
      PRINT*,'SPIRAL LOWER Q    '
      READ(5,*)SLQ
C      W0=
      W0=(SUQ+SLQ)/(2.*2*B10*SIN(.9553))
C DRB3=SAMPLE THICKNESS MM,DRB4=DETECTOR CELL THICKNESS
C DRB1=SAMPLE WIDTH DRB2=SAMPLE HEIGHT
C DRA=INCIDENT BEAM GRID DRC=DETECTOR ARRAY SPACING
      DRA=3.
      DRB1=1/5.
      DRB2=1./5.
      DRB3=1.
      DRB4=10.
      DRC=10.
C XAXIS FROM N1 TO N2;Y AXIS FROM N3 TO N4
      N1=15
      N2=19
      N3= 10
      N4= 14
      PRINT*,'X MIN(INTEGER)    '
      READ(5,*)N1
      PRINT*,'X MAX(INTEGER)    '
      READ(5,*)N2
      PRINT*,'Y MIN(INTEGER)    '
      READ(5,*)N3
      PRINT*,'Y MAX(INTEGER)    '
      READ(5,*)N4
C I=1,7 GIVES SOME MEASURE OF INCIDENT WAVELENGTH SPREAD
      DO 1 I=1,7
      B1=B10+(I-4)*B2/3
      WB1=EXP(-(B1-B10)*(B1-B10)/(2*.18*B2*B2))
      DO 2 J=-2,2
      DO 3 K=-2,2
      R1X=J*DRA
      R1Y=K*DRA
      SR1=R1X*R1X+R1Y*R1Y
      IF(SR1.GT.64.)GOTO 3
```

```
      DO 4 L=-2,2
      DO 5 M=-2,2
      R2X=L*DRB1
      R2Y=M*DRB2
C      SR2=R2X*R2X+R2Y*R2Y
C      IF(SR2.GT.16.)GOTO 5
      D1X=R2X-R1X
      D1Y=R2Y-R1Y
      R1L=1.+(D1X*D1X+D1Y*D1Y)/(R1Z*R1Z)
C NEXT 4 LINES K-SPACE,VECTOR KI.
      A1=B1/(R1Z*SQRT(R1L))
      B1X=A1*D1X
      B1Y=A1*D1Y
      B1Z=A1*R1Z
      DO 6 JA= N1,N2
      DO 7 KA= N3,N4
      IF(JA.EQ.0.AND.KA.EQ.0)GOTO 7
      R3X=JA*DRC
      R3Y=KA*DRC
      D2X=R3X-R2X
      D2Y=R3Y-R2Y
      R3L=1.+(D2X*D2X+D2Y*D2Y)/(R3Z*R3Z)
C  IF FIX KF=B1 THEN FIXES IT AS ELASTIC;NEXT 4 LINES K-SPACE
      A2=B1/(R3Z*SQRT(R3L))
      B2X=A2*D2X
      B2Y=A2*D2Y
      B2Z=A2*R3Z
C      R12=1.+(D1X*D2X+D1Y*D2Y)/(R1Z*R3Z)
C      T12=SQRT(-2*(R12)+(R1L)+(R3L))
C      N=N+1
C      T12A(N)=T12*57.296
C  NEXT 4 LINES K-SPACE
      Q1X=B2X-B1X
      Q1Y=B2Y-B1Y
      Q1Z=B2Z-B1Z
      QM=SQRT(Q1X*Q1X+Q1Y*Q1Y+Q1Z*Q1Z)
C ERROR IN Q1X= DQ1X;;DQ1Y=DQ1X
      D1M=R1L*R1Z*R1Z
      D2M=R3L*R3Z*R3Z

      D1YZ=D1Y*D1Y+R1Z*R1Z
      D1XY=D1X*D1Y
      D2YZ=D2Y*D2Y+R3Z*R3Z
      D2XY=D2X*D2Y
      D1XZ=D1X*D1X+R1Z*R1Z
      D2XZ=D2X*D2X+R3Z*R3Z
      R1ZX=R1Z*D1X
      R1ZY=R1Z*D1Y
      R3ZX=R3Z*D2X
      R3ZY=R3Z*D2Y
      D2D2=D2X*D2X+D2Y*D2Y
      DQ1X=SQRT((A1*A1*D1YZ*D1YZ*(DRA*DRA+DRB1*DRB1)/(4*D1M*D1M))+
     !          (A1*A1*D1XY*D1XY*(DRA*DRA+DRB2*DRB2)/(4*D1M*D1M))+
     !          (A2*A2*D2YZ*D2YZ*(DRC*DRC+DRB1*DRB1)/(4*D2M*D2M))+
     !          (A2*A2*D2XY*D2XY*(DRC*DRC+DRB2*DRB2)/(4*D2M*D2M))+
     !          (A2*A2*R3ZX*R3ZX*(DRB3*DRB3+DRB4*DRB4)/(4*D2M*D2M))+
     !          Q1X*Q1X*B2*B2/(6*B1*6*B1))

      DQ1Y=SQRT((A1*A1*D1XZ*D1XZ*(DRA*DRA+DRB2*DRB2)/(4*D1M*D1M))+
     !          (A1*A1*D1XY*D1XY*(DRA*DRA+DRB1*DRB1)/(4*D1M*D1M))+
```

```
     !           (A2*A2*D2XZ*D2XZ*(DRC*DRC+DRB2*DRB2)/(4*D2M*D2M))+
     !           (A2*A2*D2XY*D2XY*(DRC*DRC+DRB1*DRB1)/(4*D2M*D2M))+
     !           (A2*A2*R3ZY*R3ZY*(DRB3*DRB3+DRB4*DRB4)/(4*D2M*D2M))+
     !           Q1Y*Q1Y*B2*B2/(6*B1*6*B1))

      DQ1Z=SQRT((A1*A1*R1ZX*R1ZX*(DRA*DRA+DRB1*DRB1)/(4*D1M*D1M))+
     !           (A1*A1*R1ZY*R1ZY*(DRA*DRA+DRB2*DRB2)/(4*D1M*D1M))+
     !           (A2*A2*R3ZX*R3ZX*(DRC*DRC+DRB1*DRB1)/(4*D2M*D2M))+
     !           (A2*A2*R3ZY*R3ZY*(DRC*DRC+DRB2*DRB2)/(4*D2M*D2M))+
     !           (A2*A2*D2D2*D2D2*(DRB3*DRB3+DRB4*DRB4)/(4*D2M*D2M))+
     !           Q1X*Q1X*B2*B2/(6*B1*6*B1))
      DQM=SQRT((Q1X*Q1X*DQ1X*DQ1X/(QM*QM))+
     !          (Q1Y*Q1Y*DQ1Y*DQ1Y/(QM*QM))+
     !          (Q1Z*Q1Z*DQ1Z*DQ1Z/(QM*QM)))
C FILTER ON DQM ie ERROR ON QM BUT SPIRAL PERFECT
      QML=QM-DQM
      QMU=QM+DQM
C      IF(QML.GT.0.035.OR.QMU.LT.0.035)GOTO 7
C FILTER ON DQM ie ERROR ON QM AND ON SPIRAL
      IF(QML.GT.SUQ.OR.QMU.LT.SLQ)GOTO 7

C FOR TWO SPIRALS ;NEXT AT 70.53DEG+54.74DEG/USE ABS(Q1Y) DODGE
      AQ1Y=ABS(Q1Y)
      IF(AQ1Y.LT.1.E-3)GOTO 40
      TH=ATAN((SQRT(Q1X*Q1X+Q1Z*Q1Z))/AQ1Y)
      QTH1=Q1X*Q1X*DQ1X*DQ1X/((Q1X*Q1X+Q1Z*Q1Z)*Q1Y*Q1Y)
      QTH3=Q1Z*Q1Z*DQ1Z*DQ1Z/((Q1X*Q1X+Q1Z*Q1Z)*Q1Y*Q1Y)
      QTH2=(DQ1Y*DQ1Y/(Q1Y*Q1Y*Q1Y*Q1Y))*(Q1X*Q1X+Q1Z*Q1Z)
      DTH=COS(TH)*COS(TH)*SQRT(QTH1+QTH2+QTH3)
      GOTO 41
   40 TH=ZPI/2.
      DTH=0.
   41 THL=TH-DTH
      THU=TH+DTH
C      WRITE(1,10)TH,DTH,Q1X,Q1Y,Q1Z,B1Z
C FILTER ON DTH ie ERROR ON TH ;ANGLE DOWN FROM 001
C (.9553rad=54.74deg)
C .0017rad=0.1deg
C      IF(THL.GT.0.9553.OR.THU.LT.0.9553)GOTO 7
C FILTER ON DTH ie ERROR ON TH AND MOSAIC ON ANGLE DOWN FROM 001
      IF(THL.GT.0.9570.OR.THU.LT.0.9536)GOTO 7
C      PRINT*,'TEST  '
      W=ATAN(-Q1Z/Q1X)
      BB1X=Q1X*Q1X
      DW=COS(W)*COS(W)*SQRT((DQ1Z*DQ1Z/BB1X)+
     !                                (Q1Z*Q1Z*DQ1X*DQ1X/(BB1X*BB1X)))
      WL=W-DW
      WU=W+DW
C      WRITE(6,11)W,DW

C FILTER ON OMEGA ie ANGLE AROUND FROM STRAIGHT THROUGH
C INCLUDES BOTH DW AND MOSAIC
C W=90+.819 deg=PI/2+.01429rad+-.0017rad  THIS LINE CRAP?
      W0L=W0-.0017
      W0U=W0+.0017
C IF SET FOR POSITIVE X SIDE THEN C OUT LINES 30 & 31 AND LEAVE LINES
C 32 & 33
C IF WANT NEGATIVE X SIDE C OUT 32,33 AND LEAVE IN 30,31
C THIS CORRESPONDS TO A ROTATION OF THE SAMPLE ABOUT THE VERTICAL AXIS
C THE ANGLE CAN BE ALTERRED BY HAND TO CORRESPOND WITH SAMPLE
```

```
C ROTATION BY CHANGING W0 AT TOP OF THE PROGRAM
C  30 W0LN=ZPI-W0L
C  31 W0UN=ZPI-W0U
  32 W0LN=ZPI+W0L
  33 W0UN=ZPI+W0U
     IF(Q1X.GT.0.)GOTO 20
     IF(Q1X.LT.0.)GOTO 23
  20 IF(WL.GT.W0U.OR.WU.LT.W0L)GOTO 7
C     PRINT*,'TEST1 '
     GOTO 24
  23 W=ZPI+W
     WU=W+DW
     WL=W-DW
     IF(WL.GT.W0UN.OR.WU.LT.W0LN)GOTO 7
C     PRINT*,'TEST2 '
     GOTO 24
  24 ZDF=ZDF+1
C     C(JA,KA)=C(JA,KA)+1
     C(JA,KA)=C(JA,KA)+WB1
C  24 WRITE(1,11)QM,TH,W,R3X,R3Y,R3Z
   7 CONTINUE
   6 CONTINUE
   5 CONTINUE
   4 CONTINUE
   3 CONTINUE
   2 CONTINUE
   1 CONTINUE
C     WRITE(1,11)ZDF,ZDF
     DO 8 JA=N1,N2
     DO 9 KA=N3,N4
     WRITE(1,12)JA*1.,KA*1.,C(JA,KA)
   9 CONTINUE
   8 CONTINUE
  10 FORMAT(1H ,6E11.3)
  11 FORMAT(1H ,2E14.6)
  12 FORMAT(1H ,3E14.6)
  13 FORMAT(1H ,3E14.6)
     STOP
     END
```

Appendix D
Design and Development of a High Pressure Cell and Uniaxial Stress Device for Magnetic Measurements

D.1 Introduction

High pressure techniques are a powerful and underused tool for studying phase transitions and physical properties of solids in terms of interatomic distances. Within magnetic measurements, generally the two variables used are magnetic field and temperature with temperature range of 4.2 - 1400K and fields of 0 - 120kOe easily accessible. Thus if magnetic measurements under pressure or uniaxial stress could be developed, the scope for work is endless.

Another and more specific motive for development of magnetic measurements under pressure were the elastic neutron scattering results on MnSi at high pressure (S. Brown (1990)) which suggest strange behaviour and possible lowering of the transition temperature for pressure in the regime 10kbar.

The first considerations in any pressure cell design are (i) the type of measurements to be made, (ii) the size of the cell and (iii) the pressure required.

As experience in magnetic measurements and operation of a VSM had been obtained it was decided to perform magnetic measurements under pressure, developing the Durham VSM to do this. One of the advantages of the 180° double throw vibration mechanism apart from low noise, is the high inertial loading, in affect allowing vibration of a pressure cell.

To enable measurements to be made down to 4.2K, the cell had to be designed to fit into the Oxford CF1200 cryostat.

Finally, the pursuit of magnetic measurements under pressure was regarded as a long term development so initial pressure requirements were set in the order of kilobars.

D.2 Types of Pressure Cell

There are many types of pressure cell, each with numerous variations but only clamp type and diamond anvil cells were considerred due to their simplicity and portability. With a clamp type cell, the system is pressurised and this pressure clamped or locked in. A bore into which a piston is driven allows application of a uniaxial stress or hydrostatic pressure (by compression of a liquid medium) to a sample with the tightening of a locking nut maintaining the applied force on removal of the piston. This type is typically used for pressures upto 20kbar.

Diamond-anvil cells involve very small sample spaces and much higher pressures (in fact below 40kbars pressures are not usually known or uniform). The sample is pressurised between two diamond pieces hence the name. Due to the pressure range required, its simplicity and the desire for large sample space, a clamp cell was designed and built.

The major problems with magnetic measurements under pressure using a VSM are associated with the cell itself. Since the mass of the cell is upto 1000 times that of the sample, the size and reproducibility of the signal from the cell limit sensitivity. However, the system does have the one advantage that the sample space is entirely enclosed.

D.3 Cell Geometry and Analysis

The most common geometry used for pressure apparatus is that of the cylinder and in analysis can be considerred to be a simple, elastic, thick walled cylinder (Sherman and Stadtmuller(1987)). As the pressure increases inside the cell, the stress in the walls has radial and tangential components that give rise to a single shear stress τ which is a function of radial position (figure A4.1) and largest at the bore of the cell.

As the internal pressure is increased, all the stresses increase linearly until the resulting strain exceeds the elastic limit at some point. For thick wall cylinders, the commencement of permanent distortion at the bore comes from the shear stress reaching the allowable limit τ^* which is never greater than $\frac{\sigma}{\sqrt{3}}$ where σ is the yield stress of material used. The highest pressure which a simple cell can support elastically is

$$P_e = \frac{\tau^* K^2}{1 - K^2} \tag{D.1}$$

where K is the ratio of the inner to the outer radii $\frac{r_i}{r_o}$. This limit is not related to the bursting pressure. This condition that the boundary between idealized ($\tau = \tau^*$) overstrained material and elastic material has been pushed out to the outer circumference of the cylinder

$$P_i^* = \tau^* ln K^2 \tag{D.2}$$

The ultimate bursting pressure can be expected to exceed this value although it will cause a relatively large distortion of the cylinder.

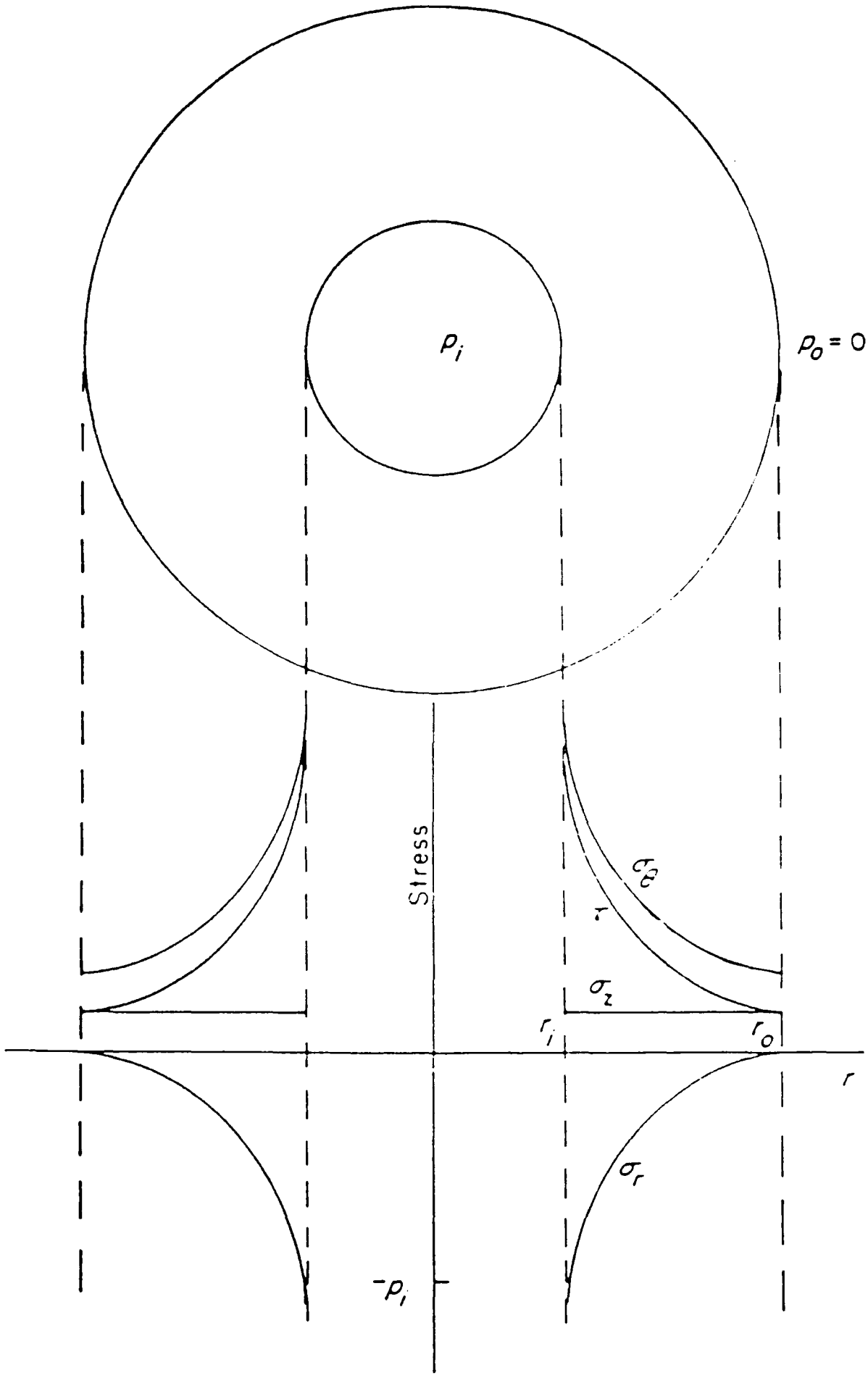

Figure A4.1 The stress distributions within an internally pressurised thick-wall cylinder as a function of radial position. (After Sherman and Stadtmuller (1987)).

D.4 Choice of Material for the Cell

The maximum internal pressure a cylinder can withstand is dependent on both the value K and more importantly σ_{max}. (In principle it will always be possible to reach a particular pressure by using sufficiently small K however there is little advantage in using a value $K < \frac{1}{3}$ since the increase in mass far outweighs the additional strength, important considerations when the cell is to be cooled and vibrated.) Obviously a strong material is necessary, but other factors include ease of machining, small magnetisation so as not to swamp the signal from the sample and a relatively high resistance at low temperatures to restrict the production of eddy currents.

The cell was made from Beryllium Copper (BeCu) supplied by Brushwellman Ltd., Reading, infact Brush Alloy 25. BeCu contains less than 2% Be but this has a large affect on some properties of the Cu, particularly its strength. It is supplied in a half-hard condition enabling ease of machining and then is heat treated (2 hours at $315°C$) which dramatically increases its strength. It also has a high thermal conductivity, reducing the possibility of temperature gradients across the cell and a low specific heat which is advantageous for cooling purposes.

Unfortunately BeCu has magnetic binders Fe, Co and Ni within the lattice however this is only 0.6% by weight and tests showed the signal from these were not significant and also reproducible. Other ways around the problem are include using BeCu without magnetic binders (Foner (1974)) or alteration of coil geometry and use of a 'dummy cell' if residuals were too large.

D.5 Strength of the Cell

Since the pressure cell was required to work at low temperatures. it had to fit down an Oxford CF1200 cryostat thus limiting the external diameter. The internal diameter of the cell was fixed at 4mm and the external at 12mm so that after heat treatment the maximum pressure the cell could support elastically was 6.5kbar. The design of the pressure cell is shown in figure A4.2. (N.B. Heat treatment of the half-hard BeCu is accompanied by a slight volume change of about 0.5 volumetric %.)

D.6 Strengthening the Cell

The maximum pressure which can be applied to a sample and supported elastically by the cell can be increased by putting the BeCu at the bore in a state of compression. One technique for achieving this is autofrettage.

Autofrettage is used to increase the elastic operating pressure of a cylinder. The cell is intentionally over pressurised beyond the elastic breakdown pressure so that non-uniform plastic flow occurs beginning at the bore extending radially outward to a radius that depends on the applied pressure. This leaves the unloaded cylinder

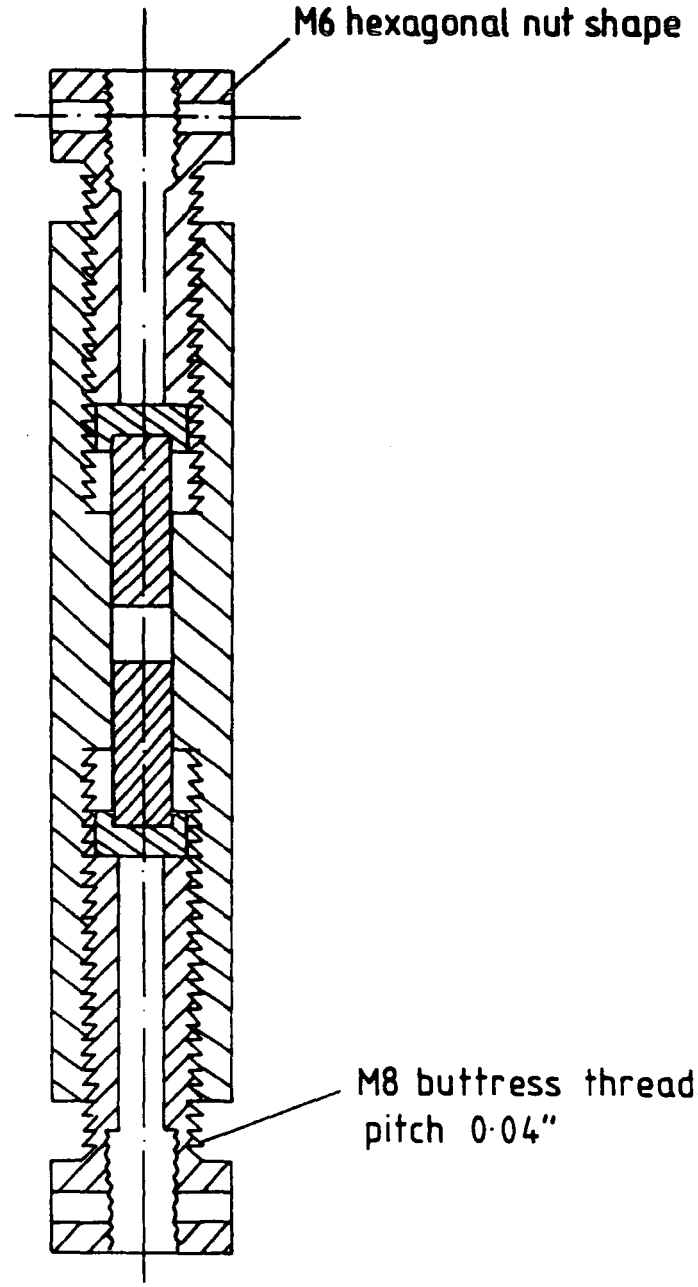

Figure A4.2 Design of the pressure cell. The cell is made of heat treated BeCu and is vibrated together with the sample on the V.S.M. Scale 2:1.

under tangential compression at the bore and permits elastic operation up to the pressure that was applied during autofrettage. The pressure required to autofrettage a cylinder is upto twice the elastic range of the same cylinder before this process. (N.B. The autofrettage process produces changes in the dimension of the cylinder but were calculated to be negligible in this case.

D.7 Pressure Vessel Closures

In a clamp type device, the locking nut is used to clamp the applied pressure and the stresses and their distributions on the threads are complicated by numerous factors. The first thread picks up the load initially and as it deforms elastically, it transfers the load to the next thread and so on until the entire thread system is loaded. With conventional Acme thread design machined into the wall of the vessel, the first few threads carry the majority of the load and under cyclic pressure loading most thread failures occur in this region as shown in figure A4.3.

To overcome the numerous problems associated with the Acme thread, one of Buttress form was used. The contacting flank of the thread which takes the thrust is so nearly perpendicular to the tread axis that the radial component of the trust is reduced to a minimum. Because of this small radial thrust, the form of the thread is advantageous when involving exceptionally high stresses along the thread axis in one direction only. The use of Buttress threads also results in a more uniform stress distribution along all the threads (figure A4.3).

Finally the nut has an M6 hexagonal head as well as a hole for a tommy bar offering two seperate methods of tightening to clamp the applied force.

D.8 Temperature Induced Stress

The pressure cell was designed to fit into the CF1200 Oxford cryostat and be used on the VSM at temperatures as low as 4.2K. However its heating or cooling produces temperature gradients which in turn set up stress gradients. With the bore at a higher temperature than the outside, thermal stresses cause a lower resultant stress and the reverse occurs for the bore at lower temperatures. The magnitude of stresses induced in BeCu is 3.5bars/K (which compares favourably to that of steel at 45bars/K) and the high thermal conductivity reduces these to a minimum. However care was taken when cooling or heating the cell.

The cell behaves as a large thermal mass and therefore a temperature sensor attaching directly to it. A calibrated AuFe(0.07%)Cr thermocouple was used.

D.9 Homogeneous Pressure Transfer

Hydrostatic pressure is transferred to the sample by compression of a liquid medium and a sealing arrangement is thus necessary. There are many methods for sealing

a cell at high pressure and an important consideration in the design is that they have to work at low pressures while the cell is being pressurised, as well as at high pressures. The basic principle of most seals is that an elastic material must be compressed to a higher pressure than the fluid that is being confined.

The most important characteristic of any pressure transmitting fluid is that it should be hydrostatic to the maximum pressure required in the experiment. To prevent crystallisation of the fluid on freezing, a mixture of liquids is used, often 1:1 n-pentane:isopentane which is hydrostatic to 70kbar.

The cell was designed to contain a 'teflon-cup' seal, first developed by Hamann and Teplitzky (Hamann and Teplitzky (1956)). This system is descibed in detail together with 1:1 n-pentane:isopentane as hydrostatic medium by Delaplace (Delaplace et. al. (1976)). Given that the cap will seal only if the pressure in the teflon is greater than the liquid, it is necessary to calculate the pressure when designing the cap. The pressures turn out to be simple functions of the ratios of the lengths, diameters and compressibilities of the fluid and teflon.

D.10 Uniaxial Stress Device

When measurements were made under uniaxial stress, the BeCu plunger in the central bore attaches directly to the sample. The ends of the pluger were machined flat and sample edges were also prepared carefully.

D.11 Pressure Measurement

One of the few advantages of using a VSM for performing magnetic measurements under pressure is that the sample space is entirely enclosed. In order to maintain this, the system was designed to measure the pressure contained within the cell in terms of expansion of the outside surface using a strain gauge. A manganin coil could be used as a primary sensor to calibrate the strain gauge.

D.12 Pressure Transfer Device

A steel vice was designed to be incorporated into a ten tonne press. The cell is centrally held whilst a pluger applies pressure to the sample space. The locking nut is then tightened to clamp the force. The most critical time for a cell when considering failure is the pressurising and in order to provide protection for the user, the cell is entirely enclosed by steel surrounds.

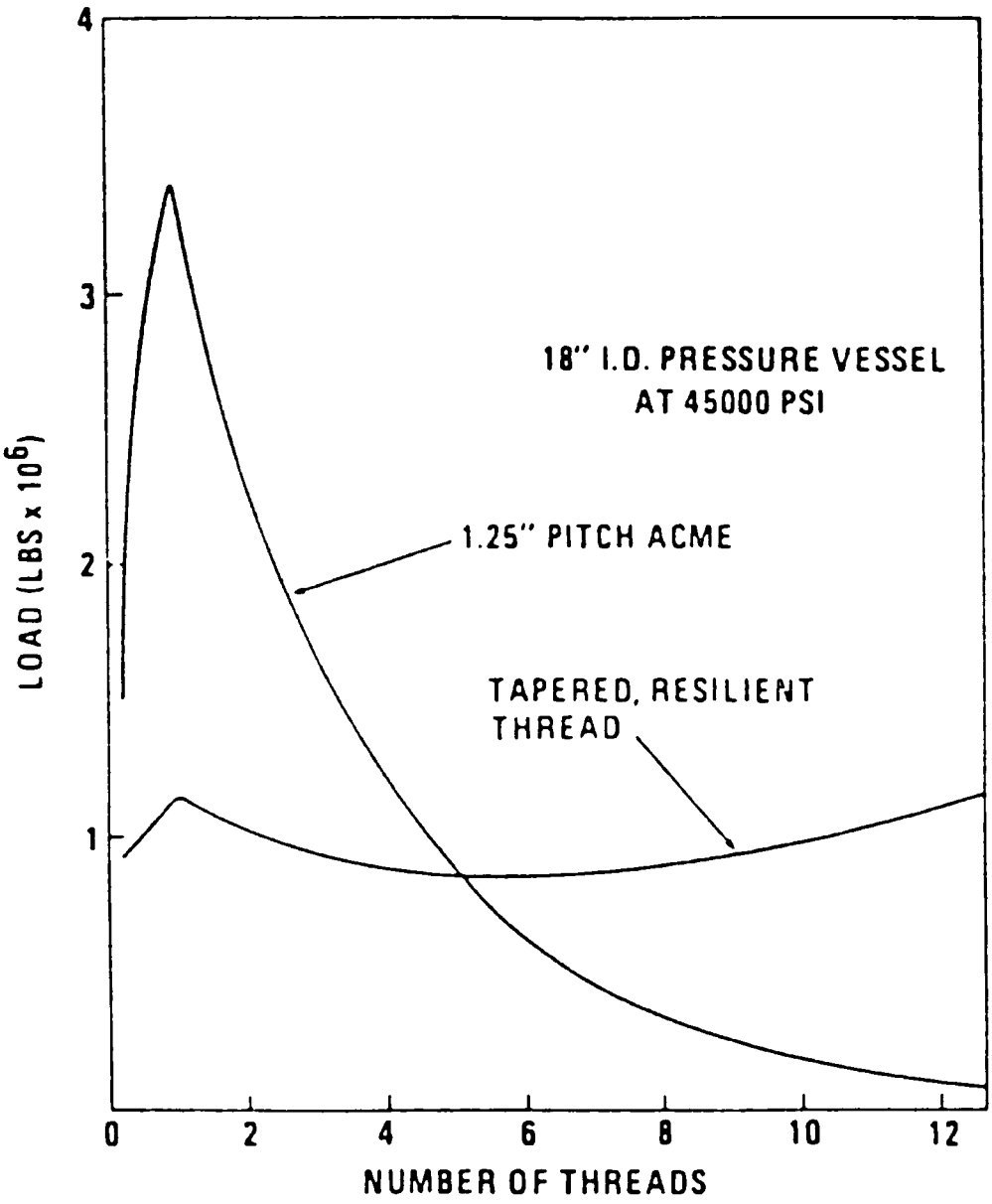

Figure A4.3 Load distribution in conventional thread closure and in a tapered Buttress thread.

D.13 Magnetic Measurements made using the BeCu Pressure Cell

D.13.1 Unpressurised measurements at room temperature

Figure A4.4 shows the magnetisation of the BeCu pressure cell at room temperature. In order that magnetic measurements could be performed under pressure, this signal has to be reproducible. The voltage and hence magnetisation appears to be initially diamagnetic and then saturates however the reason for this is that the lockin amplifier was 'phased' on the induced voltage from a 0.0737g piece of nickel put in the pressure cell. When a residual measurement was recorded without the nickel, there was and 'out of phase' signal on the lockin suggesting that this did not correspond to the 'magnetic centre' of the cell. Hysteresis exists and is evidence of the magnetic binders in the BeCu. Comparison of the signal from the cell residual and cell containing the nickel are shown in figure A4.5 at room temperature.

D.13.2 Unpressurised measurements made at lower temperatures

Similar residual measurements were made at lower temperatures and are shown in figure A4.6. From this it is evident that not only the gradient of the residual but also the amount of hysterisis in low fields are both sensitive to changes in temperature. Figure A4.7 shows the magnetisation of nickel recorded in the pressure cell as a function of field at 80K.

D.13.3 Low temperature magnetic measurements made under pressure

In order to investigate the magnetic response of the pressure cell as a function of pressure and temperature, a sample of $YBa_2Cu_3O_{7-\delta}$ (made by Mr. C.M. Friend (92% dense, T_c = 92K)) was ground into a powder and 0.121g put into the sample space of the pressure cell. Klotz *et al.* (1991) have made a.c. susceptibility measurements on a single crystal of $YBa_2Cu_3O_{7-\delta}$ under hydrostatic pressure upto 13GPa. The hydrostatic pressure was applied to the sample using a diamond-anvil cell loaded with liquid helium. The superconducting transition temperature of the crystal initially increases at a rate of $0.65 \pm 0.15 KGpa^{-1}$ before passing through a maximum at 4GPa. This pressure regime is far greater than that exerted by the BeCu cell (1GPa=10kbar) and since magnetisation is a bulk volume measurement, then no variation in the magnetisation of $YBa_2Cu_3O_{7-\delta}$ was predicted using the BeCu cell. This enabled the magnetisation of the BeCu cell to be studied as a function of applied pressure and temperature. A powder was used so that the pressure within the sample would be approximately homogeneous without requiring a pressure transfer medium or seal. The force was applied to the sample via the steel vice

using a ten tonne press, the pressure exerted being displayed on a dial and recorded at room temperature, the locking nut then being tightened.

Figure A4.8 shows the results obtained at 80K with the locking nut only hand tight on the pressure cell. The cell was cooled in a field of less than three gauss to prevent flux penetrating the sample. The results obtained are typical of a 'high T_c' polycrystalline sample and can be interpreted in terms of flux penetration and trapping in the sample via Bean's model (1964). Below the lower critical field B_{c1}, magnetic flux only penetrates into a surface layer. The bulk of the superconductor excludes all the applied field and behaves as a perfect diamagnet until the field at the surface reaches B_{c1} . Above the lower critical field the magnetic field penetrates the specimen in the form of quantised flux lines (fluxons), each containing a magnetic flux quantum $\frac{h}{2e}$. The superconductor loses its diamagnetic behaviour and its magnetisation decreases. As the field is reversed, hysterisis is observed and can be explained in terms of Bean (1964) through his 'Critical State Model'.

Figures A4.9 and A4.10 show the same measurements, but performed after pressurising the cell to 1 and 2kbar at room temperature. Fig-a consists of the raw data together with BeCu cell residual at 80K while fig-b is the data with the residual subtracted. The shape of the hysterisis curve is identical to that recorded at ambient pressure in the cell as expected. However, as the pressure is increased (see for example figure A4.11: pressure set at room temperature 4kbar) although the low field properties (less than 1kOe) of the magnetisation remain similar, the high field susceptibility increases with pressure, i.e. there is an increasing paramagnetic component. Figure A4.12 shows the magnetisation data recorded at 95K (i.e. above the transition temperature of the superconductor) for various pressures applied at room temperature and clamped with the 'locking nut'. From this it is evident that the increase in paramagnetic component with pressure is dramatic and probably a characteristic of the BeCu used and not the superconductor. It is also apparent that the low field properties of the BeCu cell vary with pressure as the low field 'kink' observed about zero field at ambient pressure reduces and disappears at a pressure of 3kbar (applied at room temp.).

In order to overcome this problem, the magnetisation recorded at 95K and at a particular pressure was used as a residual measurement for the remaining data recorded at lower temperatures but the same initial pressure. Figures A4.13 - A4.16 show the results of this obtained for ambient, 1, 2 and 4kbar respectively at 85K. From these it is evident that using this technique the results are again typical of a polycrystalline 'high T_c' superconductor, very similar to those obtained by subtracting the ambient pressure cell residual. However, the results obtained at lower presssures, particularly ambient and 1kbar have too large paramagnetic components, particularly noticable at high fields.

Initially the magnetisation of the cell does not alter with pressure (for pressures of and below 1kbar) and the residual is best represented by the true unpressurised cell residual, recorded at the same temperature. Using measurements taken at 95K i.e. above the transition temperature of the superconductor as a residual at low pressures result in the data having too large a paramagnetic moment, again particularly evident at high fields ($> 1kOe$). The reason for this is that the actual

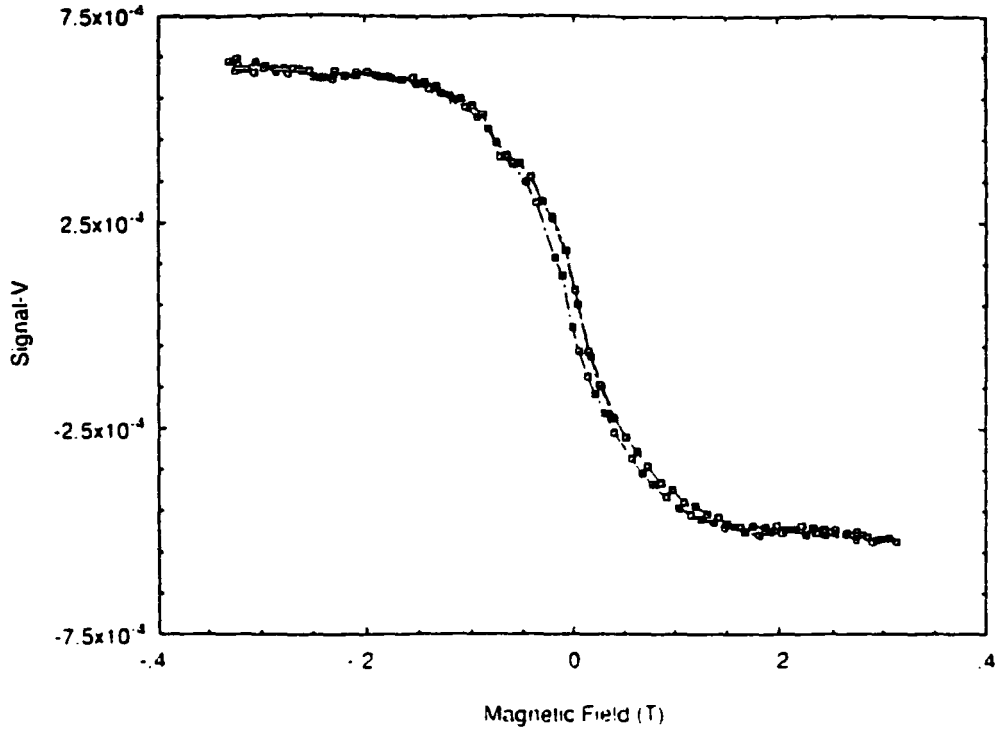

Figure A4.4 BeCu cell residual recorded at room temperature. The lockin amplifier was 'phased' when the cell contained a nickel sample.

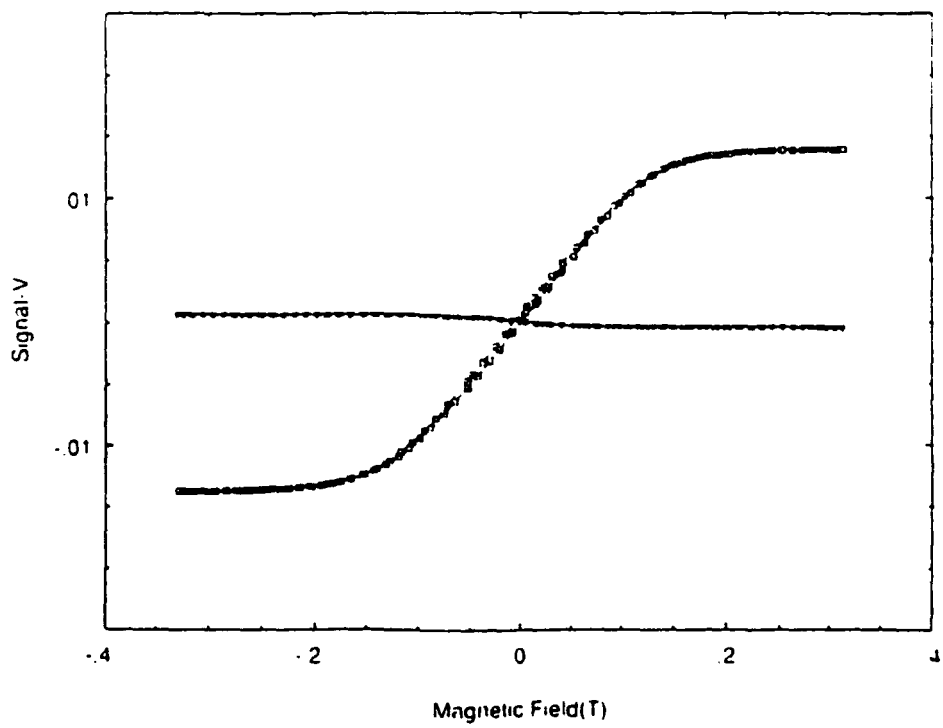

Figure A4.5 The signal obtained from 0.0737g of nickel in the BeCu cell (unpressurised) at room temperature together with the cell residual.

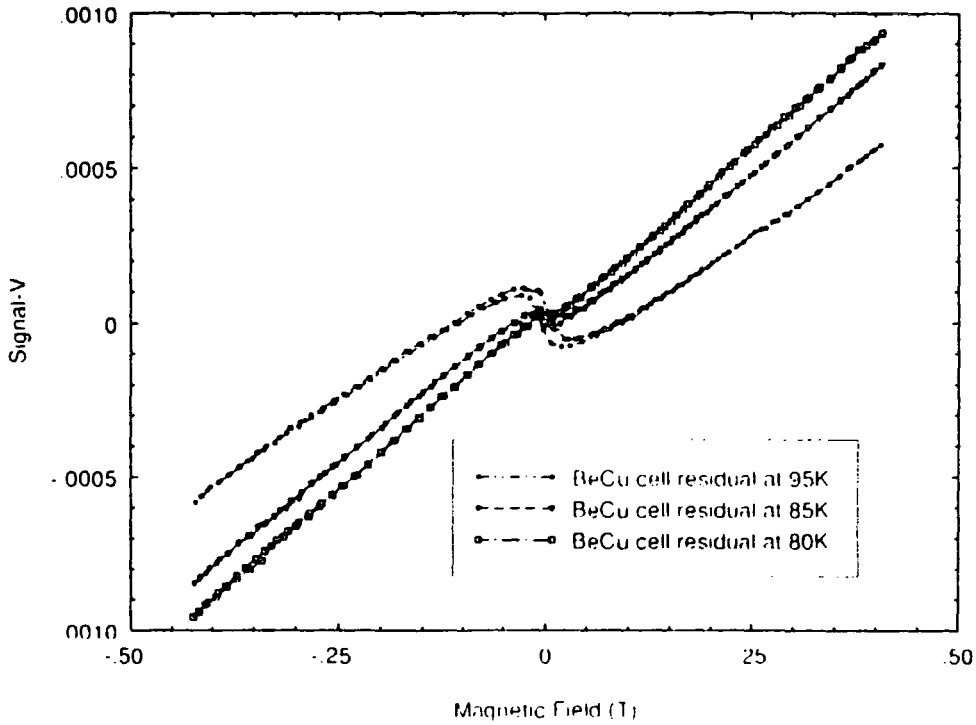

Figure A4.6 The signal obtained from the BeCu cell at 95K (circles), 85K (triangles) and 80K (squares).

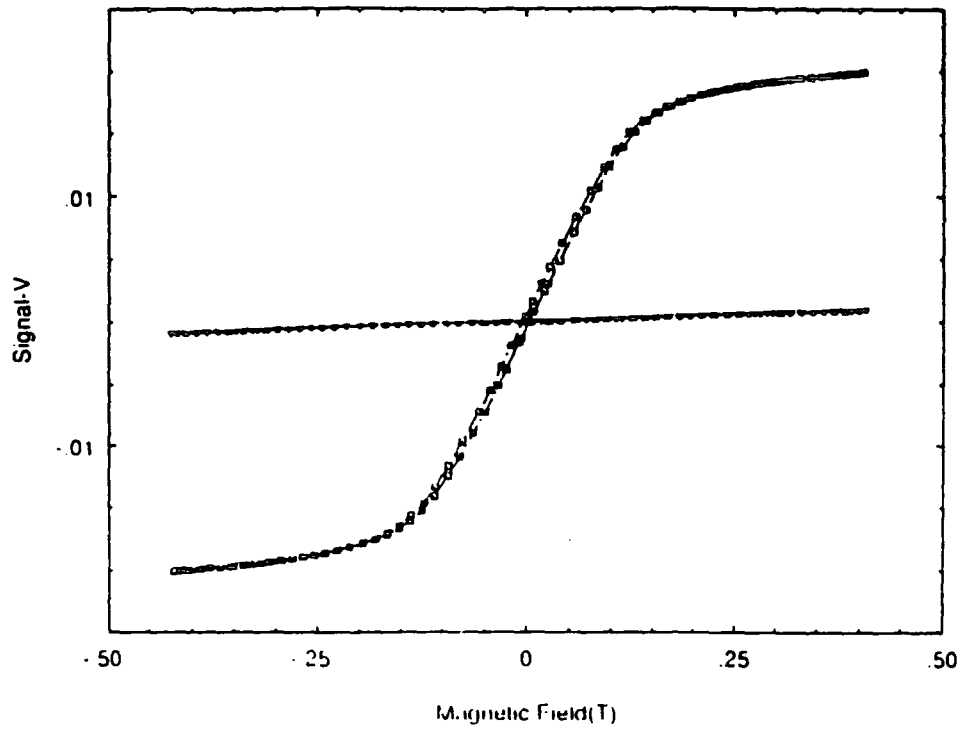

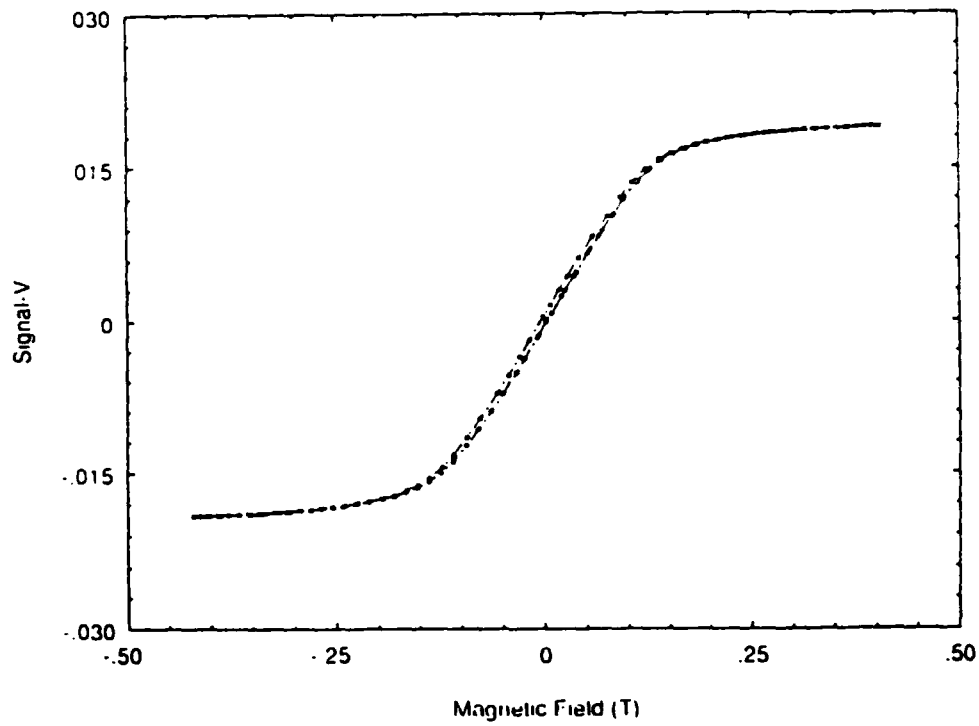

Figure A4.7 (a) The signal obtained from 0.0737g of nickel in the BeCu pressure cell (unpressurised) at 80K together with the cell residual at that temperature. (b) The corrected signal from 0.0737g of nickel with the cell residual subtracted.

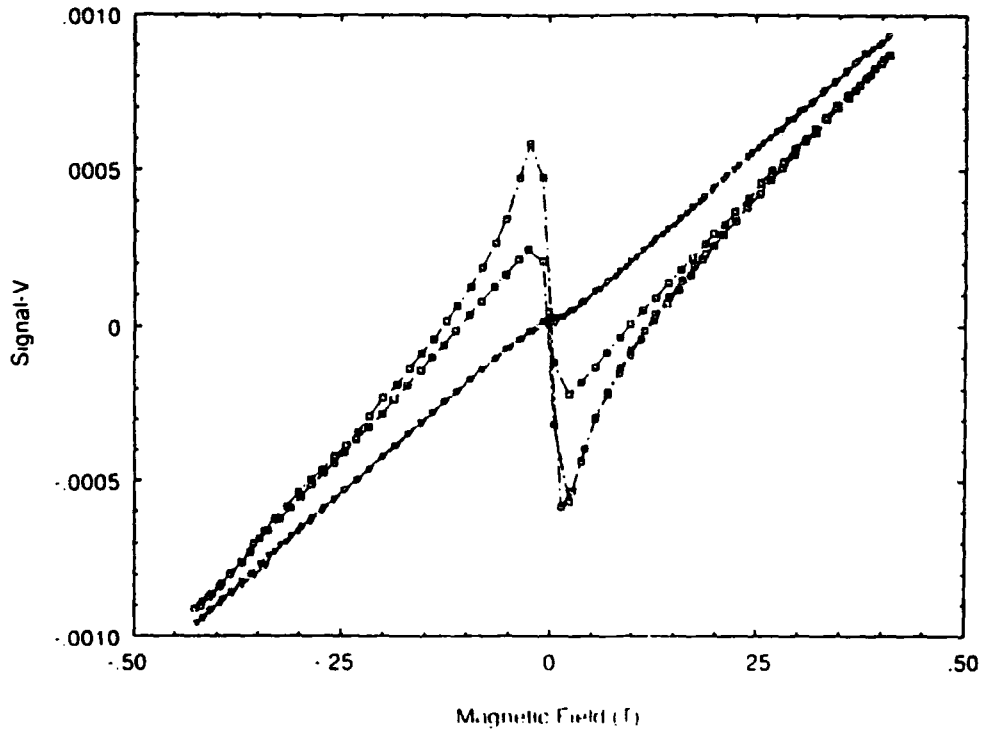

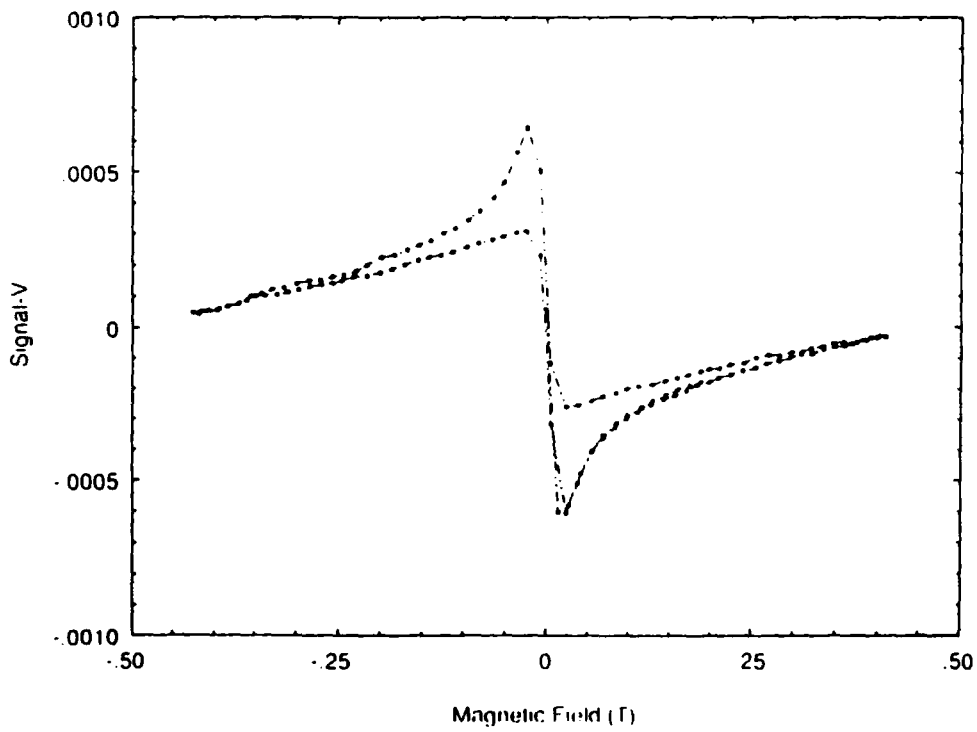

Figure A4.8 (a) The signal obtained from 0.121g of 'YBCO' in the BeCu cell at 80K (squares), where the cell had been pressurised 'hand tight' at room temperature before cooling, together with the unpressurised BeCu cell residual (triangles), at that temperature. (b) The corrected signal from the 'YBCO' at 80K with the unpressurised BeCu cell residual subtracted.

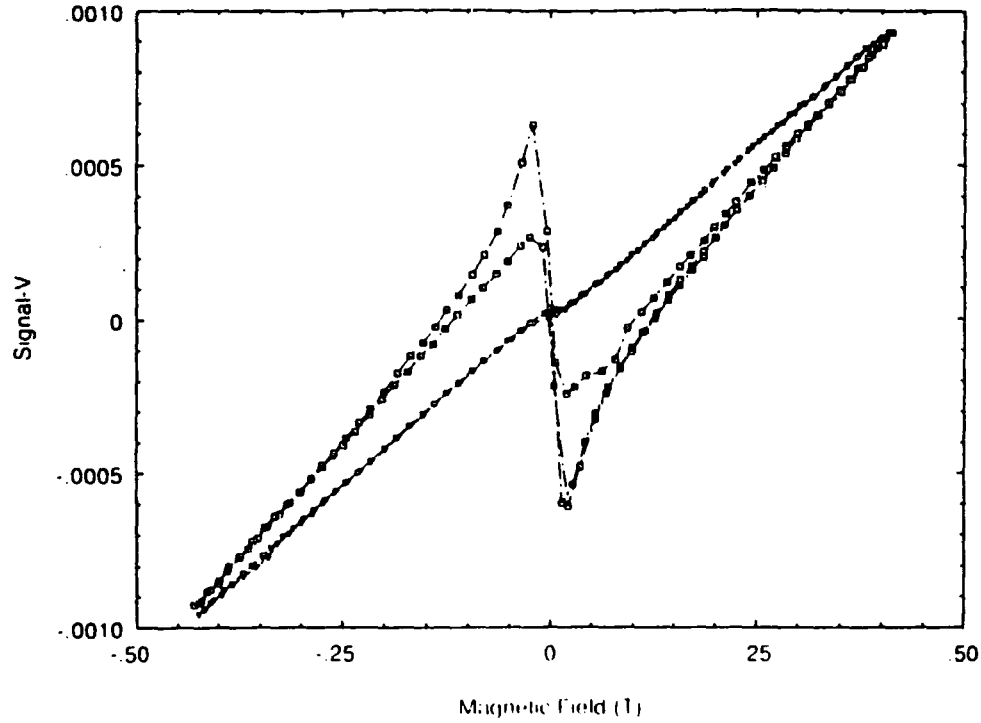

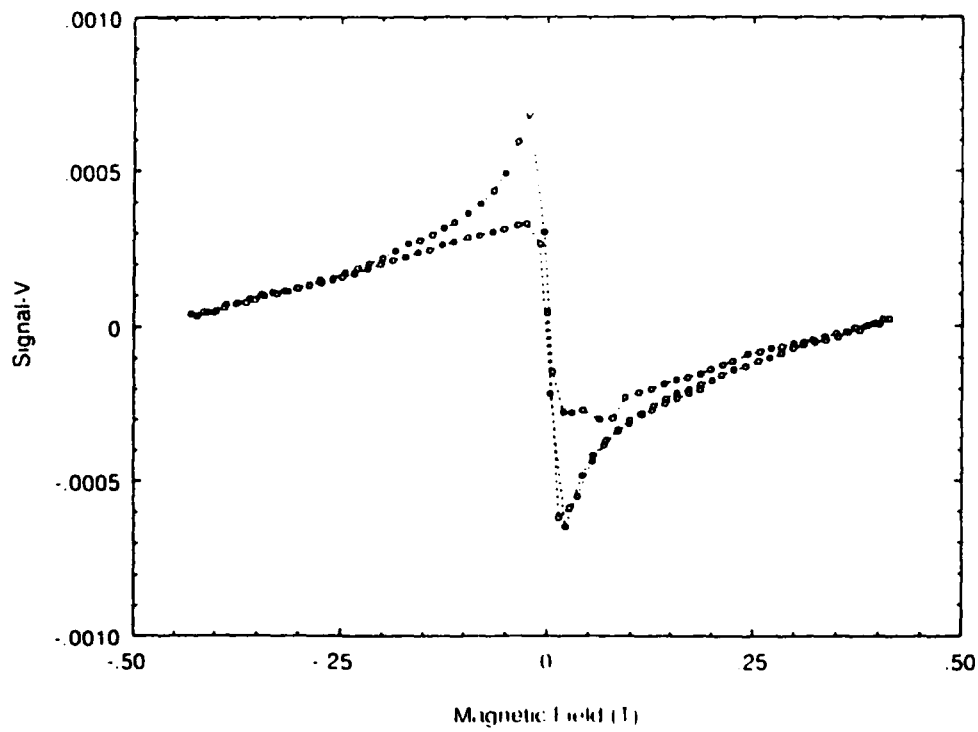

Figure A4.9 (a) The signal obtained from 0.121g of 'YBCO' in the BeCu cell at 80K (squares), where the cell had been pressurised to 1kbar at room temperature before cooling, together with the unpressurised BeCu cell residual (triangles), at that temperature. (b) The corrected signal from the 'YBCO' at 80K with the unpressurised BeCu cell residual subtracted.

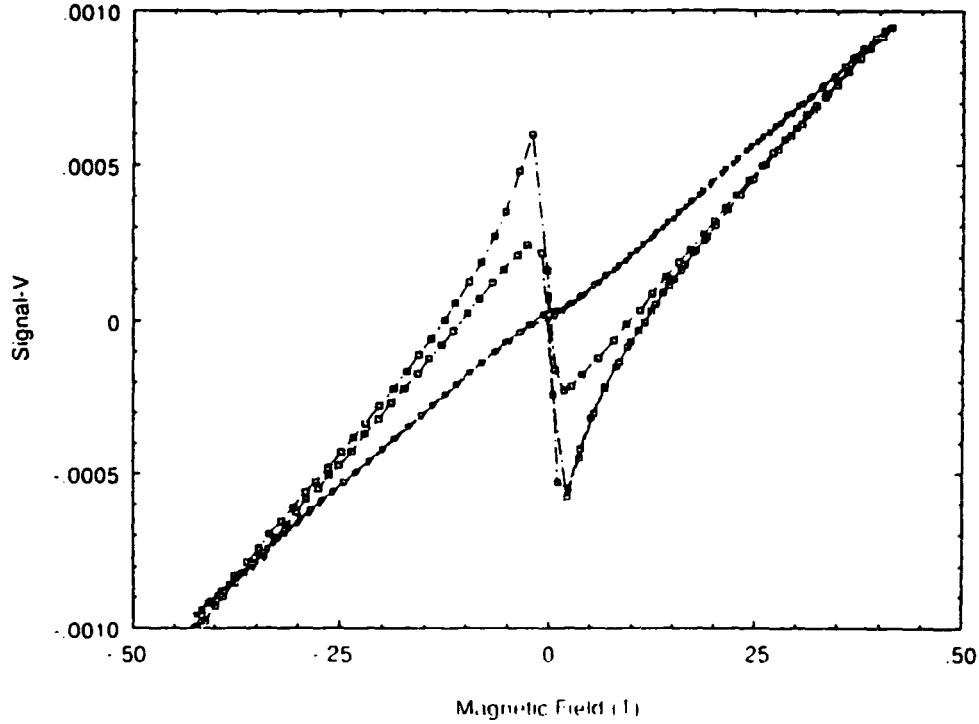

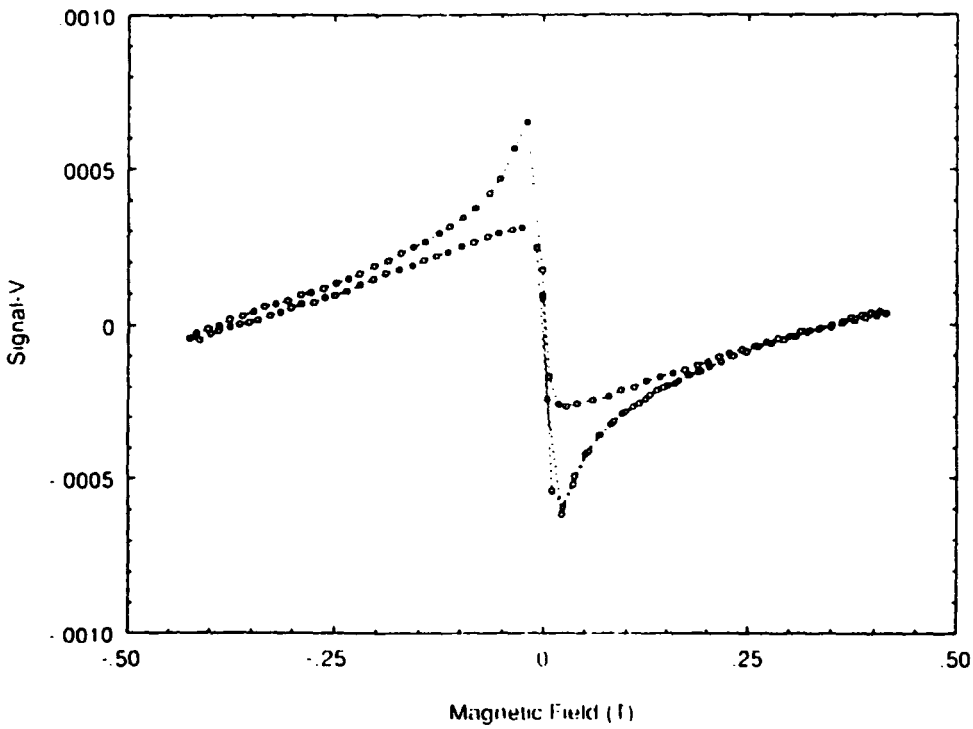

Figure A4.10 (a) The signal obtained from 0.121g of 'YBCO' in the BeCu cell at 80K (squares), where the cell had been pressurised to 2kbar at room temperature before cooling, together with the unpressurised BeCu cell residual (triangles), at that temperature. (b) The corrected signal from the 'YBCO' at 80K with the unpressurised BeCu cell residual subtracted.

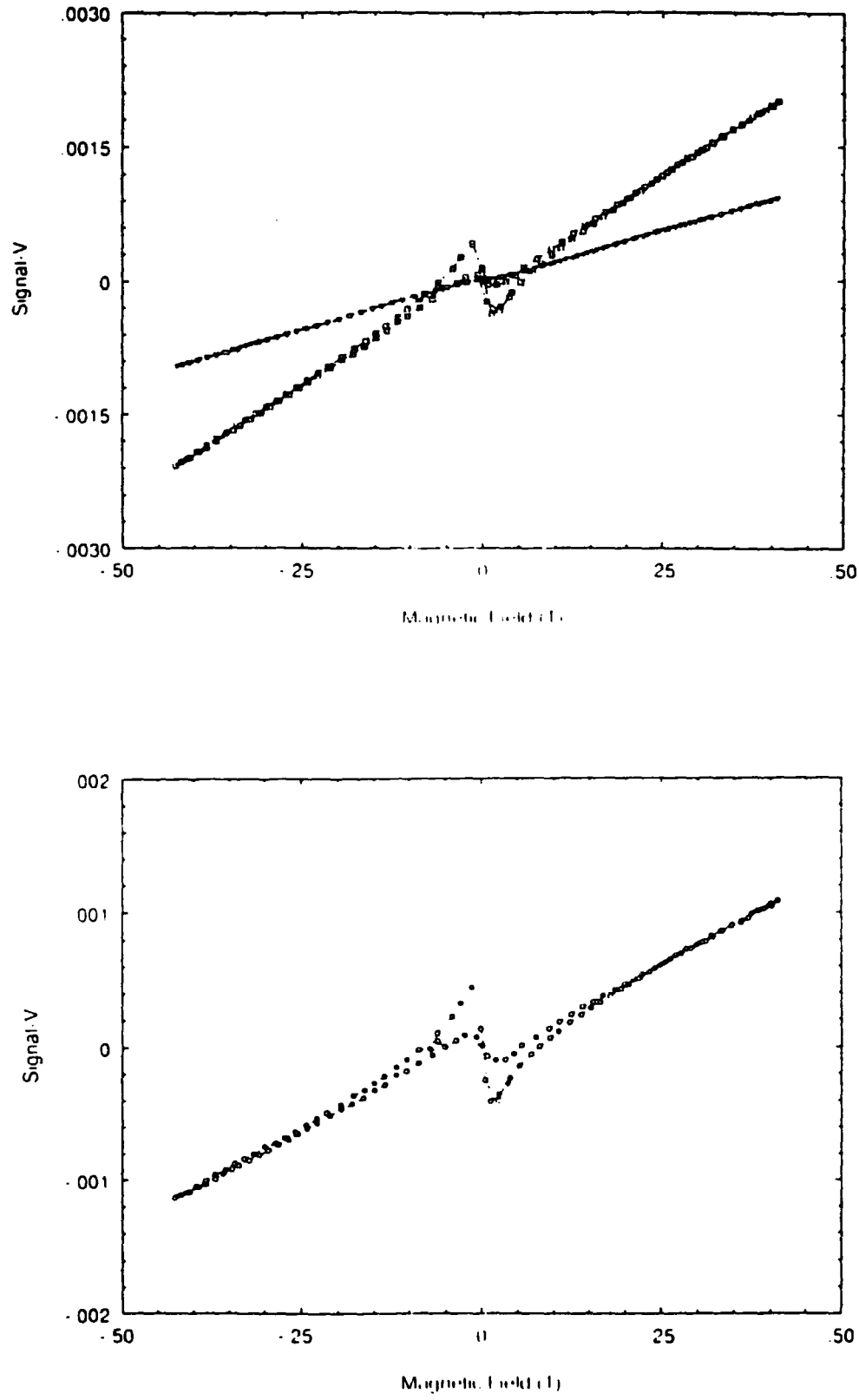

Figure A4.11 (a) The signal obtained from 0.121g of 'YBCO' in the BeCu cell at 80K (squares), where the cell had been pressurised to 4kbar at room temperature before cooling, together with the unpressurised BeCu cell residual (triangles), at that temperature. (b) The corrected signal from the 'YBCO' at 80K with the unpressurised BeCu cell residual subtracted.

data is taken at a lower temperature (infact 10K lower) where the paramagnetic component of the magnetisation from both sample and cell will be greater. As the pressure within the cell is increased, the paramagnetic component of the magnetisation of the cell increases. When the unpressurised BeCu cell residual is subtracted, it gives the impression that the sample has too large a paramagnetic component. For pressures of 2kbar and above, this affect is greater than that of the increasing paramagnetic component due to reduction in temperature so the residual is better represented by the magnetisation of the sample and cell at that particular pressure but at a temperature of 95K.

Naturally the fact that the magnetisation of BeCu cell varies so dramatically with temperature and pressure is a great disappointment and sets limitations on the usefulness of the cell. From figure A4.12 it is evident that the low field 'kink' in the magnetisation of the BeCu cell, observed at low applied pressures disappears as well as the paramagnetic component increasing as the pressure is increased in the cell. However, a combination of using the magnetisation of the pressurised cell but at a higher temperature, coupled with the assumption of Curie-Weiss behaviour of the BeCu enables the problem to be overcome though this is not entirely satisfactory. Despite this, the cell was able to withstand applied pressures of upto 6kbar and close inspection of the cell afterwards showed no sign of damage.

D.14 Further Developments

The next suggested development is application of a strain gauge to the cell, in order to measure the applied pressure within the cell and study how it varies with temperature. From figure A4.12, it is evident that for applied pressures of 2kbar and above, the icrease in the paramagnetic component of magnetisation is approximately linear with increasing pressure apart from 3kbar. The reason for this may have been the fact that although the press applied 3kbar at room temperature, the locking nut may not have been tightened enough on the cell to maintain this pressure on the sample. In order to enable measurement of the pressure applied to the sample, application of a strain gauge to the BeCu will enable the resulting deformation of the cell and hence internal pressure to be measured. Variation of this pressure with cell temperature could then also be investigated. Following this, development of sample enviroment and sealing to apply hydrostaic pressure to the sample could commence. Because of the success of the cell to withstand applied pressures, the production of a further cell with same design but made of 'nonmagnetic steel' is recommended in an attempt to discover a more suitable material where magnetic properties are not so pressure dependant.

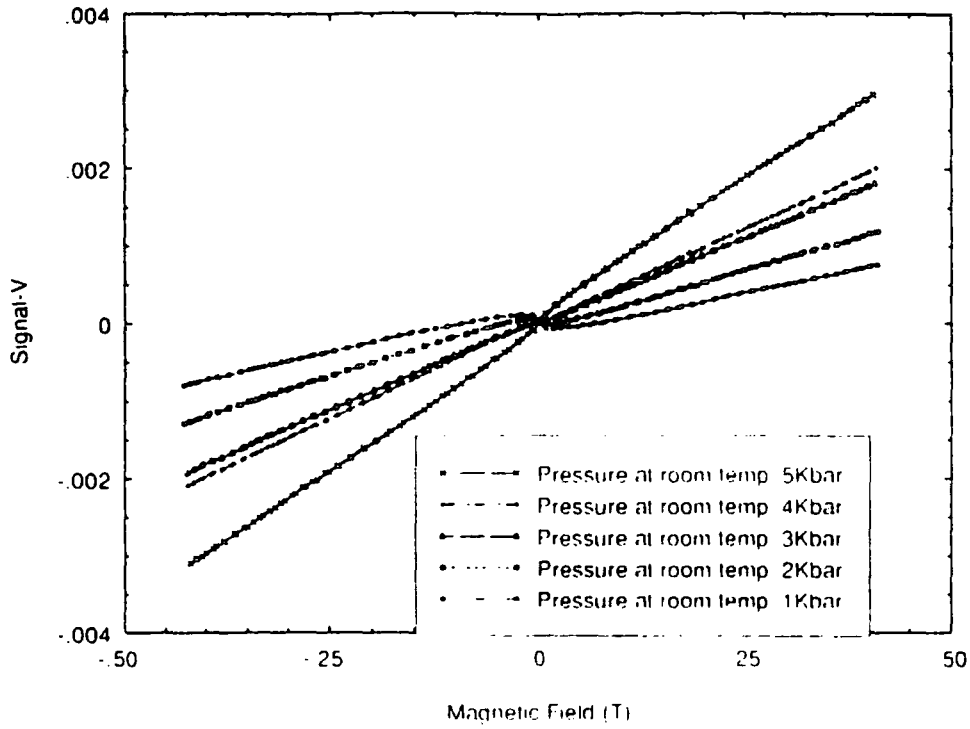

Figure A4.12 The signal obtained from 0.121g of 'YBCO' in the BeCu pressure cell at 95K (i.e. above T_c) after application of various pressures at room temperature.

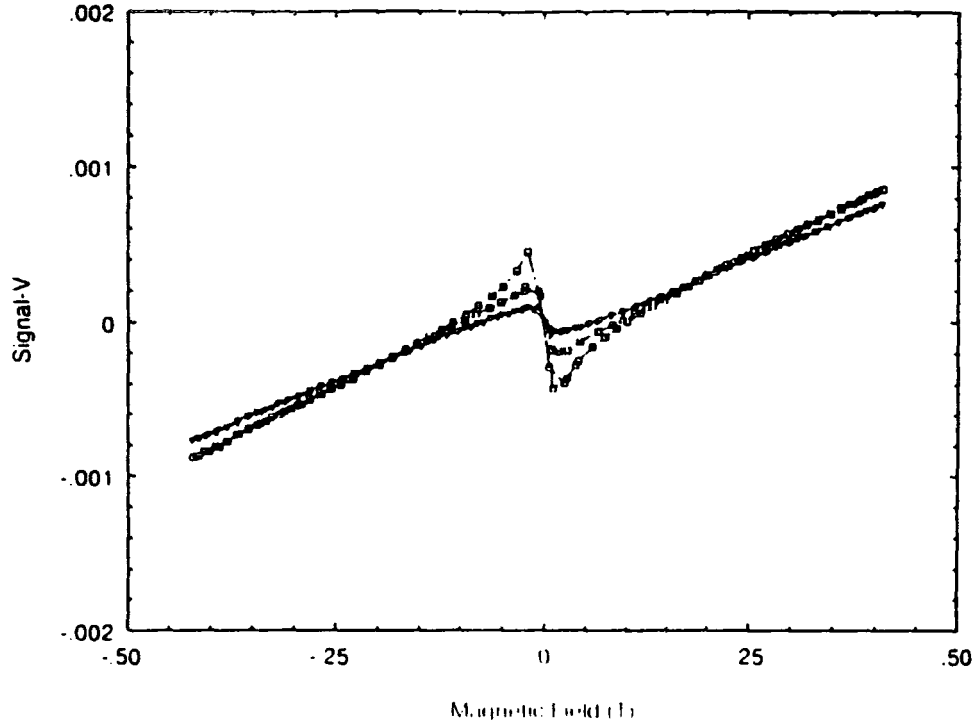

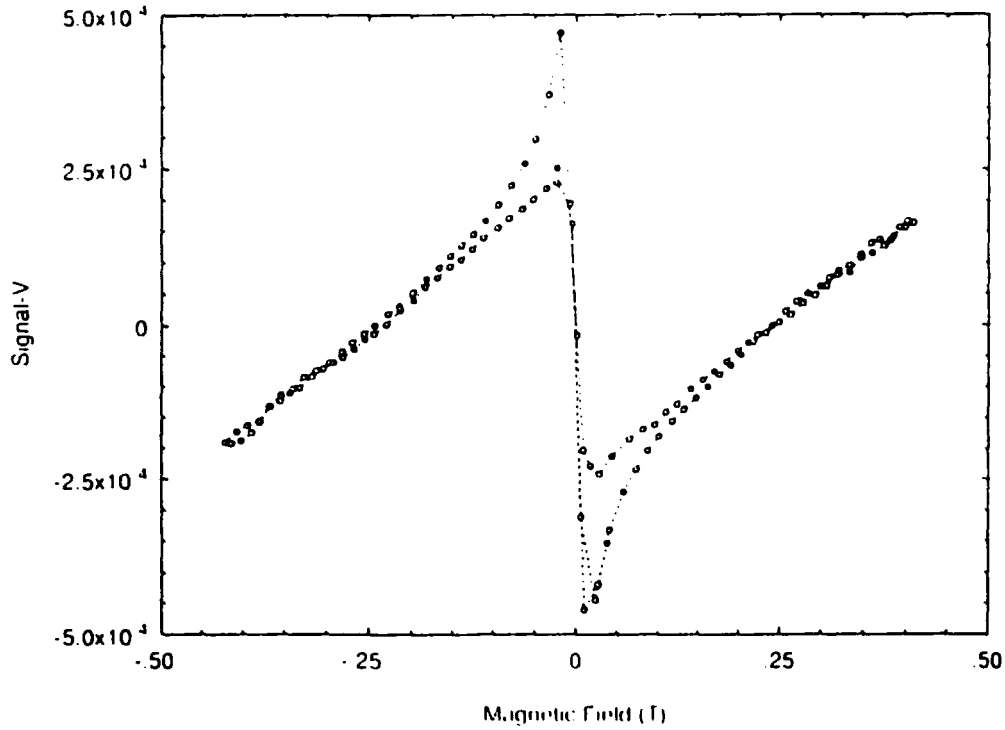

Figure A4.13 (a) The signal obtained from 0.121g of 'YBCO' in the BeCu cell at 85K (squares), where the cell had been pressurised hand tight at room temperature before cooling, together with the signal obtained from 0.121g of 'YBCO' under identical conditions apart from at 95K (triangles). (b) The corrected signal from the 'YBCO' at 85K with signal obtained at 95K subtracted.

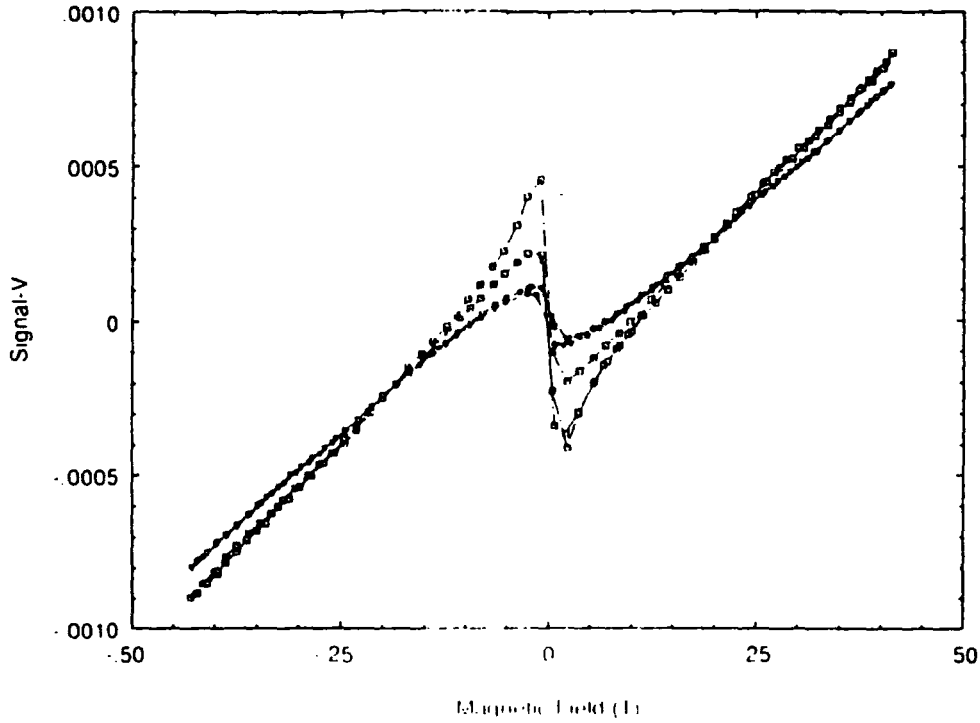

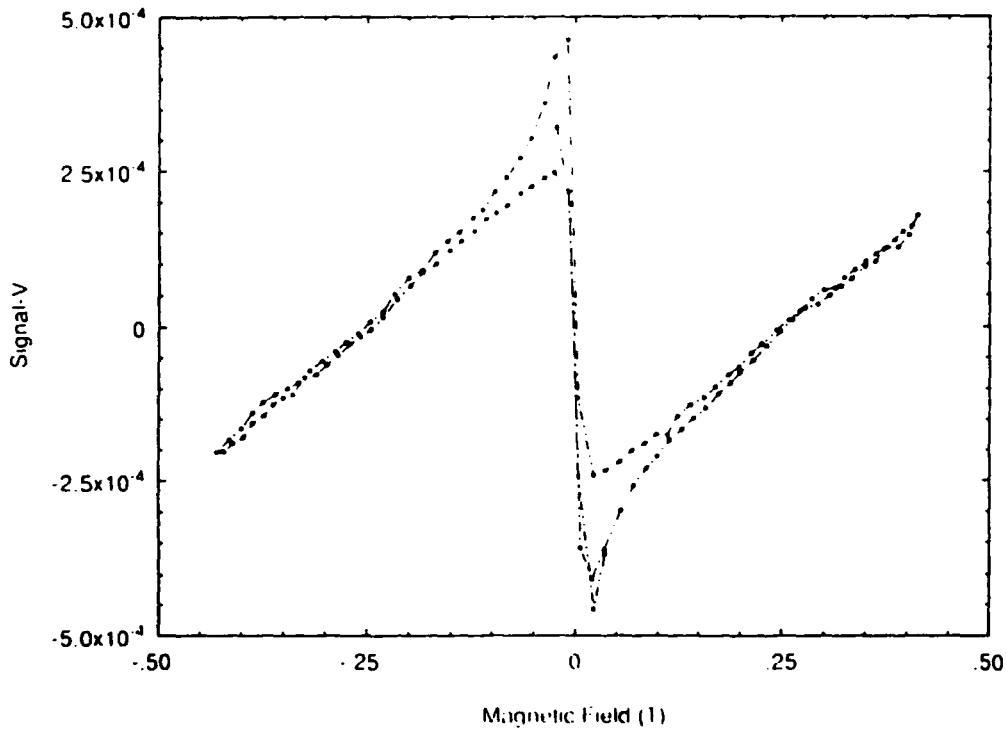

Figure A4.14 (a) The signal obtained from 0.121g of 'YBCO' in the BeCu cell at 85K (squares), where the cell had been pressurised to 1kbar at room temperature before cooling, together with the signal obtained from 0.121g of 'YBCO' under identical conditions apart from at 95K (triangles). (b) The corrected signal from the 'YBCO' at 85K with signal obtained at 95K subtracted.

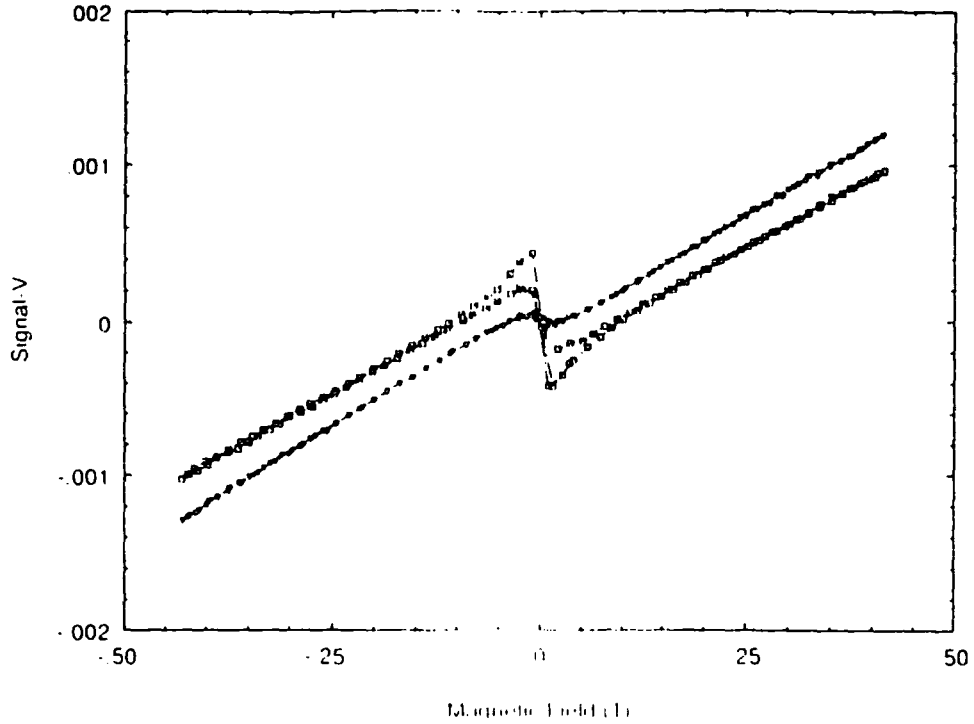

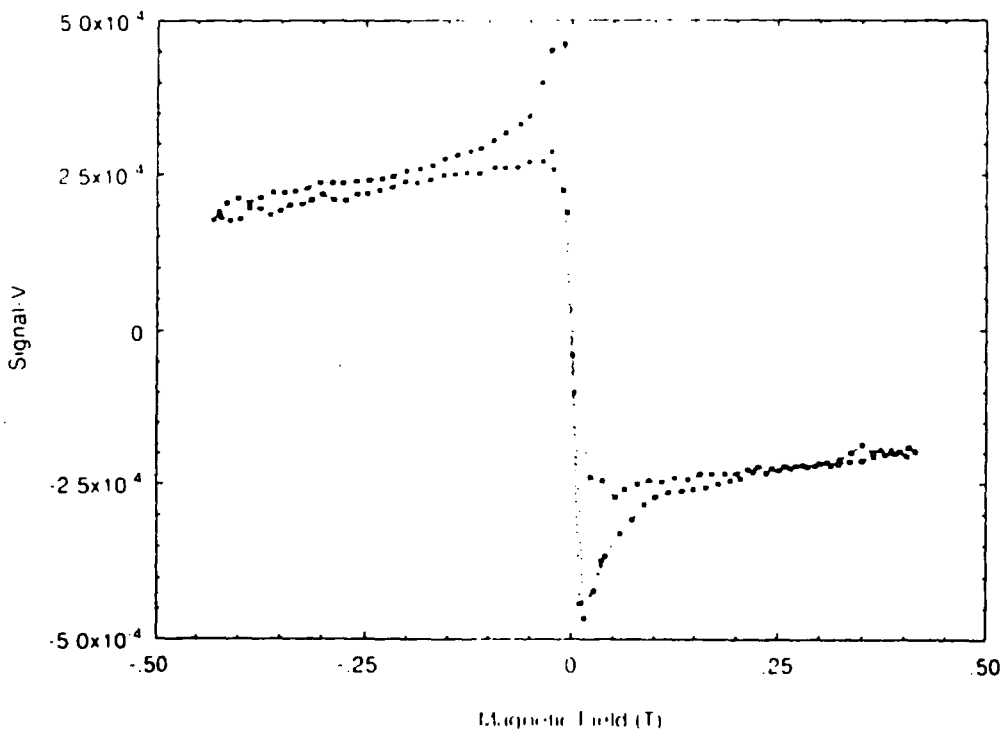

Figure A4.15 (a) The signal obtained from 0.121g of 'YBCO' in the BeCu cell at 85K (squares), where the cell had been pressurised to 2kbar at room temperature before cooling, together with the signal obtained from 0.121g of 'YBCO' under identical conditions apart from at 95K (triangles). (b) The corrected signal from the 'YBCO' at 85K with signal obtained at 95K subtracted.

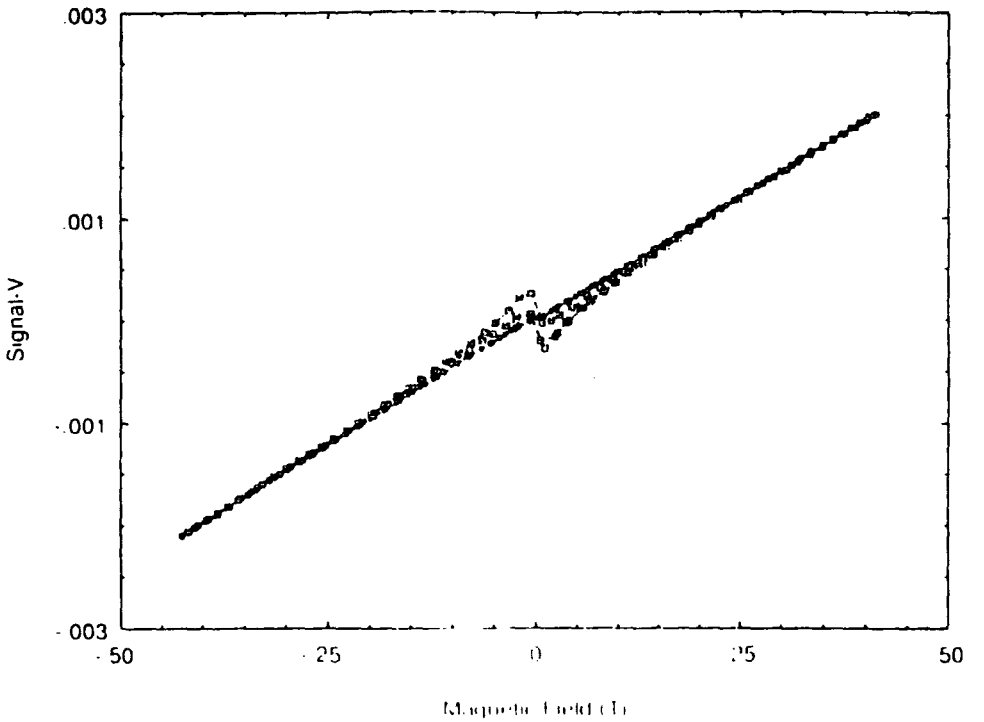

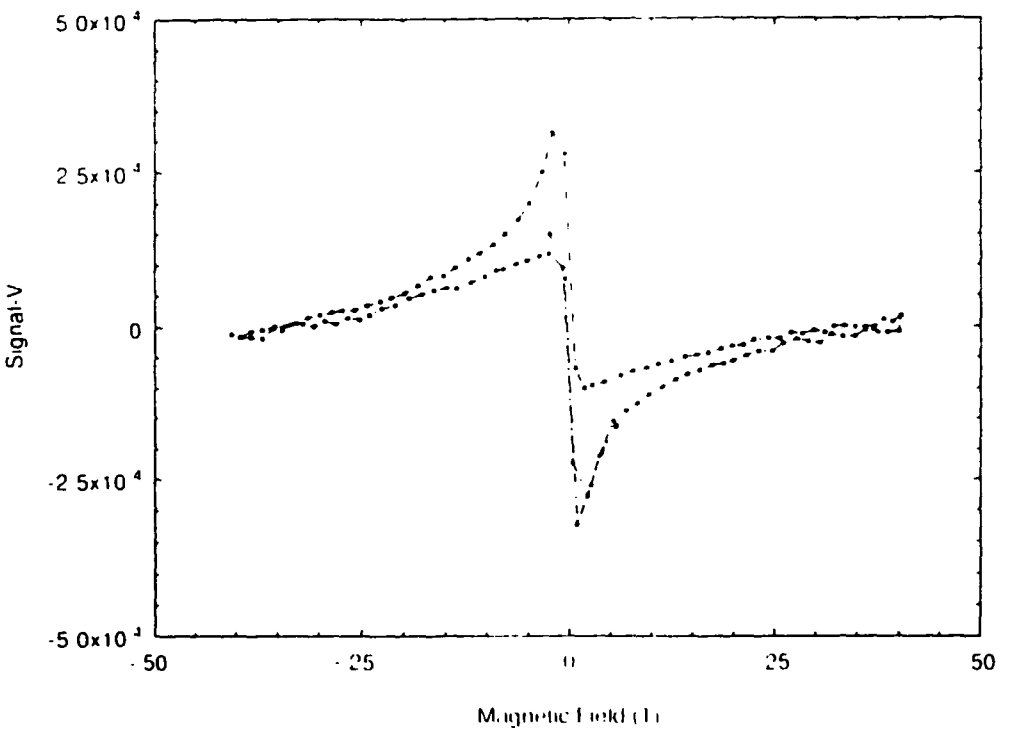

Figure A4.16 (a) The signal obtained from 0.121g of 'YBCO' in the BeCu cell at 85K (squares), where the cell had been pressurised to 4kbar at room temperature before cooling, together with the signal obtained from 0.121g of 'YBCO' under identical conditions apart from at 95K (triangles). (b) The corrected signal from the 'YBCO' at 85K with signalobtained at 95K subtracted.

D.15 References

Bean C.P.(1964), Review of Modern Physics **36**, 31.
Brown S. (1990), Ph. D. Thesis, University of Cambridge.
Delaplace R. *et al.*(1976), Rev. Phys. Appliquee **11**, 327.
Hamann S.D. and Teplitzsky D.R.(1956), Discuss. Faraday Soc. **22**, 114.
Klotz S. *et al.*(1991), Physica C **172**, 423.
Sherman W.F. and Stadtmuller (1987), *'Experimental Techniques in High Pressure ——Research'*, Publ. Wiley and Sons, Chichester.